# Selected Papers in the Hydrologic Sciences 1988–92

December 1992


Comparisons of Ground-Water Quality in Selected Land Use Area, Central Florida

Quantification of Natural Ground-Water Evapotranspiration in Smith Creek Valley, Lander County, Nevada

Climatological and Hydrological Factors Affecting the Lake Thompson Chain of Lakes in Eastern South Dakota

Automatic System for Measuring and Recording Fluorometry Data from Multiple Sources, South Cascade Glacier, Washington

Model Analysis of Hydraulic Properties of a Leaky Aquifer System, Sarasota County, Florida

Maximizing Sustainable Ground-Water Withdrawals—Comparing Accuracy and Computational Requirements for Steady-State and Transient Digital Modeling Approaches

Hydrology and Water-Level Fluctuations of Devils Lake, North Dakota

Geochemical Indicators Used to Determine Source of Saline Water in Mesozoic Aquifers, Montezuma Canyon Area, Utah

Using the Area of Diversion for Pumping Centers to Estimate Potential Freshwater Production in Coastal Aquifers, East-Central Florida

Identification of Net-Flux Rates for Ground-Water Models

A Method for Estimating Velocity and Depth of Streams at Low Flow in Southeastern Louisiana

Issues in Debris–Flow Research: Personal Views

An Examination of Spatially Representative Water-Quality Sampling Methods in the Tidal Potomac River

Modeling Flood Flows From a Hypothetical Failure of the Glacial Moraine Impounding Carver Lake Near Sisters, Oregon

Ground-Water-Flow Modeling and Optimization Techniques Applied to High-Ground-Water Problems in San Bernardino, California

Hydrogeochemical Evidence for Subsurface Inflow to Stagecoach Valley, Lyon County, Nevada

A Comparision of the Brune and Churchill Methods for Computing Sediment Yields Applied to a Reservoir System

Bubble-Gage Registration Errors Caused by Gas Column Density



United States Geological Survey Water-Supply Paper 2340


# AVAILABILITY OF BOOKS AND MAPS OF THE U.S. GEOLOGICAL SURVEY

Instructions on ordering publications of the U.S. Geological Survey, along with prices of the last offerings, are given in th current-year issues of the monthly catalog "New Publications of the U.S. Geological Survey." Prices of available U.S. Geologica Survey publications released prior to the current year are listed in the most recent annual "Price and Availability List." Publication that may be listed in various U.S. Geological Survey catalogs (**see back inside cover**) but not listed in the most recent annual "Pric and Availability List" may be no longer available.

Prices of reports released to the open files are given in the listing "U.S. Geological Survey Open-File Reports," update monthly, which is for sale in microfiche from U.S. Geological Survey Book and Open-File Report Sales, Box 25286, Denver, C 80225. Reports released through the NTIS may be obtained by writing to the National Technical Information Service, U.S Department of Commerce, Springfield, VA 22161; please include NTIS report number with inquiry.

Order U.S. Geological Survey publications **by mail** or **over the counter** from the offices given below.

## BY MAIL

### Books

Professional Papers, Bulletins, Water-Supply Papers, Techniques of Water-Resources Investigations, Circulars, publications of general interest (such as leaflets, pamphlets, booklets), single copies of Earthquakes & Volcanoes, Preliminary Determination of Epicenters, and some miscellaneous reports, including some of the foregoing series that have gone out of print at the Superintendent of Documents, are obtainable by mail from

**U.S. Geological Survey, Book and Open-File Report Sales**
**Box 25286**
**Denver, CO 80225**

Subscriptions to periodicals (Earthquakes & Volcanoes and Preliminary Determination of Epicenters) can be obtained ONLY from the

**Superintendent of Documents**
**Government Printing Office**
**Washington, D.C. 20402**

(Check or money order must be payable to Superintendent of Documents.)

### Maps

For maps, address mail orders to

**U.S. Geological Survey, Map Sales**
**Box 25286**
**Denver, CO 80225**

Residents of Alaska may order maps from

**U.S. Geological Survey, Map Sales**
**101 Twelfth Ave. - Box 12**
**Fairbanks, AK 99701**

## OVER THE COUNTER

### Books and Maps

Books and maps of the U.S. Geological Survey are availabl over the counter at the following U.S. Geological Survey Offices, all c which are authorized agents of the Superintendent of Documents:

- **ANCHORAGE, Alaska**—Rm. 101, 4230 University Dr.
- **LAKEWOOD, Colorado**—Federal Center, Bldg. 810
- **MENLO PARK, California**—Bldg. 3, Rm. 3128, 345 Middle field Rd.
- **RESTON, Virginia**—USGS National Center, Rm. 1C402, 1220 Sunrise Valley Dr.
- **SALT LAKE CITY, Utah**—Federal Bldg., Rm. 8105, 125 Sout State St.
- **SPOKANE, Washington**—U.S. Post Office Bldg., Rm. 135 West 904 Riverside Ave.
- **WASHINGTON, D.C.**—Main Interior Bldg., Rm. 2650, 18t and C Sts., NW.

### Maps Only

Maps may be purchased over the counter at the following U.S Geological Survey offices:

- **FAIRBANKS, Alaska**—New Federal Bldg., 101 Twelfth Ave
- **ROLLA, Missouri**—1400 Independence Rd.
- **STENNIS SPACE CENTER, Mississippi**—Bldg. 3101

# Selected Papers in the Hydrologic Sciences 1988–92

*Edited by* Seymour Subitzky

## December 1992


Comparisons of Ground-Water Quality in Selected Land Use Area, Central Florida
By A.T. Rutledge

Quantification of Natural Ground-Water Evapotranspiration in Smith Creek Valley, Lander County, Nevada
By L.B. Hines

Climatological and Hydrological Factors Affecting the Lake Thompson Chain of Lakes in Eastern South Dakota
By D.S. Hansen and W.A. Miller

Automatic System for Measuring and Recording Fluorometry Data from Multiple Sources, South Cascade Glacier, Washington
By A.G. Fountain

Model Analysis of Hydraulic Properties of a Leaky Aquifer System, Sarasota County, Florida
By C.B. Hutchinson and J.T. Trommer

Maximizing Sustainable Ground-Water Withdrawals—Comparing Accuracy and Computational Requirements for Steady-State and Transient Digital Modeling Approaches
By R.C. Peralta, R.R.A. Cantiller, and G.L. Mahon

Hydrology and Water-Level Fluctuations of Devils Lake, North Dakota
By G.J. Wiche

Geochemical Indicators Used to Determine Source of Saline Water in Mesozoic Aquifers, Montezuma Canyon Area, Utah
By B.A. Kimball

Using the Area of Diversion for Pumping Centers to Estimate Potential Freshwater Production in Coastal Aquifers, East-Central Florida
By Michael Planert

Identification of Net-Flux Rates for Ground-Water Models
By Peter Martin and T.J. Durbin

A Method for Estimating Velocity and Depth of Streams at Low Flow in Southeastern Louisiana
By F.N. Lee

Issues in-Debris-Flow Research: Personal Views
By Cheng-lung Chen

An Examination of Spatially Representative Water-Quality Sampling Methods in the Tidal Potomac River
By R.H. Coupe, Jr.

Modeling Flood Flows From a Hypothetical Failure of the Glacial Moraine Impounding Carver Lake Near Sisters, Oregon
By Antonius Laenen, K.M. Scott, J.E. Costa, and L.L. Orzol

Ground-Water-Flow Modeling and Optimization Techniques Applied to High-Ground-Water Problems in San Bernardino, California
By W.R. Danskin and J.R. Freckleton

Hydrogeochemical Evidence for Subsurface Inflow to Stagecoach Valley, Lyon County, Nevada
By J.R. Harrill, A.H. Welch, and A.M. Preissler

A Comparision of the Brune and Churchill Methods for Computing Sediment Yields Applied to a Reservoir System
By S.W. Trimble and W.P. Carey

Bubble-Gage Registration Errors Caused by Gas Column Density
By Winchell Smith



U.S. GEOLOGICAL SURVEY WATER-SUPPLY PAPER 2340

U.S. DEPARTMENT OF THE INTERIOR
MANUEL LUJAN, Jr., Secretary

U.S. GEOLOGICAL SURVEY
Dallas L. Peck, Director




UNITED STATES GOVERNMENT PRINTING OFFICE: 1992

For sale by
Book and Open-File Report Sales
U.S. Geological Survey
Federal Center, Box 25425
Denver, CO 80225

Selected Papers in the Hydrologic Scienes
ISSN 0892–3450

# PREFACE

*Selected Papers in the Hydrologic Sciences*, a U.S. Geological Survey-managed journal-type publication in the Water-Supply Paper series, is aimed at meeting widespread public and professional needs for results of state-of-the-art broad-based hydrologic studies. The results of these studies are derived from integrated water-resource projects of the Federal research program, Federal-State cooperative program, and, to some extent, work done on behalf of other Federal agencies.

This is the sixth issue of the series and consists of 18 topical papers that address a broad array of topics, including ground- and surface-water hydrology, hydrogeochemistry, land use, and selected hydrologic, geologic, and climatologic techniques for Water-Resources studies.

*Selected Papers* is intended to serve as a forum that encourages dialog between readers and authors. Participation in such dialog among hydroscientists within and outside the Federal sector would be beneficial. Discussion papers by all members of the hydroscience community are desired. A discussion section for readers' comments and authors' replies will be included in each issue. Such discussion papers for this issue will be open until December 1994.

Address comments to:
Editor, Selected Papers in the Hydrologic Sciences
U.S. Geological Survey
12201 Sunrise Valley Drive, MS 443
Reston, VA 22092

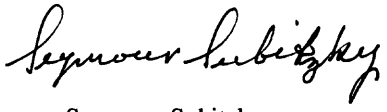

Seymour Subitzky
Editor

## SI AND INCH-POUND UNIT EQUIVALENTS

International System of Units (SI), a modernized metric system of measurement. All values have been rounded to four significant digits. Use of hectare (ha) as an alternative name for square hectometer ($hm^2$) is restricted to measurement of land or water areas. Use of liter (L) as a special name for cubic decimeter ($dm^3$) is restricted to the measurement of liquids and gases.

| Multiply SI units | By | To obtain inch-pound units |
|---|---|---|
| **Length** | | |
| micrometer (μm) | 0.000 039 37 | inch (in) |
| millimeter (mm) | 0.039 37 | inch (in) |
| centimeter (cm) | 0.393 7 | inch (in) |
| meter (m) | 3.281 | foot (ft) |
| | 1.094 | yard (yd) |
| kilometer (km) | 0.621 4 | mile (mi) |
| **Area** | | |
| centimeter$^2$ ($cm^2$) | 0.155 0 | inch$^2$ ($in^2$) |
| meter$^2$ ($m^2$) | 10.76 | foot$^2$ ($ft^2$) |
| | 1.196 | yard$^2$($yd^2$) |
| | 0.000 247 1 | acre |
| hectometer$^2$ ($hm^2$) | 2.471 | acre |
| kilometer$^2$ ($km^2$) | 0.386 1 | mile$^2$ ($mi^2$) |
| **Volume** | | |
| centimeter$^3$ ($cm^3$) | 0.061 02 | inch$^3$ ($in^3$) |
| milliliter (mL) | 0.061 02 | inch$^3$ ($in^3$) |
| liter (L) | 61.02 | inch$^3$ ($in^3$) |
| | 0.035 31 | foot$^3$ ($ft^3$) |
| | 33.82 | ounce, fluid (oz) |
| | 2.113 | pint (pt) |
| | 1.057 | quart (qt) |
| | 0.264 2 | gallon (gal) |
| meter$^3$ ($m^3$) | 35.31 | foot$^3$ ($ft^3$) |
| | 1.308 | yard$^3$ ($yd^3$) |
| | 264.2 | gallon (gal) |
| | 0.000 810 7 | acre-foot (acre-ft) |
| hectometer$^3$ ($hm^3$) | 810.7 | acre-foot (acre-ft) |
| kilometer$^3$ ($km^3$) | 0.239 9 | mile$^3$ ($mi^3$) |
| **Volume per unit time (includes flow)** | | |
| gram per minute (g/min) | 0.035 27 | ounce (avoirdupois) per minute (oz/min) |
| milliliter per minute (mL/min) | 0.033 82 | ounce (fluid) per minute |
| | 0.035 31 | foot$^3$ per second ($ft^3/s$) |
| liter per second (L/s) | 15.85 | gallon per minute (gal/min) |
| meter per second (m/s) | 3.281 | foot per second (ft/s) |
| meter per day (m/d) | 3.281 | foot per day (ft/d) |
| meter$^2$ per day ($m^2/d$) | 10.76 | foot$^2$ per day ($ft^2/d$) |
| meter$^3$ per second ($m^3/s$) | 35.31 | foot$^3$ per second ($ft^3/s$) |
| | 15 850 | gallon per minute (gal/min) |
| **Mass** | | |
| microgram (μg) | 0.000 015 43 | grain (gr) |
| gram (g) | 0.035 27 | ounce, avoirdupois (oz avdp) |
| kilogram (kg) | 0.002 205 | pound, avoirdupois (lb avdp) |
| **Mass per unit volume** | | |
| microgram per liter (μg/L) | 0.000 058 41 | grain per gallon (gr/gal) |
| milligram per liter (mg/L) | 0.058 41 | grain per gallon (gr/gal) |
| **Transmissivity** | | |
| meter$^2$ per day ($m^2/d$) | 10.76 | foot$^2$ per day ($ft^2/d$) |
| **Temperature** | | |
| degree Celsius (°C) | Temp °F = 1.8 temp °C + 32 | degree Fahrenheit (°F) |
| **Specific conductance** | | |
| microsiemens per centimeter at 25 degrees Celsius (μS/cm at 25°C) | 1.000 | micromho per centimeter at 25 degrees Celsius (μmho/cm at 25°C) |
| millisiemens per meter at 25 degrees Celsius (mS/m at 25°C) | 1.000 | millimho per meter at 25 degrees Celsius (mmho/m at 25°C) |

*Sea level*: In this report, "sea level" refers to the National Geodetic Vertical Datum of 1929—a geodetic datum derived from a general adjustment of the first-order level nets of the United States and Canada, formerly called *Sea Level Datum of 1929*.

# CONTENTS

Preface **iii**

SI and Inch-Pound Unit Equivalents **iv**

Comparisons of Ground-Water Quality in Selected Land Use Area, Central Florida
By A.T. Rutledge **1**

Quantification of Natural Ground-Water Evapotranspiration in Smith Creek Valley, Lander County, Nevada
By L.B. Hines **9**

Climatological and Hydrological Factors Affecting the Lake Thompson Chain of Lakes in Eastern South Dakota
By D.S. Hansen and W.A. Miller **21**

Automatic System for Measuring and Recording Fluorometry Data from Multiple Sources, South Cascade Glacier, Washington
By A.G. Fountain **39**

Model Analysis of Hydraulic Properties of a Leaky Aquifer System, Sarasota County, Florida
By C.B. Hutchinson and J.T. Trommer **49**

Maximizing Sustainable Ground-Water Withdrawals—Comparing Accuracy and Computational Requirements for Steady-State and Transient Digital Modeling Approaches
By R.C. Peralta, R.R.A. Cantiller, and G.L. Mahon **63**

Hydrology and Water-Level Fluctuations of Devils Lake, North Dakota
By G.J. Wiche **75**

Geochemical Indicators Used to Determine Source of Saline Water in Mesozoic Aquifers, Montezuma Canyon Area, Utah
By B.A. Kimball **89**

Using the Area of Diversion for Pumping Centers to Estimate Potential Freshwater Production in Coastal Aquifers, East-Central Florida
By Michael Planert **107**

Identification of Net-Flux Rates for Ground-Water Models
By Peter Martin and T.J. Durbin **119**

A Method for Estimating Velocity and Depth of Streams at Low Flow in Southeastern Louisiana
By F.N. Lee **131**

Issues in Debris-Flow Research: Personal Views
By Cheng-lung Chen **137**

An Examination of Spatially Representative Water-Quality Sampling Methods in the Tidal Potomac River
By R.H. Coupe, Jr. **145**

Modeling Flood Flows From a Hypothetical Failure of the Glacial Moraine Impounding Carver Lake Near Sisters, Oregon
By Antonius Laenen, K.M. Scott, J.E. Costa, and L.L. Orzol **151**

Ground-Water-Flow Modeling and Optimization Techniques Applied to High-Ground-Water Problems in San Bernardino, California
By W.R. Danskin and J.R. Freckleton **165**

Hydrogeochemical Evidence for Subsurface Inflow to Stagecoach Valley, Lyon County, Nevada
By J.R. Harrill, A.H. Welch, and A.M. Preissler **179**

A Comparision of the Brune and Churchill Methods for Computing Sediments Yields Applied to a Reservoir System
By S.W. Trimble and W.P. Carey **195**

Bubble-Gage Registration Errors Caused by Gas Column Density
By Winchell Smith **203**

# Comparisons of Ground-Water Quality in Selected Land Use Areas, Central Florida

*By* A.T. Rutledge

**Abstract**

Comparisons are made among ground-water-quality conditions at three test areas in central Florida: (1) a control area, (2) a citrus growing area, and (3) a phosphate mining area. The focus of comparisons is on physical properties, major ions, nutrients, and trace elements in water from the surficial aquifer that underlies the study areas. The level of significance, $\alpha$, was set at 0.05 for all statistical comparisons. Parametric statistical procedures are found to be effective only for comparative analysis of physical properties and major ions, whereas they are of limited use for analysis of nutrient and trace elements because the data do not exhibit normal distributions. Except for pH, all water-quality data analyzed by the parametric statistical procedure required logarithmic data transformation to achieve a normal distribution of the data. Nonparametric statistical procedures can be used for comparative analysis on all types of data because the procedure does not require data that are normally distributed.

The constituents that occur in significantly higher levels in the citrus area than in the control area include potassium and nitrate plus nitrite (both occur at higher levels than in the mining area) in addition to boron, alkalinity, sodium, cobalt, and manganese. The constituents that occur in significantly higher levels in the mining area than in the control area include pH, fluoride, ammonia, orthophosphorus, arsenic, iron, nickel, alkalinity, sodium, cobalt, and manganese (all occur at higher levels than in the citrus area), in addition to zinc and potassium. Conductance and concentrations of calcium, chloride, hardness, magnesium, sulfate, chromium, and strontium are significantly higher in both developed areas than in the control area, yet show no significant difference between the developed areas. Concentrations of barium, cadmium, copper, lead, mercury, molybdenum, selenium, and silver show no significant differences among the three test areas.

On the basis of statistical comparisons, demonstrable relations exist between land use and the concentrations or numerical values at which water-quality constituents occur in ground water.

## INTRODUCTION

### Background and Purpose

Human activities at land surface can affect the quality of water that recharges ground-water systems. Because ground water is the principal source of drinking water in many areas, it is important to know the relation between land use and ground-water quality. This study is one of seven being conducted throughout the country as part of the Toxic Substances Hydrology Program of the U.S. Geological Survey to assess nonpoint source ground-water contamination. The overall objective of the program is to assess the current quality of the Nation's ground-water resources and the nature and extent of the ground-water contamination problem (Helsel and Ragone, 1984).

This report documents statistical comparisons of ground-water-quality conditions at three test areas in Florida: (1) a control area where land use is minimal, (2) a citrus growing area where effects of agriculture on ground water may be expected, and (3) a phosphate mining area where effects of mining activities on ground water may be expected. Because the two developed areas are representative of land uses that are much more extensive than the test areas used, and the control area is similarly representative of near pristine conditions that exist over a larger area, results of this study may be transferable to other areas. This study addresses water-quality conditions in the surficial aquifer, which consists of sand and clay beds of Pleistocene and Holocene age, that underlies the three test areas. The constituents of interest include physical properties such as specific conductance and pH, major ions, nutrients, and trace elements.

### Geohydrologic Setting

The climate in central Florida is subtropical humid and is characterized by relatively wet summers and mild, relatively dry winters. The average annual temperature is 71 °F, and average annual rainfall is about 53 in.

The topography in most of the control area and the citrus growing area is characterized as karst. This is the name applied to the undulating, pitted land surface where sinkholes are numerous and drainage is primarily downward into deep aquifers instead of laterally into streams. The topography of the phosphate mining area is modified flatlands.

All three study areas are underlain first by the surficial aquifer, composed of sand and clay beds of Pleistocene and Holocene age, and at depth by the Floridan aquifer system, composed of fractured limestone and dolomitic limestone of Paleocene to early Miocene age. Between these units lies a sequence of generally discontinuous beds of clay, marl, sand, and limestone of Miocene age. Where the limestone is thick and laterally extensive enough to constitute an aquifer, as it is in the phosphate mining area, the sequence is known as the intermediate aquifer. In the other two study areas, the limestone is missing, and the sequence of beds is primarily a confining unit. The thickness of the surficial aquifer ranges from 0 to 180 ft and averages about 60 ft in these study areas. The depth to the water table in the surficial aquifer ranges from 0 to 100 ft and averages about 20 ft. The intermediate aquifer has an average thickness of 120 ft in the mining area and is absent in the other two areas. The Floridan aquifer system is from 1,500 to 3,500 ft thick in central Florida. The most important unit for water supply in central Florida is the Floridan aquifer system. In the phosphate mining area, the intermediate aquifer is also important for water supply. Most of each study area may be characterized as areas of recharge to the Floridan aquifer system. Thus, there is potential for movement of contaminants from the land surface to this aquifer system.

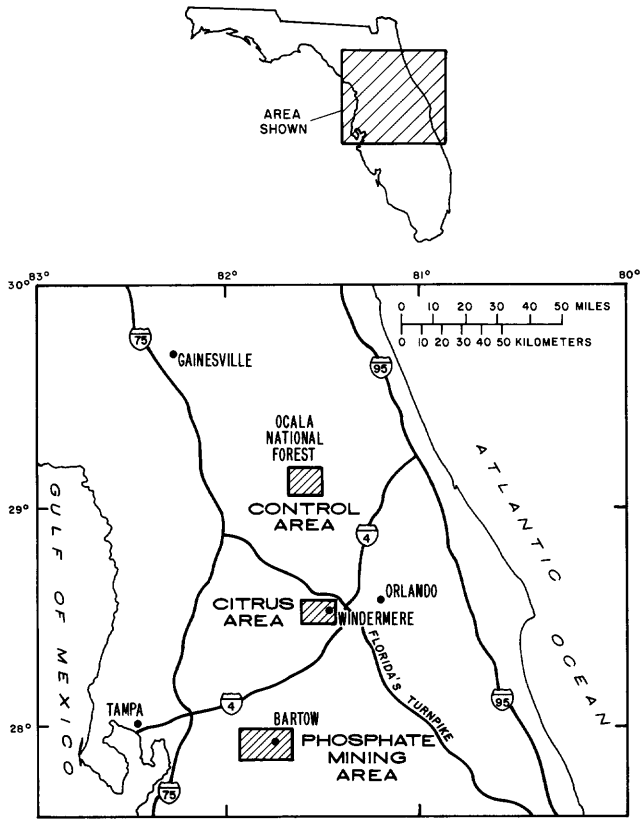


**Figure 1.** Locations of study areas.

## Descriptions of Study Areas

### Control Area

The control area is 30 mi north-northwest of Orlando (fig. 1) in the southern part of the Ocala National Forest and is one of the least developed areas in central Florida. Most (65 percent) of this study area is upland forest, and the remainder consists of wetlands, lakes, and rangeland in approximately equal parts. The control area has only been studied to a limited extent in the past, so little ground-water quality data were available before the present study.

Large parts of the control area are periodically subjected to logging activities. A small subarea within the control area is used as a military bombing range, but no water-quality samples were taken within this subarea.

### Citrus Growing Area

The citrus growing area (fig. 1) is about 15 mi west-southwest of downtown Orlando and is bounded on the east by the town of Windermere. Approximately 40 percent of the area is occupied by citrus groves, and the remainder is cropland, pastures, wetlands, lakes, and barren land. Citrus farming is one of the largest industries in Florida.

Optimal production of citrus in this area requires large withdrawals of water from the Floridan aquifer system for irrigation and requires the use of numerous agricultural chemicals, including fertilizers and pesticides. Methods of application of these chemicals include spraying and direct application to the soil and trees. The chemicals applied at the land surface include nitrogen, phosphorus, potassium, calcium, magnesium, sulfur, iron, copper, manganese, zinc, boron, and molybdenum and represent potential contaminants that can degrade the quality of water in the underlying surficial aquifer. Another potential source of chemicals that can change the quality of water in the surficial aquifer may be infiltration of mineralized irrigation water from the Floridan aquifer system. Such water includes high concentrations especially of calcium, chloride, magnesium, sodium, and dissolved solids. Little water-quality data from the surficial aquifer were collected in this area before this study.

### Phosphate Mining Area

The phosphate mining area (fig. 1) is 25 mi east of Tampa and includes the town of Bartow. This study area is one of the most heavily mined areas in central Florida, where about one-fifth of the world's phosphate production occurs. Land cover includes barren land, rangeland, industrial complexes, lakes, and wetlands. Most of the barren land and rangeland are mined areas in various stages of reclamation.

Phosphate ore is found in a confining layer between the surficial aquifer and the intermediate aquifer. Mining is accomplished by dragline excavation of the overburden (the surficial aquifer) followed by removal of phosphate ore for processing.

Upon excavation, the ore is mixed with water, and the resulting slurry is transported through pipes to an ore processing plant. The processing plant separates the phosphate from the unwanted sands and clays. A sand slurry and a clay slurry are then disposed of in sand tailings and slime ponds, respectively. The phosphate is transported to a chemical processing plant where a reaction with sulfuric acid produces phosphoric acid. A voluminous byproduct of gypsum is transported as slurry to gypsum stacks for disposal. Water used at the ore processing plants and the chemical processing plants is obtained from the intermediate aquifer and the Floridan aquifer system. The water used at the plants is recycled.

Activities associated with the phosphate industry can create potential sources of contamination of ground water in several ways. These sources, which consist of sand tailings, slime ponds, recirculation ditches, gypsum stacks, and cooling ponds near gypsum stacks, can degrade the quality of water in the surficial aquifer. Furthermore, because chemical reactions between acidic process waters and aquifer materials will dissolve many substances, some elements may have increased mobility in ground water. Some organic compounds may enter ground water because mixtures of organic compounds are used in processing plants to facilitate separation processes. Another possible alteration in the chemical composition of water in the surficial aquifer may result from withdrawal of mineralized water from deeper carbonate aquifers. Such water is applied to the land surface at sand tailings and slime ponds and may percolate to the water table.

Two reports by Miller and Sutcliffe (1982; 1984) addressed the effects of activities in an ore processing plant and a chemical processing plant on water quality. At the ore processing plant, clay-waste discharges to slime ponds were found to contain high concentrations of trace elements such as iron, manganese, and zinc; water in the slime ponds was found to contain high concentrations of sulfate and sodium. At the chemical plants, process waters were found to have higher concentrations of most ions than natural waters. Water in a well completed in the surficial aquifer and located one-third mile from a gypsum stack had concentrations of sulfate, sodium, silica, ammonium, and orthophosphorus that were significantly above background concentrations. Two other wells completed in the surficial aquifer and adjacent to the gypsum stack yielded water having elevated concentrations of iron, manganese, cadmium, chromium, cobalt, copper, molybdenum, nickel, strontium, zinc, arsenic, and boron.

## SAMPLING PROGRAM

The ground-water sampling program was undertaken to determine prevailing chemical characteristics of surficial aquifer water under each of the three areas having different land uses and to ensure that results would be representative of conditions for each area. In the control area, sites were chosen that would not be affected by human activity such as buildings, roads, agriculture, excavations, logging areas, or livestock feeding lots. Sites were chosen that were widely distributed over the study area and that would represent differing geohydrologic environments (to the extent possible in this relatively homogeneous area). In the citrus area, sites were chosen that were within or immediately downgradient of citrus groves. Most were inside groves but within a few feet of the downgradient edge. Sites were widely distributed over the study area in many different geohydrologic environments, and the groves in which sites were located represent various degrees of crop age and growth condition. In the mining area, sites were selected to represent as many of the mining and ore processing activities as possible, so that the site distribution would be representative of the distribution of the activities. For example, because most of the study area is located on reclaimed land, many of the sites were on reclaimed land, but there were a few sites selected on new sand tailings, a few near slime ponds, and a few next to cooling ponds and gypsum stacks.

Existing wells tapping the surficial aquifer were pumped and sampled. Because there were few existing wells, additional water samples were obtained from a portable drive-point sampler. Evacuation of water from existing wells was accomplished with a centrifugal pump, and final sampling from wells and from the portable drive-point sampler was accomplished with a peristaltic pump.

Samples were analyzed for physical properties, major ions, nutrients, and trace elements (table 1). Conductance and pH were determined in the field on the raw water sample. Nutrients and trace elements were analyzed on unfiltered samples, so results represent total concentrations (dissolved plus suspended). The major ions and the trace elements iron and manganese were analyzed on filtered samples, so results represent dissolved concentrations. Samples were analyzed by standard U.S. Geological Survey procedures described by Skougstad and others (1979).

**Table 1.** Physical properties and chemical constituents used in the comparison analysis

| Physical properties | | Trace elements (total) |
|---|---|---|
| Specific conductance, field | | Arsenic. |
| Specific conductance, lab | | Barium. |
| pH, field | | Boron. |
| Alkalintry, lab | | Cadmium. |
| Hardness | | Chromium. |
| | | Cobalt. |
| | | Copper. |
| Major ions (dissolved) | Nutrients (total) | Iron.[1] |
| | | Lead. |
| | | Manganese.[1] |
| Calcium | Ammonia | Mercury. |
| Chloride | Nitrate plus | Molybdenum. |
| Fluoride | nitrite. | Nickel. |
| Magnesium | Orthophosphorus | Selenium. |
| Potassium | | Silver. |
| Sodium | | Strontium. |
| Sulfate | | Zinc. |

[1]These trace elements also were analyzed for dissolved concentration.

## METHODS OF DATA ANALYSIS

Study areas were compared by pairs to evaluate their similarity or difference in chemical constituent occurrence. For each constituent, three statistical comparisons were made between the (1) control area and citrus area, (2) control area and mining area, and (3) citrus area and mining area. The purpose of each statistical comparison was to ascertain whether there was a significant difference between the means or the mean ranks.

The structure of each statistical comparison consists of (1) a null hypothesis $H_o$—that no significant difference exists—and (2) the alternate hypothesis $H_1$—that a significant difference exists. The level of significance, $\alpha$, was set at 0.05 for all analyses. Procedures used are those described by Iman and Conover, 1983.

A significant difference between results from a developed area and the control area may indicate an effect of that particular land use. Furthermore, if a constituent occurs at significantly higher levels at one developed area than it does at the other developed area and the control area, then there is stronger support for the possible effect. If a constituent occurs at higher levels in both developed areas than it does in the control area, whereas there is no difference between the developed areas, then it may be an effect of both land uses and, possibly, an effect that many land uses would have on water quality. Overall conclusions such as these, which are based on simultaneous results from three statistical comparisons, have less accuracy associated with them than the individual comparisons. Therefore, an overall statistical comparison method is also used to ascertain whether there is a significant difference among the three study areas at the 0.05 level of significance.

### Parametric Methods

Parametric statistical comparisons are attempted twice for each group pair—once on the raw data and once on the logarithms of raw data. For each of these analyses, a set of procedures that includes a test for normality, a comparison of variances, and a comparison of means is used. These steps are described here and diagramed in figure 2.

Before the statistical comparisons described here can be executed, it must be confirmed that both data groups come from populations that show normal distributions. Normality is ascertained by using the Lilliefors test (Iman and Conover, 1983, p. 153–155).

Before a test comparing the means of each group can be used, it is necessary to determine if the sample variances for each group are significantly different or not. The test for equality of variances between two sample groups involves the F-distribution. If the variances are not significantly different, then the two-sample T-test can be used to compare means. If the variances of the two sample groups are significantly different, then the Satterthwaite approximation must be used to compare means. The two-sample T-test is considered more reliable than the Satterthwaite approximation.

### Nonparametric Methods

To identify differences between the pairs of data groups, the Wilcoxon-Mann-Whitney rank sum test is used (Iman and Conover, 1983, p. 280–285). This procedure has the advantage of not requiring that the data be normally distributed. Furthermore, it is regarded as a good approximate test even when the assumption of equal variances is not valid.

A nonparametric analysis of variance, known as the Kruskal-Wallis test (Iman and Conover, 1983, p. 418–421), is used to determine if there are significant overall differences among the three data groups. This procedure has the same advantages of not requiring normality nor equal variances.

## DISCUSSION OF RESULTS

Generally, parametric analysis is possible only on the physical properties (pH and conductance) and major ions. Most parametric analyses are accomplished on the logs of raw data, whereas the pH is the only property for which

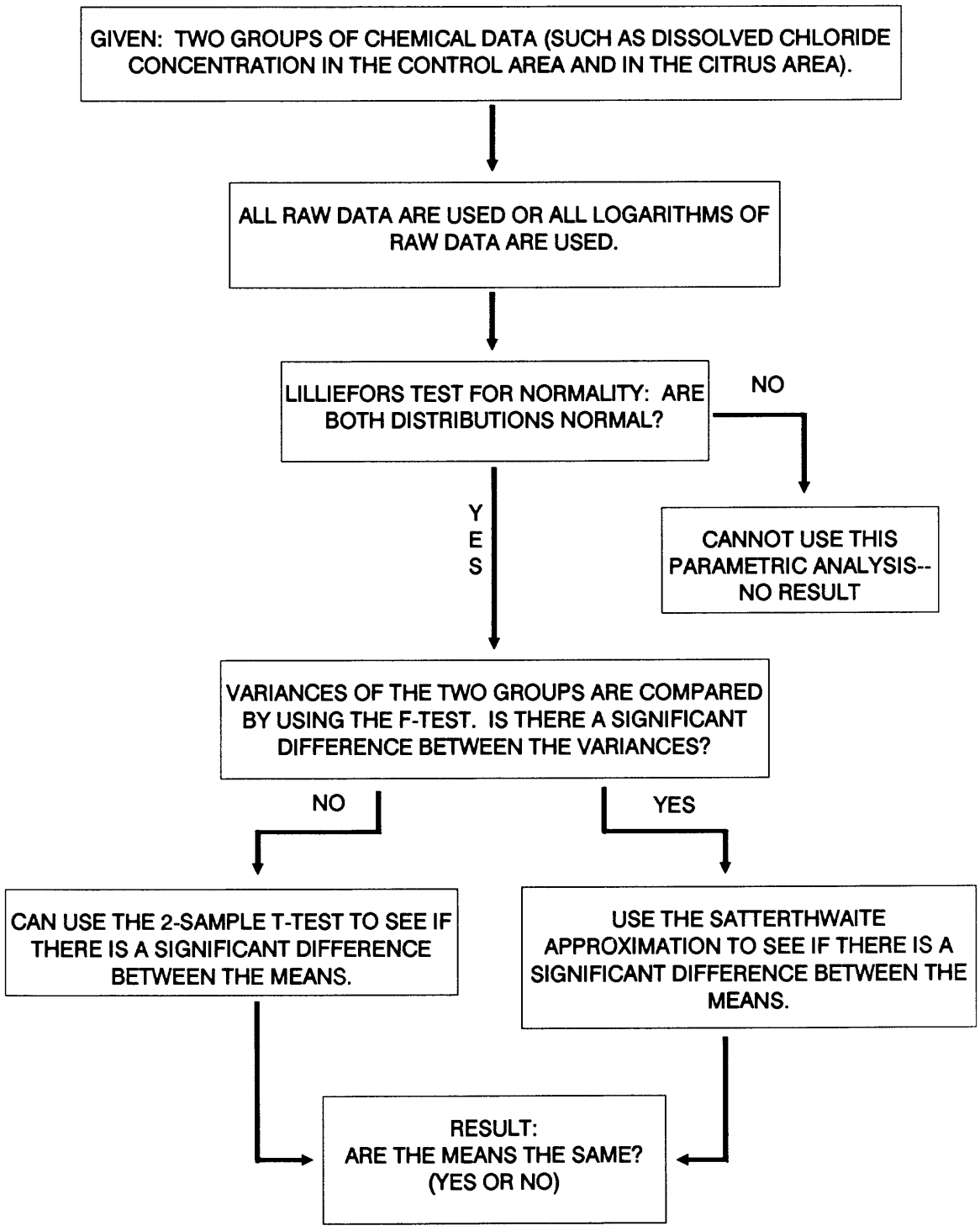


**Figure 2.** Steps used to conduct a parametric analysis to detect a difference in the means between two groups.

three complete parametric pair comparisons of raw data are possible. The nutrients and trace elements are not conducive to parametric methods because of the absence of normality in their distributions (both raw and log data).

Because of the absence of requirements for normality and for equal variance, nonparametric analysis can be conducted on all possible group pairs by using the Wilcoxon-Mann-Whitney rank sum test. Results of this test are in

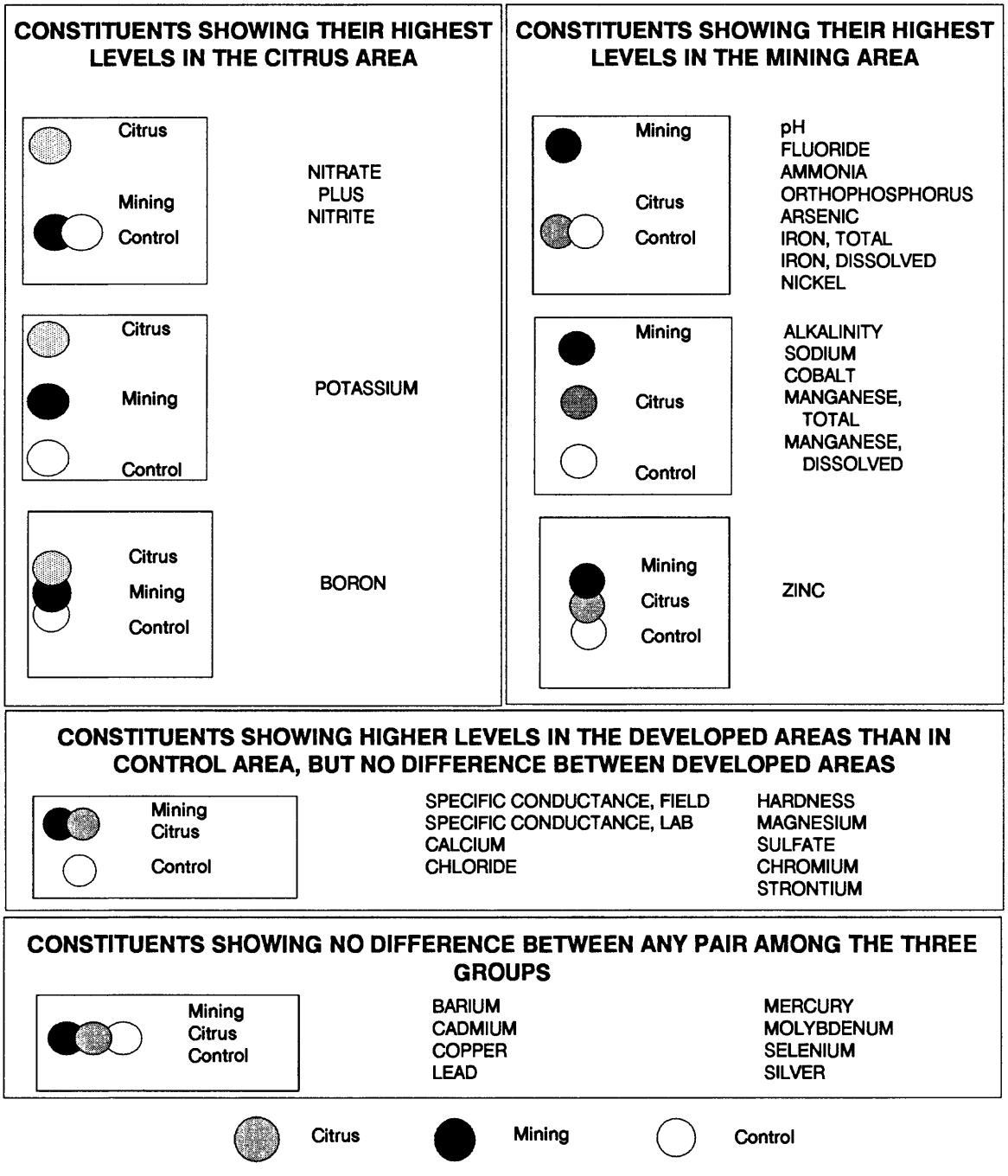


**Figure 3.** Differences in ground-water quality among the three study areas.

reasonable agreement with those from parametric analysis, with only 1 conflict out of 42 comparisons. There were no conflicts between results of the Kruskal-Wallis test and any results obtained by other tests.

Schematic representations of the results of all statistical comparisons are shown in figure 3. Relative vertical position of circles represent relative constituent levels for comparisons between land-use areas. Higher position indi-

cates higher constituent levels, and complete separation of circles indicates that a statistically significant difference exists. A summary of findings follows.

No constituents occur at significantly higher levels in the control area than in either of the developed areas.

The constituents that occur in significantly higher levels in the citrus area than in the control area include potassium and nitrate plus nitrite (which occurred at higher levels than in the mining area) and boron, alkalinity, sodium, cobalt, and manganese. Elevated levels of these constituents may be related to chemicals used in citrus growing.

The constituents that occur in significantly higher levels in the mining area than in the control area include pH, fluoride, ammonia, orthophosphorus, arsenic, iron, nickel, alkalinity, sodium, cobalt, and manganese (which occurred at higher levels than in the citrus area) and zinc and potassium. These elevated levels may be related to phosphate mining and processing activities such as the disruption of the surficial aquifer, the disposal of sand and clay in sand tailings and slime ponds, and the acidification of process water used at chemical processing plants.

Constituents that occur at significantly higher levels in both developed areas than in the control area, yet show no significant difference between the developed areas, are conductance, calcium, chloride, hardness, magnesium, sulfate, chromium, and strontium. This may indicate that the reason for their higher levels is a process that is common to both areas, such as withdrawals from deeper carbonate aquifers and subsequent application of this water to the land surface.

Constituents that show no significant differences among the three test areas are barium, cadmium, copper, lead, mercury, molybdenum, selenium, and silver. It may be that concentrations of these constituents in ground water are not affected by the land uses studied or that the variance of the data is so large that differences in means cannot be detected.

There are demonstrable relations between land use and the levels at which chemical constituents occur in ground water. This report documents findings resulting from early phases of study. Ongoing work is expected to enhance the understanding of mechanisms by which land use affects ground-water quality and reveal why some chemicals introduced at the surface affect ground-water quality whereas others do not. The scope of future work at these sites is expected to include organic compounds.

## SELECTED REFERENCES


Helsel, D.R., and Ragone, S.E., 1984, Evaluation of regional ground-water quality in relation to land use: U.S. Geological Survey Toxic Waste—Ground-Water Contamination Program: U.S. Geological Survey Water-Resources Investigations Report 84–4217, 33 p.

Hutchinson, C.B., 1978, Appraisal of shallow ground-water resources and management alternatives in the upper Peace and eastern Alafia River basins, Florida: U.S. Geological Survey Water-Resources Investigations Report 77–124, 57 p.

Iman, R.L., and Conover, W.J., 1983, A modern approach to statistics: New York, John Wiley and Sons, 497 p.

Knapp, J.L., Tucker, D.P.H., and Fasulo, T.R., 1984, Florida citrus spray guide: Florida Cooperative Extension Service, Institute of Food and Agricultural Sciences, University of Florida, 14 p.

Knochenmus, D.D., and Hughes, G.H., 1976, Hydrology of Lake County, Florida: U.S. Geological Survey Water-Resources Investigations Report 76–72, 100 p.

Lichtler, W.F., Anderson, Warren, and Joyner, B.F., 1968, Water resources of Orange County, Florida: Florida Division of Geology Report of Investigations 50, 150 p.

Miller, J.A., 1982a, Thickness of the Tertiary limestone aquifer system, southeastern United States: U.S. Geological Survey Open-File Report 81–1124, 1 sheet.

———1982b, Thickness of the upper permeable zone of the Tertiary limestone aquifer system, southeastern United States: U.S. Geological Survey Open-File Report 81–1179, 1 sheet.

Miller, R.L., and Sutcliffe, Horace, Jr., 1982, Water-quality and hydrogeologic data for three phosphate industry waste-disposal sites in central Florida, 1979–80: U.S. Geological Survey Water-Resources Investigations Report 81–84, 77 p.

———1984, Effects of three phosphate industrial sites on ground-water quality in central Florida: U.S. Geological Survey Water-Resources Investigations Report 83–4256, 184 p.

Robertson, A.F., and Mills, L.R., 1974, Ground-water withdrawals in the upper Peace and upper Alafia River basins, Florida: Florida Bureau of Geology Map Series 67, 1 sheet.

Rutledge, A.T., 1987, Effects of land use on ground-water quality in central Florida—preliminary results: U.S. Geological Survey Toxic Waste—Ground-Water Contamination Program: U.S. Geological Survey Water-Resources Investigations Report 86–4163, 49 p.

Skougstad, M.W., Fishman, M.J., Friedman, L.C., Erdmann, D.E., and Duncan, S.S., eds., 1979, Methods for determination of inorganic substances in water and fluvial sediments: U.S. Geological Survey Techniques of Water-Resources Investigations, book 5, chap. A1, 626 p.

Stewart, H.G., Jr., 1966, Ground-water resources of Polk County: Florida Geological Survey Report of Investigations 44, 170 p.

U.S. Geological Survey, 1979a, Land use and land cover, 1972, Daytona Beach, Florida: U.S. Geological Survey L–6, 1 sheet, scale 1:250,000.

———1979b, Land use and land cover, 1972, Fort Pierce, Florida: U.S. Geological Survey L–7, 1 sheet, scale 1:250,000.

———1979c, Land use and land cover, 1972, Orlando, Florida: U.S. Geological Survey L–12, 1 sheet, scale 1:250,000.

———1979d, Land use and land cover, 1972, Tampa, Florida: U.S. Geological Survey L–16, 1 sheet, scale 1:250,000.

University of Florida, 1981, Florida statewide pesticide use survey: Office of the Pesticide Coordinator, Institute of Food and Agricultural Sciences, University of Florida, April 1981, 112 p.

# Quantification of Natural Ground-Water Evapotranspiration in Smith Creek Valley, Lander County, Nevada

*By* Lawrence B. Hines

**Abstract**

Natural evapotranspiration rates from the ground-water reservoir in 1983 at Smith Creek Valley, Nevada, were estimated by using foliage-volume density. These rates are based on earlier lysimeter measurements near Winnemucca, Nevada. Native vegetation in Smith Creek Valley was grouped into five zones on the basis of foliage-volume density and plant-species composition. Evapotranspiration rates for three zones dominated by greasewood (*Sarcobatus vermiculatus)* ranged from 0.1 to 0.9 foot per year, whereas the rate for stands of pure rabbitbrush (*Chrysothamnus*) was 0.3 foot per year. A value of 0.5 foot per year used in previous work was applied to grass (*Distichlis spicata* and *Elymus cinerous*). Discharge from the bare playa soil was estimated by discretizing the vertical hydraulic-head gradient into zones bounded by equal-gradient lines at a 0.05-foot-per-foot interval, and then applying a form of Darcy's Law. Evaporation rates for bare soil ranged from less than 0.1 to 0.5 foot per year. Estimated annual evapotranspiration is 5,700 acre-feet for natural vegetation and 2,400 acre-feet for bare soil; thus, total ground-water discharge by natural evapotranspiration is approximately 8,100 acre-feet per year.

## INTRODUCTION

Water budgets for hydrologically closed rural valleys in the Great Basin are typically dominated by recharge to basin-fill aquifers from rainfall and discharge from these aquifers by evaporation and transpiration of ground water from bare-soil playas and adjacent phreatophytic vegetations. For these budgets, evapotranspiration discharge can be used to corroborate recharge estimates and to determine the amount of water that might be diverted for beneficial use. Although many studies have been conducted to determine the effects of vegetation on rivers and lakes supplying water to major urban and agricultural areas in the Southwest, results of such studies commonly are difficult to apply to hydrologic systems in the Great Basin. The difficulty in quantifying evapotranspiration discharge stems from the absence of algorithms that relate evapotranspiration rates to differences in climate, plant species, and soil properties. A study near Winnemucca, Nev. (Robinson and Wannanen, 1970), related ground-water evapotranspiration rates to foliage-volume density for woody phreatophytes common to Nevada and Utah; the results of this study allowed some uncertainties associated with variance of climate and plant morphology to be circumvented. This report shows how results of the Winnemucca study were combined with knowledge about evaporation and transpiration of ground water by plants and evaporation of water from bare soil to estimate total evapotranspiration from the aquifer in Smith Creek Valley, Nev.

Smith Creek Valley, which is near the center of Nevada (fig. 1), contains a closed-basin aquifer system where virtually all inflow and outflow of water occurs within the watershed. The valley occupies an area of 583 $mi^2$ and ranges in altitude from about 6,000 ft to about 10,000 ft above sea level. The valley floor contains two adjacent playas. The main playa (fig. 1) covers about 19 $mi^2$. It occupies the lowest part of the valley floor and is underlain by a shallow water table. Several small thermal springs are present along the southwest margin of the main playa. The north playa (fig. 1) is a bare-soil area of about 1.6 $mi^2$ that formed after a gravel bar blocked the surface drainage just north of the main playa.

The surface drainage is from the mountains that border the valley toward the main playa. Flow across the valley floor is ephemeral and reaches the main playa only during spring runoff periods of wet years or after high intensity precipitation. The major drainages are Smith Creek and Campbell Creek from the Desatoya Mountains and Peterson Creek from the Shoshone Mountains (fig. 1). Annual precipitation on the valley floor is about 6 in. (Thomas and others, 1989, p. E5).

Ground water in Smith Creek Valley is discharged by evapotranspiration from naturally vegetated areas adjacent to the playas and by evaporation from bare playa soil (combined area, 47 $mi^2$). Also, ground-water discharge

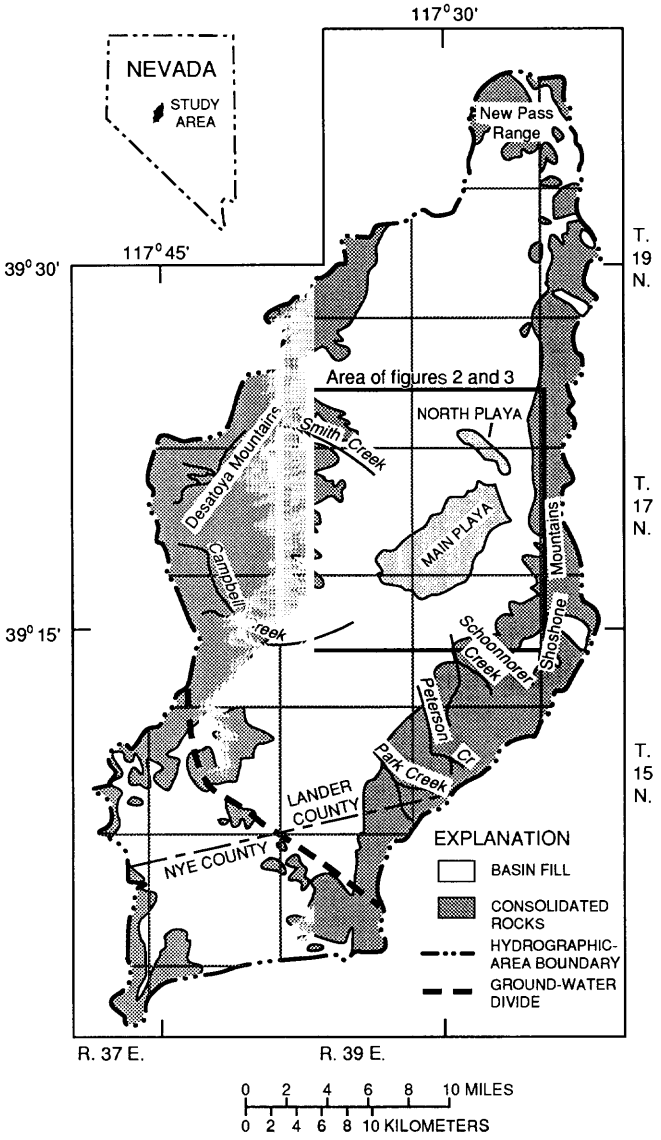


**Figure 1.** Location of Smith Creek Valley, Nev.

includes withdrawals to irrigate four alfalfa fields, but this discharge is not considered in this study. Additionally, some water discharges from thermal springs, but it is accounted for in this report as evapotranspiration by saltgrass near these springs.

The purpose of this report is to estimate ground-water discharge by evaporation from bare soil and evapotranspiration by indigenous vegetation in Smith Creek Valley, Nev. During the initial attempt to accomplish this purpose, it was discovered that appropriate methods were either nonexistent or undocumented. Consequently, the scope of work was extended to include the development and documentation of a method that could be applied to other valleys in the Great Basin as well as to Smith Creek Valley.

The scope of the study described herein was confined to combining vegetation mapping and lysimeter data from previous studies (Horton and others, 1964; Robinson, 1970) in a nonideal setting. The study is intended to relate directly to closed basins more than 5,000 ft above sea level in the Northern Great Basin having big greasewood [*Sarcobatus vermiculatus* (Hook.) Torr.], rabbitbrush [*Chrysothamnus*], and saltgrass [*Distichlis spicata* (L.) Greene] as their principal vegetation types. It assumes that specific evapotranspiration rates as a function of foliage-volume density are known at the outset. It does not discuss the determination of those rates, so application of this method to settings significantly differing in climate or species types may not be appropriate.

This work was done in support of the Great Basin Regional Aquifer-System Analysis (RASA) study begun by the U.S. Geological Survey in 1981 (Harrill and others, 1983, p. 42). As a part of the RASA study, hydrologic data were collected for use in calibration of a mathematical ground-water flow model. Some of these data form the basis of this report.

## EVAPOTRANSPIRATION IN PHREATOPHYTE AREAS

The study of evapotranspiration in phreatophyte areas comprises three parts: (1) identification of zones where evapotranspiration of ground water occurs, (2) identification and mapping of plant-type and density zones within those areas, and (3) estimation of zone-specific phreatophyte discharge rates.

### Types and Distribution of Vegetation

Plants in the study area were divided into two hydrologic groups: xerophytes and phreatophytes. A xerophyte derives water primarily from surface-water infiltration, whereas a phreatophyte derives most of its water from the underlying aquifer (Meinzer, 1927, p. 1). Commonly, phreatophyte species can exist in xerophytic areas where surface-water runoff infiltrates and is temporarily stored as soil moisture or perched ground water, so a rigorous definition of phreatophytic evapotranspiration is required to avoid incorporation of xerophytic areas in the phreatophytic ground-water discharge zone. In this study, the term "phreatophyte" refers to a plant using water whose hydraulic-head-gradient tensor has virtually no downward component normal to land surface. This constraint includes plants growing where ground water flows parallel to or toward the land surface but excludes plants maintained by shallow perched water or surface-water runoff.

The distribution of phreatophytes is a function of their ability to obtain ground water and is directly related to root depth, depth to the water table, and hydraulic characteristics of the soil. This relation is distorted by the infiltration of surface-water runoff, which allows phreatophytes to prop-

agate into areas where the depth to ground water is greater than the common depth penetration of phreatophyte roots. Xerophytic areas of this type are prevalent in the west-central and southwest parts of Smith Creek Valley at the effluences of Smith and Campbell Creeks. In contrast to these areas having surface-water augmentation, the east side of the valley has little runoff, and the extent of phreatophyte distribution is better defined.

Three principal genera of natural phreatophytes in Smith Creek Valley are big greasewood, rabbitbrush, and saltgrass (fig. 2). Great Basin wildrye (*Elymus cinerus* Scirbn. and Merr.), a phreatophytic grass, is also present in two abandoned fields, but wildrye appears to be yielding to rabbitbrush incursion. Because grasses constitute a minor part of the total discharge area and because useful information on evapotranspiration rates for native phreatophytic grasses is minimal, areas of wildrye were included with areas of saltgrass in this study.

Of the three principal phreatophyte genera, greasewood has roots that penetrate deepest, commonly reaching water at approximately 15 to 20 ft below land surface. It has been argued (Meinzer, 1927, p. 41) that greasewood may obtain water from depths greater than 50 ft, but this condition is rare and probably indicates an atypical growth pattern. Greasewood is commonly found several miles from the main playa in Smith Creek Valley, but in these areas it achieves a height of only 1 ft and has a shrubby appearance with muted coloration—a morphology presumed to be indicative of an environment lacking water. Within half a mile of the east margin of the main playa, the outer phreatophytic boundary occurs where the depth to water is approximately 25 ft. Plants outside of this boundary exhibit a uniformly scrubby appearance, whereas plant vigor changes distinctly at the boundary, and areas of decreasing depth to water within the zone exhibit a dramatic enhancement of color, height, and density of vegetation. Adjacent to the main playa, greasewood leaves are darker, greener, and longer (at typically three-fourths of an inch they have twice the length exhibited by plants growing in the xeric region), and maximum plant height exceeds 2 ft.

Greasewood dominates the east and north sides of the discharge area and shows greatest foliage density in the southeast and least foliage density in the northeast. Scattered plants grow on the north and east sides of the north playa (fig. 2), but their vigor is believed to result from water pooled during sporadic storm events. The depth to water along the east edge of the main playa is approximately 12 ft, therefore, little phreatophytic grass survives. Rabbitbrush on the east side of the valley only grows along stream channels.

In contrast to the more arid east side of valley, the south, west, and northwest sides are heavily wetted during the spring and early summer by Smith and Campbell Creeks as well as by numerous other small streams. Much of this area is dominated by dense stands of rabbitbrush (fig. 2) that commonly exceed 3 ft in height. No rabbitbrush species have been specified in this report because the number of species and subspecies is great and time did not allow detailed taxonomic investigations. At least two species (*Chrysothamnus nauseosus* and *C. pumilus*) have phreatophytic subspecies (Robinson, 1958, p. 53), and only *C. nauseosus* is documented in States other than Idaho. In Smith Creek Valley, phreatophytic and xeric areas support rabbitbrush with differing morphologic characteristics. This condition seems related to differences in moisture availability, rather than to different species, and is a criterion used to identify zone boundaries. Phreatophytic rabbitbrush has a broomlike appearance produced by slender secondary branches radiating from primary branches and leafed only at the tips. In xeric areas, rabbitbrush branches are short, leafy, and generally more intricately branched.

Phreatophytic grasses in Smith Creek Valley grow where the depth to water is least—typically less than 7 ft. Great Basin wildrye grows in an abandoned hay field at the terminus of Campbell Creek and in another field at the terminus of Smith Creek. Information regarding former crop types and length of abandonment was not available at the time of the study, but the size of rabbitbrush companion plants suggests that at least a decade has elapsed since the most recent cultivation. This wildrye may have been cultivated as "natural" hay, or it may be only an intermediate successor plant type. At both locations, rabbitbrush is propagating into the grass area and presumably will ultimately replace it. In its current state, wildrye grows in varying density ranging from lush stands to scattered clumps, with heads reaching 4 to 5 ft in height.

Saltgrass is restricted to the area adjacent to thermal springs at the southwest edge of the main playa where the water table is shallow. Cover ranges from moderate to heavy, but most blades are less than 5 in. tall, and the most vigorous growth approaches only 1 ft in height along the margins of spring openings. Some saltgrass extends onto the southwest margin of the main playa for approximately 1 mi but is so sparse that its role in evapotranspiration seems negligible.

## Identification and Mapping of Phreatophytic Areas

Phreatophyte assemblages and densities were mapped to determine zones having similar composition (fig. 2). The outer boundary of the phreatophytic area was mapped first by driving along the perimeter and recording its location with a radio navigation instrument. Visual identification of this perimeter was complicated by frequently encountered propagation of normally phreatophytic plants into xerophytic regions. In contrast, sagebrush, the principal xerophyte in the study area, seldom grows in phreatophytic areas, so identification of the discharge boundary was most

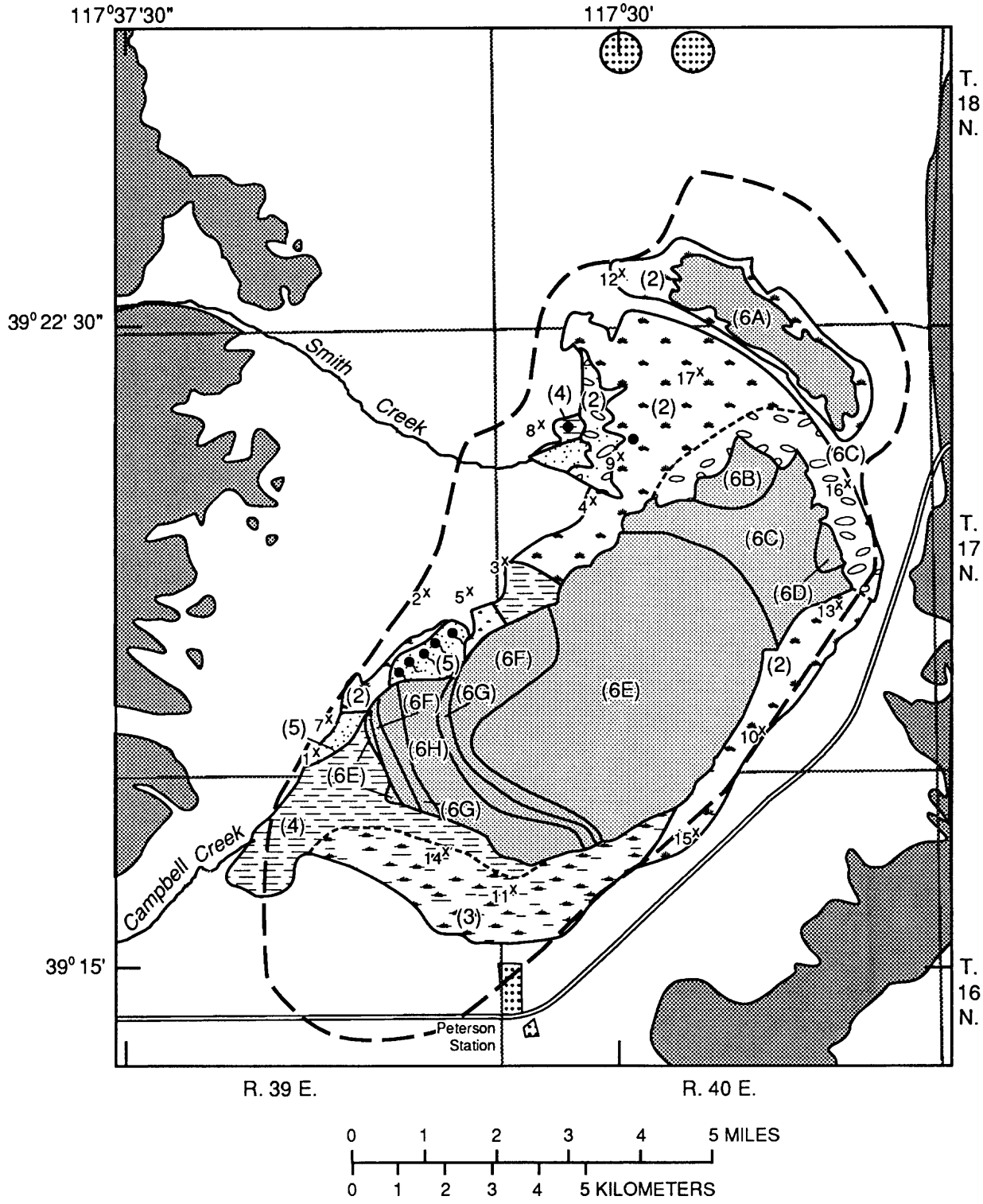


**Figure 2.** Generalized geology and areas of ground-water evapotranspiration.

readily initiated by isolating and excluding areas in which sagebrush is present. Application of this criterion to Smith Creek Valley produced a boundary that is generally concentric to the main playa margin and is in close agreement with known relations between phreatophyte distribution and depth to water. This criterion for mapping the inner xeric boundary failed in a small area northwest of the main playa where sporadic flooding from Smith Creek reduces near-

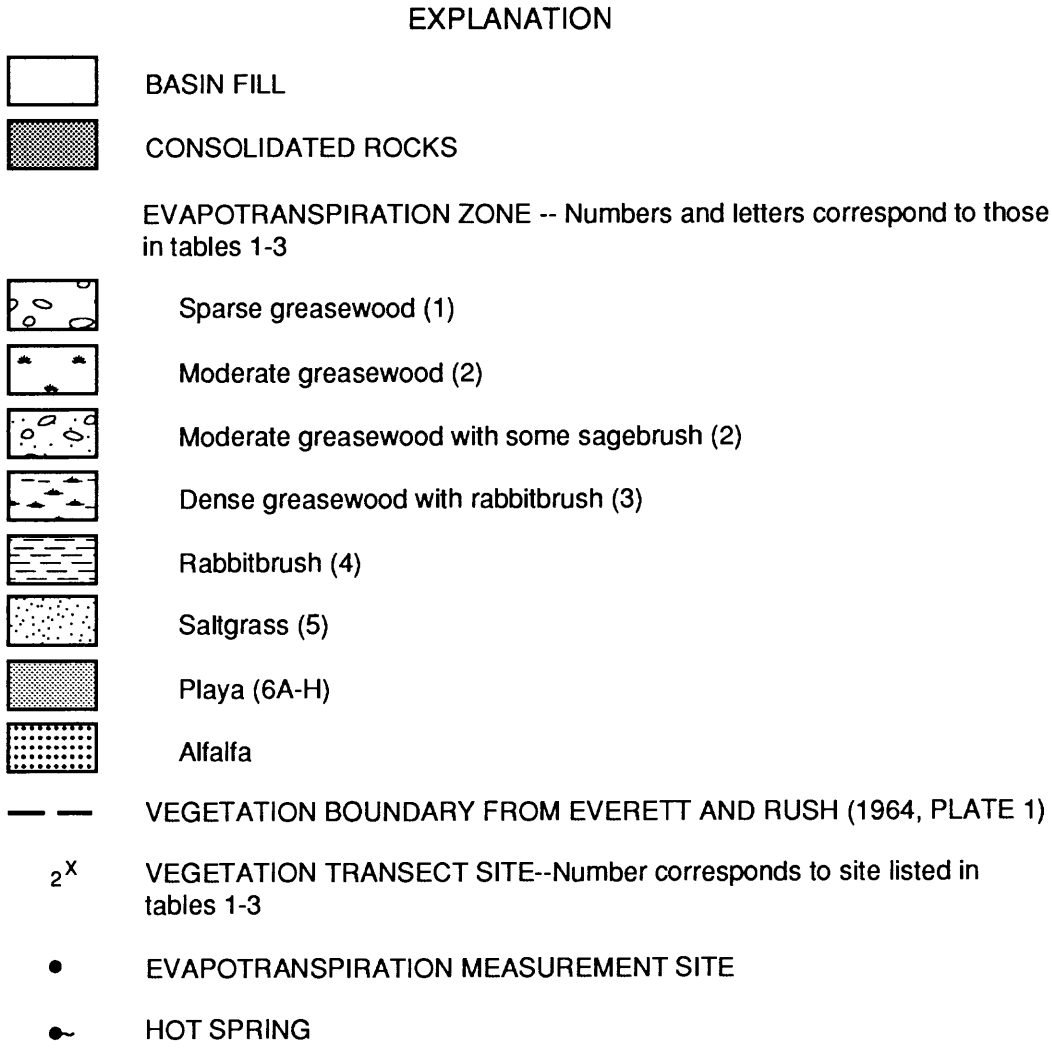


**Figure 2.**—Continued

surface soil salinity, allowing mixed stands of sagebrush and phreatophytes. The method is also weak when applied to the east side of the valley where xeric areas near the main playa are dominated by scrubby greasewood. However, abrupt and dramatic changes in vegetation vigor with proximity to the main playa make boundary demarcation on the east side visually obvious.

In general, woody phreatophytes in Smith Creek Valley consist exclusively of greasewood where the depth to water is less than 20 ft but greater than 12 and of a rabbitbrush-dominated mixture with greasewood along stream channels where nearby recharge maintains the water table at less than 12 ft. Areas occupied by a single species are uncommon, and subdivision of the discharge area was facilitated by first identifying areas where species dominance is most apparent and then partitioning these areas into zones of homogeneous foliage density.

The boundaries of areas occupied by grass were most obvious. Saltgrass is generally dominant in the zones mapped as grass (fig. 2, zone 5).

Identification of rabbitbrush-dominated stands (fig. 2, zone 4) required a judgment as to where rabbitbrush density exceeded that of greasewood. The boundaries presented in this report represent an estimation of the position at which the relative proportions of greasewood and rabbitbrush are equal.

Greasewood-dominated zones (fig. 2, zones 1 and 2) comprise significant changes in foliage-volume densities dictating further subdivision of greasewood areas on the basis of density. Delineation of zonal boundaries was based on visual estimates and on transect information discussed in the following section (tables 1 and 2). This subdivision was somewhat nebulous because changes in foliage volume are subtle within each phreatophytic zone. The uncertainty of

**Table 1.** Aerial characteristics of vegetation from transects, 1983

[—, indicates transect where vegetation densities were not determined]

| Zone in fig. 2 | Phreatophyte category[1] | Transect site[2] | Apparent crown height[3] | Crown cover (percentage of total area) | | | | | Percentage of phreatophyte cover | |
|---|---|---|---|---|---|---|---|---|---|---|
| | | | | Greasewood | Rabbitbrush | Combined phreatophytes | Xerophytes | All plants | Greasewood | Rabbitbrush |
| 1..... | Sparse greasewood | 16 | 1.3–2.4 | 11 | 0 | 11 | 10 | 21 | 100 | 0 |
| 2..... | Moderate greasewood. | [4]1 | 2.3–3.3 | — | — | 16 | 22 | 38 | — | — |
| | | 4 | 2.3–2.9 | 26 | 5 | 31 | 1 | 32 | 84 | 16 |
| | | 6 | 2.8–3.0 | 17 | 3 | 20 | 0 | 20 | 85 | 15 |
| | | 7 | 2.2–2.7 | 7 | 11 | 18 | 12 | 30 | 39 | 61 |
| | | 9 | 2.3–2.9 | 21 | 0 | 21 | 0 | 21 | 100 | 0 |
| | | 10 | 2.2–2.3 | 28 | 2 | 30 | 13 | 43 | 93 | 7 |
| | | 12 | 2.3–3.1 | 15 | 5 | 20 | 2 | 22 | 75 | 25 |
| | | 13 | 1.9–2.8 | 27 | 0 | 27 | 3 | 30 | 100 | 0 |
| | | 15 | 2.3–3.3 | 21 | 8 | 29 | 6 | 35 | 72 | 28 |
| | | 17 | 2.2–3.0 | 13 | 8 | 21 | 5 | 26 | 62 | 38 |
| 3..... | Dense greasewood and rabbitbrush. | 11 | 2.3–2.7 | 16 | 21 | 37 | 1 | 38 | 43 | 57 |
| 4..... | Rabbitbrush | 8 | 2.7–3.9 | 0 | 11 | 11 | 6 | 17 | 0 | 100 |
| | | 14 | 1.8–2.2 | 8 | 16 | 24 | 0 | 24 | 33 | 67 |

[1]Grasses not measured. See explanation in text.

[2]Site locations are shown in figure 3. Sites 2, 3, and 5 are omitted from table because they are outside the discharge area.

[3]Height range, in feet, associated with the tallest 15 percent of the plants along transect.

[4]Nonfoliated; transect performed before advent of growing season.

zone partitions may be as great as half a mile, but the impact upon total discharge calculations is believed to be negligible due to the small difference between evapotranspiration rates for related adjacent areas.

## Determination of Foliage Cover and Volume

A vegetation survey was conducted to aid in the identification of woody phreatophyte zones and to provide quantitative data for the determination of zone-specific evapotranspiration rates. No attempt was made to quantify evapotranspiration rates for grasses because available data were from studies conducted in environments significantly different from that of Smith Creek Valley. Instead, an average annual rate of 0.5 $ft^3$ of water per square foot of vegetated area was arbitrarily chosen as an approximation (Everett and Rush, 1964, p. 11).

Vegetation surveying employed the line-intercept method of sampling (Horton and others, 1964, p. 7), in which a steel measuring tape is stretched horizontally over the shrubbery to form a sampling transect. The transect was oriented in a random geographic direction and was of sufficient length to intersect both the spatial and species variations in the local plant community. A standard transect (tape) length of 300 ft was adopted for use in Smith Creek Valley, on the basis of previous experience by the author in both Smith Creek Valley and Dixie Valley, which is approximately 40 mi west of Smith Creek Valley. Vertical projection of the foliage crown onto the tape (termed the intercept) and its height were measured for each plant along the transect. Parts of intercepts occupied by more than one plant are distributed among the contributing individuals. The height-intercept pairs are tabulated by plant type for use in calculating fractional amounts of areal cover and foliage-volume densities.

In all, 17 transects were sampled in Smith Creek Valley (fig. 3). Preliminary sampling was first conducted to help isolate generalized discharge zones. As these zones became defined, additional transects were examined at sites that seemed to better represent the species composition and foliage-volume density for each zone. Transects number 2, 3, and 5 proved to lie outside the discharge area, leaving data for 14 transects on which to base the evaluation of vegetation characteristics. Data from transect number 1, although incomplete, were retained for height and density information.

Calculations were based on two features: aerial characteristics and foliage-volume densities. Aerial characteristics consisted of cover composition (1) by vegetation type and (2) as a fraction of the total area and apparent crown height; the latter term is defined here as the height range associated with the tallest 15 percent of the plants along a transect. These characteristics helped to quantify and verify visual impressions used to approximate vegetation zone boundaries. Foliage-volume densities were then used to

**Table 2.** Foliage-volume densities from vegetation transects, 1983

[—, indicates transect where phreatophyte types were not differentiated]

| Zone in fig. 2 | Phreatophyte category[1] | Transect site[2] | Volumetric density ($ft^3/ft^2$) | | | | | Percent of combined phreatophyte density | |
|---|---|---|---|---|---|---|---|---|---|
| | | | Greasewood | Rabbitbrush | Combined phreatophytes | Xerophytes | Total foliage | Greasewood | Rabbitbrush |
| 1..... | Sparse greasewood | 16 | 0.15 | 0.00 | 0.15 | 0.11 | 0.26 | 100 | 0 |
| 2..... | Moderate greasewood | [3]1 | — | — | .37 | .39 | .76 | — | — |
| | | 4 | .51 | .10 | .61 | .03 | .64 | 84 | 16 |
| | | 6 | .38 | .06 | .44 | .00 | .44 | 86 | 14 |
| | | 7 | .13 | .21 | .34 | .20 | .54 | 38 | 62 |
| | | 9 | .40 | .00 | .40 | .01 | .41 | 100 | 0 |
| | | 10 | .53 | .05 | .58 | .18 | .76 | 91 | 9 |
| | | 12 | .29 | .15 | .44 | .17 | .61 | 66 | 34 |
| | | 13 | .43 | .00 | .43 | .04 | .47 | 100 | 0 |
| | | 15 | .38 | .17 | .55 | .13 | .68 | 69 | 31 |
| | | 17 | .22 | .21 | .43 | .05 | .48 | 52 | 48 |
| 3..... | Dense greasewood and rabbitbrush. | 11 | .31 | .44 | .75 | .02 | .77 | 41 | 59 |
| 4..... | Rabbitbrush | 8 | .00 | .24 | .24 | .13 | .37 | 0 | 100 |
| | | 14 | .13 | .26 | .39 | .00 | .39 | 33 | 67 |

[1]Grasses not measured. See explanation in text.

[2]Site locations are shown in figure 3. Sites 2, 3, and 5 are omitted from table because they are outside the discharge area.

[3]Nonfoliated; transect performed before advent of growing season.

refine these boundaries and to estimate evapotranspiration rates for each vegetation zone.

Crown cover was determined by summing the intercepts of the group or groups of plants under consideration and expressing the total as a fraction of the transect length. Multiplication of this proportion by a unit width resulted in an area ratio of square feet of foliage cover per square foot of land surface area ($ft^2/ft^2$). Results of the computations are presented in table 1.

Foliage volumes were required for each vegetation type to compute weighted evapotranspiration rates for zones of mixed genera. First, the average weighted height was computed by summing the products of the individual plant height and intercept and by dividing this total by the sum of the intercepts (footnote 1, table 3). Multiplying the average weighted height (ft) by the fraction of cover ($ft^2/ft^2$) produces an average density value with units of cubic feet of foliage per square foot of area ($ft^3/ft^2$). Because the lower parts of most plants are devoid of foliage, this averaged density is excessive, but the method was employed as originally devised to preserve the transfer value of previous study by Robinson (1970). Results of the density computations are presented in table 2.

## Estimation of Evapotranspiration Rates

After establishing vegetation-zone boundaries and assigning foliage densities for each plant species, evapotranspiration rates were estimated for each zone comprising greasewood, rabbitbrush, or both based on foliage volume. In a lysimeter study near Winnemucca, Nev., Robinson (1970, p. 28) determined evapotranspiration rates for greasewood and rabbitbrush. Averaging the rates for the years 1963 through 1967 produces annual evapotranspiration volumes of 0.7 and 1.1 $ft^3$ of water per cubic foot of foliage for greasewood and rabbitbrush, respectively. These rates were adjusted to accommodate zones of mixed vegetation by multiplying each value by the fractional amount of foliage volume present, then summing the products to produce an evapotranspiration rate for the zone. Annual evapotranspiration from a zone was determined by multiplying the associated amount of evapotranspiration by the respective area. Results of these rate computations are presented in table 3.

Evapotranspiration estimated from phreatophyte volumes by using rates developed by Robinson (1970, p. 28) is in general agreement with evapotranspiration calculations based on the eddy-correlation technique used at two sites in Smith Creek Valley (fig. 3), by R.L. Carman (U.S. Geological Survey, written commun., 1983). The term "eddy correlation" refers to the covariance of atmospheric fluxes near land surface. Measurements of vertical windspeed, vapor density, air temperature, net solar radiation, and soil-heat flux can be used to evaluate evaporation rates (Goltz and others, 1970). Computations based on measure-

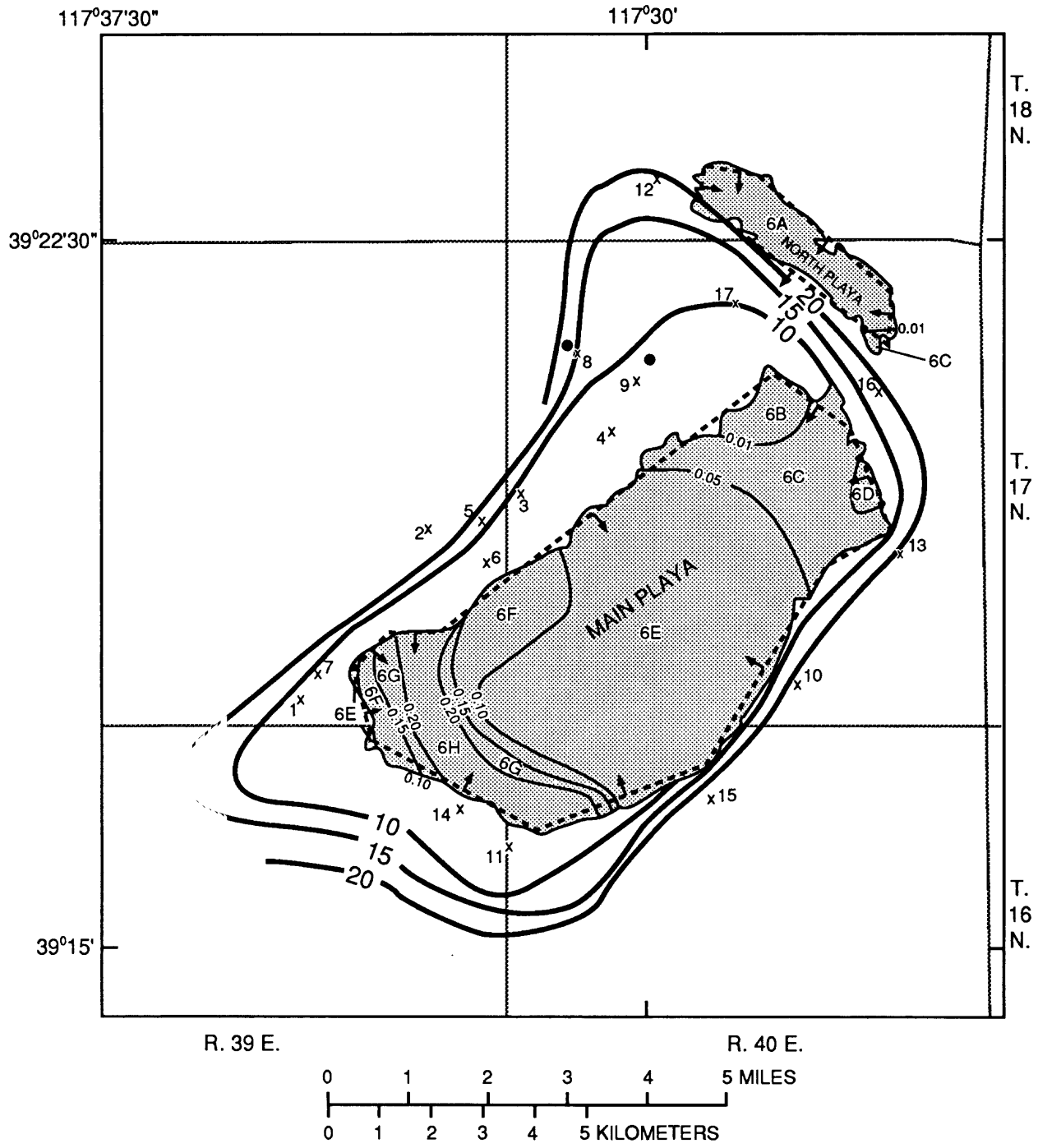


**Figure 3.** Vertical hydraulic-head gradients and evapotranspiration zones on playa, vegetation-transect and eddy-correlation measurement sites adjacent to playa, and depth to water table.

ments of these fluxes yield quasi-instantaneous evaporation-rate values that, when integrated over time, provide estimates of cumulative evaporation from plant and soil surfaces, calibrated to both diurnal and monthly levels and configurations of energy. Carman's data were collected in 1982 during the frost-free season, which constitutes approximately 180 days per year in Smith Creek Valley. Transpiration virtually ceases during the winter months, so the measurements during the 180-day period account for most of the annual evapotranspiration.

Measurements were collected at one rabbitbrush-dominated site and at one greasewood-dominated site used by Carman. Evapotranspiration for the rabbitbrush site was calculated to be 0.5 ft/yr (R.L. Carman, U.S. Geological

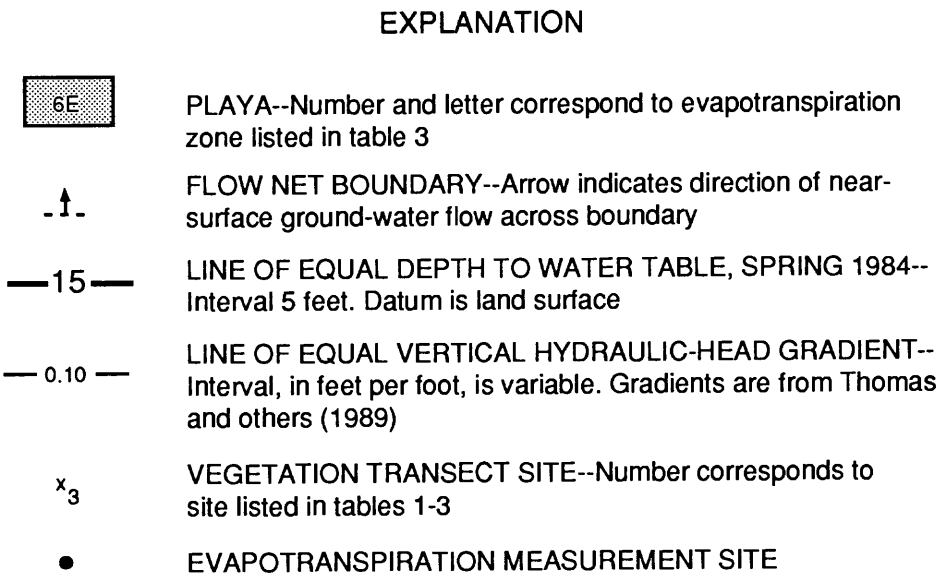


**Figure 3.**—Continued

**Table 3.** Annual natural discharge from the basin-fill aquifer, 1983

[—, areas where vegetation densities were not determined]

| Zone in fig. 2 | Zone type | Phreatophyte density[1] ($ft^3/ft^2$) | | Annual evapotranspiration (ft) | Zone area (acres) | Annual discharge (acre-ft) |
|---|---|---|---|---|---|---|
| | | Greasewood | Rabbitbrush | | | |
| 1..... | Sparse greasewood | 0.15 | 0.00 | 0.11 | 1,170 | 130 |
| 2..... | Moderate greasewood | .36 | .11 | [2].37 | 6,370 | 2,400 |
| 3..... | Dense greasewood and rabbitbrush. | .75 | .31 | .87 | 2,460 | 2,100 |
| 4..... | Rabbitbrush | .07 | .25 | .32 | 2,150 | 690 |
| 5..... | Grass | — | — | .50 | 670 | 340 |
| 6A ..... | North playa | — | — | [3].01 | 1,040 | 10 |
| 6B..... | Main playa | — | — | [3].02 | 380 | 8 |
| 6C..... | Main playa, small area of north playa. | — | — | [3].05 | 1,860 | 90 |
| 6D ..... | Main playa | — | — | [3].11 | 120 | 13 |
| 6E..... | Main playa | — | — | [3].17 | 6,790 | 1,200 |
| 6F..... | Main playa | — | — | [3].28 | 1,240 | 350 |
| 6G ..... | Main playa | — | — | [3].39 | 560 | 220 |
| 6H ..... | Main playa | — | — | [3].50 | 1,130 | 570 |
| — | Main playa, lateral inflow | — | — | — | — | 7 |
| Total (rounded) | | | | | 25,900 | 8,100 |

[1]Statistical mean.

[2]Example: Evapotranspiration rate = (0.36 × 0.7) + (0.11 × 1.1) = 0.37 ft per year, where 0.7 and 1.1 are annual unit discharge rates for greasewood and rabbitbrush, respectively. Annual evapotranspiration = 0.37 × 6,370 = 2,360 acre-ft.

[3]Evapotranspiration rates for the playa were calculated from Darcy's Law using the equation: Q = K × I × A, where Q = hydraulic flow rate; K = directional hydraulic conductivity; I = directional hydraulic head gradient; and A = zone area orthogonal to flow.

Survey, written commun., 1983), as compared with a value estimated during this study of 0.32 ft/yr on the basis of an average rabbitbrush foliage volume for a comparable phreatophyte area of 0.25 $ft^3/ft^2$ (table 3). Evapotranspiration at Carman's greasewood site was calculated to be 0.4 ft/yr (R.L. Carman, U.S. Geological Survey, written commun., 1983) as compared to a value of 0.37 ft/yr estimated herein from an average greasewood foliage volume of 0.36 $ft^3/ft^2$ for moderate density greasewood areas (table 2).

## EVAPORATION FROM THE PLAYAS

Discrete evaporation rates for the bare soil playa surface were estimated by using variations of Darcy's Law for flow velocities calculated from an average saturated vertical hydraulic conductivity of $7\times10^{-8}$ ft/s and extended vertical hydraulic gradients within the playa deposits (fig. 3). The hydraulic conductivity of fine-grained deposits in the basin was determined from core samples and from water-temperature gradients in a well near the center of the larger playa by using four techniques: (1) a laboratory test of a core sample by using a falling-head permeameter (Freeze and Cherry, 1979, p. 335), (2) an algorithm relating hydraulic conductivity to a soil-moisture retention curve (Marshall, 1958, p. 1–8), (3) the Kozeny-Carmen equation (Bear, 1972, p. 166) relating hydraulic conductivity to porosity and particle-size distribution, and (4) an energy-dissipation function relating water-temperature changes to vertical flow velocities (Michael L. Sorey, U.S. Geological Survey, written commun., 1971). Estimates of vertical hydraulic conductivity range from $1\times10^{-7}$ to $3\times10^{-9}$ ft/s, with a mean value of $7\times10^{-8}$ ft/s. This mean value was assumed to apply throughout the playa areas and was employed in all computations of water volumes lost through direct evaporation.

Vertical hydraulic gradients vary throughout the playas with values ranging from virtually zero to 0.2 ft/ft, which results in differing discharge rates. This continuous rate function was discretized by partitioning the playa area into zones having uniform discharge rates, with lines of equal gradient at intervals of 0.05 ft/ft (fig. 3). Additional zones bounded by a 0.01 ft/ft line were required for the north playa and small portions of the main playa to prevent exclusion of much area having small gradients. Hydraulic gradients of bounding lines were averaged to provide a single gradient value for each intervening zone. The average value was then multiplied by the saturated hydraulic conductivity and area to determine discharge.

Total discharge from the two playas, based on the data for 1983, is estimated to average approximately 2,400 acre-ft/yr (table 3). However, discharge from the aquifer may be less during wet years, when a significant part of the main playa and all the north playa are covered with surface-water runoff for approximately 3 months.

Significant errors in estimates of the annual evaporation rate can result from uncertainties in (1) the determination of vertical hydraulic conductivity and (2) the precise location of lines of equal vertical hydraulic-head gradient (zonal boundaries). Evaporation rates are directly proportional to hydraulic conductivity, so the propagation of this type of error can be intuitive. However, the nonproportionality of total evaporation rates to individual zone areas causes a nonlinear change in total discharge to result from linear errors in area estimates. Relocation of a boundary within the discharge area does not change the total area but causes new values from the stepped-rate function to apply to the area reallocated. Two simulations were performed to test the sensitivity of predicted discharge to these factors: the shape of the vertical-gradient surface was assumed to remain unchanged, but its overall magnitude was allowed to vary by the algebraic addition of a constant, thereby generating hypothetic surfaces above and below the estimated actual position. Specifically, the surface was raised such that 15 percent of the area of each zone was reallocated to the zone having the next greater evaporation rate, while the total area of bare soil was held constant. Similarly, a second simulation lowered the surface such that areas were reapportioned to lesser rate zones. The result of these simulations was that total discharge increased by only 3 percent for the elevated gradients and diminished by only 5 percent for the lowered gradients. Thus, the effects of errors introduced by uniform redistribution of area seem to have minor effects on the computation of total discharge.

Another source of error results from using a subsurface depth interval for the measurement of vertical hydraulic-head gradient. A saturated near-surface layer subjected to lateral inflow of water is unaccounted for in the foregoing analysis. Vertical hydraulic-head gradients were determined by drilling adjacent wells of differing depths and measuring the difference in height between the piezometric surface in each. The shallowest wells were 22 ft deep, so if the water-table depth were 10 ft, lateral inflow of water in the uppermost 12 ft of saturated playa would be unaccounted for in the flow regime described above. To address this discrepancy, a rudimentary planimetric flow-net analysis was implemented along the playa margin (fig. 3). Due to anisotropy in the playa sediments, the horizontal hydraulic conductivity was assumed to be approximately two orders of magnitude greater than the vertical conductivity; therefore, a value of $1\times10^{-5}$ ft/s was used. The boundaries of the two playas were simulated as straight-line polygons, and the hydraulic-head gradient for each segment was determined as the arithmetic mean of the gradients at each end of, and perpendicular to, that segment. Flow volume across the vertical plane subtended by the segment was calculated as the product of the horizontal hydraulic conductivity, average head gradient, saturated thickness, and segment length. Summation of the values for all faces of the polygon produced an additional discharge of 7

acre-ft/yr for total net lateral inflow to both playas—a small value when compared to 2,400 acre-ft/yr of total evaporation from bare soil.

## SUMMARY AND CONCLUSIONS

This study shows how natural ground-water discharge by plants can be estimated on the basis of evapotranspiration rates determined at an alternate location if the only significant difference between the two sites is the distribution and density of plants. It also shows how the principle of hydraulic continuity can be used to estimate ground-water evaporation from bare-soil playas.

To determine natural evapotranspiration, the vegetative discharge zone was identified by mapping the lowland area not containing sagebrush and then contracting this boundary to exclude seemingly phreatophytic areas caused by the infiltration of surface-water runoff. The phreatophytic area was subsequently partitioned into zones having homogeneous plant properties—species proportion, areal cover, and foliage-volume density—beginning with obvious grass zones and ending with the approximated subdivision of greasewood zones. The purpose of this division was to obtain discrete evapotranspiration rates to apply to varying vegetation. Mapping vegetation into zones was based primarily on visual identification of plant properties and was refined according to the results of 17 sampling transects. The principal purpose of these transects was to provide data for the calculation of foliage-volume densities and evapotranspiration rates. Annual evapotranspiration for each phreatophyte zone was estimated on the basis of the foliage volume of each species, a corresponding unit value of evapotranspiration determined by Robinson (1970), and an area. Evapotranspiration from the grass zone was estimated by using a nominal value of 0.5 ft/yr (Everett and Rush, 1964, p. 11). The total evapotranspiration for all phreatophytes was estimated to be 5,700 acre-ft/yr.

Ground-water evaporation from the playas was determined indirectly by recognizing that the volume of water discharged was equal to the volume of water emerging from the water table into the unsaturated soil zone. This amount, in turn, was equal to the amount of inflow into an aquifer zone bounded on the top by the water table, on the bottom by the minimum depth of observation wells used to estimate vertical hydraulic gradients (12 ft below the water table), and laterally by the playa sediment boundaries. Inflow to this aquifer was determined by using data on vertical hydraulic gradients (derived from piezometric-surface differences in paired test wells of differing depths) to partition the playas into zones with gradients varying less than 0.05 ft/ft. Inflow to each zone was estimated by using average vertical hydraulic gradients, a vertical hydraulic-conductivity value of $7\times10^{-8}$ ft/s, and area. Total ground-water evaporation from the playas was estimated to be 2,400 acre-ft/yr. All but 10 acre-ft/yr was from the main playa.

A simplified flow-net analysis also was conducted to ascertain the amount of error due to lateral inflow. On the basis of a horizontal hydraulic conductivity value of $1\times10^{-5}$ ft/yr, the total lateral inflow was only 7 acre-ft/yr.

An earlier study estimated that the total natural discharge was approximately 6,600 acre-ft/yr, as compared to the 8,100 acre-ft estimated in this report (both values rounded to the nearest 100 acre-ft). The previous value was obtained by treating woody phreatophytes as a single zone and applying lumped-parameter evapotranspiration rates to this zone and to the playas. However, the earlier study produced results within 21 percent of those in this report, the discharge area used was much larger than seems warranted by this study, and assumed evapotranspiration rates were lower.

At the outset of the current investigation, the author was somewhat skeptical of the ability to apply lysimeter data to the study of evapotranspiration in undisturbed soil environments. Water levels maintained in lysimeters are generally closer to land surface than are naturally occurring water levels in semiarid valleys; therefore, evapotranspiration rates associated with the artificial settings would seem excessive. However, the close agreement of current results with the data obtained through other techniques indicates that foliage density is a more reliable index than depth to water when attempting to transfer evapotranspiration-rate information from one site to another. The general agreement of the results of this study with those of the Everett-Rush reconnaissance indicates that the methods applied in this study, with only small modification, might provide a means for assessing evapotranspiration in similar systems throughout the Great Basin.

## SELECTED REFERENCES


Bear, Jacob, 1972, Dynamics of fluids in porous media: New York, American Elsevier, 764 p.

Everett, D.E., and Rush, F.E., 1964, Ground-water appraisal of Smith Creek and Ione Valleys, Lander and Nye Counties, Nevada: Nevada Department of Conservation and Natural Resources, Ground-Water Resources-Reconnaisance Report 28, 19 p.

Freeze, R.A., and Cherry, J.A., 1979, Groundwater: Englewood Cliffs, N.J., Prentice-Hall, 604 p.

Goltz, S.M., Tanner, C.B., and Thurtell, G.W., 1970, Evaporation measurements by an eddy correlation method: Water Resources Research, v. 6, no. 2, p. 440–446.

Harrill, J.R., Welch, A.H., Prudic, D.E., Thomas, J.M., Carman, R.L., Plume, R.W., Gates, J.S., and Mason, J.L., 1983, Aquifer systems in the Great Basin region of Nevada, Utah, and adjacent States—a study plan: U.S. Geological Survey Open-File Report 82–445, 49 p.

Horton, J.S., Robinson, T.W., and McDonald, H.R., 1964, Guide to surveying phreatophyte vegetation: U.S. Department of Agriculture Handbook 266, 37 p.

Marshall, T.J., 1958, A relation between permeability and size distribution of pores: Journal of Soil Science, v. 9, no. 1, p. 1–8.

Meinzer, O.E., 1927, Plants as indicators of ground water: U.S. Geological Survey Water-Supply Paper 577, 95 p.

Robinson, T.W., 1970, Evapotranspiration by phreatophytes in the Humboldt River Valley near Winnemucca, Nevada, *with* a section on Soil moisture determinations, by A.O. Waananen: U.S. Geological Survey Professional Paper 491–D, 41 p.

Stewart, J.H., McKee, E.H., and Stager, H.K., 1977, Geology and mineral deposits of Lander County, Nevada: Nevada Bureau of Mines and Geology Bulletin 88, 106 p.

Thomas, J.M., Carlton, S.M., and Hines, L.B., 1989, Groundwater flow and simulated response to selected developmental alternatives in Smith Creek Valley, a hydrologically closed basin in Lander County, Nevada: U.S. Geological Survey Professional Paper 1409–E, 57 p.

# Climatological and Hydrological Factors Affecting the Lake Thompson Chain of Lakes in Eastern South Dakota

*By* Donald S. Hansen *and* Wayne A. Miller

**Abstract**

The Lake Thompson chain of lakes is located in a 494-square-mile noncontributing subbasin within the Vermillion River drainage basin in eastern South Dakota. Prior to 1986, Lake Thompson was a terminal lake; in October 1986, the lake began to drain into the East Fork Vermillion River. Lake-level fluctuations in the chain of lakes region are caused primarily by changes in precipitation and runoff. Parts of the Lake Thompson chain of lakes subbasin received as much as 35.13 inches of cumulative excess precipitation from 1982 through 1987. Greater than normal precipitation and runoff in the basin have caused water levels in Lake Thompson to rise 23 feet, in Lake Whitewood to rise 9 feet, and in Lake Preston to rise 5 feet. The rate of lake-surface expansion and the extent of land inundated from 1977 to 1988 were determined by analysis of satellite imagery. Lake Thompson expanded from 0.53 square mile in 1977 to 22.64 square miles in 1987; Lake Whitewood expanded from 0.56 square mile in 1977 to 11.16 square miles in 1986, and Lake Preston expanded from nearly dry conditions in 1977 to 9.37 square miles in 1986. From 1977 to 1987, 42 square miles of land were inundated by rising lake levels in the Lake Thompson drainage basin.

A mass-balance equation was used to describe water-level fluctuations of Lake Thompson. The result of the mass-balance equation is the ratio of change in lake volume to the corresponding change in rate of discharge from the lake and has the dimension of time. This ratio is referred to as the response time of a lake. The computed response time for Lake Thompson as a terminal lake ranged from 8 to 18 years. The computed response time for Lake Thompson as a draining lake, which began to drain into the East Fork Vermillion River in October 1986, is 3 months.

## INTRODUCTION

About 5 percent of the landmass of North America drains into terminal lakes, which are lakes that are located at the lowest point within a closed drainage basin (de Martonne, 1927). Closed basins have no surface outlet to the oceans of the world. Water-level fluctuations in lakes throughout the United States are becoming an increasing problem as residential and recreational development along lakeshores increases. A recent investigation to determine the cause of water-level fluctuations in Devils Lake, North Dakota, and in other terminal lakes in the United States, was conducted by Wiche (1986).

From 1982 through 1987, greater than normal precipitation at many locations in eastern South Dakota caused greater than normal runoff. Rising water levels in lakes from 1982 to 1987 have caused flooding of lakeshore homes and businesses, agricultural land, farmsteads, and outbuildings and have damaged roads and bridges. Estimates of total damage caused by the rising water levels are in the millions of dollars.

This report presents the results of a study that was designed to (1) determine the relation between water-level fluctuations in the Lake Thompson chain of lakes and precipitation trends; (2) determine the most likely cause of large lake-level fluctuations; and (3) determine the water-surface areas of lakes during droughts and floods, and the expansion and contraction of small sloughs in the Lake Thompson drainage basin from 1977 to 1988 by using satellite images. Although the results presented in this report pertain only to the Lake Thompson chain of lakes, the results may be applicable to other lakes with similar glacial hydrogeologic settings in eastern South Dakota.

## DESCRIPTION OF THE STUDY AREA

The study area is located within the Vermillion River drainage basin of eastern South Dakota (fig. 1). The study area, 494 $mi^2$, comprises the drainage area of the Lake Thompson chain of lakes. Prior to 1986, the study area was thought to be a noncontributing subbasin of the Vermillion River basin (total drainage area of 2,655 $mi^2$). The topography in the chain of lakes area is of glacial origin and is characterized by shallow closed depressions, sloughs, pot-

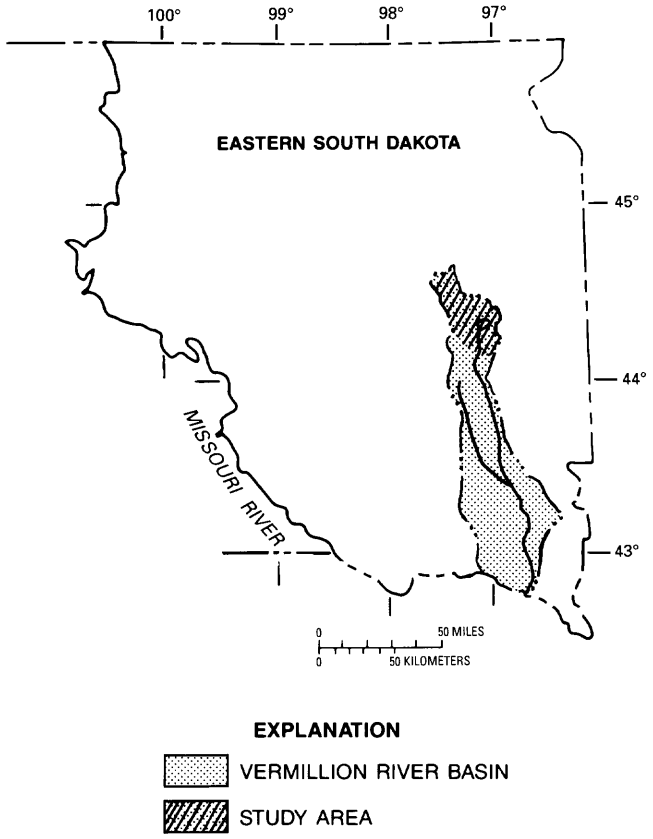


**Figure 1. Index map of eastern South Dakota.**

holes, and lakes. Many of these depressions are connected by poorly defined channels and swales. The western part of the noncontributing drainage area is a well-defined ridge that separates the Coteau des Prairies from the James River lowland. The northern, eastern, and southern boundaries of the basin are poorly defined low divides.

The geology and ground-water resources of the chain of lakes subbasin have been described by Hamilton (1989). Cretaceous bedrock is covered by as much as 700 ft of glacial drift. The principal bedrock aquifers in the area are the Codell and the Dakota aquifers in the Codell Sandstone Member of the Carlile Formation and Dakota Sandstone, respectively. Depth from land surface to the top of the aquifers ranges from 630 to 1,040 ft. Few wells have been completed in the aquifers because of the availability of adequate water supplies from shallower aquifers.

Aquifers in the glacial drift occur principally as buried-valley outwash deposits and undifferentiated sand and gravel deposits associated with glacial till. The most significant of these outwash deposits is the Vermillion East Fork aquifer (fig. 2). The aquifer trends southeasterly from north of Spirit Lake to south of Lake Thompson. The aquifer ranges from 2 to 7 mi wide; potential well yields are as much as 1,000 gal/min. Recharge to the aquifer is by infiltration of precipitation through the overlying topsoil. Water in the aquifer generally is unconfined, except near Spirit Lake where the aquifer is overlaid by till. The aquifer may be hydraulically connected to Spirit, Mud, and Silver Lakes, and to Lakes Henry and Thompson, but not to Lakes Preston and Whitewood.

## HYDROLOGY OF THE LAKE THOMPSON CHAIN OF LAKES REGION

### Historic Water-Level Fluctuations

The earliest accounts of lake levels for the Lake Thompson chain of lakes region are found in John Charles Fremont's memoirs (1887). The memoirs contain a letter, dated February 13, 1884, that Fremont received from C.W. Irish, an engineer who surveyed and located the Chicago & Northern railroad in the area. The letter from C.W. Irish states

> On the west side of the Big Sioux River is a lake region. These lakes bear the names Thompson, Whitewood, Preston, Te-tonka-ha, Poinsett, and Kampeska. When the Dakota Central railway was built in 1879–80 all these lakes excepting Thompson, Poinsett and Kampeska were dry, and it took me a long time and no small research to ascertain when they last held water. They had been known to be dry for the 25 years preceding 1879 or at least persons who had lived there or in the vicinity for 25 years said that the lakes were dry when they came into the locality, but I found an old Frenchman who had seen these lakes full of water in 1843–46, and I, in studying over the matter, found that you had seen and named them in 1836–38. I came very near locating the railroad line through Lake Preston; for the head men of the railroad company believed that it had dried up for all time; but on my presenting the testimony of certain reliable voyagers, they allowed me to go around it. It was well that they did, for the winter of 1880–81 gave a snow-fall such as had not been seen since the years 1843–44 and in the spring of 1881 all these lakes filled up, bank full, and have contained so ever since, signed C.W. Irish CE.

Assuming from C.W. Irish's letter that the Lake Thompson chain of lakes were full in 1843 and 1880, the level of the lakes may have been Lake Preston, about 1,696 ft above sea level; Lake Whitewood, 1,695 ft above sea level; Lake Henry, about 1,690 ft above sea level; and Lake Thompson, about 1,689 ft above sea level. Regular annual lake level measurements for the chain of lakes did not begin until 1983.

### Hydrologic and Climatologic Analysis

There are many conflicting theories about the cause of water-level fluctuations in terminal lakes. The most prevalent of these theories are (1) evaporation rates; (2)

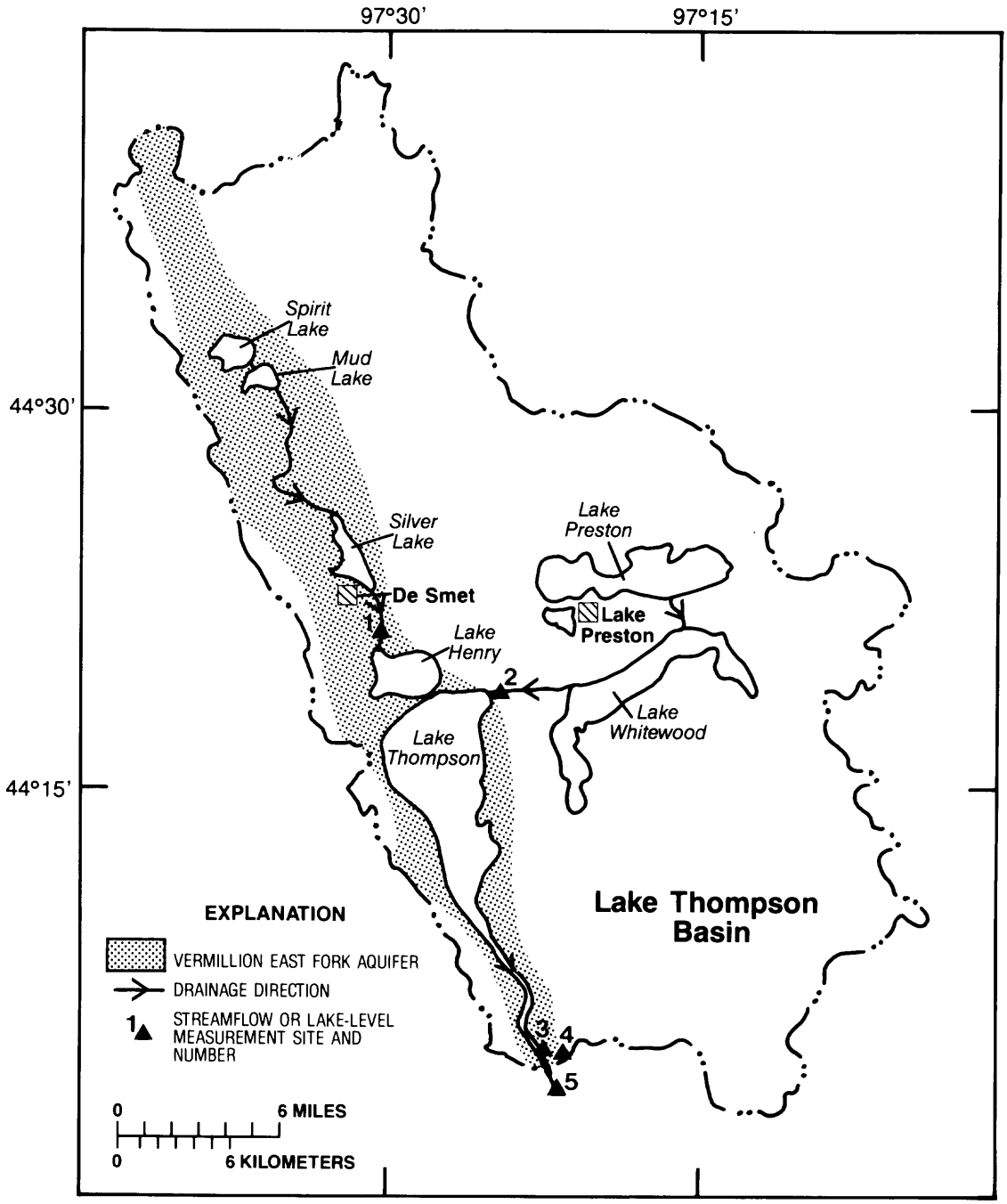


**Figure 2.** Lake Thompson basin, drainage direction of Lake Thompson chain of lakes, and Vermillion East Fork aquifer.

precipitation variability, alternating periods of greater than and less than normal precipitation; (3) breaking of the prairie sod in the Dakotas during the 1880's that exposed permeable soil, thus increasing infiltration and decreasing runoff to tributaries that flow to terminal lakes; and (4) changes in the ground-water elevation relative to the lake surface, thus affecting recharge and discharge to the terminal lakes.

Precipitation and runoff from 1982 through 1987 were greater than normal at many locations in eastern South Dakota. Records of annual precipitation at six meteorologic stations (De Smet, Huron, Howard, Watertown, Brookings, and Sioux Falls) are shown in figure 3. At all six stations, less than normal precipitation in 1980 and 1981 was followed by near-normal and greater than normal precipitation from 1982 to 1986. The normal precipitation and

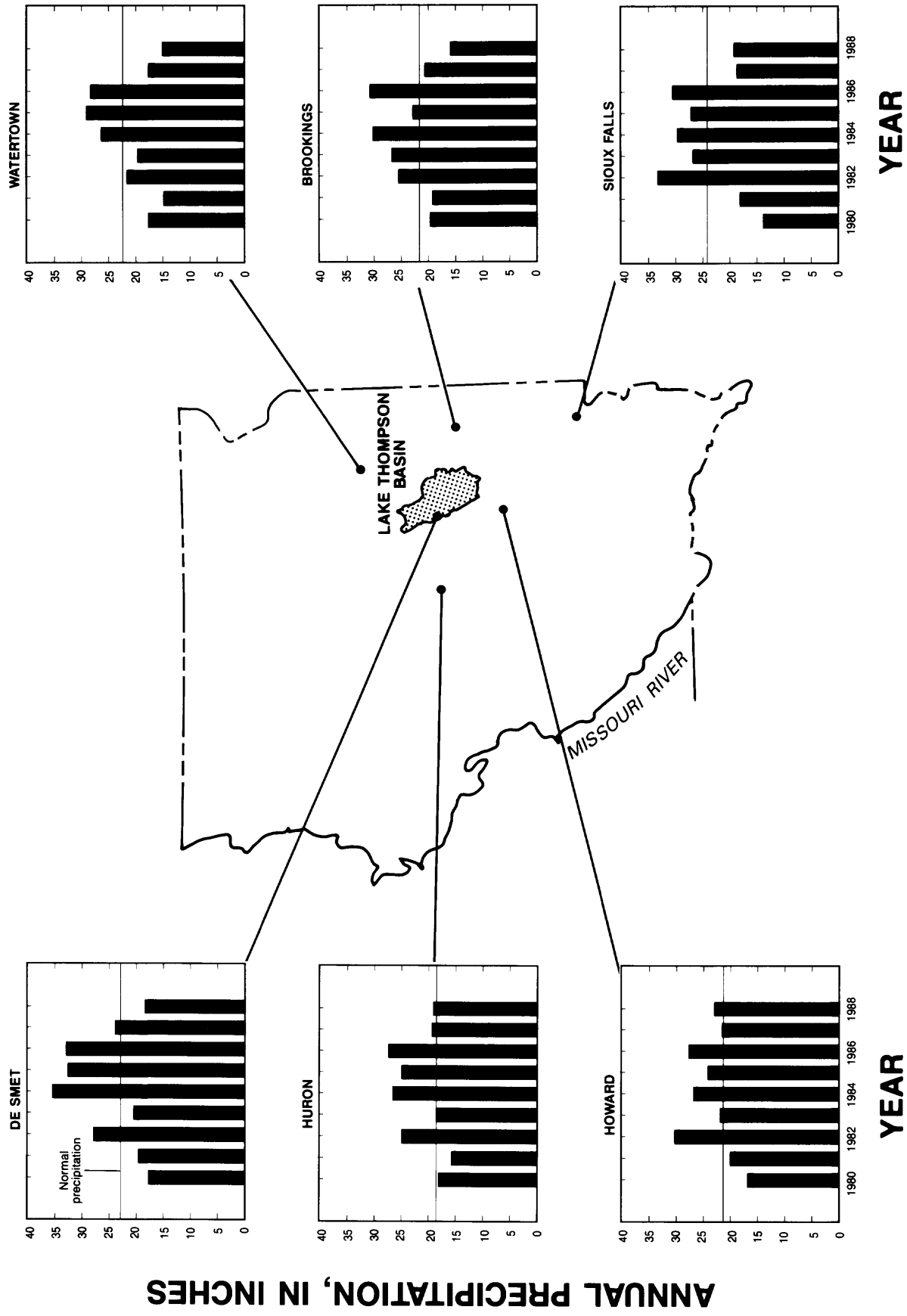


**Figure 3.** Annual precipitation (1980–88) for selected sites in eastern South Dakota.

**Table 1.** Normal precipitation and cumulative departure from normal precipitation at De Smet, Huron, Howard, Watertown, Brookings, and Sioux Falls

| City | Normal precipitation[1] (in.) | Cumulative departure from normal precipitation (in.) | |
|---|---|---|---|
| | | 1982–86 | 1982–87 |
| De Smet | 22.78 | +34.07 | +35.13 |
| Huron | 18.66 | +31.57 | +32.31 |
| Howard | 21.16 | +22.63 | +21.53 |
| Watertown | 22.33 | +6.87 | +2.14 |
| Brookings | 21.69 | +26.74 | +25.65 |
| Sioux Falls | 24.12 | +26.20 | +20.74 |

[1]Base period 1951–80.

cumulative departure from normal precipitation at these stations from 1982 to 1986 and from 1982 to 1987 are given in table 1.

Greater than normal precipitation has caused increased runoff in the study area and probably is the principal cause for the rapid rise of water levels in the Lake Thompson chain of lakes and surrounding small lakes and sloughs. The percentage of average annual streamflow for water years 1980 through 1988 was computed for the James River at Huron, the James River near Forestburg, the James River near Scotland, the Little Vermillion River near Salem, the West Fork Vermillion River near Parker, the Big Sioux River near Watertown, the Big Sioux River near Brookings, and the Big Sioux River at North Cliff Avenue at Sioux Falls (fig. 4). The percentage of average annual streamflow was computed by dividing the streamflow for a given year by the average annual streamflow for the period of record and multiplying by 100. Thus, the graphs are not a plot of actual streamflow or of a single flood. If the percentage of average annual streamflow is equal to 100, then streamflow during that year was equal to the long-term average. Streamflow at the eight streamflow-gaging stations during water year 1986 ranged from 320 to 520 percent of the long-term average.

Levels of Lakes Preston and Whitewood (fig. 5) rose rapidly in 1984, either declined slightly or remained about level in 1985, rose rapidly in early 1986, declined rapidly in the rest of 1986 and in 1987, and began to rise again in early 1988. In contrast, the level of Lake Thompson (fig. 5) rose gradually in 1984 and 1985, rose rapidly in 1986, rose slightly in early 1987, declined slightly in the rest of 1987, and began to rise again in early 1988. Lake Preston rose about 5 ft, Lake Whitewood rose about 8 ft, and Lake Thompson rose about 20 ft from 1984 to 1986. The lake-level rises from 1984 to 1986 corresponded to the greater than average streamflow in major streams surrounding the study area during 1984 and 1986. Lake Preston rose above its outlet and began to drain into Lake Whitewood in April 1986. Lake Whitewood subsequently rose above its outlet in April 1986 and began to drain into Lake Thompson. The rapid rise of Lake Thompson (about 15 ft) occurred in April 1986 and was caused by discharge from Lake Whitewood. Tributary inflow to the chain of lakes was not measured until October 1986; however, streamflow during 1984 and 1986 in major streams surrounding the study area was as much as five times the long-term average. Thus, it can be concluded that tributary inflow to the chain of lakes during 1984 and 1986 probably also was substantially greater than average.

Discharge and lake-level measurements for the chain of lakes region from October 1986 to June 1988 are listed in table 2. Measured inflow to Lake Thompson from Lakes Henry and Preston decreased from about 200 $ft^3/s$ in October 1986 to about 24 $ft^3/s$ in May 1987, and levels in Lakes Preston and Whitewood declined about 3 to 4 ft during the same period. The decline corresponded to less than normal precipitation and less than average runoff during that period. Lake Thompson, the last lake in the chain of lakes, rose about 1.25 ft from November 1986 to April 1987.

From the late 1890's through March 1986, all lakes in the Lake Thompson basin were unconnected, terminal lakes with no outlet. Tributary inflow and direct precipitation were the only sources of surface-water inflow to the lakes. Drainage areas of the lakes, determined from U.S. Geological Survey 7.5-min topographic maps, are (1) Spirit Lake, 82 $mi^2$; (2) Lake Henry, 92 $mi^2$; (3) Lake Preston, 84 $mi^2$; (4) Lake Whitewood, 151 $mi^2$; and (5) Lake Thompson, 85 $mi^2$. In April 1986, Spirit Lake overflowed, draining into Mud Lake. Mud Lake overflowed and drained into an unnamed drainage channel that emptied into Silver Lake. Silver Lake overflowed and began to drain into Lake Henry. Lake Henry overflowed and drained into Lake Thompson. Lake Preston overflowed and began to drain into Lake Whitewood, which subsequently began to drain into Lake Thompson. In October 1986, Lake Thompson overflowed and began to drain into the East Fork Vermillion River; thus, an additional 494 $mi^2$ of drainage area was added to the drainage area of the Vermillion River.

## SATELLITE DATA COLLECTION AND HYDROLOGIC CHARACTERISTICS

The United States and France have each launched and maintain a series of sun-synchronous, polar-orbiting satellites that carry multispectral instruments designed to measure the intensity of radiant energy reflected or emitted from the surface of the Earth and to transmit this information to ground receiving stations equipped for disseminating the satellite data (fig. 6).

For this study, satellite imagery was used to (1) determine the surface-area change of the Lake Thompson chain of lakes and of other small lakes and sloughs from 1977 to 1988; (2) identify topographic depressions susceptible to flooding; (3) determine the area of Lake Thompson

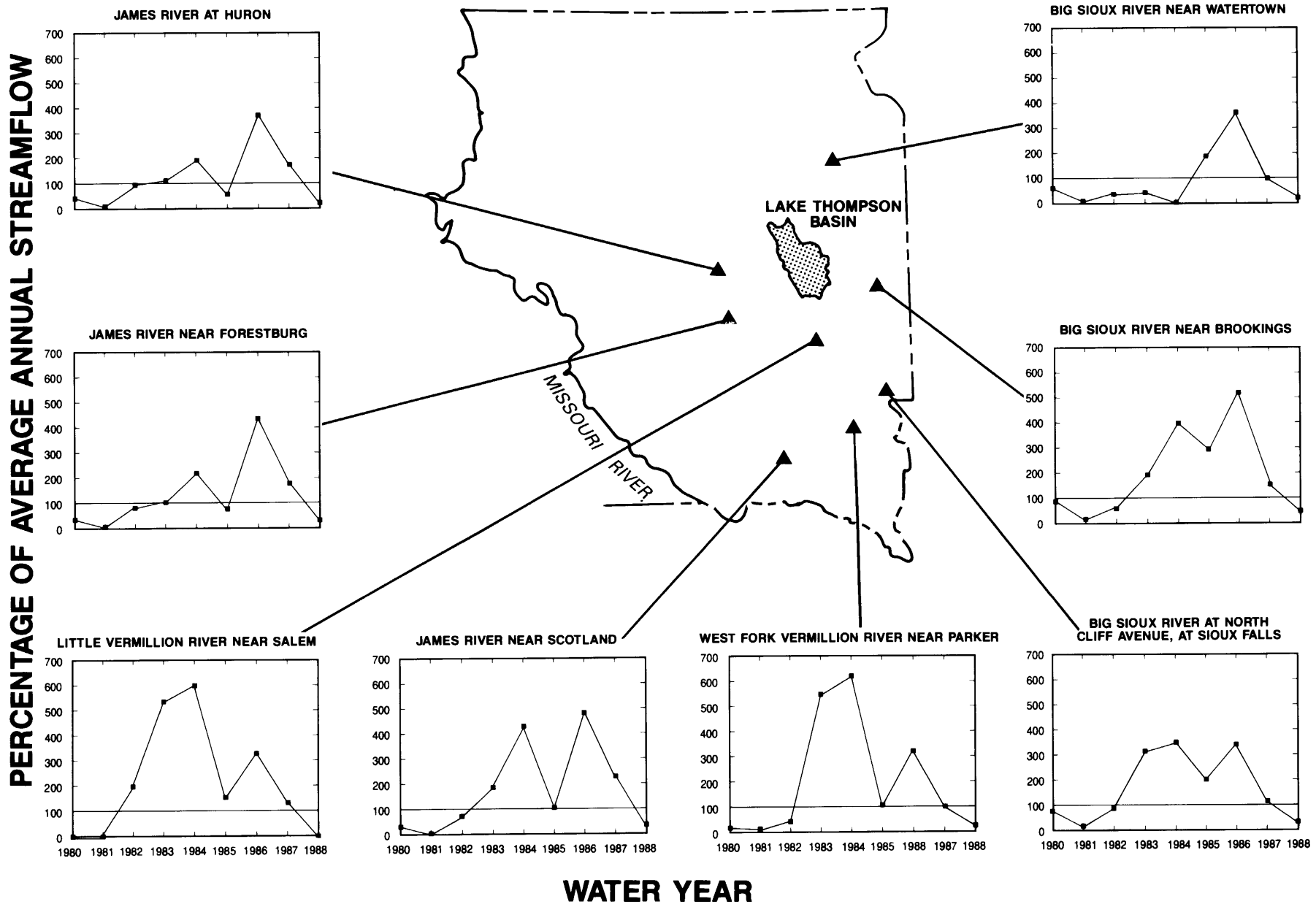


**Figure 4.** Percentage of average annual streamflow at selected streamflow-gaging stations in eastern South Dakota, water years 1980–88.

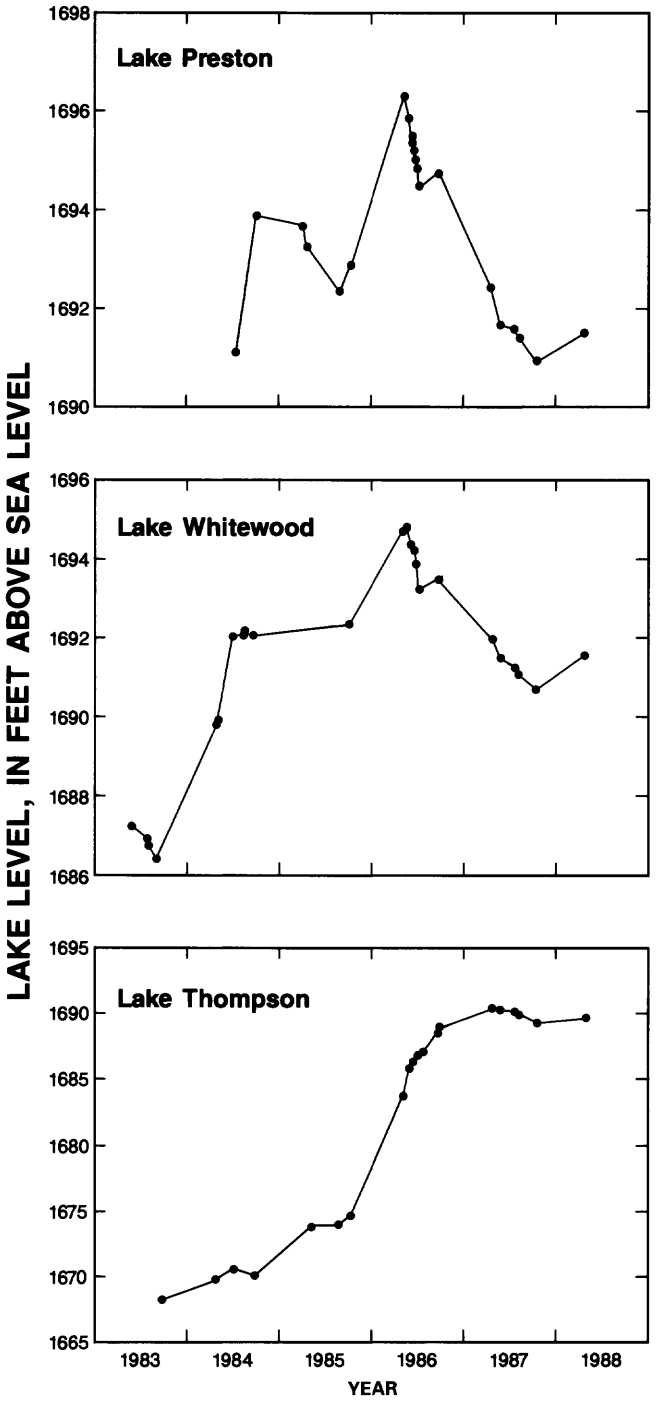


**Figure 5.** Lake levels for principal lakes in the Lake Thompson chain of lakes (1983–88).

at various lake stages under various climatic conditions; and (4) determine the extent of flooding from lakes and streams in eastern South Dakota from 1984 to 1986.

The National Oceanic and Atmospheric Administration's (NOAA) series of meteorological satellites carry an Advanced Very High Resolution Radiometer (AVHRR). The AVHRR is a five-channel radiometer having a ground resolution of 1,100 m at nadir (Kidwell, 1983). The AVHRR system has a swath width of about 2,400 km and provides daily global coverage. Sufficient cloud-free data can be obtained to support a variety of monitoring programs. These data have been available since the launch of NOAA 6 in 1972.

The Landsat series of United States satellites carries a Multispectral Scanner (MSS) system and a Thematic Mapper (TM) sensor system. The MSS is a four-channel scanner (fig. 6) having a ground resolution of 80 m (U.S. Geological Survey and National Oceanic and Atmospheric Administration, 1984). Landsat MSS data have been used for mapping land cover of large geographic areas since the launch of Landsat 1 in 1972. The TM sensor system is a seven-channel scanner (fig. 6) having a ground resolution of 30 m (U.S. Geological Survey and National Oceanic and Atmospheric Administration, 1984). The greater resolution and additional channels provided by the TM sensor system provides land-use managers with an opportunity to support a variety of applications using satellite data since the launch of Landsat -4 in 1983.

The French Systeme Probatoire d'Observation de Terre (SPOT) series of satellites carries two High-Resolution Visible (HRV) scanners. Each HRV scanner has the ability of being used as either a three-channel or one-channel system having a ground resolution of 20 or 10 m, respectively. Selective positioning of the scanning mirror on contiguous passes of the satellite allows imaging of the same area at different angles to provide sufficient parallax to produce stereoscopic images (French Systeme Probatoire d'Observation de Terre, 1987). The improvement in spatial resolution and the capability of acquiring stereoscopic imagery have made HRV data useful for mapping small areas in greater detail. These data have been available since the launch of SPOT 1 in 1985.

Eight satellite images, acquired from 1977 to 1988 (figs. 7–14), were used in this investigation. In general, red areas on the satellite images indicate green vegetation, light-blue and gray areas indicate dark-toned soils, black to dark-blue areas indicate water surfaces, and dark-gray to black areas indicate areas with substantial soil moisture and almost saturated soils (Lillesand and Kiefer, 1987). A Landsat 2 MSS image (fig. 7) acquired June 6, 1977, shows the chain of lakes during the most severe stage of the 1970's regional drought. The area of Lake Thompson on June 6, 1977, was 0.53 $mi^2$ (table 3). Lake Whitewood contained some water (black areas) and supported cattail growth. Lake Preston appears to have been completely dry and contained little green vegetation as indicated by the light blue and gray areas.

A TM image, acquired May 9, 1984, is shown in figure 8. The surface area of Lake Thompson increased from 0.53 $mi^2$ in 1977 to 9.15 $mi^2$ in 1984 (table 3). The surface area of Lake Whitewood increased from 0.56 $mi^2$ in

**Table 2.** Discharge and lake-level data in the Lake Thompson chain of lakes (fall 1986 through spring 1988)

[—, no data]

| Number of measurement site (fig. 2) | Location and type of data | Date | Discharge ($ft^3/s$) | Lake-level elevation (ft) |
|---|---|---|---|---|
| 1 | Lake Henry (inflow) | 10–06–86 | 30.8 | — |
| | | 01–14–87 | 2.42 | — |
| | | 02–10–87 | 5.49 | — |
| | | 03–23–87 | 60.5 | — |
| | | 04–02–87 | 82.9 | — |
| | | 04–15–87 | 52.7 | — |
| | | 05–11–87 | 10.7 | — |
| 2 | Lake Whitewood (outflow) | 10–06–86 | 168 | — |
| | | 11–05–86 | 125 | — |
| | | 01–14–87 | 46.6 | — |
| | | 02–10–87 | 28.3 | — |
| | | 03–23–87 | 25.5 | — |
| | | 04–02–87 | 77.5 | — |
| | | 04–15–87 | 97.8 | — |
| | | 05–11–87 | 12.9 | — |
| 3 | Lake Thompson (stage) | 11–04–86 | — | 1,689.52 |
| | | 02–10–87 | — | 1,689.88 |
| | | 04–15–87 | — | 1,690.77 |
| | | 10–11–87 | — | 1,689.68 |
| | | 11–01–87 | — | 1,689.37 |
| | | 03–01–88 | — | 1,689.88 |
| | | 06–01–88 | — | 1,689.19 |
| 4 | Davis Slough, a tributary of the East Fork Vermillion River (outflow). | 11–07–86 | 2.49 | — |
| | | 12–10–86 | .27 | — |
| | | 02–10–87 | .90 | — |
| | | 03–23–87 | 4.80 | — |
| | | 04–02–87 | .83 | — |
| | | 04–15–87 | 3.51 | — |
| | | 05–11–87 | .04 | — |
| 5 | East Fork Vermillion River near Ramona. | 11–05–86 | 2.94 | — |
| | | 02–10–87 | 2.64 | — |
| | | 03–23–87 | 11.30 | — |
| | | 04–15–87 | 50.80 | — |
| | | 05–11–87 | 24.60 | — |
| | | 10–01–87 | 1.9 | — |
| | | 06–01–88 | .63 | — |

1977 to 6.18 $mi^2$ in 1984. Lake Preston had an area of 5.18 $mi^2$. From 1982 to 1984, the Lake Thompson drainage basin received about 12 in. of cumulative excess precipitation.

Topographic depressions and areas where soils were almost saturated are prevalent in figure 8. Topographic lows are indicated by narrow, dark-gray rings surrounding circular, light-gray to white areas. The light-gray to white circular areas are topographic highs or mounds and are ice disintegration ridges (Christensen, 1977). This particular pattern of stagnation-moraine topography is referred to as "coral" or "brain" patterns (Christensen, 1977). Topographic depressions are within the circular, light-gray to white areas. These depressions are indicated by dark-gray tones. The absence of red areas in figure 8 compared to figure 7 is caused by the lack of green vegetation.

A TM image, acquired May 31, 1986, is shown in figure 9. Comparison of figures 8 and 9 shows that the surface area of Lake Thompson increased from 9.15 $mi^2$ on May 9, 1984, to 21.21 $mi^2$ on May 31, 1986 (table 3). The area of Lake Whitewood increased from 6.18 $mi^2$ on May 9, 1984, to 11.16 $mi^2$ on May 31, 1986. The area of Lake Preston increased from 5.18 $mi^2$ on May 9, 1984, to 9.37 $mi^2$ on May 31, 1986. The water surface area, excluding the chain of lakes, on May 9, 1984, was about 12.4 $mi^2$ (fig. 8) and on May 31, 1986, it was about 28.6 $mi^2$ (fig. 9) (a net increase of 16.2 $mi^2$). The total additional land inundated in the Lake Thompson drainage basin from May 1984 to May

# SATELLITE CHARACTERISTICS

| SATELLITE | SENSOR | MODE | ALTITUDE (kilometers) | GROUND RESOLUTION (meters) | SWATH WIDTH (kilometers) | REPEAT CYCLE (days) | BANDS |
|---|---|---|---|---|---|---|---|
| NOAA | AVHRR | Multispectral | 833 | 1,100 | 2,400 | 0.5 | 5 |
| Landsat | MSS | Multispectral | 705 | 80 | 185 | 16 | 4 |
| Landsat | TM | Multispectral | 705 | 30 | 185 | 16 | 7 |
| SPOT | HRV | Multispectral | 832 | 20 | 60 | 26 | 3 |
| | | Panchromatic | 832 | 10 | 60 | 26 | 1 |

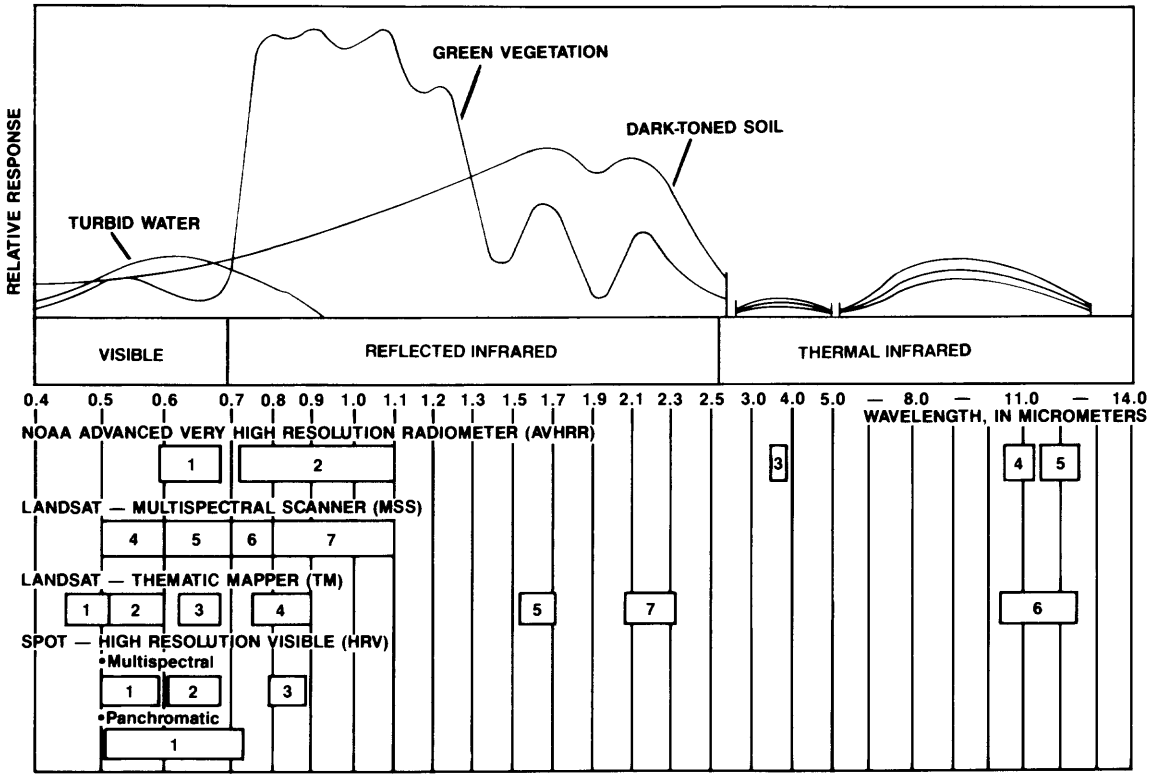


**Figure 6.** Satellite spectral characteristics.

1986 was 39.2 mi², or about 25,000 acres. The absence of red areas and abundance of dark-gray-blue areas in most parts of figure 9 indicate that little vegetation had emerged and that soils were probably almost saturated. Under normal climatic conditions, small-grain and row crops should emerge by June 1.

The outlet of Lake Whitewood was partially blocked with debris from 1984 to 1987, which compounded flooding problems on Lakes Preston and Whitewood and subsequently delayed flooding of Lake Thompson. As tributary inflow to the chain of lakes decreased, the lake levels of Lake Preston and Lake Whitewood declined about 1.3 ft between the May 1986 image (fig. 9) and the September 1986 image (fig. 10). The level of Lake Thompson continued to rise (2.6 ft from May 1986 to September 1986) because the lake had not reached the altitude of the outlet. In October 1986, the level of Lake Thompson reached an altitude of about 1,689 ft above sea level and began to drain into the East Fork Vermillion River. The surface-area changes of the chain of lakes from May 31, 1986, to June 5, 1988, were determined from figures 9–12 and are listed in table 3.

## RESPONSE TIME OF LAKE THOMPSON

Langbein (1961) developed a mass-balance equation (eq 1) that describes water-level fluctuations of terminal lakes:

$$I + PA = E_G A \qquad (1)$$

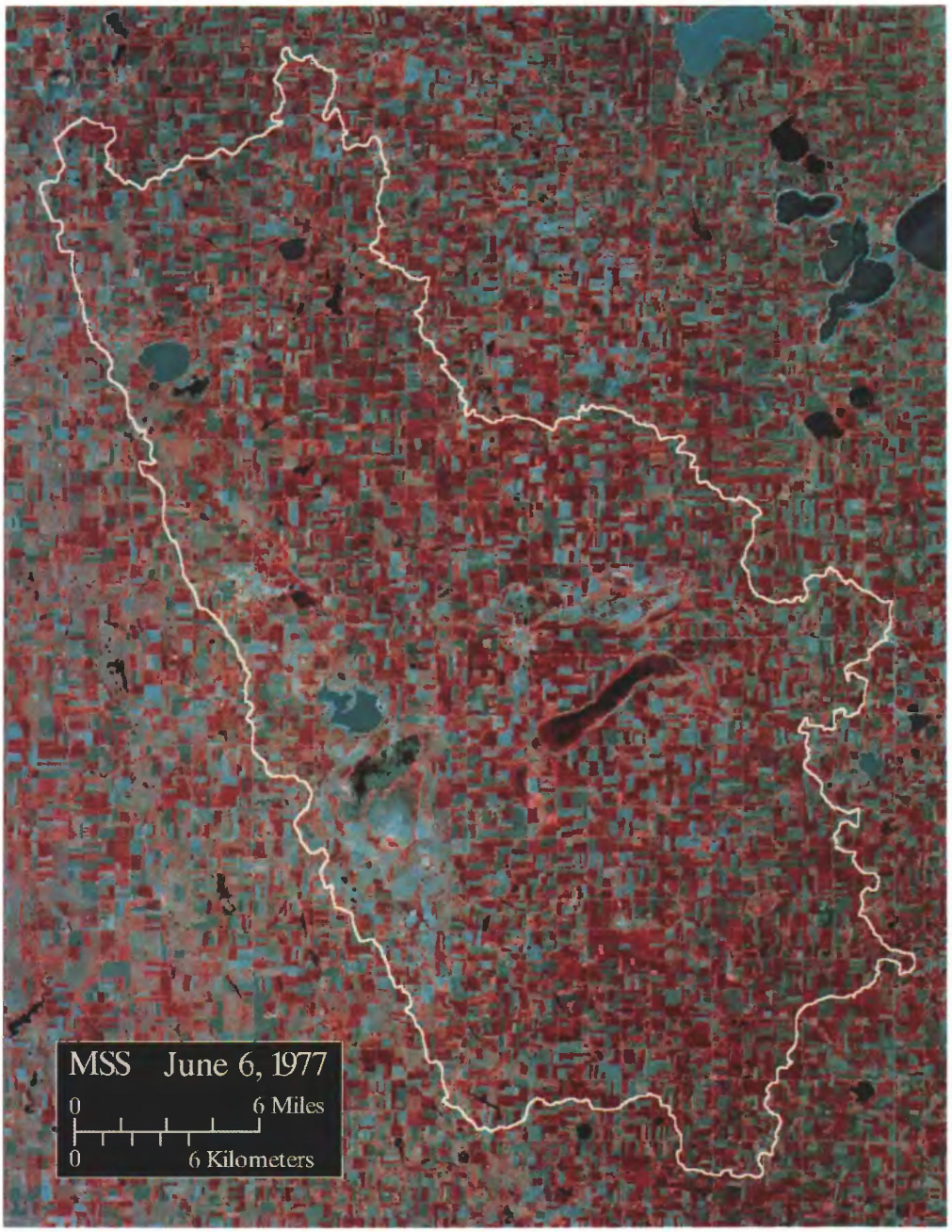


**Figure 7.** Landsat 2 Multispectral Scanner image of the Lake Thompson basin and vicinity, June 6, 1977.

where $I$= inflow from the tributary area, in acre-feet per year;
$P$= precipitation on the lake surface, in feet per year;
$A$= lake area, in acres; and
$E_G$= gross evaporation rate from the lake, in feet per year.

Year-to-year variations in $I$ and $P$ produce fluctuations in water level with corresponding variations in surface area. Equation 1 may be rewritten as:

$$\Delta H = I/A - E_N \quad (2)$$

where $\Delta H$= the change in lake stage, in feet, and
$E_N$= net evaporation, in feet per year. (Equal to $E_G$ minus precipitation on the lake surface.)

**Table 3.** Surface area, in square miles, of selected lakes in the Lake Thompson chain of lakes as determined from satellite images (1976–88)

[—, no data]

| Date | Lake Thompson | Lake Whitewood | Lake Preston | Lake Henry | Spirit Lake |
|---|---|---|---|---|---|
| June 6, 1977 | 0.53 | 0.56 | — | 1.70 | 1.43 |
| May 9, 1984 | 9.15 | 6.18 | 5.18 | 1.97 | 1.25 |
| May 31, 1986 | 21.21 | 11.16 | 9.37 | 3.05 | 1.98 |
| Sept. 3, 1986 | 21.31 | 9.67 | 8.39 | 3.21 | Cloud cover |
| June 3, 1987 | 22.64 | 9.20 | 7.66 | 3.31 | 1.86 |
| June 5, 1988 | 21.30 | 8.50 | 7.00 | 3.10 | 1.66 |

From these mass-balance equations, Langbein (1961) derived equation 3:

$$k=\frac{V_H-V_L}{E_N(A_H-A_L)} \quad (3)$$

where $k$= the response time of a lake, which is the ratio of a change in lake volume to the corresponding change in rate of discharge with time;
$V_H$= lake volume at high stage, in cubic feet;
$V_L$= lake volume at low stage, in cubic feet;
$A_H$= lake area at high stage, in square feet; and
$A_L$= lake area at low stage, in square feet.

Because volume may be expressed as:

$$V = AD,$$

where $D$ = mean lake depth, in feet, then

$$k=\frac{A_HD_H-A_LD_L}{E_N(A_H-A_L)} \quad (4)$$

where $D_H$= lake depth at high stage, in feet, and
$D_L$= lake depth at low stage, in feet.

The value of $k$ can explain the nature of fluctuations in the levels of terminal lakes. For example, a terminal lake with a $k$ value of 1 fills and dries up in 1 yr, such as a playa lake (Langbein, 1961); however, a lake with a large value of $k$ responds slowly to precipitation patterns and may maintain a high lake level even during a period of less than normal precipitation.

To calculate a response time for Lake Thompson, the lake volume, lake area, and average depth were determined at low and high lake stages. Figure 8 was used to determine the area (9.15 mi$^2$) of Lake Thompson at low lake stage (May 9, 1984), and figure 9 was used to determine the area (21.2 mi$^2$) of Lake Thompson at high lake stage (May 31, 1986). The lake volume was calculated by constructing cross sections across the lake at 1-mi intervals, using U.S. Geological Survey 7.5-min topographic maps. The average area between cross sections was multiplied by length (1 mi), and these products were summed to compute a total lake volume. The lake volume at both high and low stages was divided by the corresponding area to obtain the average depth. The average depth at a lake stage of 1,669.8 ft above sea level (May 9, 1984) was 1 ft, and the average depth at a lake stage of 1,685.9 ft above sea level (May 31, 1986) was 11.0 ft.

The net evaporation was calculated by subtracting the average annual precipitation (22.8 in/yr) from the gross evaporation from the lake. Evaporation from lake surfaces in eastern South Dakota is about 70 to 75 percent of evaporation from a class A pan. The average May through September evaporation from a class A pan at Brookings during 1970–80 was 40.64 in/yr (Farnsworth and Thompson, 1982). Using 72 percent of the average evaporation, the evaporation from the lake surface from May through September was 29.26 in. Because pan evaporation from May to September accounts for 78 percent of the annual lake evaporation (Wiche, 1986), the annual lake evaporation is equal to 29.26 in/yr divided by 0.78, or 37.51 in/yr. Farnsworth and Thompson (1982) lists average lake evaporation for the study area at 33 in. Thus, the average annual lake evaporation for the Lake Thompson drainage basin was computed as an average ((37.5+33)/2 = 35.25 in.). The net evaporation from lakes is equal to 35.25 in/yr −22.8 in/yr = 12.45 in/yr, or 1.04 ft/yr. Mean depth, areas, and net evaporation were entered into equation 4. The computed response time ($k$) for Lake Thompson using figures 8 and 9 (May 9, 1984, and May 31, 1986) was 18 yr. Comparison of two different images can yield a different response time for Lake Thompson. Using figure 7 (MSS image acquired June 6, 1977) and figure 10 (SPOT 1 HRV image acquired Sept. 3, 1986), the calculated response time was 11 yr. The calculated response time for Lake Thompson, thus, also is dependent on the particular image used to determine lake area.

Errors in estimating discharge from the lake surface (net evaporation) and lake volume can affect the calculated response time significantly. Net lake evaporation computed using various percentages of class A pan evaporation and corresponding calculated response time are listed in table 4. If the average depth at high lake stage, determined from the lake cross section, is in error by 20 percent, the lake response time would change by 6 yr. It should be emphasized that the computed lake response time in years is not a time period in which a lake will go dry, but a measure of how lake levels will respond to climatic conditions.

For comparison to Lake Thompson, the response time computed by Langbein (1961) for the Great Salt Lake, Utah, was 9 yr; for Pyramid Lake, Nev., the response time was 5 yr; and for Devils Lake, N. Dak., the response time was 14 yr.

The response time of a lake may be affected by the interaction of a hydraulically connected aquifer. Groundwater recharge may have a stabilizing effect on lake levels and, thus, increase the lake response time. Discharge from the lake to an aquifer may decrease the lake response time.

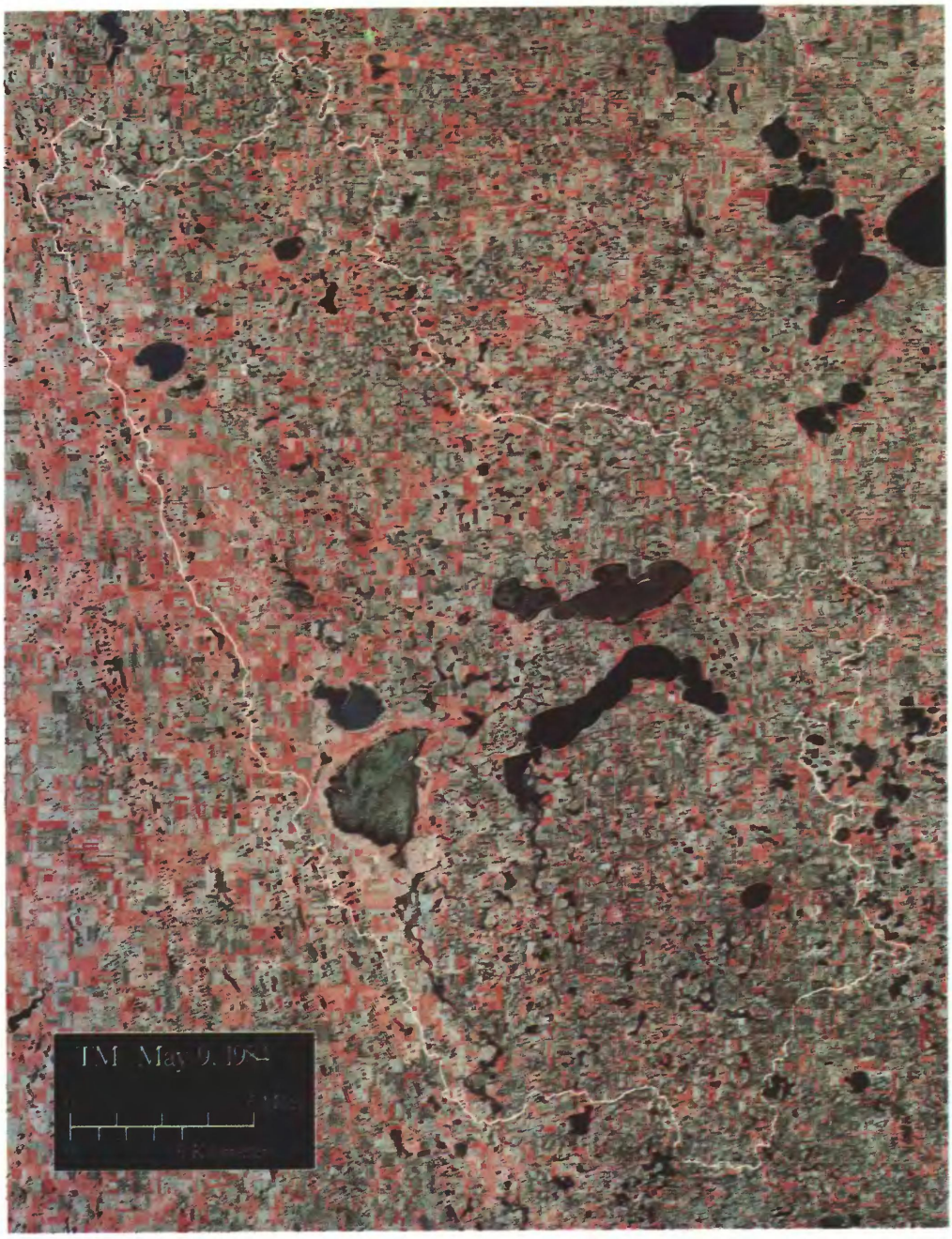

**Figure 8.** Landsat 5 Thematic Mapper image of the Lake Thompson basin and vicinity, May 9, 1984.

**Table 4.** Calculated response times of Lake Thompson

| Percentage of class A pan evaporation | Net lake evaporation (ft per year) | Response time, *k*, (yr) determined from | |
|---|---|---|---|
| | | Figures 8 and 9 | Figures 7 and 10 |
| 70 | 0.49 | 16 | 10 |
| 72 | .56 | 18 | 11 |
| 75 | .65 | 14 | 8 |

Test-hole data indicate that Lake Thompson is hydraulically connected to the Vermillion East Fork aquifer; however, the recharge-discharge interaction and rates between the lake and the aquifer are unknown.

The response time of draining lakes is considerably different than that of terminal lakes because of the method of discharge from the lake (Langbein, 1961). During times when Lake Thompson drains into the East Fork Vermillion

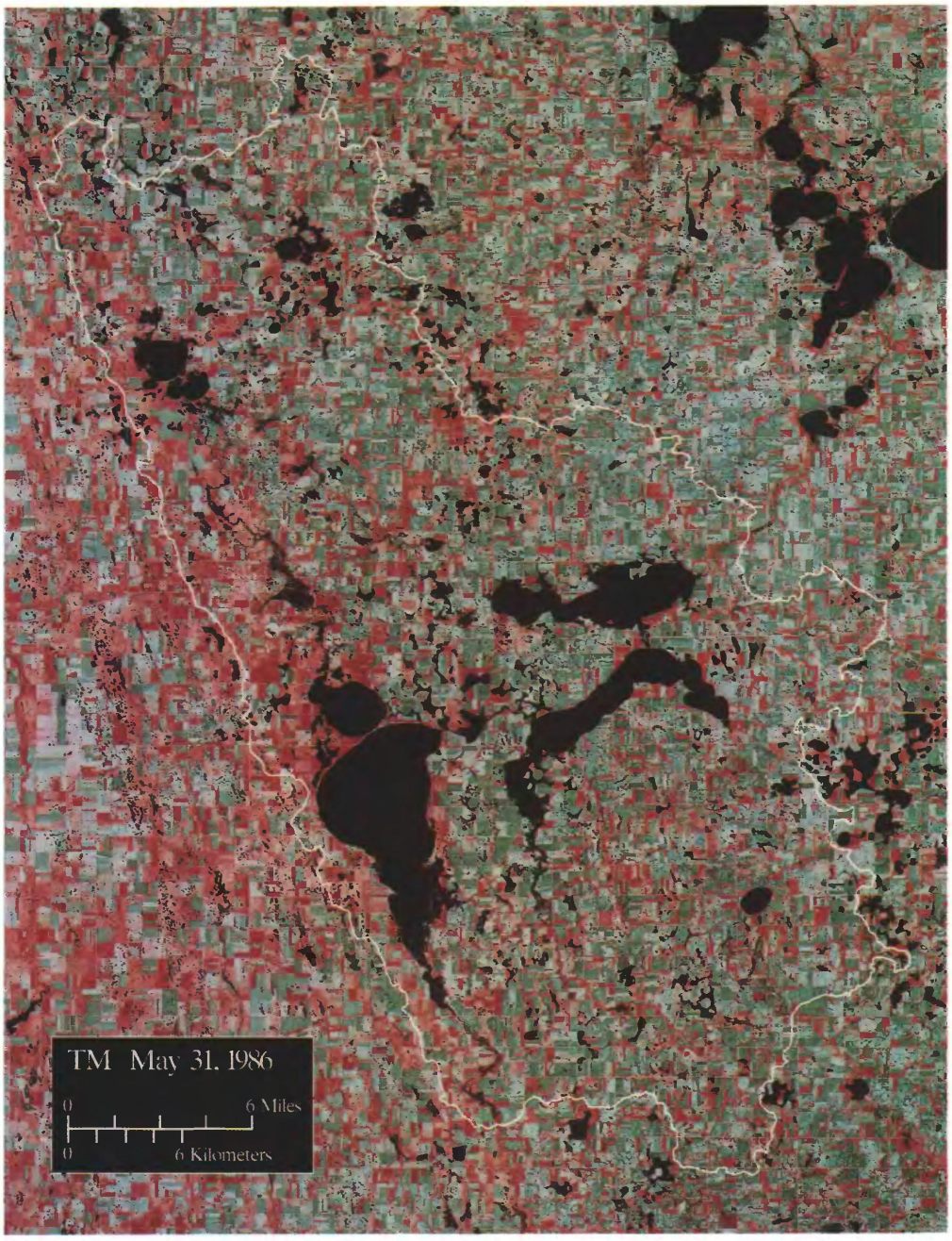


**Figure 9.** Landsat 5 Thematic Mapper image of the Lake Thompson basin and vicinity, May 31, 1986.

River and is, therefore, a draining lake, the response time, $k$, may be calculated by using the following equation:

$$k = 0.06\ A/Q^{0.6} \quad (5)$$

where

$A$ = lake area, in square miles; and

$Q$ = mean discharge, in cubic feet per second.

The calculated response time for Lake Thompson as a draining lake, using equation 5, is about 0.2 yr or 3 months.

As long as Lake Thompson remains a draining lake, lake levels will respond more rapidly to greater than or less than normal precipitation, and lake-level fluctuations will be less than if the lake level declines below the outlet and Lake Thompson becomes a terminal lake. Lakes Preston and Whitewood, which have been draining lakes since November 1984, have responded to less than normal precipitation from November 1986 through May 1988 (lake levels have declined about 3 to 4 ft).

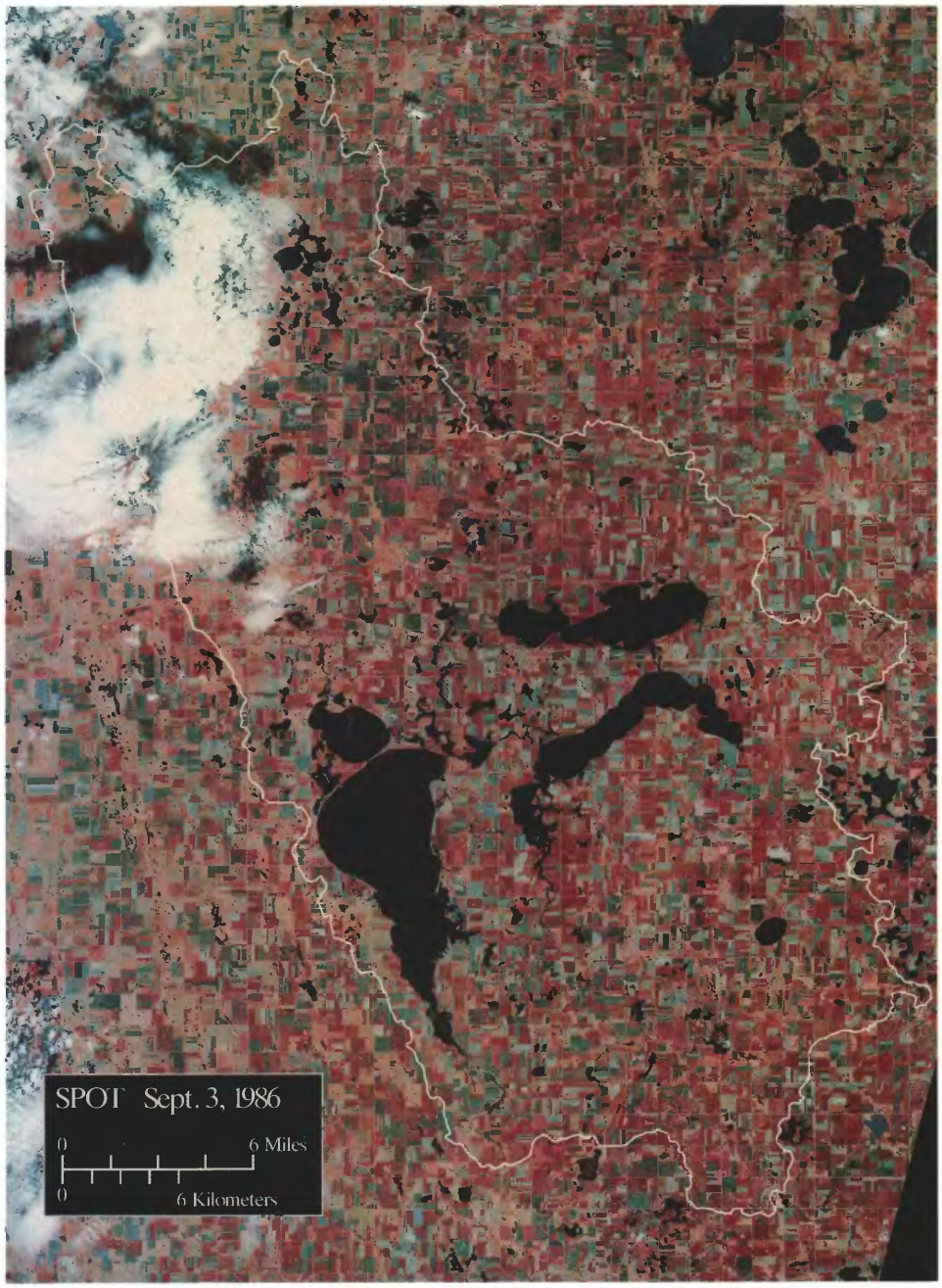


**Figure 10.** SPOT 1 High-Resolution Visible scanner image of the Lake Thompson basin and vicinity, Sept. 3, 1986.

The increased lake and slough surface area and flooded rivers and creeks caused by greater than normal precipitation and greater than average runoff from 1982 through 1986 extend beyond the Lake Thompson drainage basin. A NOAA 7 AVHRR image of eastern South Dakota acquired May 30, 1984 (fig. 13), and a NOAA 7 AVHRR image acquired May 4, 1986 (fig. 14), illustrate the relative increase of the surface-water area in eastern South Dakota.

## SUMMARY

Parts of the Lake Thompson subbasin received as much as 35.13 in. of cumulative excess precipitation from 1982 through 1987. During water year 1986, total flow in major streams in the area surrounding the chain of lakes region ranged from 320 to 520 percent of the long-term average. Runoff from the greater than normal

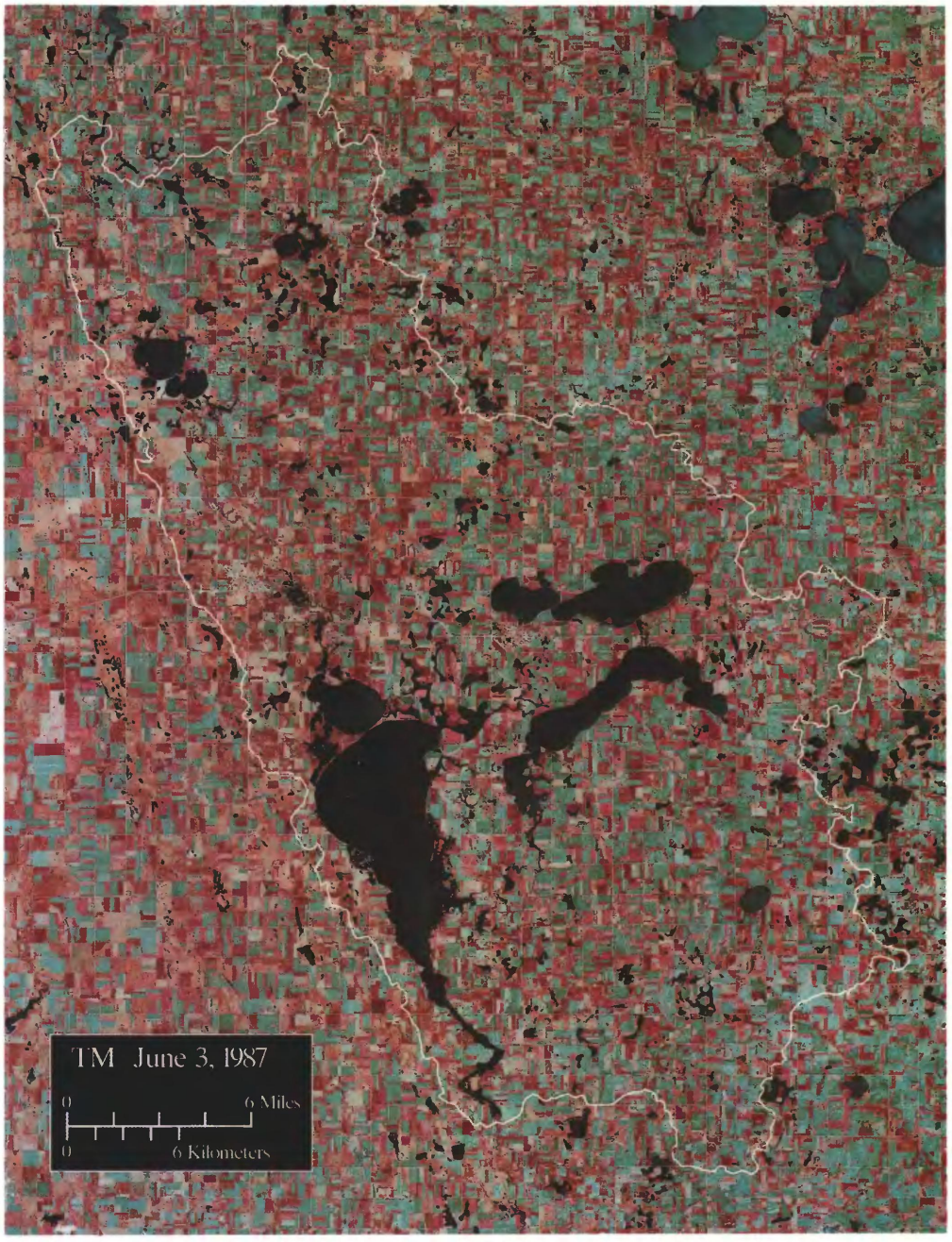


**Figure 11.** Landsat 5 Thematic Mapper image of the Lake Thompson basin and vicinity, June 3, 1987.

precipitation caused rapid rises in water levels in the lakes. Satellite data were used to determine the water surface area of lakes and sloughs during droughts and floods. The surface areas of Lake Thompson at high and low lake stages were used in Langbein's (1961) mass-balance equation to compute a response time of the lake, in years. The computed response time of Lake Thompson ranged from 8 to 18 yr.

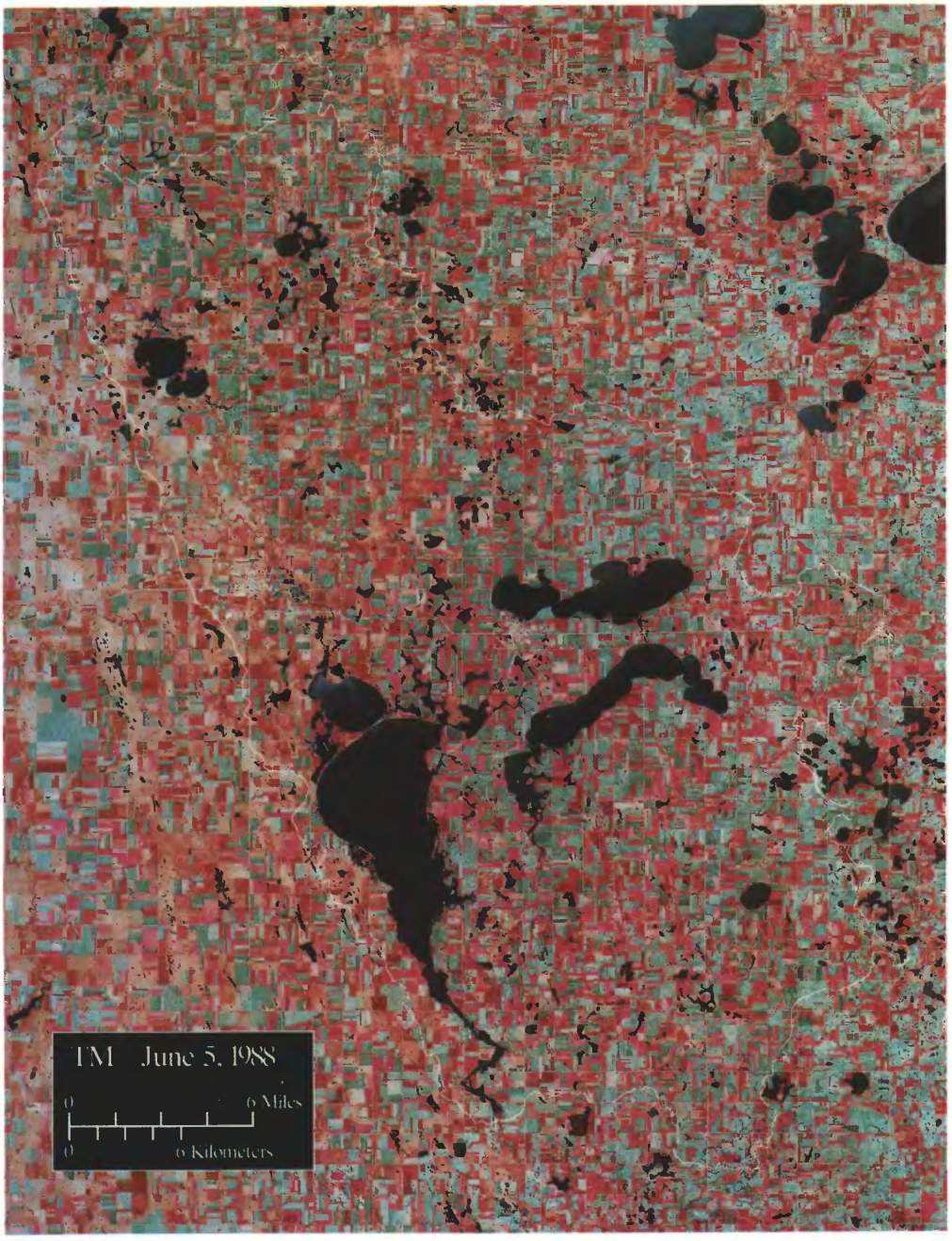


**Figure 12.** Landsat 5 Thematic Mapper image of the Lake Thompson basin and vicinity, June 5, 1988.

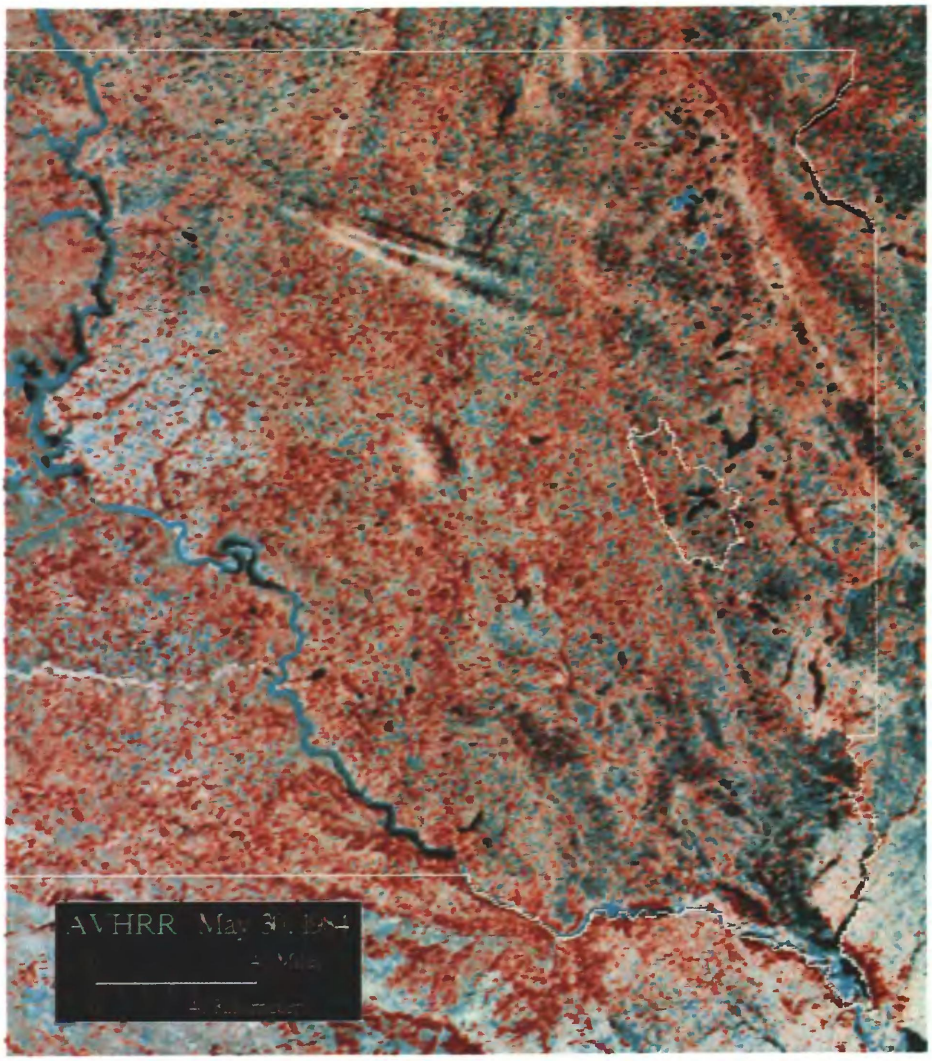


**Figure 13.** NOAA 7 image of the Lake Thompson basin and vicinity, May 30, 1984.

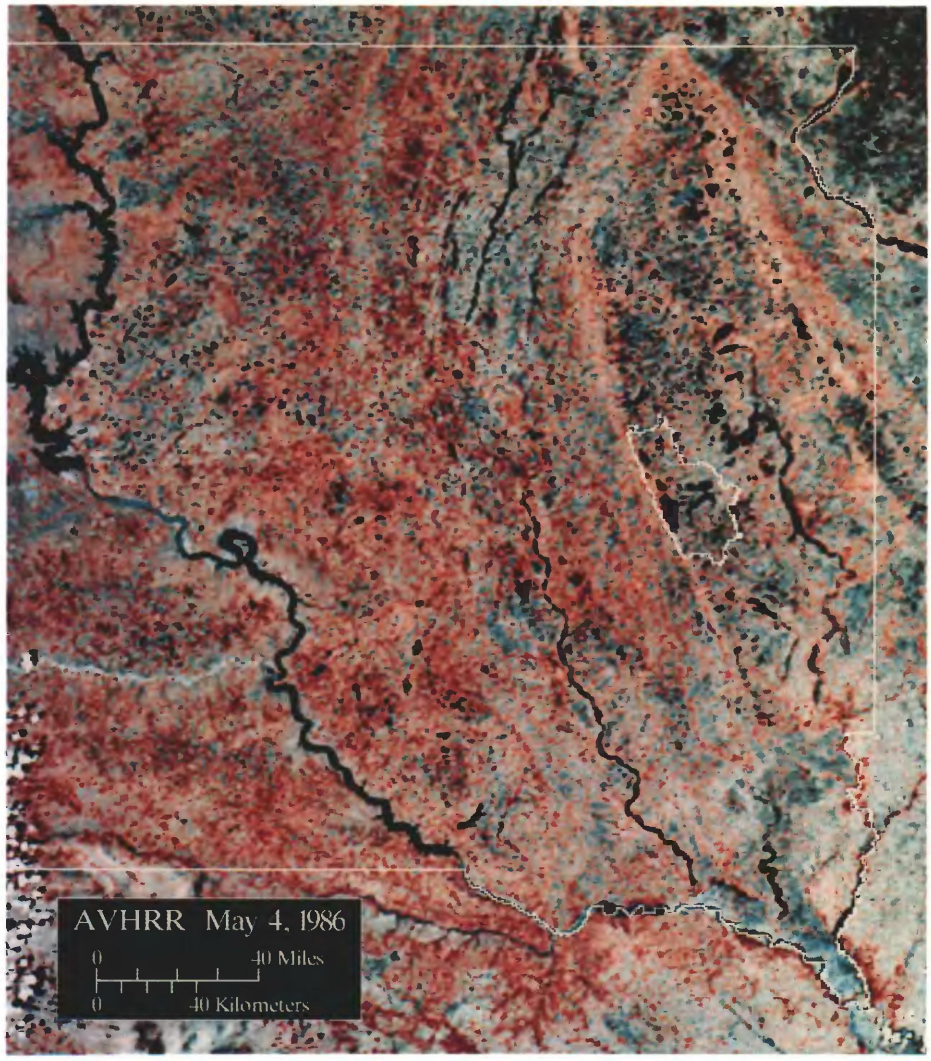


**Figure 14.** NOAA 9 image of the Lake Thompson basin and vicinity, May 4, 1986.

## REFERENCES CITED

Christensen, C.M., 1977, Geology and water resources of McPherson, Edmunds, and Faulk Counties, South Dakota, pt. I, Geology: South Dakota Geological Survey Bulletin 26, 58 p.

de Martonne, Emmanuel, 1927, Regions of interior-basin drainage: The Geographic Review, v. 27, 411 p.

Farnsworth, R.K., and Thompson, E.S., 1982, Mean, monthly, seasonal, and annual pan evaporation for the United States: National Oceanic and Atmospheric Administration Technical Report NWS 33, 26 p.

Fremont, J.C., 1887, Memoirs of my life.

French Systeme Probatoire d'Observation de Terre, 1987, SPOT data items and options: Reston, Va., SPOT Image Corp., 4 p.

Hamilton, L.J., 1989, Water resources of Brookings and Kingsbury Counties, South Dakota: U.S. Geological Survey Water-Resources Investigations Report 88–4185, 82 p.

Kidwell, K.B., 1983, NOAA polar orbiter data (TIROS-N, NOAA-6, NOAA-7, and NOAA-8)—A user guide: Washington, D.C., National Oceanic and Atmospheric Administration, Satellite Data Services Division, 100 p.

Langbein, W.B., 1961, Salinity and hydrology of closed lakes: U.S. Geological Survey Professional Paper 412, 20 p.

Lillesand, T.M., and Kiefer, R.W., 1987, Remote sensing and image interpretation (2d ed.): New York, John Wiley, 721 p.

National Oceanic and Atmospheric Administration, 1970–87, Climatological Data Annual Summary: Asheville, N.C., issued annually with variable pagination.

U.S. Geological Survey, 1991, National Water Summary 1988-89—Hydrologic events and floods and droughts: U.S. Geological Survey Water-Supply Paper 2375, 591 p.

U.S. Geological Survey and National Oceanic and Atmospheric Administration, 1984, Landsat-4 data users handbook: Sioux Falls, S. Dak., U.S. Geological Survey, EROS Data Center, 75 p.

Wiche, G.J., 1986, Hydrologic and climatologic factors affecting water levels of Devils Lake, North Dakota: U.S. Geological Survey Water-Resources Investigations 86–4320, 62 p.

# Automatic System for Measuring and Recording Fluorometry Data from Multiple Sources, South Cascade Glacier, Washington

*By* Andrew G. Fountain

**Abstract**

A system has been developed to automatically measure fluorescent tracers in multiple streams and to record the information in a digital data logger with solid-state memory. This system minimizes much of the tedium associated with making such measurements and simplifies data reduction. Automated equipment used for this system requires minimal time to set up and maintain, thereby maximizing the efficiency of the onsite personnel. An application to water-flow studies at South Cascade Glacier (Skagit County, Washington State) indicates that reliable data can be collected while the instruments are unattended. In addition to Rhodamine WT, a new tracer, Tinopal CBS-X, is used simultaneously. Interference between the two tracers is minimal. Tinopal CBS-X proved easy to work with, had sufficient fluorescence, and could be considered for other applications.

## INTRODUCTION

The use of fluorescent tracers is a common technique to measure discharge when standard methods are not applicable (Kilpatrick and Cobb, 1985) and to trace water routing in difficult situations, such as subterranean caverns (Smart and Smith, 1976) or glaciers (Krimmel and others, 1975). Usually, this technique requires at least two people, one to make the injection and one to record the information. If traveltime is either long or unknown, one person must stay with the fluorometer and make measurements for extended periods, perhaps through the night. If sampling involves multiple streams or multiple locations along a stream, the onsite effort quickly becomes labor intensive. This paper describes a system that decreases the onsite effort so that only one person is needed to set up and to run the equipment. Also, other tasks can be attended to while intermittently monitoring the instruments. The system was then used to monitor two dye tracers from three streams. Two noninterfering tracers were used simultaneously to increase the frequency of tracer injections.

Brian Cole, U.S. Geological Survey, Menlo Park, Calif., Robert Krimmel, U.S. Geological Survey, Tacoma, Wash., and James Wilson, U.S. Geological Survey, Cheyenne, Wyo., provided the fluorometers used in the study. Peter Danes of Danes Research, Tacoma, Wash., worked out the details and constructed the hydraulic-switching device that made the sampling system feasible.

## INSTRUMENTS AND OPERATION

The basic components of the system are a data logger and a flow-through fluorometer. The instruments used in this study were a Campbell Scientific 21X data logger and a Turner Designs Model 10 fluorometer. Similar type instruments may require some operation modification.

In the simplest operation, the output ports of the fluorometer are connected to the input channels of the data logger. Two input channels on the data logger are required, one for the range and the other for the meter reading. This circuitry involves three wires, one for ground and two for data. The data wires pass information about the measurable range and the meter reading. Four ranges in fluorometer units are available: 0–10, 0–31.6, 0–100, and 0–316; a constant voltage is specified for each range. A multiplier, ($\times 1$ or $\times 100$) also can be used; however, unlike the range, the multiplier needs to be operated automatically, nor is there a factory-installed output, so the multiplier needs to be operated and recorded manually. Once the relation between tracer mass being injected and resulting peak concentration is known, further results can be recorded by using one multiplier with the certainty that the readings will remain within a specified range. One advantage in measuring voltages from the fluorometer output ports, rather than reading the values from the meter, is greater accuracy. Visually reading the meter is hampered by parallax and visual interpolation.

The sampling interval is controlled by the data logger. If the fluorometer is continuously on, the data logger can sample at any desired interval. The interval may

be constant and manually changed during different periods of the experiment in order to obtain numerous samples during rapidly changing concentrations or, conversely, fewer samples during slowly changing concentrations. The data logger also can automatically change its recording frequency based on previously measured concentrations. For example, the recording interval can change if either the tracer concentration or the time rate of change in concentration exceeds a preset value. The data logger can turn on the fluorometer, through a relay, but because the warmup time is 10 min, the recording interval needs to be at least 15 min for this option to be practical.

Transporting water to a continuous-flow fluorometer can be accomplished by two methods. The first method is to pump the water to the fluorometer; this is necessary in situations of low topographic relief. The pump, if not continuously operated, needs to be turned on well in advance of a measurement to completely flush the system. This operation can be controlled by the data logger. A second method is to siphon the water to the fluorometer; this method is viable in areas of sufficient natural slope. This latter method proved particularly useful and will be described in more detail in the "Case Study" section.

A more comprehensive system than the previous example involves a data logger that controls water flow from multiple sources to multiple fluorometers and that records the measured tracer concentrations. For example, it may be desired to monitor a tracer concentration at more than one point along a stream or to monitor multiple streams. If these locations are within a few hundred yards of a central location, then in addition to a hydraulic-switching device, only one fluorometer is required. One type of switching device is a set of solenoid valves, one valve for each source of water. When the valve is normally closed (fig. 1*A*), no water is diverted to the fluorometer, and the water from each source flows across the valve and out the exit. Each valve is opened sequentially (fig. 1*B*), which diverts water to the fluorometer.

The switching device can be automatically operated. The data logger sets a control-port voltage that activates a solenoid valve and enables water to flow to the fluorometer. The control-port voltage that opens the valve needs to be maintained for a sufficient time to permit the fluorometer to stabilize. The fluorometer may have to switch among as many as three ranges before stabilizing, and the time required to do so may be appreciable, usually more than 10 s. Once the measurement is made, the data logger decreases the control-port voltage, which closes the solenoid valve, and water no longer flows to the fluorometer. Then the data logger increases the voltage of the next control port to open the next valve that diverts the water from the second source and so forth. For each source of water, one port on the data logger and one relay-solenoid set in the switching device are needed.

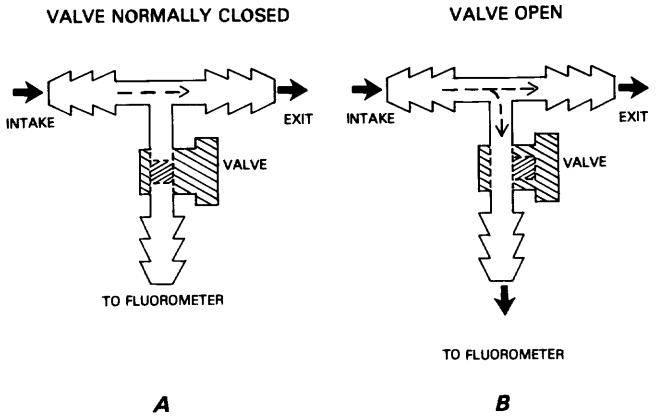


**Figure 1.** Valve arrangement in the hydraulic switching device: *A*, Normally closed valve; *B*, Power supplied to the valve, which opens it and permits flow to the fluorometer.

Data from the fluorometer are received by the same two channels, as described previously in the simplest setup, and some consideration needs to be given as to how the data are to be stored in the data logger. Fortunately, the data logger distinguishes between the "channels," where the sensor wires are attached, and the memory location. The result is that the fluorometer range and measurement for each source of water can be stored in different memory locations despite entering the logger through the same channels. The memory of most data loggers is substantial, and, with the addition of extended memory modules, the total storage can be expanded to meet almost any need.

Continuous-flow systems avoid shuttling between the source and the fluorometer location, which can become frantic if the tracer concentration is rapidly changing. Also, continuous flow minimizes sample contamination; this is particularly important when powdered tracers are used that may contaminate clothes and the sampling location.

## CASE STUDY

The automatic sampling system is being used in an ongoing study of the hydraulics of subglacial water flow at South Cascade Glacier in the North Cascade Range of Washington. Results from this study are to be applied to runoff models from glacierized basins and to understanding the nature of outburst floods from glaciers. The need for an automatic fluorometric system was to minimize the time for attending the fluorometers in order to concentrate on other, equally important, aspects of the study.

Water-flow tracing is difficult at South Cascade Glacier. A tracer injected into the glacier could appear in any one of three streams, each of which requires monitor-

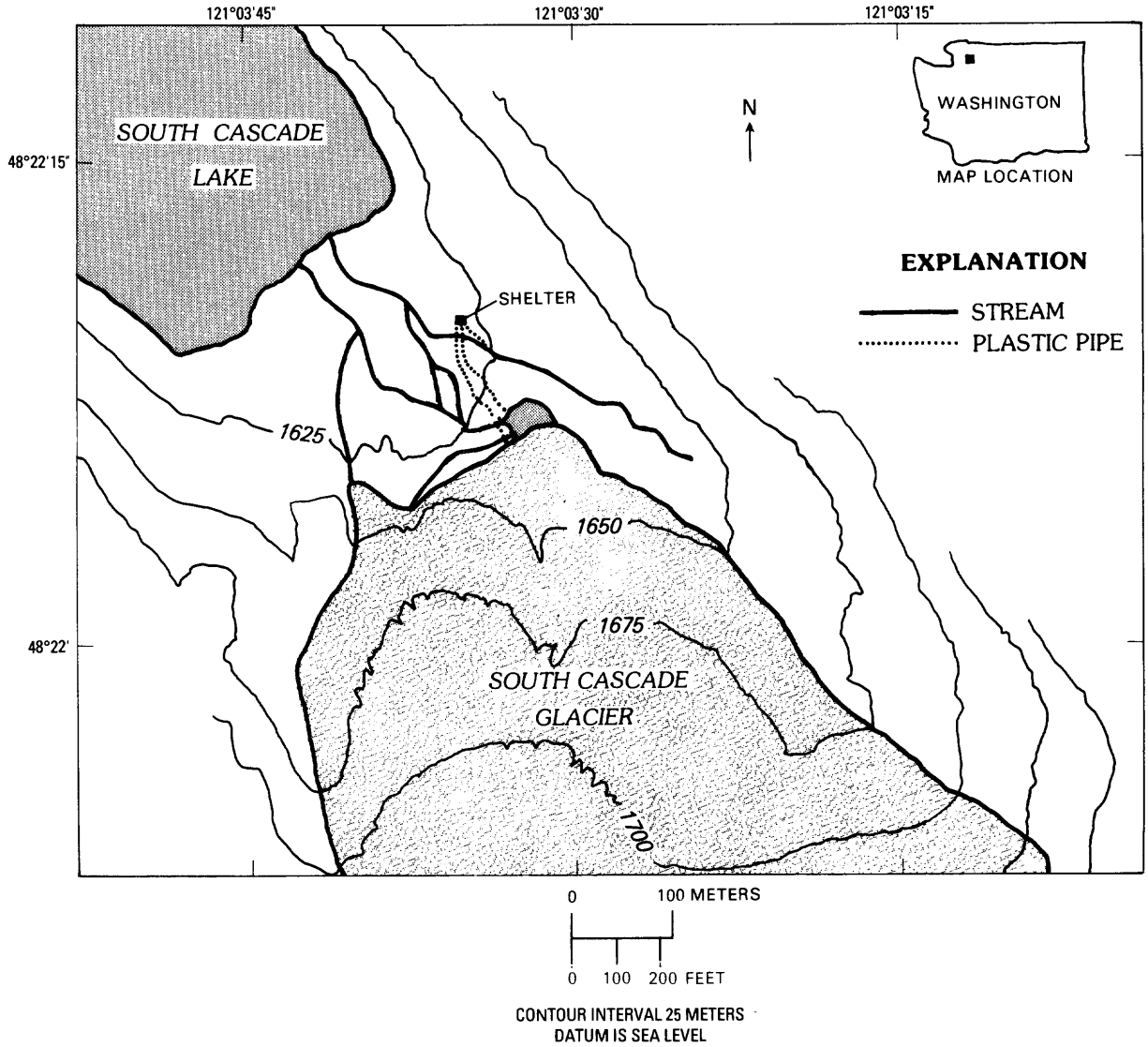


**Figure 2.** Location of the streams, siphons, and shelter for the fluorometers and data loggers, South Cascade Glacier, Wash.

ing. If grab samples are collected from each stream, it requires two people to sample and a third to measure the fluorescence. The traveltime of the main dye cloud varies depending on injection location and time of day (Krimmel and others, 1975), so this variation precludes the use of an automatic grab sampler. Also, the streams are swift and shallow, which makes installation and operation of samplers difficult. A continuous-flow, gravity-feed system was developed instead. Because of the potentially long traveltime of a tracer, two noninterfering tracers were used to maximize the number of injections. For these reasons, the sampling system was designed to detect two different fluorescent tracers in three streams by using two fluorometers to measure the tracers and a data logger to control the sampling rate and to record the information.

## Onsite Setup

Continuously flowing water from each stream was siphoned to a central location by 2.54-cm-diameter, black, plastic pipe (fig. 2). The streams flowed over a 4-m-high cascade, which provided sufficient hydraulic head to maintain the siphon for fairly long distances, about 200 m. The service required by each siphon depended on the quantity of sediment transported in the water at the depth of the siphon intake and how well the pipe was fixed in position on the streambed. The siphons worked well, requiring minimal maintenance. In one stream, the siphon required no maintenance during the entire 3-month field season; in other streams, the siphon intakes had to be cleared about once every 3 weeks.

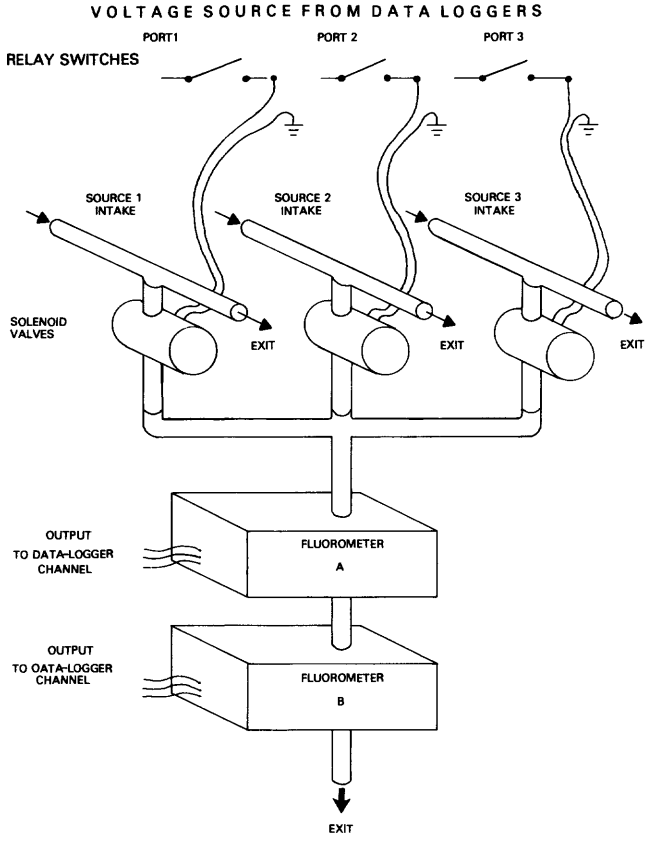


**Figure 3.** Hydraulic-switching device for three separate water sources and their flow to the fluorometers and data loggers.

Based on experience from previous field seasons, internal clogging could be prevented by installing a male-to-male connector on the pipe intake. This decreases the intake diameter so any pebble that enters the intake can flow through the system without becoming lodged at the next connector. A fine-screen intake was installed in an attempt to filter out the sediment, but it quickly became clogged and decreased the discharge through the pipe. Fine sediment occasionally was observed in the clear tubes that exited the hydraulic-switching device, but no pebbles were ever lodged in the valves or in the flow-through adapter of the fluorometer.

The sampling procedure was automated by using a hydraulic-switching device (fig. 3) that consisted of three 12-V, solenoid valves powered through relay switches. The relay switches were required because the data logger could not provide sufficient power to operate the valves. The solenoids operated on 12-V battery power because standard 110-V AC power was not available. The valves were of a T-design (fig. 1*A*), and normally were closed, so the water flows across the valves and out. When the valve opens (fig. 1*B*), water is permitted to pass through the fluorometer and out the normal exit. This arrangement was chosen rather than one that completely diverted the flow to the fluorometer to avoid pressure transients in the pipes. Lights were included in the switching device so the operator could quickly determine which valve was operating and, therefore, which stream was being sampled.

Initially, water did not flow to the fluorometer because of hydraulic resistance of the valves. This resistance problem was solved by clamping the exit tubes sufficiently to increase their resistance such that water readily flowed through the valves. Occasionally, small sediment grains, about 1.6 mm in diameter, prevented complete valve closure. This incomplete valve closure usually occurred when the siphon broke and sediment in the water settled into the valve. Flushing with clear water solved the problem.

The switching device was controlled by the data logger. In the situation of a rapidly changing tracer concentration between streams, the fluorometer required some time to cycle through each range before settling on a reading. After range selection, about 20–25 s was required before the meter stabilized. The data-logger program set a 5-V control-port voltage that tripped a relay and activated one valve. The data logger paused for 20 s, made a measurement, and then turned off the external power. The data logger repeated this procedure, activating successive control ports for each of the next two valves. The minimum sampling interval can be no shorter than the time required to cycle between the three valves. In this application, the minimum time was 60 s (three valves times 20 per valve). Because of uncertainty in traveltime of the dye cloud, the fluorometer was monitored by a person who manually changed the sampling interval by reprogramming one line in the data logger. This was a simple operation, successfully completed by people completely unfamiliar with data loggers.

The range of sampling cycles was 1–30 min. The water from the switching device was routed to two fluorometers connected in series. Each fluorometer detected a different tracer to allow increasing the frequency of injections. Black, plastic pipe also was used to connect the two fluorometers to decrease the possibility of light entering the fluorometric system.

## Tracers

The two tracers used were Rhodamine WT (Crompton and Knowles Corp.) and Tinopal CBS-X (Ciba-Geigy Corp.). Tinopal CBS-X is a fluorescent whitener used in detergents to brighten clothes. Brugman (1986) used Tinopal AMS in the melt waters flowing from Variegated Glacier, Alaska, rather than the CBS-X reported here. Tinopal CBS-X has greater emission intensity, greater solubility, and less dusting ability than does Tinopal AMS. The positive and negative aspects of Rhodamine WT, as a

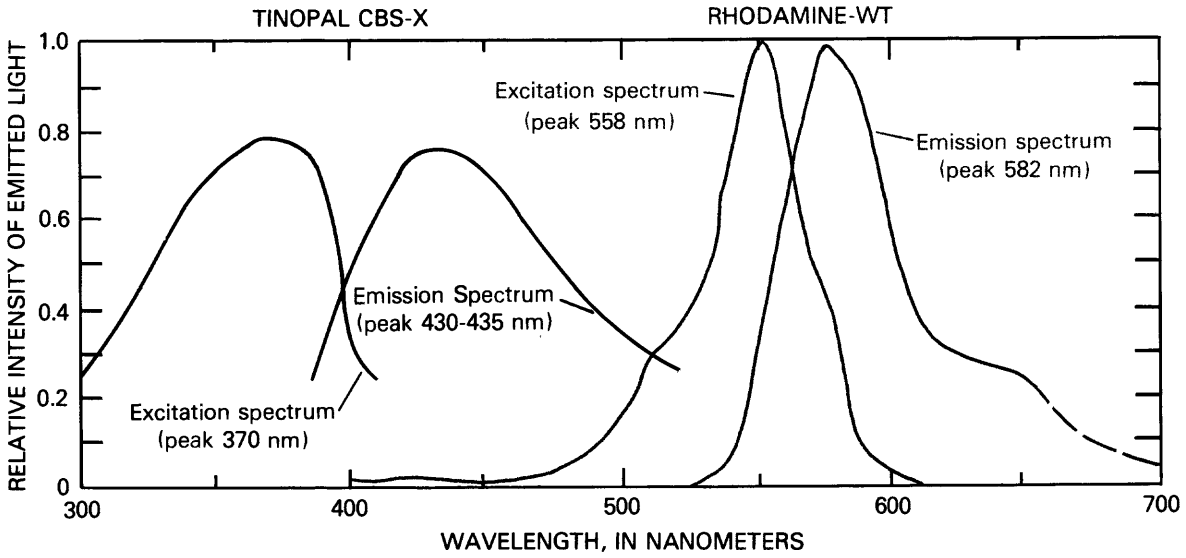


**Figure 4.** Spectral excitation and emission curves for Tinopal CBS-X (courtesy of Ciba-Geigy Corp., Greensboro, N.C., written commun., 1987) and Rhodamine WT (Wilson and others, 1986).

tracer, are well documented (Smart and Laidlaw, 1976; Abidi, 1982; Bencala and others, 1983; Smart, 1984; Abidi and others 1986, Steinheimer and Johnson, 1986). Much less is known about Tinopal CBS-X, although its toxicity was examined by Smart (1984). Natural organic compounds in the water fluoresce in the same wavelength range as Tinopal (Gaspar, 1987) and are responsible for higher background levels. One clear advantage of Tinopal CBS-X compared to Rhodamine WT is that it easily washes off hands and clothes. Rhodamine WT stains hands for days, and clothing requires bleaching to remove it.

Onsite tests of both tracers indicated that they were suitable for the conditions experienced at South Cascade Glacier. The fluorometers were calibrated onsite by using standards made from the stream water. The water temperature was fairly constant, within a few degrees of freezing. The sediment load varied between streams. The one stream in which the sediment load was monitored has an average suspended-sediment concentration of about 200 μg/L. The electrical conductivity, a measure of dissolved ion concentration, indicated a substantial diurnal variation, with peaks of 20 μS/cm coinciding with the minimum discharge. Under these conditions, the minimum detection level of Rhodamine WT was 0.1 μg/L and that of CBS-X was 1.0 μg/L . The adsorbance characteristics of Tinopal CBS-X are unknown at this time; however, tests are planned to compare the adsorbance characteristics of Rhodamine WT and Tinopal CBS-X in relation to conditions at South Cascade. Although no specific tests were done to account for suspended sediment interfering with fluorometer readings, background readings indicated no substantial variations during different sediment loads.

The expected interference between Rhodamine WT and Tinopal CBS-X is minimal based on the absorption and emission spectrum of each tracer (fig. 4). Rhodamine WT fluoresces in the yellow range of visible light and has a maximum excitation of 558 nm and a maximum emission of 582 nm (Wilson and others, 1986). Tinopal CBS-X fluoresces in the near-ultraviolet range and has maximum excitation of 370 nm and maximum emission of 430 to 435 nm (Ciba-Geigy Corp., Greensboro, N.C., written commun., 1987). Onsite tests at South Cascade Glacier, which used local stream water, indicated that the fluorometer measuring Rhodamine WT was insensitive to Tinopal CBS-X concentrations. Conversely, the fluorometer measuring Tinopal CBS-X was sensitive to Rhodamine WT concentrations of about 100 μg/L.

Brugman (1986) reported considerable difficulties in using Tinopal AMS onsite because of its powdered form. The tracer did not dissolve easily in large quantities, probably because of low water temperature. Also, it became airborne, which resulted in contamination of the sampling site. Neither difficulty occurred while using Tinopal CBS-X at South Cascade Glacier. The tracer was permitted to dissolve for 2 days prior to injection; however, only 40 g were required for most injections or about 0.03 percent of what Brugman (1986) required. Tinopal CBS-X caked if added in large quantities to water. Contamination of the sampling site was avoided by handling the tracer powder about 0.8 km downwind from the fluorometer and by the continuous flow operation of the fluorometer, which also eliminated handling and local environmental contamination.

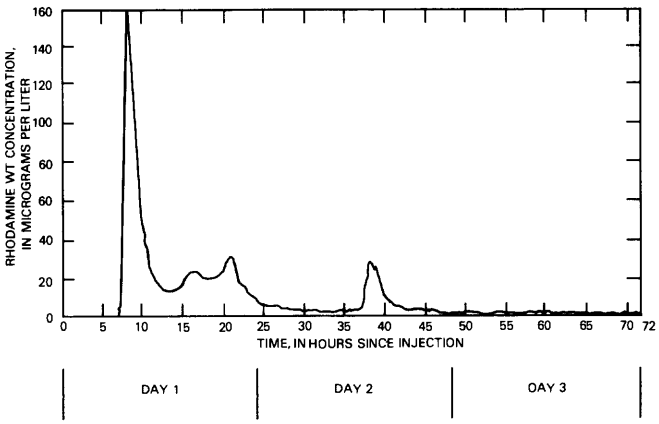


**Figure 5.** Plot of Rhodamine WT concentration as a function of time for injection 36. The different peaks within the first 24 h indicate multiple flow paths.

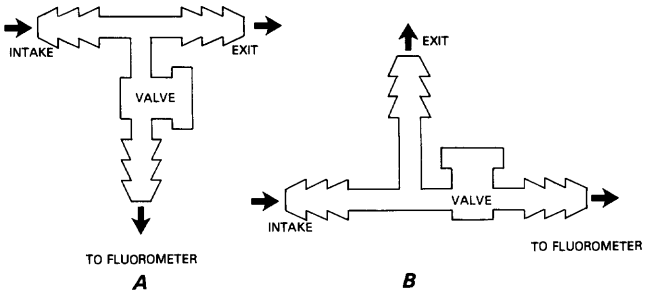


**Figure 6.** *A*, Current valve arrangement; *B*, Modification to improve flow to the fluorometer.

## Results of Study

A total of 39 injections were completed at 23 different locations during 3 months. Traveltimes ranged from 0.75 to almost 24 h. Sampling periods became quite extended, although traveltimes sometimes were short, because some of the tracers would reappear a day after the main peak had passed (fig. 5). Therefore, it was important to have a sampling system that could operate continuously for long periods. After the second hour of monitoring, information, such as that shown in figure 5, was collected without any supervision.

## POWER REQUIREMENTS

The data logger required 1 mA quiescent and about 60 mA during measurements, the switching device requires 50 mA quiescent and 1 A during operation, and the fluorometer requires 2 A at 12 V. The power supply was a bank of three 100 A-hour batteries connected to two 36-W solar panels. Also a 600-W generator occasionally was used when current drain was large and cloudy weather was persistent.

## PROBLEMS AND POSSIBLE IMPROVEMENTS

The main problem, unless a lap top computer is available, is that there is no quick method of determining visually whether the tracer peak has passed. This is a particular problem for glacier research because traveltimes can vary substantially for injection locations a short distance apart. This problem can be overcome by using a strip-chart recorder installed in parallel with the data logger provided the impedance of the recorder and data logger are matched. The strip-chart recorder also would provide a hard-copy backup of the information in the data logger. The data logger used in this study had the ability to output voltages that matched incoming ones. Although this feature was not used, it does provide an easy method of using the data logger and analog, strip-chart recorder, in conjunction.

Another problem was inadequate flow to the fluorometers through the valves. Rather than having a T-arrangement for a valve that, in its open position, requires the water to be forced downward to the fluorometers (fig. 6*A*), the T-arrangement could be inverted as shown in figure 6*B* so the water would tend to flow directly into the valve rather than over it.

The problem of sediment occasionally preventing complete closure of the solenoid valves in the switching device could be solved by installing a small sediment trap upstream from the device. The sediment trap could be inspected once or twice a day and emptied if necessary. A small-volume sediment trap would minimize trapping of the tracer.

The rapid drain of the internal batteries of the data logger also was a problem. The unusual power consumption, which normally did not occur during most data-logging applications, was caused by setting the control-port voltage at 5 V for 20 s for each valve. This power consumption can be avoided by using the external power connections to the data logger.

## DATA-LOGGER PROGRAM

The data-logger program shown on facing page is the one being used in the onsite application of the automatic sampling system at South Cascade Glacier. This program is not intended to represent the optimal program but is an example of how the data logger may be programmed. The program consists of a series of subprograms designated by "P," and each subprogram consists of one or more instructions.

```
1 P 20  PORT SET                                  [turn on first solenoid and route water from the
     1    1  set port to 5 volts                   first source to the fluorometer]
     2    1  set port #1
2 P 22  EXCITE-DELAY                              [delay for 20 seconds]
     1    1  excite channel 1
     2    0  excite with zero volts
     3 2000  excitation maintained times .01 seconds
     4    0  delay after this many .01 seconds
3 P 01  SINGLE-ENDED VOLTAGE MEASUREMENT          [measure all relevant channels]
     1    4  repetitions
     2   15  range (5 volts with fast rise)
     3    1  start at input channel 1 and increment
     4    1  storage location
     5   1.  multiplier
     6   0.  offset
4 P 20  PORT SET                                  [turn off the water flow]
     1    0  set port to 0 volts
     2    1  port #1
5 P 20  PORT SET                                  [turn on second solenoid and route the water from
     1    1  set port to 5 volts                   the second source to the fluorometer]
     2    2  set port #2
6 P 22  EXCITE-DELAY
     1    1  excite channel 1
     2    0  excite with zero volts
     3 2000  excitation maintained times .01 seconds
     4    0  delay after excitation times .01 seconds
7 P 01  SINGLE-ENDED VOLTAGE MEASUREMENT
     1    4  repetitions
     2   15  range (5 volts with fast rise)
     3    1  start at input channel 1 and increment
     4    5  first storage location
     5   1.  multiplier
     6   0.  offset
8 P 20  PORT SET                                  [turn off the water flow]
     1    0  set port to 0 volts
     2    2  set port #2
9 P 20  PORT SET                                  [turn on third solenoid and route
     1    1  set port to 5 volts                   the water from the second source
     2    3  set port #3                           to the flurometer]
10 P 22 EXCITE-DELAY
     1    1  excite channel 1
     2    0  excite with zero volts
     3 2000  excitation maintained times .01 seconds
     4    0  delay after excitation times .01 seconds
11 P 01 SINGLE-ENDED VOLTAGE MEASUREMENT
     1    4  repetitions
     2   15  range (5 volts with fast rise)
     3    1  start at input channel 1 and increment
     4    9  first storage location
     5   1.  multiplier
     6   0.  offset
12 P 20 PORT SET                                  [turn off the water flow]
     1    0  set port to 0 volts
     2    3  set port #3
13 P 86 SET FLAG                                  [start data transfer]
     1   10  set flag to zero for output
14 P 77 OUTPUT REAL TIME
     1 0110  store day, hour, minute
15 P 70 SAMPLE (send data from temporary to permanent storage)
     1   12  repetitions
     2    1  start storage location 1 and increment
```

The major programming problem to overcome was how to turn on the switching device to route the water to the fluorometer, wait until the fluorometer reading stabilized, and then record the value. There are two ways to do this: by using subprogram 4, the excite-delay-measure routine, or by using a combination of subprograms. Subprogram 4 was designed precisely for this type of situation; however, the maximum delay time is substantially less than the 20 s required. By combining subprograms 20—Port set, 22—Excite-delay, and 1—Single-ended voltage measurement, a facsimile of subprogram 4 could be produced with a longer delay time. Subprogram 20 sets the voltage of a port to a preset 5 V, which, in this application, trips a relay and opens a solenoid valve that routes the water to the fluorometer. Subprogram 22 normally is used to turn on an accessory device, such as a ventilating fan, prior to making an air-temperature measurement. In this instance, the subprogram is used to delay the sequence the required 20 s by supplying an unused channel with 0 V. The single-ended voltage measurement is made by using subprogram 1. The program then scans all the desired channels beginning with the first one. Once all the measurements are made, the next program (subprogram 20) is run, which shuts off the power to the solenoid valve and stops the water flowing to the fluorometer from the first source. This procedure is repeated for each source of water. Table 1 indicates how the data transfer was handled.

## INSTRUMENTATION NOTES

Solid-state data loggers represent a significant advance in data acquisition. Their relatively inexpensive cost compared to analog recorders, and reliability under varying weather conditions have made data collection easier than before. One drawback has been that the data modules or tapes had to be returned to the office for processing before the information could be analyzed. The advantage to analog recorders and the reason they have remained popular recording devices is that they can be quickly examined onsite and the experiment changed to meet previously unexpected results. Their main drawback is the labor-intensive and tedious digitization of the analog records. The disadvantage with the solid-state recorders of not being able to view the accumulated data now can be largely avoided with a portable computer. A lap-top computer that has disk drives and sufficient memory can run spread-sheet programs to quickly retrieve, convert, and plot the stored data. The advantages of this approach include fast processing of large data sets and the ability to alter the onsite experiment by using newly acquired results. The latter consideration is important because occasionally a measurement is not written down that later proves critical to the data processing.

**Table 1.** Sequence of events for the data logger that controls the water flow and information transfer

[The events occur from left to right in each row and from top to bottom. fluoro R indicates a fluorometer measuring Rhodamine WT; fluoro T indicates a fluorometer measuring Tinopal CBS-X]

| Control port on | Channel numbers | Memory location | Control port off |
|---|---|---|---|
| 1 (stream 1) | 1,2 (fluoro R) | 1,2 | |
| | 3,4 (fluoro T) | 3,4 | 1 |
| 2 (stream 2) | 1,2 (fluoro R) | 5,6 | |
| | 3,4 (fluoro T) | 7,8 | 2 |
| 3 (stream 3) | 1,2 (fluoro R) | 9,10 | |
| | 3,4 (fluoro T) | 11,12 | 3 |

Read all memory locations and place data into final storage.

## CONCLUSIONS

The advantages of the automated data-collection system for fluorometric projects are as follows. The automatic collection minimizes the number of personnel and, therefore, the cost of the project. The system provides accurate and numerous data at short time intervals that enable improved analysis. The required personnel can attend to other aspects of the project while giving cursory attention to the fluorometers. The accuracy of the information collected is increased because errors due to parallax, visual interpolation and manual recording are avoided. By using additional improvements, as outlined, the reliability is increased.

The automated data-collection system was useful for onsite measurements of tracers flowing in multiple streams. Applications other than for glacier research include braided-stream studies and transverse or longitudinal profiles in a single stream. Combining this system with recent technological advances in data loggers and laptop computers decreases the effort expended in data reduction and analysis and enables personnel at the study site to quickly determine whether additional tracer injections are required.

Tinopal CBS-X was successfully used as a tracer. It did not substantially interfere with Rhodamine WT when present, and it is easier to handle than is Rhodamine WT. More tests with Tinopal CBS-X need to be made to determine its characteristics under a variety of conditions.

## SELECTED REFERENCES


Abidi, S.L., 1982, Detection of diethylnitrosamine in nitrite-rich water following treatment with Rhodamine flow tracers: Water Research, v. 16, p. 199–204.

Abidi, S.L., Dawon, V.K., and Hubley Jr., R.C., 1986, Potential for nitrosamine formation in seven fishery chemicals: The Progressive Fish-Culturist, v. 48, p. 301–302.

Bencala, K.E., Rathburn, R.E., Jackman, A.P., Kennedy, V.C., Zellqeger, G.W., and Avanzino, R.J., 1983, Rhodamine WT dye losses in a mountain stream environment: Water Resources Bulletin, v. 19, no. 6, p. 943–950.

Brugman, M.M., 1986, Water flow at the base of a surging glacier: Pasadena, California Institute of Technology, Department of Geology, unpub. Ph. D. dissertation, 267 p.

Gaspar, Emilian, 1987, Modern trends in tracer hydrology, v.1: Boca Raton, Fla., CRC Press, Inc. 105 p.

Kilpatrick, F.A., and Cobb, E.D., 1985, Measurement of discharge using tracers: U.S. Geological Survey Techniques of Water-Resources Investigations, book 3, chap. A16, 52 p.

Krimmel, R.M., Meier, M.F., and Tangborn, W.V., 1975, Water flow through a temperate glacier, *in* The role of snow and ice in hydrology, International Association of Hydrological Sciences publication 107, p. 401–416.

Smart, P.L., 1984, A review of the toxicity of twelve fluorescent dyes used for water tracing: The NSS Bulletin, October 1984, p. 21–33.

Smart, P.L., and Laidlaw, I.M.S., 1976, An evaluation of some fluorescent dyes for water tracing: Water Resources Research, v. 13, no. 1, p. 15–33.

Smart, P.L., and Smith, D.I., 1976, Water tracing in tropical regions, the use of fluorometric techniques in Jamaica: Journal of Hydrology, v. 30, p. 79–195.

Steinheimer, T.R., and Johnson, S.M., 1986, Investigation of the possible formation of diethylnitrosamine resulting from the use of Rhodamine WT dye as a tracer in river waters, *in* Subitzky, Seymour, ed., Selected papers in the hydrologic sciences, 1986: U.S. Geological Survey Water-Supply Paper 2290, p. 37–49.

Wallis, S.G., Blakeley, C., and Young, P.C., 1987, A microcomputer based fluorometric data logging system for flow and dispersion measurements: Journal of the Institution of Water Engineers and Scientists, v. 41, p. 122–134

Wilson, J.F., Cobb, E.D., and Kilpatrick, F.A., 1986, Fluorometric procedures for dye tracing: U.S. Geological Survey Techniques of Water-Resources Investigations, book 3, chapt. A12, 34 p.

# Model Analysis of Hydraulic Properties of a Leaky Aquifer System, Sarasota County, Florida

By C.B. Hutchinson *and* J.T. Trommer

**Abstract**

A three-dimensional model is used in a radial mode to simulate water-level response in monitor wells during a multistage-discharge test of a leaky limestone aquifer system. The test was conducted at a group of multizone observation wells in central Sarasota County, Florida. Transmissivity of the Suwannee permeable zone, determined analytically, is 13,000 feet squared per day. Hydraulic conductivity of the overlying and underlying semiconfining units, estimated through model calibration, are 10 feet per day and 0.1 foot per day, respectively. The estimated compressibility of the limestones, also determined through model calibration, is $1.5\times10^{-5}$ square inch per pound. Model-derived hydraulic properties fall within ranges of properties reported from standard aquifer tests in west-central Florida. In contrast to analytical approaches, the model analysis was not constrained by multiple phases of discharge and recovery, length of testing, assumptions concerning storage within a semiconfining unit, or number of layers in the hydrogeologic system. The model was sensitive to changes in hydraulic conductivity and rock compressibility.

## INTRODUCTION

Hundreds of aquifer tests are conducted annually in Florida to define the hydraulic properties of aquifer systems. In tests of leaky aquifers, determination of hydraulic properties of the semiconfining units is desired in addition to determination of aquifer properties. Leakance, hydraulic conductivity, and specific storage of the semiconfining beds can sometimes be determined by using analytical methods (Hantush, 1967; Neuman and Witherspoon, 1972). However, application of such analytical methods may be limited if the duration of the test is too short, if the hydrologic system being analyzed is multilayered, if observation wells are not strategically placed, and by the assumption that the semiconfining units do not store water.

The purpose of this report is to describe a means of analyzing aquifer-test data by using numerical modeling rather than an analytical method. A multistage-discharge test of a complex multiple-aquifer system in Sarasota County, Fla., was selected to demonstrate modeling procedures used to derive hydraulic properties of semiconfining units above and below a pumped zone. A finite-difference model, HST3D, for simulating heat and solute transport in three dimensions (Kipp, 1986), was selected because of its versatility in simulating the flow field in a cylindrical (R-Z) coordinate system. The analysis is based on a 44-h withdrawal test from the Regional Observation and Monitor-Well Program (ROMP) TR5–2 Suwannee well in Sarasota County.

Sarasota County, Fla., is underlain by six water-bearing zones separated by semiconfining units constituting a 2,075-ft-thick aquifer system (Sutcliffe and Thompson, 1982, p. 6). In addition to the complex hydrogeologic framework, there exists a diversity of water quality, with potable supplies occurring only in shallow zones. Increases in both municipal water use and wastewater discharges have prompted feasibility studies of disposal of reverse-osmosis reject brines and treated sewage into the lower zones of the aquifer system.

The test was conducted as part of a regional study in cooperation with the Southwest Florida Water Management District (SWFWMD) to assess the potential for upward migration of wastewater from deep injection zones. An estimate of potential for wastewater migration is required by the Florida Department of Environmental Regulation in its permitting procedure.

## APPROACH

Observation wells were drilled and an aquifer test was conducted to obtain data for input into a multilayered, digital ground-water-flow model. To achieve the study objectives, the following project elements were completed:

1. The hydrogeologic framework was defined from lithologic and geophysical logs;
2. Previous pumping tests were analyzed to estimate hydraulic properties of permeable zones in the aquifer system at the test site;
3. Information on hydraulic properties of semiconfining units was compiled from engineering reports of nearby test-injection wells;

4. A multistage-discharge test was conducted with drawdown and recovery measured in observation wells above and below the pumped zone;
5. A radial-flow model that simulates water-level responses in the observation wells was calibrated against tidal-corrected observed water-level responses;
6. The model was tested to demonstrate its sensitivity to large changes in input parameters; and
7. Constraints of the model analysis that limit reliability were defined.

## HYDROGEOLOGIC FRAMEWORK

An improved understanding of the hydrogeologic framework of southwest Florida is being developed through a systematic program of well drilling, logging, sampling, and testing by the SWFWMD. ROMP consists of a network of single and cluster wells at approximately 150 sites in the 10,200-mi² Water Management District. Data from ROMP cluster TR5–2 (fig. 1) were used to delineate the hydrogeologic framework in west-central Sarasota County.

Hydrogeologic units at ROMP TR5–2 consist of thick carbonate rock sequences overlain by clastic deposits. Units, in descending order, are an unconfined surficial aquifer system, a multilayered intermediate aquifer system, and a very thick carbonate aquifer, which has been referred to as the Floridan aquifer system (table 1). Miller (1986, p. 2) defines the Floridan aquifer system to include the Upper Floridan aquifer, the middle confining unit, and the Lower Floridan aquifer. Observation and test wells at ROMP TR5–2 penetrate the surficial and intermediate aquifer systems and the upper part of the Upper Floridan aquifer. Water levels (heads) in fully cased wells at the test site generally increase with depth and range from near land surface in the surficial aquifer to about 17 ft above land surface in the Upper Floridan aquifer.

The surficial aquifer system at ROMP TR5–2 consists of undifferentiated terrace deposits, clay, and shell beds of Holocene and Pleistocene age and is about 50 ft thick. The aquifer in the area is recharged primarily from local precipitation.

The intermediate aquifer system consists of interbedded limestone, sand, and clays of Pliocene and Miocene age. Two aquifer units recognized in the system at the test site are the Tamiami-upper Hawthorn aquifer and the lower Hawthorn-upper Tampa aquifer (Wolansky, 1983, p. 20). Tops and bottoms of the aquifers are based on producing zones denoted on flow logs during a 700-gal/min test of a 480-ft deep well. The Tamiami-upper Hawthorn aquifer occurs between 60 and 100 ft below land surface and is separated from the surficial aquifer system by overlying beds of sandy clay, clay, and marl in the Caloosahatchee Marl and the upper part of the Tamiami Formation. It is

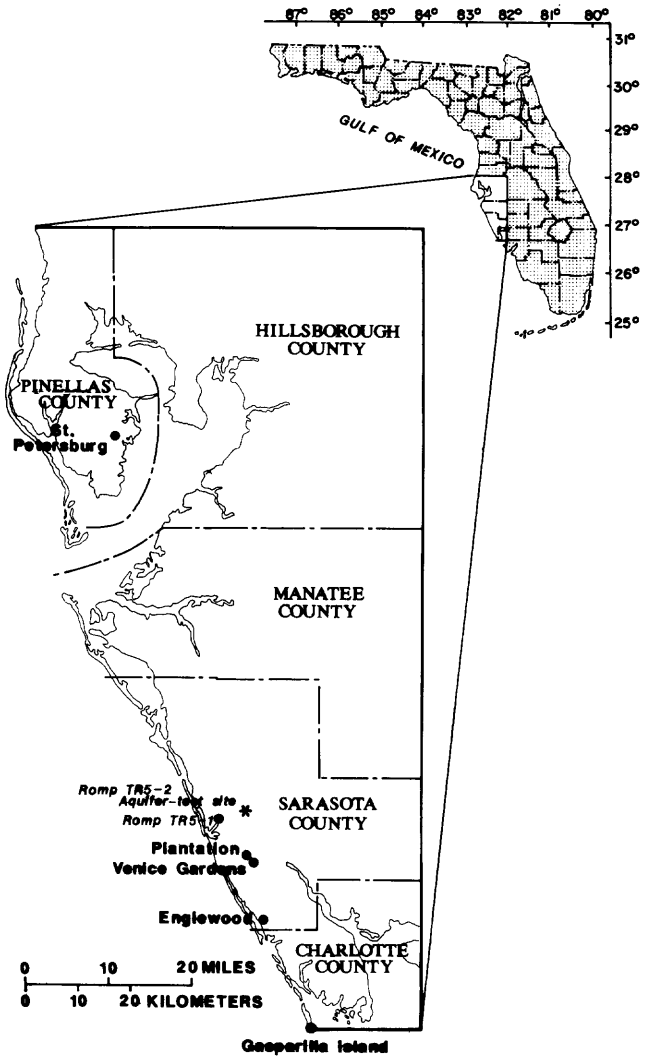


**Figure 1.** Aquifer-test site and related data sites, west-central Florida.

separated from the lower Hawthorn-upper Tampa aquifer (240–410 ft) by a clay and sandy clay semiconfining unit in the middle of the Hawthorn Formation. Clay and sandy clay beds that regionally occur in the lower part of the Tampa Formation and form the semiconfining unit between the intermediate aquifer system and the Upper Floridan aquifer were not observed in drill cuttings (table 1). The semiconfining unit between 410 and 500 ft is composed of limestone with small percentages of clay and sand. A "gamma kick" between 480 and 500 ft, which often denotes a clay cap over the Floridan aquifer system, corresponds with phosphatic sands in the carbonate formations at the test site. Transmissivities, as determined from tests at the site, are 5,100 ft²/d for the Tamiami upper Hawthorn aquifer and 9,600 ft²/d for the lower Hawthorn-upper Tampa aquifer.

The Upper Floridan aquifer is a thick, regionally extensive sequence of limestone and dolomite consisting of,

**Table 1.** Hydrogeologic framework at ROMP TR5-2 test site

| System | Series | Stratigraphic unit | Hydrogeologic unit | | Depth below land surface (ft) | Use of zone |
|---|---|---|---|---|---|---|
| Quaternary | Holocene and Pleistocene | Terrace deposits | Surficial aquifer system[3] | Surficial aquifer | 0-50 | Domestic and municipal supplies |
| | | Caloosa-hatchee Marl | Intermediate aquifer system or intermediate confining unit[3] | Semiconfining unit | 50-60 | |
| Tertiary | Pliocene | Tamiami Formation | | Tamiami-upper Hawthorn aquifer[1] | 60-100 | |
| | Miocene | Hawthorn Formation | | Semiconfining unit | 100-240 | |
| | | Tampa Formation | | Lower Hawthorn-upper Tampa aquifer[1] | 240-410 | Reverse osmosis feed and irrigation supplies. |
| | | | | Lower Tampa semiconfining unit | 410-500 | |
| | Oligocene | Suwannee Limestone | Floridan aquifer system[2] / Upper Floridan aquifer[2] | Suwannee permeable zone | 500-750 | |
| | Eocene | Ocala Limestone | | Lower Suwannee-Ocala semiconfining unit | 750-1,100 | |
| | | Avon Park Formation[1] | | Avon Park upper permeable zone | 1,100-1,400 | Injection of treated sewage and reverse osmosis reject water |
| | | | | Avon Park highly permeable dolomite | 1,400-2,075 | |
| | | Oldsmar and Cedar Keys Formations | | Middle confining unit[2] | 2,075-2,400 | Unused |
| | Paleocene | | | Lower Floridan aquifer[2] | 2,400-? | |

[1]Based on nomenclature of Wolansky (1983).
[2]Based on nomenclature of Miller (1986).
[3]Based on nomenclature of Southeastern Geological Society (1986).

in ascending order, the Avon Park Formation and the Ocala and Suwannee Limestones (table 1). At the test site, the Upper Floridan aquifer is estimated to be 1,575 ft thick. A permeable zone was identified between 500 and 750 ft within the Suwannee Limestone. From 750 to 810 ft, the lower Suwannee Limestone and, from 810 to 1,100 ft, the Ocala Limestone comprise poorly transmissive carbonate rocks that act as a semiconfining unit between more permeable zones of the upper Suwannee Limestone and the Avon Park Formation. In this area, the Avon Park Formation (1,100–2,075 ft) contains saltwater and is used as a receptacle for injection of effluent from wastewater treatment plants and reject water from reverse-osmosis supply plants in western Sarasota County. Knowledge concerning

the confining characteristics of the lower Suwannee and Ocala Limestones is critical to regional utilization of the injection zone along with the safeguarding of freshwater supplies.

The occurrence of persistent gypsiferous dolomites within the Avon Park Formation marks the top of the middle confining unit of the Floridan aquifer system and the base of the injection zone. At the test site, this occurs at about 2,075 ft below land surface (Wolansky and others, 1979). The gypsum is largely intergranular and appears to fill preexisting pore spaces in the rock to form a virtually nonleaky confining bed (Miller, 1986, p. 56).

Little is known of the rocks that compose the Lower Floridan aquifer beneath Sarasota County. Ryder (1985, p. 5) characterized the aquifer as one having relatively low permeability and containing poor quality water. This paper is not concerned with the Lower Floridan.

## AQUIFER-TEST DESIGN

An aquifer test was designed to discharge water from the Suwannee permeable zone and to observe water-level changes in observation wells above and below the pumped aquifer. A picture of the test site is shown in figure 2. A 6-in.-diameter test well was constructed, open from 510 to 700 ft in the Suwannee permeable zone (fig. 3). The potentiometric surface of the Suwannee permeable zone is about 16 ft above land surface or 31 ft above sea level. Observation wells 9 ft away were constructed open from 360 to 400 ft in the bottom of the lower Hawthorn-upper Tampa aquifer and from 850 to 890 ft in the middle of the lower Suwannee-Ocala semiconfining unit (table 1). The observation wells were instrumented with continuous water-level recorders 4 days before testing began. During this time, water levels in observation wells of the lower Hawthorn-upper Tampa aquifer and lower Suwannee-Ocala semiconfining unit averaged 29.5 ft and 31.8 ft above sea level, respectively. Both wells showed small fluctuations in water level (about 0.1 ft) due to barometric pressure and tidal influences. Natural fluctuations observed during the test were adjusted using the ROMP TR5–1 Suwannee observation well, 3 mi east of the test site (fig. 1). Adjustments consisted of using a lag time of 1 h with 100-percent and 50-percent efficiencies in observation wells of the lower Suwannee-Ocala semiconfining unit and lower Hawthorn-upper Tampa aquifer, respectively.

The multistage-discharge schedule consisted of letting the well flow naturally at rates between 250 and 220 gal/min for 26 h, then pumping at 500 gal/min for 18 h. The drawdown in the discharge well was assumed to be constant during the flow phase of the test, and discharge was measured periodically by using a 55-gal drum and a stopwatch. During the pumping phase, discharge was held constant; flow through a 6-in. discharge pipe was measured with a 5-in. orifice plate, and drawdown was measured by using an electric tape. Spinner flow-meter logs indicated that 97 percent of the discharge was produced from an interval between 510 and 640 ft under natural-flow conditions. Under pumping conditions, 80 percent of the discharge was produced from this interval, and 20 percent of the water was produced from the 640- to 700-ft zone. Recovery was recorded after the test stopped.

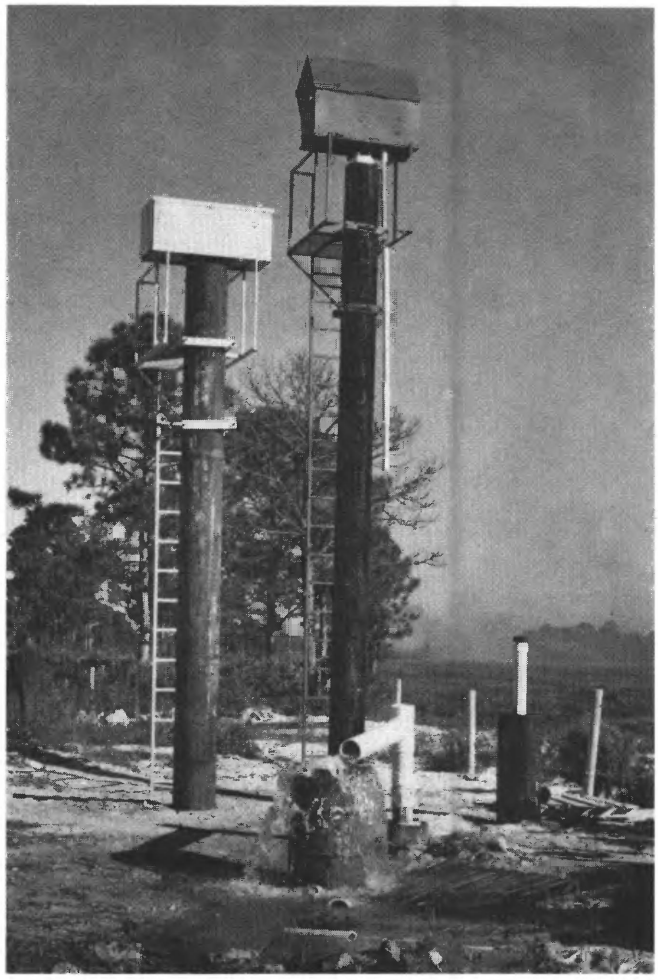

**Figure 2.** ROMP TR5–2 aquifer-test site.

## TRANSMISSIVITY OF THE SUWANNEE PERMEABLE ZONE

Transmissivity of the Suwannee permeable zone was calculated analytically by the Jacob and Lohman method (Lohman, 1972, p. 23) for the flowing part of the test and by the Cooper and Jacob method (Lohman, 1972, p. 19) for the pumping segment. Semilogarithmic plots (fig. 4) represent time-drawdown straight-line analyses for flow and pumping segments of the test as measured in the test well. Transmissivity of the Suwannee permeable zone was calculated to be

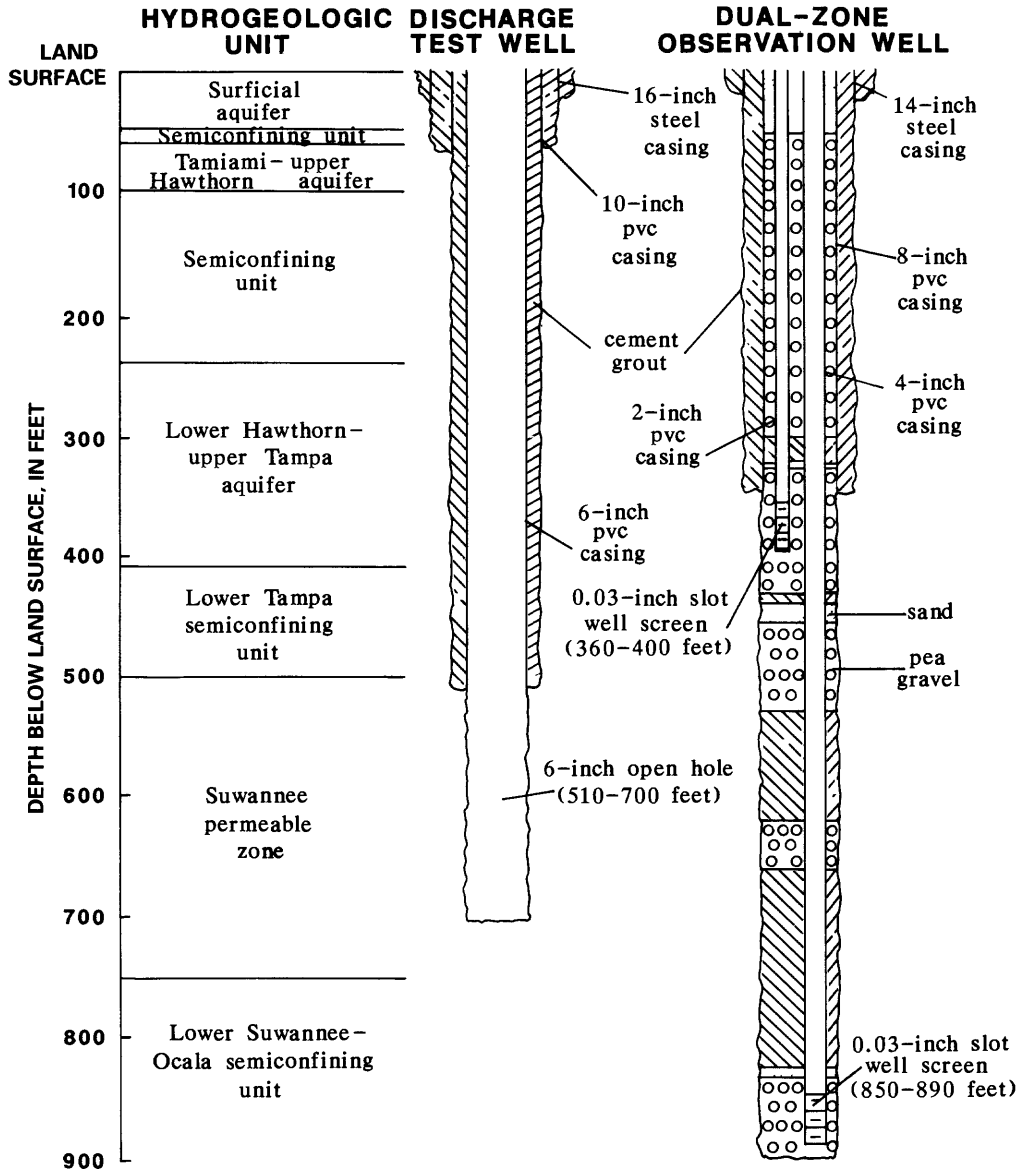


**Figure 3.** Construction characteristics of test and observation wells.

13,000 ft²/d. The average hydraulic conductivity calculated by dividing transmissivity by the open-hole interval of 190 ft is 70 ft/d and falls near the 75-ft/d average value reported for the Upper Floridan aquifer in the Sarasota-Charlotte County area (Wolansky, 1983, p. 18). Because permeable zones are indicated by drill cuttings and geophysical logs to be below the open-hole interval, the calculated hydraulic conductivity was assigned to the interval between 500 and 750 ft. The adjusted transmissivity is 17,500 ft²/d.

## MODEL ANALYSIS OF SEMICONFINING UNITS

Hydraulic properties of semiconfining units were estimated by using a numerical model to simulate water-level changes in observation wells above and below the Suwannee permeable zone. The model equations for pressure are approximated with finite-difference techniques in which the aquifer is represented as a two-dimensional, logarithmically spaced, block-centered grid.

### Calibration

The model of the test site includes a cylindrical coordinate system gridded into 40 columns that extend radially from the borehole face to a distance of 30,000 ft and 40 rows that represent 9 hydrogeologic units totaling 2,075 ft thick (fig. 5). Distances between columns increase logarithmically to produce a fine rectangular grid near the well and a coarse grid at the outer boundary. Spacing of rows is controlled by thickness and position of individual

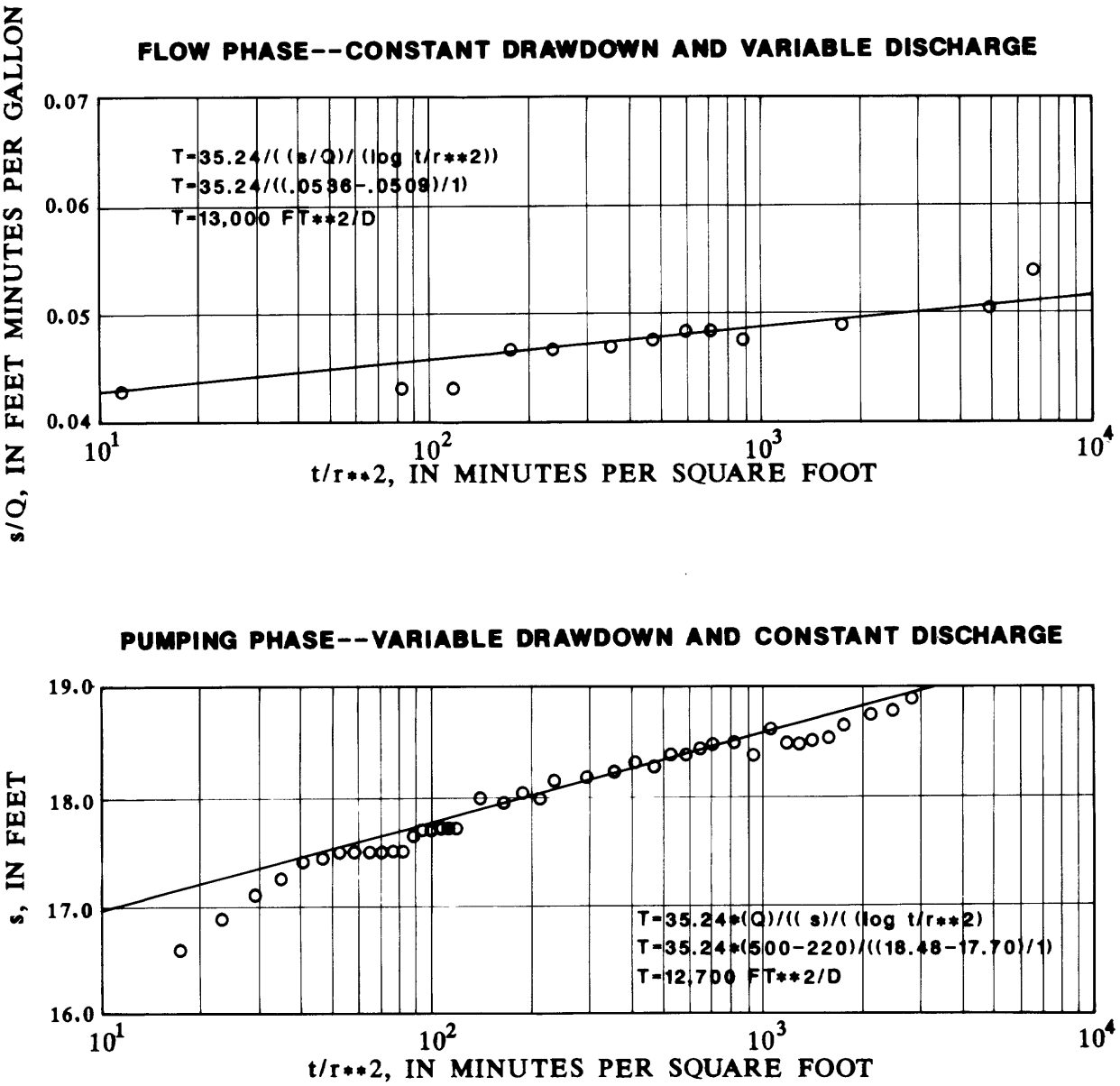


**Figure 4.** Semilogarithmic plots used to determine transmissivity of the Suwannee permeable zone. (T = transmissivity; s = drawdown; Q = discharge rate; t = time; and r = well radius.)

hydrogeologic units and monitor wells. The 44-h discharge phase and the 120-h recovery phase were divided into twenty-two 2-h and thirty 4-h discrete time steps, respectively. The model calculates (and can plot) head at 1,600 grid intersections at the end of each time step. Constant-pressure boundaries were imposed at land surface and the 30,000-ft cylindrical face. A no-flow boundary was applied to the base of the model, corresponding with the gypsiferous dolomites. Discharge from the well at the radial origin was as a specified flow rate from the open-hole section. The discharge was allocated to specific depth intervals by adjusting a well-completion factor until the distribution of flow approximated that observed in the flow-meter survey. Individual hydrogeologic units were considered to be isotropic. Vertical and horizontal hydraulic conductivities derived from aquifer tests and model analysis (Wolansky, 1983, p. 18) were used as initial estimates of aquifer and confining unit properties. The model was calibrated by systematically adjusting (1) hydraulic conductivities of the lower Tampa and lower Suwannee-Ocala semiconfining units and (2) rock compressibilities of various units. The calibration focused on matching simulated water-level changes within approximately 0.1 ft of observed changes at selected times.

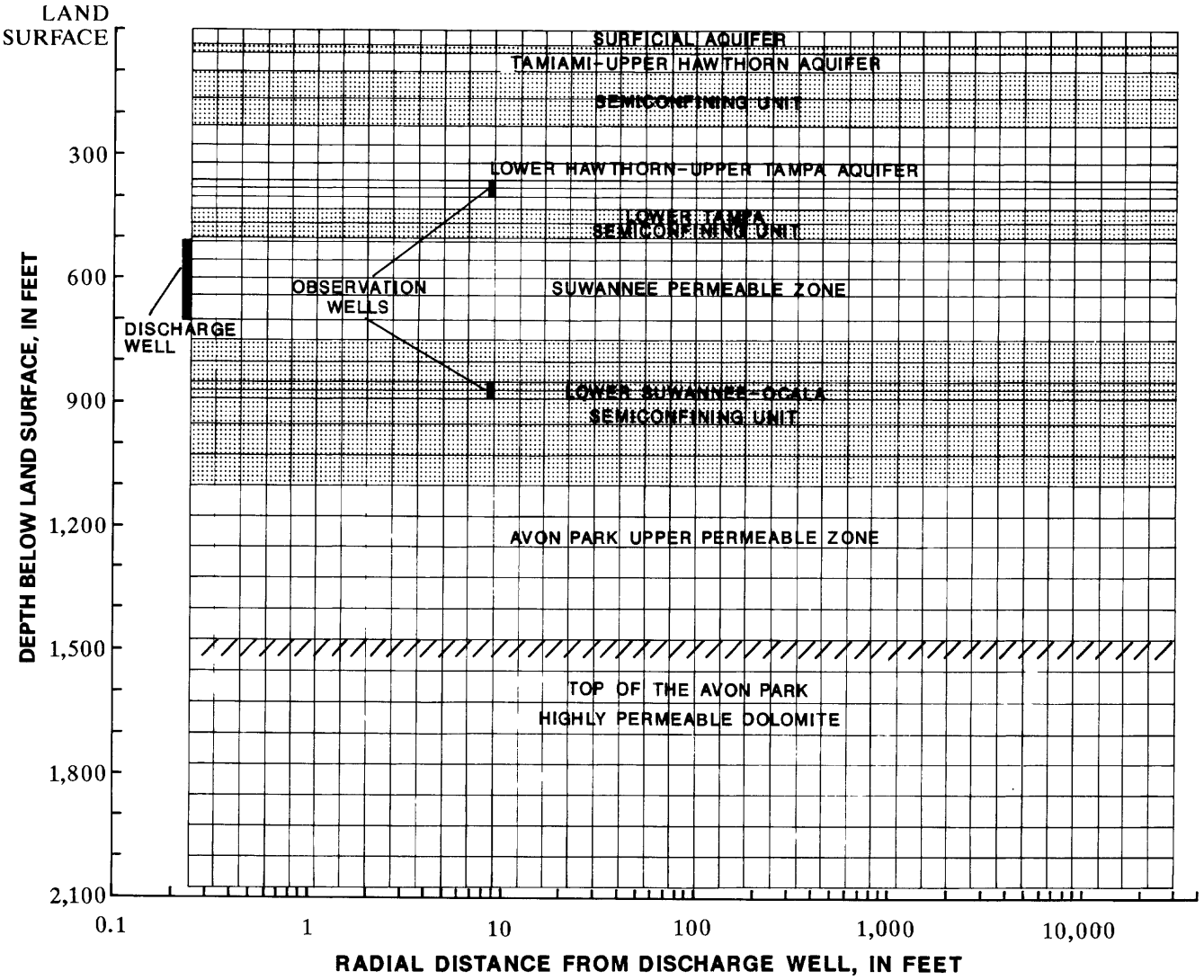


**Figure 5.** Radial-model grid, hydrogeologic framework, and configuration of pumping and observation wells.

Figure 6 depicts observed water levels and model-simulated changes in observation wells 9 ft from the test well. Model-simulated changes in the lower Suwannee-Ocala semiconfining unit parallel those observed in the observation well during all five phases of the test (flow, restricted flow, pumping, restricted flow, and recovery). Because the test began on a tidal low water level, recovery (phase 5) matches daily low water levels rather than daily average water levels. The observed daily low and model-simulated water levels must eventually recover to the zero drawdown starting level. In the lower Hawthorn-upper Tampa aquifer, simulated water-level changes parallel observed changes during the first, second, and fifth phases. The observed water levels are apparently influenced by stresses in the vicinity of the test area, and the model does not accurately simulate the 500-gal/min pumping phase of the observed hydrograph. Possible causes of the anomalously early water level stabilization during the 500-gal/min discharge phase are interception of a recharge boundary, a nearby pumped well being shut down, change in distribution of yield from the open borehole from that of phase 1, or problems with well construction. The model calibration was accepted for early and late phases of the test.

Calibrated model-input parameters are listed in table 2. Because hydraulic properties of the aquifers in the multilayered system were considered to be known from independent tests, the model calibration focused on unknown attributes of semiconfining units above and below the pumped aquifer. The simulated hydraulic conductivity for the 90-ft-thick lower Tampa semiconfining unit above the Suwannee permeable zone is 10 ft/d and is about one-sixth to one-seventh the hydraulic conductivity of adjacent aquifers. The rapid response to pumping and relatively high model-derived hydraulic conductivity indicates good hydraulic connection between the intermediate and Floridan aquifer systems at the test site. Average

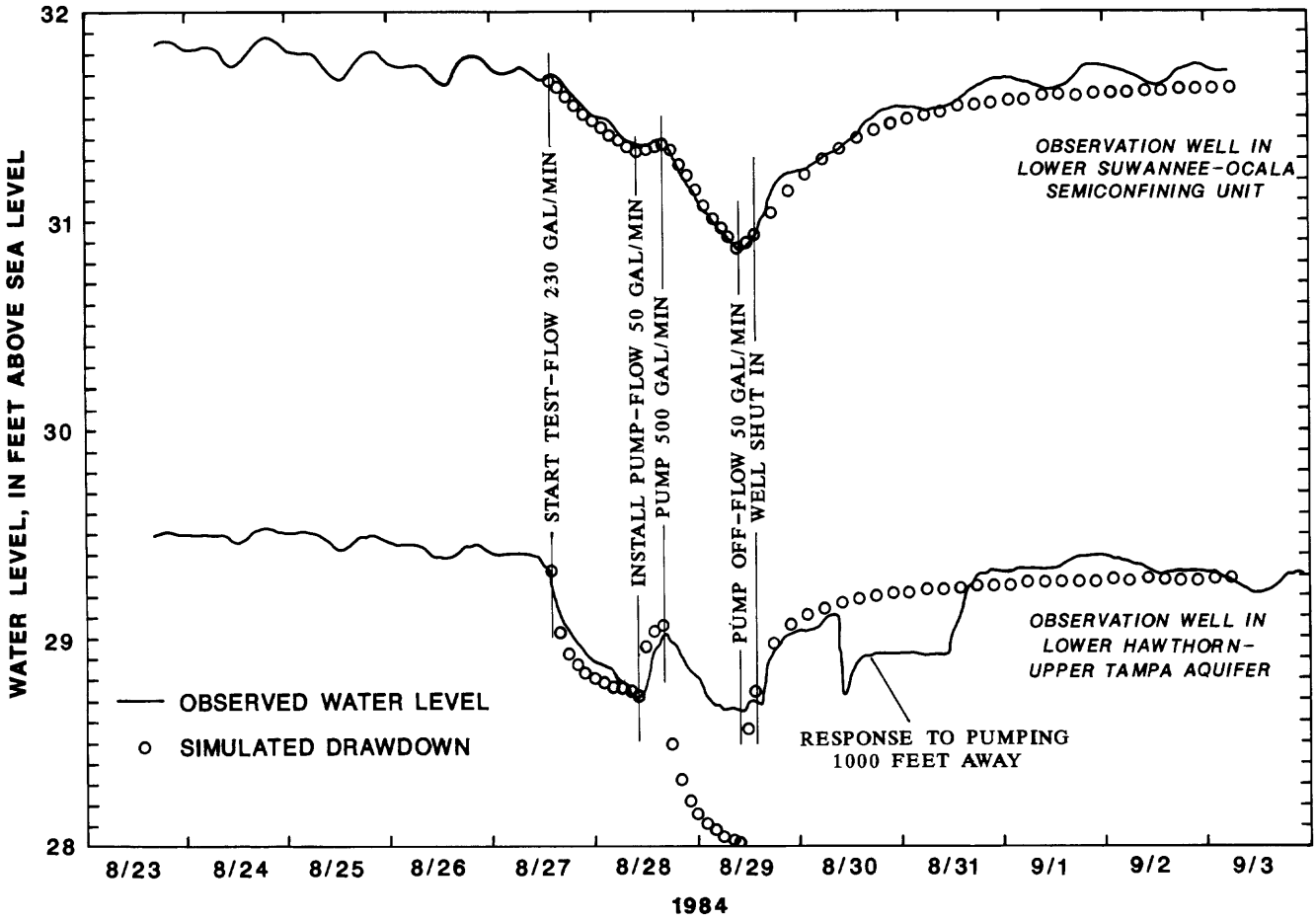


**Figure 6.** Observed and model-simulated water levels in observation wells.

hydraulic conductivity for the 330-ft thick lower Suwannee-Ocala semiconfining unit is 0.1 ft/d. This value is less than one one-hundredth of the hydraulic conductivity of adjacent aquifers and falls at about the midpoint of a range of hydraulic conductivities measured in tests at nearby injection-well sites (table 3). Hydraulic conductivities of both semiconfining units fall within the probable range of 0.01 to 100 ft/d reported for units within the Upper Floridan aquifer (Wolansky and Corral, 1985, p. 6).

**Table 2.** Model input values of selected physical and hydraulic parameters

[Constant parameters: water density, 62.4 lb/ft$^3$; water temperature, 77 degrees Fahrenheit; porosity, 0.2; and viscosity, 0.8705 centipoise. Feet per day, ft/d; square inch per pound, in$^2$/lb]

| Hydrogeologic unit | Hydraulic conductivity (ft/d) | Compressibility (in$^2$/lb) |
|---|---|---|
| Surficial aquifer system | 10 | $5.5\times10^{-5}$ |
| Semiconfining unit | 0.005 | $5.5\times10^{-5}$ |
| Tamiami-upper Hawthorn aquifer | 125 | $5.5\times10^{-5}$ |
| Semiconfining unit | 0.1 | $5.5\times10^{-5}$ |
| Lower Hawthorn-upper Tampa aquifer | 59 | $1.5\times10^{-5}$ |
| Lower Tampa semiconfining unit | 10 | $1.5\times10^{-5}$ |
| Suwannee permeable zone | 70 | $1.5\times10^{-5}$ |
| Lower Suwannee-Ocala semiconfining unit | 0.1 | $1.5\times10^{-5}$ |
| Avon Park upper permeable zone | 25 | $3.0\times10^{-7}$ |
| Avon park highly permeable dolomite | 100 | $3.0\times10^{-7}$ |

Rock compressibility was estimated from measurements reported for similar rocks from nearby test wells and from published literature (table 4). A relatively high compressibility of $5.5\times10^{-5}$ in$^2$/lb was assigned to the clay-rich upper zones between land surface and 240 ft. A compressibility of $1.5\times10^{-5}$ in$^2$/lb was assigned to the zone of nearly pure limestone between 240 and 1,100 ft. Below 1,100 ft, dolomization is suspected; therefore, a relatively low rock compressibility of $3.0\times10^{-7}$ in$^2$/lb was assigned to lower zones. Specific storage, the volume of water released from or taken into storage per unit volume of confined aquifer by a 1-ft drop in head, is related to rock compressibility by the equation (Eagleson, 1970, p. 270):

$$Ss=\gamma(\alpha+\eta\beta)$$

**Table 3.** Packer test and core hydraulic conductivities for the lower Suwannee-Ocala semiconfining unit

[—, no data; feet per day, ft/d]

| Site | Type | Depth (ft) | Hydraulic conductivity (ft/d) | |
|---|---|---|---|---|
| | | | Vertical | Horizontal |
| Englewood[1] | Packer | 916–926 | — | 0.25 |
| | Core | 922–923 | 0.01 | .03 |
| | Core | 926–927 | .01 | .03 |
| | Core | 931–932 | .09 | .11 |
| Plantation[2] | Core | 913 | — | .23 |
| Gasparilla Island[3] | Packer | 1,218–1,269 | — | .03 |
| Venice Gardens[4] | Core | 1,215.7–1,216.2 | .71 | — |
| | Core | 1,261.2–1,261.5 | .54 | — |
| | Core | 1,329.0–1,329.3 | .37 | — |

[1]CH2M Hill, 1986, p. 3–23 and 3–27.
[2]Post, Buckley, Schuh, and Jernigan, Inc., 1984, table 7–6.
[3]Geraghty and Miller, Inc., 1986, table 2.
[4]Geraghty and Miller, Inc., written commun., June 11, 1987.

**Table 4.** Laboratory measurements of rock compressibility

[Square inch per pound, $in^2/lb$]

| | Number of samples | Range in compressibility ($in^2/lb$) | Average compressibility ($in^2/lb$) |
|---|---|---|---|
| Limestone core samples[1] (representing Tampa Formation to Ocala Limestone). | 5 | $3.1\times10^{-7}$ to $1.2\times10^{-5}$ | $6.2\times10^{-6}$ |
| Dolomite core samples (representing Avon Park Formation) | 6 | $6.4\times10^{-8}$ to $2.2\times10^{-6}$ | $5.5\times10^{-7}$ |
| Fissured rock[2] | | $2.2\times10^{-6}$ to $4.9\times10^{-5}$ | |
| Medium-hard clay[2] | | $4.9\times10^{-4}$ to $9.0\times10^{-4}$ | |

[1]Core samples from wells near St. Petersburg (Hickey, 1982, p. 7).
[2]Domenico, 1972, p. 231.

where $Ss$= specific storage (1/ft);
$\gamma$= specific weight of water (62.4 $lb/ft^3$);
$\alpha$= rock compressibility ($ft^2/lb$);
$\eta$= porosity; and
$\beta$= compressibility of water ($2.1\times10^{-8}$ $ft^2/lb$).

Specific storage of the limestone, calculated from model-derived compressibility, is about $1\times10^{-5}$/ft. This results in an artesian storage coefficient of 0.002 for the 250-ft thick Suwannee permeable zone. By comparison, the storage coefficient of an equivalent zone, derived from a test in northwest Manatee County, is 0.0011 (Wolansky and Corral, 1985, p. 98). The probable range for the storage coefficient of units that compose the Upper Floridan aquifer is reported to be 0.0005 to 0.002 (Wolansky and Corral, 1985, p. 6).

Figure 7 depicts the flow field along a vertical plane radiating out from the discharging well at the end of the 500-gal/min test phase. It supports the calibration by demonstrating that:

1. Flow to the well in the Suwannee permeable zone diminishes to less than 10 ft/d beyond a 55-ft radius and to less than 0.001 ft/d beyond 10,000 ft;
2. The 30,000-ft radial simulation boundary does not influence flow to the well;
3. Flow is nearly vertical in the lower Suwannee-Ocala semiconfining unit because of a relatively high permeability contrast between it and the Suwannee permeable zone;
4. The lower Tampa semiconfining unit between the lower Hawthorn-upper Tampa aquifer and the Suwan-

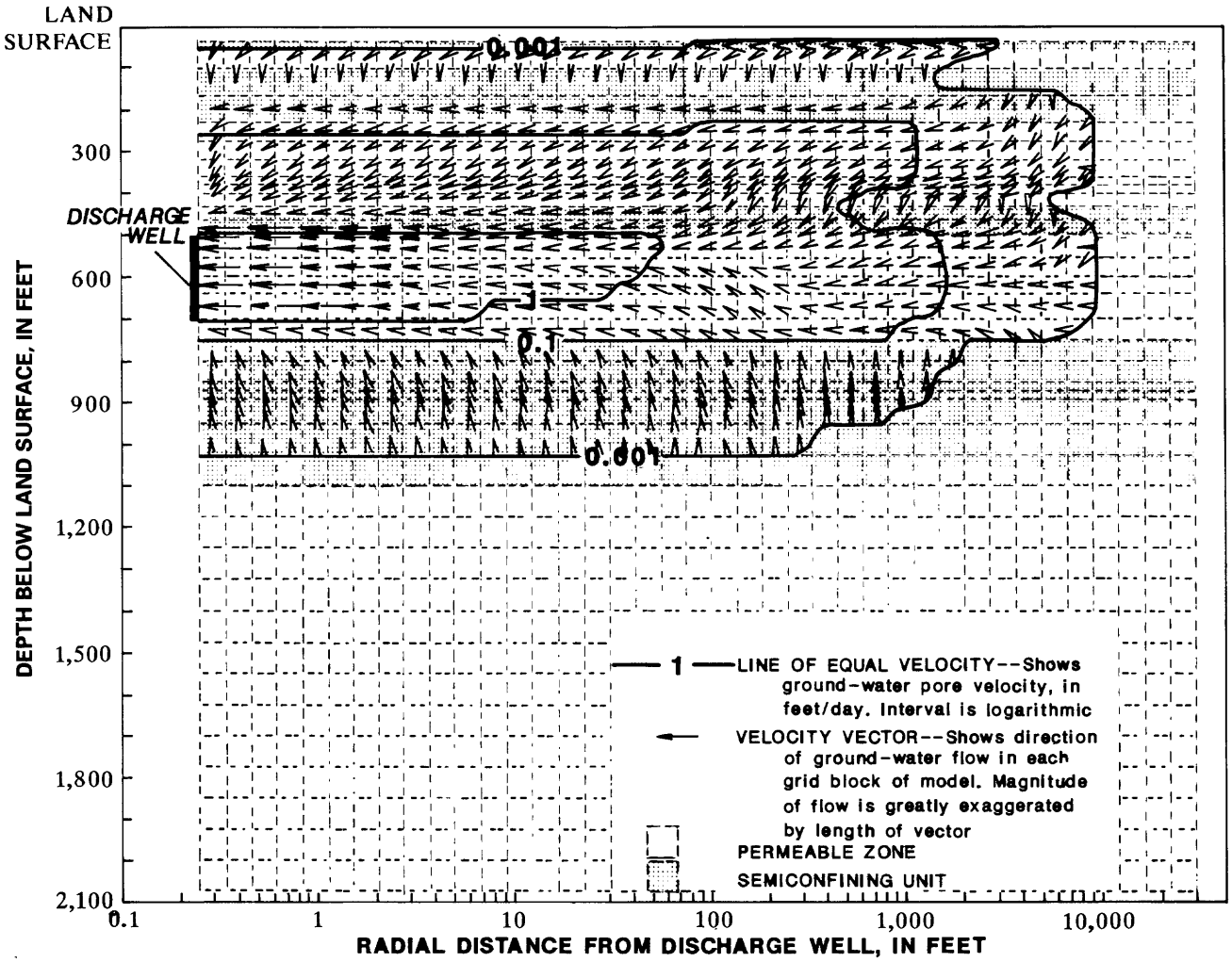


**Figure 7.** Velocity-vector flow field in a plane perpendicular to the discharge well at the end of the 500-gal/min pumping phase of the test.

nee permeable zone does not have a low enough hydraulic conductivity to noticeably alter the flow field; and

5. A stable solution is achieved. Vectors uniformly point to the discharging interval in the area where velocities are greater than 0.001 ft/d. Beyond this area, the flow field is somewhat erratic, which may be attributed to numerical roundoff or truncation errors where velocities are extremely low.

## Sensitivity Analysis

Sensitivity analysis shows model response to changes in input parameters. Separate model simulations were made with a single parameter varied over a reasonable range of values that occur in the area while holding the other parameters at their calibrated values. Relative changes in water levels provide insight as to the degree that changes in parameters may affect results of model simulation. The sensitivity analysis is used to assess the degree of reliability of various input parameters. Because hydraulic properties of beds above the injection zone of the Avon Park Formation were of primary interest, sensitivity tests focused on varying the hydraulic conductivity of the lower Suwannee-Ocala semiconfining unit and the compressibility of rock units between the top of the lower Hawthorn-upper Tampa aquifer and the bottom of the lower Suwannee-Ocala semiconfining unit. The sensitivity analysis demonstrates the effects of parameter changes on simulated water levels at the middle of the screened interval (row 18, column 13 of model grid) in the observation well of the lower Suwannee-Ocala semiconfining unit.

The model calibrated hydraulic conductivity of the lower Suwannee-Ocala semiconfining unit of 0.1 ft/d was increased and decreased by an order of magnitude, bracketing the field values listed in table 3. Results, shown in

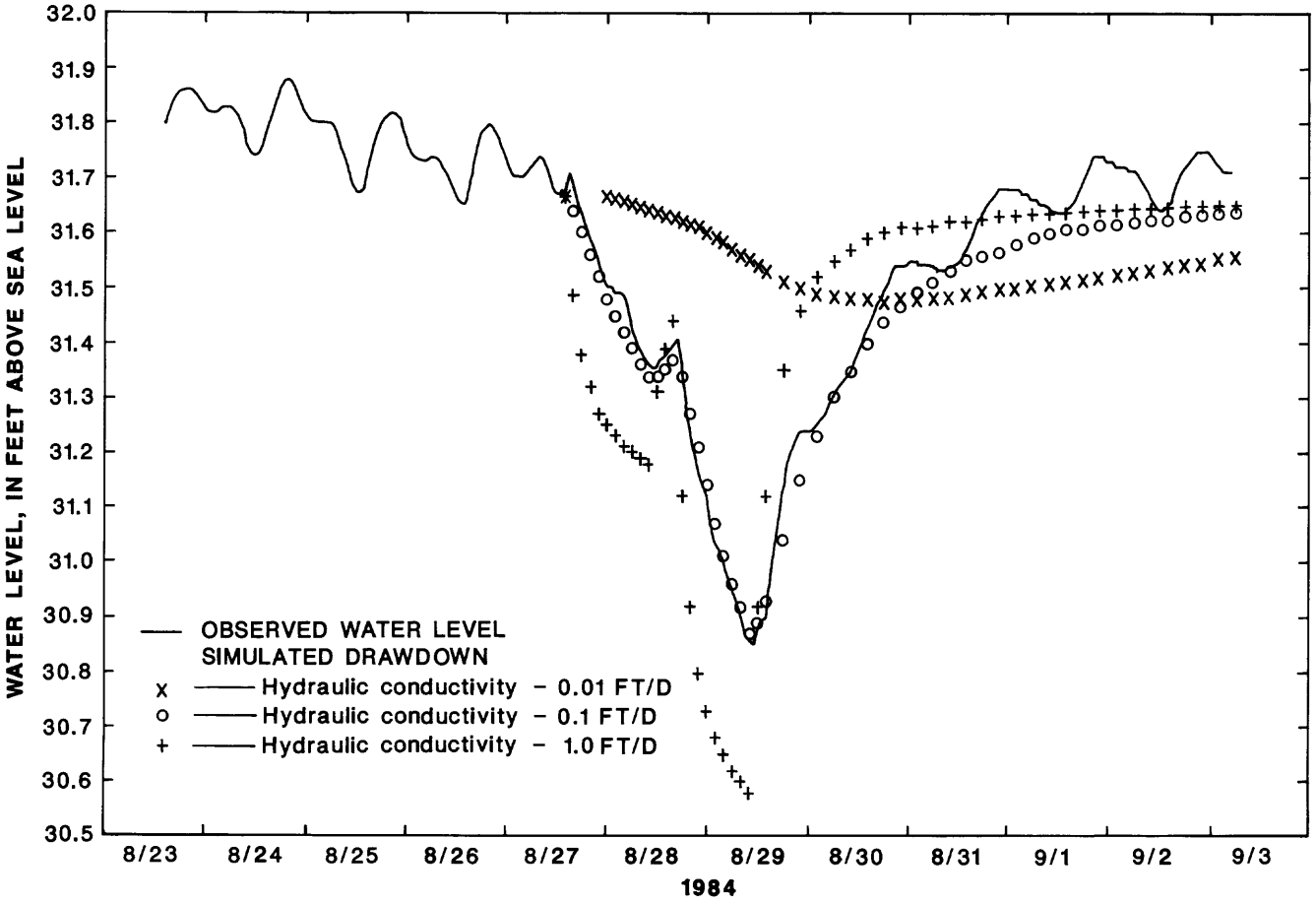


**Figure 8.** Effects of varying hydraulic conductivity on the simulated water-level change in the lower Suwannee-Ocala semiconfining unit.

figure 8, indicate that, if the lower Suwannee-Ocala semiconfining unit had a much lower (0.01 ft/d) hydraulic conductivity, response to pumping from the Suwannee permeable zone would be sluggish compared to the observed response and maximum drawdown would be only about 0.2 ft compared to 0.8 ft for the calibration. A much higher (1.0 ft/d) hydraulic conductivity for the unit would result in a much more responsive hydrograph than was observed. Maximum drawdown (1.1 ft) would be about 0.3 ft more than observed drawdown, and water-level changes would occur much faster than observed. Contrasting response is obvious in the recovery curve where water levels recover to within 0.2 ft of the starting level about 10 h after pumping ceased, compared to 24 h when a hydraulic conductivity of 0.1 ft/d was assigned.

Compressibility of the limestone was adjusted from the calibration level of $1.5\times10^{-5}$ in$^2$/lb to a high of $1.5\times10^{-4}$ in$^2$/lb and a low of $1.5\times10^{-6}$ in$^2$/lb. The low value is within the range of laboratory compressibilities for limestone in table 4, and the high value represents compressibility of medium-hard clay. The comparison of hydrographs in figures 8 and 9 indicates that an order-of-magnitude change in rock compressibility brackets the calibrated change in water level at about the same magnitude as the changes in hydraulic conductivity.

An understanding of uncertainties in the ranges of rock compressibility and hydraulic conductivity was useful in assessing the reliability of model-derived aquifer characteristics. Sensitivity-test hydrographs demonstrate that, for the range of variables tested, a change in hydraulic conductivity requires a directly proportional change in rock compressibility to maintain the water level. The calibration rock compressibility of $1.5\times10^{-5}$ in$^2$/lb approaches the upper limit observed for limestone cores, and hydraulic conductivity of 0./1 ft/d is in about the middle of the measured range (tables 3 and 4). If hydraulic conductivity is raised to 1.0 ft/d, it will be necessary to raise compressibility proportionately to about $1.5\times10^{-4}$ in$^2$/lb, which is higher than the value expected for a limestone aquifer. Based on this analysis, the derived hydraulic conductivity of 0.1 ft/d approaches a maximum value for the semiconfining unit that limits upward migration of wastewater from the underlying injection zone to the overlying potable aquifer.

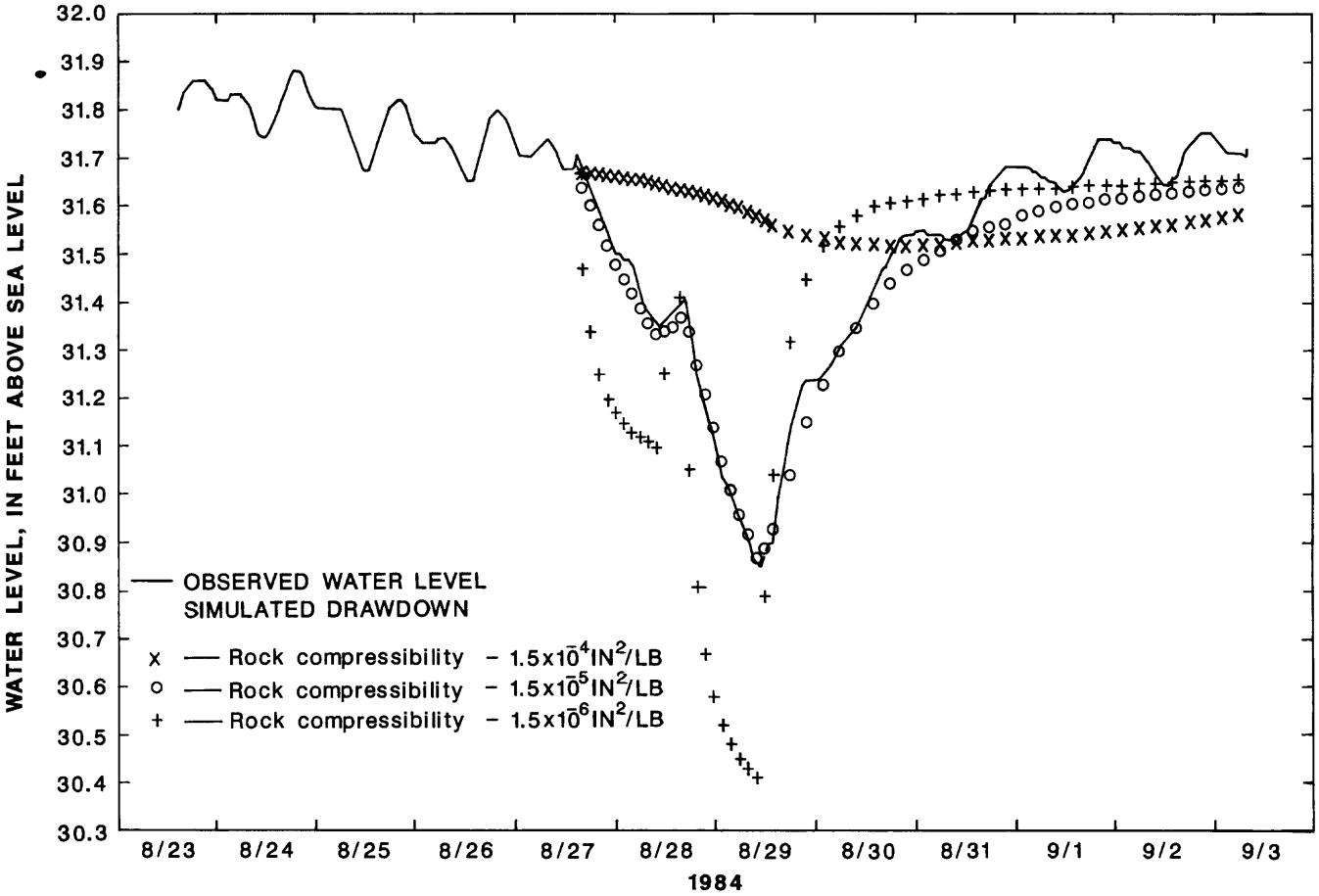


**Figure 9.** Effects of varying rock compressibility on the simulated water-level change in the lower Suwannee-Ocala semiconfining unit.

Sensitivity of the spatial discretization was checked to see if the 40 by 40 radius by depth model grid was too coarse to produce an accurate simulation. The check consisted of model runs with 40 by 79, 80 by 40, and 80 by 79 grids of the model region. In all cases, the test simulations replicated water-level changes of the calibration. Because this explicit check indicated no telling differences in results, the coarser simulation used for the calibration indeed was adequately discretized.

## Limitations of Model Application

A conceptual approach to ground-water modeling was used in the application of the HST3D model. The hydrogeologic framework was conceptualized from lithologic and geophysical logs, its parameters were identified and estimated, and then it was transformed to the mathematical analog. The mathematical model represents a simplification of the complex physical processes that control the conceptual model and is an approximate representation of the prototype.

The model does not account for tidal and barometric effects. Combined water-level fluctuations caused by these phenomena were generally less than 0.1 ft. The 500-gal/min discharge phase (44 h) ended 5 h short of two complete tide cycles (49 h) at the midpoint of a tidally induced water-level recession. The water level recorded in an observation well at ROMP TR5–1 in the Suwannee permeable zone, 3 mi west (fig. 1), was 0.05 ft higher at the end of the discharge phase than at the beginning of the test. The simulated water level in an observation well of the lower Suwannee-Ocala semiconfining unit was about 0.05 ft lower than the observed level. The calibration was improved when observed water levels were corrected for natural fluctuations.

An important factor that influenced the model application is that the water level in the underlying lower Suwannee-Ocala semiconfining unit observation well began to rise immediately after the test began, whereas the water level in the monitor well in the overlying lower Tampa semiconfining unit declined. Wolff (1970) attributed this type of response to the transference of strain across a confining layer, thereby compressing it and accounting for

reverse water-level changes. The water level in the lower Suwannee-Ocala semiconfining unit observation well rose 0.03 ft within 15 min after flow of 230 gal/min started and 0.04 ft within 15 min after pumping at 500 gal/min started. When the pump was shut off, the water-level decline in the observation well of the lower Suwannee-Ocala semiconfining unit accelerated 0.03 ft in 15 min, demonstrating another reverse water-level change.

Water levels in the observation well of the lower Hawthorn-upper Tampa aquifer (fig. 6) and the pumping well stopped declining about 12 h after the 500-gal/min test began and were stable for about 10 h. Of the probable causes listed earlier, the most likely is shutting off an unknown, distant irrigation pump. The aquifer's response to pumping from a 1,000-ft distant well is clearly shown in the hydrograph of figure 6. The water level in the lower Suwannee-Ocala semiconfining unit observation well continued to decline throughout the test and was not affected by pumping for irrigation, thereby indicating that the unknown stresses originated in shallower hydrogeologic units.

The model simulated relatively large head differentials between tops and bottoms of intervals tapped by the observation wells. At the end of the 500-gal/min test segment, simulated drawdown of the observation well in the lower Hawthorn-upper Tampa aquifer was 1.28 ft at the bottom of the casing and 1.36 ft at the bottom of the well. At the observation well in the lower Suwannee-Ocala semiconfining unit, simulated drawdowns were 0.96 ft at the bottom of the casing and 0.66 ft at the bottom of the well. Hantush (1964, p. 351) states, "The water level in an observation well reflects the average head, and consequently the average drawdown in the aquifer profile that is occupied by the water-entry section of the well." Under this assumption, the model calibration was based on matching simulated head changes at the midpoint of each observation well screen (node 13, 18 and 13, 31) with observed head changes.

Horizontal hydraulic conductivity in the Upper Floridan aquifer has been reported to be as much as 75 times greater than the vertical hydraulic conductivity (Wolansky, 1983, p. 18). Anisotropy could significantly affect the calibration. However, packer and laboratory core tests indicate that horizontal and vertical hydraulic conductivity in the lower Suwannee-Ocala semiconfining unit are similar (table 3). For modeling purposes, each hydrogeologic unit was assumed to be isotropic.

## CONCLUSIONS

This report documents a multistage-discharge test in a multiple aquifer system at a site in Sarasota County and use of the HST3D model to estimate aquifer and semiconfining unit properties. Estimated hydraulic and physical properties derived from the test and model are given below:

| Hydrogeologic unit | Depth interval (ft) | Hydraulic conductivity (ft/d) | Compressibility ($in^2/lb$) |
|---|---|---|---|
| Lower Tampa semiconfining unit | 410–500 | 10 | $1.5\times10^{-5}$ |
| Suwannee permeable zone | 500–750 | 70 | $1.5\times10^{-5}$ |
| Lower Suwannee-Ocala semiconfining unit | 750–1,100 | 0.1 | $1.5\times10^{-5}$ |

Based on sensitivity tests of relations between hydraulic conductivity and compressibility, the hydraulic conductivity of 0.1 ft/d apparently is a maximum value for the semiconfining unit at the test site. The hydraulic conductivity of this unit limits upward migration of wastewater from the underlying injection zone to the overlying potable aquifer.

A radial-flow model is a versatile tool for analysis of hydraulic properties of semiconfining units above and below the pumped aquifer. Modeling procedures involve adjusting hydraulic properties of the units within reasonable ranges of values until the model adequately simulates observed water-level hydrographs in the units. The digital model has advantages over analytical solutions because the user is not constrained by multiphase discharge, storage within confining units, change with time, or number of layers in the hydrogeologic system. Sensitivity tests demonstrate the proportionality between hydraulic conductivity and rock compressibility and the range of reasonable values of these parameters for use in models in Sarasota County.

## REFERENCES CITED


CH2M Hill, 1986, Results of the reverse osmosis injection well investigation for the Englewood Water District: Consultant's report to Florida Department of Environmental Regulation, file no. UD58–097806.

Domenico, P.A., 1972, Concepts and models in ground-water hydrology: New York, McGraw-Hill, 405 p.

Eagleson, P.E., 1970, Dynamic hydrology: New York, McGraw-Hill, 462 p.

Geraghty and Miller, Inc., 1986, Construction and testing of the injection and monitoring wells at Gasparilla Island Water Association, Inc., wastewater treatment plant, Boca Grande, Florida: Report to Florida Department of Environmental Regulation, file no. D036–121561.

Hantush, M.S., 1964, Hydraulics of wells, *in* Chow, Ven Te, ed., Advances in hydroscience, v. 1: New York, Academic Press Inc., p. 281–442.

———1967, Flow in wells in aquifers separated by semipervious layers: Journal of Geophysical Research, v. 72, no. 6, p. 1709–1720.

Hickey, J.J., 1982, Hydrogeology and results of injection tests at waste-injection test sites in Pinellas County, Florida: U.S. Geological Survey Water-Supply Paper 2183, 42 p.

Kipp, K.L., 1986, HST3D, A computer code for simulation of heat and solute transport in three-dimensional ground-water flow systems: U.S. Geological Survey Water-Resources Investigations Report 86–4095, 517 p.

Lohman, S.W., 1972, Ground-water hydraulics: U.S. Geological Survey Professional Paper 708, 70 p.

Miller, J.A., 1986, Hydrogeologic framework of the Floridan aquifer system in Florida and in parts of Georgia, Alabama, and South Carolina: U.S. Geological Survey Professional Paper 1403–B, 91 p.

Neuman, S.P., and Witherspoon, P.A., 1972, Field determination of the hydraulic properties of leaky multiple aquifer systems: Water Resources Research, v. 8, no. 5, p. 1284–1298.

Post, Buckley, Schuh, and Jernigan, Inc., 1984, Deep injection test well, the Plantation, Sarasota County, Florida: Consultant's report to Florida Department of Environmental Regulation, file no. UD58–109386.

Ryder, P.D., 1985, Hydrology of the Floridan aquifer system in west-central Florida: U.S. Geological Survey Professional Paper 1403–F, 63 p.

Southeastern Geological Society, 1986, Hydrogeological units of Florida: Florida Bureau of Geology Special Publication 28, 9 p.

Sutcliffe, H., Jr., and Thompson, T.H., 1982, Occurrence and use of ground water in the Venice-Englewood area, Sarasota and Charlotte Counties, Florida: U.S. Geological Survey Open-File Report 82–700, 59 p.

Wolansky, R.M., 1983, Hydrogeology of the Sarasota-Port Charlotte area, Florida: U.S. Geological Survey Water-Resources Investigations Report 82–4089, 48 p.

Wolansky, R.M., Barr, G.L., and Spechler, R.M., 1979, Generalized configuration of the bottom of the Floridan aquifer, Southwest Florida Water Management District: U S. Geological Survey Water-Resources Investigations Open-File Report 79–1490, 1 sheet.

Wolansky, R.M., and Corral, M.A., Jr., 1985, Aquifer tests in west-central Florida: U.S. Geological Survey Water-Resources Investigations Report 84–4044, 127 p.

Wolff, R.G., 1970, Relationship between horizontal strain near a well and reverse water level fluctuation: Water Resources Research, v. 6, no. 6, p. 1721–1728.

# Maximizing Sustainable Ground-Water Withdrawals—Comparing Accuracy and Computational Requirements for Steady-State and Transient Digital Modeling Approaches

*By* Richard C. Peralta,[1] R.R.A. Cantiller,[2] *and* Gary L. Mahon[3]

**Abstract**

Rigorous models for maximizing sustainable ground-water withdrawals may require more computer memory for their constraint set than is available. In some situations, alternative constraint formulations yield similar or identical answers resulting in great saving in computer memory requirements. In order to evaluate the efficiency of using alternative constraints, maximum ground-water withdrawal pumping strategies were computed by three digital models for a hypothetical area for a five-decade period. Model A maximized steady ground-water withdrawal. Model B maximized unsteady ground-water mining. Model C maximized unsteady ground-water mining subject to a constraint that final pumping be sustainable after the end of the 50-year period. Change in pumping with time was forced to be monotonic (variably increasing or decreasing but not oscillating) in time. The models were tested by assuming constant transmissivity and by using a range of recharge constraints for four scenarios—with stressed and unstressed initial potentiometric surfaces and with constant and changing upper limits on pumping. In situations where upper limits on pumping changed with time, Model A was run repetitively, by using monotonicity constraints. In those situations, optimality of solution is not assured in all cells. Models A and C computed pumping strategies sustainable after the end of the 50-year period. Model C was the most detailed in that it allowed pumping to vary in time and recharge constraints were based both on unsteady-state flow at 50 years and on steady flow after that time. Model A considered only steady pumping and recharge constraints. Pumping strategies from Model B were not necessarily sustainable because it considered only recharge constraints at 50 years. Results indicate that, when recharge through the study area periphery is unconstrained, all models compute identical pumping. For an initially undeveloped aquifer, or for a developed aquifer if steady pumping is assumed, Model A computes strategies very similar to those computed with Model C and requires only 28 percent of the computer memory and 38 percent of the execution time. For an initially overdeveloped aquifer, Model B computes identical pumping strategies to those computed with Model C and requires 73 percent of the computer memory and 78 percent of the computation time. For that situation, Model A is more conservative and computes less pumping than Model C if pumping in Model C is permitted to vary. Although Model A may compute lower pumping rates during the first 50 years, the sustainable pumping rate thereafter may be greater for Model A than for Model C.

## INTRODUCTION

Ground-water availability is an important consideration for agricultural and land-use planners in the United States and abroad. Ensuring the long-term availability of ground water contributes to developing sustainable production. Computer models are used to develop regional land-use plans and agronomic cropping strategies that consider the restraints on ground-water use posed by the physical system. Such models simulate ground-water flow and compute development strategies optimal for particular policy objectives and physical or nonphysical constraints. This paper compares the accuracy and computer-resource requirements of three optimization model formulations to determine their appropriateness for estimating maximum sustainable regional ground-water withdrawals. Each model computes optimal future withdrawals for each decade of a 50-yr planning period. Optimal pumping was computed for a hypothetical region consisting of finite difference cells, each 3 mi by 3 mi in size (fig. 1). Distributed pumping is assumed within the block-centered nodes. Because of the large cell sizes and time steps, the models are more

[1]Utah State University, Logan, Utah
[2]University of Arkansas, Fayetteville, Ark.
[3]U.S. Geological Survey, Little Rock, Ark

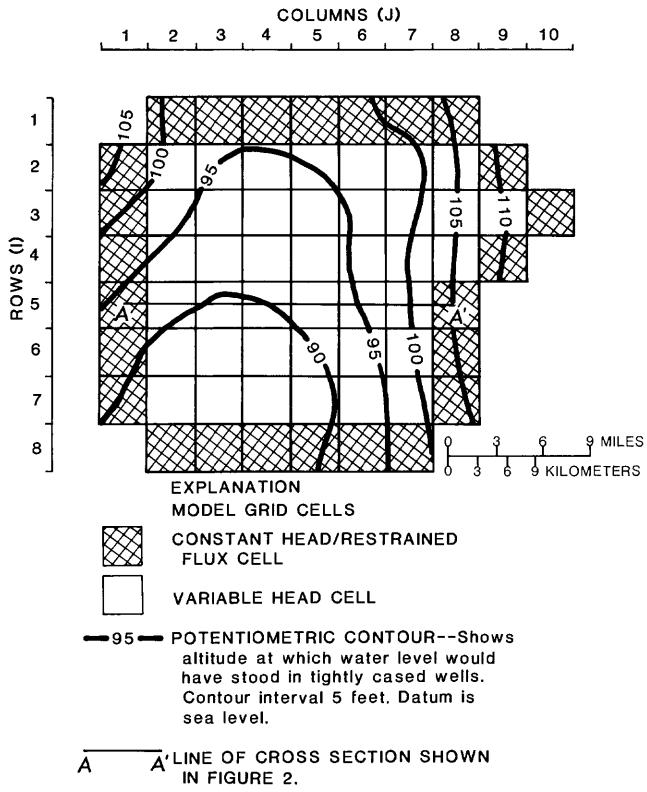


**Figure 1.** Model grid and initial potentiometric surface in hypothetical study area.

appropriate for planning future crop acreages supportable by ground water than for managing daily pumping operations.

Early uses of distributed parameter computer models to develop optimal volumetric ground-water management strategies are summarized by Domenico (1972), Bear (1979), and Gorelick (1983). Gorelick describes both linear and nonlinear programming models. Because this paper deals only with linear programming to optimize volumetric withdrawals, no studies utilizing quadratic or nonlinear models are cited. Applications of optimization based on economic or water-quality considerations also are omitted, even though several have been reported.

Recent studies using the linear objective function of maximizing ground-water withdrawal are reported by Tung and Koltermann (1985), Tung (1986), Peralta and others (1987), and Yazicigil and others (1987). Other efforts have included maximizing withdrawal within multiobjective optimization (Datta and Peralta, 1986; Peralta and Killian, 1987; Yazicigil and Rasheeduddin, 1987).

For several reasons, planners might prefer to use the linear objective function of maximizing ground-water withdrawal rather than a quadratic function of maximizing economic benefits. The first reason is that a strategy maximizing withdrawal volume may be almost identical to a strategy maximizing net return, depending on the planning period, cost coefficients, bounds on variables (head, pumping, recharge, streamflow, and so forth), and other restrictions. In fact, a linear objective function is sometimes considered a surrogate for the quadratic function of maximizing net economic return of crop production resulting from ground-water use. For example, Peralta and Kowalski (1988) obtained total ground-water withdrawal and economic value differences of less than 2 percent between strategies that maximize withdrawal and those that maximize economic value. Casola and others (1986) also reported little difference between volumetric and economic solutions. Their optimal economic pumping strategy consisted of pumping at or near its upper bound until the final time steps. A second reason for using the linear objective functions is that the terminology used by a legislature or court, in mandating water management directives, generally is related to volumetric rather than economic constraints. For example, "maximizing use" does not imply economic optimization. A third reason for using linear objective functions is that they require less computer memory and time than similar quadratic problems, since no matrix of quadratic coefficients is needed. Even though quadratic problems are readily solved by using commercially available optimization algorithms, linear objective functions are used to ensure that formulated problems can be solved practically on hardware such as microcomputers.

The central issue of this paper is how to best incorporate equations of ground-water flow within models for maximizing volume withdrawal during a hypothetical planning period. The purpose is to compare the accuracy and computational requirements of alternative approaches and to demonstrate situations where one set of simulation constraints is preferable to another.

Three finite-difference digital models were used to test the alternative approaches. Model A incorporated steady-state flow equations embedded directly as constraints (embedding method). The systems engineering concept of not simulating in more detail than is necessary for a particular situation is employed in Model A. Model B utilizes superposition and linear systems theory (response matrix method) to represent unsteady flow. It maximizes ground-water mining, withdrawing in excess of what is recharged for a period of time, and does not assure sustainability of pumping beyond the 50-yr planning period. Model C incorporated both steady-state embedding and transient-response matrix approaches. Model C is a combination of Models A and B. It simulates unsteady flow for the planning period and has additional steady-state flow constraints to ensure that pumping in the final time step can be continued beyond the end of the planning period (50 yr in this test). Model C is the most physically rigorous model and is used as the basis for comparison.

Constraints were tested for a range of acceptable boundary recharge rates by using combinations of four scenarios—with constant and varying upper limits on

pumping and with stressed and unstressed initial potentiometric surfaces. Pumping strategy sensitivity to aquifer parameters and transmissivity was demonstrated.

## DESCRIPTION OF MODELS

Two-dimensional saturated ground-water flow is assumed in a hypothetical 585 $mi^2$ study area (fig. 1). The aquifer in the study area is merely part of a surrounding, much larger aquifer system. The surrounding aquifer can provide recharge to the study area through each of the boundary cells in the study area. The hypothetical simulations and parameters are representative of alluvial aquifers.

Simulation of the flow system is accomplished by using the finite-difference model code AQUISIM, an acronym for aquifer simulation (Verdin and others, 1981). This model code solves the linearized Boussinesq equation and also is utilized to compute influence coefficients (the drawdown that results at a particular cell at a certain time in response to a unit pumping at some other cell and time) in optimization Models B and C. Finite-difference optimization models have been developed to compute maximum sustainable ground-water withdrawal volumes using the boundary conditions, constraints, and assumptions given below.

The use of constant-head/restrained-flux (CH/RF) cells exhibiting a modified Dirichlet boundary condition has been justified previously (Peralta and Killian, 1985; Yazdanian and Peralta, 1986) and applied to the developed models along their lateral outer limits. For the models tested, boundary heads are assumed to remain at constant elevations as long as the rate of ground-water movement across the boundary does not change significantly. Because of the application of this boundary condition in the models, boundary flow is not permitted to exceed predetermined limiting values, thus justifying applicability of the model computed strategies to field conditions.

In this study, aquifer transmissivity is assumed constant for a particular scenario for comparisons between models. Transmissivity is the same for Scenarios I and II; it is the same for Scenarios III and IV; however, transmissivity of Scenarios I and II differs from that of Scenarios III and IV. In general, transmissivity is assumed to be constant if the aquifer is confined or if the change in saturated thickness with time is small with respect to the initial saturated thickness. The effect of changes in transmissivity in response to changes in assumed saturated thickness is presented later in the section discussing simulation accuracy and sensitivity analysis.

The aquifer is assumed to be overlain by a completely impermeable cap (fig. 2). Except for ground-water pumping from wells, all recharge to or discharge from the aquifer in the study area enters or leaves through the 25 boundary CH/RF cells. No stream-aquifer hydraulic connection or

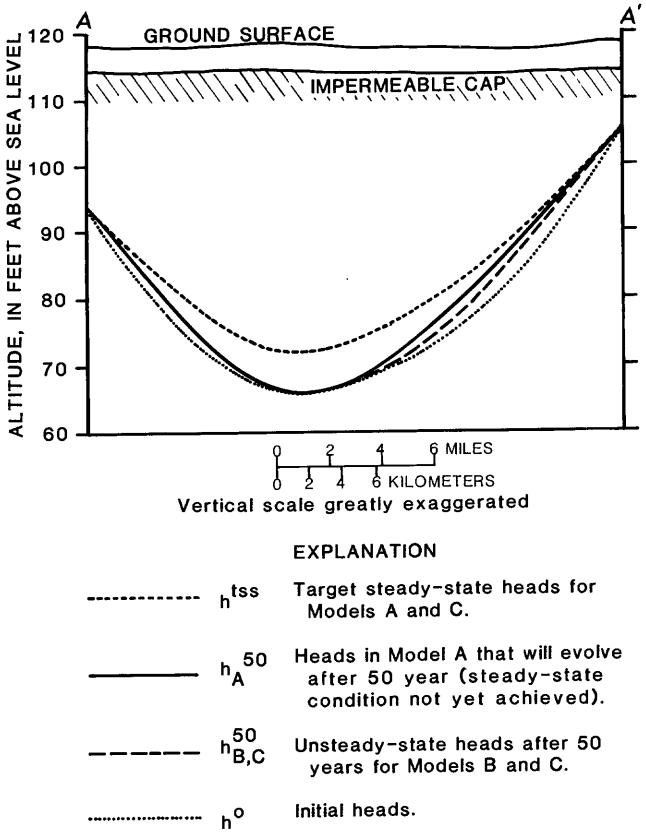


**Figure 2.** Geologic section *A-A'* showing initial and ultimate steady-state potentiometric surfaces for strategies developed for Scenario IV by using Models A, B, and C.

surface recharge occurs in any internal cells. Pumping constitutes the only discharge from the aquifer at the 40 internal cells. Because their heads can change with time, all interior cells are termed variable-head (VH) cells.

The technical development of steady-state embedded and unsteady response matrix models are presented below. In the literature, embedded models usually use a row-column notation to identify cells, while transient response matrix models usually include a running-string notation. For clarity, when merging both formulations, a row-column notation was used for all models.

Discussion of each model begins with presentation of the objective function, constraint equations, and bounds. Even though the study area used to compare the models is irregularly shaped, models are described as if they are being applied to a rectangular area of I rows and J columns. The total I×J cells is comprised of some inactive cells and active VH and CH/RF cells. Ground-water pumping occurs only at the internal VH cells, and recharge occurs only at the boundary cells.

## Model A (Steady-State Embedded Constraints)

Using a steady-state modeling approach is appropriate if one wishes to compute maximal pumping rates that will cause acceptable heads, sustainable for an infinite length of time. The objective function of this model maximizes sustainable ground-water withdrawals (eq 1), while simultaneously satisfying constraints in the ground-water flow equation (eq 2) and bounds on variables (head, recharge, and withdrawal) (eqs 3–5).

$$\max Q=\sum_{i=1}^{I}\sum_{j=1}^{J} q_{i,j}^{tss} \qquad \text{cell i,j is a VH cell} \tag{1}$$

Subject to:

$$T^{i}_{i,j}h^{tss}_{i+1,j}+T^{i}_{i-1,j}h^{tss}_{i-1,j}+T^{j}_{i,j-1}h^{tss}_{i,j-1}+T^{J}_{i,j}h^{tss}_{i,j+1} -h^{tss}_{i,j}(T^{i}_{i,j}+T^{i}_{i-1,j}+T^{j}_{i,j}+T^{j}_{i,j-1})-q^{tss}_{i,j}-r^{tss}_{i,j}=0 \qquad i=1,2,\ldots,I,\ j=1,2,\ldots,J \tag{2}$$

$$h^{Ltss}_{i,j} \le h^{tss}_{i,j} \le h^{Utss}_{i,j} \qquad i=1,2,\ldots,I,\ j=1,2,\ldots,J, \text{ and cell i,j is a VH cell} \tag{3}$$

$$r^{Ltss}_{i,j} \le r^{tss}_{i,j} \le r^{Utss}_{i,j} \qquad i=1,2,\ldots,I,\ j=1,2,\ldots,J, \text{ and cell i,j is a CH/RF cell} \tag{4}$$

$$q^{Ltss}_{i,j} \le q^{tss}_{i,j} \le q^{Utss}_{i,j} \qquad i=1,2,\ldots,I,\ j=1,2,\ldots,J, \text{ and cell i,j is a VH cell} \tag{5}$$

where

$Q$ = total ground-water pumping ($L^3/T$);

I and J = number of rows and columns of the area grid system;

$q^{tss}_{i,j}$ and $r^{tss}_{i,j}$ = ground-water pumping (+) and recharge (−) in cell i,j that will maintain $h^{tss}_{i,j}$ ($L^3/T$); there is only one ground-water flux variable per cell;

$h^{tss}_{i,j}$ = target steady-state potentiometric head that will ultimately evolve at each internal cell i,j if each is stressed by rate $q^{tss}_{i,j} + r^{tss}_{i,j}$ (L);

$T^{i}_{i,j}$ = geometric mean transmissivity between cells i,j and i+1, j ($L^2/T$); $= K[(b_{i,j})\,(b_{i+1,j})]^{1/2}$

$T^{j}_{i,j}$ = geometric mean transmissivity between cells i,j and i, j+1 ($L^2/T$); $= K[(b_{i,j})\,(b_{i,j+1})]^{1/2}$

L and U = lower and upper bounds on superscripted variables.

The model simulates steady-state flow (eq 2) to compute constant ground-water withdrawal rates. Stressing internal cells at a particular constant rate ($q^{tss}$) ultimately produces a unique "target" head ($h^{tss}$) for each cell. Acceptable final target heads are assured by equation 3, and equations 2 and 4 assure that final steady-state recharge rates are acceptable.

Heads for a specified time and location can be predicted by using a transient simulation model after optimal withdrawals have been determined. Heads might not attain their steady-state values for many years. It can be assumed that if initial and final heads are acceptable, transitional heads also will be satisfactory if withdrawals are constant in time. For purposes of comparing model performance, transient flow was simulated with the optimum withdrawals for a 50-yr period. The simulated heads and boundary flows were then used in evaluating the performance of the various models.

## Model B (Transient Response Matrix Constraints)

The response matrix method (Morel-Seytoux and Daly, 1975) in Model B uses the linear systems theory, analogous to well image theory or superposition, where a simulation model or set of equations is used to compute the head change that occurs at a specific cell at a specific time in response to a unit pumping at some cell at some time. The computed head change may reflect the result of pumping at a different location and time.

The objective function of Model B (eq 6) maximizes ground-water mining (withdrawal of more water than is recharged for a period of time), subject to constraints and bounds (eqs) 7–12).

$$\max Q=\sum_{k=1}^{K}\sum_{i=1}^{I}\sum_{j=1}^{J} q_{i,j,k} \qquad \text{cell i,j is a VH cell} \tag{6}$$

Subject to:

$$h_{i,j,K}+\sum_{k=1}^{K}\sum_{m=1}^{I}\sum_{n=1}^{J}\delta_{i,j,m,n,K-k+1}(q_{m,n,k}-q^{ass}_{m,n})=h^{o}_{i,j} \qquad i=1,2,\ldots,I,\ j=1,2,\ldots,J, \text{ and cell i,j is a VH cell and cell m,n is a pumping cell} \tag{7}$$

Boundary flows are computed by:

$$T^{i}_{i,j}h_{i+1,j,k}+T^{i}_{i-1,j}h_{i-1,j,k}+T^{j}_{i,j-1}h_{i,j-1,k}+T^{j}_{i,j}h_{i,j+1,k} -h_{i,j,k}(T^{i}_{i,j}+T^{i}_{i-1,j}+T^{j}_{i,j}+T^{j}_{i,j-1})-r_{i,j,k}=0 \qquad i=1,2,\ldots,I,\ j=1,2,\ldots J, \text{ and cell i,j is a CH/RF cell} \tag{8}$$

$$q_{i,j,k} \le q_{i,j,k+1} \qquad i=1,2,\ldots,I,\ j=1,2,\ldots,J,\ k=1,2,\ldots,(K-1),\ q_{i,j,1} \ge q^{o}_{i,j} \text{ and cell i,j is a VH cell} \tag{9a}$$

$$q_{i,j,k} \ge q_{i,j,k+1} \qquad i=1,2,\ldots,I,\ j=1,2,\ldots,j,\ k=1,2,\ldots,(K-1),\ q_{i,j,1} \le q^{o}_{i,j} \text{ and cell i,j is a VH cell} \tag{9b}$$

$$h^{L}_{i,j,K} \le h_{i,j,k} \le h^{U}_{i,j,K} \qquad i=1,2,\ldots,I,\ j=1,2,\ldots,J, \text{ and cell i,j is a VH cell} \tag{10}$$

$$r^{L}_{i,j,K} \leq r_{i,j,K} \leq r^{U}_{i,j,K} \qquad \begin{array}{l} i=1,2,\ldots,I,\ j=1,2,\ldots,J, \\ \text{and cell i,j is a CH/RF cell} \end{array} \quad (11)$$

$$q^{L}_{i,j,k} \leq q_{i,j,k} \leq q^{U}_{i,j,k} \qquad \begin{array}{l} i=1,2,\ldots,I,\ j=1,2,\ldots,J, \\ k=1,2,\ldots,K, \\ \text{and cell i,j is a VH cell} \end{array} \quad (12)$$

where

K=total number of time steps;

$h^{o}_{i,j}$=initial potentiometric surface elevation, (L);

$\delta_{i,j,m,n,K-k+1}$=nonnegative-valued influence coefficient describing the effect on hydraulic head in cell i,j by period K of a unit pumping in cell m,n in period k ($T/L^2$). The computed influence coefficient includes the effect of storage in the hydraulic behavior of the aquifer;

$q^{ass}_{m,n}$=ground-water pumping that must occur in each time step in cell m,n for that cell to maintain its initial head ($L^3/T$);

$q^{o}_{i,j}$=pumping prior to beginning of planning period ($L^3/T$).

Arrays and equations containing the time dimension are analogous to some found in Model A. As in Model A, no pumping occurs in CH/RF cells, and no recharge occurs in VH cells.

Superposition is used (eq 7) to compute the total head change or response at a particular cell and time to the pumping in all active cells. The head change is termed an influence coefficient and is used in equation 7. The response matrix is the matrix of influence coefficients as they are found within the constraint equations of an optimization model.

The head change caused by two units of pumping will be twice the head change caused by one unit of pumping. To determine the head response to a particular pumping rate of $q$ (some multiple of unit pumping), the influence coefficient is multiplied by $q$. In equation 7, however, the influence coefficients are multiplied by $q-q^{ass}$ to account for the initially stressed potentiometric surface used in Scenarios III and IV. In Scenarios I and II, when the initial potentiometric surface is unstressed, $q^{ass}=0$, and the influence coefficient is multiplied by $q$ in equation 7. Equations 8 and 11 assure that the heads resulting by the end of the planning period do not induce unacceptable values of recharge through CH/RF cells.

Although ground-water withdrawal can vary with time, equation 9a or 9b assures that acceptable pumping rates do not oscillate. From an agricultural planning and management perspective, if ground-water withdrawals are expected to change with time, the change generally is monotonic. If the aquifer is initially undeveloped (no prior pumping) pumping might be expected to increase with time. Thus equation 9a applies to Scenarios I and II discussed later. If the aquifer is initially overdeveloped, pumping might be expected to decrease with time. Therefore equation 9b applies to Scenarios III and IV.

### Model C (Transient Response Matrix Constraints With Embedded Terminal Steady-State Constraints)

This model is designed to maximize unsteady pumping during the planning period, while assuring that the pumping values of the final time step are sustainable beyond that period. It is a combination of approaches used in Models A and B. It includes the same objective function (eq 6) as Model B, equations 2–5 from Model A, and equations 7–12 from Model B. It also contains an embedding method (Tung and Koltermann, 1985) that includes finite difference or finite element equations describing ground-water flow included directly as a constraint equation (eq 13) within the optimization model, assuring that pumping in period K does not exceed a hypothetical steady pumping value, $q^{tss}$.

$$q_{i,j,K} \leq q^{tss}_{i,j} \qquad \begin{array}{l} i=1,2,\ldots,I,\ j=1,2,\ldots J, \\ \text{and cell i,j is VH cell} \end{array} \quad (13)$$

It is assumed that $q^{tss}$ can be sustained by feasible recharge rates (eqs 2 and 4) and will cause acceptable heads to develop (eqs 2 and 3). By using this model, a management agency can avoid having to reduce ground-water withdrawal after the end of the planning period.

## APPLICATION AND RESULTS

### Tested Scenarios and Utilized Data

Optimal regional ground-water withdrawal strategies were developed for a five-decade planning period using all three models. Each model was tested for a range of recharge constraints for four scenarios. The scenarios differ depending on whether the aquifer was already being utilized and whether upper limits on ground-water withdrawal might change with time. These scenarios are as follows:

I. Initially undeveloped aquifer, constant limits on pumping,
II. Initially undeveloped aquifer, changing limits on pumping,
III. Initially developed aquifer, constant limits on pumping, and
IV. Initially developed aquifer, changing limits on pumping.

In all optimizations, except some performed for sensitivity analysis, transmissivities were assumed to be constant in time (fig. 3). These values were used to compute the finite difference terms in equations 2 and 8 and also were used, in conjunction with a specific yield of 0.3, to compute the influence coefficients for equation 7.

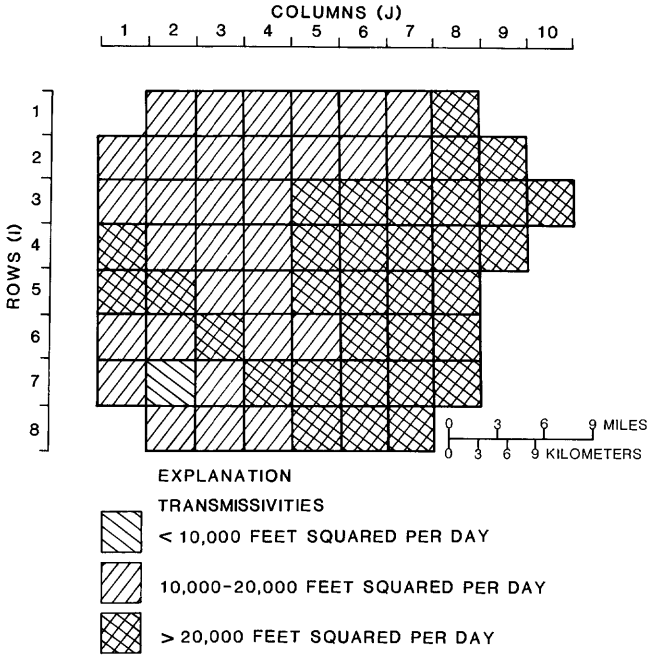


**Figure 3.** Transmissivities used in model comparisons.

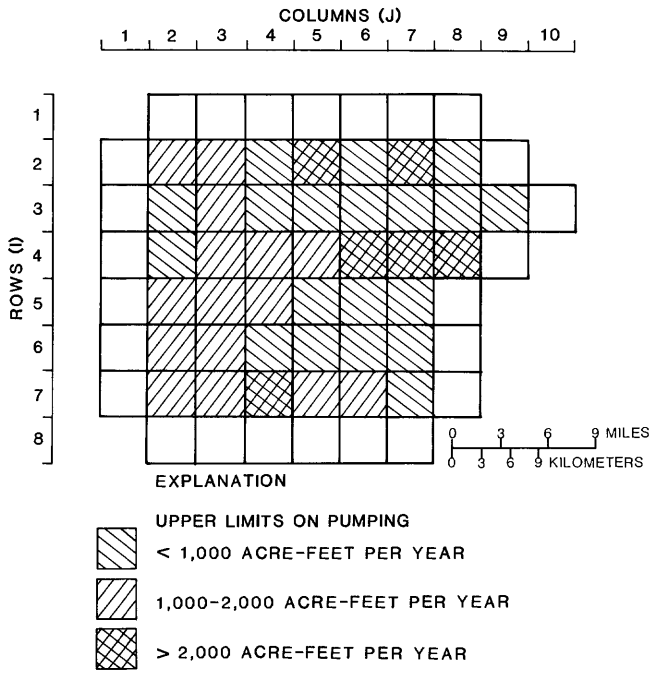


**Figure 4.** Assumed upper limits on ground-water pumping for Scenarios I and III. No pumping exists in boundary cells.

Target steady-state and transient heads are constrained by equations 3 and 10. The initial unstressed potentiometric surface, $h^{o}$ in equation 7, for Scenarios I and II is shown in figure 1. Initial heads for Scenarios III and IV (initially developed aquifer) are the $h^{tss}$ computed by using Model A for Scenario II and unconstrained recharge.

The lower limit on pumping, $q^{Ltss}$ and $q^{L}$, is 0.0 in equations 5 and 12 for all optimizations. The constant upper limits on pumping in equations 5 and 12 for Scenarios I and III are shown in figure 4. The arbitrary upper limits on pumping in Scenario II for the five decades are 0.8, 0.95, 1.0, 1.05, and 1.2 times the constant values of Scenarios I and III; the upper limits for Scenario IV are 1.2, 1.05, 1.0, 0.95, and 0.8 times the constant values, respectively. In other words, the constant upper bounds on pumping in Scenarios I and III are the same as the upper bounds of the third decade for Scenarios II and IV and also are the average values of all five decades for Scenarios II and IV. The total upper limit on pumping for all five decades is the same for all Scenarios.

The goal of having a monotonic change in pumping applies additional lower limits on pumping in Scenarios I and II (initially underdeveloped aquifer) and additional upper limits on pumping for Scenarios III and IV (initially developed aquifer). For Scenarios I and III, which have constant upper bounds on pumping, monotonicity is assured by Model A since it can compute only a single steady withdrawal for each cell.

In order to use Model A for Scenarios with changing bounds on pumping (II and IV), it is run sequentially, one distinct optimization after the other in five separate optimizations. In this process, the optimal pumping from one optimization affects the bounds on pumping in the next optimization. The lower bound on pumping in a cell for decade k in Scenario II is the pumping in decade k−1 (an equivalent of eq 9a). The upper bound on pumping in Scenario IV in decade k is the pumping in decade k−1 (equivalent to eq 9b).

This repetitive optimization is similar but not the same as a "staircase" procedure mentioned by Dantzig (1963), Gorelick, (1983), and Tung and Koltermann (1985), because the heads at the end of one decade are not used as the initial condition of the second decade (the optimal steady-state heads from one decade could not be used as the initial heads of the next decade because heads in a real system probably may not evolve to equilibrium by the end of a decade). This results from the fact that for constant transmissivity a volumetrically optimal steady-state strategy is independent of the initial heads of the internal VH cells. When using this approach, the "target" steady-state potentiometric surface changes every decade. None of the target surfaces was attained during the five-decade management period. However, the actual surface that would result from strategy implementation during the management era would always be evolving toward the target.

Because recharge is negative in sign, the greatest volume of flow permitted to enter the study area through a CH/RF cell is $r_{i,j}^{Ltss}$ in equation 4 or $r_{i,j,K}^{L}$ in equation 11. Upper limits on recharge are large positive numbers to

permit discharge if it enhances the value of the objective function. The lower limits on recharge through each cell are specified for each optimization and range from being unconstrained to being fairly restrictive at −2,000 acre-ft/yr per CH/RF cell.

## Volumetric Comparison of Optimal Strategies

Models A, B, and C are compared below on the basis of optimized pumpage and not pumping rate. The optimized constant pumping rate for Model A has been converted to a 50-yr volume for comparison with volumes calculated in Models B and C. Optimal total pumping volumes computed by each model (table 1) are shown in figure 5. Recharge constraints of unconstrained, 5,000, 3,750, and $2{,}500 \times 10^3$ acre-ft shown in the first column are the product of unconstrained, 4,000, 3,000, or 2,000 acre-ft/yr per CH/RF cell recharges times 50 yr times 25 CH/RF cells, respectively. These total maximum conceivable recharges are used to aid comparison with total pumping. As previously described, the actual constraints in the models are on a cell-by-cell basis. No constraint on total recharge is used.

Before comparing models, some general observations are in order. Care must be used when making comparisons because the assumed transmissivities and initial heads of Scenarios I and II are different than those of III and IV. Also it should be noted that, as available recharge is reduced (as the recharge constraint becomes increasingly restrictive), pumping decreases for all models.

Comparing strategies in table 1, it is apparent that the pumped volume from Model A is greater for scenarios in which there are constant upper bounds on pumping (I and III) than for those with varying upper bounds (II and IV), even though the total of all upper bounds is the same. This occurs because in Scenarios I and III pumping is effectively restricted primarily by the recharge constraint since the upper bound is an average value as previously stated. On the other hand, in Scenarios II and IV, pumping in the decades with a large upper bound on pumping is restricted by the recharge constraint, and pumping in the decades with a small upper bound on pumping is restricted by that upper bound.

If the initial potentiometric surface is unstressed, Models B and C also compute greater pumping if bounds are constant than if they are varying. The reasoning is the same as that presented for Model A. However, if the initial surface is stressed, the opposite trend is observed for those two models. This probably results from the fact that Models B and C emphasize pumping as early in the planning period as possible in order to have as much time as possible for the water levels to adjust to recharge constraints. Scenario IV permits the models to accomplish this because the upper bounds on pumping are greatest in the early decades.

Induced recharge/pumping ratios at the end of a 50-yr simulation period describe the proportion of total pumping that is replaced by recharge through the boundaries and are given in table 1, and trends in these and other ratios are given in table 2. It should be emphasized that Model A simulated transient flow for a 50-yr period using optimum withdrawals from a steady-state optimization model. In table 1, these ratios are less than 1.0 for a decrease in aquifer volume (Scenarios I and II) and greater than 1.0 for an increase (Scenarios III and IV). Within a Scenario, as total pumping increases, the recharge/pumping ratio decreases.

Other ratios in tables 1 and 2 describe differences in results with respect to those from Model C. The pumping ratio describes the ratio between total pumping for Model A or B and that of Model C. For unconstrained recharge, the pumping ratio of all models are virtually identical. Subsequent discussion deals only with optimizations in which recharge is constrained.

Note that the pumping ratios of Models A and B in table 1 are never both less than 1.0 for any single situation. This indicates, as does table 2, that Model C never computes higher total pumping than Models A or B for the same situation—an expected result since C includes the constraints of Models A and B.

In all but one Scenario, Model B computes at least as much total pumping as Models A and C, because it optimizes mining, rather than sustainable withdrawal (table 1). The difference in pumping between B and A or C increases as the recharge is progressively constrained. For an unstressed initial surface, Model B may compute pumping that is up to 12 percent greater than that from Model C and 11 percent greater than that from Model A. For these Scenarios (I and II), Model B is not useful for sustained yield analysis. However, for Scenarios III and IV, pumping from Model B is distributed identically with that from Model C (fig. 6). Although it is difficult to predict exactly when this degree of similarity will occur, Model B may in some instances be used in place of Model C. However, if sustainable pumping rates after the management era are to be at least as great as the rates in the final decade, then Model C must be used.

Total pumping in Model A is always within 2 percent (greater) of that of Model C for Scenarios I and II. Distribution of pumping in time also is similar. Dissimilarity is partially due to Model C having more constraints. It may result also from difference in the form of the flow constraints in Models A and C, despite the fact that in both models these constraints link all cells. In Model A, the steady-state equation 2 for a particular cell includes heads and transmissivities of only five cells. In Model C, equation 7 for each cell potentially includes influence coefficients for all cells in the study area.

For Scenarios III and IV, Model A withdrawals are much less than Models B or C. The major reason for the

**Table 1.** Summary of ground-water pumping and ratios of recharge/pumping and sustainable pumping

[NA, not available]

| Maximum total recharge constraints for a 50-yr period ($10^3$ acre-ft) | Model | Total pumped volume in 50 yr ($10^3$ acre-ft) | Induced recharge/ pumping ratio at the end of a 50-yr simulation | Pumping ratio Model (A or B) / Model C | Sustainable pumping ratio |
|---|---|---|---|---|---|
| | | **Scenario I** | | | |
| Unconstrained | A | 2,265 | 0.62 | 1.00 | 1.00 |
| | B | 2,265 | .62 | 1.00 | NA |
| | C | 2,265 | .62 | NA | NA |
| 5,000 | A | 2,131 | .62 | 1.01 | 1.01 |
| | B | 2,112 | .62 | 1.00 | NA |
| | C | 2,112 | .62 | NA | NA |
| 3,750 | A | 1,936 | .64 | 1.00 | 1.00 |
| | B | 1,954 | .64 | 1.01 | NA |
| | C | 1,936 | .64 | NA | NA |
| 2,500 | A | 1,499 | .71 | 1.02 | 1.02 |
| | B | 1,601 | .71 | 1.09 | NA |
| | C | 1,468 | .75 | NA | NA |
| | | **Scenario II** | | | |
| Unconstrained | A | 2,265 | 0.60 | 1.00 | 1.00 |
| | B | 2,265 | .60 | 1.00 | NA |
| | C | 2,265 | .60 | NA | NA |
| 5,000 | A | 2,067 | .61 | 1.00 | 1.00 |
| | B | 2,105 | .60 | 1.02 | NA |
| | C | 2,067 | .61 | NA | NA |
| 3,750 | A | 1,867 | .64 | 1.00 | 1.00 |
| | B | 1,952 | .62 | 1.05 | NA |
| | C | 1,867 | .64 | NA | NA |
| 2,500 | A | 1,436 | .72 | 1.01 | 1.03 |
| | B | 1,593 | .69 | 1.12 | NA |
| | C | 1,416 | .74 | NA | NA |
| | | **Scenario III** | | | |
| Unconstrained | A | 2,265 | 1.02 | 1.00 | 1.00 |
| | B | 2,265 | 1.02 | 1.00 | NA |
| | C | 2,265 | 1.02 | NA | NA |
| 5,000 | A | 2,145 | 1.04 | .96 | 1.00 |
| | B | 2,239 | 1.03 | 1.00 | NA |
| | C | 2,239 | 1.03 | NA | NA |
| 3,750 | A | 1,970 | 1.09 | .92 | 1.06 |
| | B | 2,139 | 1.07 | 1.00 | NA |
| | C | 2,139 | 1.07 | NA | NA |
| 2,500 | A | 1,574 | 1.28 | .85 | 1.02 |
| | B | 1,855 | 1.19 | 1.00 | NA |
| | C | 1,855 | 1.19 | NA | NA |
| | | **Scenario IV** | | | |
| Unconstrained | A | 2,263 | 1.04 | 1.00 | 1.00 |
| | B | 2,265 | 1.04 | 1.00 | NA |
| | C | 2,265 | 1.04 | NA | NA |
| 5,000 | A | 2,084 | 1.07 | .93 | .99 |
| | B | 2,248 | 1.05 | 1.00 | NA |
| | C | 2,248 | 1.05 | NA | NA |
| 3,750 | A | 1,905 | 1.13 | .88 | 1.07 |
| | B | 2,152 | 1.08 | 1.00 | NA |
| | C | 2,152 | 1.08 | NA | NA |
| 2,500 | A | 1,513 | 1.33 | .81 | .96 |
| | B | 1,874 | 1.20 | 1.00 | NA |
| | C | 1,874 | 1.20 | NA | NA |

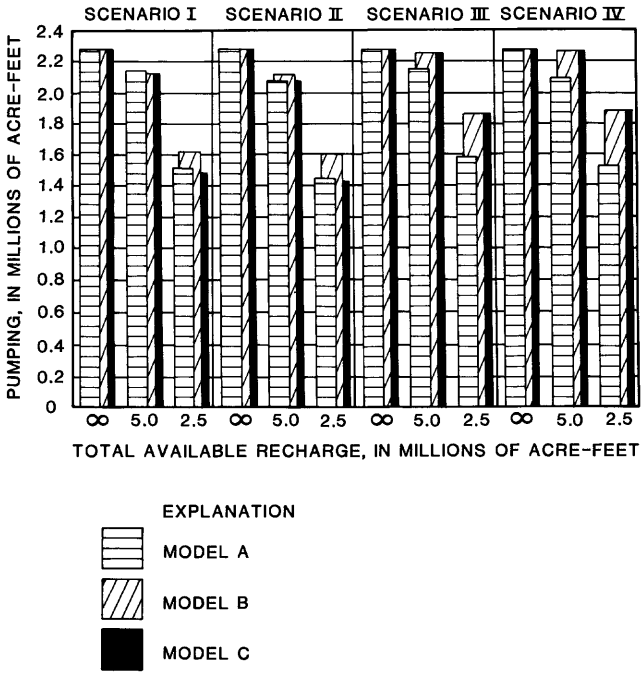


**Figure 5.** Total 50-yr ground-water pumping for all models and scenarios.

**Table 2.** Trends of pumping, recharge/pumping, and sustainable pumping ratios for optimizations using constrained recharge

| | Scenario | | | |
|---|---|---|---|---|
| | I | II | III | IV |
| Pumping ratio | C≤B<br>C≤A | C≤A≤B | A≤B=C | A≤B=C |
| Recharge/pumping ratio. | A=B≤C | B≤A≤C | B=C≤A | B=C≤A |
| Sustainable pumping ratio. | C≤A | C≤A | C≤A | no trend |

difference in pumping between Models A and C is that pumping can vary with time in Model C. An additional optimization was performed by using a modified Model C for Scenario III and each of the three recharge-constraint situations. In these three optimizations, pumping in Model C was forced to be constant in time. The resulting pumping totals are 2,144,614, 1,969,710, and 1,544,491 acre-ft for recharge constraints of 4,000, 3,000, and 2,000 acre-ft/yr per CH/RF cell, respectively. Model A computes pumping identical to that computed in Model C for recharge constraints of 5,000 and $3{,}750 \times 10^3$ acre-ft. For the $2{,}500 \times 10^3$ acre-ft recharge constraint, Model A pumping is 2 percent higher than that from Model C. This illustrates that, if temporally constant pumping is assumed, Model A is a viable substitute for Model C whether the initial surface is stressed or unstressed.

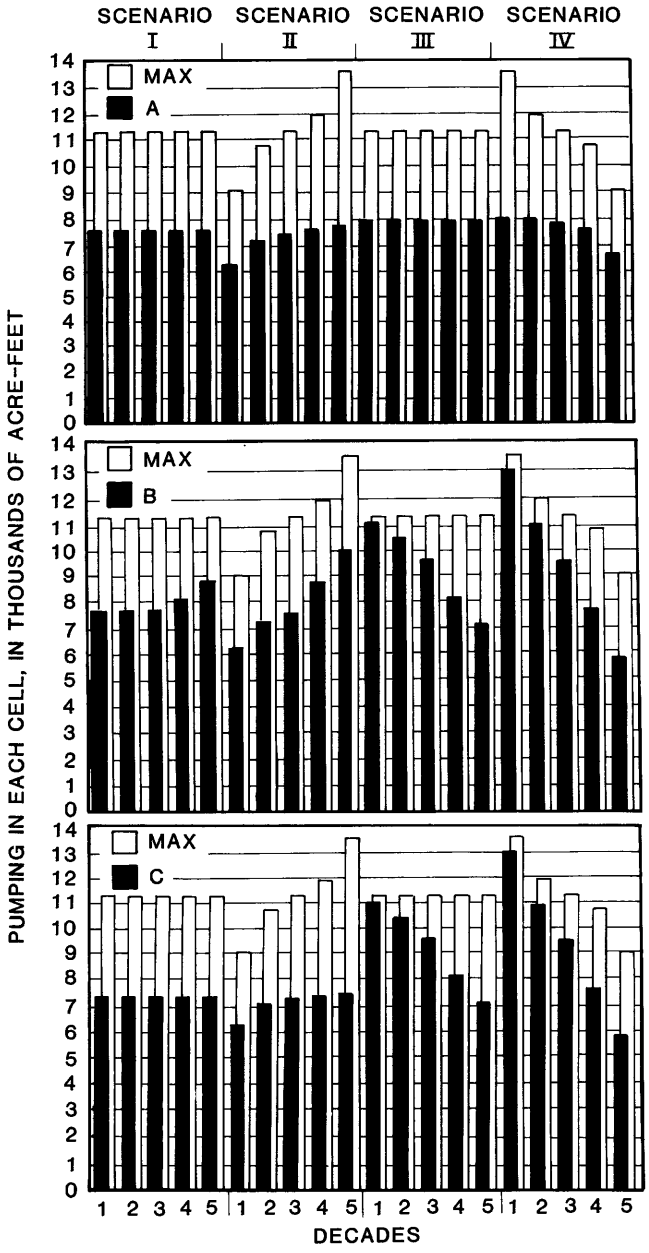


**Figure 6.** Average pumping by decade for Models A, B, and C and all scenarios for recharge not exceeding 2,000 acre-ft/yr in each boundary cell. "Max" pumping is the upper limit on pumping in a decade.

Trends in sustainable pumping ratios are evident from the data in tables 1 and 2. These ratios compare the steady pumping ratio that can continue after the 50-yr planning period as computed by Model A, with that computed by Model C. No value is shown for Model B because it includes no steady-state constraints. For Scenarios I and II, sustainable pumping for Model A is no more than 3 percent greater than that for Model C. For Scenarios III and IV,

sustainable pumping for Model A ranges between 96 and 107 percent of that for Model C.

The trends in table 2 do not show results of runs using unconstrained recharge because coefficients are identical for all three models. Also, no sustainable pumping is computed for Model B. If sustainable pumpage was computed, it would not exceed that for Model A.

## Simulation Accuracy and Sensitivity Analysis

The accuracy of the unsteady head computation achieved by Models B and C through equation 7 was verified by comparing predicted heads from Scenario I with simulated values from AQUISIM. All heads predicted by equation 7 to exist after 50 yr are within 0.002 to −0.046 ft of the heads (0.01 percent to −0.4 percent) predicted by AQUISIM.

The sensitivity of optimization models to changes in parameters is sometimes unexpected. For example, note the 2,131,000 acre-ft pumping volume obtained in Scenario I by Model A constrained such that recharge never exceeds 4,000 acre-ft/yr at any boundary cell. Analysis of the sensitivity of that strategy shows that if, transmissivity is globally decreased by 25 percent, optimal pumping increases slightly by 0.9 percent. Optimal heads are lower but do not reach the lower limits. The new transmissivity coefficients in equation 2 are apparently better for the objective of optimizing pumping than the previous values. If optimal heads had reached their lower limits in the run using a reduced transmissivity, total pumping would be expected to be less. A more intuitively consistent result occurs when transmissivity is globally reduced by 50 percent. Heads reach their lower limits, and pumping is decreased by 4 percent.

## Computational Considerations

All models are written by using the Generalized Algebraic Modeling System (GAMS) (Kendrick and Meeraus, 1985). Linked to GAMS is (MINOS) (Murtagh and Saunders, 1987), which accomplishes the optimization. Processing is performed within a VM/SP environment by using a conversational operating system (CMS) (International Business Machines Corp., 1980).

Table 3 indicates that Model A requires significantly less processing time than the others (62 percent less than Model C). This is the result of having fewer constraints and variables (such as rows and columns in a linear programming constraint set). Using the equations in table 4, Model A requires only 28 and 27 percent of the variables and constraints required by Model C, respectively, for the test problem. In contrast, Model B requires 72 and 73 percent of the variables and constraints used by Model C.

**Table 3.** Average computer processing time of optimization algorithm

[In seconds; processing time for Model A is the total for five separate optimizing runs (one for each decade)]

| Model | Scenario | | | |
|---|---|---|---|---|
| | I | II | III | IV |
| A | 29.97 | 32.1 | 30.4 | 32.4 |
| B | 63.3 | 63.2 | 63.1 | 62.2 |
| C | 81.7 | 81.4 | 80.4 | 80.1 |

**Table 4.** Comparison of number of decision variables and constraint equations

[*Mc* = number of constant-head cells; *Mv* = number of variable-head cells; K = total number of time periods; number of variables and equations reported for A is the number required to perform a single optimization, not the cumulative number required to perform separate optimizations for K time periods]

| Model | Number of decision variables | Number of constraint equations |
|---|---|---|
| A | $Mc+2Mv$ | $2Mc+5Mv$ |
| B | $Mc+(K+1)Mv$ | $2Mc+(3K+1)Mv$ |
| C | $2Mc+(K+3)Mv$ | $4Mc+(3K+6)Mv$ |

Note that transient heads in Models B and C are computed and constrained only for the end of the final time step. To constrain heads at other points in time, more computer memory and processing time are required. As long as heads do not need to be constrained at particular finite times, Model A offers a computational advantage. A user wishing to know the interim heads that result from implementing an optimal strategy can always compute them by using a transient simulation model after optimization is performed.

Presented in table 4 is a comparison of the total number of decision variables and constraint equations used in the simulations of Models A, B, and C. The variable *Mc* is the number of constant-head cells; variable *Mv* is the number of variable-head cells; variable *M* is the sum of the constant-head and variable-head cells ($M = Mc + Mv$). For example:

For *Model A*,

For *Mc* cells, recharge is a variable,

For *Mv* cells, pumpage and heads are variables,

Sum = $Mc + 2Mv$ = total number of decision variables.

Model A consists of one objective function (eq 1), *M* of equation 2, *Mv* of equations 3 and 5, and *Mc* of equation 4. Model B consists of one objective function (eq 6), *Mv* of equation 7, *Mc* of equation 8, $Mv \times (K-1)$ of equation 9, *Mv* of equation 10, *Mc* of equation 11, and *Mv* of equation 12 if ground-water pumping is to be constant or $Mv \times K$ of

equation 12 if ground-water pumping is to vary with time. Model C has the objective function of equation 6 plus all variable bounds and constraints mentioned for A and B, as well as $Mv$ of equation 13.

The fairly small system described in this paper represents a Model A problem of 250 rows and 105 columns of decision variables. Model B uses 690 rows and 265 columns, while Model C requires 940 rows and 370 columns of decision variables. For a larger imaginary system of 300 CH/RF cells and 1,300 VH cells, Model C requires 27,300 rows and 11,000 columns of decision variables. Model A needs only about 26 percent of that, 7,000 rows and 2,900 columns. Yazdanian and Peralta (1986) report that processing time increases exponentially with problem size for tested optimization models. Thus, Model A becomes increasingly attractive as problem size increases. In preliminary testing, an IBM/AT with 640 K of Random Access Memory had inadequate memory to run Model C, although it could easily run Model A for one decade at a time.

Depending on the optimization solution algorithm that is used, Models A and C may be subject to a weakness sometimes ascribed to the embedding technique—susceptibility to computational instability for large systems. The tendency for the model to fail to converge increases as the size of the pentadiagonal constraint matrix (containing steady flow constraint equations) increases. This possible limitation may affect C more than Model A because Model C has $(2Mc+Mv)$ such equations while A has only $Mc+Mv$.

Models B and C compute globally optimal solutions for all situations. Model A solutions are globally optimal for Scenarios I and III. For Scenarios where upper bounds on pumping change and Model A is run for each decade, solutions may not be globally optimal.

## SUMMARY

Three management model formulations (Models A, B, and C) were compared to evaluate which are appropriate for computing maximum sustained yield ground-water withdrawal strategies for alternative scenarios and a range of recharge constraints. Model A contains embedded steady-state flow equations. Model B contains only response matrix-type transient equations. Model C combines constraints from both models plus a restriction that pumping in the final time period is sustainable. The models were tested for four Scenarios that included the combinations of having an initially unstressed or stressed potentiometric surface and having constant or changing upper limits on withdrawal.

Model C is the most rigorous model and is preferred for computing sustained yield strategies when sufficient data and computer capability are available. However, in some cases, Models A and B compute comparable strategies while offering significant reduction in computational effort. To evaluate whether Models A or B can be substituted for Model C, results from both were compared with the results from Model C.

A five-decade planning period was used in all models. Models B and C can optimize for the entire period even if upper bounds on pumping change with time. For situations in which these bounds change, Model A can be run for each consecutive decade. In this situation, an optimal balance between withdrawal and recharge of Model A cannot be assured in every cell. All other scenarios in this study achieved optimal solutions in every cell.

If the initial potentiometric surface is relatively unstressed, Model A is an appropriate substitute for Model C. Pumping strategies computed by Model A are almost identical to those computed by C but require much less computer processing execution time and memory. Pumping strategies from Model B exceed those from Model C. Because they are not sustainable, Model B is not appropriate for this situation.

Model A is a conservative substitute for Model C for the situation where the initial potentiometric surface is stressed to the extent that pumping rates cannot be sustained for specified recharge constraints. If pumping in Model C is forced to be constant in time, pumping strategies from Models A and C are very similar. Pumping in Model A is less than that in Model C because pumping in Model A is not allowed to vary with time. Pumping strategies computed by Model A are sustainable and provide the same reduction in computational effort mentioned previously.

For situations where the potentiometric surface is initially stressed, optimal pumping strategies from Model B are almost identical to those from Model C. However, because Model B contains no sustained-yield constraints, there is no guarantee that pumping will always be sustainable. Therefore, Model B may not be appropriate, even though it requires less computational resources than Model C.

Pumping rates computed by Models A and C to be sustainable beyond the 50-yr planning period also were compared. For the initially unstressed aquifer, rates from Model A may be slightly greater than those computed by Model C. For the initially stressed aquifer, sustainable pumping computed by Model A is within several percent of that computed by Model C.

For computing maximum sustained-yield ground-water withdrawal strategies, a model that employs only embedded steady-state equations compares favorably with a more detailed model that combines steady-state and unsteady response-matrix formulations. In this comparison, the attempt was made to constrain heads during the planning period. Interim heads during the planning period can of course be computed by using transient modeling subsequent to the optimization modeling.

The steady-state formulation is especially competitive when available computer time or memory is limited, a condition that frequently occurs in projects in which computations are performed on personal computers. In the presented example, time requirements were 62 percent lower with the embedded steady-state equation approach relative to the more complex response matrix approach. The number of variables and constraints (affecting computer memory) were 72 and 73 percent, respectively, lower with the steady-state equation approach.

## SELECTED REFERENCES


Bear, J., 1979, Hydraulics of ground water: New York, McGraw-Hill, chap. 12.

Bredehoeft, J.D., Papadopulos, S.S., and Cooper, H.H., Jr., 1982, Ground water: the water-budget myth, *in* Scientific basis of water-resource management: Washington, D.C., National Academy Press, p. 51–57.

Casola, W.H., Narayanan, R., Duffy, C., and Bishop, A.B., 1986, Optimal control model for ground-water management: American Society of Civil Engineers Journal of Water Resources Planning and Management, v. 112, no. 2, p. 183–197.

Dantzig, G.B., 1963, Linear programming and extensions: Princeton, New Jersey, Princeton University Press.

Datta, B., and Peralta, R.C., 1986, Interactive computer graphics-based multiobjective decision-making for regional ground-water management: Agricultural Water Management, v. 11, p. 91–116.

Domenico, P.A., 1972, Concepts and models in ground-water hydrology: New York, McGraw-Hill, chap. 3.

Gorelick, S.M., 1983, A review of distributed parameter ground-water management modeling methods: Water Resources Research, v. 19, p. 305–319.

Illangasekare, T.H., Morel-Seytoux, H.J., and Verdin, K.L., 1984, A technique of reinitialization for efficient simulation of large aquifers using the discrete kernel approach: Water Resources Research, v. 20, no. 11, p. 1733–1742.

International Business Machines Corporation, 1980, IBM Virtual Machine/System Product: CMS User's Guide, White Plains, New York, 466 p.

Kendrick, D., and Meeraus, A., 1985, GAMS, an introduction: The World Bank, Washington, D.C.

Knapp, K.C., and Feinerman, E., 1985, The optimal steady-state in ground-water management: Water Resources Bulletin, v. 21, no. 6, p. 967–975.

McDonald, M.G., and Harbaugh, A.W., 1984, A modular three-dimensional finite-difference ground-water flow model: Washington, D.C., Scientific Publications Co.

Morel-Seytoux, H.J., and Daly, C.J., 1975, A discrete kernel generator for stream-aquifer studies: Water Resources Research, v. 11, no. 2, p. 253–260.

Morel-Seytoux, H.J., Illangasekare, T.H., Bittinger, M.W., and Evans, N.A., 1980, Potential use of a stream-aquifer model for management of a river basin-case of the South Platte River in Colorado: Progressive Water Technology, v. 13, p. 175–187.

Murtagh, B.A., and Saunders, M.A., 1987, MINOS 5.1 user's guidelines: Technical Report SOL 83–20r, Stanford University.

Peralta, R.C., and Killian, P.J., 1985, Optimal regional potentiometric surface design, least-cost water supply/sustained ground-water yield: Transactions of the American Society of Agricultural Engineers, v. 28, no. 4, p. 1098–1107.

———1987, Decision support for optimal regional ground-water management strategy modification: Transactions of the American Society of Agricultural Engineers, v. 30, no. 2, p. 400–410.

Peralta, R.C., and Kowalski, K., 1988, Optimal volumetric and economic ground-water mining for the Arkansas Grand Prairie: Agricultural Water Management, v. 15, no. 1, p. 1–17.

Peralta, R.C., Kowalski, K., and Morel-Seytoux, H.J., 1987, Ground-water recharge planning using resolvent discrete kernels: Transactions of the American Society of Agricultural Engineers, v. 30, no. 6, p. 1694–1699.

Tung, Y., 1986, Ground-water management by chanceconstrained model: Journal of Water Resources Planning and Management, v. 112, no. 1, p. 1–19.

Tung, Y., and Koltermann, C.E., 1985, Some computational experiences using embedding technique for ground-water management: Groundwater, v. 23, no. 4, p. 455–464.

Verdin, K.L., Morel-Seytoux, H.J., and Illangasekare, T.H., 1981, User's manual for AQUISIM: FORTRAN IV programs for discrete kernels generation and for simulation of an isolated aquifer behavior in two dimensions: HYDROWAR Program, Fort Collins, Colorado, Colorado State University, 199 p.

Yazdanian, A., and Peralta, R.C., 1986, Maintaining target ground-water levels using goal-programming, linear and quadratic methods: Transactions of the American Society of Agricultural Engineers, v. 29, no. 4, p. 995–1004.

Yazicigil, H., Al-Layla, R.I., and de Jong, R.L., 1987, Optimal management of a regional aquifer in eastern Saudi Arabia: Water Resources Bulletin, v. 23, no. 3, p. 423–434.

Yazicigil, H., and Rasheeduddin, M., 1987, Optimization model for ground-water management in multi-aquifer systems: Journal of Water Resources Planning and Management, v. 113, no. 2, p. 257–273.

# Hydrology and Water-Level Fluctuations of Devils Lake, North Dakota

*By* Gregg J. Wiche

**Abstract**

Rising water levels of Devils Lake, North Dakota, and other terminal lakes, have, in recent years, threatened flooding of highways, agricultural land, recreational cabins, and communities located near these lakes. This study was undertaken to describe the hydrology of the Devils Lake basin and to determine probabilities of future water levels.

The average annual net storage gain to Devils Lake has varied from 86.3 cubic hectometers during 1969–84 to 5.58 cubic hectometers during 1931–40. An interconnected chain of lakes upstream of Devils Lake retains runoff and functions as an evaporation basin, which significantly decreases inflow to Devils Lake. For example, 138 cubic hectometers of water was stored and subsequently evaporated in the upstream lakes from 1965 through 1967.

Exceedance probability for a given water-level rise was obtained by computing the exceedance probability for a net storage gain and then converting the net storage gain value to a water-level rise. The higher the starting water level, the lower the associated water-level rise for a given net storage gain. For example, a net storage gain of 89.1 cubic hectometers has an exceedance probability of 10 percent. This gain results in a 1.22-meter water-level rise if Devils Lake is at a starting water level of 429.8 meters above the National Geodetic Vertical Datum of 1929 (NGVD of 1929), but the water-level rise is only 0.37 meter if the starting water level is 435.9 meters above NGVD of 1929.

A water-balance model was developed to account for the gains and losses in discharge that occur as water moves through the chain of lakes upstream from Devils Lake. Based on previously recorded hydrologic and climatologic data, a "high-runoff" and "low-runoff" condition was simulated for 1985–90. The high-runoff simulation indicates that the maximum water level in Devils Lake would be 436.30 meters above NGVD of 1929. The low-runoff simulation indicates that the minimum water level in Devils Lake would be 433.04 meters above NGVD of 1929.

## INTRODUCTION

About 5 percent of the landmass of North America drains into terminal lakes, which are lakes that are located at the lowest point within a closed drainage basin (de Martonne, 1927). Closed drainage basins have no outlet to the oceans of the world. Rising water levels of many of these terminal lakes have, in recent years, threatened flooding of highways, agricultural land, recreational cabins, and communities located near these lakes. The current high water levels of Devils Lake, N. Dak., pose a flood threat to the city of Devils Lake, a National Guard camp, roads, and sewer and lagoon systems of several other communities.

The U.S. Army Corps of Engineers (1984) is conducting a feasibility study of possible flood-control projects to protect the cities, roads, and other properties around Devils Lake. An understanding of the hydrology of Devils Lake and some knowledge of the probability of future lake levels are needed as a basis for implementation of the flood-control project. For data collected at streamflow stations, the standard procedure most commonly used to compute probabilities is to fit the annual series of discharge data to a log-Pearson Type III distribution. However, problems arise when an annual series of lake levels is applied to a frequency distribution, such as the log-Pearson Type III, because the primary assumption of independence is violated. Future lake levels of all terminal lakes are dependent to varying degrees on the previous years' lake level.

The purposes of this study are to describe the hydrology of the Devils Lake basin and to determine how to estimate probabilities of future water levels in Devils Lake. The description of the hydrology of the Devils Lake basin is limited to currently (1983) available data.

## DESCRIPTION OF THE STUDY AREA

Devils Lake basin (fig. 1), in northeastern North Dakota, is a 9,870-km$^2$ closed basin within the drainage basin of the Red River of the North. About 8,600 km$^2$ of the basin is tributary to Devils Lake, and about 1,270 km$^2$ is tributary to Stump Lake. The topographic relief and surficial landforms are of glacial origin. A large number of

shallow depressions and potholes occur throughout the basin. Many of these depressions are connected by poorly defined channels and swales.

The eastern, western, and northern boundaries of the Devils Lake basin are poorly defined low divides. The southern boundary is a series of recessional moraines that lie between Devils Lake and the Sheyenne River. The major subbasins within the Devils Lake basin and the principal streams draining them are shown in figure 1, and the drainage areas are listed in table 1. Edmore, Starkweather, and Calio Coulees originate in southern Cavalier County and flow in a south-southwesterly direction. Mauvais Coulee originates along the southern flanks of the Turtle Mountains 90 to 120 m above the elevation of Devils Lake and flows in a southerly direction.

Prior to 1979, discharge from the tributaries flowed into the interconnected chain of lakes shown in figure 1 and then, starting with the upstream lake, flowed through Sweetwater Lake, Morrison Lake, Dry Lake, Mikes Lake, Chain Lake, Lac aux Mortes (Lake Alice), Lake Irvine, and then into Big Coulee. Prior to 1979, most of the discharge entering Devils Lake flowed through Big Coulee, which is the only principal stream discharging directly to Devils Lake. A small quantity of runoff entered Devils Lake by overland flow from drainage areas adjacent to the lake. In 1979, the Ramsey County and Cavalier County Water Management Boards completed construction of channel A, which connects Dry Lake to Six Mile Bay on Devils Lake. Channel A changed the drainage area of Big Coulee downstream of Churchs Ferry; drainage from Sweetwater, Morrison, and Dry Lakes is conveyed by channel A, and the remaining discharge follows the natural watercourse.

## HYDROLOGY OF THE DEVILS LAKE BASIN

### Prehistoric Water-Level Fluctuations

Since the retreat of the Pleistocene glaciation, the water level of Devils Lake has fluctuated between about 442.9 m above NGVD of 1929, the spill elevation, to less than 427 m above NGVD of 1929 (Aronow, 1957). Callender (1968) analyzed sediment samples from Devils Lake for their physical, chemical, and mineralogical properties and concluded that Devils Lake has fluctuated in response to changing climatic and hydrologic conditions. Callender (1968) reached the conclusion that Devils Lake was dry sometime between 8,500 to 6,000 yr B.P.

Aronow (1955, 1957) analyzed abandoned strand lines, lacustrine sand and gravel deposits containing buried soils and vertebrate remains, and rooted stumps uncovered by receding water around Stump Lake. Aronow (1957) indicated that a lowering of water levels of lakes in the Devils Lake basin occurred during a dry period in the 15th and 16th centuries, as evidenced by the growth of burr oak in Stump Lake. According to Brooks (1951), this dry period occurred throughout most of western North America. After this dry period, there was a general rise in water levels from the mid-1500's until the mid- to late 1800's (Aronow, 1957). The period of rising water levels was contemporaneous with the expansion of the glaciers in the Alps, Scandinavia, and Iceland and commonly is referred to as the Little Ice Age (Brooks, 1951; Wahl, 1968).

### Historic Water-Level Fluctuations

Upham (1895, p. 595) indicated that the water level of Devils Lake was 439.2 m above NGVD of 1929 in 1830. He based this water level on a large and dense stand of timber that grew at and above 439.2 m above NGVD of 1929. Below 439.2 m above NGVD of 1929, scattered trees and brush existed. Captain H.H. Heerman informed Upham that, based on tree-ring chronology, the largest tree cut below 439.2 m above NGVD of 1929 was 57 yr old in 1887. Thus, Upham concluded that 57 yr prior to 1887, or 1830, the water level of Devils Lake was 439.2 m above NGVD of 1929. No water levels were recorded from 1830 to 1867.

Water levels of Devils Lake have been recorded, albeit somewhat sporadically, from 1867 to 1901 (fig. 2), and these records have been authenticated by the U.S. Geological Survey (USGS). In 1901, the USGS established a gage at Devils Lake. For the period of record at Devils Lake, the maximum water level occurred in 1867; the water level was 438.3 m above NGVD of 1929, and the lake had a surface area of about 360 $km^2$. From 1867, the water level of Devils Lake declined almost continuously until 1940 when it reached a recorded low of 427.0 m above NGVD of 1929, and the lake was a shallow brackish body of water covering 26.4 $km^2$ (North Dakota State Engineer, 1944). From 1940 to 1956, Devils Lake rose; from 1956 to 1968, it again declined, and in 1983, it reached a peak of 435.28 m above NGVD of 1929, which is the highest water level in about 100 yr.

## HYDROLOGIC ANALYSIS

### Statistical Analysis of the Discharge Record

Discharge data collected at three long-term gaging stations (table 2) were used to describe the temporal variability in discharge of the major tributaries to Devils Lake. Monthly streamflow statistics computed for these long-term gaging stations (table 3) indicate a large variability in discharge from month to month. Most of the runoff occurs in April and May in Edmore and Mauvais Coulees. The maximum monthly mean and median flows occur in April in Edmore and Mauvais Coulees and in May in Big

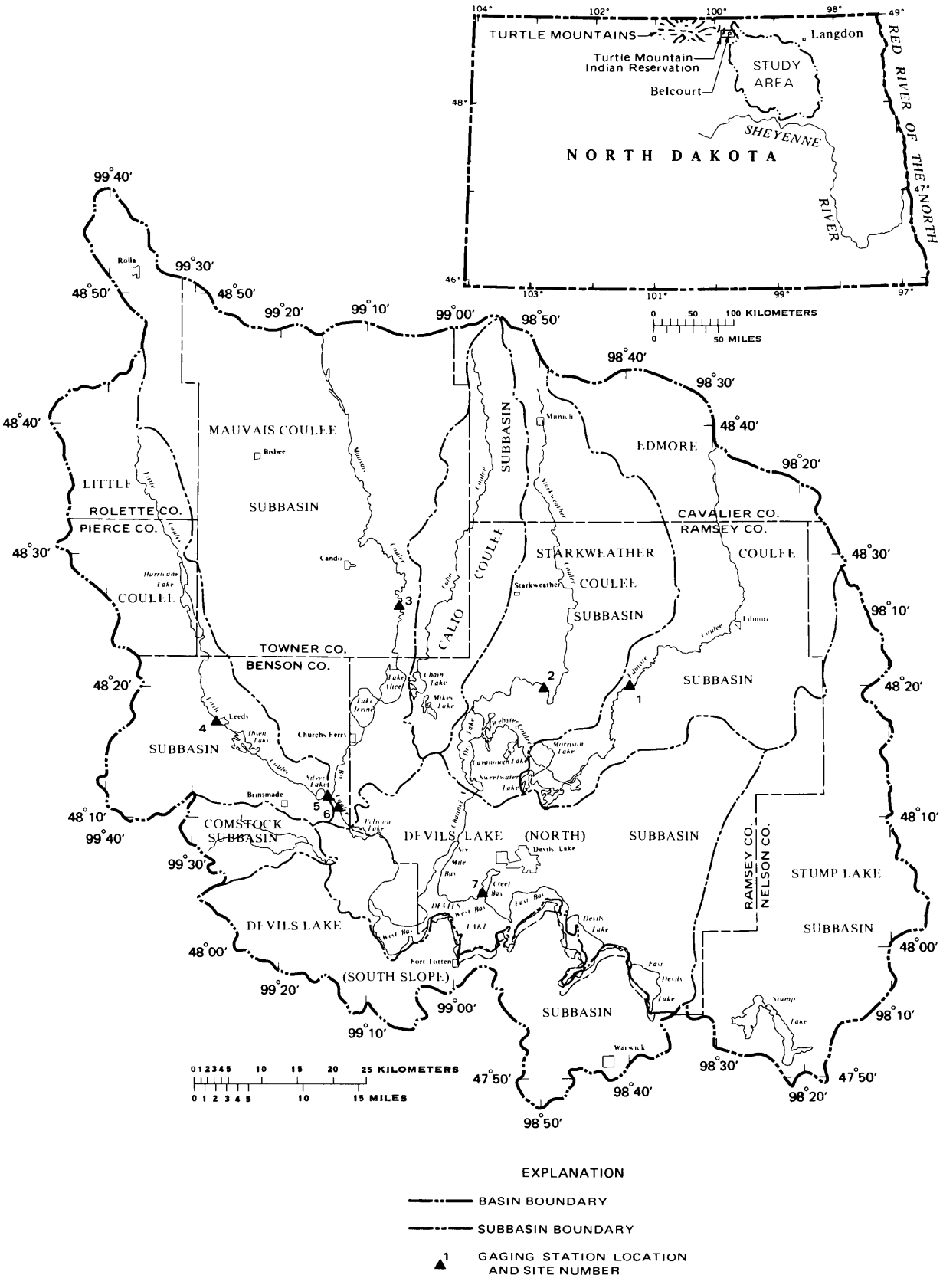


**Figure 1.** Devils Lake basin.

**Table 1.** Drainage areas of subbasins in the Devils Lake basin

[Modified from Devils Lake Basin Advisory Committee, 1976; —, no data]

| Subbasin | Drainage area ($km^2$) | | |
|---|---|---|---|
| | Contributing[1] | Non-contributing[1] | Total |
| Edmore Coulee | 1,008 | 290 | 1,298 |
| Starkweather Coulee | 754 | [2]259 | [3]1,013 |
| Calio Coulee | 603 | — | [3]603 |
| Mauvais Coulee | 2,258 | 26 | 2,284 |
| Little Coulee | 681 | 409 | 1,090 |
| Comstock | 150 | — | [3]150 |
| Devils Lake (north) | 1,326 | — | [3]1,326 |
| Devils Lake (south slope) | 850 | — | [3]850 |
| Stump Lake | 1,264 | — | [3]1,264 |

[1]Contributing and noncontributing drainage areas are based on current conditions. Unusually large quantities of precipitation or runoff could cause some noncontributing areas to contribute runoff temporarily; similarly, unusually dry conditions may decrease the drainage area that would contribute runoff during normal conditions.

[2]The noncontributing drainage area within the subbasin of Starkweather Coulee was not determined by the Devils Lake Basin Advisory Committee (1976). The noncontributing area indicated was estimated for this investigation.

[3]The contributing and noncontributing drainage areas have not been determined for the subbasin.

Coulee. The later peak on Big Coulee is caused by the relatively long traveltime of the flow passing through the interconnected chain of lakes upstream of the Big Coulee near Churchs Ferry gage.

The large differences between the mean and median monthly discharges (table 3) indicate that the monthly discharge distribution is skewed substantially. The mean discharge is a result of a relatively few high-flow events. The mean and median discharges for October through February at the Edmore and Mauvais Coulee gages indicate that little discharge ever occurs during the winter. Apparently there is little ground-water contribution in the Edmore and Mauvais Coulee drainages.

The monthly flow statistics (table 3) indicate that lakes upstream from Devils Lake affect the timing and quantity of discharge that passes the Big Coulee gage. A mass-balance approach was used to estimate the quantity of discharge passing the Big Coulee gage. The annual discharge for the period of record for five gaging stations is listed in table 4. The annual discharge at the Starkweather Coulee gage from 1957 through 1979 was estimated by adding the average annual runoff at the Edmore Coulee gage and the Mauvais Coulee gage, dividing the sum by 2, and then multiplying the quotient by the contributing drainage area at the Starkweather Coulee near Webster gage.

Of the contributing drainage area of the Big Coulee near Churchs Ferry gage, about 36 percent (1,700 $km^2$) is from Edmore Coulee near Edmore and Mauvais Coulee near Cando; 12 percent is from Starkweather Coulee near Webster; and 10 percent is from Little Coulee near Brinsmade. Thus, 58 percent of the contributing drainage area upstream from the Big Coulee gage is gaged.

A conservative estimate of the losses in lakes upstream of the Big Coulee gage was made by subtracting the sum of the annual discharge recorded at the four gages upstream from the Big Coulee gage from the annual discharge recorded at the Big Coulee gage (table 4). A negative number in the gain or loss column indicates more discharge flowed past the upstream gages than arrived at the Big Coulee gage. A positive number indicates an increase in discharge at the Big Coulee gage.

The chain of lakes upstream from Devils Lake provides substantial storage capacity in many years. From 1965 through 1967, the upstream lakes provided at least 138 $hm^3$ of storage. The water going into storage eventually is removed from the upstream lakes by evaporation and any ground-water seepage that might occur. To illustrate the effect of this upstream storage, the level of Devils Lake was computed as if the storage was not available for 1965–67. The maximum water level of Devils Lake in 1967 would have been 432.72 m above NGVD of 1929 instead of 430.65 m if the upstream storage had not been available from 1965 through 1967. Therefore, the water level without upstream storage would have been 2.1 m higher than the recorded water level of Devils Lake. For illustrative purposes, the assumption was made that the increase in net evaporation from Devils Lake would be equal to the inflow from the 42 percent of the ungaged drainage area not included in the storage estimate. If discharge records were available for all contributing drainage areas upstream from the Big Coulee near Churchs Ferry gage, the losses from, or storage in, the upstream lakes probably would be larger in most years (larger negative values and smaller positive values).

## Temporal Variability of Inflow to and Outflow From Devils Lake

A water-balance model was used to estimate the variability of inflow to Devils Lake for time periods ranging from 1 month to 10 yr or more. The following water-balance model was used:

$$Q_I = S_C + (E_{LS}A_{LS}) - (P_{LS}A_{LS}) - G \quad (1)$$

where

$Q_I$=surface-water inflow to Devils Lake, in cubic hectometers;

$S_C$=storage change, in cubic hectometers;

$E_{LS}$=evaporation from the lake surface, in meters;

$A_{LS}$=lake-surface area, in hectares;

$P_{LS}$=precipitation falling on the lake surface, in meters; and

$G$=ground-water inflow to the lake, in meters.

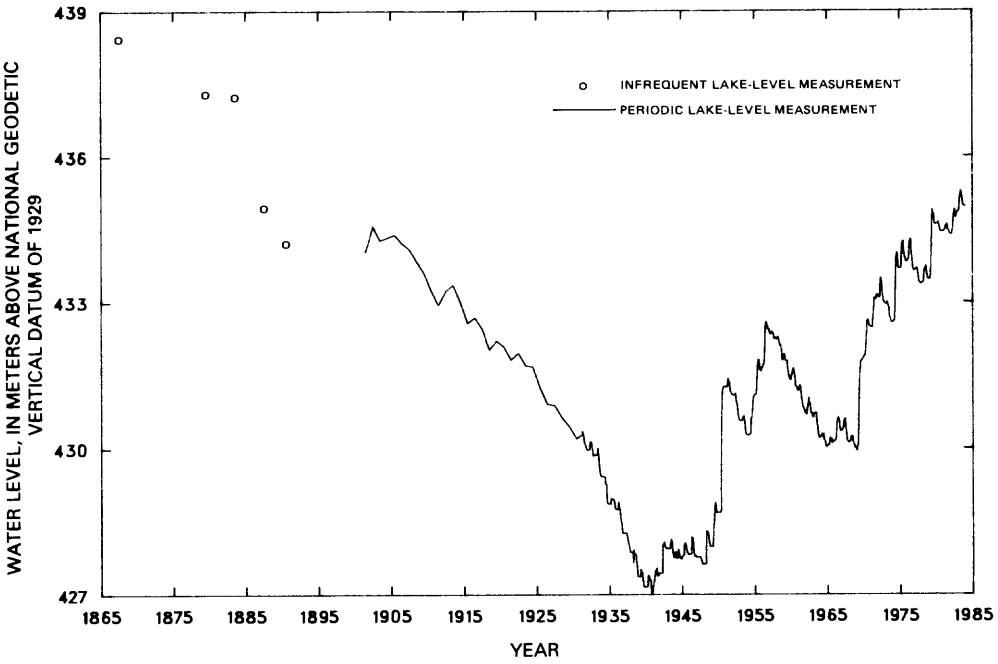


**Figure 2.** Historic water levels for Devils Lake, 1867–1983.

**Table 2.** Drainage areas and period of record for gaging stations in the Devils Lake basin

| Site number | Station name | Drainage area ($km^2$) | | Period of record |
|---|---|---|---|---|
| | | Contributing | Noncontributing | |
| 1 | Edmore Coulee near Edmore. | 730 | 259 | Apr. 1956 to June 1956, June 1957–83 |
| 2 | Starkweather Coulee near Webster. | 803 | 259 | Oct. 1979–83 |
| 3 | Mauvais Coulee near Cando. | 976 | 26 | May 1956–83 |
| 4 | Little Coulee at Leeds. | 363 | 363 | Oct. 1955–73 |
| 5 | Little Coulee near Brinsmade. | 492 | 414 | Oct. 1975–83 |
| 6 | Big Coulee near Churchs Ferry. | 4,714 | 1,787 | Mar. 1950–83 |

The inflow ($Q_I$) enters Devils Lake in three ways: (1) inflow through Big Coulee (the major tributary to Devils Lake), (2) inflow through channel A, and (3) inflow from the 1,326-$km^2$ drainage area surrounding Devils Lake. The 850-$km^2$ Devils Lake south slope drainage subbasin is comprised of numerous small closed drainage basins. These closed drainage basins have no defined drainage network and, thus, contribute no runoff to Devils Lake. In this study, inflow from the Devils Lake south slope drainage subbasin to Devils Lake was assumed to be zero.

The combination of the dynamic processes described in equation 1 results in fluctuations in water levels from month to month and year to year. An annual hydrologic model can be outlined as follows: (1) During late fall the water level in Devils Lake declines to a minimum and remains relatively constant from freezeup until spring thaw. (2) Snowmelt and rain in March-May produce runoff from the basin into Devils Lake. The maximum water level occurs in April or May in drier years and June or July in wetter years. (3) Sometime in April through July, outflow (primarily evaporation) exceeds the inflow, and the water level starts to decline to a minimum in late fall or early winter. Then the cycle is repeated. Deviations from the annual hydrologic model undoubtedly occur.

The terms "net storage gain" and "net storage loss" have a specific meaning in this report. Net storage gain is used to denote the change in storage volume between the fall or winter minimum water level and the following spring or summer maximum water level; this storage change represents the excess of inflow compared to other subtractions. Conversely, the net storage loss is defined as the change in storage volume between the seasonal maximum water level and the succeeding seasonal minimum.

An attempt was made to compute the annual net storage gain to and the annual net storage loss from Devils Lake (tables 5 and 6) by using equation 1. Net storage gain was substituted for inflow ($Q_I$) in equation 1. Annual net storage gain is equal to the capacity of the lake at maximum water level minus the capacity of the lake at minimum water level. The precipitation ($P_{LS}$) falling on the lake surface and the evaporation ($E_{LS}$) from the lake surface are assumed to be equal between the time that the minimum water level and the maximum water level were recorded. The ground-water

**Table 3.** Monthly flow statistics, in cubic meters per second, for selected gaging stations in the Devils Lake basin

| Month | Station name | | | | | |
|---|---|---|---|---|---|---|
| | Edmore Coulee | | Mauvais Coulee | | Big Coulee | |
| | Mean | Median | Mean | Median | Mean | Median |
| January | 0 | 0 | 0 | 0 | 0.03 | 0 |
| February | .01 | 0 | .01 | 0 | .02 | 0 |
| March | .38 | 0 | .44 | 0 | .11 | .02 |
| April | 2.77 | 2.31 | 3.85 | 1.8 | 2.25 | .72 |
| May | .84 | .25 | 1.35 | .38 | 4.59 | 1.03 |
| June | .18 | .04 | .28 | .08 | 3.31 | .74 |
| July | .15 | 0 | .21 | .02 | 2.02 | .16 |
| August | .14 | 0 | .11 | .01 | .89 | .01 |
| September | .01 | 0 | .12 | 0 | .37 | .01 |
| October | .01 | 0 | .05 | 0 | .25 | .01 |
| November | .01 | 0 | .03 | 0 | .19 | .01 |
| December | 0 | 0 | .01 | 0 | .08 | 0 |

contribution (*G*) was assumed to be negligible. Thus, the net storage gain is equal to the storage change (*SC*) in equation 1. No net storage gain or loss was computed for the years prior to 1931 because water-level measurements were too infrequent to determine the minimum water level prior to spring breakup.

The conceptual model does not fit in some years. As an example, in the dry years of 1934, 1935, and 1937, there is no net storage gain to Devils Lake. In these years, the water level either remained unchanged or actually declined. Thus, in these dry years of the 1930's, the inflow to Devils Lake plus the precipitation falling on the lake apparently always was less than the evaporation from the lake surface.

The net storage loss was computed by subtracting the capacity of Devils Lake at its seasonal minimum water level from the capacity of the lake at the preceding seasonal maximum water level. The assumption was made that precipitation falling on the lake surface and evaporation from the lake surface are equal between the time the minimum and maximum water levels are recorded. Also, the assumption was made that losses to ground water are negligible. The net storage loss from Devils Lake has not been as variable as the net storage gain to the lake. From 1931 through 1969, the net storage loss ranged from zero in 1950, 1954, and 1969 to 41.6 $hm^3$ in 1952 (table 6). Since 1969, the net storage loss has averaged about 66.4 $hm^3$ per year. The large increase in net storage loss since 1969 primarily is the result of the large increase in the surface area of Devils Lake during the 1970's.

The water-balance model also was used to estimate the variability of inflow to Devils Lake that has occurred during 10- to 20-yr intervals. Equation 1 was used along with the following assumptions: (1) The average precipitation recorded at the city of Devils Lake is representative of the precipitation falling on Devils Lake, (2) the average evaporation from shallow ponds and lakes (U.S. Department of Commerce, 1959) is representative of the evaporation from the surface of Devils Lake, (3) the average surface area of Devils Lake for the period was computed using the average water level for the period, and (4) the total storage change that occurred during the period was assumed to occur in equal increments during the period.

Undoubtedly, there are uncertainties in these assumptions, but an analysis of how errors in the assumptions would affect the water-balance variables was outside the scope of this study. A comprehensive discussion of the errors associated with the variables used to estimate the water balance of lakes can be found in a report by Winter (1981).

Inflow from 1867 through 1884 and from 1931 through 1940 was computed by using equation 1. The years 1867–84 represent a wet period that had the highest sustained lake levels for the period of record (1867–1983). The years 1931–40 represent a dry period that had the lowest sustained lake levels. Although the selection of the wet and dry periods is subjective, the inflow computed for each period indicates the large differences in runoff that occurred in the Devils Lake basin for 10 yr or more. The water-balance equations for the two periods are listed in table 7. It is interesting to note that an average annual inflow of 71.9 $hm^3$ to Devils Lake from 1867 through 1884 occurred during a period of declining water levels. This occurs in part because the evaporative draft is a function of the surface area of the lake, and the surface area from 1867 through 1884 was much greater than the surface area from 1931 through 1940.

The inflow to Devils Lake for the more recent period of rising water levels (1969–83, fig. 2) can be compared to the relatively wet and dry periods listed in table 7. Annual net storage gain to Devils Lake averaged 86.3 $hm^3$ from 1969 through 1983 as compared to an average annual inflow of 71.9 $hm^3$ from 1867 through 1884. Average annual net storage gain of 86.3 $hm^3$ for 1969 through 1983

**Table 4.** Annual discharge at gaging stations in the Devils Lake basin

[The gain or loss (−) is equal to the discharge of Big Coulee minus the sum of the discharge of Mauvais Coulee, Little Coulee, Edmore Coulee, and Starkweather Coulee; —, no data]

| Calendar year | Discharge ($hm^3$) | | | | | Gain or loss ($hm^3$) |
|---|---|---|---|---|---|---|
| | Edmore Coulee | Starkweather Coulee | Mauvais Coulee | Little Coulee | Big Coulee | |
| 1956 | — | — | 9.38 | 9.38 | 69.79 | — |
| 1957 | 0.036 | 0.13 | .40 | — | .69 | 0.124 |
| 1958 | .005 | .014 | .045 | 0 | .060 | −.004 |
| 1959 | 1.23 | .52 | .22 | 0 | .091 | −1.88 |
| 1960 | 11.18 | 7.41 | 14.30 | .69 | .35 | −33.23 |
| 1961 | .18 | .070 | .004 | 0 | .002 | −.25 |
| 1962 | 9.58 | 4.75 | 4.24 | .80 | .73 | −18.64 |
| 1963 | 7.98 | 2.98 | .028 | 0 | .14 | −10.85 |
| 1964 | 3.23 | 1.88 | 2.39 | .35 | .13 | −7.72 |
| 1965 | 8.09 | 11.01 | 28.73 | 1.12 | 1.62 | −47.33 |
| 1966 | 30.09 | 15.54 | 15.41 | 6.63 | 18.00 | −45.67 |
| 1967 | 35.51 | 16.40 | 11.44 | — | 18.25 | −45.10 |
| 1968 | 1.03 | 2.06 | 6.02 | — | .48 | −8.63 |
| 1969 | 17.02 | 21.21 | 53.39 | — | 123.30 | 31.68 |
| 1970 | 4.51 | 10.27 | 30.82 | — | 72.99 | 27.39 |
| 1971 | 17.51 | 16.15 | 34.65 | — | 95.44 | 27.13 |
| 1972 | 16.28 | 12.58 | 23.43 | — | 58.08 | 5.79 |
| 1973 | .74 | .44 | .60 | — | 2.58 | .80 |
| 1974 | 42.54 | 33.66 | 63.99 | — | 197.77 | 57.58 |
| 1975 | 9.19 | 9.05 | 20.22 | — | 68.06 | 29.60 |
| 1976 | 8.29 | 13.07 | 35.88 | 7.86 | 65.23 | .13 |
| 1977 | .26 | .115 | .065 | .005 | 2.64 | 2.19 |
| 1978 | 13.81 | 7.02 | 6.71 | .035 | 30.70 | 3.12 |
| 1979[1] | 32.55 | 27.62 | 55.73 | 31.94 | [2]281.00 | 133.16 |
| 1980 | 1.65 | 1.38 | 2.76 | .17 | [3]2.66 | — |
| 1981 | 5.92 | 5.30 | 11.12 | 1.53 | [3].28 | — |
| 1982 | 18.74 | 13.07 | 21.95 | 2.37 | [3]42.66 | — |
| 1983 | 14.06 | 9.53 | 15.41 | 4.94 | [3]35.63 | — |

[1]Construction of channel A completed, and channel A put into operation.

[2]Discharge conveyed in channel A was 66.88 $hm^3$.

[3]Discharge conveyed in channel A was unknown; therefore, gain or loss is not given.

is greater than the total net storage gain of 55.8 $hm^3$ for the drought years of 1931 through 1940 (table 5).

## ESTIMATES OF FUTURE LAKE LEVELS

### Exceedance Probabilities of Net Storage Gains

Although problems are encountered when trying to predict the probability of a future lake level, it is possible to assign a probability to a given water-level rise if the starting water level has been determined. As an example, the annual exceedance probability is plotted against the water-level rise for three starting water levels in figure 3. The exceedance probability for a given water-level rise was obtained by first computing the exceedance probability for the net storage gains listed in table 5 and then converting the net storage gains value to a water-level rise by using the water-level-capacity table for the desired starting water level.

The exceedance probability for a given net storage gain to Devils Lake was computed by using the procedures outlined by the U.S. Water Resources Council (1981). The recommended technique for fitting a log-Pearson Type-III distribution to the annual net storage gain is to compute the base-10 logarithms of the net storage gain, $Q$, at the selected exceedance probability, $P$, by the equation:

$$\text{Log } Q = X + KS, \tag{2}$$

where

$X$=mean,

$K$=a factor that is a function of the skew coefficient and the selected exceedance probability, and

$S$=standard deviation.

The station skew coefficient was used because the map-skew and the weighted-skew options are based on peak discharge and not on net storage gain. The final exceedance probabilities plotted in figure 3 were adjusted for the 5 yr out of the 55 yr when the net storage gain was 0 based on procedures described by the U.S. Water Resources Council (1981).

Analysis of figure 3 indicates that, the lower the starting water level of Devils Lake, the greater the water-

**Table 5.** Annual net storage gain to Devils Lake

[After examining the water-level records to obtain the minimum water level before spring breakup and then obtaining the maximum water level after spring breakup, net storage gain was computed by subtracting the capacity of the lake at minimum water level from the capacity of the lake at maximum water level; —, no data]

| Yr | Net storage gain ($hm^3$) | Yr | Net storage gain ($hm^3$) |
|---|---|---|---|
| 1931 | 3.08 | 1961 | 1.36 |
| 1932 | 16.5 | 1962 | 22.8 |
| 1933 | 7.52 | 1963 | 2.34 |
| 1934 | — | 1964 | 4.44 |
| 1935 | — | 1965 | 9.00 |
| 1936 | 6.17 | 1966 | 33.2 |
| 1937 | — | 1967 | 20.2 |
| 1938 | 8.88 | 1968 | 9.00 |
| 1939 | 5.92 | 1969 | 109.7 |
| 1940 | 7.65 | 1970 | 68.5 |
| 1941 | 19.0 | 1971 | 78.7 |
| 1942 | 22.0 | 1972 | 44.4 |
| 1943 | 8.63 | 1973 | 1.60 |
| 1944 | 9.87 | 1974 | 187.5 |
| 1945 | 9.87 | 1975 | 80.2 |
| 1946 | 15.3 | 1976 | 73.3 |
| 1947 | .99 | 1977 | 7.40 |
| 1948 | 24.7 | 1978 | 33.2 |
| 1949 | 37.0 | 1979 | 306.0 |
| 1950 | 135.7 | 1980 | 19.5 |
| 1951 | 8.63 | 1981 | 38.1 |
| 1952 | 2.71 | 1982 | 118.0 |
| 1953 | 11.2 | 1983 | 128.4 |
| 1954 | 56.9 | | |
| 1955 | 34.7 | | |
| 1956 | 78.2 | | |
| 1957 | 8.14 | | |
| 1958 | — | | |
| 1959 | — | | |
| 1960 | 10.1 | | |

**Table 6.** Annual net storage loss from Devils Lake

[After examining the water-level records to obtain the maximum water level after spring breakup and the minimum water level at winter freezeup, net storage loss was computed by subtracting the capacity of the lake at minimum water level from the capacity of the lake at maximum water level]

| Yr | Net storage loss ($hm^3$) | Yr | Net storage loss ($hm^3$) |
|---|---|---|---|
| 1931 | 18.1 | 1961 | 33.3 |
| 1932 | 22.6 | 1962 | 31.9 |
| 1933 | 27.4 | 1963 | 37.0 |
| 1934 | 22.2 | 1964 | 15.4 |
| 1935 | 8.63 | 1965 | 9.25 |
| 1936 | 25.9 | 1966 | 22.4 |
| 1937 | 15.5 | 1967 | 32.4 |
| 1938 | 18.7 | 1968 | 15.4 |
| 1939 | 11.5 | 1969 | 0 |
| 1940 | 13.1 | 1970 | 26.8 |
| 1941 | 5.92 | 1971 | 22.3 |
| 1942 | 6.17 | 1972 | 89.6 |
| 1943 | 14.6 | 1973 | 66.4 |
| 1944 | 7.89 | 1974 | 70.9 |
| 1945 | 9.87 | 1975 | 78.1 |
| 1946 | 18.2 | 1976 | 133.2 |
| 1947 | 5.92 | 1977 | 72.9 |
| 1948 | 12.3 | 1978 | 59.2 |
| 1949 | 9.87 | 1979 | 80.3 |
| 1950 | 0 | 1980 | 64.0 |
| 1951 | 16.6 | 1981 | 50.8 |
| 1952 | 41.6 | 1982 | 47.2 |
| 1953 | 29.4 | 1983 | 67.7 |
| 1954 | 0 | | |
| 1955 | 17.6 | | |
| 1956 | 22.2 | | |
| 1957 | 14.7 | | |
| 1958 | 35.3 | | |
| 1959 | 32.1 | | |
| 1960 | 23.6 | | |

level rise that will occur for any given exceedance probability. As an example, a net storage gain of 89.1 $hm^3$ has an exceedance probability of 10 percent (10-yr return period) in any given year. This net storage gain would result in a 1.22-m water-level rise if Devils Lake is at a starting water level of 429.8 m above NGVD of 1929, but the water-level rise would be only 0.37 m if the starting water level is 435.9 m above NGVD of 1929. The net storage gain of 306 $hm^3$ in 1979 was the largest net storage gain from 1931 through 1984 and has an exceedance probability of 1.8 percent (return period of about 56 yr).

## Water-Balance Model

### Conceptual Design

A monthly water-balance model was developed, based on equation 1, that accounts for the gains and losses in discharge that occur as water moves through the chain of lakes upstream from Devils Lake. The monthly water-balance model operates on monthly values of inflow, precipitation, and evaporation. Monthly values of inflow available at gaging stations in the different subbasins were adjusted, by using drainage-area ratio techniques to account for the intervening drainage area in a basin downstream of the monthly gage. Comparison of recorded and simulated monthly water levels indicates that the simulated monthly water levels may be distorted because excess water above the spill elevation is assumed to immediately discharge. Thus, the model does not lag the outflows as would reservoir routing.

Discharge from Edmore Coulee is added to the capacity of Sweetwater and Morrison Lakes. The precipitation falling on a lake surface is added, and the evaporation from a lake surface is subtracted from the capacity of a lake. Sweetwater and Morrison Lakes are treated as a combined lake in the water-balance model. The spill elevation of

**Table 7.** Computed water-balance equations for Devils Lake for 1867 through 1884 and for 1931 through 1940

| Period | Annual average ($hm^3$) | | | | | | |
|---|---|---|---|---|---|---|---|
| | Storage change | | Inflow | | Precipitation | | Outflow |
| 1867–84 | −25.6 | = | 71.9 | + | 143.9 | − | 241.4 |
| 1931–40 | −13.4 | = | 3.5 | + | 15.5 | − | 32.4 |

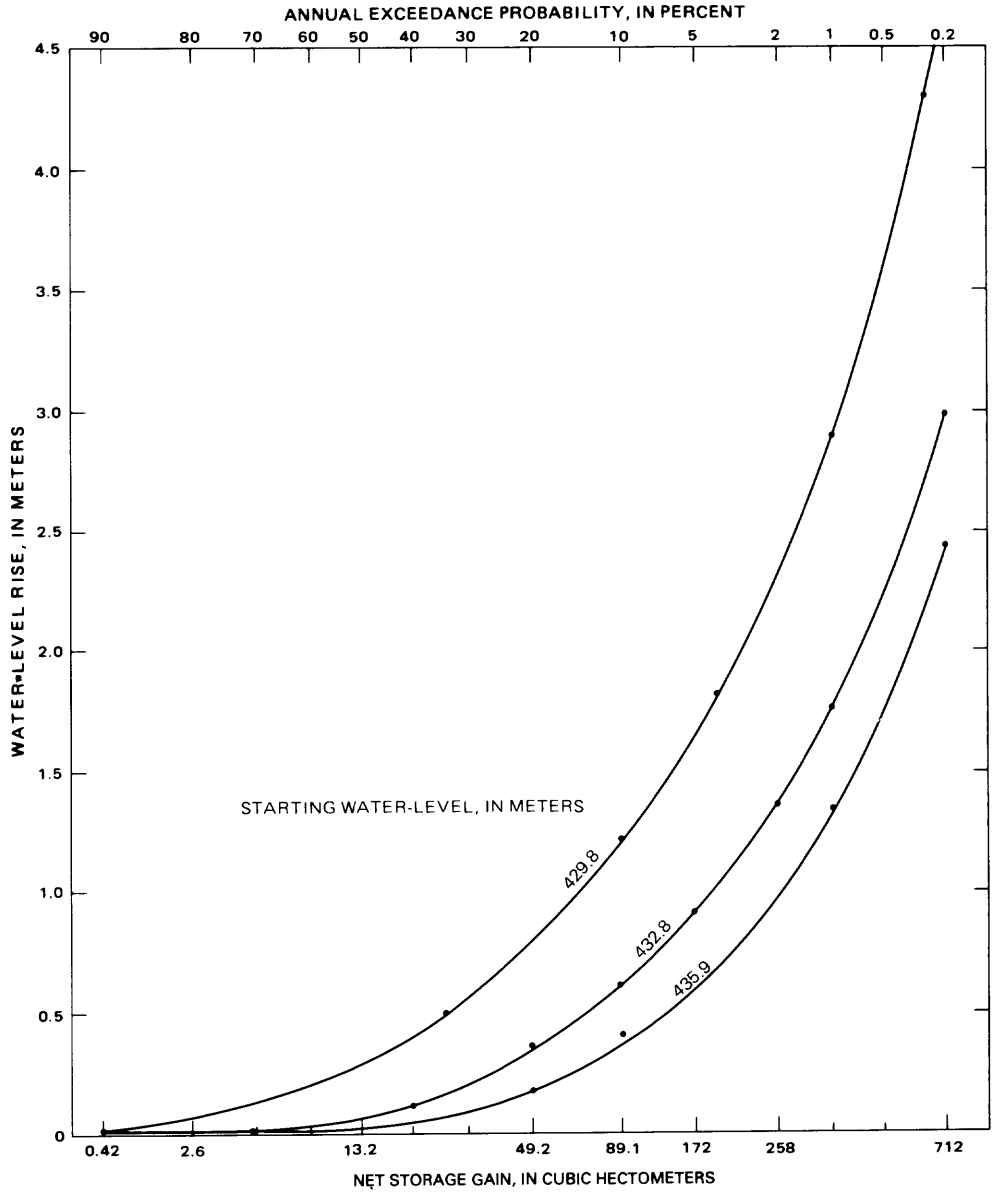


**Figure 3.** Relation between the annual exceedance probabilities of net storage gains and water-level rise of Devils Lake.

Morrison Lake into Webster Coulee is about 444.55 m above NGVD of 1929. If the capacity of the lake at the end of the month is above the spill-elevation capacity, the difference is treated as outflow from Sweetwater and Morrison Lakes to Webster Coulee.

Dry Lake receives inflow from Webster Coulee and Starkweather Coulee in addition to precipitation falling on the lake surface. Water is lost to the atmosphere by evaporation. If the capacity of Dry Lake at the end of the month is greater than the capacity of Dry Lake at the spill

elevation, then all excess water is treated as outflow to channel A. The operating criteria for the control structure that regulates the water level of Dry Lake were incorporated into the water-balance model. From October through April, the spill elevation of Dry Lake is set at 440.4 m above NGVD of 1929, and from May through September the spill elevation is set at 441.20 m above NGVD of 1929.

Chain Lake receives inflow from Mikes Lake, Calio Coulee, and precipitation falling on the lake surface. Water is removed from Chain Lake through evaporation. All water in Chain Lake above the spill elevation of 439.2 m above NGVD of 1929 is released to Lake Alice.

Lake Alice receives inflow from Chain Lake, Mauvais Coulee, and precipitation falling on the lake surface. In 1968, the U.S. Fish and Wildlife Service constructed a control structure in the channel between Lake Alice and Lake Irvine that allows them to control the water level of Lake Alice. The sill elevation of the control structure is about 437.69 m above NGVD of 1929, and the outlet elevation from Lake Irvine to Big Coulee is 438.79 m above NGVD of 1929. From November through April the gates at the control structure are open, and Lake Alice and Lake Irvine virtually are one lake. Thus, when the gates are open, the water-balance model treats the lakes as a combined lake with a uniform water level. From May through October the gates are closed, and the water level for Lake Alice is held at 439.52 m above NGVD of 1929. Thus, separate lake levels are computed from May through October in the water-balance model. In November the gates are open, and Lake Alice and Lake Irvine operate as a combined lake in the water-balance model.

Inflow enters Lake Alice-Lake Irvine via Chain Lake and Mauvais Coulee. From May through October flow from Lake Alice to Lake Irvine occurs only during months when the computed water level is greater than 439.52 m above NGVD of 1929. From May through October flow out of Lake Irvine occurs when the computed water level is greater than 438.79 m above NGVD of 1929. From November through April outflow from Lake Irvine-Lake Alice occurs whenever the computed water level is greater than 438.79 m above NGVD of 1929.

Three tributaries, channel A, Big Coulee, and an unnamed tributary draining the Comstock subbasin, provide most of the inflow to Devils Lake. A small quantity of inflow probably enters Devils Lake from the Devils Lake north subbasin adjacent to Devils Lake (fig. 1). Precipitation falling on the lake surface is treated as an inflow in the water-balance model. Evaporation from Devils Lake is the only way that water can be removed from Devils Lake. No accounting is made for ground-water inflow or outflow from Devils Lake in the water-balance model. Therefore, a declining lake level can occur only when evaporation from the lake exceeds inflows to Devils Lake plus precipitation falling on the lake surface.

### Analysis of Simulations

The water-balance model requires, as input, monthly precipitation, evaporation, and discharge. Monthly precipitation, lake-evaporation, and discharge values were used as inputs to the water-balance model to simulate monthly water levels of Devils Lake from 1968 through 1983. The water-balance model was validated by comparing the computed water levels to the recorded water levels. The recorded water level of Devils Lake of 430.15 m above NGVD of 1929 was used as the initial water level in the simulation. Estimates of initial water levels for the upstream chain of lakes were based on the water levels at freezeup in 1984. No monthly water levels were simulated prior to 1968 because hydraulic changes in the upstream chain of lakes cannot be determined with any degree of certainty.

Comparison of the simulated water levels and the recorded water levels is shown in figure 4, and in general there is good agreement between the simulated and recorded water levels. Maximum deviation between the simulated and the recorded water level occurs in April 1969 when the simulated water level is 1.58 m greater than the recorded water level. This relatively large difference between the computed and recorded water level is caused by the inability of the water-balance model to account for traveltime required for flow to pass through the upstream chain of lakes. By August 1969 the simulated water level is 0.15 m greater than the recorded water level. The annual maximum deviation between the simulated and recorded water level occurs in April or May when the simulated water level usually is greater than the recorded water level. The maximum simulated water level of 435.28 m above NGVD of 1929 occurred in April 1983, and the maximum recorded water level of 435.28 m above NGVD of 1929 occurred in June 1983. Based on this comparison, no further model validation was considered necessary. Although many assumptions have been made regarding model inputs, the water-balance model seems to provide reasonable results.

The water-balance model was used to simulate possible water-level fluctuations for two different sets of input data; a high-runoff or wet condition and a low-runoff or dry condition. Water levels for the high-runoff condition were simulated from January 1985 through December 1990 by using the monthly values of precipitation, lake evaporation, and discharge from 1974 through 1979. The recorded water level of 434.68 m above NGVD of 1929 in January 1985 was used as the initial water level for the high-runoff simulation. Thus, the simulated water levels of Devils Lake are based on the assumption that the precipitation, lake evaporation, and the discharge will have the same timing and magnitude from 1985 through 1990 as that which occurred from 1974 through 1979.

Based on the computed net storage gain to Devils Lake (table 6), 1974–79 has the greatest 6-yr net storage

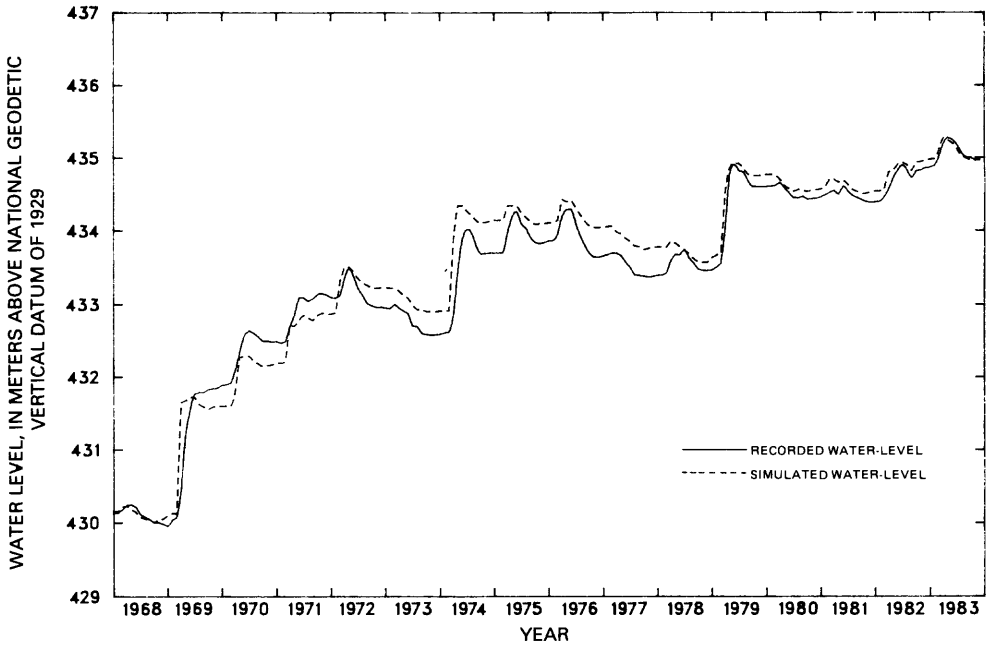


**Figure 4.** Monthly recorded and simulated water levels of Devils Lake, 1968–83.

gain for the period of record, 1931 through 1983. Total net storage gain for 1974–79 was 687.6 $hm^3$, or 115 $hm^3$ per year. The annual precipitation at Devils Lake was 404 mm in 1974, 437 mm in 1975, 330 mm in 1976, 554 mm in 1977, and 363 mm in 1979 (U.S. Department of Commerce, National Oceanic and Atmospheric Administration, Environmental Data Service, 1975–80). The computed lake evaporation is 719 mm/yr for the period.

The maximum simulated water level of 436.30 m above NGVD of 1929 would occur in April of 1987, and after a decline in water levels in 1988 and 1989 a secondary peak of 436.14 m above NGVD of 1929 would occur in June of 1990 (fig. 5). There is about a 1.6-m difference between the initial water level of Devils Lake and the maximum water level for this simulation. The maximum difference of the recorded water levels between 1974 and 1979 is 2.4 m. The recorded water level in January of 1974 is about 1.5 m lower than the initial water level used for the high-runoff simulation. Therefore, the volume of water needed to increase the water level of Devils Lake for a given increment is greater for the high-runoff simulation than for the recorded water levels of 1974 through 1979.

The low-runoff condition was simulated by using the monthly values of precipitation, lake evaporation, and discharge from 1958 through 1963. Total net storage gain from 1958 through 1963 was 36.6 $hm^3$. The annual precipitation at Devils Lake averaged 399 mm during this period as compared to normal precipitation of 420 mm (U.S. Department of Commerce, National Oceanic and Atmospheric Administration, Environmental Data Service, 1959–64, and 1982). The computed annual lake evaporation for this period is 730 mm.

Total net storage gain from 1933 through 1938 was 22.6 $hm^3$. The annual precipitation at Devils Lake averaged 351 mm during this period (U.S. Department of Agriculture, Weather Bureau, 1934–39). Although 1933 through 1938 probably represents a more extreme low-runoff condition than the period 1958 through 1963, no gaging stations were in operation in the Devils Lake basin; thus, all discharges needed as input for the water-balance model would have to be synthesized. Therefore, data limitations associated with 1933 through 1938 were used to eliminate this period for selection as the low-runoff condition.

Water levels for the low-runoff simulation are plotted in figure 5. There generally would be a steady decline in water levels from 1985 through 1990, although a minor increase in water levels would occur in the spring of 1987 and 1989. The simulated water level would decline 1.65 m from 434.68 m above NGVD of 1929 in January of 1985 to 433.04 m above NGVD of 1929 in October of 1990. Based on recorded water levels, Devils Lake declined 2.0 m from January 1950 through December 1963.

## CONCLUSIONS

Discharge data collected in the Devils Lake basin were analyzed by using statistical and graphical techniques in order to gain a better understanding of the hydrologic factors affecting the water-level fluctuations of Devils Lake. The monthly flow statistics indicate that the chain of

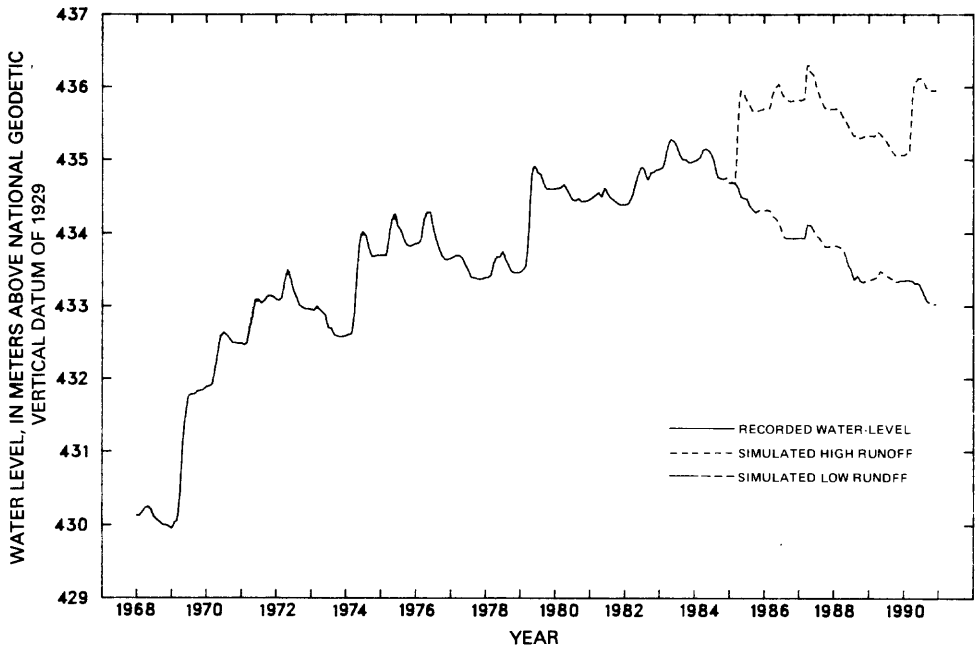


**Figure 5.** Recorded water levels, 1968–84, and simulated water levels of Devils Lake, 1985–90.

lakes upstream from Devils Lake affects the timing and quantity of discharge that passes the Big Coulee gage about 5 mi upstream from Devils Lake. The maximum mean monthly discharge of coulees that are tributary to the upstream chain of lakes, such as Edmore Coulee and Mauvais Coulee, occurs in April followed by relatively rapid decrease in mean monthly discharge. The maximum mean discharge on Big Coulee occurs in May, followed by a gradual decrease in mean monthly discharge as water drains out of the chain of lakes. The upstream chain of lakes has enough storage capacity that they significantly decrease the discharge that reaches Devils Lake. For example, 138 $hm^3$ of water was stored and subsequently evaporated in the upstream lakes from 1965 through 1967. Large variations in inflow to Devils Lake have occurred in periods of 10 yr or more. For example, the total net storage gain to Devils Lake during 1931–40 was 55.8 $hm^3$; however, based on water-balance computations, total inflow during 1867–84 was 1,290 $hm^3$. During 1969–83 the total net storage gain also was 1,290 $hm^3$.

The exceedance probability for a given water-level rise was computed by first developing the exceedance probability for the net storage gains and then converting the net storage gain value to a water-level rise based on the starting water level of Devils Lake. The analysis indicates that, the higher the starting water level, the lower the associated water-level rise for a given net storage gain. As an example, a net storage gain of 89.1 $hm^3$ has an exceedance probability of 10 percent, and this gain results in a 1.22-m water-level rise if Devils Lake is at a starting water level of 429.8 m above NGVD of 1929, but the water-level rise is only 0.37 m if the starting water level is 435.9 m above NGVD of 1929.

A water-balance model was developed that accounts for the gains and losses in discharge that occur as water moves through the chain of lakes upstream from Devils Lake. Monthly values of precipitation, lake evaporation, and discharge were used to simulate a high-runoff and low-runoff condition from 1985 through 1990. Inputs to the water-balance model for the high-runoff simulation were based on hydrologic and climatologic data recorded from 1974 through 1979. Under the high-runoff conditions the maximum water-level of 436.30 m above NGVD of 1929 would occur in April 1987. The low-runoff simulation was based on hydrologic and climatologic data recorded from 1958 through 1963. Under the low-runoff simulation the water level of Devils Lake generally would decline steadily from 434.68 m above NGVD of 1929 in January 1985 to 433.04 m above NGVD of 1929 in August 1990.

## REFERENCES CITED

Aronow, Saul, 1955, Problems in late Pleistocene and Recent history of the Devils Lake region, North Dakota: Madison, University of Wisconsin, unpub. Ph.D. dissertation, 125 p.

———1957, On the postglacial history of the Devils Lake region, North Dakota: Journal of Geology, v. 65, no. 4, p. 410–427.

Brooks, C.E.P., 1951, Geological and historical aspects of climatic change, *in* Malone, T.F., ed., Compendium of meter-

ology: Boston, American Meterological Society, p. 1004–1018.
Callender, Edward, 1968, The postglacial sedimentology of Devils Lake, North Dakota: Grand Forks, University of North Dakota, unpub. Ph.D. dissertation, 312 p.
de Martonne, Emmanuel, 1927, Regions of interior-basin drainage: The Geographic Review, v. 27, 411 p.
Devils Lake Basin Advisory Committee, 1976, The Devils Lake basin study: Bismarck, North Dakota, v. 1, 235 p.
North Dakota State Engineer, 1944, Fourth biennial report of State Water Commission and 21st biennial report of State Engineer of North Dakota: p. 1661–1872.
U.S. Army Corps of Engineers, 1984, Reconnaissance report—Devils Lake Basin, North Dakota: St. Paul, Minnesota, 31 p.
U.S. Department of Agriculture, Weather Bureau, 1934–39, Climatological data, North Dakota, annual summaries 1933–38: v. 42–47, no. 15.
U.S. Department of Commerce, 1959, Evaporation maps for the United States: U.S. Department of Commerce Technical Paper 37, pl. 3.
U.S. Department of Commerce, National Oceanic and Atmospheric Administration, Environmental Data Service, 1959–64, 1975–80, Climatological data, North Dakota, annual summaries 1958–63, 1974–79: Asheville, North Carolina.
U.S. Water Resources Council, 1981, Guidelines for determining flood flow frequency: Washington, D.C., Hydrology Committee Bulletin 17B, 28 p.
Upham, Warren, 1895, The glacial Lake Agassiz: U.S. Geological Survey Monograph no. 25, 658 p.
Wahl, E.W., 1968, A comparison of the climate of the eastern United States during the 1830's with the current normals: Monthly Weather Review, v. 96, no. 2, p. 73–82.
Winter, T.C., 1981, Uncertainties in estimating the water balance of lakes: Water Resources Bulletin, v. 17, no. 1, p. 82–115.

# Geochemical Indicators Used to Determine Source of Saline Water in Mesozoic Aquifers, Montezuma Canyon Area, Utah

*By* Briant A. Kimball

**Abstract**

Saline water occurs in samples of water from the Navajo Sandstone, which is part of the middle Mesozoic aquifer, in the Montezuma Canyon area, Utah, where water in the aquifer usually is fresh. This saline water may result from natural vertical leakage of brine from the underlying middle Paleozoic aquifer or from injection of oil-field brine.

Three hydrochemical facies determined by Q-mode factor analysis are identified: (1) recharge water, (2) diagenetic water that has evolved from the recharge water through chemical reactions, and (3) saline water resulting from mixing between diagenetic water and a brine. Major changes in hydrochemical facies and isotopic composition of the water indicate that the source of the saline water may be the middle Paleozoic aquifer. Sulfur-34 values in the aquifer vary from about −10 to +10 per mil, progressively approaching the value of +12.4 per mil found in salts of the Paradox Member of the Hermosa Formation. Deuterium and oxygen-18 also indicate mixing of local recharge water with deeper basin waters.

However, no saline water occurs in the upper Paleozoic aquifer, even though the water chemistry probably would be affected by upward leakage of brine from the middle Paleozoic aquifer to the middle Mesozoic aquifer. Also, hydraulic-head data indicate downward movement of water in Paleozoic rocks; these data suggest that injection of oil-field brine is the source of the saline water in the Navajo Sandstone.

## INTRODUCTION

In ground-water systems, changes in water chemistry usually are steady-state changes (Berner, 1980; Plummer and others, 1983). This hypothesis assumes that the chemistry of ground water systematically changes, as a result of chemical and physical processes, as it moves along a flow path at constant flow rates. As water flows past a particular point in the flow path, the water usually acquires the same chemistry as water that was at that same point at an earlier time. A flow-path model offers the possibility to investigate water-rock interactions and to identify processes that alter and control water chemistry in an aquifer.

Aquifers of the Upper Colorado River basin have been investigated as part of the Regional Aquifer-System Analysis (RASA) program of the U.S. Geological Survey (Taylor and others, 1983). Areas of relatively saline water have been identified in the Navajo Sandstone, part of the middle Mesozoic aquifer (Freethey and others, 1984). Normally, dissolved-solids concentrations in water from this aquifer are less than 1,000 mg/L. Possible causes of the saline water include (1) dissolution of evaporite minerals in the Carmel Formation of Jurassic age, which overlies the Navajo Sandstone; (2) upward leakage of brine from underlying Paleozoic rocks; (3) water-rock interactions within the Navajo Sandstone; or (4) injection of oil-field produced brine. The occurrence of this saline water provides an opportunity to investigate the geochemical processes along a flow path.

The purpose of this paper is to present geochemical evidence about the source of the saline water in the Navajo Sandstone. In developing this evidence, the use of two geochemical models is illustrated. The first model is a computer program, called SNORM (Bodine and Jones, 1986), that recasts water-quality analyses into normative salt percentages. The use of SNORM has been combined with a second, multivariate statistical model, extended Q-mode factor analysis (Miesch, 1976), that defines principal hydrochemical facies and quantifies the percentage of each of these facies in each sample.

Twenty ground-water samples, representative of the middle Mesozoic aquifer, collected near the flow path were used in the geochemical-facies analysis. Twelve additional samples of water from wells completed in the Navajo and Entrada Sandstones were collected along a flow path that trends to the south in the area of Montezuma Canyon, Utah (fig. 1). Chemical determinations included major ions, trace elements, and isotopes of carbon, sulfur, oxygen, and hydrogen. A total of 32 sites represent a vertical profile through three formations (Wingate, Navajo, and Entrada

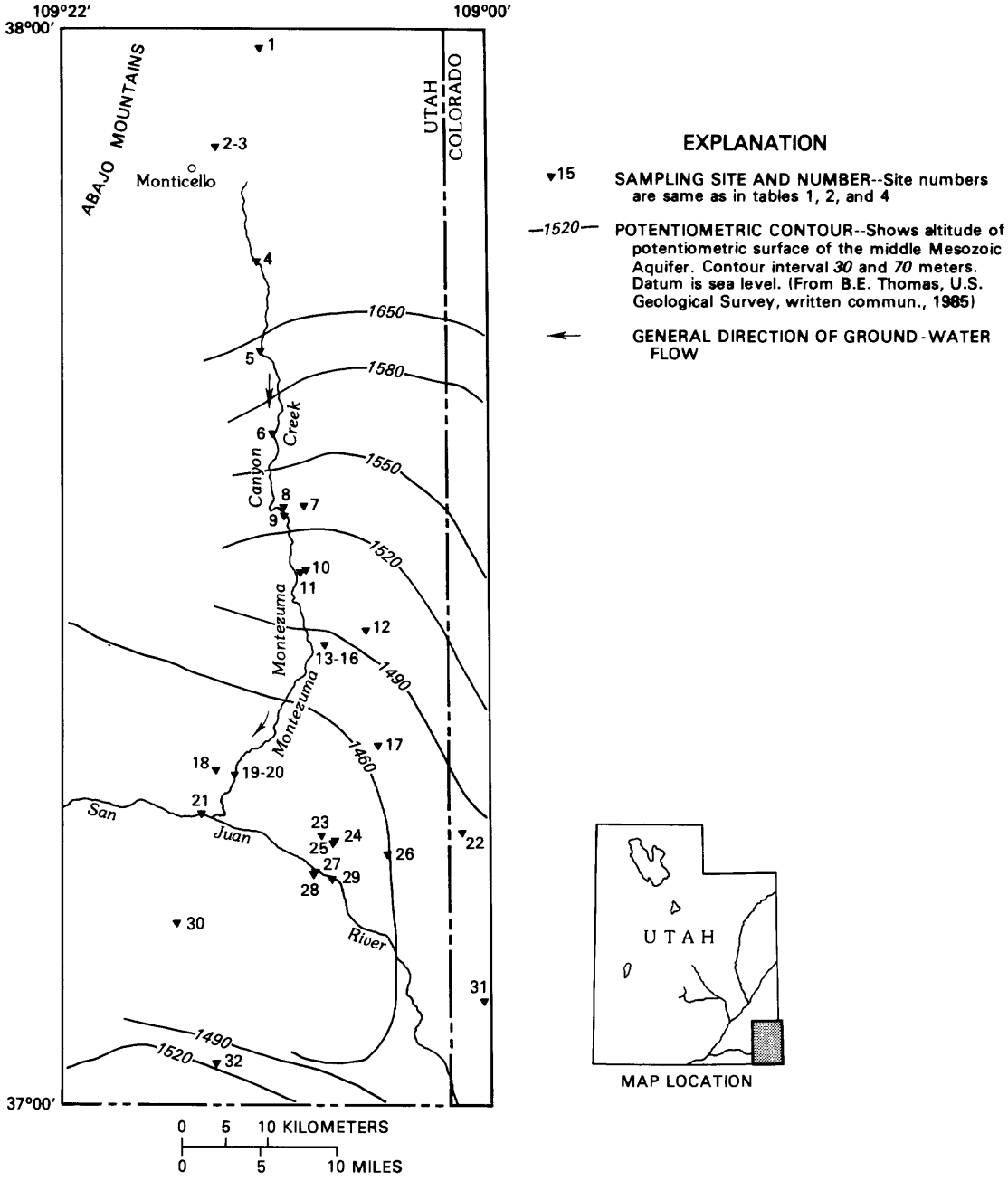


**Figure 1.** Location of sampling sites and altitude of potentiometric surface of the middle Mesozoic aquifer.

Sandstones) that are part of the middle Mesozoic aquifer along the flow path. Chemical analyses of the 32 samples collected from the 32 sites are presented in table 1. Three samples are identified as belonging to the Glen Canyon Group. This means the wells are open to both the Wingate and Navajo Sandstones, or that neither formation was identified.

Results of the trace-element and isotope determinations of samples collected for this study are given in table 2. Isotope determinations are presented in the delta notation [$\delta$, using per mil (‰) units] (Fritz and Fontes, 1980, p. 4–19), except for carbon-14 and tritium. Carbon-14 is presented as percent modern carbon-14. This age determination indicates a relative age, when converted to years before present. Corrections have not been applied to the analytical values of carbon-14 to obtain absolute ages, but the reported values probably indicate relative ages (Kimball, 1984).

**Table 1.** Chemical determinations

[Site number, relative position along the flow path (fig. 1); site numbers with asterisk indicate samples collected for this study. Lat, latitude, in decimal degrees; Long, longitude, in decimal degrees. Unit, geologic formation sampled: 221ENRD, Entrada Sandstone, 220GLCN, Glen Canyon Group undivided; 220NVJO, Navajo Sandstone of Glen Canyon Group; 231WNGT, Wingate Sandstone of Glen Canyon Group. T, °C, temperature in degrees Celsius; DS, dissolved solids; Ca, calcium; Mg, magnesium; Na, sodium; K, potassium; Cl, chloride; $SO_4$, sulfate; Alk, titration alkalinity as $CaCO_3$; $SiO_2$, silica; --, not determined]

| Site number | Lat | Long | Unit | pH (units) | T (°C) | Major ions, in milligrams per liter | | | | | | | | |
|---|---|---|---|---|---|---|---|---|---|---|---|---|---|---|
| | | | | | | DS | Ca | Mg | Na | K | Cl | $SO_4$ | Alk | $SiO_2$ |
| 1 | 37.9819 | 109.267 | 231WNGT | 8.60 | 16.0 | 765 | 7.9 | 3.5 | 280 | 6.7 | 12.0 | 150.0 | 495 | 5.8 |
| 2 | 37.8911 | 109.320 | 221ENRD | 8.80 | 15.5 | 816 | 6.2 | 5.6 | 301 | 5.1 | 7.5 | 130.0 | 544 | 21.0 |
| 3 | 37.8911 | 109.320 | 220NVJO | 8.50 | 20.0 | 329 | 37.0 | 18.0 | 57 | -- | 4.0 | 48.0 | 235 | 19.0 |
| 4* | 37.7833 | 109.271 | 220NVJO | 7.59 | 14.5 | 506 | 61.0 | 33.0 | 71 | 6.4 | 22.0 | 130.0 | 281 | 11.0 |
| 5* | 37.7000 | 109.267 | 220NVJO | 7.50 | 14.5 | 480 | 48.0 | 50.0 | 67 | 9.6 | 6.4 | 77.0 | 363 | 5.5 |
| 6* | 37.6233 | 109.252 | 220NVJO | 7.89 | 15.1 | 281 | 26.0 | 16.0 | 57 | 4.5 | 3.5 | 31.0 | 218 | 9.5 |
| 7 | 37.5564 | 109.216 | 221ENRD | -- | -- | 510 | 15.0 | 4.8 | 161 | 15.0 | 26.0 | 80.0 | 310 | -- |
| 8 | 37.5553 | 109.240 | 221ENRD | 7.50 | 17.0 | 351 | 19.0 | 10.0 | 86 | 20.0 | 13.0 | 52.0 | 235 | 9.3 |
| 9* | 37.5472 | 109.239 | 220NVJO | 8.02 | 15.6 | 419 | 14.0 | 7.7 | 130 | 15.0 | 15.0 | 51.0 | 290 | 9.1 |
| 10* | 37.4964 | 109.213 | 221ENRD | 8.30 | 17.3 | 361 | 6.2 | 2.6 | 120 | 9.6 | 10.0 | 54.0 | 243 | 9.1 |
| 11 | 37.4942 | 109.220 | 221ENRD | -- | -- | 380 | 5.8 | 3.4 | 122 | 3.9 | 13.0 | 58.0 | 261 | -- |
| 12* | 37.4411 | 109.144 | 220NVJO | 8.04 | 18.6 | 713 | 6.7 | 2.7 | 260 | 13.0 | 57.0 | 62.0 | 494 | 8.8 |
| 13 | 37.4280 | 109.191 | 220GLCN | 8.25 | -- | 785 | 20.0 | 6.7 | 276 | 19.0 | 38.0 | 99.0 | 542 | 12.0 |
| 14 | 37.4280 | 109.191 | 221ENRD | 7.93 | 15.3 | 486 | 18.0 | 9.2 | 146 | 21.0 | 10.0 | 55.0 | 363 | 10.0 |
| 15* | 37.4278 | 109.193 | 221ENRD | 7.81 | 19.8 | 500 | 13.0 | 7.0 | 160 | 21.0 | 5.6 | 56.0 | 372 | 9.0 |
| 16* | 37.4275 | 109.193 | 220NVJO | 7.99 | 19.3 | 1,010 | 11.0 | 4.0 | 360 | 16.0 | 190.0 | 110.0 | 504 | 10.0 |
| 17 | 37.3352 | 109.130 | 220NVJO | 7.70 | 18.8 | 10,400 | 172.0 | 77.0 | 3,470 | 61.0 | 3,040.0 | 2,940.0 | 1,060 | 12.0 |
| 18 | 37.3120 | 109.320 | 221ENRD | 7.50 | 21.0 | 362 | 30.0 | 20.0 | 80 | -- | 4.0 | 48.0 | 274 | 13.0 |
| 19* | 37.3083 | 109.297 | 220NVJO | 7.70 | 15.6 | 2,440 | 27.0 | 10.0 | 850 | 18.0 | 760.0 | 300.0 | 754 | 10.0 |
| 20* | 37.3083 | 109.297 | 220NVJO | 7.56 | 15.6 | 2,460 | 28.0 | 11.0 | 880 | 17.0 | 720.0 | 300.0 | 805 | 6.7 |
| 21 | 37.2720 | 109.337 | 221ENRD | 7.60 | -- | 7,350 | 224.0 | 136.0 | 2,210 | -- | 2,110.0 | 2,330.0 | 512 | 11.0 |
| 22 | 37.2550 | 109.033 | 221ENRD | -- | 20.2 | 11,600 | 167.0 | 45.0 | 3,770 | .0 | 2,100.0 | 5,280.0 | 410 | .0 |
| 23 | 37.2519 | 109.195 | 220GLCN | 7.80 | -- | 3,820 | 30.0 | 5.8 | 1,160 | -- | 581.0 | 675.0 | 1,110 | -- |
| 24* | 37.2486 | 109.180 | 220NVJO | 7.55 | 19.0 | 3,030 | 30.0 | 13.0 | 1,000 | 16.0 | 760.0 | 690.0 | 839 | 10.0 |
| 25 | 37.2453 | 109.182 | 220GLCN | 7.60 | 20.0 | 3,090 | 35.0 | 13.0 | 1,100 | 15.0 | 680.0 | 710.0 | 868 | 12.0 |
| 26* | 37.2342 | 109.120 | 221ENRD | 8.40 | 19.0 | 2,150 | 4.3 | 3.0 | 750 | 4.6 | 100.0 | 820.0 | 741 | 8.0 |
| 27 | 37.2178 | 109.201 | 220NVJO | 7.90 | -- | 7,080 | 85.0 | 41.0 | 2,510 | -- | 2,810.0 | 1,360.0 | 448 | 10.0 |
| 28 | 37.2159 | 109.203 | 220NVJO | 7.75 | -- | 7,360 | 112.0 | 44.0 | 2,590 | -- | 3,020.0 | 1,250.0 | 504 | 7.5 |
| 29 | 37.2102 | 109.184 | 220GLCN | 7.90 | 18.5 | 8,220 | 105.0 | 74.0 | 2,940 | 28.0 | 3,500.0 | 1,640.0 | 564 | 10.0 |
| 30 | 37.1695 | 109.366 | 220NVJO | 9.00 | 16.5 | 500 | 1.3 | .7 | 195 | .8 | 21.0 | 52.0 | 355 | 14.0 |
| 31 | 37.0992 | 109.009 | 221ENRD | -- | -- | 4,690 | 22.0 | 11.0 | 1,590 | 8.1 | 920.0 | 1,910.0 | 340 | .0 |
| 32 | 37.0405 | 109.319 | 231WNGT | -- | 19.0 | 404 | 2.0 | 1.3 | 161 | -- | 5.0 | 9.5 | 337 | 17.0 |

**Table 2.** Trace-element and isotope determinations

[Site number, relative position along the flow path (fig. 1); only sites sampled for this study are included in the table. Unit, geologic formation sampled; 221ENRD, Entrada Sandstone; 220NVJO, Navajo Sandstone; Al, aluminum; Ba, barium; B, boron; Br, bromide; Fe, iron; Li, lithium; Mn, manganese; Sr, strontium; Zn, zinc; $\delta^{13}C$, del carbon-13 ratio, in per mil; $^{14}C$, carbon-14 activity in percent modern carbon; $\delta^{34}S$, del sulfur-34 ratio, in per mil; $\delta^{18}O$, del oxygen-18, in per mil; δD, del deuterium, in per mil; TU, tritium activity, in tritium units; --, not determined]

| Site number | Unit | (Micrograms per liter) Al | Ba | B | Br | Fe | Li | Mn | Sr | Zn | $\delta^{13}C$ | $^{14}C$ | $\delta^{34}S$ | $\delta^{18}O$ | δD | TU |
|---|---|---|---|---|---|---|---|---|---|---|---|---|---|---|---|---|
| 4 | 220NVJO | < 10 | 49 | 60 | 47 | 62 | 85 | 250 | 2,700 | 19 | -9.0 | 40.2 | -10.5 | -14.5 | -107.0 | 18 |
| 5 | 220NVJO | < 10 | 65 | 50 | 15 | 26 | 85 | 150 | 3,800 | 24 | -6.2 | 6.6 | -7.8 | -15.1 | -111.0 | 5 |
| 6 | 220NVJO | < 10 | 66 | 90 | 10 | 53 | 55 | 21 | 1,900 | 110 | -8.2 | 5.9 | -11.4 | -14.5 | -114.0 | 3 |
| 9 | 220NVJO | 20 | 66 | 410 | 25 | 62 | 330 | 15 | 1,200 | 13 | -7.2 | 1.8 | -4.6 | -15.7 | -117.0 | 2 |
| 10 | 221ENRD | < 10 | 50 | 510 | 10 | 20 | 240 | 8 | 470 | 10 | -6.0 | 3.4 | -9.5 | -16.0 | -119.0 | 3 |
| 12 | 220NVJO | < 10 | 64 | 850 | 88 | 42 | 480 | 8 | 620 | 5 | -6.0 | 1.8 | - .2 | -15.4 | -114.0 | 3 |
| 15 | 221ENRD | < 10 | 56 | 460 | 24 | 4 | 300 | 9 | 1,100 | 6 | -6.1 | 5.0 | -3.5 | -14.7 | -111.0 | 2 |
| 16 | 220NVJO | < 10 | 38 | 650 | 550 | 86 | 560 | 8 | 2 | 54 | -5.7 | 1.6 | .0 | -15.0 | -112.0 | < 1 |
| 19 | 220NVJO | < 10 | 100 | 1,400 | 1,900 | 470 | 1,100 | 20 | 3,100 | 20 | -4.9 | .9 | 9.7 | -14.6 | -110.0 | 2 |
| 24 | 220NVJO | 20 | 100 | 160 | 330 | 1,600 | 820 | 50 | 3,800 | 40 | -5.4 | .8 | 6.1 | -13.3 | -104.0 | < 1 |
| 26 | 221ENRD | 30 | 100 | 350 | 84 | 70 | 490 | 20 | 640 | 10 | -4.9 | -- | 6.1 | -13.5 | - 98.5 | < 1 |

## SNORM Model

Back (1966) advanced the concept of hydrochemical facies in terms of percentages of milliequivalents of cations and anions. Many genetic relations and evolutionary trends in water chemistry can be described by changes in hydrochemical facies. A new approach to identifying hydrochemical facies has been used for this study. Hydrochemical facies are identified in terms of normative salts, rather than in terms of dominant, unassociated cations and anions. A normative salt composition represents a unique salt assemblage that would result if the given water were evaporated to dryness at 25 °C, 1 atmosphere (atm) total pressure, and atmospheric carbon-dioxide pressure; that is, at earth-surface conditions. In calculating this normative-salt assemblage, the cations and anions of the solution are quantitatively associated in the salt minerals. A computer model, SNORM, has been used to recast the chemical compositions of water samples into normative-salt compositions (Bodine and Jones, 1986).

Normative salts can be recast into 12 simple salts for the statistical model and for describing hydrochemical facies. These 12 simple salts include the alkaline-earth (calcium and magnesium) and alkali (sodium and potassium) salts of carbonate, sulfate, and chloride. To make reacting or equivalent concentrations the same for each simple salt, the sodium and potassium salts of chloride are doubled, as with $Na_2Cl_2$. Each simple salt then has a cation charge of 2. Hydrochemical facies can be described in terms of the principal simple salts that they contain, such as a $CaCO_3$ water or a $Na_2CO_3$ water. Changes among the simple-salt compositions along the flow path indicate changes in the hydrochemical facies that in turn, indicate processes affecting the water chemistry.

## Q-mode Factor Analysis

Mixing of different water types can be compared to petrologic mixing of end-member rock compositions. However, for water compositions, end members usually are called hydrochemical facies, with a characteristic chemistry that results from the sum of geochemical processes that have produced that chemistry. For example, weathering of a particular rock type can produce a distinct chemical character (Garrels, 1975). For water sampled along a flow path, end members likely will represent stages in the geochemical evolution of the water.

Factor analysis has been used in many geologic applications. The mathematics and theory of factor analysis, with references to many studies, are discussed by Joreskog and others (1976). Briefly, when water analyses are expressed as percentages of simple salts, the percentage of each simple salt gives a direction to a data vector. Each composition has a direction and magnitude that can be compared to other compositions by using the cosine of the angle between their data vectors. Similar compositions have similar directions, and the cosine approaches 1. This result is analogous to a correlation coefficient, but it is a comparison among individual sample compositions, rather than among variables. A matrix of these cosines has been called a cosine-theta matrix, or a similarity matrix.

Q-mode factor analysis uses the principal components of the similarity matrix to calculate factors that represent the major water types. Generally, for a large set of samples, only a few factors are needed to describe the dominant types of water, thereby expressing the variability among the samples as a much smaller number of descriptive end members. These end members are related to the major hydrochemical facies and represent reactions with particular solute-source minerals, or they may be the result of geochemical processes, like mineral precipitation or sulfate reduction. Each sample is related to the end member by a loading on the factor.

An extended Q-mode factor analysis model has been developed by Miesch (1976). When compositional data sum to a constant value, like 100 percent for the simple salts, factor loadings can be transformed to percentages of end-member compositions. This transformation can help classify samples, indicate changes in hydrochemical facies along flow paths, and quantify mixing proportions of characteristic water types. Q-mode factor analysis, without the extended model, will produce misleading results if it is done on data that sum to a constant value, because of forced correlations.

## CHEMICAL CHARACTER OF WATER IN THE HYDROGEOLOGIC UNITS

The geology and structure of the Paradox Basin have been described by Ohlen and McIntyre (1965). A more detailed description of the Montezuma Canyon area has been given by Huff and Lesure (1965). The rocks have been grouped into seven hydrogeologic units, including four aquifer units and three confining units (B.E. Thomas, U.S. Geological Survey, written commun., 1985). The hydrogeologic units of importance and the geologic formations comprising them are detailed in table 3. The table also diagrammatically indicates the dissolved-solids concentrations and the chemical character of water in the units. Chemical data have not been given here for each of these units, but a summary of the salinity and general chemical character follows.

Ranges of dissolved-solids concentrations of the hydrogeologic units are compared using box plots. The box plots show the minimum, lower quartile, median, upper quartile, and maximum of the data for each unit. Distributions of dissolved-solids concentrations in water from the upper three aquifers, the Lower Cretaceous through the upper Paleozoic aquifers, generally are in the same range. However, water in the middle Paleozoic aquifer is much more saline; many samples have dissolved-solids concentrations exceeding 100,000 mg/L. Some water samples from both the Lower Cretaceous and middle Mesozoic aquifers have dissolved-solids concentrations near 10,000 mg/L. Dissolved-solids concentrations in water samples from the upper Paleozoic aquifer are less than 3,500 mg/L. Detailed geochemical interpretations are being prepared as part of the Upper Colorado River basin RASA study (Taylor and others, 1983).

The Redwall Limestone is the only geologic formation in the middle Paleozoic aquifer. Hanshaw and Hill (1969) described some geochemical aspects of the regional middle Paleozoic aquifer. The chemical composition of individual water samples from the middle Paleozoic aquifer varies from nearly pure NaCl water to a mixed $CaCl_2$-$MgCl_2$-NaCl water. The NaCl component of the water exceeds that of seawater (78 percent NaCl), indicating that the brine samples result from resolution of overlying marine salts in the upper Paleozoic confining unit (Bodine and Jones, 1986). However, the water samples also have been affected by diagenetic reactions in the aquifer.

Water samples from the upper Paleozoic confining unit have a very large percentage of NaCl and large percentages of alkaline-earth chloride components. The Paradox Member of the Hermosa Formation contains potash salts that produce this brine and affect the water quality of the underlying middle Paleozoic aquifer. The potash salts include halite, NaCl; sylvite, KCl; carnallite, $KMgCl_3 \cdot 6H_2O$; and anhydrite, $CaSO_4$ (Hite and Gere, 1958). These salts also may be the source of saline water in the middle Mesozoic aquifer. Salt anticlines have formed north of the study area (Shoemaker and others, 1958) but probably do not affect water quality in the Montezuma Canyon area.

Formations composing the upper Paleozoic aquifer in ascending order are the Cedar Mesa Sandstone Member, the De Chelly Sandstone Member or the correlative, White Rim Sandstone Member of the Cutter Formation, and the Kaibab Limestone. The chemical composition of individual water samples from the upper Paleozoic aquifer is quite different from that in samples from the two underlying units. Only slightly saline water occurs, with a small NaCl component and no $MgCl_2$ or $CaCl_2$ components. The water predominantly is a $CaSO_4$-$Na_2SO_4$ type.

**Table 3.** Summary of water quality in hydrogeologic units of the Montezuma Canyon area

[Distribution of dissolved-solids concentrations: Box plots have +, median value [, lower quartile;], upper quartile; −, extending from minimum value to lower quartile and from upper quartile to maximum value. Water-quality type: percentages of simple salts calculated from mean values of major ions]

| Hydrogeologic unit | Geologic formations | Distribution of dissolved-solids concentrations log scale | Water-quality type |
|---|---|---|---|
| Lower Cretaceous aquifers | Dakota Sandstone<br>Cedar Mesa Formation<br>Burro Canyon Formation | 100 1,000 10,000 100,000<br>------[ + ]------ | 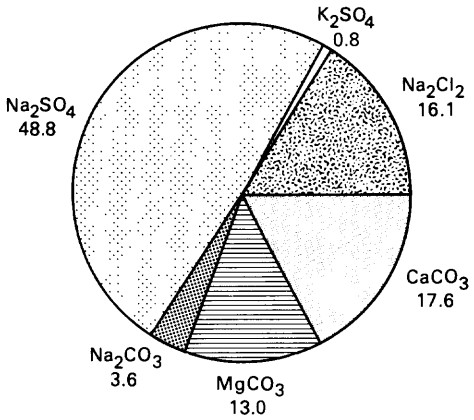 |
| Upper Jurassic confining unit | Morrison Formation<br>Bushy Basin Member<br>Salt Wash Member<br>Bluff Sandstone<br>Summerville Formation<br>Curtis Formation | 100 1,000 10,000 100,000<br>----[+ ]-- | 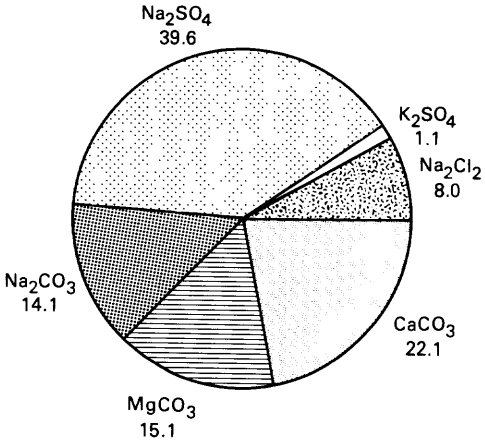 |

| | Number of samples | Minimum | Lower quartile | Median | Upper quartile | Maximum |
|---|---|---|---|---|---|---|
| Lower Cretaceous aquifers | 36 | 116 | 411 | 731 | 2,548 | 9,810 |
| Upper Jurassic confining unit | 30 | 139 | 289 | 433 | 911 | 1,920 |

**Table 3.** Summary of water quality in hydrogeologic units of the Montezuma Canyon area—Continued

| Hydrogeologic unit | Geologic formations | Distribution of dissolved-solids concentrations log scale | Water-quality type |
|---|---|---|---|
| | | 100 1,000 10,000 100,000 | |
| Middle Mesozoic aquifer | Entrada Sandstone<br>Carmel Formation<br>Navajo Sandstone<br>Kayenta Formation<br>Wingate Sandstone | ----[ + ]---------- | |
| | | Number of samples 81<br>Minimum 103<br>Lower quartile 264<br>Median 419<br>Upper quartile 946<br>Maximum 11,600 | 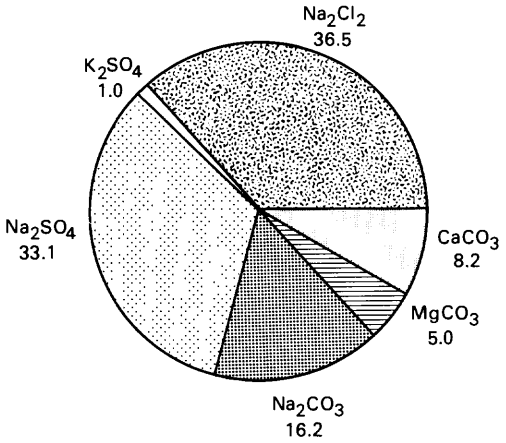 |
| | | 100 1,000 10,000 100,000 | |
| Lower Mesozoic confining unit | Chinle Shale<br>Shinarump Conglomerate Member<br>Moenkopi Formation | --+]- | |
| | | Number of samples 4<br>Minimum 218<br>Median 234<br>Maximum 471 | 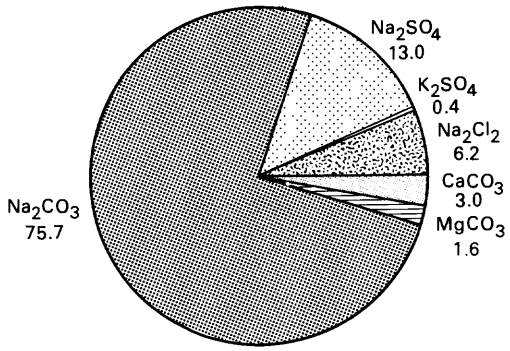 |

**Table 3.** Summary of water quality in hydrogeologic units of the Montezuma Canyon area—Continued

| Hydrogeologic unit | Geologic formations | Distribution of dissolved-solids concentrations log scale | | Water-quality type |
|---|---|---|---|---|
| | | 100 1,000 10,000 100,000 | | |
| Upper Paleozoic aquifers | Kaibab Limestone<br>White Rim Sandstone<br>De Chelly Sandstone<br>Cedar Mesa Sandstone | --[ + ]- | | |
| | | Number of samples | 8 | |
| | | Minimum | 393 | |
| | | Lower quartile | 628 | |
| | | Median | 1,095 | |
| | | Upper quartile | 2,502 | |
| | | Maximum | 3,070 | |
| | | 100 1,000 10,000 100,000 | | |
| Upper Paleozoic confining units | Organ Rock Shale<br>Halgaito Formation<br>Elephant Canyon Formation<br>Hermosa Formation<br>Honaker Trail Member<br>Paradox Member<br>Pinkerton Trail Member | ----------[ + ]-- | | |
| | | Number of samples | 34 | |
| | | Minimum | 3,180 | |
| | | Lower quartile | 66,600 | |
| | | Median | 118,000 | |
| | | Upper quartile | 212,750 | |
| | | Maximum | 308,000 | |

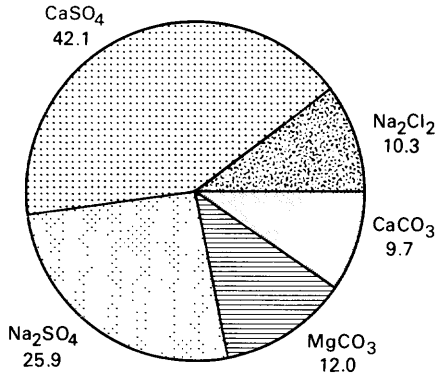


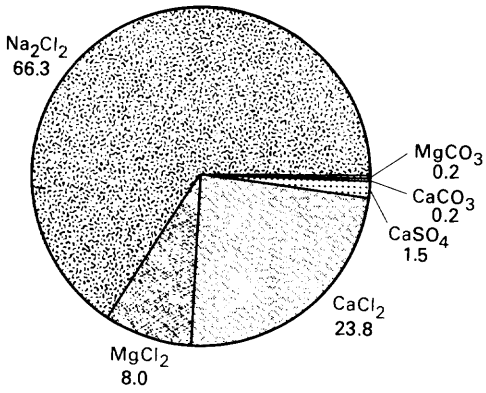

**Table 3.** Summary of water quality in hydrogeologic units of the Montezuma Canyon area—Continued

| Hydrogeologic unit | Geologic formations | Distribution of dissolved-solids concentrations log scale | Water-quality type |
|---|---|---|---|
| | | 100 1,000 10,000 100,000 | |
| Middle Paleozoic aquifer | Redwall Limestone | ----[ +--- | |
| | | Number of samples 14 | |
| | | Minimum 18,400 | |
| | | Lower quartile 54,675 | |
| | | Median 74,250 | |
| | | Upper quartile 86,975 | |
| | | Maximum 161,000 | |

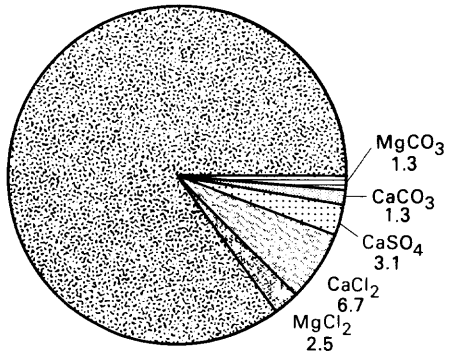


The oldest Mesozoic rocks, the Moenkopi Formation and the overlying Chinle Formation, including the Shinarump Member, form a confining unit between the upper Paleozoic aquifer and the middle Mesozoic aquifer. Only samples from the Shinarump Member were available. These indicated only dilute $NaCO_3$-$Na_2SO_4$ water in this member.

Formations composing the middle Mesozoic aquifer in ascending order are the Wingate Sandstone, the Kayenta Formation, and the Navajo Sandstone, all of the Glen Canyon Group; the Carmel Formation, a confining unit in some parts of the area; and the Entrada Sandstone. Formations in the middle Mesozoic aquifer are mostly quartz sandstone. The Navajo Sandstone in the Montezuma Canyon area is about 98 percent quartz (Huff and Lesure, 1965). The remaining minerals include orthoclase, plagioclase, chert, and calcite. Some local, cherty limestone lenses occur (Wright and Dickey, 1958, p. 173). The other sandstones have similar compositions. The Carmel Formation is mostly a sandy siltstone, loosely cemented with calcite. This formation also has a limestone facies and local beds of evaporite deposits.The chemical character of water in the middle Mesozoic aquifer shown in table 3 reflects both the dilute $CaCO_3$-$MgCO_3$-$Na_2CO_3$ water and the more concentrated NaCl-$Na_2SO_4$ water. Concentrations of dissolved solids generally increase toward the south, with a large increase in the area near the San Juan River, where some concentrations of dissolved solids are greater than 10,000 mg/L. The details of these changes are described in this report.

The Dakota Sandstone is the principal unit of the upper Mesozoic aquifer. It is separated from the middle Mesozoic aquifer by the middle Mesozoic confining unit that consists of the Wanakah Formation and Morrison Formation. The Bluff Sandstone Member at the base of the Morrison is a local aquifer within this confining unit. A considerable range in dissolved-solids concentration occurs in water from the upper middle Mesozoic confining unit and the upper Mesozoic aquifer; concentrations range from 116 to 9,810 mg/L. The more dilute water varies from a $CaCO_3$-$MgCO_3$ type to a $Na_2CO_3$ type. Water with larger dissolved-solids concentration is a NaCl-$Na_2SO_4$ type, similar to the saline water in the middle Mesozoic aquifer. A few water samples from the Dakota Sandstone contain $CaCl_2$ and $MgCl_2$ components.

## GEOCHEMICAL INDICATORS FOR DETERMINING SOURCES OF SALINE WATER

Several types of evidence have been used to identify the source of saline water in the middle Mesozoic aquifer. The geochemical indicators include variations in hydrochemical facies, trace element concentrations, and stable-isotope-ratios.

### Hydrochemical Facies

To define the hydrochemical facies, the chemical analyses in table 1 were recast into simple-salt equivalent

percentages (table 4), using the SNORM model. Simplesalt percentages indicate that general changes in chemical character of the water occur along the flow path. There is a large variation among the samples. To account for the variation, Q-mode factor analysis was used to decrease the variability of the 32 samples to 3 descriptive end-member compositions.

Factor analysis indicated that 82 percent of the variance among the samples can be described by these three end members. Only the $Na_2SO_4$ component is poorly represented; the other simple salt components are almost completely accounted for by the three end members. The chemical character of the end members is shown by pie diagrams in figure 2. Each sample can be described as a percentage of the three end members. These percentages, which are compositional loadings from the factor analysis, are reported in table 4 and are plotted in figure 2.

The first end member is a $CaCO_3$-$MgCO_3$-$Na_2SO_4$ water representing the composition of dilute recharge in the Navajo Sandstone aquifer. The second end member consists of two groups of samples, both with a $Na_2CO_3$-$Na_2SO_4$ water. The first group consists of dilute recharge samples from the Wingate and Entrada Sandstones. The second group consists of samples from the Navajo Sandstone that have changed from recharge compositions through diagenetic reactions in the aquifer. The third end member is a NaCl-$Na_2SO_4$ brine. The progression of changes along the flow path is indicated by arrows in figure 2. Generally, concentrations of dissolved solids increase in the direction of the arrows, but a few exceptions are discussed below. Chemical reactions that account for these changes are described below.

There are two types of recharge waters in the area. Samples from the Navajo and Entrada Sandstones collected at the beginning of the flow path (sites 3, 4, 5, 6, 8, 14, and 18; table 4) are predominantly composed of the $CaCO_3$-$MgCO_3$-$Na_2SO_4$ end member. This water type results from hydrolysis of calcium sodium feldspars and dissolution of carbonate minerals in the Navajo Sandstone. It appears that calcium and magnesium are acquired in nearly equal mole percentages; the $CaCO_3$ and $MgCO_3$ components are approximately equal for these samples. Carbonate cements occur in the Navajo Sandstone (Huff and Lesure, 1965), but the source of this carbonate in the water also may be the overlying Carmel Formation. Magnesium in recharge waters may come from weathering of more mafic minerals in the area of the Abajo Mountains (fig. 1). Weathering can be attributed to both $CO_2$- and $SO_2$-enriched waters. The $SO_2$ most likely comes from oxidizing pyrite and results in a $Na_2SO_4$ component. The light $\delta^{34}S$ of water near recharge areas (see table 2) indicates this sulfur source. Dissolution of gypsum, if it were present in the aquifer, would produce a $\delta^{34}S$ much heavier than this, nearer to +15 to +20 ‰, determined for marine Jurassic rocks (Holser and Kaplan, 1966).

Samples from the Wingate, Navajo, and Entrada Sandstones near the recharge area (sites 1, 7, 9, 10, 11, 14, 15, 30, and 32; table 4) also are very dilute and are composed mostly of the $Na_2CO_3$-$Na_2SO_4$ end member. The sample from the Wingate Sandstone at site 32 represents recharge flowing toward the north (see fig. 1, potentiometric surface). The difference in salt norms indicates that calcium and magnesium carbonate minerals, associated with the other recharge samples, are not present to affect dissolution reactions producing the $Na_2CO_3$-$Na_2SO_4$ water. Instead, water chemistry in these areas reflects silicate hydrolysis, enhanced by $SO_2$ weathering. In summary, the chemical character of recharge water depends on the availability of carbonate minerals during infiltration and subsequent percolation.

After water in the Navajo and Entrada Sandstones acquires solutes from dissolution of carbonate minerals, feldspars, and sulfides, the water changes from an alkaline-earth carbonate water to an alkali-carbonate water, through chemical reactions. Arrow 1 in figure 2 shows the direction of this change Thus, the water in the Navajo and Entrada Sandstones tends to become chemically similar to the $Na_2CO_3$-$Na_2SO_4$ recharge water. Precipitation of carbonate minerals in the aquifer, removing the alkaline-earth metals from solution, could cause this change. Cation exchange is another possibility, with calcium and magnesium exchanging for sodium. However, the sandstones are relatively free of clay minerals (Huff and Lesure, 1965). Sodium also is gained from the hydrolysis of alkali feldspars and probably not from cation exchange. This may be the main source of sodium in water from the Entrada Sandstone.

After obtaining a $Na_2CO_3$-$Na_2SO_4$ character, water in the Navajo and Entrada Sandstones is affected by mixing with a brine, generally having the composition of the third end member in figure 2 (indicated by arrow 2). This composition is similar to that of water in the middle Paleozoic aquifer (table 3). This is a two-component mixing between the altered or diagenetic aquifer water and the brine. The percentage of this brine end member in the samples increases substantially along the flow path.

The Navajo Sandstone generally is considered an eolian deposited sandstone (Selley, 1970, p. 52–58). Marine fluids may have circulated through the formation during later times, but subsequent subareal exposure has most likely removed any remnants of these fluids. Thus, it is not likely that there is a source of NaCl within the Navajo Sandstone.

At site 16 (table 4), the change to a NaCl-$Na_2SO_4$ water has become very significant in the Navajo Sandstone, but much less of a change occurs in the Entrada Sandstone, site 15. The change to a NaCl-$Na_2SO_4$ water in the Navajo Sandstone is accompanied by a change in the bromide concentration (table 2). Again, a much smaller increase in bromide concentration occurs in the Entrada Sandstone at

## Table 4. Simple-salt percentages

[Site number, refers to relative position along the flow path, used for reference to figure 2; numbers followed by asterisk are sites where samples were collected for this study. Unit, geologic formation sampled: 221ENRD, Entrada Sandstone; 220GLCN, Glen Canyon Group undivided; 220NVJO, Navajo Sandstone; 231WNGT, Wingate Sandstone of Glen Canyon Group; DS, mg/L, dissolved-solids concentration in milligrams per liter; End-member percentages, percent of end-member compositions; percentages less than 20 are omitted: Rech., Recharge waters; Diagen., Diagenetic waters; Brine, Brine input; --, less than 20 percent]

| Site number | Unit | DS | Simple salts, in percent equivalents | | | | | | | End-member percentages | | |
|---|---|---|---|---|---|---|---|---|---|---|---|---|
| | | | $CaCO_3$ | $MgCO_3$ | $Na_2CO_3$ | $Na_2SO_4$ | $K_2SO_4$ | $CaSO_4$ | NaCl | Rech. | Rech. Entrada; Navajo diagen. | Brine |
| 1 | 231WNGT | 765 | 3.0 | 2.2 | 69.3 | 21.6 | 1.3 | 0.0 | 2.5 | -- | 74.8 | -- |
| 2 | 221ENRD | 816 | 2.2 | 3.3 | 74.0 | 18.1 | .9 | .0 | 1.5 | -- | 79.6 | -- |
| 3 | 227NVJO | 329 | 31.8 | 25.5 | 23.8 | 16.9 | .0 | .0 | 1.9 | 58.1 | 23.7 | -- |
| 4 | 227NVJO | 506 | 32.7 | 30.1 | .0 | 27.3 | 1.8 | 1.1 | 6.9 | 61.4 | -- | 31.8 |
| 5 | 227NVJO | 480 | 24.8 | 42.6 | 13.0 | 15.2 | 2.5 | .0 | 2.0 | 65.4 | 20.6 | -- |
| 6 | 227NVJO | 281 | 24.9 | 25.3 | 35.3 | 10.4 | 2.2 | .0 | 1.9 | 48.9 | 41.7 | -- |
| 7 | 221ENRD | 510 | 8.8 | 4.6 | 58.7 | 14.9 | 4.5 | .0 | 8.5 | -- | 67.7 | -- |
| 8 | 221ENRD | 351 | 15.7 | 13.7 | 47.0 | 9.1 | 8.5 | .0 | 6.0 | 29.5 | 63.6 | -- |
| 9 | 227NVJO | 419 | 9.5 | 8.6 | 61.6 | 9.3 | 5.2 | .0 | 5.8 | -- | 71.9 | -- |
| 10 | 221ENRD | 361 | 5.2 | 3.6 | 69.0 | 13.7 | 4.1 | .0 | 4.5 | -- | 77.3 | -- |
| 11 | 221ENRD | 380 | 4.8 | 4.7 | 67.3 | 16.1 | 1.7 | .0 | 5.4 | -- | 73.0 | -- |
| 12 | 227NVJO | 713 | 2.7 | 1.8 | 72.9 | 7.3 | 2.7 | .0 | 12.5 | -- | 79.0 | -- |
| 13 | 220GLCN | 785 | 7.1 | 3.9 | 66.7 | 11.2 | 3.5 | .0 | 7.6 | -- | 74.0 | -- |
| 14 | 221ENRD | 486 | 10.5 | 8.9 | 64.3 | 6.8 | 6.3 | .0 | 3.2 | 20.7 | 75.7 | -- |
| 15 | 221ENRD | 500 | 7.4 | 6.6 | 70.9 | 7.1 | 6.2 | .0 | 1.8 | -- | 81.7 | -- |
| 16 | 227NVJO | 1010 | 3.2 | 1.9 | 51.8 | 10.5 | 2.4 | .0 | 30.1 | -- | 56.3 | 39.4 |
| 17 | 227NVJO | 10400 | 5.1 | 3.8 | 3.7 | 35.4 | .9 | .0 | 51.0 | -- | -- | 83.8 |
| 18 | 221ENRD | 362 | 22.6 | 24.8 | 35.7 | 15.1 | .0 | .0 | 1.7 | 47.5 | 36.7 | -- |
| 19 | 227NVJO | 2440 | 3.4 | 2.1 | 29.8 | 13.4 | 1.2 | .0 | 50.1 | -- | 31.1 | 65.9 |
| 20 | 227NVJO | 2460 | 3.4 | 2.2 | 32.2 | 13.6 | 1.1 | .0 | 47.6 | -- | 33.2 | 63.7 |
| 21 | 221ENRD | 7350 | .0 | 8.7 | .0 | 30.8 | .0 | 9.4 | 50.3 | -- | -- | 96.9 |
| 22 | 221ENRD | 11600 | 2.5 | 2.1 | .0 | 59.8 | .0 | 2.2 | 33.4 | -- | -- | 88.5 |
| 23 | 220GLCN | 3820 | 2.9 | .9 | 38.5 | 26.6 | .0 | .0 | 31.1 | -- | 38.6 | 59.0 |
| 24 | 227NVJO | 3030 | 3.2 | 2.3 | 26.4 | 26.4 | .9 | .0 | 40.7 | -- | 28.6 | 66.8 |
| 25 | 220GLCN | 3090 | 3.4 | 2.1 | 28.4 | 28.0 | .8 | .0 | 37.3 | -- | 30.6 | 64.6 |

Table 4. Simple-salt percentages—Continued

| Site number | Unit | DS | Simple salts, in percent equivalents | | | | | | | End-member percentages | | |
|---|---|---|---|---|---|---|---|---|---|---|---|---|
| | | | $CaCO_3$ | $MgCO_3$ | $Na_2CO_3$ | $Na_2SO_4$ | $K_2SO_4$ | $CaSO_4$ | NaCl | Rech. | Rech. Entrada; Navajo diagen. | Brine |
| 26 | 221ENRD | 2150 | .6 | .7 | 41.8 | 48.4 | .4 | .0 | 8.1 | -- | 46.0 | 50.3 |
| 27 | 227NVJO | 7080 | 3.6 | 2.9 | 1.2 | 24.3 | .0 | .0 | 68.0 | -- | -- | 96.7 |
| 28 | 227NVJO | 7360 | 4.6 | 3.0 | .8 | 21.4 | .0 | .0 | 70.2 | -- | -- | 96.7 |
| 29 | 220GLCN | 8220 | 3.5 | 4.4 | .0 | 22.9 | .5 | .2 | 68.4 | -- | -- | 94.8 |
| 30 | 227NVJO | 500 | .8 | .7 | 80.3 | 11.5 | .2 | .0 | 6.4 | -- | 85.0 | -- |
| 31 | 221ENRD | 4690 | 1.5 | 1.3 | 6.6 | 54.6 | .3 | .0 | 35.8 | -- | -- | 83.9 |
| 32 | 231WNGT | 404 | 1.4 | 1.5 | 92.3 | 2.8 | .0 | .0 | 2.0 | -- | 99.2 | -- |

site 15; such data do not indicate substantive mixing of water between the two sandstones at these sites.

Some water in the Entrada Sandstone has a $NaCl\text{-}Na_2SO_4$ character with greater concentrations of dissolved solids not only where water with this character occurs in the Navajo Sandstone but also in an area to the southeast (site 22; table 4; fig. 2). The Dakota Sandstone has an area with $NaCl\text{-}Na_2SO_4$ water directly north of the San Juan River and west of Montezuma Creek (fig. 1, samples from Les Dobson, U.S. Bureau of Land Management, written commun., 1985, not included in tables 1 and 4). If a brine were leaked upward along a fault zone, the brine would be lined up vertically in the aquifers, so that it would occur in the same location in each aquifer. The fact that the brine occurs in different geographic areas indicates that the brine is introduced by another process, and not by upward leakage along a common fault zone.

Along a steady-state flow path, in the absence of freshwater recharge, salinity is likely to increase as ground water acquires solutes from aquifer minerals. Samples from the Navajo Sandstone collected at sites 4 and 5 have concentrations of dissolved solids larger than samples collected at sites 6 and 9 (table 1). The samples from sites 4 and 5 may be along a slightly different flow path than samples from sites 6 and 9; however, the larger dissolved-solids concentration in a sample from site 4 also could be from local injection of oil-field brine. The sample from site 4 (fig. 2) appears to be along a tie line between the most dilute water and the brine hydrochemical facies. Otherwise, it would be the sample most similar in composition to the $MgCO_3\text{-}CaCO_3$ recharge water. The possibility that this sample contains some oil-field brine also is indicated by relatively larger bromide concentration (table 2). Values of carbon-13 and carbon-14 in the sample from site 4 are typical of recharge waters (Kimball, 1984, p. 277), despite the larger dissolved-solids concentration.

In the absence of mixing processes, solute ratios in dilute water determine the composition of a more saline water after geochemical evolution (Eugster and Jones, 1979; Drever, 1982, fig. 9–3). Processes that add solutes to water, such as hydration of aluminosilicates or dissolution of salts, have the same effect as evaporation on the chemical evolution of water. Chemical divides, based on solute ratios, limit the possible trends a water can follow as its chemistry evolves. Recharge water in the Navajo Sandstone characteristically has calcium to alkalinity-plus-sulfate ratios of less than 1; the equivalents of alkalinity are greater than those of sulfate. Such a water can evolve to have any major anion predominate: carbonate, sulfate, or chloride. However, mass-action controls of the concentration of calcium by carbonate and gypsum equilibria will decrease calcium concentrations as salinity increases.

The only way to obtain a calcium-enriched water from such a recharge water is through mixing with water of very different chemical composition. This mixing appears to be the means of increasing the calcium concentration in water from the Navajo Sandstone. The mole ratio of calcium to bromide virtually is constant, indicating that calcium is being added to the solution in the same ratio as

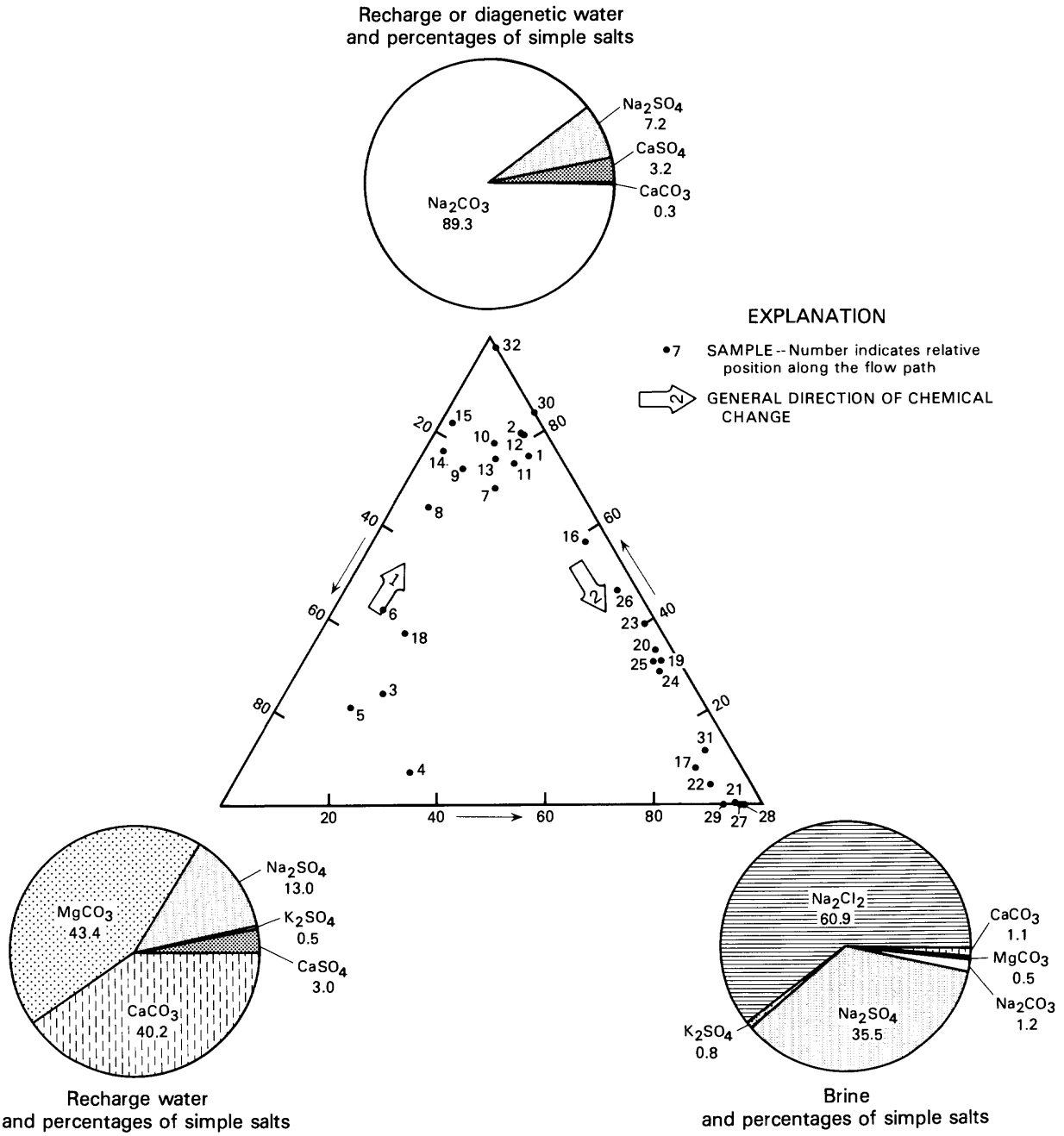


**Figure 2.** Q-mode trilinear diagram for middle Mesozoic aquifer. Compositions of end members are indicated by pie diagrams. Site numbers indicate position along flow path and are referenced to tables 1, 2, and 4.

bromide. Calcium is introduced as $CaCl_2$, which is a component of the Paleozoic brine.

The sodium-to-bromide ratio in water from the Navajo Sandstone decreases along the flow path. Sodium usually is a conservative element during geochemical evolution of a saline water. The ratio of sodium to bromide may increase through hydrolysis or ion-exchange reactions. However, sodium does not readily precipitate from solution in water with small concentrations. Perhaps the formation of zeolites, such as analcime, or albitization may cause a decrease in sodium at concentrations less than halite saturation in some aquifers, but it is not likely in the middle Mesozoic aquifer because of the small solute concentrations. At these small solute concentrations, mixing is a better explanation for the decreasing sodium-to-bromide ratio than is mineral precipitation.

The percentage of brine mixing with water in the Navajo Sandstone, calculated by mass balance of sodium,

chloride, and bromide, ranges from 1.5 to 3 percent. Other solutes, especially calcium, magnesium, bicarbonate, and sulfate are not conservative in solution. Their concentrations are affected by chemical reactions, principally mineral precipitation, and cannot be used for the mixing calculations. The percentages of the $NaCl$-$Na_2SO_4$ end member differ from the percentages indicated by mass-balance calculations, which are based on absolute concentrations rather than end member percentages.

## Trace Elements

Concentrations of trace elements (table 2) also give some indications of mixing. Boron, bromide, and lithium concentrations markedly increase along the flow path; no likely sources of these trace elements occur in the Navajo or Entrada Sandstones, so these increases indicate mixing rather than chemical reaction with aquifer minerals. Bromide concentrations increase linearly with chloride concentrations at virtually a 1:1 slope (in logarithmic units). Carpenter (1978, fig. 7) determined that mixing of brine with freshwater likely would result in a linear increase of bromide and chloride concentrations.

Other trace elements either have no trend of increasing or decreasing concentrations or they tend to decrease down the flow path. In general, aluminum, barium, iron, and zinc concentrations have no defined trends along the flow path; concentrations of these trace elements may be controlled by various mineral equilibria, and not by mixing processes. Manganese and strontium concentrations decrease down the flow path; concentrations of these two trace elements could be controlled by carbonate-mineral equilibria. As carbonate minerals precipitate, these two trace elements apparently coprecipitate and are removed from solution.

## Thermodynamic Constraint

Thermodynamic calculations can indicate which of the proposed chemical reactions are plausible. Saturation states of the water, expressed as a saturation index with respect to given aquifer minerals, were calculated by using the chemical-equilibrium model WATEQF (Plummer and others, 1976). Mineral equilibrium is indicated by a saturation index (as defined by Plummer and others, 1983, p. 667) that is almost zero, undersaturation by a negative index, and supersaturation by a positive index.

Water in the Entrada Sandstone, in the recharge area, is slightly undersaturated with respect to calcite and dolomite. With no carbonate minerals dissolving, there should be no carbonate saturation in the dilute water. In the Navajo Sandstone, the water generally is supersaturated at the beginning of the flow path, where $CaCO_3$ and $MgCO_3$ components dominate. This may just be an apparent supersaturation, resulting from a calcite equilibrium constant used in WATEQF, that does not account for the actual composition of these carbonate minerals. With an increasing $Na_2CO_3$ component in the water, similar to the water in the Entrada Sandstone, saturation indices decrease, approaching equilibrium with respect to calcite and dolomite. This may occur because the alkalinity increases to a point where there is sufficient activation energy, driven by disequilibrium to cause precipitation. Magnesium could be depleted by incorporation into carbonate minerals, but also could be removed as a brucite layer [$Mg(OH)_2$], associated with clays. The NaCl water farther along the flow path is supersaturated with respect to calcite and dolomite.

The partial pressure of carbon dioxide ($P_{CO_2}$), calculated by WATEQF for the 11 sites in table 2, varies from $-2.89$ to $-1.69$ atm, in logarithmic units. The two most concentrated samples from the Navajo Sandstone sampled during the study, collected from sites 20 and 24, have the largest $P_{CO_2}$ pressures, about $-1.8$ atm. Greater $P_{CO_2}$ pressures may result from carbonate precipitation or from oxidation of organic acids associated with oil-field brine (Kharaka and others, 1983).

These saturation calculations indicate a chemical front, with an area of carbonate dissolution producing the $CaCO_3$ and $MgCO_3$ components in the water, followed by carbonate precipitation. Because silicate hydrolysis continues along the flow path, producing sodium and bicarbonate in solution, the loss of alkaline earths changes the water to a $Na_2CO_3$-$Na_2SO_4$ type. This type of water evolves in the Wingate and Entrada Sandstones without a carbonate dissolution-precipitation step. These saturation calculations agree with the proposed reactions in the aquifer that are indicated by the changes in simple salts.

## Stable-Isotope Ratios

Stable isotopes, like thermodynamic calculations, help limit the possible choice of reactions that account for changes in water quality by providing constraints on mass-balance calculations (Plummer and others, 1983). Systematic changes in carbon and sulfur isotopes result from chemical and physical processes affecting the solutes in the aquifer water; their isotope ratios change in response to water-rock interactions. Hydrogen and oxygen isotopes, on the other hand, reflect the origin and history of the water more than the origin of solutes, because the large mass transfer of hydrogen and oxygen from rock to water that would be required to affect the ratios generally is not seen under normal aquifer conditions. Shifts in the hydrogen and oxygen isotope ratios generally only are seen in hydrothermal system (Taylor, 1979). Frape and others (1984), in their study of Canadian Shield water, have illustrated how

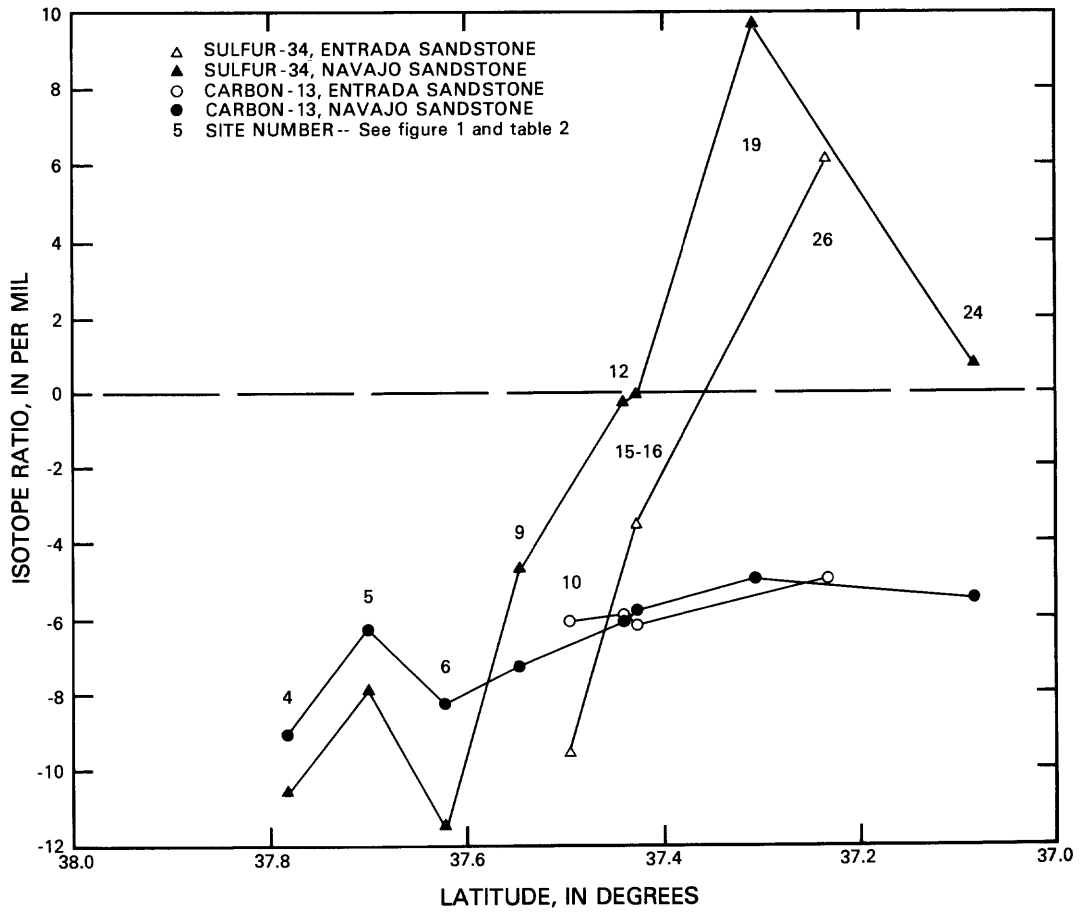


**Figure 3.** Variations in $\delta^{34}S$ and $\delta^{13}C$ along the flow path. Number by plot symbol indicates site number in figure 1 and table 2.

the differences in stable isotope ratios can be used to study water-rock interactions, and particularly the effects of mixing with brines.

Water in the middle Mesozoic aquifer, at the beginning of the flow path, contains about −10 ‰ $\delta^{34}S$. Values of $\delta^{34}S$ generally increase along the flow path (table 2), with a large increase in the sample from wells where mixing with the Paleozoic brine may occur (fig. 3). The Abajo Mountains provide a source of light $\delta^{34}S$ as igneous rocks are weathered. Field titration for sulfide in the water indicated no evidence of sulfate reduction along the flow path; thus, changes in $\delta^{34}S$ are not the result of sulfate reduction in the aquifer. Instead, the increase may be from mixing with the Paleozoic brine or from injection of oil-field brine.

A well sampled near Moab, Utah (north of the study area), that produces brine by injecting freshwater to dissolve salts had a $\delta^{34}S$ of +12.4‰. This value probably represents the value of salt from the Paradox Member of the Hermosa Formation, because sulfate concentrations in the injected water are small. The large increase in $\delta^{34}S$ from −10 to +10 ‰ and the increase in sulfate concentration along the flow path indicate that most of the sulfate, and, consequently, the $\delta^{34}S$ in samples from sites 16, 19, and 24 is the result of mixing.

A mixing calculation is possible using the $\delta^{34}S$ values. This calculation can be compared to the mixing calculation that is based on input of NaCl salts. An isotope mass balance of $\delta^{34}S$ indicates that 7 percent of the water may be from the Paleozoic brine or from injection of oil-field brine.

Ratios of $\delta^{13}C$ range from −9.0 to −4.9 ‰ (fig. 3). Samples from sites 4 and 6 (Navajo Sandstone) are light in $\delta^{13}C$, reflecting recharge waters least affected by dissolution of carbonate minerals in the aquifer. Samples from sites 10 and 15 (Entrada Sandstone) have heavier $\delta^{13}C$, but they do not reflect carbonate-mineral dissolution; they are part of the $Na_2CO_3$-$Na_2SO_4$ hydrochemical facies (fig. 2). Vegetation in the outcrop area is sparse in this region, and the initial signature of $\delta^{13}C$ from the atmosphere might be unaltered. A general value of about −7 ‰ has been reported for atmospheric carbon dioxide (Pearson and Friedman, 1970). Thus, in the absence of carbonate weathering and with little biogenic carbon dioxide in a soil zone,

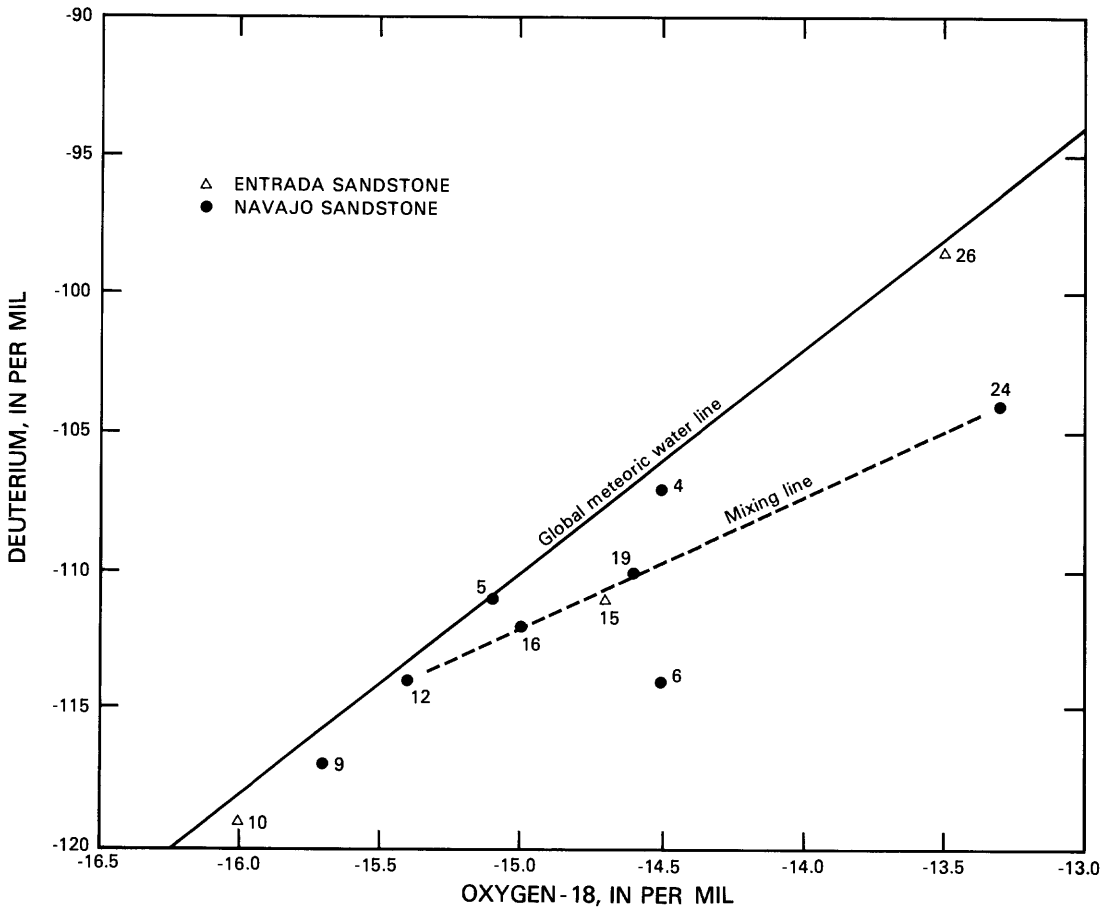


**Figure 4.** Variation of δD with $\delta^{18}O$. Number by plot symbol indicates site number in figure 1 and table 2.

the water in these sandstones may obtain and retain an atmospheric $\delta^{13}C$. The $\delta^{13}C$ is less affected by mass balance during mixing than is $\delta^{34}S$ because the alkalinity of water resulting from dissolved salt in the Paradox Member is smaller than the alkalinity of water in these sandstones [only 1.17 millimoles per liter (mM/L)]. Samples from sites 19, 24, and 26 have slightly heavier carbon-13 values that could indicate some effect of mixing with the Paleozoic or oil-field brine.

The sample from site 4 has the lightest $\delta^{13}C$, the second lightest $\delta^{34}S$, the largest carbon-14 activity, and measureable tritium (table 2). Each of these isotopes indicates that the sample from site 4 is a recharge water. However, the bromide concentration is larger than that in water from other wells with heavier carbon-isotope values. The chemistry of this water appears to have been modified by mixing in that local area, which would explain why it does not appear to be an end member in the steady-state flow-path model.

Six of the 11 δD and $\delta^{18}O$ ratios (fig. 4) plot along the trend determined for global meteoric water by Craig (1961). A second linear trend extends from site 12 to site 24 and includes sites 15, 16, and 19. These samples are affected by mixing, and the linear trend is typical of meteoric recharge waters mixed with an evaporite basin water, such as the water that deposited the salt in the Paradox Member salt (Clayton and others, 1966). The different value for site 6, which plots below both lines, may result from exchange with mineral $\delta^{18}O$ near the Tertiary igneous intrusion of the Abajo Mountains.

High-temperature isotopic exchange can cause such an $\delta^{18}O$ shift without shifting deuterium (Frape and Fritz, 1982, fig. 2). The sample from site 25, which shows chemical and isotopic indications of mixing for $\delta^{34}S$ and $\delta^{13}C$, does not show mixing for δD and $\delta^{18}O$. It appears that water at site 25 has obtained solutes from either Paleozoic brine or injection of the oil-field brine, but most of the water is from local recharge. This could result if a small quantity of brine were injected into a very dilute water.

Along with the geochemical evidence, hydrologic evidence presented by E.M. Weiss (U S. Geological Survey, written commun., 1985) indicates that the difference in hydraulic heads between the upper Paleozoic and middle Paleozoic aquifers is greater than 200 m, with the middle

Paleozoic aquifer having the lower hydraulic head. The possibility of upward leakage from the middle Paleozoic aquifer to the middle Mesozoic aquifer is, therefore, small. Factor analysis, trace elements (boron, bromide, and lithium), and the stable isotopes indicate that the saline water in the Navajo Sandstone is a result of mixing brine from the middle Paleozoic aquifer, but the hydrologic data indicate that the saline water is most likely a result of mixing with reinjected oil-field brine and not natural upward leakage.

## CONCLUSIONS

A large difference in salinity between the middle Paleozoic and middle Mesozoic aquifers occurs in the Montezuma Canyon area. The middle Paleozoic aquifer contains brine derived from the resolution of salts in the overlying Paradox Member of the Hermosa Formation. The upper Paleozoic aquifer does not contain water with the same chemical character or dissolved-solids concentration present in either the middle Paleozoic or the middle Mesozoic aquifers. The middle Mesozoic aquifer contains water that is chemically and isotopically similar to the brine in the middle Paleozoic aquifer. The upper Mesozoic aquifer also contains some areas with water chemically similar to the brine in the middle Paleozoic aquifer.

Extended Q-mode factor analysis distinguishes three major hydrochemical facies. Recharge waters are of two types: a $CaCO_3$-$MgCO_3$-$Na_2SO_4$ water that is typical of recharge in the Navajo Sandstone and a $Na_2CO_3$-$Na_2SO_4$ water that is typical of recharge water in the Entrada and Wingate Sandstones. As water moves through the Navajo Sandstone along the flow path, the chemical character changes through carbonate-mineral precipitation and silicate hydrolysis reactions to a $Na_2CO_3$-$Na_2SO_4$ water, similar to the recharge water in the Entrada and Wingate Sandstones. Farther along the flow path, a third end member becomes dominant, a NaCl-$Na_2SO_4$ water, that results from mixing normal aquifer water with brine either from the middle Paleozoic aquifer or from injection of oil-field wastes. Each of these chemical changes is indicated by determining the percentages of the three end members in samples along the flow path (fig. 2).

Because the upper Paleozoic aquifer in the same area does not contain any of the same type of water present in the middle Paleozoic aquifer, and because hydraulic-head data indicate downward, rather than upward, movement of water from the Paleozoic rocks, the source of saline water in the middle Mesozoic and upper Mesozoic aquifers is most likely from injection of oil-field brine. The extent of contamination by injection appears to be limited to small areas in the Dakota, Entrada, and Navajo Sandstones.

## REFERENCES CITED


Back, William, 1966, Hydrochemical facies and ground-water flow patterns in northern part of the Atlantic Coastal Plain: U. S. Geological Survey Professional Paper 448–A, 42 p.

Berner, R.A., 1980, Early diagenesis—A theoretical approach: Princeton, New Jersey, Princeton University Press, 241 p.

Bodine, M.W., Jr., and Jones, B.F., 1986, THE SALT NORM: A quantitative chemical-mineralogical characterization of natural waters: U.S.. Geological Survey Water-Resources Investigations Report 86–4086, 130 p.

Carpenter, A.B., 1978, Origin and chemical evolution of brines in sedimentary basins: Oklahoma Geological Survey Circular 79, 77 p.

Clayton, R.N., Friedman, I., Graf, D.L., Mayeda, T.K., Meents, W.F., and Schimp, N.F., 1966, The origin of saline formation waters. 1. Isotopic composition: Journal of Geophysical Research, v. 71, p. 3869–3882.

Craig, Hugh, 1961, Isotopic variations in meteoric waters: Science, v. 133, p. 1702–1703.

Drever, J.I., 1982, The geochemistry of natural waters: Englewood Cliffs, New Jersey, Prentice-Hall, 388 p.

Eugster, H.P., and Jones, B.F., 1979, Behavior of major solutes during closed-basin brine evolution: American Journal of Science, v. 279, p. 609–631.

Frape, S.K., and Fritz, Peter, 1982, The chemistry and isotopic composition of saline ground-waters from the Sudbury Basin, Ontario: Canadian Journal of Earth Science, v. 19, p. 645–661.

Frape, S.K., Fritz, Peter, and McNutt, R.H., 1984, Water-rock interaction and chemistry of ground waters from the Canadian Shield: Geochimica et Comochimica Acta, v. 48, p. 1617–1627.

Freethey, G.W., Kimball, B.A., Wilberg, D.E., and Hood, J.W., 1984, General hydrogeology of the aquifers of Mesozoic age, Upper Colorado River basin—Excluding the San Juan basin, Colorado, Utah, Wyoming, and Arizona: U.S. Geological Survey Open-File Report 84–716, 11 p.

Fritz, Peter, and Fontes, J.C., 1980, Handbook of environmental isotope geochemistry: New York, Elsevier Scientific Publishing Company, 545 p.

Garrels, R.M., 1975, A survey of low temperature water-mineral relations, *in* Interpretation of environmental isotopes and hydrochemical data in ground water: Vienna, Austria, International Atomic Energy Association special volume, p. 65–84.

Hanshaw, B.B., and Hill, G.A., 1969, Geochemistry and hydrodynamics of the Paradox Basin region, Utah, Colorado, and New Mexico: Chemical Geology, v. 4, p. 263–294.

Hite, R.J., and Gere, W.C., 1958, Potash deposits of the Paradox Basin: Intermountain Association of Petroleum Geologists Guidebook 9, p. 221–225.

Holser, W.T., and Kaplan, I.R., 1966, Isotope geochemistry of sedimentary sulfates: Chemical Geology, v. 1, p. 93–135.

Huff, L.C., and Lesure, F.G., 1965, Geology and uranium deposits of Montezuma Canyon area San Juan County, Utah: U.S. Geological Survey Bulletin 1190, 102 p.

Joreskog, K.G., Klovan, J.E., and Reyment, R.A., 1976, Geological factor analysis: New York, Elsevier Scientific Publishing Company, 178 p.

Kharaka, Y.K., Carothers, W.W., and Rosenbauer, R.J., 1983, Thermal decarboxylation of acetic acid—Implications for

origin of natural gas: Geochimica et Cosmochimica Acta, v. 47, p. 397–402.

Kimball, B.A., 1984, Ground water age determinations, Piceance Creek basin, Colorado, *in* Hitchon, Brian, and Wallick, E.I., eds., 1984, Proceedings First Canadian/American Conference on Hydrogeology, Practical Applications of Ground Water Geochemistry, Banff, Alberta, Canada, 1984: Worthington, Ohio, National Water Well Association, p. 267–283.

Miesch, A.T., 1976, Q-mode factor analysis of geochemical and petrologic data matrices with constant row-sums: U.S. Geological Survey Professional Paper 574–G, 47 p.

Ohlen, H. R., and McIntyre, L.B., 1965, Stratigraphy and tectonic features of Paradox Basin, Four Corners area: Bulletin of the American Association of Petroleum Geologists, v. 49, p. 2020–2040.

Pearson, F.J., Jr., and Friedman, I., 1970, Sources of dissolved carbonate in an aquifer free of carbonate minerals: Water Resources Research, v. 6, p. 1775–1781.

Plummer, L.N., Jones, B.F., and Truesdell, A.H., 1976, WATEQF—A FORTRAN IV version of WATEQ, a computer program for calculating chemical equilibrium of natural waters: U.S. Geological Survey Water-Resources Investigations 76–13, 70 p.

Plummer, L.N., Parkhurst, D.L., and Thorstenson, D.C., 1983, Development of reaction models for ground-water systems: Geochimica et Cosmochimica Acta, v. 47, p. 665–686.

Selley, R.C., 1970, Ancient sedimentary environments—A brief survey: Ithaca, New York, Cornell University Press, 237 p.

Shoemaker, J.E., Case, J.E., and Elston, D.P., 1958, Salt anticlines of the Paradox Basin: Intermountain Association of Petroleum Geologists Guidebook 9, p. 39–59.

Taylor, H.P., Jr., 1979, Oxygen and hydrogen isotope relationships in hydrothermal mineral deposits, *in* Barnes, H.L., ed., Geochemistry of hydrothermal ore deposits (2d ed.): New York, John Wiley, p. 236–277.

Taylor, O.J., Hood, J.W., and Zimmerman, E.A., 1983, Plan of study for the regional aquifer systems analysis of the Upper Colorado River basin in Colorado, Utah, Wyoming, and Arizona: U. S. Geological Survey Water-Resources Investigations Report 83–4184, 23 p.

Wright, J.C., and Dickey, D.D., 1958, Pre-Morrison Jurassic strata of southeastern Utah: Intermountain Association of Petroleum Geologists Guidebook 9, p. 172–181.

# Using the Area of Diversion for Pumping Centers to Estimate Potential Freshwater Production in Coastal Aquifers, East-Central Florida

*By* Michael Planert

**Abstract**

To estimate the probability of obtaining water with a chloride concentration of less than 250 milligrams per liter, heads derived from a digital model were used to define the area of diversion for ground-water flow surrounding well fields. The areas were plotted on a map of chloride concentrations establishing a relation between the extent of the area and the occurrence of high chloride water. Thus, model-derived heads would be used to evaluate particular pumping schemes.

Four pumping schemes representing potential well fields in east-central Florida are presented to demonstrate this technique. Two schemes having pumping centers in Osceola and Orange Counties produced water in quantities that ranged from 50 to 65 million gallons per day. The scheme that produced 65 million gallons per day intercepted a zone of water having chloride concentrations greater than 250 milligrams per liter, but the percentage of the zone within the area of diversion was small. Of the other two schemes, both in Brevard County, water of acceptable quality is limited to an additional 5 million gallons per day.

## INTRODUCTION

### Background

The Floridan aquifer system (limestone and dolomite) is the primary source of water supply for east-central Florida. In most of Brevard County though, the Floridan aquifer system contains water with chloride concentrations that exceed the recommended limit of 250 mg/L for public supplies (U.S. Environmental Protection Agency, 1977, p. 17146). Therefore, much of Brevard County has difficulty in obtaining acceptable public water supplies. Small amounts of ground water are available from shallow aquifers, but the quantity is not sufficient for large public supply.

Northern Brevard County obtains most of its water from a well field in neighboring Orange County that was established in 1956 by the city of Cocoa (fig. 1). The well field taps the Floridan aquifer system and produces about 15 Mgal/d.

The source of water for southern Brevard County is Lake Washington (fig. 1), which supplies the city of Melbourne and adjacent areas. The lake water is subject to periodic algae blooms, and seasonal increases in chloride concentrations have exceeded 200 mg/L. An analysis by the County's engineering consultants (Post, Buckley, Schuh, and Jernigan, Inc., 1980, p. 5–12) indicated the maximum sustained yield of Lake Washington should be 14 to 15 Mgal/d. To meet the projected water demand, southern Brevard County seeks a source of water similar to that which supplies northern Brevard County.

### Purpose and Scope

This paper addresses a hydraulic solution to lateral saltwater intrusion in coastal aquifers. By modeling the area of diversion (Brown, 1963) for a pumping center, this area can be superimposed over the chloride distribution within an aquifer to determine whether water with unacceptable chloride concentrations will be drawn to the wells.

This paper also examines the probability of obtaining a dependable source of freshwater from ground water for southern Brevard County and is excerpted from Planert and Aucott (1985). The projected demand for water in southern Brevard County is about 45 Mgal/d by the year 2000. The source investigated was the Floridan aquifer system, and the probability of obtaining this amount of water was estimated by using a digital model to simulate various pumping schemes.

## ANALYTICAL TECHNIQUE

A general indication of the water quality to be expected from a well field developed in a coastal aquifer

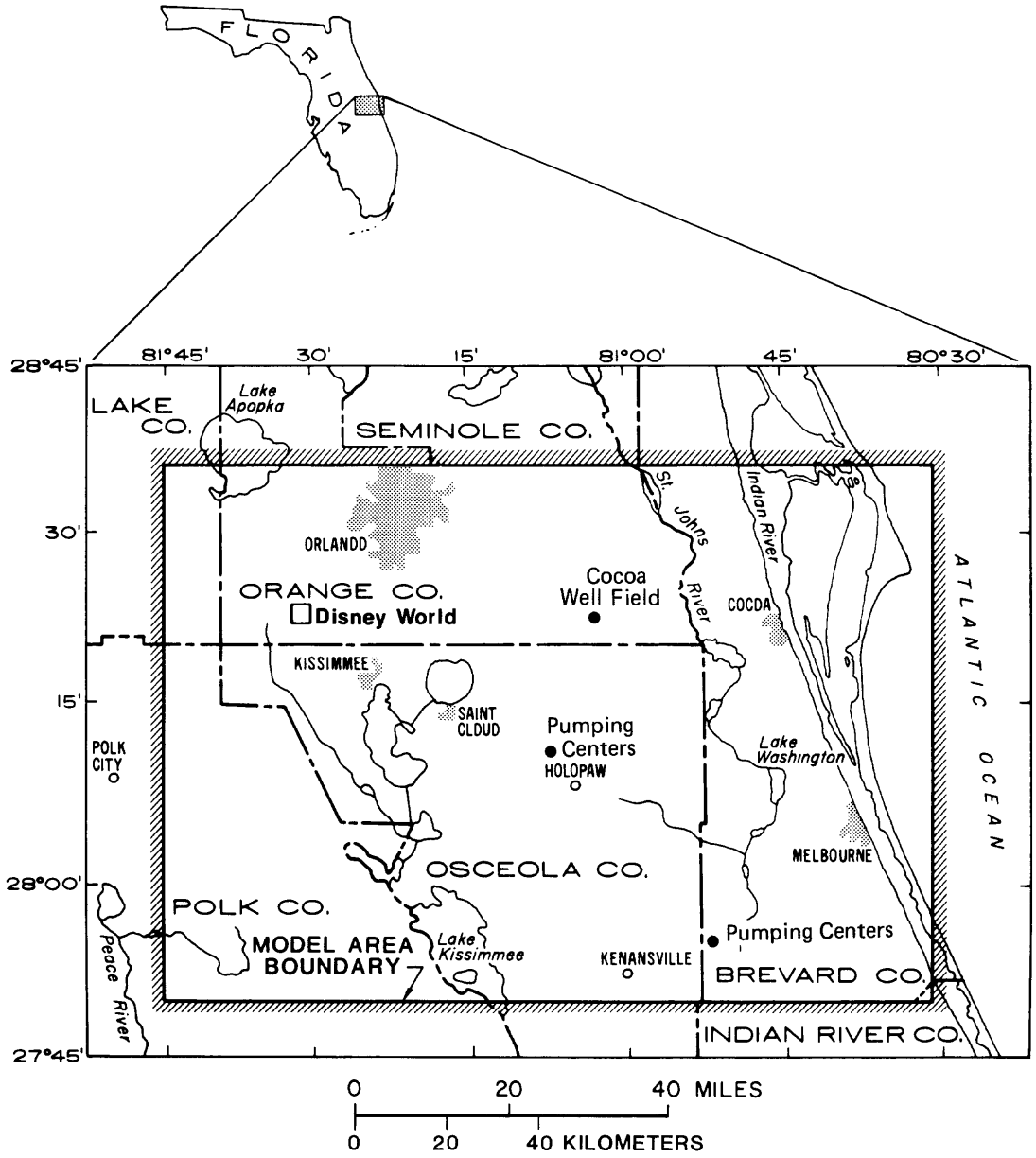


**Figure 1.** Location of the study area.

can be estimated by superimposing the equilibrium potentiometric surface for a proposed pumping scheme upon the known areal distribution of chloride concentration. From the existing potentiometric surface and the calculated cone of depression, the area of diversion (Brown, 1963) can be defined for a given pumping scheme. Thus, for several different pumping schemes, the areas of diversion can be mapped and compared, the result showing in a quantitative way the extent to which zones of high chloride (chloride concentrations greater than 250 mg/L) are being penetrated.

The area of diversion around a well or well field is the area from which the pumping center actually draws its water. In a ground-water system with natural head gradients, the area of diversion as described by Brown (1963) is not coincident with the cone of depression caused by pumping. Brown used an infinite strip aquifer bounded by fully penetrating streams (fig. 2) to illustrate this point. Figure 3 shows the contour map and profile of the water table for the infinite strip aquifer based on a transmissivity of 10,000 $ft^2/d$ and a uniform recharge rate of 6 in/yr. Because of the symmetry of the system, only one quadrant is presented. Placing a pumping well at the ground-water divide, Brown presented data for pumping the well at a constant rate of 200 gal/min for selected periods of time to show the difference between the cone of depression and area of diversion. Figure 4 shows a contour map and

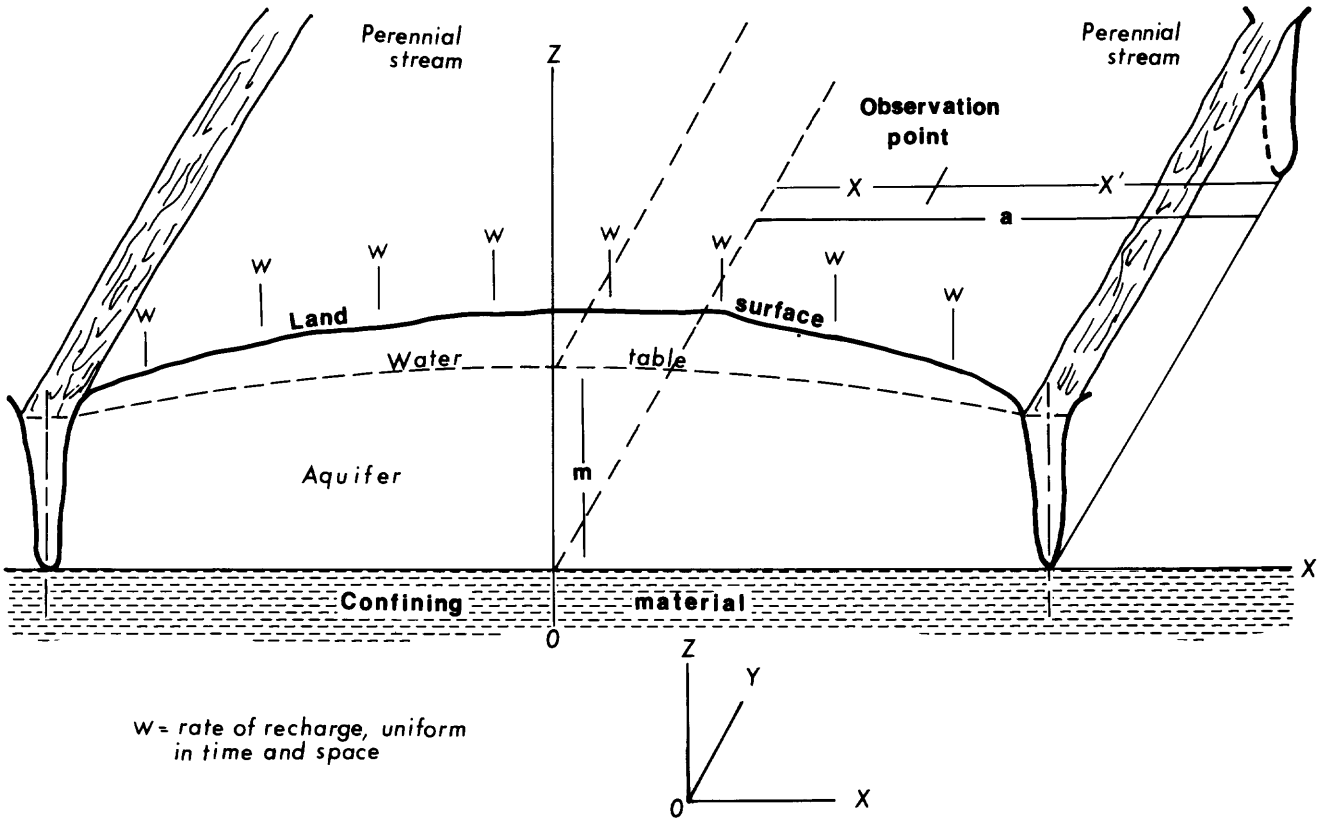


**Figure 2.** Cross section and oblique view of part of an infinite strip aquifer bounded by two parallel streams (from Brown, 1963, p. C 71).

profile of the water table after 30 days. The cone of depression (arbitrarily defined by a limiting drawdown of 0.01 ft) has reached a radius of almost 4,000 ft, but the area of diversion covers a lesser area. Figure 5 shows a contour map and profile of the water table at equilibrium. Pumping effects have reached the stream, but, in the original downgradient direction of flow, the area of diversion extends to 2,000 ft from the well. The area of diversion parallel to the divide has expanded to about 7,000 ft, but this is due to placing the well at the natural ground-water divide. Placing the well downgradient toward the stream would change the lateral extent of the area of diversion.

Figure 6 is a map of the potentiometric surface within the study area for the Floridan aquifer system in September 1980, with the area of diversion outlined for the Cocoa well field in Orange County. The lateral and downgradient limits of the area of diversion are in relative close proximity to the pumping center, as opposed to the pattern for the pumping well placed on the ground-water divide in Brown's example. The limit for the area upgradient from the well is the natural ground-water divide in the recharge area for the aquifer and can be difficult to define depending on the location of the pumping center and complexity of the flow pattern. Most important are the downgradient limits because the initial quality of water is based on the water flowing from the recharge area. It is important to understand that any changes in quality will be from water derived downgradient from a well field.

## GENERAL DESCRIPTION OF THE STUDY AREA

### Location

The study area, located in east-central Florida (fig. 1), consists of most of Osceola and Brevard Counties and parts of Lake, Orange, and Polk Counties. The Cocoa well field and the two hypothetical pumping centers, one near Holopaw and the other in southwestern Brevard County, used in the simulation of the areas of diversion are shown in figure 1.

Most of Brevard County is a discharge area for the Floridan aquifer system, as the potentiometric surface is above land surface, and there is little local recharge of freshwater to the aquifer. Most recharge occurs in adjacent Orange and Osceola Counties.

### Geohydrology

The ground-water system has been divided into three layers: a surficial aquifer, an underlying confining layer,

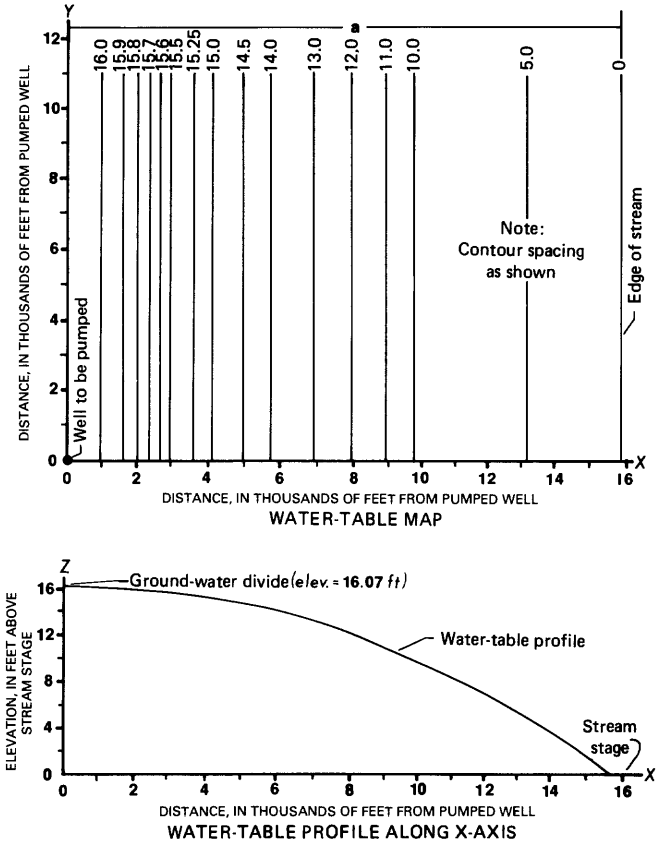


**Figure 3.** Contour map and profile of the water table before pumping begins (from Brown, 1963, p. C 73).

and below these two layers, the Floridan aquifer system. The surficial aquifer is comprised mainly of sand; it is present throughout the study area. The confining layer, which includes the Hawthorn Formation of Miocene age, separates the two aquifers and is comprised chiefly of clays, silts, marls, dense limestone, and fine sediments that do not readily transmit water. This restriction of flow, especially where the Hawthorn is present, causes artesian conditions in the Floridan aquifer system.

The Floridan aquifer system consists of a series of limestone and dolomite formations that have a total thickness of several thousand feet. However, the thickness containing potable water (less than 250 mg/L chloride) rapidly diminishes in Brevard County. The limestones of Eocene age that compose the Floridan aquifer system in east-central Florida, in descending order, are the Ocala Limestone and the Avon Park Formation (Miller, 1985). Dense and less permeable zones that probably restrict the vertical movement of water in the Floridan aquifer system are common.

## Distribution of Saline Waters in the Floridan Aquifer System

A map of chloride concentrations (fig. 7), primarily for the upper 500 ft of the Floridan aquifer system, shows that high chlorides occur along the St. Johns River and farther east. A line of equal concentration of 50 mg/L is the lowest concentration line that can be drawn in the study area; west of this line only individual concentrations can be shown because of their wide range.

Data are insufficient to define the regional vertical interface between fresh and nonpotable water within the study area. The only definitive information available is from the Cocoa well field (fig. 1) in Orange County, but these data support the assumption of no vertical movement of saline waters. Thirteen wells were constructed between 1956 and 1961, and many wells experienced problems of high chloride concentrations soon after they were placed in operation. Beginning in 1962, six wells were drilled 4 mi west of the original well field, and in 1965, a salinity monitor well was constructed to monitor four zones in the Floridan aquifer system—approximately 1,000, 1,050, 1,200, and 1,400 ft below land surface. At a depth of about 1,400 ft, the chloride concentration was more than 1,000 mg/L, but at a depth of 1,200 ft, the concentration was less than 100 mg/L. As of 1981, the new well field has not experienced the chloride increases that occurred in the old well field, although there has been some increase in chloride concentration for the two easternmost wells in the new well field (Tibbals and Frazee, 1976, p. 26). Tibbals and Frazee (1976, p. 46) speculated that the easternmost wells in the new well field were becoming increasingly salty because of westward movement of salty water from the old well field area.

Records of water levels during 16 yr show that the deep zone is not severely affected by pumping from the new well field, probably due to a low vertical hydraulic conductivity in the area of the new well field. The fluctuations in water levels are controlled mainly by regional variations in the potentiometric surface (Tibbals and Frazee, 1976).

## MODEL ANALYSIS OF PUMPING SCHEMES

A model was developed to evaluate various pumping schemes for the Floridan aquifer system. By comparing the impact of the pumping schemes on the aquifer to nearby areas of water with chloride concentrations in excess of 250 mg/L, those schemes could be identified in which the pumped water would have chloride concentrations less than 250 mg/L.

The model (Trescott, 1975) consisted of five units: (1) a surficial aquifer, (2) an upper confining layer, (3) an upper flow layer that represents the upper 500 ft of the Floridan aquifer system, (4) a confining layer that repre-

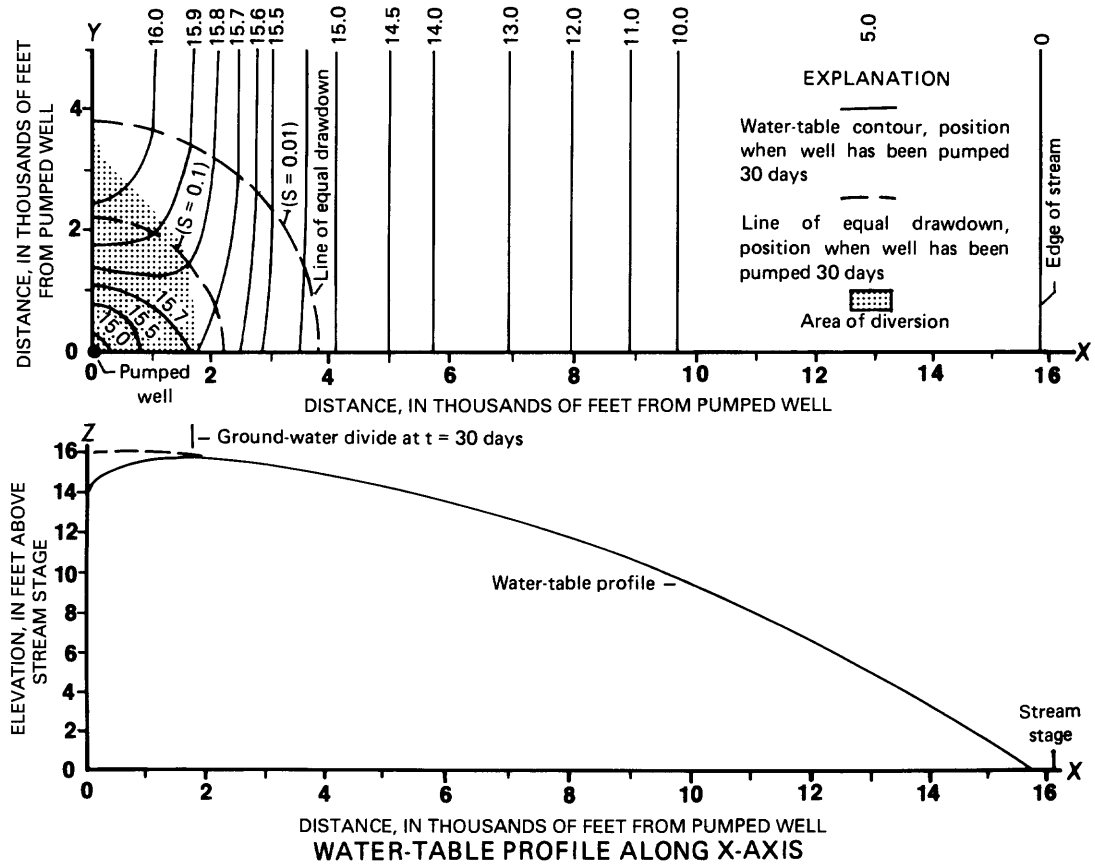


**Figure 4.** Contour map and profile of the water table after pumping 30 days (from Brown, 1963, p. C 78).

sents the vertical resistance to flow in the Floridan, and (5) a lower flow layer that represents another 500 ft of the Floridan aquifer system.

The Floridan aquifer system was simulated as two layers, each 500 ft thick, because pumpage in Orlando indicates that there are two zones in the Floridan aquifer system. (Pumpage from the deeper 500-ft layer has no effect on the upper 500 ft layer in the Orlando area.) This analysis considered lateral movement of water. Little is known about the areal vertical distribution of chloride concentration; consequently, no analysis of upconing from depth will be attempted. Monitoring of the well designed to detect upward movement of high chloride waters in the Cocoa well field has shown no dramatic increase in chloride concentrations over 16 yr and is the only datum point in the study area to evaluate the possibility of upconing. Based on this information and the fact that the wells in Orlando have not had a problem with increasing chloride concentrations, a well field placed in central Osceola County is judged to be quite safe from migration of high chloride water from below, provided the well depths are restricted to the upper 500 ft of the Floridan aquifer system.

Five major public water supply systems in the study area obtain water from the Floridan aquifer system. Three systems (Cocoa, St. Cloud, Walt Disney World complex) tap the upper 500 ft of the Floridan. Kissimmee has one of two wells drilled to almost 1,200 ft, and the city of Orlando withdraws most of its water from a zone below 1,000 ft. The 1978 yearly average pumpage for each system is as follows:

1. City of Cocoa averages 15 Mgal/d from its well field in eastern Orange County.
2. City of St. Cloud averages 1.1 Mgal/d.
3. City of Kissimmee averages 2.5 Mgal/d.
4. Disney World complex averages 7.5 Mgal/d.
5. City of Orlando averages 40 Mgal/d from seven pumping centers throughout the city.

These pumping centers were used in the calibration of the model.

Four pumping schemes with wells simulating pumping from the upper part of the Floridan aquifer system will be examined by using a model to illustrate this technique. Two schemes simulated a hypothetical well field near Holopaw, Osceola County, and an increase in pumpage at the Cocoa well field that yielded an additional 35 and 50 Mgal/d, and two schemes simulated yields of 5 and 20 Mgal/d from a hypothetical well field in southwest Brevard County.

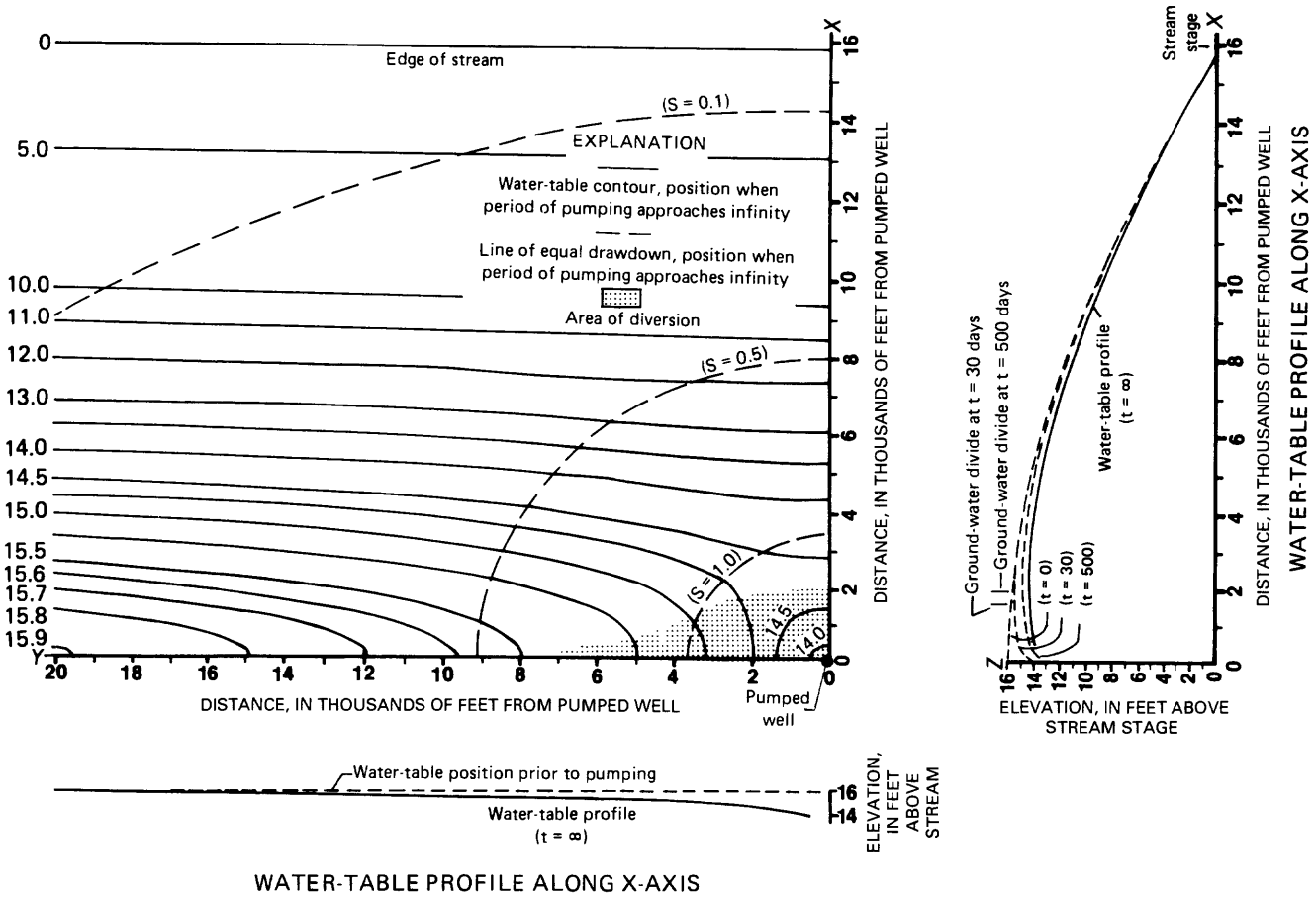


**Figure 5.** Contour map and profiles of the water table when pumping approaches equilibrium (from Brown, 1963, p. C 82).

Scheme 1 simulated an increase of 5 Mgal/d at Cocoa plus pumpage of 30 Mgal/d from four pumping centers at a site west of Holopaw. The yield from two westernmost pumping centers in the Cocoa well field was increased 2.5 Mgal/d each for a total production of 20 Mgal/d, and the Holopaw well field pumpage was simulated at 30 Mgal/d. Each center at Holopaw yielded an equal amount. Figure 8 shows the area of diversion for the Cocoa and Holopaw well fields. The upgradient extent of the areas of diversion in this study was arbitrarily drawn to the 80-ft contour on each potentiometric surface. The results show the Cocoa well field is surrounded by a 30-ft contour and the boundary of the area of diversion contacts the area of 250 mg/L chloride concentration. The increase of 35 Mgal/d in Osceola and Orange Counties (a total production of 50 Mgal/d) should provide water at a chloride concentration below 250 mg/L.

Scheme 2 simulated the largest withdrawal—an increase of 20 Mgal/d (total production of 35 Mgal/d) at the Cocoa well field that included two new pumping centers plus Holopaw pumpage at a rate of 30 Mgal/d—for a total production of 65 Mgal/d. The area of diversion for the Holopaw well field (fig. 9) remained practically the same as that in scheme 1 (fig. 8), but the area of diversion for the Cocoa well field moved slightly into the area of high chloride water. Production of water with this pumping scheme approaches potentially unacceptable effects, but mixing of waters could still produce potable water and render this scheme acceptable.

The potential of the southwest corner of Brevard County was tested because chloride concentrations are less than 250 mg/L. Caution should be used, however, in evaluating the results because the model was not designed to test southwest Brevard. A head-controlled flux boundary condition was added to the model to allow this analysis. Although the analysis will give an indication of the groundwater potential, the pumping is too close to the border of the model for the results to be unconditionally reliable. Variations in transmissivity or water quality outside the modeled area could drastically change the results described in the following two experiments.

Scheme 3 simulated 5 Mgal/d being pumped from one pumping center in southwest Brevard County, and figure 10 shows the potentiometric surface and the area of diversion. The area of diversion contacts the high chloride area. Because the water at the pumping center location has a chloride concentration greater than 200 mg/L, 5 Mgal/d would be the approximate limit for production at this site.

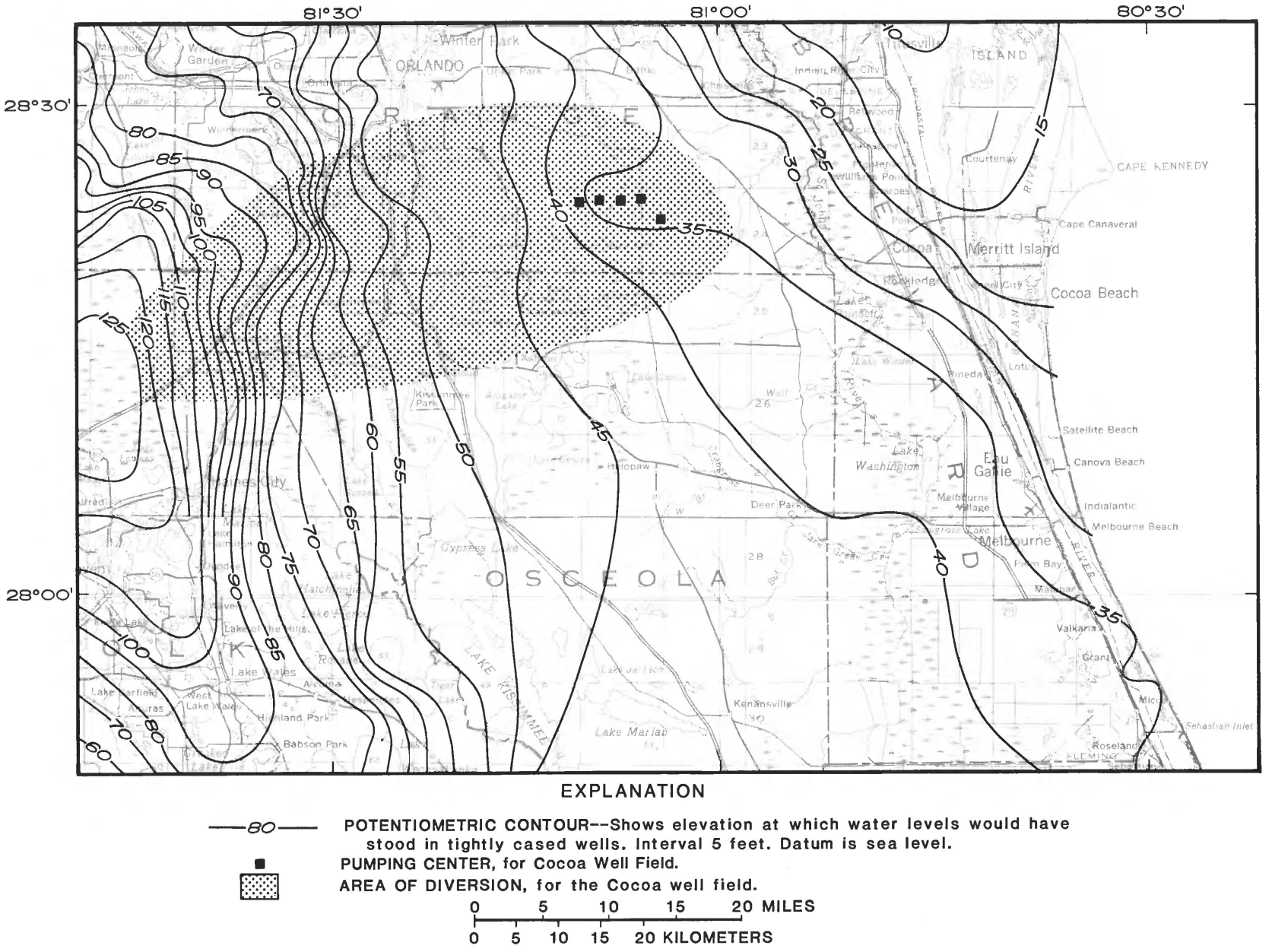


**Figure 6.** Potentiometric surface of the Floridan aquifer system, September 1980, and the area of diversion for the Cocoa well field.

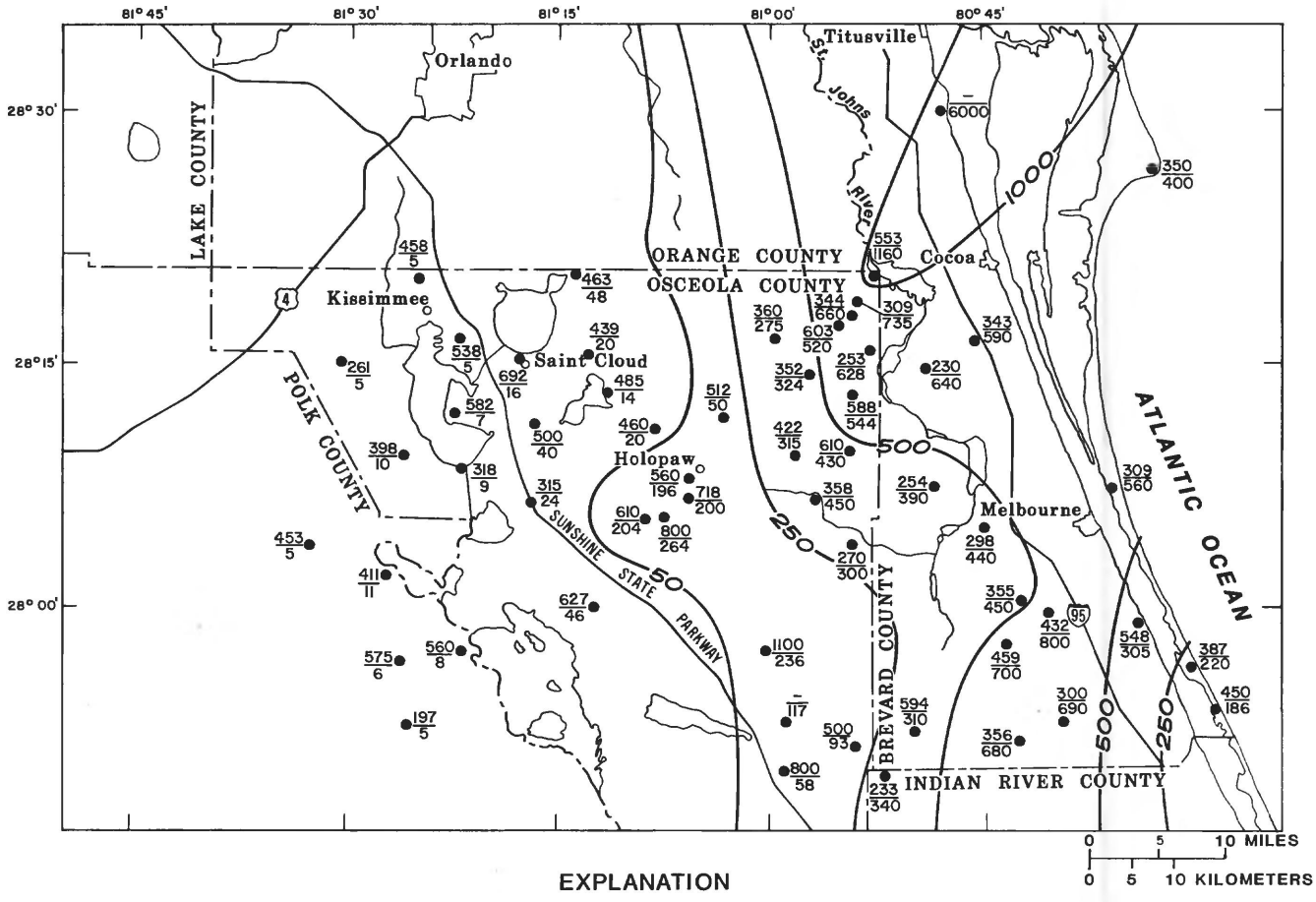


**Figure 7.** Chloride concentrations, in milligrams per liter, for the study area in the Floridan aquifer system, September 1979.

Scheme 4 simulated three north-south pumping centers in the same area of southwestern Brevard County, pumping at a combined rate of 20 Mgal/d. The area of diversion for this pumping scheme incorporates a substantial area of high chloride water (fig. 11) and includes a zone where chloride concentrations are greater than 500 mg/L. This pumping scheme would probably not succeed in maintaining chloride concentrations at less than 250 mg/L.

## CONCLUSIONS

By applying the concept of the area of diversion to a map of chloride concentrations, an estimate of lateral intrusion of saltwater to well fields can be obtained. This method was used to evaluate four pumping schemes in Osceola, Orange, and Brevard Counties. Three of the schemes could produce water of suitable quality. The results show an additional 50 Mgal/d could be produced from the Floridan aquifer system in Orange and Osceola Counties in addition to the 15 Mgal/d presently pumped from the Cocoa well field in Orange County. The maximum amount of water available from a hypothetical well field in Osceola County was not determined.

The technique of superimposing the area of diversion for a well field on the areal distribution of chloride concentrations can be used semiquantitatively to ascertain the quality of water produced by the well field. This technique evaluates lateral intrusion only but should be valid for most artesian situations where low vertical hydraulic conductivities restrict the vertical flow of water. This technique is not restricted to saltwater intrusion problems but should be a viable tool in any evaluation of lateral movement of poor quality water due to pumpage.

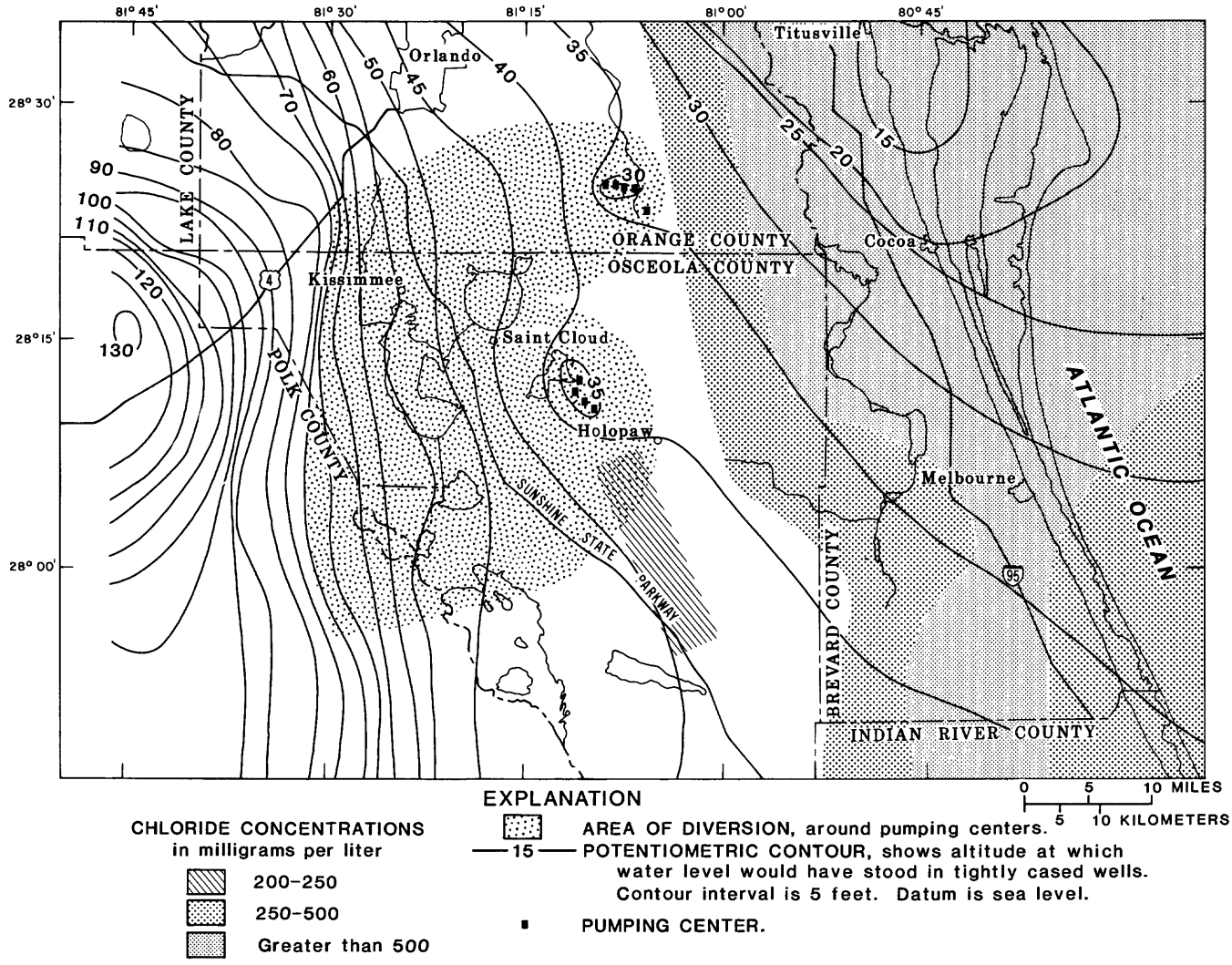


**Figure 8.** Potentiometric surface of the upper limestone layer at a new equilibrium for scheme 1, Cocoa pumpage 20 Mgal/d and Holopaw pumpage 30 Mgal/d, and the areas of diversion around the pumping centers.

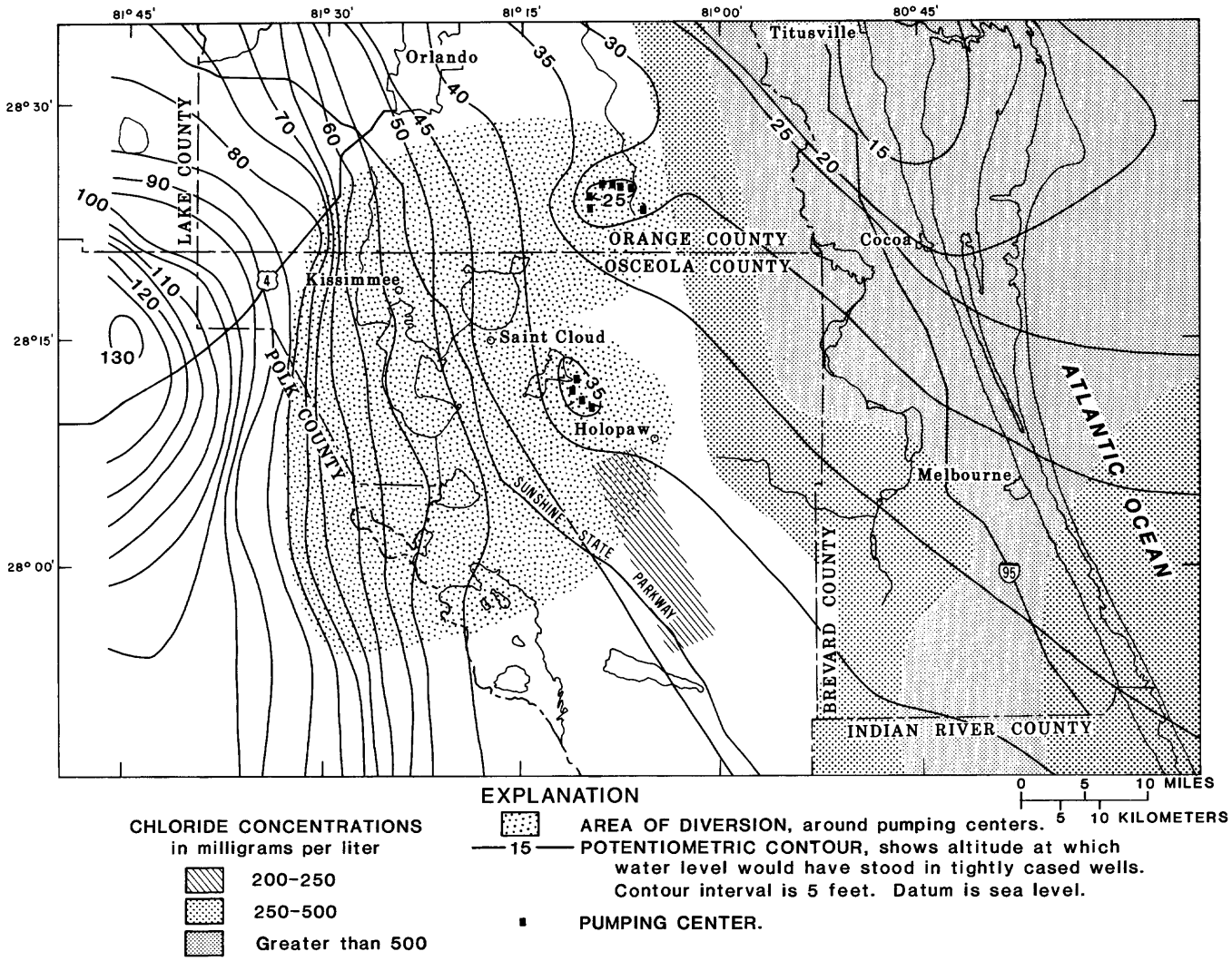


**Figure 9.** Potentiometric surface of the upper limestone layer at a new equilibrium for scheme 2, Cocoa pumpage 35 Mgal/d and Holopaw pumpage 30 Mgal/d, and the areas of diversion around the pumping centers.

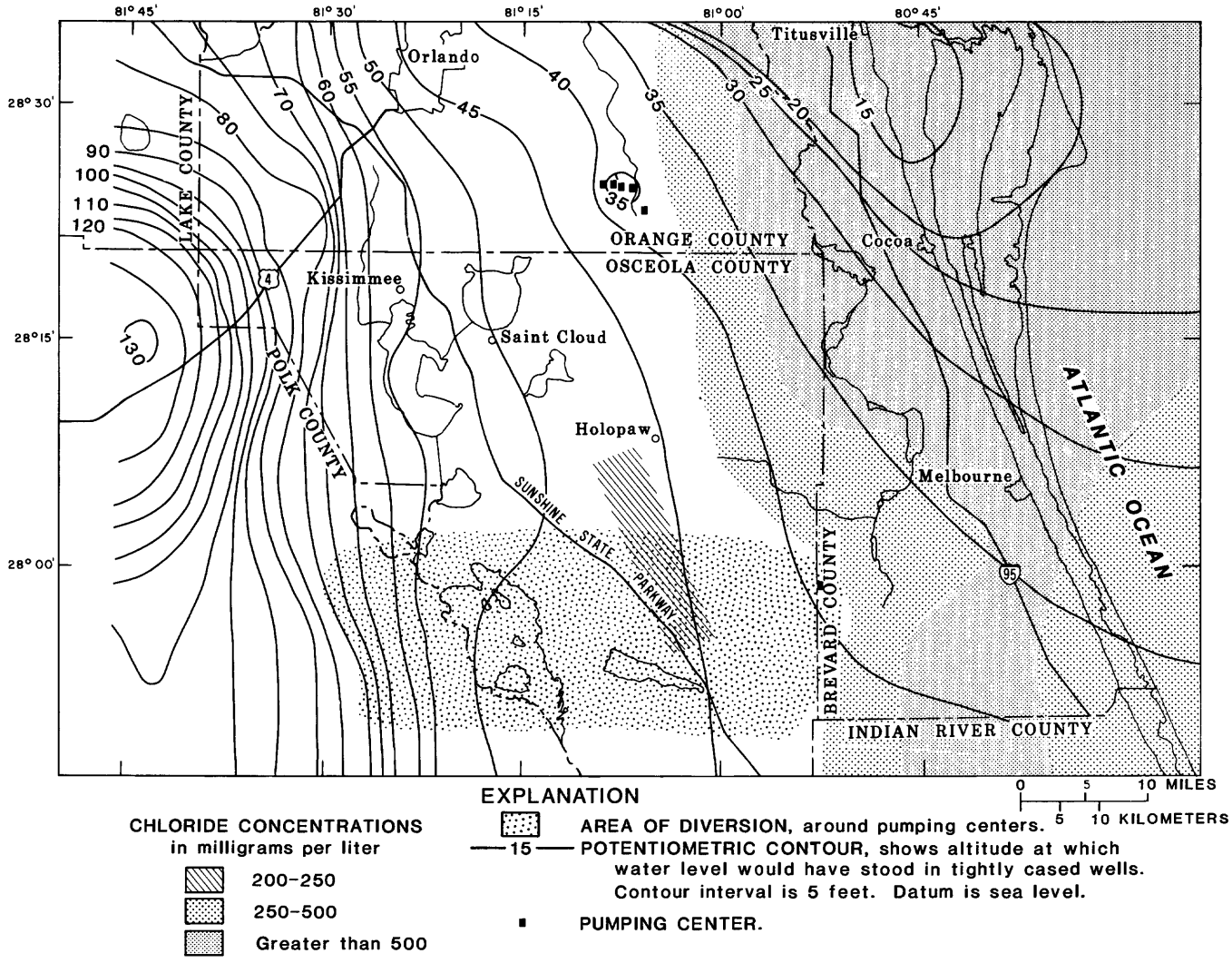


**Figure 10.** Potentiometric surface of the upper limestone layer at a new equilibrium for scheme 3, southwest Brevard pumpage 5 Mgal/d, and the area of diversion around the pumping center.

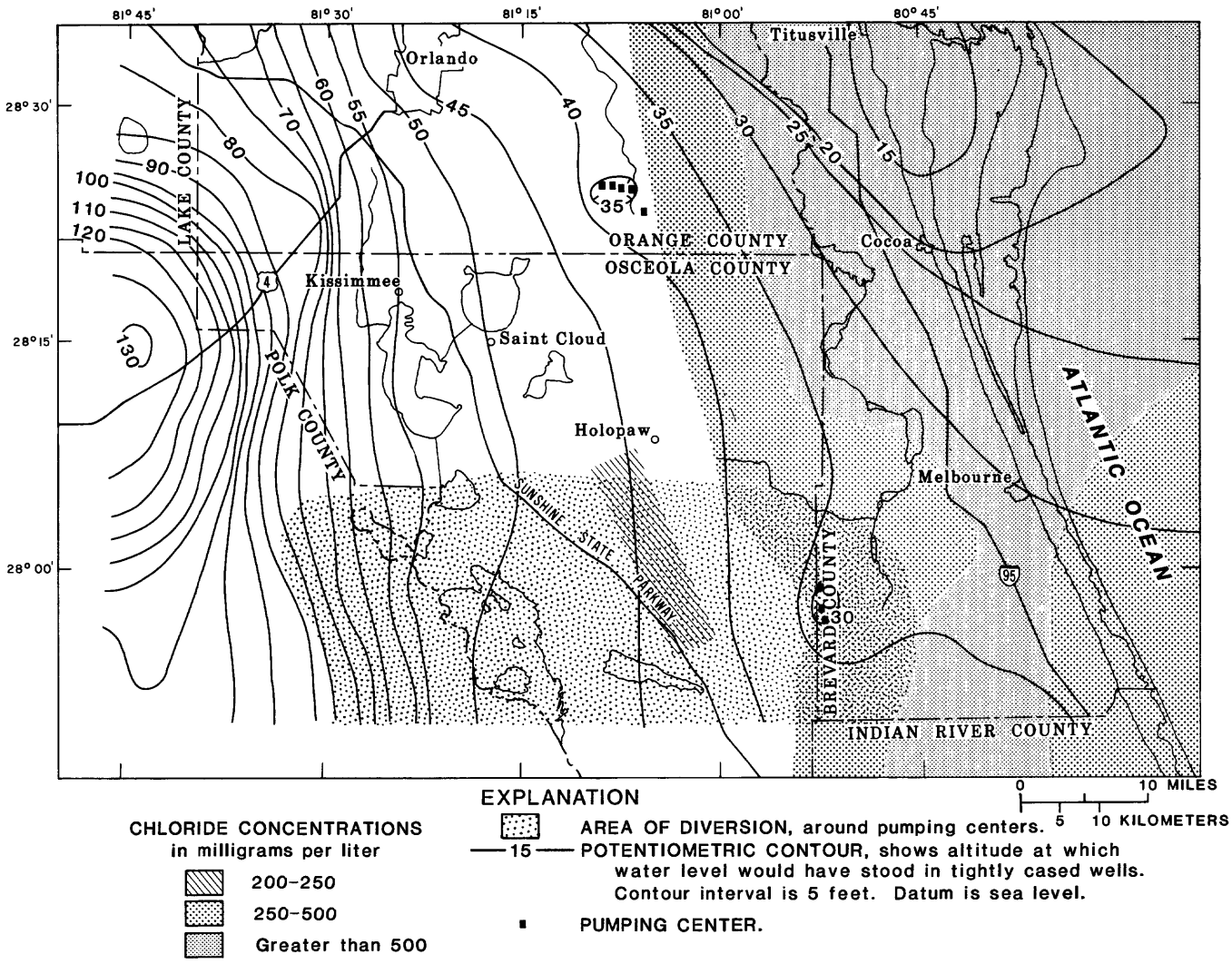


**Figure 11.** Potentiometric surface of the upper limestone layer at a new equilibrium for scheme 4, southwest Brevard pumpage 20 Mgal/d, and the area of diversion around the pumping center.

## REFERENCES


Brown, R.H., 1963, The cone of depression and the area of diversion around a discharging well in an infinite strip aquifer subject to uniform recharge, *in* Bentall, Ray, Shortcuts and special problems in aquifer tests: U.S. Geological Survey Water-Supply Paper 1545–C, p. 69–85.

Miller, J.A., 1985, Hydrogeologic framework of the Floridan aquifer system in Florida and in parts of Georgia, South Carolina and Alabama: U.S. Geological Survey Professional Paper 1403–B, 91 p.

Planert, Michael, and Aucott, W.R., 1985, Water-supply potential of the Floridan aquifer in Osceola, eastern Orange and southwestern Brevard Counties, Florida: U.S. Geological Survey Water-Resources Investigations Report 84–4135, 69 p.

Post, Buckley, Schuh, and Jernigan, Inc., 1980, Brevard county water supply phase A report: Interim Report 776–001.17, 60 p.

Schiner, G.R., and Hayes, E.C., 1981, Potentiometric surface map of the Floridan aquifer in the St. Johns River Water Management District and vicinity, Florida, September 1980: U.S. Geological Survey Open-File Report 81–136.

Tibbals, C.H., and Frazee, J.M., 1976, Ground-water hydrology in the Cocoa well-field area: U.S. Geological Survey Open-File Report 75–676, 67 p.

Trescott, P.C., 1975, Documentation of finite-difference model for simulation of three-dimensional ground-water flow: U.S. Geological Survey Open-File Report 75–438, 32 p.

U.S. Environmental Protection Agency, 1977, National secondary drinking water regulations: Federal Register, v. 42, no. 62, Thursday, March 31, 1977, pt. 1, p. 17143–17147.

# Identification of Net-Flux Rates for Ground-Water Models

*By* Peter Martin[1] *and* Timothy J. Durbin[2]

**Abstract**

A least-squares method can be used to identify net-flux rates (the difference between recharge and net discharge) for a linear or approximately linear distributed-parameter ground-water model. The method will estimate net-flux rates by using known aquifer characteristics, measured water levels, and the geographic location of recharge and discharge. This is accomplished by using the model to generate water-level response coefficients that result from unit pumpage or recharge. These coefficients, along with measured water levels, are assembled into a system of linear equations with net-flux rates as the unknown quantity. This system of equations can then be solved for the unknown net-flux rates. The least-squares method was applied as a practical problem to the identification of net-flux rates for the San Antonio Creek valley ground-water basin in southern California.

## INTRODUCTION

Distributed-parameter ground-water models commonly are used by hydrologists to evaluate ground-water resources. Such models are based on the numerical solution of a one- , two- , or three-dimensional partial-differential equation of steady or unsteady ground-water flow (Prickett and Lonnquist, 1971; Remson and others, 1971; Trescott, 1975; Pinder and Gray, 1977; and Wang and Anderson, 1982). For the governing equation, numerical solutions typically are obtained by application of the finite-difference or finite-element method. The geographic distribution of aquifer characteristics and net-flux rates (the difference between recharge and net discharge) are represented in the model by assigning values of these and other properties of the ground-water system to specific locations in the finite-difference or finite-element grid used to obtain a numerical solution.

The design and construction of a ground-water model involve system characterization and parameter identification. System characterization is the process of developing a conceptual model and translating that conceptual model into mathematical terms. Decisions are made regarding determination of the flow domain to be incorporated into the model, the use of a one- , two- , or three-dimensional mathematical representation, the location and rate of net flux, the distribution and range of aquifer characteristics, and the boundary conditions of the flow domain. Parameter identification is the process of estimating system characteristics such as transmissivity or storage coefficient. This is accomplished by finding parameter values that are physically acceptable, and, when input in the model, adequately reproduce the measured water levels of the ground-water system.

For models of regional ground-water systems, important uncertainties in the development of the model frequently result from errors in characterization or in estimating recharge and pumpage. Adequate water-level data usually are available; however, data on recharge and pumpage may be inadequate to define these processes with a high degree of certainty. Furthermore, the contribution of these errors to the overall uncertainty in the model commonly is larger than that owing to other aspects of the model, such as aquifer characteristics. Consequently, net-flux values commonly are treated by ground-water hydrologists, in practical applications, as system parameters to be identified.

This paper describes a simple method for the identification of net-flux rates applicable to distributed-parameter ground-water models that treat the ground-water system as a linear or approximately linear system. The approach involves model generation of water-level response coefficients that result from recharge or pumpage and the use of these response coefficients in a least-squares method of parameter identification. The approach is applied as a practical problem to the identification of net-flux rates for the San Antonio Creek valley ground-water basin in southern California.

The application of least-squares methods to ground-water problems is not new. Cooley (1977 and 1979), Durbin (1978), and others have designed or applied nonlinear least-squares methods to the problems of identifying aquifer parameters, recharge and pumping, and initial

[1]U.S. Geological Survey, San Diego, Calif.
[2]S.S. Papadopulos and Assoc., Inc., Davis, Calif.

conditions. The method described herein is a special case of this previous work, where the identification problem is linear in the quantity to be identified.

## MATHEMATICAL FORMULATION

### Response Functions

A generalized linear-response lumped-parameter model of a ground-water system is given by the relation

$$\bar{h}=\bar{h}_o+\bar{\alpha}^T\bar{q}, \tag{1}$$

where

$\bar{h}\equiv[h_1,h_2,\ldots,h_n]^T$ is a vector of computed water levels,

$\bar{h}_o\equiv[h_{o_1},h_{o_2},\ldots,h_{o_n}]^T$ is a vector of relaxed initial water levels,

$\bar{q}\equiv[q_1,q_2,\ldots,q_m]^T$ is a vector of net-flux values, and

$T$ indicates that the matrix or vector is transposed.

$$\bar{\alpha}\equiv\begin{bmatrix}\alpha_{11} & \alpha_{12} & \cdots & \alpha_{1n}\\ \alpha_{21} & \alpha_{22} & \cdots & \alpha_{2n}\\ . & . & & .\\ . & . & & .\\ . & . & & .\\ \alpha_{m1} & \alpha_{m2} & \cdots & \alpha_{mn}\end{bmatrix}$$

is a matrix of unit-response coefficients. In the simplest case, $\alpha_{ij}$ is the ratio of $h_j$ to $q_i$. Alternatively, $\bar{\alpha}$ can be expressed as

$$\bar{\alpha}=\bar{\nabla}_q\bar{h}^T, \tag{2}$$

where

$\bar{\nabla}_q\equiv[\partial/\partial q_1,\partial/\partial q_2,\ldots,\partial/\partial q_m]^T$.

The elements of vectors $\bar{h}$ and $\bar{q}$ can arbitrarily be distributed in space and time. These elements correspond to locations and time periods where measured water levels are available and recharge or discharge occur. The elements of vector $\bar{h}_o$ usually represent water levels, corresponding to $\bar{h}$ in space and time, that would occur in the absence of recharge or pumpage. Stated differently, the vector $\bar{h}_o$ represents the relaxation of the initial conditions, but it can additionally represent the effects on water levels of net flux not included in $\bar{q}$. The elements of $\bar{h}_o$ and $\bar{\alpha}$ embed factors such as the geometry of the flow domain, the aquifer characteristics, and the boundary conditions on the flow domain.

Unit-response coefficients ($\alpha_{ij}$) are generated from the distributed-parameter model of the ground-water system. Separate model runs are made for each location represented by the elements of $\bar{q}$. For a particular location, a unit net flux, distributed in space and time proportionally to the distribution of a selected element of $\bar{q}$, is used as input to the distributed-parameter model. The water levels computed from the distributed-parameter model, corresponding in time and space to $\bar{h}$, are the unit-response coefficients.

The vector $\bar{h}_o$ also can be obtained from the distributed-parameter model by letting $\bar{q}=\bar{o}$ and computing water levels for specified initial conditions. The computed water levels corresponding in space and time to $\bar{h}$ are the elements of $\bar{h}_o$. Additionally, the vector $\bar{h}_o$ may be intended to represent more complex situations where, for example, the vector $\bar{h}_o$ may embed the effects of net flux other than that represented by $\bar{q}$. In such cases, water levels are computed for the specified initial conditions and net-flux rates. Again, the computed water levels corresponding in space and time to $\bar{h}$ are the elements of $\bar{h}_o$.

### Least-Squares Method

The least-squares method is used to identify net-flux rates such that the sum of squared residuals between computed and measured water levels is minimized. The sum of squared residuals is given by the relation

$$S_{LS}=(\bar{Y}-\bar{h})^T(\bar{Y}-\bar{h}), \tag{3}$$

where

$S_{LS}$ is the sum of squared residuals and

$\bar{Y}\equiv[Y_1,Y_2,\ldots,Y_n]^T$ is a vector of measured water levels corresponding in time and space to $\bar{h}$, the computed water levels.

$S_{LS}$ is minimized when

$$\bar{\nabla}_q S_{LS}=\bar{0}, \tag{4}$$

where

$\bar{\nabla}_q\equiv[\partial/\partial q_1,\partial/\partial q_2,\ldots,\partial/\partial q_m]^T$.

Several steps are followed to solve equation 4 for $q$. First, equation 3 is substituted into equation 4 to obtain

$$\bar{\nabla}_q(\bar{Y}-\bar{h})^T(\bar{Y}-\bar{h})=\bar{0}, \tag{5}$$

which can be expanded to obtain

$$\bar{\nabla}_q\bar{Y}^T-\bar{\nabla}_q\bar{h}^T)(\bar{Y}-\bar{h})=\bar{0}. \tag{6}$$

Second, because $\bar{\nabla}_q\bar{Y}^T=0$ and $\bar{\nabla}_q\bar{h}^T=\bar{\alpha}$ (eq 2), equation 6 reduces to

$$\bar{\alpha}(\bar{Y}-\bar{h})=\bar{0}. \tag{7}$$

Third, upon rearrangement of equation 7 and substitution of equation 1 for $\bar{h}$, the relation

$$\bar{\alpha}\bar{\alpha}^Tq=\bar{\alpha}(\bar{Y}-\bar{h}_O) \tag{8}$$

is obtained. However, equation 8 can be restated as

$$\bar{A}\bar{q}=\bar{b}, \tag{9}$$

where

$\bar{A}\equiv\bar{\alpha}\bar{\alpha}^T$ and $\bar{b}\equiv\bar{\alpha}$ $(\bar{Y}-\bar{h}_o)$, and equation 9 can be readily solved for $\bar{q}$ by any one of many standard methods for solving systems of linear equations (Forsythe and Moler, 1967).

An important point to be made regarding equation 9 is that the unit-response coefficients are independent of the least-squares algorithm. Consequently, the unit-response coefficients can be computed once, separate from the algorithm, which is not the case for general problems of parameter identification for ground-water models. The

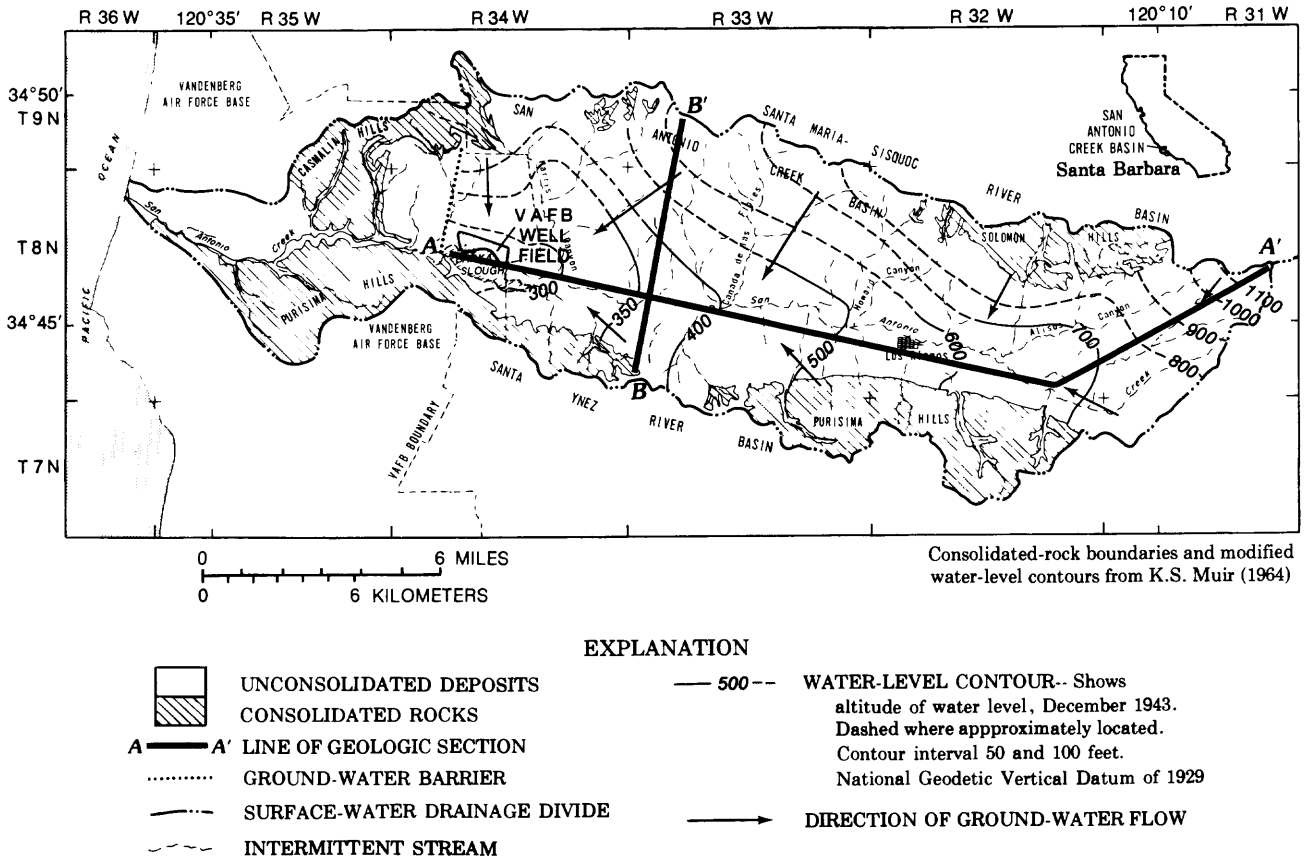


**Figure 1.** Generalized geology and December 1943 water-level contours in the San Antonio Creek valley.

unit-response coefficients are independent of the least-squares algorithm because the computed heads are linearly related to the net flux for a confined aquifer, and they are approximately linearly related for an unconfined aquifer.

## APPLICATION TO SAN ANTONIO CREEK VALLEY GROUND-WATER BASIN

The least-squares method was used to identify net-flux values for the San Antonio Creek valley ground-water basin in the west-central part of Santa Barbara County, Calif. The steady-state condition was used to estimate the geographic distribution of transmissivity from knowledge of natural net flux and ground-water levels. For the transient--state condition, information was available on the geographic distribution of the storage coefficient for the ground-water basin. Little information, however, was available for net flux. Due to the lack of adequate net-flux data, the least-squares method was used to estimate net-flux values from knowledge of aquifer characteristics and ground-water levels.

### Hydrologic Setting

The San Antonio Creek valley ground-water basin (fig. 1), which has an area of 154 $mi^2$, is contained within a northwestward-trending synclinal trough that is filled with a series of marine and continental sediments, Miocene to Holocene in age, that total about 10,000 ft in thickness. The lithology of the sediments has been generalized by Muir (1964) into the hydrologic units of unconsolidated water-bearing deposits and consolidated nonwater-bearing rocks. The consolidated rocks are sedimentary rocks, predominantly marine in origin. The consolidated rocks that are nearly impermeable, except for slightly permeable sandstone and for fracture zones, form the lower and lateral boundaries of the ground-water basin (fig. 2). The unconsolidated deposits of mostly sand and gravel blanket the central part of the valley and form the ground-water basin. The unconsolidated deposits range in thickness from 3,000 ft in the central part of the basin to nonexistent along its perimeter.

Natural recharge to the ground-water basin is derived from rainfall within the San Antonio Creek valley. As rain falls on the unconsolidated deposits of the valley, it either (1) is held as soil moisture, (2) infiltrates past the root zone to recharge the ground-water basin, or (3) runs off to stream channels where it may contribute to recharge by seepage through permeable streambeds. For steady-state conditions, Martin (1985) estimated that ground-water recharge by deep percolation of rainfall averaged 4,700 acre-ft/yr and ground-

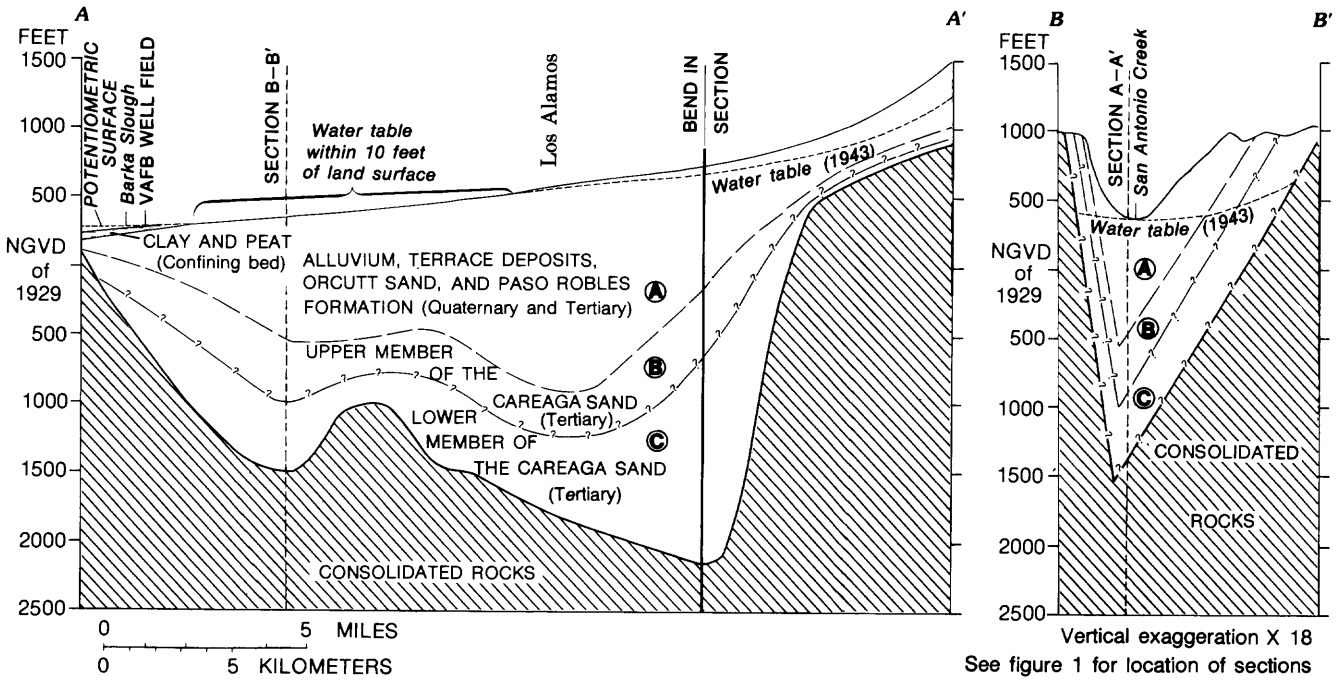


**Figure 2.** Diagrammatic geologic sections of the San Antonio Creek valley. Modified from Hutchinson (1980).

water recharge by streamflow infiltration averaged 1,500 acre-ft/yr. Steady-state conditions are represented by the period prior to the early 1940's.

Ground water in the basin is discharged naturally by evapotranspiration and base flow along the lower reach of San Antonio Creek valley and artificially by pumpage. In the middle and lower parts of the ground-water basin, ground-water gradients are toward San Antonio Creek (fig. 1), and ground water discharges by evapotranspiration along the stream channel. At the lower end of the basin, a subsurface ridge of consolidated rock creates a ground-water barrier (fig. 1) that forces ground water to discharge into Barka Slough, which is a marsh area. For steady-state conditions, Martin (1985) estimated that natural ground-water discharge was 400 acre-ft/yr along San Antonio Creek valley and 4,300 acre-ft/yr in Barka Slough.

Ground-water development since the early 1940's, primarily for agricultural and military use, has produced a transient-state condition. The increased pumpage, which in 1977 was 8,950 acre-ft/yr, has resulted in ground-water-level declines of as much as 15 ft beneath the San Antonio Creek valley channel from 1944 to 1977. During this period, ground-water pumpage was in excess of the natural recharge, and the water was derived from either aquifer storage or from a reduction in the amount of ground water naturally discharged from the aquifer.

## Ground-Water Model

Martin (1985) developed a ground-water flow model for the San Antonio Creek valley ground-water basin. The basin was represented by the two-dimensional equation of ground-water flow for an isotropic heterogeneous aquifer. The governing equation was solved by the finite-difference method using an algorithm developed by McDonald and Harbaugh (1984). The finite-difference grid is shown in figure 3. The boundary conditions on the flow domain represented by the grid are a no-flow boundary on the contact between the unconsolidated deposits and consolidated rocks, and for part of the northern boundary, a ground-water divide.

From estimated natural recharge and measured water levels, the geographic distribution of transmissivity was identified from steady-state conditions. A trial-and-error procedure was used in the identification, which involves the adjustment of transmissivity values until the ground-water model reasonably reproduces the measured water levels. Figure 4 shows a comparison between computed and measured water levels, and figure 5 shows the final distribution of transmissivity. Model-calibrated transmissivity ranged from less than 100 to 20,000 $ft^2/d$. The transmissivity values used in this model do not change with water-level fluctuations, even though the ground-water system is mostly unconfined. This was done because water-level changes (less than 15 ft) are small compared to the thickness of unconsolidated deposits (as much as 3,000 ft) and had little effect on the transmissivity values used in the model. It was also done because head-independent transmissivities result in a linear ground-water model.

The aquifer is unconfined, except in the area of Barka Slough where it is confined by a near-surface layer of clay.

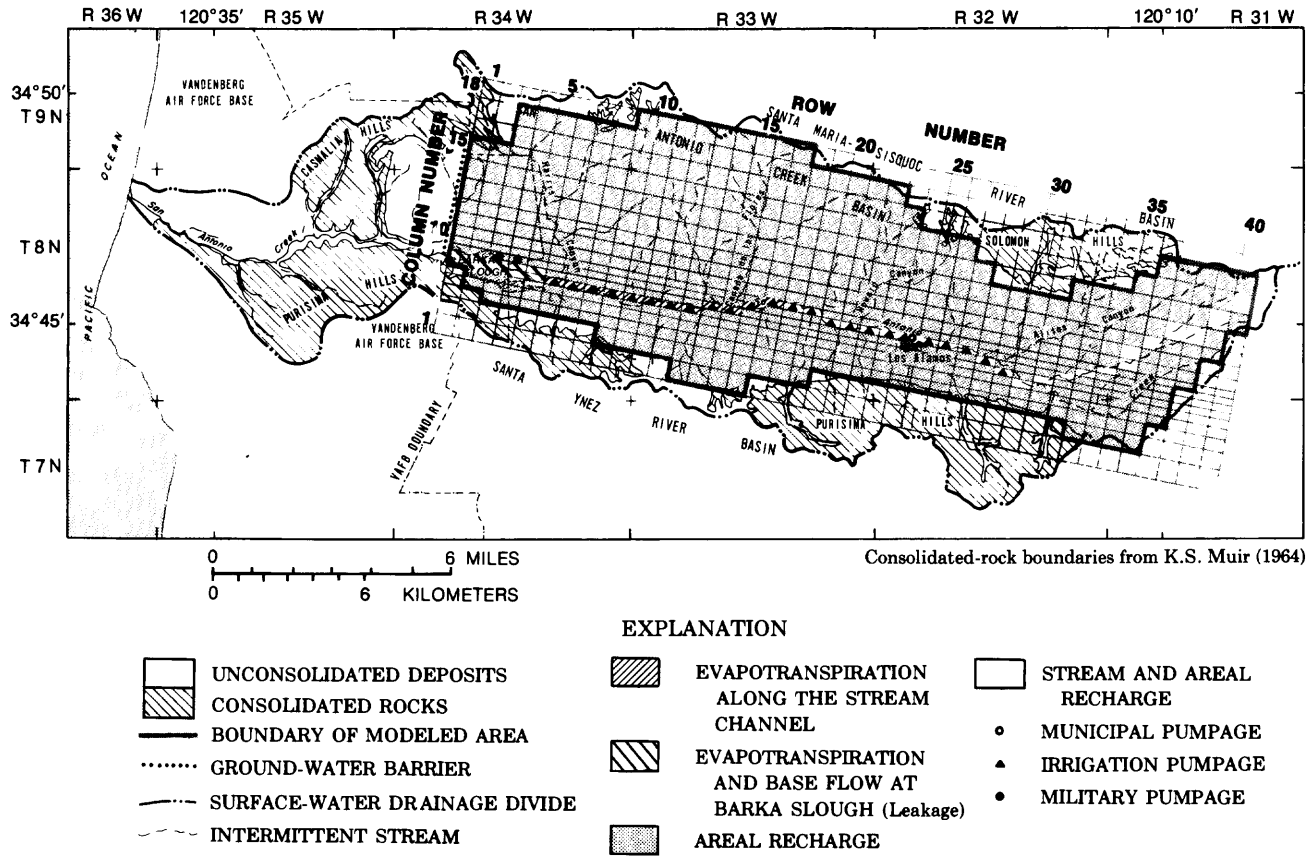


**Figure 3.** Finite-difference grid with model blocks used to simulate recharge and discharge.

An aquifer test at Barka Slough indicated a storage coefficient of 0.001 (Hutchinson, 1980), and this value was used in the model. A specific-yield value of 0.15 was used in other parts of the modeled domain; this value was determined for the nearby Cuyama and Santa Ynez Valleys (Singer and Swarzenski, 1970; and Miller, 1976). On the assumption that the aquifers in the Cuyama Valley, San Antonio Creek valley, and Santa Ynez Valley are similar, the specific-yield value of 0.15 was used in the model.

## Identification of Net-Flux Rates

To quantify net flux for the ground-water model, information is needed on ground-water levels and aquifer characteristics. In a practical sense, information also is needed on the general geographic distribution of net flux. Therefore, application of the method involves the steps of (1) establishing possible net-flux locations based on knowledge of recharge and discharge sites such as streams and wells, (2) selecting a set of reliably measured water levels that allow identification of net-flux rates, (3) computing unit-response coefficients from the distributed-parameter model based on knowledge of aquifer characteristics, and (4) assembling this information into the terms of equation 9 for solution of the net-flux rates.

The net-flux rates ($\bar{q}$) can be written as a [42×1] vector as follows:

$$\bar{q} = \begin{bmatrix} q_1^1 \\ q_2^1 \\ \vdots \\ q_7^1 \\ q_1^2 \\ q_2^2 \\ \vdots \\ q_7^2 \\ \vdots \\ q_1^6 \\ q_2^6 \\ \vdots \\ q_7^6 \end{bmatrix}$$

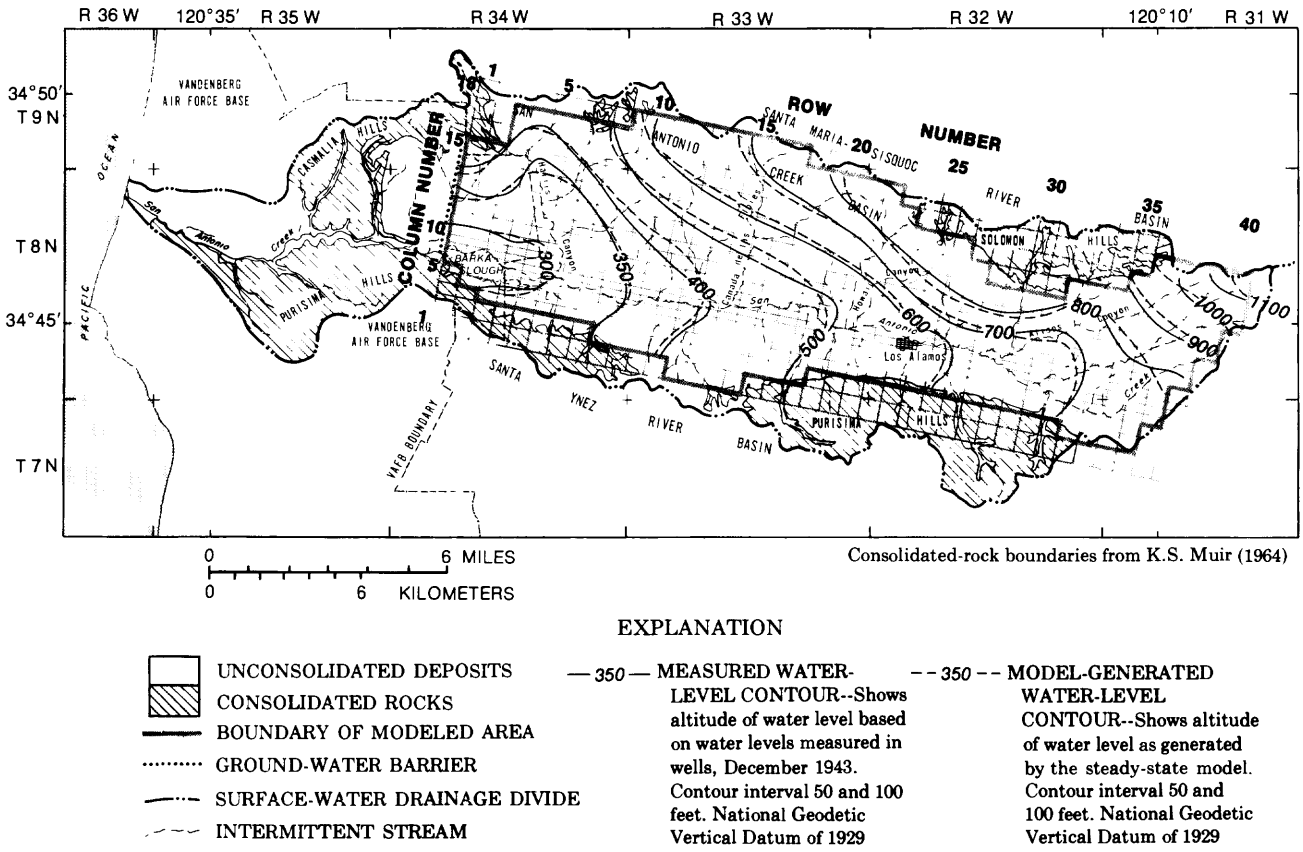


**Figure 4.** Comparison of measured and model-generated water levels for steady-state conditions (1943).

where the element $q_i^k$ represents the net-flux rate in the $k$th stress period at the $i$th subreach.

*Geographic distribution of net flux* ($\bar{q}$).—Almost all of the ground water used for agricultural, municipal, and military purposes is withdrawn from the aquifer in the narrow corridor beneath San Antonio Creek valley from about 2 mi east of Los Alamos to the western edge of Barka Slough (fig. 1). Historically, this was a reach of natural ground-water discharge into the channel of San Antonio Creek including base flow and evapotranspiration. After 1943, ground-water pumpage along the channel lowered water levels below the channel, thereby increasing the quantity of recharge from streamflow seepage and reducing the quantity of ground water naturally discharged from the aquifer. Data are not available to separate the effects of recharge, natural discharge, and pumpage. Consequently, only net quantities of pumpage, evapotranspiration, and ground-water exchanges with streamflow were identified.

The transient-state simulation of the ground-water basin was used to estimate net-flux rates for seven subreaches along San Antonio Creek valley (fig. 6) and six stress periods by the least-squares method. Each of the subreaches was one model grid-block wide and from two to five grid-blocks long. The six stress periods ranged from 4 to 9 yr as follows: 1944–52, 1953–57, 1958–63, 1964–67, 1968–73, and 1974–77. Within a subreach and stress period, the net-flux rate was assumed to be uniform in space and time, and each of these net-flux rates is an element of the vector $\bar{q}$; therefore, $\bar{q}$ is a [42×1] vector.

*Measured water levels* ($\bar{Y}$).—Forty-two measured water levels were used in the identification of net-flux values. A water level was selected to represent each subreach at the end of each pumping period from composite water-level hydrographs constructed from available data for each subreach (fig. 7). Because few water-level data were available, water levels selected for subreaches 4, 5, and 7 were estimated from hydrographs prepared for adjacent subreaches. In cases where available measured water levels appeared to be from pumping or recently pumped wells, the water-level trend determined from measurements prior to and subsequent to the affected measurements were used to estimate the representative water level. Equation 9 includes the measured water levels within the term $(\bar{Y}-\bar{h}_o)$ where $\bar{Y}$ is the vector of measured water levels and $\bar{h}_o$ is the vector of relaxed initial conditions. For the San Antonio Creek valley ground-water basin, the initial conditions represent steadystate conditions. Concomitantly, $\bar{h}_o$ is constant in time, and $(\bar{Y}-\bar{h}_o)$ is the water-level change from steadystate condition.

The measured water-level changes can be written as a [42×1] vector as follows:

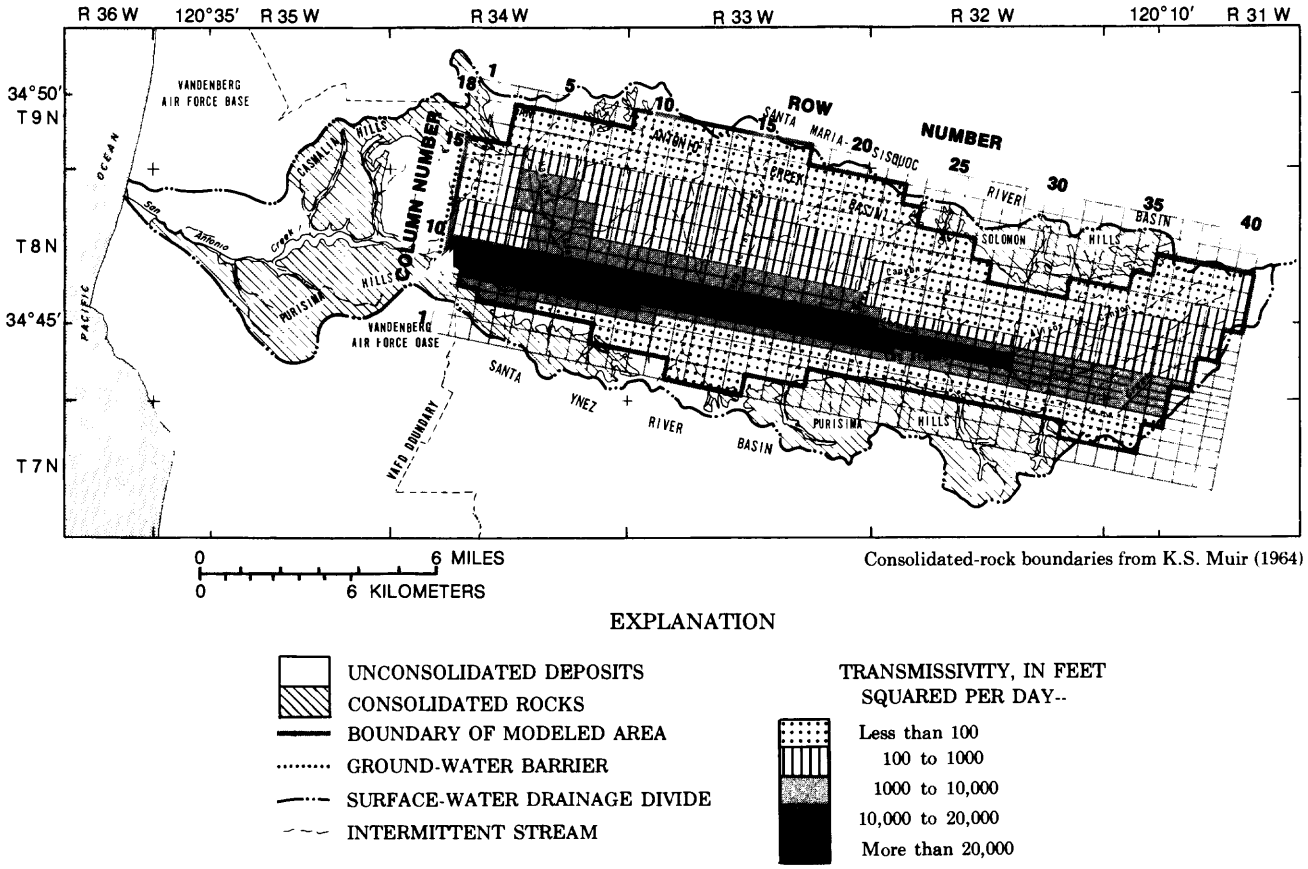


**Figure 5.** Distribution of transmissivity as calibrated by the model.

$$\bar{Y}-\bar{h}_o = \begin{bmatrix} (Y-h_o)_1^1 \\ (Y-h_o)_1^2 \\ \vdots \\ (Y-h_o)_1^6 \\ (Y-h_o)_2^1 \\ (Y-h_o)_2^2 \\ \vdots \\ (Y-h_o)_2^6 \\ \vdots \\ (Y-h_o)_7^1 \\ (Y-h_o)_7^2 \\ \vdots \\ (Y-h_o)_7^6 \end{bmatrix}$$

where the element $(Y-h_o)_i^k$ represents the water-level change from steady-state conditions to the end of the $k$th stress period measured in the $i$th subreach.

For the application of the method to the San Antonio Creek valley ground-water basin, the vector $\bar{Y}-\bar{h}_o$ has the same dimension as the vector $\bar{q}$. Consequently, the solution of equation 9 for $\bar{q}$ will produce a set of net fluxes such that, when substituted into the ground-water model, the computed heads will exactly match the measured water levels represented in the vector $\bar{Y}$. Then, the application is equivalent to the problem of fitting a straight line through two data points, which has particular statistical consequences owing to the zero degrees of freedom. In more general application, the number of measured water levels will exceed the number of net-flux values to be identified. Then, the substitution of the identified net-flux values into the ground-water model will not, in general, produce computed heads that exactly match the measured water levels. Furthermore, such an application is equivalent to the problem of fitting a straight line through a group of three or more data points.

*Unit-response coefficient* ($\alpha$).—The unit-response coefficients were determined for the different stress periods by inputting a 1.0-ft$^3$/s negative flux (unit pumpage) into a

designated subreach for the length of the stress period and recording the water-level change in response to the unit net flux in each of the seven subreaches at the end of each stress period. For subreaches represented by more than one block of the finite-difference grid, the unit net flux was distributed equally over all the blocks with a cumulative rate of −1 $ft^3/s$. While the unit response for a particular subreach was being determined, all other fluxes were kept the same as steady-state conditions. This procedure was repeated for each of the six stress periods. By this approach, 42 model runs were required to produce all the unit-response values. The computed unit-response values can be written as a [42×42] matrix as follows:

$$\bar{\alpha} = \begin{bmatrix} \alpha_{11}^{11} \alpha_{11}^{12} \cdots \alpha_{11}^{16} & \alpha_{12}^{11} \alpha_{12}^{12} \cdots \alpha_{12}^{16} & \cdots & \alpha_{17}^{11} \alpha_{17}^{12} \cdots \alpha_{17}^{16} \\ \alpha_{21}^{11} \alpha_{21}^{11} \cdots \alpha_{21}^{16} & \alpha_{22}^{11} \alpha_{22}^{12} \cdots \alpha_{22}^{16} & \cdots & \alpha_{27}^{11} \alpha_{27}^{12} \cdots \alpha_{27}^{16} \\ \vdots & & & \vdots \\ \alpha_{71}^{11} \alpha_{71}^{12} \cdots \alpha_{71}^{16} & \alpha_{72}^{11} \alpha_{72}^{12} \cdots \alpha_{72}^{16} & \cdots & \alpha_{77}^{11} \alpha_{77}^{12} \cdots \alpha_{77}^{16} \\ \alpha_{11}^{21} \alpha_{11}^{12} \cdots \alpha_{11}^{26} & \alpha_{12}^{21} \alpha_{12}^{22} \cdots \alpha_{12}^{26} & \cdots & \alpha_{17}^{21} \alpha_{17}^{22} \cdots \alpha_{17}^{26} \\ \alpha_{21}^{21} \alpha_{21}^{22} \cdots \alpha_{21}^{26} & \alpha_{22}^{21} \alpha_{22}^{22} \cdots \alpha_{22}^{26} & \cdots & \alpha_{27}^{21} \alpha_{27}^{22} \cdots \alpha_{27}^{26} \\ \vdots & & & \vdots \\ \alpha_{71}^{21} \alpha_{71}^{22} \cdots \alpha_{71}^{26} & \alpha_{72}^{21} \alpha_{72}^{22} \cdots \alpha_{72}^{26} & \cdots & \alpha_{77}^{21} \alpha_{77}^{22} \cdots \alpha_{77}^{26} \\ \vdots & \vdots & \vdots & \vdots \\ \alpha_{11}^{61} \alpha_{11}^{62} \cdots \alpha_{11}^{66} & \alpha_{12}^{61} \alpha_{12}^{62} \cdots \alpha_{12}^{66} & \cdots & \alpha_{17}^{61} \alpha_{17}^{62} \cdots \alpha_{17}^{66} \\ \alpha_{21}^{61} \alpha_{21}^{62} \cdots \alpha_{21}^{66} & \alpha_{22}^{61} \alpha_{22}^{62} \cdots \alpha_{22}^{66} & \cdots & \alpha_{27}^{61} \alpha_{27}^{62} \cdots \alpha_{27}^{66} \\ \vdots & & & \vdots \\ \alpha_{71}^{61} \alpha_{71}^{62} \cdots \alpha_{71}^{66} & \alpha_{72}^{61} \alpha_{72}^{62} \cdots \alpha_{72}^{66} & \cdots & \alpha_{77}^{61} \alpha_{77}^{62} \cdots \alpha_{77}^{66} \end{bmatrix}$$

where the element $\alpha_{ij}^{kl}$ represents the computed water-level change in the $j$th subreach at the end of the $l$th stress period in response to a unit net flux in the $i$th subreach during the $k$th stress period. For a particular element, where $(l-k)<0$ then $\alpha_{ij}^{kl}=0$.

*Solution for net flux ($\bar{q}$).*—When the values of $\bar{\alpha}$ and $(\bar{Y}-\bar{h}_o)$ are assembled into equation 8, a system of 42 linear equations and 42 unknown $\bar{q}$'s is obtained. This system was solved for $\bar{q}$ by an elimination method (Forsythe and Moler, 1967). The computed net-flux rates represent the net effects of pumping, irrigation returns, evapotranspiration, and stream-aquifer interactions.

The computed net-flux rates were input into the distributed-parameter model to test the reasonableness of the computed values. Figure 8 shows water-level contours produced from measured and computed data for the entire ground-water basin at the end of 1977. Comparison of the measured and computed water-level contours shows similar regional patterns of ground-water flow indicating that the computed net-flux rates closely simulate the hydrologic response of the regional ground-water system, as well as the response in the immediate area of the calibrated reach of the San Antonio Creek valley channel.

Another test of the reasonableness of the computed net-flux rates was to compare the computed net-flux rates in subreach 1 to measured rates (table 1). This was possible in subreach 1 because this subreach simulates military pumpage at Barka Slough, which is a metered supply. As shown in table 1, the computed and measured values compare well.

**Table 1.** Comparison of computed net-flux values to measured military pumpage in subreach 1

[All values in acre-ft/yr: Negative sign indicates water being removed from the aquifer system]

| Stress period | Computed net flux | Military pumpage |
|---|---|---|
| 1 (1944–52) | +10 | 0 |
| 2 (1953–57) | −30 | 0 |
| 3 (1958–63) | −10 | 0 |
| 4 (1964–67) | −1,310 | −1,390 |
| 5 (1968–72) | −1,220 | −1,230 |
| 6 (1973–77) | −1,900 | −1,830 |

To verify the model and the computed net-flux rates, the model was used to simulate the period from 1978 to 1982 using the annual change in net-flux rates determined by Martin (1985). During the verification period, military and net irrigation pumpage increased by more than 70 percent (6,310 acre-ft/yr). Water-level changes computed by the model during the verification run are compared to measured values on the later part of the hydrographs in figure 7. As shown in the hydrographs, the model closely duplicates the measured water levels during the verification period. The results of this run substantiate that the model and the computed net-flux rates are capable of duplicating the measured response of the aquifer.

## CONCLUSIONS

A simple least-squares method can be used to identify net-flux values for a linear or approximately linear distributed-parameter ground-water model. The method is independent of the algorithm used in the distributed-parameter model because the model is used externally from

the least-squares algorithm. From knowledge of aquifer characteristics, measured water levels, and the geographic location of recharge and discharge, the method will estimate net-flux rates. This is accomplished by using the model to derive unit-response coefficients for water levels in terms of unit pumpage or recharge. These coefficients, along with measured water levels, are assembled into a system of linear equations with net-flux rates as the unknown quantity. This system of equations can then be solved for the unknown net-flux rates.

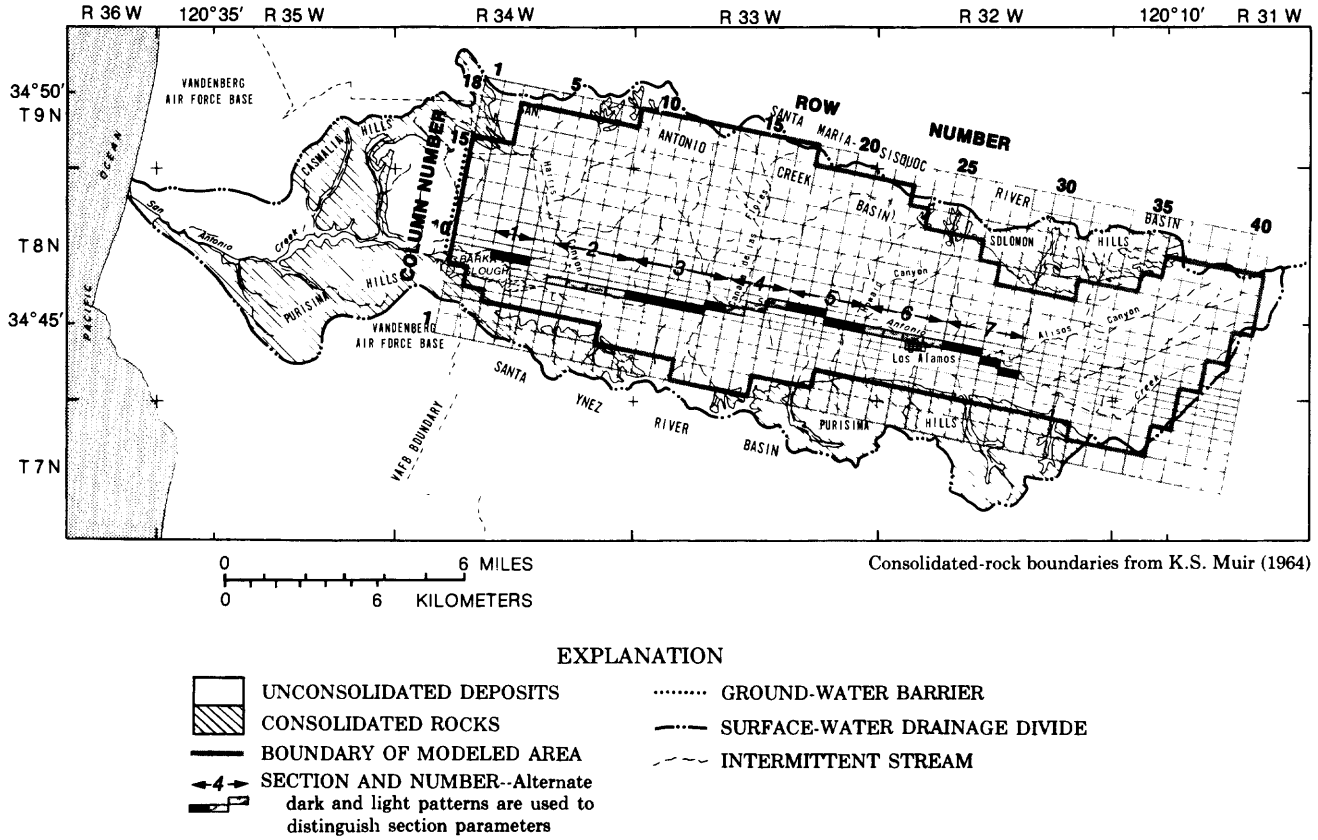


**Figure 6.** Location of subreaches used in the net-flux calibration.

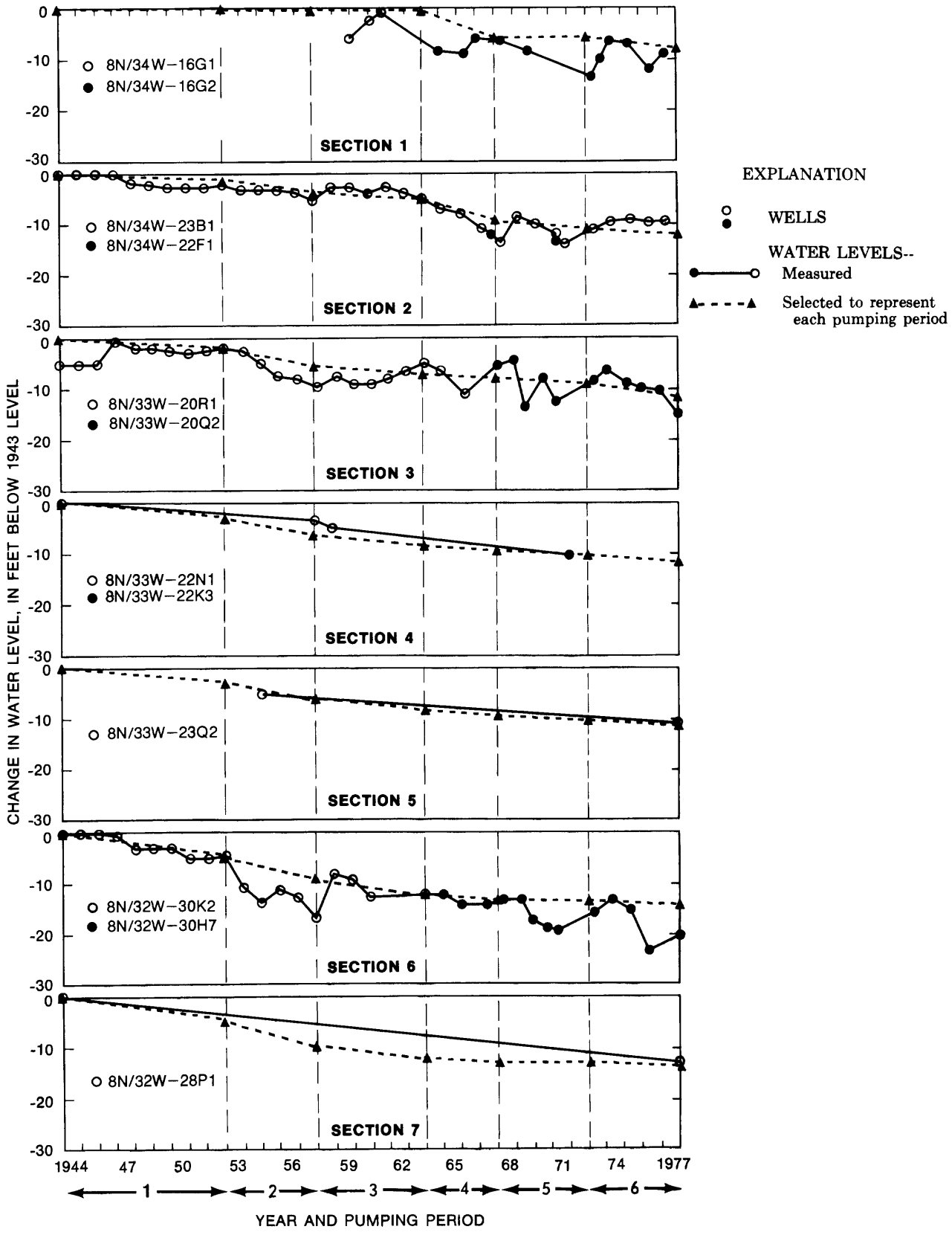


**Figure 7.** Comparison of historical measured water levels and water levels selected to be representative of a particular subreach and pumping period.

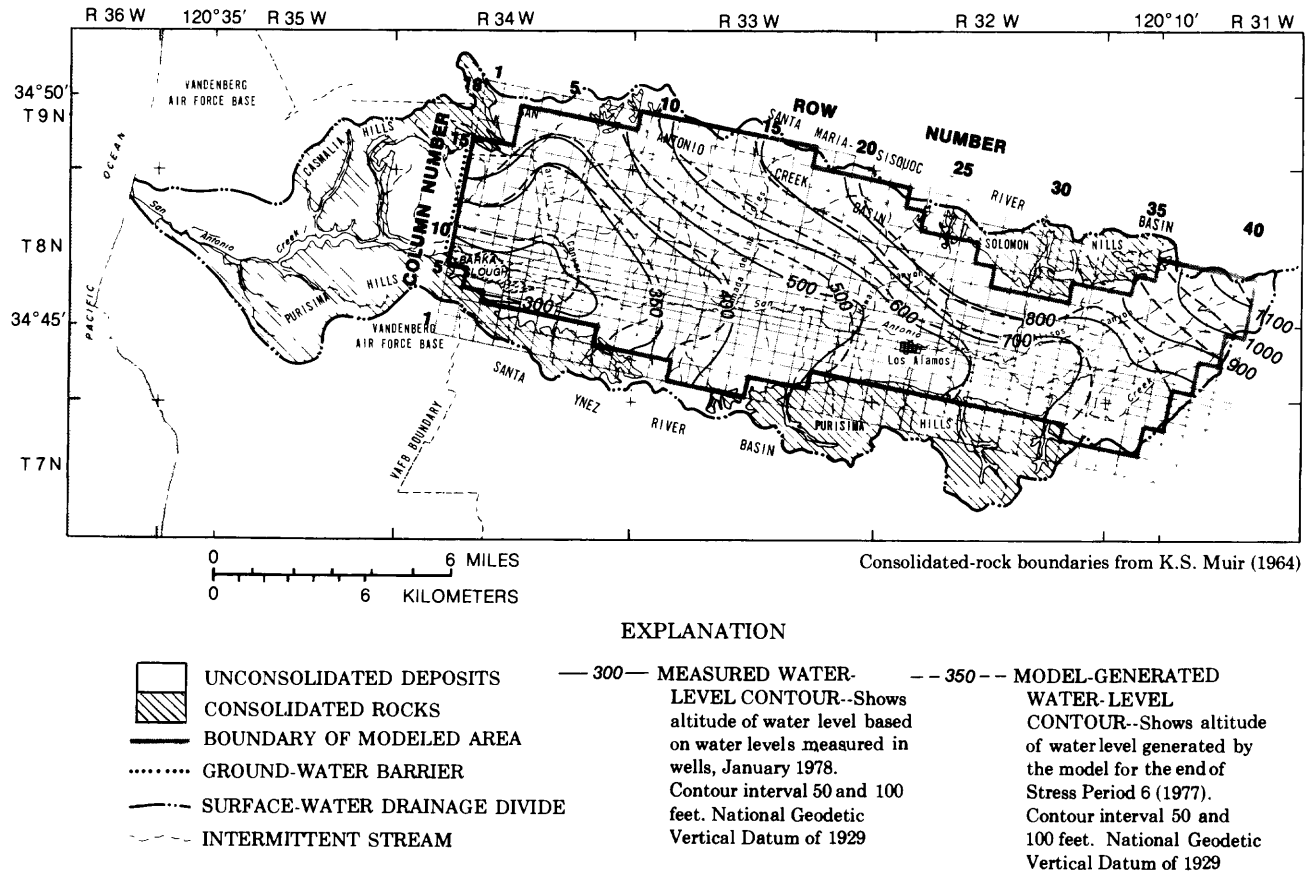


**Figure 8.** Comparison of water-level contours from field data for January 1978 and those from model results for the end of 1977.

## REFERENCES CITED


Cooley, R.L., 1977, A method of estimating parameters and assessing reliability for models of steady-state ground-water flow. Part 1, Theory and numerical properties: Water Resources Research, v. 13, no. 2, p. 318–324.

———1979, A method of estimating parameters and assessing reliability for models of steady-state ground-water flow. Part 2, Application of statistical analysis: Water Resources Research, v. 15, no. 3, p. 603–617.

Durbin, T.J., 1978, Application of Gauss algorithm and Monte Carlo simulations to the identification of aquifer parameters, *in* Verification of mathematical and physical models in hydraulic engineering: American Society of Civil Engineers 26th Annual Hydraulic Division Speciality Conference, College Park, Maryland, Proceedings, p. 101–111.

Forsythe, G.E., and Moler, C., 1967, Computer solution of linear algebraic equations: Englewood Cliffs, N.J., Prentice-Hall, 375 p.

Hutchinson, C B., 1980, Appraisal of ground-water resources in the San Antonio Creek valley, Santa Barbara County, California: U.S. Geological Survey Open-File Report 80–750, 48 p.

Martin, Peter, 1985, Development of a two-dimensional model for the analysis of the ground-water flow system in the San Antonio Creek valley, Santa Barbara County, California: U.S. Geological Survey Water-Resources Investigations Report 84–4340, 68 p.

McDonald, M.G., and Harbaugh, A.W., 1984, A modular three-dimensional finite-difference ground-water flow model simulation in three dimensions: U.S. Geological Survey Open-File Report 83–875, 528 p.

Miller, G.A., 1976, Ground-water resources in the Lompoc area, Santa Barbara County, California: U.S. Geological Survey Open-File Report 76–183, 78 p.

Muir, K.S., 1964, Geology and ground water of San Antonio Creek valley, Santa Barbara County, California: U.S. Geological Survey Water-Supply Paper 1664, 53 p.

Pinder, G.F., and Gray, W.G., 1977, Finite element simulation in surface and subsurface hydrology: New York, Academic Press, 295 p.

Prickett, T.A., and Lonnquist, C.G., 1971, Selected digital computer techniques for ground-water-resource evaluation: Illinois State Water Survey Bulletin 55, 62 p.

Remson, Irvin, Hornberger, G.M., and Moltz, F.J., 1971, Numerical methods in subsurface hydrology: New York, Wiley-Interscience, 389 p.

Singer, J.S., and Swarzenski, W.V., 1970, Pumpage and ground-water storage depletion in Cuyama Valley, California, 1947–66: U.S. Geological Survey Open-File Report, 22 p.

Trescott, P.C., 1975, Documentation of finite-difference model for simulation of three-dimensional ground-water flow: U.S. Geological Survey Open-File Report 75–438, 32 p.

Wang, H.F., and Anderson, M.P., 1982, Introduction to ground water modeling: Finite difference and finite element methods: San Francisco, W.H. Freeman and Co., 237 p.

# A Method for Estimating Velocity and Depth of Streams at Low Flow in Southeastern Louisiana

*By* Fred N. Lee

**Abstract**

An analysis of 222 low-flow discharge measurements from 20 streamflow sites in southeastern Louisiana indicated that a relation exists between the 7-day, 10-year, low-flow discharge and stream channel cross-sectional width. The equation developed from this relation had a standard error of estimate of ± 23 percent with an adjusted coefficient of determination of 0.84.

The traveltime for a 7-day, 10-year, low-flow discharge through a stream reach of an unregulated stream in southeastern Louisiana can be estimated by using an equation that estimates peak traveltime (*TP*) of a solute. This traveltime, when converted to a mean velocity ($V_A$), can be used in empirical reaeration equations, along with an estimated mean depth of the stream reach ($H_A$) to estimate the reaeration coefficient ($K_2$) of the stream reach.

## INTRODUCTION

The Louisiana Department of Environmental Quality is charged with issuing permits for injection of waste into streams in Louisiana. Before these permits can be issued, an assessment of the effect of the waste on the water quality of the stream has to be made to assure that the resultant water quality meets recommended State standards. The 7-day, 10-yr, low-flow discharge ($7Q_{10}$) is the design discharge for all permits. The reaeration coefficient ($K_2$) also is needed to determine rate of oxygen recovery in an individual stream.

To estimate the $K_2$ of a stream, costly data-collection activities (streamflow measurements, dye-tracer study, water samples, and mean depth of stream reach) are needed. These activities can last for an extended period of time and require the services of experienced field personnel. The manpower cost can be high, depending on the time required to collect the data. In addition, laboratory analysis of the water samples to determine the desorption rate of the stream is costly.

Several investigators have developed empirical equations for estimating the $K_2$ of natural streams. Bennett and Rathbun (1972, p. 48–57) summarized the regression equations developed by many of these investigators and showed that the general form of these equations is

$$K_2 = x(V_A^{\,y}/H_A^{\,z}), \qquad (1)$$

where

$K_2$=reaeration coefficient at 20 °C, in reciprocal days;
$x$=regression coefficient;
$V_A$=mean velocity of stream reach, in feet per second;
$H_A$=mean depth of stream reach, in feet;
$y$=exponent for mean velocity of stream reach; and
$z$=exponent for mean depth of stream reach.

The equation recommended by Bennett and Rathbun (1972, p. 56) for estimating the $K_2$ for natural streams is

$$K_2 = 8.76(V_A^{\,0.607}/H_A^{\,1.689}) \; . \qquad (2)$$

Although symbols used in this equation are different from those shown by Bennett and Rathbun, the definitions are the same.The purpose of this report is to present a simple and inexpensive method for estimating the flow parameters $V_A$ and $H_A$ for the $7Q_{10}$ for natural stream reaches in southeastern Louisiana (East and West Feliciana, St. Helena, Tangipahoa, Washington, St. Tammany, Livingston, and East Baton Rouge Parishes) shown in figure 1. Parameter values estimated from the method presented in this report can be used in equations such as equation 2 to give an estimate of the $K_2$ for stream reaches within the study area. The scope of the study includes:

1. Use of an equation by Lee (1985, p. 16) to estimate the $7Q_{10}$ at ungaged stream reaches within the study area,
2. Use of an equation by Calandro (1978, p. 5) to estimate $V_A$ for ungaged stream reaches in Louisiana, and
3. Evaluation of low-flow discharge measurements (1948–67) made at 20 selected partial-record sites throughout most of southeastern Louisiana (fig. 1). This evaluation is used to define an equation to compute the channel cross-sectional width ($W$) for the $7Q_{10}$ at ungaged stream reaches. The cross-sectional width is then used to estimate the mean depth of the stream reach.

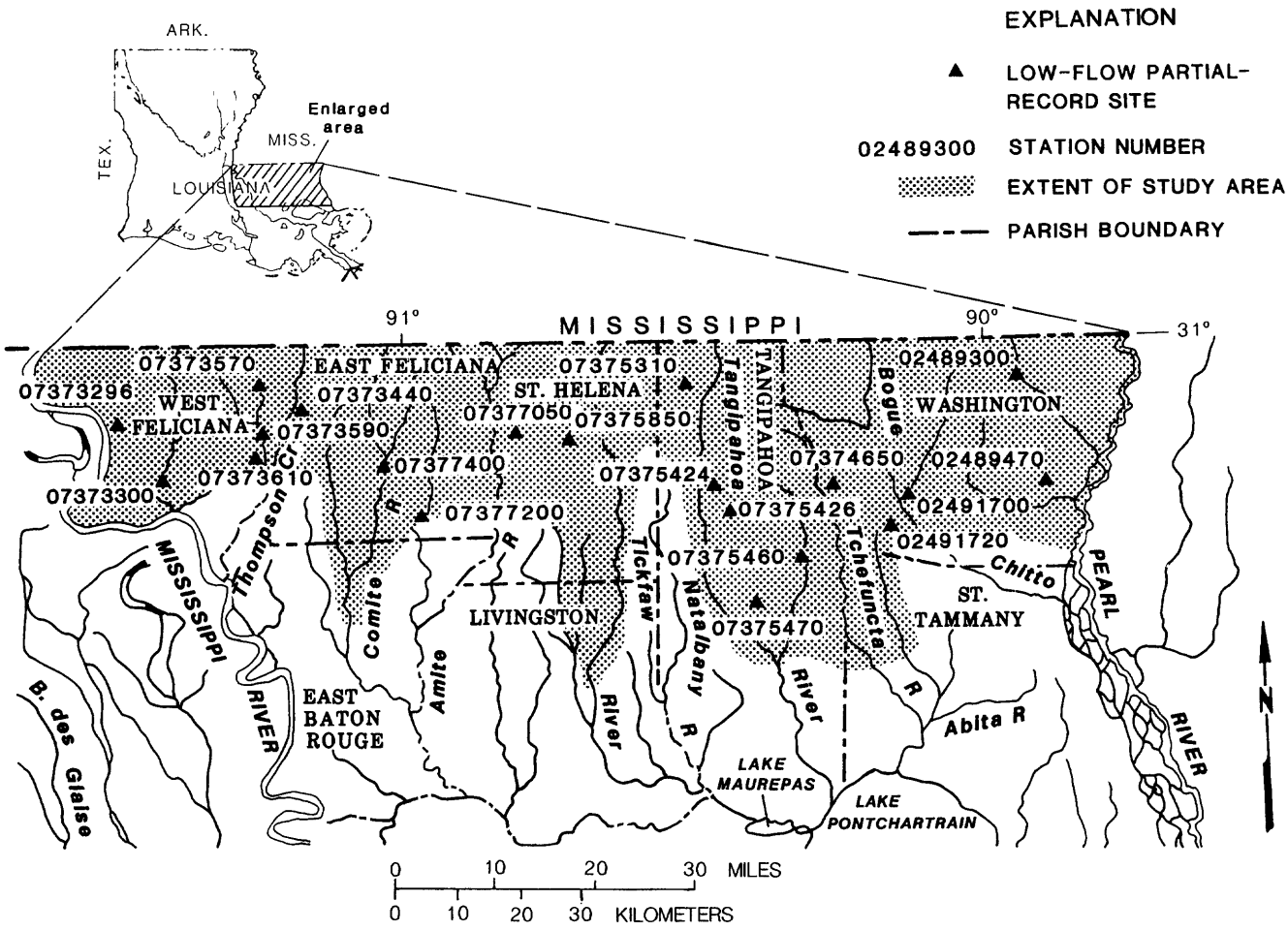


**Figure 1.** Location of streamflow sites and extent of study area.

## DESCRIPTION OF STUDY AREA

The study area is located in southeastern Louisiana (fig. 1). The boundary of the study area extends from the Mississippi River on the west to the Pearl River on the east. The northern boundary is the Mississippi State line. The southern boundary is represented by a line defined by Lee (1985, p. 3) that separates an area where the $7Q_{10}$ is equal to zero and an area of sustained low flow.

Most streams below the southern boundary line are typically shallow, and channel beds are, for the most part, underlain by clay and silt. Soils are underlain by a relatively impermeable subsoil that serves as a barrier between stream channels and the underlying aquifer systems. Large streams crossing the southern boundary are exceptions. These streams are relatively deep, cutting into the underlying aquifer systems, and, thus, have sustained flow year round (Lee, 1987, p. 4–5).

Major streams draining the area are Thompson Creek, Comite River, Amite River, Tickfaw River, Natalbany River, Tangipahoa River, Tchefuncta River, and Bogue Chitto. Thompson Creek drains into the Mississippi River, and the Bogue Chitto drains into the Pearl River. The other six streams drain either into Lake Maurepas or Lake Pontchartrain.

The entire study area is within the Southern Pine Hills belt of the Coastal Plain province (Fenneman, 1938). Characteristic features are the forests of long-leaf pine that cover most of the area. Small patches of cultivated land and many small stock ponds are scattered throughout the area. Soils are generally permeable sandy loams that allow rapid infiltration of rainfall. Stream channels consist of sand and gravel bed material and have numerous pools and riffles throughout. The channels meander back and forth across the wide, heavily vegetated flood plains.

The climate is humid subtropical. Average annual temperature is about 19 °C with the average monthly temperature ranging from about 11 °C during the winter months to about 27 °C during the summer months. Average midmonthly stream temperatures range from about 9 °C in January to about 27 °C in July (Calandro, 1973, p. 5).

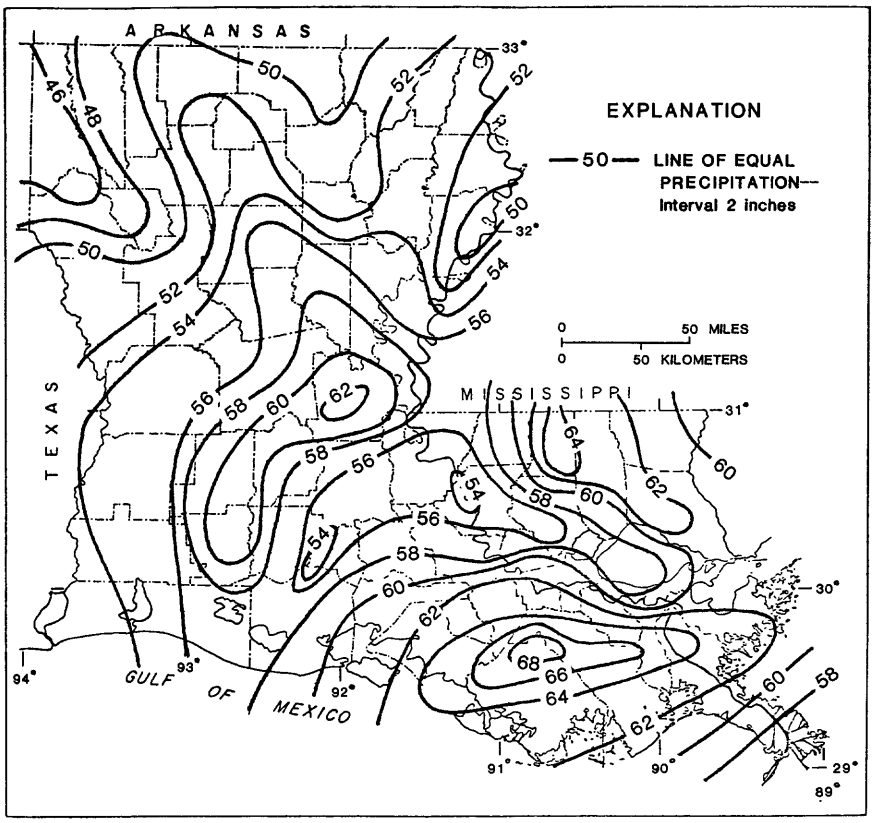


**Figure 2.** Mean annual precipitation for Louisiana for the period 1931–60. (From Neely, 1976.)

## ESTIMATION OF THE 7-DAY, 10-YR, LOW-FLOW DISCHARGE

Solution of equation 2 does not directly involve the need to know the $7Q_{10}$. This discharge is needed, however, to estimate $V_A$ included in that equation. The $7Q_{10}$ at ungaged sites with drainage areas less than 525 mi$^2$ in the study area can be computed by the following equation from Lee (1985, p. 16):

$$7Q_{10} = 1.22 \times 10^{-6}(DA)^{1.10}(P-35)^{3.15}(S)^{0.68}, \quad (3)$$

where

$7Q_{10}$ = 7-day, 10-yr, low-flow discharge, in cubic feet per second;
$DA$ = contributing drainage area, in square miles;
$P$ = mean annual precipitation, in inches; and
$S$ = main channel slope between the 10 and 85 percent channel distance upstream from the ungaged site, in feet per mile.

The $DA$ for most streams is listed in a report by Sloss (1971, p. 7–27). The $DA$ for those streams not shown by Sloss can be delineated on U.S. Geological Survey topographic maps and estimated by using planimetric techniques. Precipitation is taken from figure 2, and $S$ can be estimated by using U.S. Geological Survey topographic maps. Equation 3 is based on a log-linear regression analysis of low-flow discharge data for 90 streamflow sites (20 continuous-gaging stations and 70 partial-record stations). The standard error of estimate between the $7Q_{10}$ determined by equation 3 and the actual $7Q_{10}$ was ± 50 percent.

Figures 3, 4, and 5 show the relation between $DA$ and the $7Q_{10}$ for Bogue Chitto, Tangipahoa River, and Amite River, respectively. Because these streams have $DA$'s larger than 525 mi$^2$ at the farthest downstream gaged site, use of equation 3 to estimate the $7Q_{10}$ does not apply. Instead, figures 3, 4, and 5 can be used to estimate the $7Q_{10}$ for any reach along these three streams.

## MEAN VELOCITY IN STREAM REACH

Calandro (1978) used the results of time-of-travel measurements made on unregulated streams in Louisiana, from 1968 to 1977, to develop equations to estimate the leading edge, peak, and trailing edge traveltimes of a slug-injected solute through stream reaches in the State. Discharges of streams used in his studies ranged between the 50 and 99 percent duration. The equation that was developed to estimate the traveltime of the peak concentration of a solute is

$$TP = 7.01(L^{0.984}(DA)^{0.291}/Q^{0.553}), \quad (4)$$

where

$TP$=traveltime of the peak concentration through the stream reach, in hours;

$L$=stream reach length, in miles;

$Q$=discharge at downstream boundary of reach, in cubic feet per second; and

$DA$=contributing drainage area at downstream boundary of reach, in square miles.

Calandro (1978, p. 5) reported that the accuracy of $TP$ as determined by using equation 4 is within ± 25 percent of the field-measured $TP$. The mean reach velocity ($V_A$) can be computed by noting that by definition velocity = distance/time. From the traveltime of the peak concentration, $V_A$ can be computed as

$$V_A = 1.47(L/TP), \text{ in feet per second.} \quad (5)$$

To adapt equation 4 to estimate the traveltime of the $7Q_{10}$ through a stream reach, simply replace $Q$ with the $7Q_{10}$ estimated by equation 3. The $V_A$ for the $7Q_{10}$ is then computed by equation 5.

## MEAN DEPTH OF FLOW

For this study, the stream reach mean depth of flow for the 7-day, 10-yr, low-flow discharge is assumed to be equal to the stream reach mean hydraulic depth ($H_A$) as computed by the equation

$$H_A = A_A/W_A, \quad (6)$$

where

$H_A$=mean hydraulic depth of the stream reach, in feet, coinciding with the 7-day, 10-yr, low-flow discharge;

$A_A$=average cross-sectional area for the stream reach, in square feet, coinciding with the 7-day, 10-yr, lowflow discharge; and

$W_A$=average top width for the stream reach, in feet, coinciding with the 7-day, 10-yr, low-flow discharge.

The area ($A_A$) as used in equation 6, is computed by the continuity equation

$$A_A = 7Q_{10}/V_A, \quad (7)$$

where $A_A$ is as previously defined; $7Q_{10}$ is the 7-day, 10-yr, low-flow discharge as computed by using equation 3; and $V_A$ is the mean velocity for the stream reach computed by equation 5. A total of 222 low-flow discharge measurements, made at 20 low-flow partial-record sites (not the 20 continuous-record sites previously mentioned) within the study area, were used to define an equation to estimate the channel width ($W$) coinciding with the 7-day, 10-yr, low-flow discharge, at ungaged sites. For these 222 discharge measurements, made from 1948 to 1967, discharges ranged from 0.7 to 88 ft$^3$/s, and widths ranged from 2.5 to 91 ft. The values for widths ($W$) as shown in table 1 are the average top width for the low-flow discharge measurements made at each partial-record site. They were obtained by assuming that the true value for $W$, corresponding to the $7Q_{10}$, is the average width of the channel for measurements having discharge values within ± 50 percent of the $7Q_{10}$ computed by equation 3. Table 1 shows the $7Q_{10}$ and average $W$ for each of the 20 sites. These data were used in a log-linear regression analysis to develop an equation to estimate the cross-sectional width for ungaged sites. The equation defined by this analysis is

**Table 1.** Data used in regression analysis to develop method to estimate channel widths

| Partial record station number (fig. 1) | $DA$, contributing drainage area (mi$^2$) | $7Q_{10}$, discharge (cubic ft per second) (by eq. 3) | Average measured channel width, $W$ (ft) |
|---|---|---|---|
| 02489300 | 72.3 | 19 | 26 |
| 02489470 | 12.8 | 3.4 | 12 |
| 02491700 | 44.2 | 13 | 24 |
| 02491720 | 9.4 | 3.5 | 9.0 |
| 07373296 | 4.3 | 1.0 | 5.4 |
| 07373300 | 104 | 13 | 36 |
| 07373440 | 11.1 | 2.0 | 8.4 |
| 07373570 | 31.3 | 5.2 | 13 |
| 07373590 | 66.6 | 8.5 | 24 |
| 07373610 | 10.4 | 1.2 | 7.2 |
| 07374650 | 16.4 | 4.7 | 12 |
| 07375310 | 59.6 | 17 | 35 |
| 07375424 | 38.4 | 12 | 13 |
| 07375426 | 31.2 | 9.7 | 16 |
| 07375460 | 24.4 | 8.0 | 22 |
| 07375470 | 27.9 | 7.6 | 22 |
| 07375850 | 136 | 44 | 44 |
| 07377050 | 54.3 | 17 | 21 |
| 07377200 | 27.3 | 5.8 | 15 |
| 07377400 | 88.0 | 13 | 33 |

$$W = 6(7Q_{10})^{0.60}, \quad (8)$$

where

$W$ = estimated channel cross-sectional width, in feet, for the $7Q_{10}$ and

$7Q_{10}$ = the 7-day, 10-yr, low-flow discharge as estimated from equation 3.

Results of the log-linear regression analysis give a standard error of estimate of ± 23 percent with an adjusted coefficient of determination of 0.84. Figure 6 shows the relation between $W$ determined from equation 8 and $W$ as shown in table 1.

## LIMITATIONS

Equations shown in this publication have certain limitations of use. These limitations are shown below and should be adhered to when using these equations. Equation 3 was based on the following data: drainage area between 2.1 and 510 mi$^2$, precipitation between 46 and 64 in/yr, and

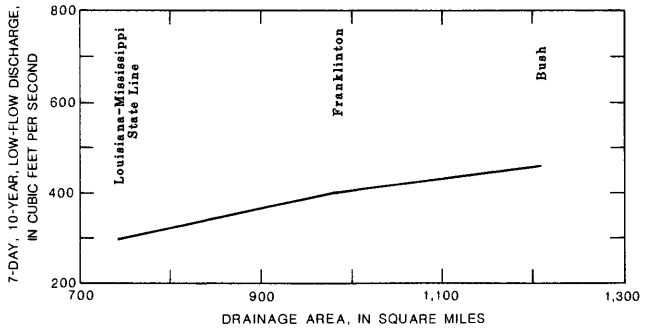


**Figure 3.** The 7-day, 10-yr, low-flow discharge as a function of drainage area for Bogue Chitto.

slope between 2.2 and 47.8 ft/mi (Lee, 1985, p. 17); this equation should not be extrapolated beyond the limits of these data.

Equation 4 was developed by using a wide range of discharges, drainage areas, and stream lengths. Calandro (1978, p. 4) states that this equation is applicable for all unregulated streams in Louisiana with drainage areas less than 2,000 $mi^2$.

Equation 8 was developed by using calculated data shown in table 1. This table shows a range in $7Q_{10}$ between 1.0 and 44 $ft^3/s$ and average measured channel widths between 5.4 and 44 ft. However, the data in table 1 are based on field measurements of discharge ranging between 0.7 and 88 $ft^3/s$ and widths between 2.5 and 91 ft. It is suggested that equation 8 be used for discharges and widths within the range of these field measurements.

## USE OF TECHNIQUE TO COMPUTE THE REAERATION COEFFICIENT

Equations 3 through 8 can be used to estimate $V_A$ and $H_A$ needed to solve reaeration coefficient equations such as equation 2. Six steps are required:

1. Compute the $7Q_{10}$ at the upstream and downstream boundary of the study reach by using equation 3 for streams with *DA* less than or equal to 525 $mi^2$, or figures 3, 4, or 5 for the three streams with *DA* greater than 525 $mi^2$, whichever applies.
2. Compute $V_A$ for the $7Q_{10}$ by using equations 4 and 5.
3. Compute $W_A$ by estimating $W$ at the upstream and downstream boundaries of the $L$, using equation 8, and average the results.
4. Estimate $A_A$ by using equation 7.
5. Compute $H_A$ by using equation 6.
6. Compute $K_2$ by using equation 2.

## EXAMPLE PROBLEM

To illustrate this procedure, a sample problem is given. Parameters used in the method (*DA*, *L*, *P*, and *S*) are assumed:

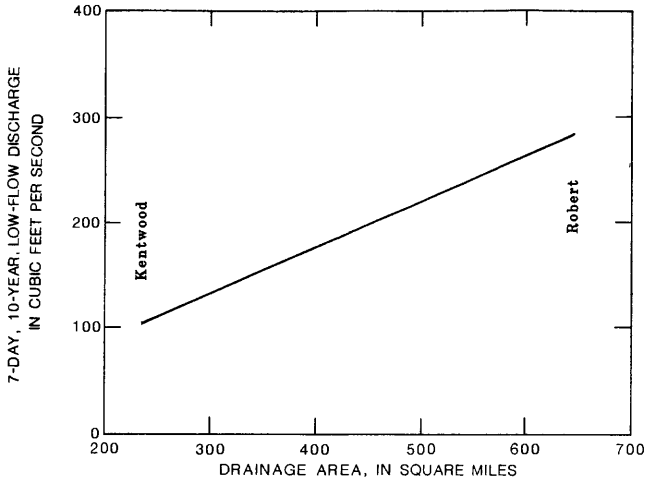


**Figure 4.** The 7-day, 10-yr, low-flow discharge as a function of drainage area for Tangipahoa River.

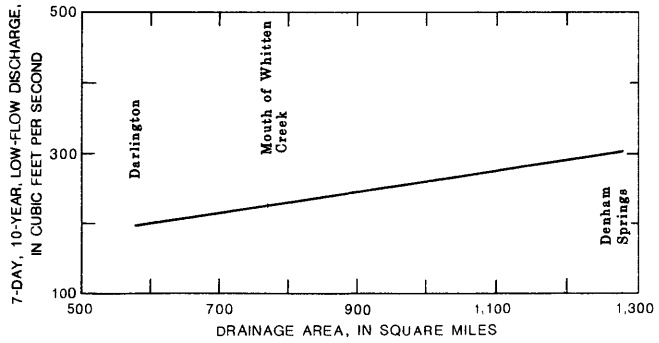


**Figure 5.** The 7-day, 10-yr, low-flow discharge as a function of drainage area for Amite River.

1. *DA* at the upstream boundary (us) of the reach is 90 $mi^2$.
2. *DA* at the downstream boundary (ds) of the reach is 100 $mi^2$.
3. $L$ is 1.0 mi.
4. $P$ is 60 in/yr.
5. $S$ is 7 ft/mi.

Step 1. Compute the $7Q_{10}$:

$$7Q_{10}\ (\text{us}) = 1.22 \times 10^{-6}(90)^{1.10}(60-35)^{3.15}(7)^{0.68}$$

$$7Q_{10}\ (\text{us}) = \underline{16.4}$$

$$7Q_{10}\ (\text{ds}) = \underline{1.22} \times 10^{-6}(100)^{1.10}(60-35)^{3.15}(7)^{0.68}$$

$$7Q_{10}\ (\text{ds}) = \underline{18.4}\ ft^3/s$$

Step 2. Compute the $V_A$:

$$TP = 7.01(1)^{0.984}(100)^{0.291}/18.4)^{0.553}$$

$$TP = 5.3\ h$$

$$V_A = 1.47\ (1/5.3) = \underline{0.28}\ ft/s$$

Step 3. Compute $W$ at the upstream and downstream boundaries and average the results:

$$W\ (\text{us}) = 6(16.4)^{0.60}$$

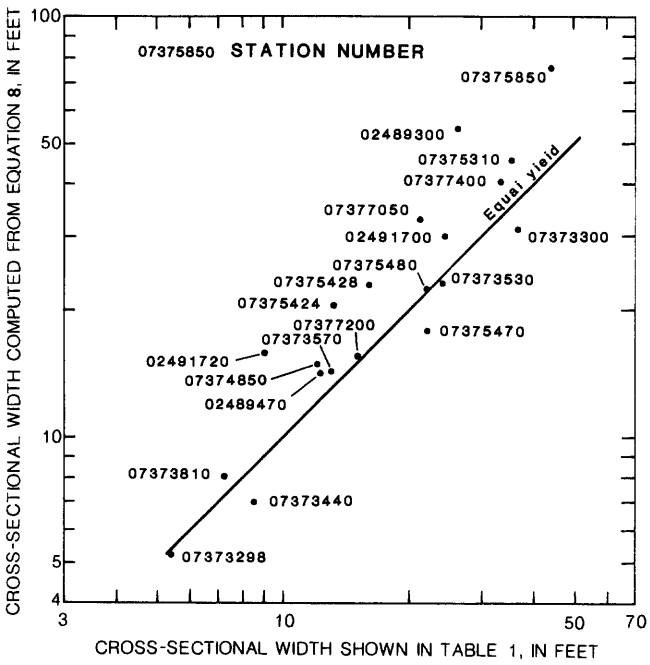


**Figure 6.** Relation between measured and computed cross-sectional width.

$W$ (us) = 32 ft
$W$ (ds) = $6(18.4)^{0.60}$
$W$ (ds) = 34 ft
$W_A$ = 33 ft

Step 4. Compute $A_A$ by using equation 7:
$A_A = 7Q_{10}/V_A$
$A_A = 18.4/0.27$
$A_A$ = 68 ft$^2$

Step 5. Compute $H_A$ by using equation 6:
$H_A = A_A/W_A$
$H_A = 68/33$
$H_A$ = 2.0 ft

Step 6. Compute $K_2$ by using equation 2:
$K_2 = 8.76(V_A^{0.607}/H_A^{1.689})$
$K_2 = 8.76(0.27^{0.607}/2.0^{1.689})$
$K_2$ = 1.2 days$^{-1}$.

## SUMMARY AND CONCLUSIONS

Methods presented in this report provide a way to estimate parameters needed to satisfy certain empirical equations for estimating the $K_2$ for natural streams in part of southeastern Louisiana. Analysis of 222 low-flow discharge measurements from 20 streamflow sites indicated that a relation exists between the $7Q_{10}$ and stream channel cross-sectional width. This relation had a standard error of estimate of ± 23 percent with an adjusted coefficient of determination of 0.84.

The $7Q_{10}$ at ungaged and unregulated sites in the study area can be estimated by an equation given by Lee (1985). This equation had a standard error of estimate of ± 50 percent.

An equation by Calandro (1978) to estimate the time-of-travel of a slug of water through a reach of an unregulated stream in the study area can be used to estimate the average velocity for the $7Q_{10}$ flow rate. This equation had a standard error of estimate of ± 25 percent and is applicable to drainage areas less than 2,000 mi$^2$.

Equations shown in this publication have certain limitations of use. These limitations should be adhered to when using these equations.

This report was prepared in cooperation with the Louisiana Department of Environmental Quality, office of Water Resources.

## REFERENCES CITED

Bennett, J.P., and Rathbun, R.E., 1972, Reaeration in open-channel flow: U.S. Geological Survey Professional Paper 737, 75 p.

Calandro, A.J., 1973, An analysis of stream temperatures in Louisiana: Louisiana Department of Public Works Technical Report no. 6, 16 p.

———1978, Time of travel of solutes in Louisiana streams: Louisiana Department of Transportation and Development, Office of Public Works Water Resources Technical Report no. 17, 32 p.

Fenneman, N.H., 1938, Physiography of eastern United States: New York, McGraw-Hill Book Co., 714 p.

Lee, F.N., 1985, Analysis of the low-flow characteristics of streams in Louisiana: Louisiana Department of Transportation and Development, Office of Public Works Water Resources Technical Report no. 35, 41 p.

———1987, Evaluation of techniques for measuring streamflow and for estimating flow characteristics of streams in the Mississippi River Delta, prairies, and coastal marshes of Louisiana: Louisiana Department of Transportation and Development, Office of Public Works Water Resources Technical Report no. 40, 72 p.

Neely, B.L., Jr., 1976 [1977], Floods in Louisiana, magnitude and frequency (3d ed.): Louisiana Department of Highways, 340 p.

Sloss, Raymond, 1971, Drainage area of Louisiana streams: Louisiana Department of Public Works Basic Records Report no. 6, 117 p.

# Issues in Debris-Flow Research: Personal Views

*By* Cheng-lung Chen

**Abstract**

This report addresses critical issues in debris-flow research and their possible resolutions. Because debris flows are non-Newtonian, a rheological model is needed prior to the formulation of a routing model. Formulation of a generally applicable rheological model based on the macroscopic (continuum-mechanics) approach is more practical than that of a similar one based on the microscopic (statistical-mechanics) approach. To evaluate the rheological parameters requires measurement of the material constants of the sediment-water mixtures as well as the velocity and concentration distributions of flow. How to develop equipment and associated instrumentation for such accurate measurements is a critical issue. The hydraulics-based routing model for debris flow is in principle similar to the one for clear-water flow, except using different values in flow parameters. How to determine such flow parameters is another critical issue in debris-flow research.

## INTRODUCTION

Debris flows are perhaps the most hazardous gravity-induced mass movement on hillslopes and (or) in river channels. They occur in response to rapid disturbances such as torrential storms, sudden snow or glacier melt, dam break, volcanic eruptions, and earthquakes. The devastation caused by catastrophic debris flows is enormous, but their causes, occurrences, and mechanisms are not completely understood. Effective methods for hazard evaluation, warning systems, and countermeasures of debris flows cannot be developed without first fully understanding their various processes and then knowing how to model them mathematically or physically, or both. Because the various stages of debris flow, namely from its initiation to its termination, are complex phenomena, studying them requires a broad knowledge of the concepts used in hydrology, fluid mechanics, soil and rock mechanics, geology, and geomorphology. In general, modeling concepts adopted in mechanics of granular flow (Savage, 1984), a new branch of hydroscience, basically cover what is needed in the investigation of the debris-flow process. Success in applying such concepts to solving debris-flow problems, however, is somewhat uncertain because there remain many technical issues yet to be resolved prior to application, as far as debris-flow modeling and routing are concerned. In this paper, major issues in these areas and their possible resolutions are subsequently addressed from the writer's points of view. Hopefully, this brief paper will serve as a starting point for future debris-flow research.

## MAJOR ISSUES IN DEBRIS-FLOW MODELING

For convenience in our discussions, issues in debris-flow modeling are classified into three categories: those pertaining to the theoretical, experimental, and field aspects. Some of the issues addressed in each of the three aspects are nevertheless related to each other. Therefore, resolving one issue in one aspect may have in effect resolved its counterpart in the remaining two aspects. The major issues and their possible resolutions in each aspect are discussed in the following.

### Theoretical Aspect

Modeling debris flows requires a rheological model (or constitutive equation) for sediment-water mixtures. Various models relating stress, strain, and time, among other variables, have been proposed. Theoretically, two approaches are capable of formulating a rheological model for debris flow. In the order of refinement, they may be called the microscopic (or molecular) approach and the macroscopic (or hydromechanic) approach. In the microscopic approach, which is primarily based on statistical mechanics, one analyzes in detail the dynamics of individual particle collisions (namely describing in a statistical manner the microstructure of a fluid-solid mixture). In the macroscopic approach, however, which is based on continuum mechanics, one simply describes the bulk behavior of fluid-solid particle movement and interaction without any detailed reference to the microstructure of the mixture. Despite this conceptual difference in the approaches, the final expressions of the constitutive equation obtained from both approaches can be readily shown to be related to each other. In other words, making additional assumptions about the values for the material properties, such as the coefficient

of restitution, and using different methods for the statistical averaging and evaluation of the collisional integrals in the statistical-mechanics-based equations, one can in principle determine all the continuum properties explicitly (Ogawa and others, 1980; Shen, 1982; Jenkins and Savage, 1983; Lun and others, 1984). For example, by using the microscopic approach the ratio of shear stress to normal stress for the case of simple shear flow has been shown by Lun and others (1984) to decrease with increasing value of the coefficient of restitution and increasing volume concentration (or fraction) of solid particles. Unfortunately, this theoretical result is not fully supported by Bagnold's (1954) experimental data. The apparent disagreement of theoretical predictions from observed values as well as the required presumptions on the values of the coefficient of restitution and (or) a dimensionless parameter characterizing the ratio of mean shear to fluctuation velocity has clearly indicated the incompleteness or defect in existing theories based on the microscopic approach. Therefore, while the development of more theoretical, detailed statistical-mechanics--based constitutive equations should be continued, our research efforts in the future should be concentrated on the development of a general continuum-mechanics-based constitutive equation with the rheological parameters to be determined from experiments. For focusing our discussions on the practical usefulness and applicability of such a macroscopic model, issues in debris-flow research hereafter will be confined to those related to the macroscopic approach only, unless otherwise stated.

Many rheological models have been developed on the basis of continuum-mechanics approach. Forms of such models vary in the degree of complexity or simplicity. Highly theoretical models, despite their general validity and applicability, are too complicated to be useful in practice, whereas the use of simpler semiempirical constitutive equations is limited to a narrow range of application for lack of adaptability. Selection of a rheological model thus constitutes the most urgent issue in debris-flow modeling. For example, one of the most general constitutive equations applied so far to modeling debris flows is a Reiner-Rivlin type (Savage, 1979; McTigue, 1979; Sayed, 1981). This highly theoretical model has been used by theoreticians in non-Newtonian fluid mechanics to study rapid, dry, noncohesive granular flows in the grain-inertia regime. On the other hand, the earliest, perhaps the simplest, of all empirical non-Newtonian fluid models appears to be the classical Bingham (1922) model, which merely expresses a linear algebraic relation between the shear stress and the shear rate with two parameters (that is, yield stress and viscosity) used to link the two variables together. A compromise between the two is apparently needed.

A generally applicable model that can realistically describe the rheological properties of debris flow should possess three major features: (1) it should describe the dilatancy of sediment-water mixtures; (2) it should describe the soil yield criteria, such as those developed by Mohr-Coulomb (Terzaghi, 1943) and Drucker and Prager (1952); and (3) it should describe the role of intergranular or interstitial fluid. Satisfying the first two requirements indispensably calls for the form of a model to be composed of a rate-independent part and a rate-dependent part. In other words, the rate-dependent part mathematically would express the first feature, while the rate-independent part would describe the second feature. Therefore, as debris flows approach the dynamic state, the rate-independent part would vanish, and the remaining rate-dependent part would be represented by a relation such as the one empirically developed by Bagnold (1954). In another limit, as debris flows approach the quasi-static (or impending flow) state, the rate-dependent part disappears and the remaining rate--independent part simply expresses a limiting stress state characterized by the Mohr-Coulomb criterion. How to link both parts in the model is an issue yet to be investigated, but not so critical at present because the linear superposition of the two parts, as first proposed by Goodman and Cowin (1971 and 1972), works quite well in the analysis of simple shear flow (McTigue, 1979 and 1982; Sayed and Savage, 1983). Inclusion of the third feature of the major rheological properties of debris flow, namely the role of interstitial fluid, in the model is more difficult to handle in the macroscopic approach than in the microscopic approach. In the microstructural description of particle collisions, for example, Shen (1982) used the additional particle friction coefficient to describe interstitial-fluid drag effects, while in the continuum description, the similar effects of interstitial fluid could be expressed only through the rheological parameters by relating their parameter values to the property of interstitial fluid and unknown particle concentration (McTigue, 1979).

Extending McTigue's macroscopic formulation, Chen (1986a) formulated a generalized viscoplastic fluid (GVF) model:

$$T_{ij} = -\rho\,\delta_{ij} + s\,D_{ij}/\sqrt{II_{D'}} + 2\,\mu_1 |4\,II_{D'}|^{(\eta-1)/2} D_{ij} + 4\,\mu_2 |4\,II_{D'}|^{(\eta-2)/2} D_{ik}D_{kj}\,,$$

in which $T_{ij}$ is the total stress tensor in indicial notation; $\rho$ is the thermodynamic pressure; $\delta_{ij}$ is the Kronecker delta; s (that is, c cos $\phi$ + $\rho$ sin $\phi$) is the yield stress (c is the cohesion and $\phi$ is the "static" angle of internal friction); $D_{ij}$ is the rate-of-deformation tensor in indicial notation; $II_{D'}$ [that is, $(\frac{1}{2})\,D'_{ij}D'_{ij}$] is the second invariant of the deviatoric rate-of-deformation tensor [$D'_{ij}$ being expressed as $D_{ij} - (\frac{1}{3})D_{ii}$]; $\mu_1$ is the consistency index; $\eta$ is the flow behavior index; $\mu_2$ is the cross-consistency index; and $D_{ik}D_{kj}$ is the tensor product of the rate-of-deformation tensors in indicial notation. Note that the first, second, third, and fourth terms on the right-hand side of the equation are, respectively, the expressions of the pressure, plasticity, viscosity, and dilatancy of the mixture. The GVF model, which has both

rate-independent and rate-dependent parts with concentration-dependent parameters, probably is sufficiently accurate, yet practical, for general use in debris-flow modeling.

Although the GVF model so formulated can be simplified to the Bingham plastic fluid model for debris flow in the macroviscous regime ($\eta = 1$), the model so simplified differs somewhat from the classical form of the Bingham model (Chen, 1986a). Unlike the classical Bingham model, which uses only the shear stress versus shear rate relation to describe the rheological properties of debris flow without taking account of the normal stress effect (or "Weissenberg" effect), the GVF model makes use of both expressions of the shear and normal stresses. The GVF model can also be reduced to Bagnold's dilatant fluid model in the case that debris flow is in the grain-inertia regime ($\eta = 2$). Because both Bingham and Bagnold versions (or submodels) of the GVF model would describe the rheological properties of flow at the dynamic state, how to evaluate the flow behavior index, $\eta$, is a subsequent major issue in debris-flow modeling.

Determining the relative importance of rate-dependent versus rate-independent processes in debris-flow modeling has received little attention, because the major factors that affect the behavior of debris flows are poorly understood. A review of literature reveals that the sediment concentration and composition (such as, particle size distribution and clay mineral species) appear to be two of the major factors in the evaluation of $\eta$ and the other rheological parameters. In China, for example, modeling hyperconcentrated streamflows and mudflows having a relatively large amount of very fine sediment particles relies almost exclusively on the Bingham model (Chen, 1986b), while applying Bagnold's dilatant model to modeling debris flows carrying much higher concentrations of coarser sediment is common in Japan (Chen, 1987). Despite such differences in sediment properties (namely concentration and composition) between mudflows and debris flows, an analysis of theoretical solutions obtained from both Bingham and Bagnold versions (or submodels) of the GVF model indicates that the velocity profile for steady uniform debris flow in wide channels based on the Bingham submodel differs little from that based on Bagnold's dilatant submodel (Chen, 1986a). Regardless of which submodel is used, the evaluation of all the rheological parameters in the GVF model is required prior to its application. The rheological parameters in the GVF model include the yield stress index in addition to the flow behavior index ($\eta$) and the consistency and cross-consistency indices ($\mu_1$ and $\mu_2$). Determining the values of such rheological parameters thus constitutes a major task in the future debris-flow research. Unfortunately, this task can be undertaken only through laboratory experiments and (or) field measurements unless one is purposely resorting to more theoretical microscopic approaches, such as numerical experiments conducted by Walton (1980), Campbell (1982), and Campbell and Brennen (1985).

## Experimental Aspect

Four important issues in the experimental aspect of debris-flow modeling are (1) how to express the rheological parameters in terms of significant sediment and flow properties; (2) how to accurately measure the velocity and concentration distributions of debris flow in the laboratory; (3) how to develop equipment and associated instrumentation for such measurements; and (4) how to design an experiment so that unrealistic scale effects do not invalidate the results, namely insuring that the experiment accurately mimics nature. The first issue can be adequately handled in the context of the GVF model, whereas the second and third issues are more difficult to deal with unless there are some major breakthroughs in hydrometry of debris flow. To tackle the fourth issue, caution should be exercised during experiments to assess the scale effects caused by the peculiar behavior of non-Newtonian debris flow.

Chinese scientists, using viscometers and flumes, have found from experiments that the Bingham parameters vary with the sediment concentration and composition. For practical applications, therefore, they have developed numerous empirical expressions for the yield stress and the Bingham viscosity in terms of the sediment concentration and composition (Chen, 1986b). The Bingham viscosity is more amenable to theoretical treatment than the yield stress because the former can be expressed in terms of Einstein's (1956) relation of the relative viscosity, or an extension thereof, such as the power-law formula developed by Krieger and Dougherty (1959). This power-law formula can be used in the expressions of the consistency and cross-consistency indices in the GVF model (Chen, 1986a).

Regarding the accurate measurements of velocity distributions, a viable technique is flow visualization by photography of marked particles moving along a transparent side wall, as used by Japanese scientists (Takahashi, 1980). However, the accuracy of this method is dubious because the movement of sediment particles along the wall is always slower than that along the center of the flume. The velocity so measured is thus subject to a correction due to side-wall effects. Other techniques using acoustic and optical devices should be explored.

Measurement of sediment concentrations in a highly concentrated flow is probably more difficult than measuring velocity. There is no viable technique in sight, and research in this critical area is urgently needed. The normal stress and the effective pressure can be evaluated from the concentration distribution of sediment particles, and thus, with the help of the velocity distribution and other sediment data, they can be used to determine the flow behavior index as well as the consistency and cross-consistency indices.

Evaluation of the yield stress index, however, requires measured data on the shear stress and the yield stress. Theoretically the yield stress is composed of the cohesion and the static angle of internal friction, which in turn, vary with the sediment concentration and thus the state of flow (namely, their values being the largest at the quasistatic state but becoming negligibly small at the dynamic state). Therefore, the experimental determination of such material constants constitutes another major task in the future debris flow research.

One piece of equipment that can generate much data for determining the rheological parameters and material constants of prototype debris flow is a ring-shear (that is, dynamic torsional shear)-type debris-flow apparatus developed by Sassa (1984, 1985) of Kyoto University in Japan. The U.S. Geological Survey (USGS) has recently procured this apparatus and shipped it to the University of California at Berkeley (UCB) for a complete testing of its functioning, performance, and reliability.

Another piece of equipment, called a conveyor-belt-type flume, has been developed by the USGS and also shipped to UCB for the verification of rheological models assumed in the simulation of debris flow. Because the flume has the capability of immobilizing the moving snout of a debris flow simulated in the laboratory, it can be used inversely to evaluate the rheological parameters by fitting the measured velocity and snout profiles to the computed ones. The flume, however, has been hampered by the leakage of small particles and water from tiny spaces between the moving bottom conveyor-belt and the fixed side walls and thus needs improvement.

### Field Aspect

Field data on flow dynamics and rheological properties of debris flows are needed to calibrate existing rheological and flow routing models as well as to provide realistic constraints on flow behavior predicted by using such models. The USGS has monitored debris flows on the southeast flank of Mount St. Helens since its 1980 eruption (Pierson, 1985 and 1986). To facilitate the collection of valuable field data, a cooperative study of debris-flow dynamic properties at Sakurajima Volcano, Japan, was undertaken in the summer of 1986 by the USGS and the Japanese Ministry of Construction (T.C. Pierson, U.S. Geological Survey, written commun., 1986).

Debris-flow measurements in the field need to include, but are not limited to (1) velocity of flow fronts and surface velocity of flowing debris, (2) horizontal velocity profiles on flow surface, (3) vertical velocity profiles, (4) flow depth and discharge, (5) sediment properties, such as sediment concentration, particle-size distribution, entrained air content, temperature, and yield strength and viscosity of slurries, and (6) bed shear. Field equipment for monitoring debris flows, however, has not progressed very much. Measurement systems adopted in the study at Sakurajima, for example, were (1) continuous stage recorder system, (2) time-lapse camera system, (3) motion picture system, (4) in flow velocity measurement system, (5) trip wire sensors, (6) bed shear stress gages, and (7) sediment sampling system. Field instruments that can greatly improve such measurements need to be diligently developed in the future.

Monitoring debris flows is a formidable task because a debris flow never comes on demand. Strategies are needed prior to debris-flow monitoring and sampling because of the high cost of data collection and analysis. To develop the strategies, however, areas subject to debris flows and factors influencing their occurrences ought to be identified and analyzed. This requires a considerable amount of research because such factors vary widely with specific site characteristics, physiographic settings, and climatic conditions. Therefore, to increase efficiency and effectiveness of both data collection strategies and data analysis strategies, it is imperative that one develop viable procedures for optimizing the design of debris-flow monitoring and sampling networks.

## MAJOR ISSUES IN DEBRIS-FLOW ROUTING

A hydraulics-based routing model, which consists of unsteady flow equations, initial conditions, and boundary conditions, can be formulated from the equations of continuity and motion upon substitution of a rheological model. The unsteady flow equations so formulated for debris flow can be shown to be identical to those for clear-water flow, except using different values in flow parameters, such as the momentum (or energy) correction factor and the resistance coefficient. How to evaluate such flow parameters constitutes the most important issue in debris-flow routing.

### Flow Parameters

Theoretical expressions of the momentum and energy correction factors for laminar debris flow in wide channels can be obtained from the GVF model and so can the theoretical expression of the resistance coefficient. However, the latter expression can be achieved only with the additional help of a uniform flow formula, such as the Darcy-Weisbach or Manning equation. The flow parameters so obtained can thus be expressed in terms of the rheological parameters. For example, in the expression of the Darcy-Weisbach resistance coefficient, the redefined Reynolds number contains a flow behavior index and a consistency index. Theoretical expressions of the flow parameters for uniform flow in wide channels may be extended to a more general case of one-dimensional debris flow in a channel with a section of arbitrary geometric

shape. This, however, requires the basic concepts of open-channel hydraulics. In other words, it may be semi-empirically reformulated by replacing the flow depth by the hydraulic radius. Whether or not it is justified to apply such semiempirically reformulated flow parameters to routing debris flows in actual channels should be investigated. In practice, however, the flow parameters can be accurately estimated only through velocity measurements in the field. This reemphasizes the importance of the issues addressed in the field aspect of debris-flow modeling.

Another flow parameter worth investigation is the superelevation coefficient for a debris flow around a curved path. Behavior of a debris flow around a bend is complex, because the streamlines of the flow are not only curvilinear but also interwoven, resulting in spiral currents and cross waves. Furthermore, water and sediment at a certain point in a bend may be separated. Many Japanese efforts have been made to empirically determine the super-elevation and the velocity distribution of debris flow in channel sections having a bend. Japanese scientists (Mizuyama and Uehara, 1981) have found from experiments that the superelevation for debris flow is commonly more than 10 times that predicted by the highly idealized Woodward (1920) formula for clear-water flow. Significant scale effects during Japanese experiments might have caused such huge superelevation for curved debris flows. Regardless of what real causes might be, this clearly indicates that a method to reconstitute a debris flow velocity in the field by use of the Woodward formula, as adopted by most field investigators (Gallino and Pierson, 1984), needs reassessment. The value of the superelevation coefficient, like that of other flow parameters, is affected by many factors, such as the bed slope, the curvature of bend, the velocity and concentration distributions of debris flow, and the rheological properties of sediment-water mixture. Theoretical determination of the superelevation coefficient using the GVF model based on the various assumptions of the velocity distribution across the channel width in a bend is possible, but whether or not it gives a realistic value remains to be investigated.

## Stratified Sediment Gravity Flow

Determination of superelevation is further complicated by the fact that water and sediment may be separated in a bend under certain conditions. For convenience, this phenomenon is referred to in this paper as stratified sediment gravity flow. The separation of water and sediment observed in a curved channel (Mizuyama and Uehara, 1981) is also found in the deposition process of debris flow on a concave downward slope (Mizuyama and Uehara, 1983), namely a sediment process in transition from debris flow to bedload transport. A critical condition for the occurrence of stratified sediment gravity flow in a bend as well as in an alluvial fan should be developed.

## Routing Methods

Other areas of research in debris flow routing need to include, but are not limited to, (1) developing debris flow initiation criteria, such as those developed by Bagnold (1954) and Takahashi (1981), or extensions thereof, especially for cohesive granules; (2) predicting an established longitudinal profile of the snout; and (3) solving various unsteady flow problems, such as roll waves, pulsating flows, and the movement of large stones or boulders.

It is believed that the one-dimensional unsteady debris-flow equations including source-sink terms can be incorporated with the shock equations to route a debris flow through a channel from the time of its initiation to the time of its termination. The routing method is perhaps similar to that of solving the dam-break flood wave problem. At an alluvial fan, however, a two-dimensional depth-averaged flow model should be used instead. Much work remains to be done in these areas, especially the development of a generally applicable routing method to deal with two transitions in the debris-flow process, namely from landslide to debris flow and then from debris flow to bedload transport.

# CONCLUSIONS

Debris flows are a complex geomorphic process. Unlike very lightly concentrated sediment-laden flows, which are ordinarily treated as Newtonian fluids, hyperconcentrated streamflows and debris flows are non-Newtonian. A generally applicable rheological model of sediment-water mixture is thus needed prior to the formulation of a routing model for debris flow. Development or selection of a generally applicable rheological model for various sediment-water mixtures and the subsequent determination of their rheological parameters are the first and second critical issues in debris-flow research, respectively. The macroscopic (continuum-mechanics) approach taken by most practicing debris-flow researchers seems rigorous and accurate enough for practical purposes, but continued efforts need to be made on the development of more theoretical models based on microscopic (statistical-mechanics) approach. The third critical issue concerns the slow development of equipment and associated instrumentation for the accurate measurement of the material constants of the mixture (cohesion, angle of internal friction, and compressibility) and the velocity and concentration distributions of highly concentrated sediment dispersions. Difficulty in developing such equipment constitutes a major obstacle in debris-flow research. Hopefully, breakthroughs in hydrometry will give an impetus to future progress. The

hydraulics-based routing model for clear-water or lightly concentrated sediment-laden flow is well known, and a similar one can be applied to routing debris flows, except using different values in flow parameters. How to evaluate the flow parameters, especially for a channel of arbitrary geometric shape, is the fourth critical issue. Once a generally applicable routing method is developed, one can deal with unsteady flow problems, including various flow conditions and transitions in the debris-flow process. The fifth, perhaps the least urgent, critical issue in debris-flow research is the development of viable procedures for optimizing the design of debris-flow monitoring and sampling networks.

## REFERENCES CITED


Bagnold, R.A., 1954, Experiments on a gravity-free dispersion of large solid spheres in a Newtonian fluid under shear: Proceedings, Royal Society of London, Ser. A., v. 225, p. 49–63.

Bingham, E.C., 1922, Fluidity and plasticity: New York, McGraw-Hill, 440 p.

Campbell, C.S., 1982, Shear flows of granular materials: Pasadena, California, California Institute of Technology, Ph D. thesis, 260 p.

Campbell, C.S., and Brennen, C.E., 1985, Computer simulation of granular shear flows: Journal of Fluid Mechanics, v. 151, p. 167–188.

Chen, C.L., 1986a, Bingham plastic or Bagnold's dilatant fluid as a rheological model of debris flow?, *in* Proceedings of the Third International Symposium on River Sedimentation, Jackson, Mississippi: The University of Mississippi, p. 1624–1636.

———1986b, Chinese concepts of modeling hyperconcentrated streamflow and debris flow, *in* Proceedings of the Third International Symposium on River Sedimentation, Jackson, Mississippi: The University of Mississippi, p. 1647–1657.

———1987, Comprehensive review of debris-flow modeling concepts in Japan, *in* Costa, J.E., and Wieczorek, G.F., eds., Reviews in engineering geology, v. VII, Debris flows/avalanches; Process, recognition, and mitigation: The Geological Society of America , p. 13–29.

Drucker, D.C., and Prager, William, 1952, Soil mechanics and plastic analysis or limit design: Quarterly of Applied Mathematics, v. 10, p. 157–165.

Einstein, Albert, 1956, Investigations on the theory of the Brownian movement: New York, Dover, 119 p.

Gallino, G.L., and Pierson, T.C., 1984, The 1980 Polallie Creek debris flow and subsequent dam-break flood, East Fork Hood River Basin, Oregon: U.S. Geological Survey Open-File Report 84–578, 37 p.

Goodman, M.A., and Cowin, S.C., 1971, Two problems in the gravity flow of granular materials: Journal of Fluid Mechanics, v. 45, p. 321–339.

———1972, A continuum theory for granular materials: Archive for Rational Mechanics and Analysis, v. 44, p. 249–266.

Jenkins, J.T., and Savage, S.B., 1983, A theory for the rapid flow of identical, smooth, nearly elastic particles: Journal of Fluid Mechanics, v. 130, p. 187–202.

Krieger, I.M., and Dougherty, T.J., 1959, A mechanism for non-Newtonian flow in suspensions of rigid spheres: Transactions of the Society of Rheology, v. 3, p. 137–152.

Lun, C.K.K., Savage, S.B., Jeffrey, D.J., and Chepurniy, N., 1984, Kinetic theories for granular flow, inelastic particles in Couette flow and slightly inelastic particles in a general flow field: Journal of Fluid Mechanics, v. 140, p. 223–256.

McTigue, D.F., 1979, A nonlinear continuum model for flowing granular materials: Stanford, California, Stanford University, Ph.D thesis, 165 p.

———1982, A nonlinear constitutive model for granular materials, application to gravity flow: Journal of Applied Mechanics, v. 49, p. 291–296.

Mizuyama, Takahisa, and Uehara, Shinji, 1981, Debris flow in steep slope channel curves: Civil Engineering Journal, Japan, v. 23, no. 5, p. 243–248 (in Japanese).

———1983, Experimental study of the depositional process of debris flow: Transactions, Japanese Geomorphological Union, v. 4, no. 1, p. 49–64.

Ogawa, Satoru, Umemura, Akira, and Oshima, Nobunori, 1980, On the equations of fully fluidized granular materials: Journal of Applied Mathematics and Physics (ZAMP), v. 31, p. 483–493.

Pierson, T.C., 1985, Field techniques for measuring debris-flow dynamics, *in* Proceedings of the International Symposium on Erosion, Debris Flows, and Disaster Prevention: Tsukuba, Japan, p. 203–207.

———1986, Flow behavior of channelized debris flows, Mount St. Helens, Washington, *in* Abrahams, A. D., ed., Hillslope processes: Boston, Allen and Unwin, p. 269–296.

Sassa, Kyoji, 1984, The mechanism starting liquefied landslides and debris flows, *in* Proceedings of the International Symposium on Landslides: Toronto, Canada, p. 349–354.

———1985, The mechanism of debris flow, *in* Proceedings of the Eleventh International Conference on Soil Mechanics and Foundation Engineering: San Francisco, California, p. 1173–1176.

Savage, S.B., 1979, Gravity flow of cohesionless granular materials in chutes and channels: Journal of Fluid Mechanics, v. 92, p. 53–96.

———1984, The mechanics of rapid granular flows, *in* Hutchinson, J.W., and Wu, T.Y., eds., Advances in applied mechanics: Academic Press, Inc., Orlando, Florida, v. 24, p. 289–366.

Sayed, Mohamed, 1981, Theoretical and experimental studies of the flow of cohesionless granular materials: Montreal, Canada, McGill University, Ph. D thesis, pt. I, 91 p.; pt. II, 66 p.

Sayed, Mohamed, and Savage, S.B., 1983, Rapid gravity flow of cohesionless granular materials down inclined chutes: Journal of Applied Mathematics and Physics (ZAMP), v. 34, p. 84–100.

Shen, Hayley, 1982, Constitutive relationships for fluid-solid mixtures: Potsdam, New York, Clarkson College of Technology, Ph. D. thesis, 137 p.

Takahashi, Tamotsu, 1980, Debris flow on prismatic open channel: Journal of the Hydraulics Division, American Society of Civil Engineers, v. 106, no. HY3, p. 381–396.

———1981, Debris flow, *in* Van Dyke, M., Wehauser, J.V., and Lumley, J.L., eds., Annual review of fluid mechanics: Annual Reviews Inc., Palo Alto, California, v. 13, p. 55–77.
Terzaghi, Karl, 1943, Theoretical soil mechanics: New York, John Wiley, 510 p.
Walton, Otis, 1980, Particle dynamics modeling of geological materials: Lawrence Livermore Laboratory Report UCRL–52915, University of California, Lawrence Livermore National Laboratory, Livermore, California.
Woodward, S.M., 1920, Hydraulics of the Miami flood control project: Dayton, Ohio, Miami Conservancy District Technical Report, pt. VII.

# An Examination of Spatially Representative Water-Quality Sampling Methods in the Tidal Potomac River

*By* Richard H. Coupe, Jr.

**Abstract**

Representative sampling of a stream is often necessary to define the average constituent concentration in a cross section. The data are used in simulation modeling, mass-balance calculations, and in a continuing monitoring program after an initial, intensive study. Of five sampling schemes [(1) surface point samples, (2) middepth point samples, (3) bottom point samples, (4) depthintegrated samples, and (5) depth-integrated composite] examined, it was determined that a depth-integrated composite sampling scheme provided the best results, but a mid-depth sampling scheme provided acceptable results at less cost.

## INTRODUCTION

Representative sampling of a stream is necessary to accurately define the average constituent concentration in a cross section. The data are used simulation modeling, mass-balance calculations, and in the continuation of a monitoring program after an initial, intensive study. It is always desirable to minimize time and analytical costs while still obtaining reasonably accurate results. This report examines five sampling schemes to determine if any provide a reasonably accurate estimate of the representative constituent concentration.

A representative constituent concentration is defined for this study as the cross-sectional mean concentration, which is estimated by an area-weighted average concentration, calculated from point samples collected from the stream cross section.

In 1980 and 1981, the U.S. Geological Survey conducted an intensive study of the Potomac River and estuary. Data were collected to calculate the cross-sectional mean for each sampling time at six cross sections: Rosier Bluff, Hatton Point, Marshall Hall, Hallowing Point, Indian Head, and Quantico (fig. 1). These stations ranged in width from 1,600 to 2,600 m and were selected because they were sampled frequently at three or more verticals in each cross section.

The constituents and (or) physical properties used to study these cross sections are chlorophyll *a* corrected, pheophytin, and specific conductance. These were selected because they represent three different types of distributions in the water column. Chlorophyll *a*, a particulate constituent, generally is found in larger concentrations near the water surface during the daylight hours; pheophytin, a particulate constituent, is found in greater concentrations near the bottom of the water column; and specific conductance, caused by dissolved ionized constituents, is nearly uniform throughout the water column in the tidal Potomac River. A few times in late summer, a wedge of saltwater penetrated the Potomac to the Quantico and Indian Head cross sections. In these cases, the specific conductance of water became stratified with the larger values on the bottom.

The five types of sampling schemes that are examined are (1) surface point samples from the navigation channel, (2) mid-depth point samples from the navigation channel, (3) bottom point samples (3 ft off the bottom) from the navigation channel, (4) depth-integrated (DI) samples from the navigation channel, and (5) depth-integrated composite (DI-COMP) samples collected from three or more verticals. The navigation channel was chosen as the vertical in which to try to find a suitable estimate of the cross-sectional average concentration, because it is the only consistently identifiable vertical in the six cross sections.

The test of a sampling scheme was to compare each scheme's estimate of the cross-sectional mean concentration with the measured cross-sectional average concentration for all three of the constituents being tested.

## FIELD AND LABORATORY METHODS

Detailed descriptions of the methods of analyses, data collection, and the actual data used can be found in Blanchard, Coupe, and Woodward (1982); Blanchard and Coupe (1982).

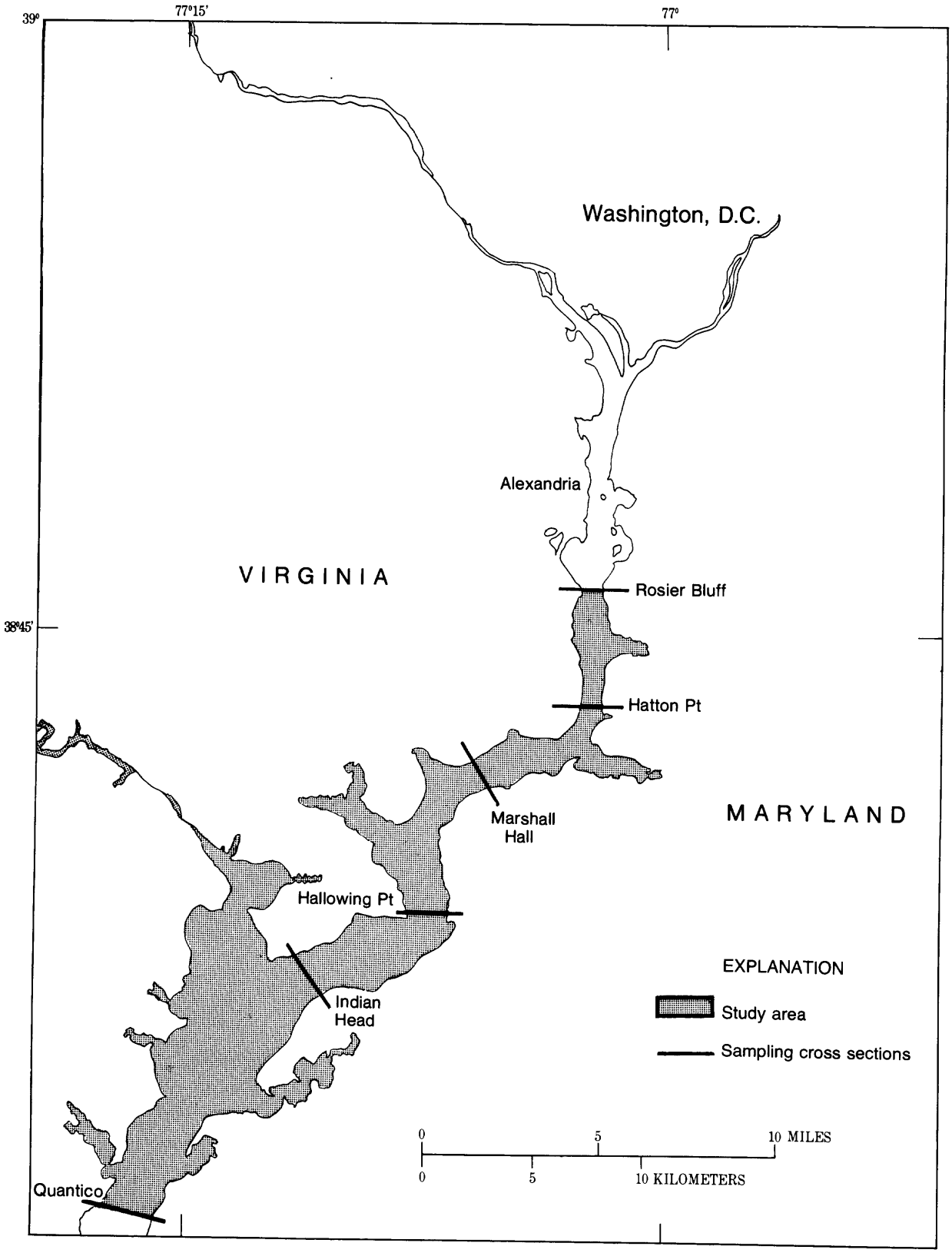


**Figure 1.** Tidal Potomac River.

Specific conductance was measured by using a Hydrolab Digital 4041 water-quality measurement system and a pumping sampler, which consists of an intake hose, a shipboard pump, and a discharge hose. The discharge from the pump is first routed into a manifold, which contains a sensor that measures specific conductance, and then through a tube from which samples may be collected. The pumping sampler intake can be positioned at any depth in the vertical.

Chlorophyll *a* and pheophytin were collected from the pumping sampler for the point samples. The analyses were based on the fluorometric, acetone extraction method of Strickland and Parsons (1972). The method was altered by two modifications described by Holm-Hansen and Riemann (1978): (1) the use of magnesium carbonate during filtration was deleted and (2) hydrochloric acid (HCL) was added to bring the sample to a concentration of 0.003 *M* in the acidification step.

An open bottle with a vent tube was used to collect depth-integrated (DI) samples. This sampler consists of a weighted 4-L capped neoprene bottle. The cap has an 8-mm-diameter hole in it, and the bottle has a hole in its shoulder. The hole in the shoulder of the bottle is fitted with a 4-mm-diameter tube that extends about 15 cm above the bottle cap. This arrangement allows air to escape from the vent tube and water to flow smoothly into the bottle through the hole in the cap. For chlorophyll *a* and pheophytin DI samples, an aliquot of water was taken from this bottle and analyzed as above. Specific conductance was not measured for the DI samples.

DI-COMP samples were collected by obtaining the DI samples from three or more verticals in the cross sections and combining them with volumes directly proportional to the depth in the vertical. Aliquots of water were then drawn and analyzed for chlorophyll *a* and pheophytin. Specific conductance of the DI-COMP samples was measured by the U.S. Geological Survey Central Laboratory in Atlanta, Ga. Both the DI samples and the DI-COMP samples were area-weighted samples.

## DATA ANALYSIS

For each sampling time, a cross-sectional mean was estimated by using the point-sample concentrations. Three or more point samples were taken from three or more verticals in each cross section.

The data are from samples collected from June 1980 through January 1981 and from June 1981 through September 1981. There were no DI channel samples for most of 1980, and there were no DI channel samples of specific conductance. In 1981, point samples for the verticals other than the channel were discontinued in favor of DI samples. In these cases, the DI concentration was used in the calculation of the cross-sectional mean in the same manner as the point samples.

There are approximately 30 observations for each constituent for each of the six cross sections; each observation ideally consists of a cross-sectional mean concentration and the concentrations from each of the five sampling schemes. The cross-sectional average is compared only to those concentrations within the same observation; therefore, the six cross sections were combined into three data sets, one for each constituent. Pertinent statistics for the constituent data sets are listed in table 1. For a given constituent, let $C_{(i,j,k,t)}$ denote the measured concentration for segment $i, j$ in the $k^{th}$ cross section at time $t$ and $A_{(i,j,k,t)}$ denote the area of segment $i, j$ in the $k^{th}$ cross section at time $t$. If the total area ($TA$) of cross section (fig. 2) at time $t$ is

$$TA_{(k,t)} = \sum_i \sum_j A_{(i,j,k,t)}, \quad (1)$$

then

$$C_{(k,t)} = \sum_i \sum_j A_{(i,j,k,t)} \, C_{(i,j,k,t)} / TA_{(k,t)} \quad (2)$$

is the cross-sectional average concentration in cross section $k$ at time $t$. Let $C_{(k,t,s)}$ denote the corresponding concentration in cross section $k$ at time $t$ for sampling method $s$. The difference in the two estimated concentrations is expressed as:

$$d_{(k,t,s)} = C_{(k,t)} - C_{(k,t,s)}. \quad (3)$$

## RESULTS

The distribution of the differences $d_{(k,t,s)}$ were studied. The differences $d_{(k,t,s)}$ for overall $k$ and $t$ were considered a random sample from some underlying population. For $C_{(k,t,s)}$ to be used as a reasonably accurate estimate of $C_{(k,t)}$, the distribution of $d_{(k,t,s)}$ would have to center around 0 and have a small variance.

For a fixed sampling method $s$ and a fixed constituent, a Wilcoxon signed-ranks test was used to test at a significance level of 0.05 the hypothesis that the median, $d_{0.5}$ of the differences $d_{(k,t,s)}$ was zero. The Wilcoxon signed-rank test is an appropriate test to use. The population need not have a normal distribution; all that is necessary is that the distribution be symmetric (Conover, 1980). In a symmetric population, the median is equal to the mean.

In table 2, confidence intervals are constructed for each of the sampling schemes. If the interval contains zero, we cannot reject the hypotheses Ho that $d=0$; that is, the median = mean of the differences is not significantly different from zero at the 5-percent significance level. Therefore, that concentration could be used as a direct estimate of the cross-sectional mean concentration.

A sampling scheme must provide a reasonably accurate estimate of the cross-sectional mean concentrations for all three constituents if it is to be accepted as providing an

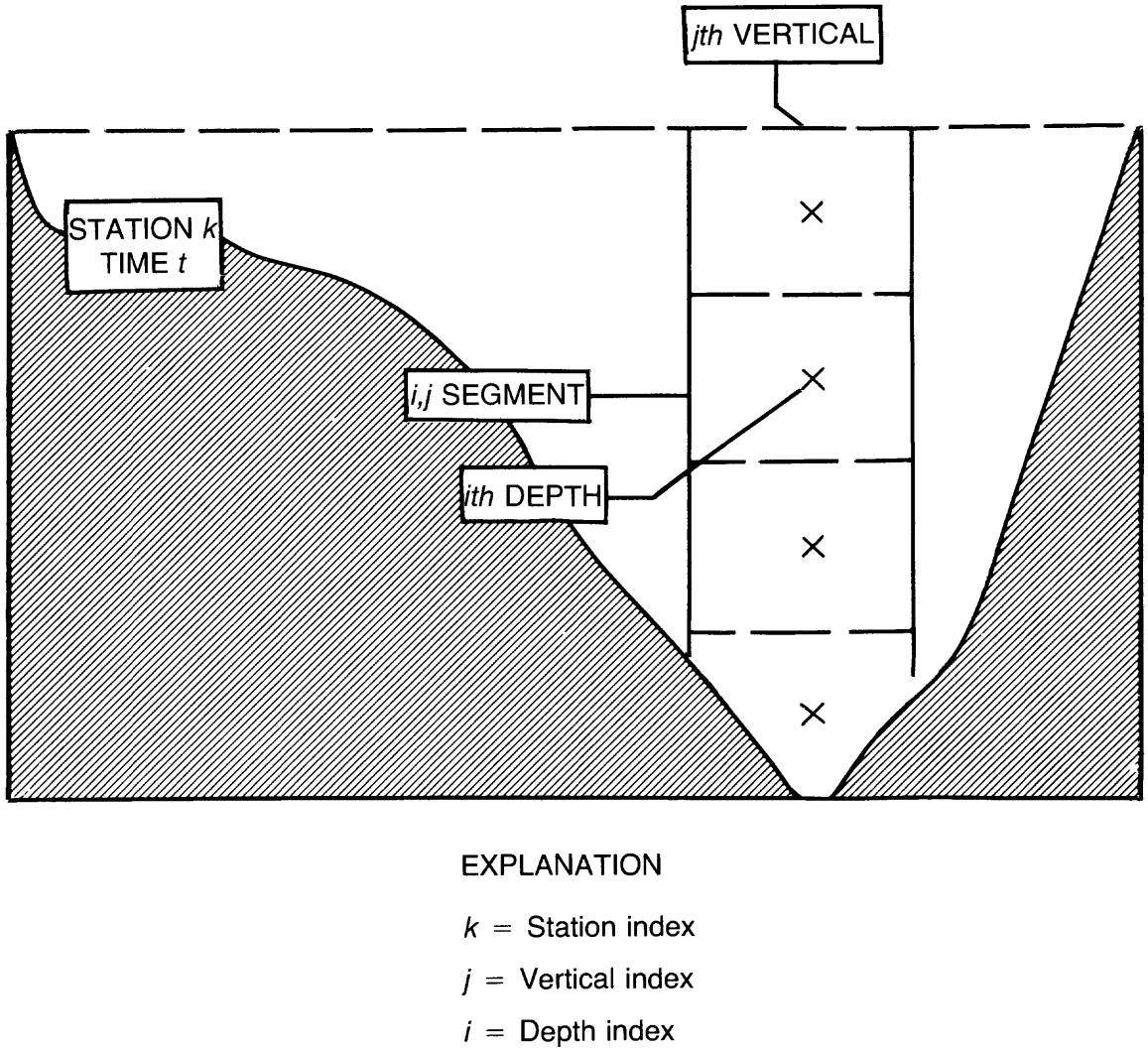


**Figure 2.** Schematic diagram of a sampling cross section.

unbiased sample at the 0.05-significance level. In examining table 1, it is obvious that this criterion is not met by any of the sampling methods.

Although it was desirable to have one sampling scheme with an interval passing through zero for all three constituents, table 2 still gives useful information on the variance of the differences $d_{(k,t,s)}$; this would correspond to the lenqth of the interval and information on the median of the $d_{(k,t,s)}$, approximately the center of the interval.

Notice the DI-COMP chlorophyll *a* and pheophytin intervals are small and close to zero; only the conductance interval seems out of place. This is the pattern for the other sampling schemes; two out of the three intervals appear acceptable, but one constituent sampling scheme interval forces us to further investigation.

The bias and mean square error of the differences $d_{(k,t,s)}$ for a fixed sampling method $s$ and each constituent are given in table 3.

The best sampling method as compared to the cross-sectional average is the one with the lowest mean square error (MSE) and with a bias close to zero.

It is interesting to note how table 3 reflects table 2, with the bias for a constituent being approximately the center of its confidence interval. This is true for most of the chlorophyll *a* and pheophytin values, but a problem arises with the bottom pheophytin and the specific conductance values. The bias is skewed outside the confidence interval. There are a few extreme values associated with surface conductivity and the bottom pheophytin samples, sometimes an order of magnitude higher than the mean, because the bias is an average of the differences. These few values could affect the bias out of proportion to their number. It will also affect the MSE in the same way. The method of calculation of the Wilcoxon confidence intervals will not be overly affected by a few extreme values. This problem is especially apparent for the bottom pheophytin, indicating

**Table 1. Pertinent statistics for the constituent data sets**

[—, no data]

| | Cross-sectional mean | DI-COMP[1] | DI[2] | Surface[3] | Mid-depth[4] | Bottom[5] |
|---|---|---|---|---|---|---|
| **Chlorophyll *a*, in micrograms per liter** | | | | | | |
| Number | 170 | 170 | 84 | 166 | 157 | 158 |
| Mean | 38.4 | 39.0 | 41.5 | 38.9 | 35.7 | 36.2 |
| Median | 38.1 | 38.7 | 41.0 | 37.9 | 36.2 | 34.9 |
| Std dev | 20.9 | 21.3 | 16.6 | 21.9 | 19.6 | 19.8 |
| Maximum | 101 | 95.2 | 84.6 | 127 | 111 | 100 |
| Minimum | 2.5 | 2.4 | 2.7 | 2.4 | 2.4 | 2.9 |
| **Pheophytin, in micrograms per liter** | | | | | | |
| Number | 168 | 168 | 70 | 164 | 156 | 161 |
| Mean | 16.8 | 16.2 | 13.9 | 13.9 | 16.0 | 23.3 |
| Median | 16.3 | 15.7 | 16.0 | 13.8 | 15.4 | 21.9 |
| Std dev | 6.03 | 6.03 | 4.45 | 5.34 | 5.42 | 11.1 |
| Maximum | 37.3 | 41.1 | 25.6 | 32.7 | 34.5 | 68.6 |
| Minimum | 5.13 | 4.50 | 6.00 | 3.50 | 5.30 | 6.00 |
| **Specific conductance, in microsiemens per centimeter** | | | | | | |
| Number | 150 | 150 | — | 149 | 146 | 148 |
| Mean | 456 | 450 | — | 420 | 454 | 469 |
| Median | 283 | 279 | — | 282 | 283 | 283 |
| Std dev | 615 | 601 | — | 491 | 614 | 673 |
| Maximum | 4,560 | 4,420 | — | 3,650 | 4,910 | 4,980 |
| Minimum | 179 | 187 | — | 177 | 178 | 168 |

[1]Depth-integrated sample composited with three or more depth-integrated samples from different verticals in the cross sections with volumes proportional to the depth of the vertical.

[2]Depth-integrated sample.

[3]Sample collected 3 ft below surface.

[4]Varies with depth of vertical.

[5]Sample collected 3 ft from the bottom.

**Table 2. 95-percent confidence intervals**

[—, no data]

| | Chlorophyll *a* | | Pheophytin | | Specific conductance | |
|---|---|---|---|---|---|---|
| DI-COMP | −0.940 | −0.195 | 0.230 | 0.925 | 2.73 | 6.61 |
| DI | 2.32 | 4.64 | −.925 | .245 | — | — |
| Surface | −1.05 | .950 | 2.30 | 3.19 | −.390 | 2.11 |
| Mid-depth | 1.03 | 3.10 | .050 | .885 | −1.03 | 1.00 |
| Bottom | .325 | 2.68 | −6.43 | −4.41 | −2.47 | −.360 |

**Table 3. Bias and mean square error**

[—, no data]

| | Chlorophyll *a* | | Pheophytin | | Specific conductance | |
|---|---|---|---|---|---|---|
| | bias | MSE | bias | MSE | bias | MSE |
| DI-COMP | −0.560 | 8.1 | 0.650 | 7.8 | 9.30 | 784 |
| DI | 3.52 | 29.6 | −.099 | 11.4 | — | — |
| Surface | −.570 | 70.9 | 2.84 | 17.5 | 38.5 | 24,530 |
| Mid-depth | 2.18 | 45.8 | .498 | 7.2 | 9.60 | 3,348 |
| Bottom | 1.66 | 55.3 | −6.68 | 113 | −9.1 | 15,690 |

significant resuspension. The surface specific conductance values denote penetration of the salt wedge throughout the water column, except for the surface layer, which remains fresh. The DI-COMP sampling scheme is the best overall sampling scheme if all three constituents are considered and compared against the other sampling schemes. A graphical representation (fig. 3) of the distribution of the differences $d_{(k,t,s)}$ that uses boxplots shows this clearly.

A consistent bias can be removed by linear regression. By regressing the cross-sectional mean concentration on the DI-COMP, DI, surface, mid-depth and bottom concentrations, a model of the form (Ingram, 1974) $Y = a + bX + e$ can be developed for each sampling scheme, where $e$ is the random error term, $Y$ is the predicted concentration, and $X$ is an estimate from a sampling scheme. The MSE's of these regressions are listed in table 4.

The DI-COMP and mid-depth sample schemes have very little improvement in their MSE's for chlorophyll *a* and pheophytin and only moderate improvement in conductivity, indicating that most of the error associated with the DI-COMP and mid-depth sampling schemes may be accounted for as random sampling error or error in the analysis. There is good improvement in the other three sampling schemes, but both the surface and bottom sampling schemes have large MSE's for two out of three

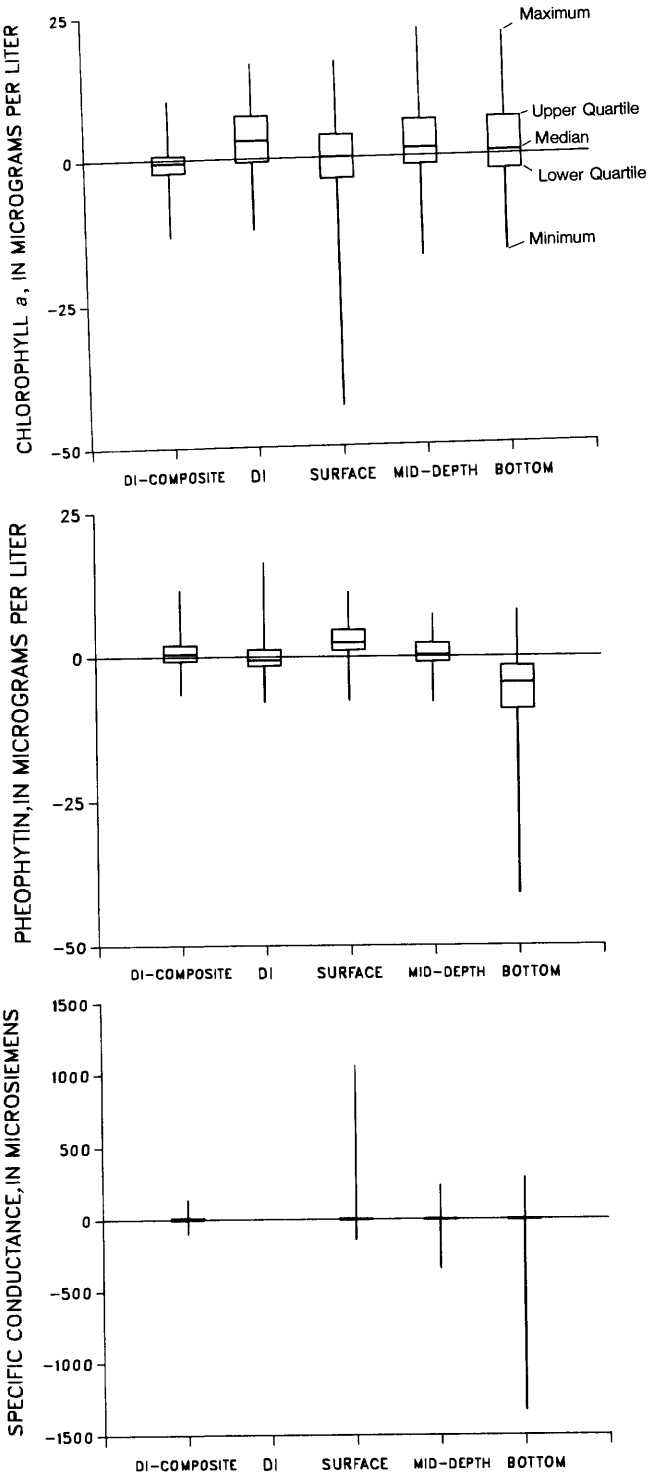


**Figure 3.** Boxplots showing distribution of $d_{(k,t,s)}$. DI-COMP representing a depth-integrated sample composited with three or more depth-integrated samples taken from different verticals in the cross sections with volumes proportional to the depths of the verticals. DI represents a depth-integrated sample. Surface represents a sample collected from 3 ft below the surface. Mid-depth represents a sample collected at the midpoint between the surface and the bottom. Bottom represents a sample collected 3 ft from the bottom.

**Table 4. —Mean square error of regression**

[—, no data]

| | Chlorophyll *a* | Pheophytin | Specific conductance |
|---|---|---|---|
| DI-COMP | 8.1 | 7.1 | 412 |
| DI | 29.6 | 10.2 | — |
| Surface | 63.1 | 9.5 | 8,690 |
| Mid-depth | 41.0 | 7.1 | 3,290 |
| Bottom | 53.1 | 19.6 | 12,000 |

constituents. These schemes will not give a satisfactory estimate of the representative sample. The DI sampling scheme has comparable results with the mid-depth scheme.

## CONCLUSIONS

The DI-COMP sampling scheme appears to be the best method for obtaining a direct estimate of the representative mean concentration of a constituent concentration in a stream. Considering the number of point samples used in the calculation of the representative sample, and the precision of the laboratory analysis of chlorophyll *a* and pheophytin, the DI-COMP predicts the representative sample accurately. The mid-depth sampling scheme gives acceptable results; it does have more variability than the DI-COMP scheme, but, considering the DI-COMP sampling scheme's considerable extra investment of time, mid-depth sampling may be the most cost-effective method to produce representative samples.

## REFERENCES CITED

Blanchard, S.F., Coupe, R.H., Jr., and Woodward, J.C., 1982, Water quality of the tidal Potomac River and estuary, hydrologic data report, 1980 water year: U.S. Geological Survey Open-File Report 82–152, 349 p.

Blanchard, S. F., and Coupe, Jr., R.H., 1982, Water quality of the tidal Potomac River and estuary hydrologic data report 1981 Water Year; *with a section on* chlorophyll-A by J.C. Woodward: U.S. Geological Survey Open-File Report 82-575, 298 p.

Conover, W.J., 1980: Practical non/parametric statistics (2d ed.): New York, John Wiley and Sons, p. 280–285.

Holm-Hansen, O., and Riemann, B., 1978, Chlorophyll-*a* determination—Improvements in methodology: Ofkiss, v. 3, no. 30, p. 438–447.

Ingram, J.A., 1974, Introductory statistics: Cummings Publishing Company, 341 p.

Strickland, J.D.H., and Parsons, T.R., 1972, A practical handbook of seawater analysis (2d ed.): Fisheries Research Board of Canada Bulletin 167, 310 p.

# Modeling Flood Flows from a Hypothetical Failure of the Glacial Moraine Impounding Carver Lake Near Sisters, Oregon

*By* Antonius Laenen, K.M. Scott, J.E. Costa, *and* L.L. Orzol

**Abstract**

A hydrologic hazard exists that could create a large-magnitude, but short-duration, flood in the Squaw Creek drainage and inundate areas in and around the community of Sisters, Oregon. Carver Lake, located at elevation 7,800 feet above sea level on the east slope of South Sister volcano, could catastrophically empty. The probability of this lake-breakout flood is estimated to be approximately 1 to 5 percent for any given year. At the U.S. Geological Survey gage (14075000) on Squaw Creek between Carver Lake and Sisters, the magnitude of the breakout flood would be 10 times that of a 1-percent probability flood from snowmelt or runoff. In Sisters, the magnitude of the breakout flood would be about five times that of a 1-percent probability flood.

Carver Lake is a potential hazard because (1) the lake contains 740 acre-feet of water and is more than 100 feet deep; (2) a large rock, snow, or ice avalanche could displace the entire lake or create a wave that would consequently overtop and erode the dam; (3) the moraine dam confining the lake, is steep faced, rendering the dam unstable, and unvegetated, making it highly erodible; (4) large amounts of readily erodible material are available for transport downstream of the dam and would increase the magnitude of a large flood; and (5) a greater-than-normal possibility exists for the area to become seismically or volcanically active—earthquakes or eruptions could cause rock and ice to fall into the lake.

A one-dimensional unsteady-state streamflow model was used to route a hypothetical flood down the Squaw Creek drainage below Carver Lake. The most extreme scenario considers the lake to be drained almost instantaneously by the displacement of lake water by a rock or ice avalanche. This scenario creates a starting hydrograph with a peak of a 180,000 cubic feet per second. The ensuing hypothetical flood could incorporate readily erodible debris and sediment in the steep canyons, consequently increasing the total volume of the flood by a factor of two. As the peak of the flood emerges from the steeper slopes into a more gently sloping valley 8 miles from the lake, it would have a magnitude of 47,000 cubic feet per second. At the U.S. Geological Survey gage 15.4 miles downstream from the lake (in a valley just upstream of an alluvial fan area), the attenuating peak would have a magnitude of 21,000 cubic feet per second. The peak would continue to attenuate as it traveled downstream and would reach the community of Sisters, about 20 miles downstream from the lake, in 2½ hours from initial breach at a magnitude of to 9,800 cubic feet per second.

## INTRODUCTION

### Background

The Three Sisters area in central Oregon (fig. 1) has one of the largest concentrations of neoglacial moraine-dammed lakes in the conterminous United States. Pleistocene volcanic rocks that form the mountains in this area are easily eroded; thus, even relatively small glaciers have been able to build large moraines. Floods that resulted from at least three moraine-dam failures in the last 50 yr have traveled down the drainages of Soda Creek, Squaw Creek, and White Branch (fig. 1). Recent fieldwork by the U.S. Geological Survey (USGS) in 1985–86 defined peak flows that reached magnitudes of at least 13,000 $ft^3/s$ and traveled as debris flows as far as 10 mi downstream from the source.

Fieldwork done in the Three Sisters area during the past 4 yr is part of a larger study assessing hydrologic hazards caused by volcanic activity. During this fieldwork, it became evident that many flows (debris and hyperconcentrated flows) had resulted from past moraine-lake breakouts, glacial outbursts, and avalanches. Later surveys (fig. 1) documented these flows. Some of the hydraulic information obtained in these later surveys is shown in table 1.

An example of a moraine-lake breakout and the behavior of its flood wave downstream occurred on September 7, 1970, in the upper North Fork Squaw Creek drainage (fig. 2). Approximately 130 acre-ft of water was released from the unnamed moraine-dammed lake, which drained entirely. This flow several times reached a magnitude in excess of 10,000 $ft^3/s$ during descent from the

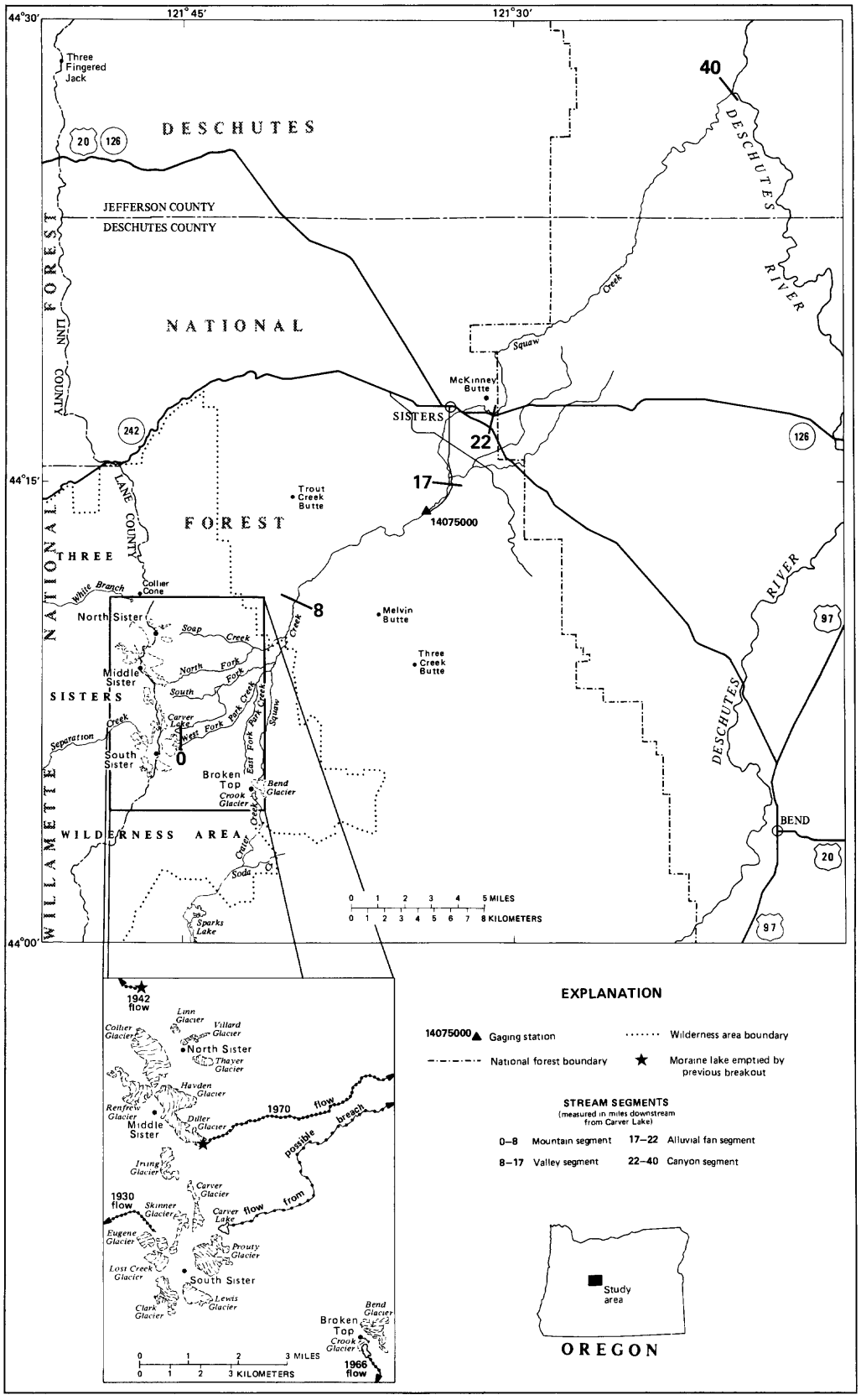


**Figure 1.** Location of study area.

**Table 1.** Hydraulic data for floods from glacial-moraine breakouts in the Three Sisters area, from U.S. Geological Survey work done in 1985–86

[ft/s, feet per second; $ft^3/s$, cubic feet per second; elevation, in feet, refers to distance above sea level]

| Stream | Date of flood | Elevation (ft) | Peak discharge ($ft^3/s$) | Velocity (ft/s) | Manning's *n* coefficient | Type of survey |
|---|---|---|---|---|---|---|
| Soda Creek | 10–07–66 | 8,500 | 3,700 | 14.7 | 0.076 | Superelevation. |
| | | 6,500 | 300 | 20.0 | .084 | Superelevation. |
| | | 5,520 | 500 | 13.0 | .032 | Critical depth. |
| Squaw Creek | 9–07–70 | 6,400 | 10,500 | 25.6 | .051 | Superelevation. |
| | | 4,720 | 11,500 | 31.6 | .039 | Superelevation. |
| | | 4,420 | 8,000 | 11.9 | .020 | Slope/area. |
| White Branch | 07–42 | 6,400 | 12,600 | 30.9 | .086 | Superelevation. |

**Figure 2.** Breached moraine that occurred in the North Fork Squaw Creek basin in 1970.

7,500-ft elevation. The peak attenuated to 8,000 $ft^3/s$ as it exited from steeply sloping canyons at elevation about 4,400 ft, 7 mi from the source. By the time the peak flow passed the USGS gage (14075000) approximately 15 mi downstream from the source, it had been drastically reduced to 1,200 $ft^3/s$ (2.5 ft of stage increase at the gage). (For comparison purposes, the highest peak of record since 1909 at the USGS gage was 2,000 $ft^3/s$, which occurred on December 25, 1980.) At Sisters the peak flow had attenuated even more drastically to a small muddy-water surge of about 1 ft in height.

Another well-documented moraine-lake breakout in the area occurred in the Soda Creek drainage (Nolf, 1966). Approximately one-half of the 300 acre-ft of total volume of Moraine Lake on Broken Top Mountain (an ancient volcano) at elevation 8,000 ft was released (fig. 3). This moraine-dam failure created a flood peak of about 8,500 $ft^3/s$ at higher elevations and a flood peak of about 2,000 $ft^3/s$ as it inundated an area marginal to Sparks Lake, 6 mi downstream. Future failure of Moraine Lake could cause a flood event of similar magnitude.

Recent fieldwork also has revealed a significant hydrologic-hazard potential at Carver Lake in the Squaw Creek basin at elevation 7,800 ft on the east flank of the South Sister volcano (fig. 1). The following factors indicate that the lake is a particular hazard:

**Figure 3.** Moraine Lake, head of Soda Creek basin, that breached in 1966.

(1) Carver Lake is large and deep. It has a maximum depth of 101 ft and contains approximately 740 acre-ft of water (about five times the volume of the moraine lake that breached in 1970). Most other lakes in the area are relatively shallow.

(2) The moraine dam is unstable and consists of sand- and gravel-size particles that are loosely consolidated. The moraine-dam face has a slope of 42 degrees and is unvegetated. The outlet channel of the lake is not significantly armored with boulder-size material and is thereby potentially erodible in the event of an overtopping wave of water.

(3) The geology of the east slope of South Sister volcano is such that avalanches of rock and ice into the lake could cause overtopping of the moraine. In August of 1930, a large avalanche occurred on the west side of South Sister volcano (fig. 1). Large volumes of potentially unstable rock and ice rise with near-vertical slopes above the headwaters of the lake. The steeply sloping and heavily crevassed Prouty Glacier also is located almost immediately above the lake.

(4) Large amounts of readily erodible material are available for transport in the channel below the lake. Debris flows attenuate differently than clear-water floodflows because debris flows increase in volume by picking up sediment and debris where channel slopes are steep. A larger breakout than that which occurred in North Fork Squaw Creek in 1970 could mobilize more material and create a larger magnitude flood. Once channel slopes become more gentle, however, debris flows generally attenuate more quickly than clear-water flows.

(5) Although the area is not now seismically active, earthquakes could be generated with renewed volcanic activity in the Three Sisters area. Basaltic eruptions in the area occurred as recently as 1,200 to 1,400 yr ago, when Belknap Crater was created (Taylor, 1965). Either volcanic or nonvolcanic seismic activity could trigger large avalanches.

## Purpose and Scope

This report presents a method for assessing potential flood hazards associated with moraine- or debris-dam failures. It identifies specific flood hazards, based on reasonable scientific assumptions and computations, for a hypothetical flooding down Squaw Creek and through the community of Sisters in the event of a catastrophic breakout

of Carver Lake. A prior Open-File Report (Laenen and others, 1987) alerted State and Federal agencies and the public of the hydrologic hazard. A computer model was used to simulate a starting flood hydrograph at the moraine dam and route the flow downstream. The failure scenario assumed total and instantaneous displacement of the lake by avalanche material. It was assumed that the simulated flood would increase in volume by two times from sediment incorporated in the flow in the steep upper reaches of the channel.

## NEOGLACIAL MORAINE DAMS

Many moraine dams occur throughout the world, but the most dangerous of these are restricted to alpine regions affected by the advances and retreats of valley glaciers. A globally synchronous readvance of glaciers during the last few centuries has been documented (Grove, 1979); this readvance has been referred to as the Little Ice Age (Matthes, 1939) or neoglacial time (Porter and Denton, 1967). More recent local glacial oscillations also have created moraine-dammed lakes. Neoglacial advances north of the Three Sisters area have been documented by Scott (1977). In the last 50 yr, mountain glaciers have retreated significantly (Porter and Denton, 1967), leaving behind many moraine-dammed lakes. In the Three Sisters Wilderness Area, at least 15 lakes were created by this glacial activity.

Neoglacial moraine-dammed lakes are hazards because (1) they are sufficiently young and located at such high elevations that ground vegetation has not completely stabilized their slopes, so that they are highly erodible; (2) slopes are steep, and some are greater than the angle of repose; (3) thermal degradation may have melted an ice or snow core in some moraines, rendering them unstable; and (4) these dams are close to the ice front and adjacent to steep, rock-walled valleys. Extensive meltwater or icefalls and (or) rockfalls into the lakes may precipitate breaching failure of these dams.

Most of the textural data from morainal dams indicate that moraine material is silty, sandy, bouldery till, commonly with 5 percent or less clay. Lake levels are controlled by seepage through the barrier and open overflow channels across the top of the moraine. The moraines may or may not have ice cores but have ground water that probably is frozen at depth for most of the year.

The most commonly reported failure mechanism of moraine dams is overtopping by a wave or series of waves generated by icefalls or rockfalls or by snow or rock avalanches into the lake basin (six examples are given by Costa and Schuster, 1987). The wave overtops the barrier, initiating erosion that is propagated by the downcutting and release of additional lake water. Settlement and subsequent failure of moraine dams accompanying earthquakes is another potential failure mechanism (one example given by Costa and Schuster, 1987). Although no documented cases are known, the failure of an ice-cored moraine dam from ice melt also is a distinct possibility.

The question of the longevity and stability of moraine dams is complex. All of the known moraine dams that have failed in the last century are of neoglacial (Little Ice Age) or younger origin. These moraine dams, formed in the last 300 yr, are steep, unvegetated, and potentially unstable. They were formed in mountainous regions, where steep valley walls or lateral moraines surround dammed lakes and the proximity of glacial ice presents the potential for excessive meltwater and mass movements into the lakes and the formation of dam-breaching waves. Ice-cored moraines or moraines of frozen soil may thaw over centuries and then may reach critical levels of instability (Ostrem, 1964; Andrews, 1975).

## POTENTIAL HYDROLOGIC HAZARD

### Moraine Failure

The moraine that contains Carver Lake is a terminal moraine of neoglacial origin (Scott, 1977). The texture of the moraine material is a silty, sandy, bouldery till. Morainal material completely encircles the lake (fig. 4). A short terminal moraine forms the downstream side of the lake. Another terminal moraine abuts the upstream end of the lake, and lateral moraines curve around and form the remaining sides.

The downstream terminal moraine shows the remains of a previous breach. The breach, which is located where the terminal moraine abuts the south lateral moraine, may have been initiated by melting glacial ice during formation. The stream that now runs in the bottom of the breach travels nearly level for about 200 ft and then plummets down the steep face of the moraine, incising a channel (figs. 4 and 5). The downcutting of the small stream on the face of the moraine gradually reduces moraine stability. The stability of the moraine is probably also dependent on the proximity to the surface of a frozen-ice or ground-water core. Techniques for identifying ice interfaces in moraines involving geophysical investigations have been developed by Haeberli (1986) but were not used in this study.

Approximately 1 mi to the southwest of Carver Lake, and about 2,600 ft above, is the peak of South Sister. A schematic geologic cross section of the South Sister volcano above Carver Lake is shown in figure 6. The upper part of the volcano consists of thin agglutinate flows and scoria of the summit cone, overlying poorly consolidated breccia, sand, and silt (W.E. Scott, U.S. Geological Survey, written commun., 1987). There occasionally is a seasonal meltwater lake in the summit crater, which may drain by seepage through poorly consolidated material of its rim.

**Figure 4.** Carver Lake from the northeast, showing encircling moraines.

The remainder of the volcano exposed in the steep headwall above Prouty Glacier consists of an upper sequence of steeply dipping, highly fractured, thin lava flows, breccias, and scoria and a lower sequence of thicker lava flows and pyroclastic material. A large mass of landslide material, probably derived from the headwall, rests on the slope just at the head of Carver Lake and is a visible reminder of instability. Undercutting of the summit-cone flows by erosion of the poorly consolidated sediment provides a continual source of landslide material.

An avalanche of ice and (or) rock into a moraine lake would be the most probable trigger causing moraine-dam failure. Vertical outcrops of highly fractured volcanic rock are observed above Carver Lake (fig. 4). Prouty Glacier, directly above the lake (but probably not directly connected because of a second terminal moraine; refer to fig. 4), is highly crevassed and has the potential for sections of ice to calve from above.

## Probability

Many Cascade Range peaks have had avalanche-caused debris flows originating from fractured rocks such as those found above Carver Lake (for example, the Mount Tom, Lake George, and Little Tahoma Peak avalanches on Mount Rainier). The Little Tahoma Peak avalanche is a well-documented example of this type of failure and resulting debris flow (Crandell and Fahnestock, 1965). In August of 1933, an avalanche of rock, snow, and ice on the west flank of South Sister evolved into a muddy flow that was channeled down the Separation Creek drainage and noticed 25 mi downstream at McKenzie Bridge (see fig. 1). The August 17, 1933, issue of "The Oregonian" carried an article that described the event and included areal photographs.

In the last 50 yr, three known neoglacial moraine dams in the Three Sisters area have breached and caused large-magnitude floods. From this evidence and the inference of other undocumented events in the last century (observed from historic coverage of areal photography), the frequency of breakouts of moraine-impounded lakes in the Three Sisters area has been greater than about one every 15 to 20 yr (an annual probability of at least 5 to 6 percent, until moraine lakes in the area no longer exist).

Standard frequency analysis is not possible in the determination of the probability of Carver Lake breaching, because the sample size is so small. Although 15 or more lakes were created during neoglaciation, at least 5 lakes in

**Figure 5.** Carver Lake outlet channel flowing down steep face of moraine.

the area (Upper Chambers Lake, Moraine Lake on Broken Top Mountain, unnamed lake on North Fork Squaw Creek, Carver Lake, and unnamed lake on Three Fingered Jack volcano) are known to still have a potential for breaching. Other lakes with this potential probably exist in the area, and future studies are needed to define them. A crude estimate of probability can be obtained by the following method: Given the number of breakouts that have occurred in the area for a given period (3), divided by the number of lakes with a potential for breakout, times the period of time in years (5×50), it is assumed that the probability of any given lake failing to be approximately 1 percent a year.

The probability of moraine failure is greater than 1 percent per year. The last 50 yr have seen a general retreat of glaciers that took 800 yr to advance (Porter and Denton, 1967). The most objective estimate of the probability of occurrence would be to adjust for the local occurrences and increase the range from 1 to 5 percent. This estimate indicates that the Carver Lake blockage could have a 1-to-5 chance in 100 of being breached in any given year.

The hazard represented by the failure of the moraine impounding Carver Lake, a probability of at least 1 percent per year, is larger (the magnitude will be higher) than a typical design hydrologic event with a recurrence frequency of 100 yr (equivalent to an annual probability of 1 percent). The topographic setting of the lake at the base of steep unstable masses of ice, snow, and rock and the steep faces of the blockage, as well as the complete drainage of other moraine-dammed lakes in the area, clearly indicate that Carver Lake dam could fail catastrophically. A worstcase event is the most appropriate design analysis for planning possible mitigating measures. All the recorded avalanches and lake breakouts appear to have occurred from June through October. It is highly probable that this is the time when another lake breakout will occur.

## MODELING THE POTENTIAL MORAINE-DAM FAILURE

A survey of Carver Lake showed the maximum depth to be 101 ft. The lake has a surface area of 15.4 acres and a volume of 740 acre-ft. The crew making the survey, while on the lake, experienced a 6-in. wave created from snow calving from the adjacent field. This minor surge probably created an instantaneous peak of about 10 $ft^3/s$ at the outlet. Assuming that a large section of rock or ice were to splash into the lake and create a 10-ft wave, the instantaneous peak

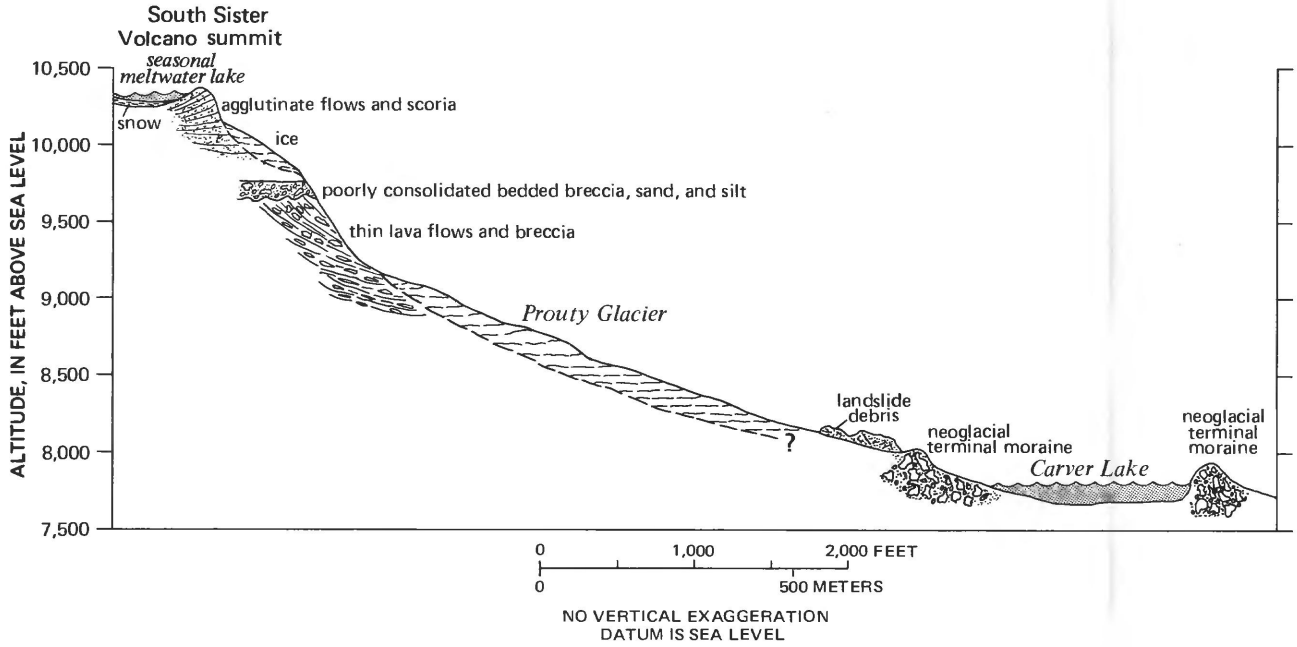


**Figure 6.** Geologic cross section of South Sister volcano from Carver Lake to summit.

would then be about 4,000 $ft^3/s$—a discharge estimated to be sufficiently large to begin rapid erosion of the channel and breaching of the moraine.

## Breach Scenario

The National Weather Service model DAMBRK (Fread, 1980) was used to simulate a number of breach scenarios for the Carver Lake moraine dam. The part of DAMBRK used for this study develops a trapezoidal breach of input dimensions over a given period of time. Breach development follows an exponential time curve, developing slowly at first and most rapidly as the total breach time draws close. The volume of water in the lake drains out accordingly, with the total volume depleting sometime later than the time of full breach development. For all scenarios, a breach side slope of 1:1 with a bottom width of 10 ft was assumed. How the outflow peak discharge varied with time of breach development over the maximum depth of breach (assumed to be 80 ft) is shown in figure 7. Figure 8 shows how different breach depths affected the peak discharge for a 3-min time-to-maximum breach. Breach volumes were included with the volume of the lake for simulation purposes. The maximum breach volume totaled less than 10 percent of the total volume.

In an analysis with DAMBRK of moraine-dam failures that occurred in the Soda Creek and North Fork Squaw Creek drainages, the time to maximum breach would have to be 3 and 5 min, respectively. Discharges for these events are found on table 1. Moraine Lake in the Soda Creek

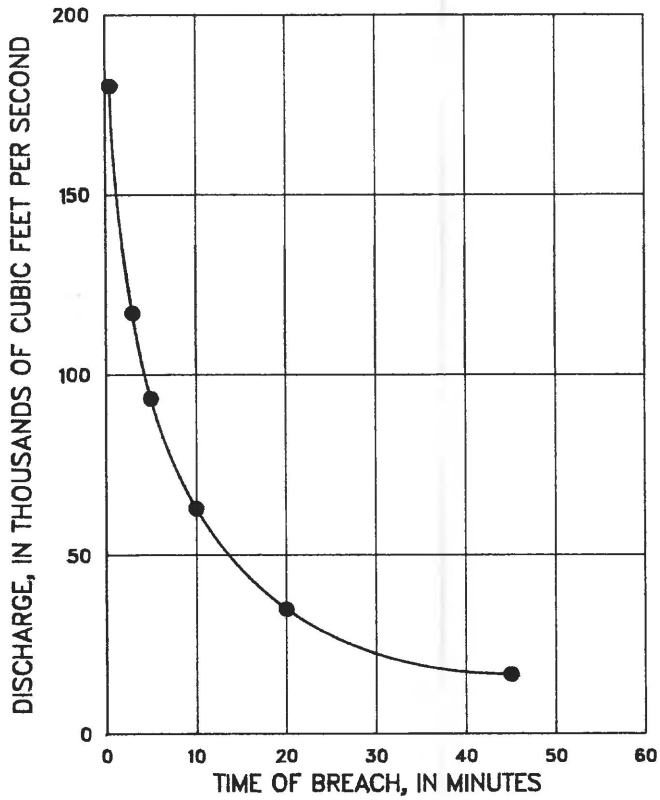


**Figure 7.** Relation of outflow peak and time-to-maximum breach for hypothetical failure of Carver Lake moraine.

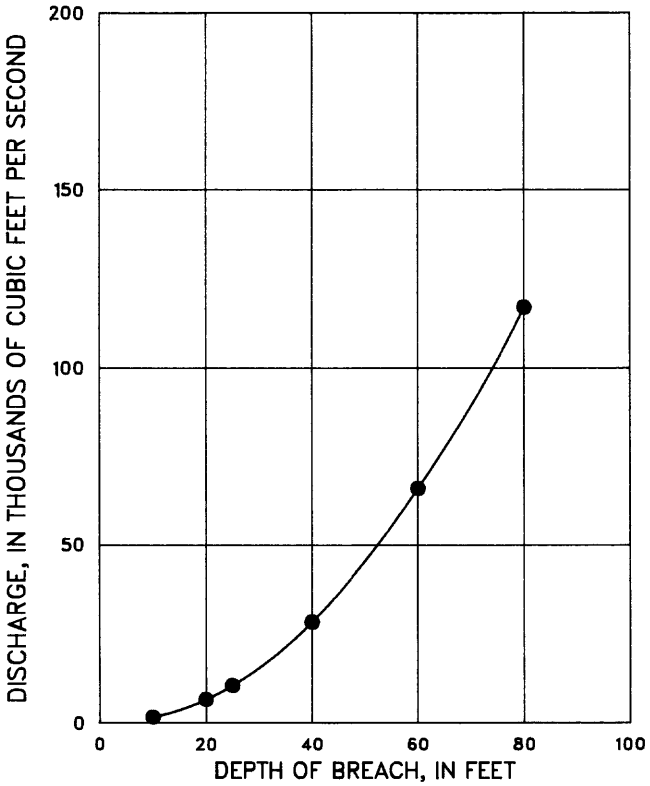


**Figure 8.** Relation of outflow peak and depth of breach for hypothetical failure of Carver Lake moraine.

drainage was only partially drained, whereas the lake in the North Fork Squaw Creek basin was drained completely. Carver Lake had drained partially in postneoglacial times, while the lake at the foot of Collier Glacier (in White Branch drainage) was drained completely in 1942. At present, there is no way to determine if the next breach of the moraine dam of Carver Lake will drain the lake partially or completely. The chances are that a small avalanche would not produce a large enough wave to start a breach but that a large avalanche would start a breach that would continue until the lake was completely (or nearly completely) drained.

The most extreme scenario for hypothetical failure therefore would be the total and almost instantaneous evacuation of the lake, caused by a large avalanche displacing all lake water. For this scenario, we can estimate 80 ft of head in a broad-crested trapezoidal-notch breach, with a 10-ft-wide bottom width and can calculate an instantaneous peak flow of about 180,000 $ft^3/s$. Should a new breach completely empty the lake, approximately 170,000 $yd^3$ of material in the moraine dam would be removed.

## Bulking and Debulking

Flows from historic lake breakouts on Mount St. Helens, Wash., have increased in magnitude and volume as they entrained erodible material. Scott (1989) has estimated instantaneous peak magnitudes in excess of 10,000,000 $ft^3/s$ (the flood flow of the Amazon River) for an ancient lake breakout of Spirit Lake on Mount St. Helens in Washington (the lake volume there is 30 times that of Carver Lake).

On the basis of the behavior of the previous flows in Squaw Creek, White Branch, and Soda Creek, the flood wave from the potential failure of the Carver Lake moraine would be expected to bulk almost continuously for about 8 mi downstream. Variations in that trend would occur, but the overall process would be the net addition of eroded sediment to the flood wave. Boulder fields 6 ft in depth could be formed below the breach but would represent only a minor part of the volume, as would aggradation in the minor valley flats in the bulking reach. A deposit thickness of about 6 ft would occur locally outside of the main channel area in valley flats but would be offset partially by erosion along the main channel. This thickness estimate is based on the deposits of previous breakout flood waves in Squaw and Soda Creeks.

Previous breakout flood waves from moraine--dammed lakes, such as the drained lake in the upper North Fork Squaw Creek basin, have remained high in the hyperconcentrated flow range (40–80 percent sediment by weight), as evidenced by the presence of a transition facies (Scott, 1988, figs. 10, 39, and 42) at a comparable point in the Squaw Creek channel.

It is assumed that the flow would bulk up to a sediment concentration of 50 percent by volume (hyperconcentration) in the reach between the breach and the end of the steeply sloping canyons, a distance of 8 mi. This value, high in the range of hyperconcentrated flow, is based on the stratigraphic and sedimentologic evidence from earlier moraine-dam failures in the area; it is based on quantitative comparisons of the textures of downstream Squaw Creek deposits with those resulting from flows having known sediment concentrations in hyperconcentrated flow in the Toutle River, Mount St. Helens, Wash. Clay content, mean size, and sorting of the deposits are all comparable.

Debris flow, if not attained at the breach, would not be attained downstream. Debris flow probably would not occur because of the noncohesive nature of the morainal deposits (less than 3–5 percent clay). Such noncohesive flows probably would not entrain sufficient sediment downstream, especially in the critical silt- and clay-size classes, to transform into a debris flow. The nature of the flow deposits from previous breakouts of Carver Lake also indicates that debris flow would not occur.

The Carver Lake flood wave would debulk continuously downstream from the end of the bulking reach, estimated to be about 8 mi downstream from the dam. At Mount St. Helens, the median thickness of debris-flow deposits on flood plains in the Toutle River system is about 2 ft. A general discussion of the formation and ratios of

deposit thickness to flow depth of hyperconcentrated flood flows is found in reports by Scott (1988, 1989). The flood wave would be a hyperconcentrated flow, based on the bulking criteria discussed above. The following debulking criteria, are based on the experience at Mount St. Helens, Wash.:

(a) If flow depth is greater than 6 ft, volume of sediment on flood-plain surfaces in feet = 2.0 × (inundated area minus area of active channel); or

(b) If flow depth is less than 6 ft, volume of sediment on flood-plain surfaces in feet = 0.35 × depth × (inundated area minus area of active channel).

As flow spreads out in the debulking interval and encounters greater roughness on the fan surface,

(c) Case (a) becomes = [3.0 + (0.3 × flow depth greater than 6 ft)] × (inundated area minus area of active channel); and

(d) Case (b) becomes = 0.50 × depth × (inundated area minus area of active channel).

The peak flood created by catastrophic breaching could mobilize additional material (bulk up) as it progressed downstream through steeply sloping canyons with available surficial deposits. In areas where canyons open to wider valleys and the channel slope decreases, the flow would begin to deposit what it had picked up (debulk). Evidence in this area shows that, in most cases (one exception: the debris flow down White Branch in 1942), flows did not commonly bulk past hyperconcentration. Therefore, by the time the peak reaches the exit of the mountain area, it is assumed that the flow would have doubled in volume to 1,480 acre-ft and would reach an approximate sediment concentration of 50 percent by volume.

Debulking would begin to occur when the channel slope decreases at the end of the mountain segment; it would begin approximately 8 mi from the breach and would occur rapidly. Debulking would be confined to the valley and alluvial-fan segments. The magnitude of the event at the exit of the mountain segment would determine the length of the major depositional reach. At the exit of the valley segment, at mile 16, the flow would become so wide that deposition would occur very rapidly. The flow probably would be out of the hyperconcentrated range and would become a water-dominated flood flow by the time it traveled 3 mi into the alluvial fan segment.

## Peak Routing

The DeLong (1986) one-dimensional, unsteady-state streamflow model HYDRAUX was used to route the breach hydrograph downstream. Assuming that the event would occur sometime from June to October, the base flow used was a maximum of 230 $ft^3/s$ (Friday and Miller, 1984). The modeled downstream flow was periodically interrupted to bulk the system with estimated volumes of sediment. An algorithm to simulate the debulking process (as described in the previous section) was used from mile 8 on downstream. No attempt was made to factor in viscosity changes due to increased sediment and debris concentrations. Considering all the other unknowns, it is not likely that this inclusion would significantly improve our assessment.

Concentration and viscosity changes are reflected in the Manning roughness coefficient(s) assigned at each cross section. This Manning's $n$ was determined from values defined by past flows in the area (table 1) and from other data obtained in the Mount St. Helens, Washington, area (Laenen and Hansen, 1986).

Carver Lake flows into an unnamed tributary of South Fork Squaw Creek. It flows for 3.1 mi in this tributary before it reaches the confluence of the South Fork Squaw Creek. In the South Fork Squaw Creek it flows for 2.5 more miles before it reaches the main stem of Squaw Creek at river mile 36.3 (fig. 1).

The channel from Carver Lake to the mouth of Squaw Creek, a total distance of 42 mi, was analyzed in four segments: (1) a mountain segment from mile 0.0 to mile 8.0, with an average channel slope of 380 ft/mi and some canyon slopes of 800 ft/mi; (2) a valley segment from mile 8.0 to 17.0, with an average channel slope of 110 ft/mi and average valley widths of 500 ft; (3) an alluvial fan from mile 17.0 to 22.0, having one major and two minor channels and an average channel slope of 50 ft/mi; and (4) a canyon segment from mile 22.0 to 42.0, having an average channel slope of 50 ft/mi. Discharge hydrographs at specific cross sections in the channel are shown in figure 9. From figure 9, flood-wave and peak arrivals, as well as flood-peak magnitude, can be determined along the entire route from the lake to the confluence with the Deschutes River. Table 2 is a summary of peak discharge, stage, time of peak, and Mannings $n$ values at all input cross sections.

A peak discharge of 180,000 $ft^3/s$, with a volume of 810 acre-ft, is used as the starting hydrograph. The model was stopped and additional volumes added to simulate bulking at river miles 0.5, 1.6, 4.2, and 7.9, on the rising limb and on one-third of the receding limb of the hydrograph. The total lake volume of 740 acre-ft was doubled by mile 8. By the end of this segment, the flood hydrograph had increased in volume, but the peak had attenuated to 53,000 $ft^3/s$ (fig. 9). The peak had taken 0.9 hours to reach this location.

The peak discharge at the Geological Survey gage at 15.4 mi from the lake would arrive in 1.65 h and have a magnitude of 21,000 $ft^3/s$. This magnitude can be compared with 2,000 $ft^3/s$, the 100-yr frequency meteorological event at this location. Modeled values of this scenario showed a stage 13 ft above the thalweg and 8 ft higher than the U.S. Army Corps of Engineers (1978) 100-yr flood elevation.

As the flood enters an alluvial fan (or fanhead valley), most flow would follow the principal channel (Squaw Creek), but some would follow two distributary channels

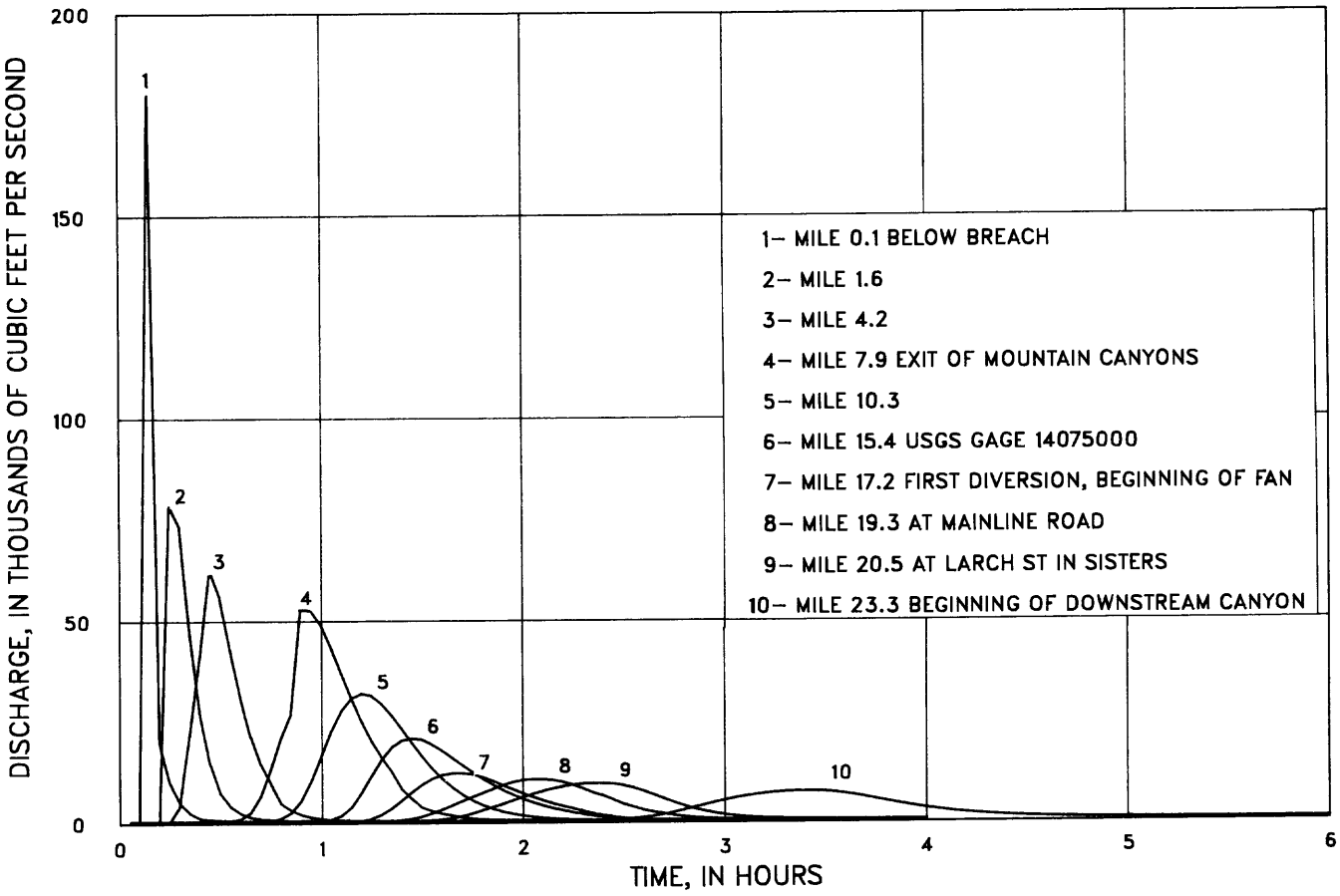


**Figure 9.** Hypothetical discharge hydrographs at selected cross sections showing progression of flood downstream.

(an abandoned channel and Squaw Creek Ditch, see fig. 1). At mile 17.2, an old diversion set in the channel diverts flow down an abandoned stream channel. At this location, flow in Squaw Creek follows a tight curve to the left; considerable flow could conceivably be diverted down the abandoned channel. It is also a distinct possibility that some new channels could be eroded on the fan because of the high stream velocities associated with the estimated flows. Certainly, flows would be overbank in this area and, if localized damming occurs, almost any location on the fan could be susceptible to flooding.

For the Squaw Creek channel, the hypothetical flood would have a magnitude of 9,800 $ft^3/s$ at mile 20.5 in the town of Sisters. The flow wave would first arrive in Sisters in about 1.8 h, with the peak arriving at about 2.4 h. This peak again can be compared to the estimated meteorological peak for the 100-yr frequency event. Stage at this location is about 10 ft above the streambed and 3 ft higher than the 100-yr event (U.S. Army Corps of Engineers, 1978). For flows in the abandoned channel and other routes in the fanhead valley upstream from Sisters, the peak magnitude would be about 2,000 $ft^3/s$ and would be attenuating rapidly.

The peak would arrive at the mouth of Squaw Creek in 5.5 h with a magnitude of 5,700 $ft^3/s$. Because flow has been confined to a canyon, the peak would not have much attenuation between Sisters and the mouth of Squaw Creek.

## Model Verification

The hyperconcentrated flood that occurred in the Squaw Creek drainage on September 7, 1970, can be used as an analog to help model and verify the prediction of the hypothetical Carver Lake breakout flood. The 1970 event resulted from a sudden moraine-dam failure that completely emptied a lake on the southeast side of Middle Sister. This lake was in a geologic setting similar to that of Carver Lake in that it was confined by a neoglacial moraine located subjacent to an active glacier (Diller) and was located at approximately the same elevation.

The volume of the lake was estimated from field measurements made in July 1985 to be about 130 acre-ft. This estimated volume is considerably smaller than the Carver Lake volume of 740 acre-ft. The breach geometry was measured as follows: length, 400 to 500 ft; perpendic-

**Table 2.** Summary of peak discharge, stage, time, and Manning's *n* for three hypothetical moraine-failure scenarios at input cross sections

[CL, Carver Lake Tributary; SF, South Fork Squaw Creek; SQ main stem Squaw Creek; $ft^3/s$, cubic feet per second;--, no data]

| Downstream mile | River mile | Peak discharge $(ft)^3/s$ | Water-surface Depth above Streambed (ft) | Time[1] (h) | Manning's *n* values used at cross section | | |
|---|---|---|---|---|---|---|---|
| | | | | | Subarea | Main channel | Subarea |
| CL 0.0 | CL 3.1 | 180,000 | 38 | 0.00 | 0.095 | 0.085 | 0.095 |
| CL 0.4 | CL 2.7 | 147,000 | 34 | -- | .090 | .080 | .090 |
| CL 0.5 | CL 2.6 | 137,000 | 12 | -- | .085 | .075 | .085 |
| CL 1.0 | CL 2.1 | 104,000 | 29 | -- | .080 | .070 | .080 |
| CL 1.6 | CL 1.5 | 78,000 | 22 | -- | .075 | .065 | .075 |
| CL 2.6 | CL 0.5 | 69,000 | 28 | -- | .070 | .060 | .070 |
| SF 4.2 | SF 1.5 | 63,000 | 13 | -- | .090 | .055 | .090 |
| SQ 6.6 | SQ 35.4 | 59,000 | 8 | -- | .080 | .050 | .090 |
| SQ 7.9 | SQ 34.1 | 53,000 | 22 | .90 | .090 | .045 | .090 |
| SQ 9.2 | SQ 32.8 | 44,000 | 13 | -- | .085 | .040 | .090 |
| SQ 10.3 | SQ 31.7 | 32,000 | 14 | -- | .090 | .045 | .080 |
| SQ 13.0 | SQ 29.0 | 24,000 | 15 | -- | .080 | .040 | .085 |
| SQ 15.4 | SQ 26.6 | 21,000 | 12 | 1.65 | .075 | .035 | .085 |
| SQ 17.2 | SQ 24.9 | 12,400 | 12 | -- | .060 | .032 | .060/.080 |
| SQ 17.3 | SQ 24.8 | 12,300 | 5 | -- | .085 | .030 | .065/.080 |
| SQ 19.1 | SQ 23.0 | 10,900 | 7 | -- | .085 | .030 | .065/.085 |
| SQ 19.3 | SQ 22.8 | 10,800 | 11 | -- | .085 | .028 | .085 |
| SQ 20.1 | SQ 22.0 | 10,000 | 8 | -- | .085 | .028 | .085 |
| SQ 20.5 | SQ 21.5 | 9,800 | 7 | 2.35 | .085 | .028 | .085 |
| SQ 20.8 | SQ 21.3 | 9,400 | 12 | -- | .085 | .028 | .085 |
| SQ 21.3 | SQ 20.8 | 9,100 | 9 | -- | .085 | .032 | .085 |
| SQ 22.0 | SQ 20.1 | 8,600 | 9 | -- | .085 | .035 | .085 |
| SQ 23.3 | SQ 18.8 | 7,600 | 7 | -- | .085 | .038 | .085 |
| SQ 28.1 | SQ 14.0 | 7,000 | 7 | -- | -- | .040 | -- |
| SQ 32.3 | SQ 9.8 | 6,500 | 5 | -- -- | | .045 | -- |
| SQ 36.4 | SQ 5.6 | 6,300 | 5 | -- | .060 | .045 | -- |
| SQ 39.1 | SQ 3.0 | 6,000 | 14 | -- | -- | .045 | -- |
| SQ 41.9 | SQ 0.2 | 5,700 | 13 | 5.50 | -- | .045 | -- |

[1]Time to peak from start of moraine breach.

ular height, 104 ft; width at moraine crest, 318 ft; width at bottom, 5 to 10 ft; lake-level drop, 64 ft. The Carver Lake moraine is about twice the thickness of the aforementioned breach. (For a hypothetical total-depth breach of the Carver Lake moraine, the length of the breach would be about 1,000 ft.)

The breaching of the 1970 event was modeled by using the breach routine in DAMBRK (Fread, 1980) for different breach-time intervals. A 5-min time interval produced a peak magnitude of 22,000 $ft^3/s$, which best matched the desired starting discharge that would in turn match the downstream flows calculated from field observations. That is, with modeled attenuation and assuming bulking of the flow as it travels downstream, we can best match the 10,500 $ft^3/s$ field-calculated flow at mile 1.42 by using a breach time of 5 min.

The hydrograph produced by the 5-min breach scenario was routed downstream using HYDRAUX (DeLong, 1986). Bulking and debulking scenarios were applied with the model routing. Three primary scenarios were run—A, B, and C—and two secondary scenarios B′ and C′ (see table 3). Material from the breach was entrained by the sudden release of water from the lake, and the volume of this material was added to the rising limb of the breach hydrograph for scenarios C and C′, but not for the other scenarios.

Scenario A routed the breach hydrograph downstream without applying bulking or debulking schemes. This scenario was run to define peak attenuation from channel friction alone for comparison purposes.

Scenario B applied a bulking scheme that doubled the flow volume by mile 8.87 and a debulking scheme that decreased volume by subtracting a portion of flow based on cross-section geometry. The bulking and debulking is discussed in earlier sections. This scenario matched field calculations well at mile 1.42, 5.53, and 8.87 (see table 3) but was considerably larger at mile 14.59 and 19.67.

Scenario C was run to see if an improved estimate of the distribution of bulking and debulking could enhance the calibration. This scenario was based on assessment of areal

**Table 3.** Summary of verification scenarios for the September 7, 1970 lake-breakout flood down the Squaw Creek channel

[CL, Carver Lake tributary; SF, South Fork Squaw Creek; SQ, main stem Squaw Creek; $ft^3/s$ cubic feet per second; --, no data]

| Downstream mile | Field-calculated discharge ($ft^3/s$) | Streamflow model scenario discharge ($ft^3/s$) | | | | |
|---|---|---|---|---|---|---|
| | | A[1] | B[2] | C[3] | B'[4] | C'[4] |
| CL 0.00 | -- | 22,000 | 22,000 | 29,400 | 22,000 | 29,400 |
| CL 1.42 | 10,500 | 7,120 | 10,100 | 10,900 | 10,100 | 10,900 |
| SF 5.53 | 11,500 | 4,250 | 11,500 | 7,110 | 11,500 | 7,110 |
| SQ 8.87 | 8,000 | 3,650 | 8,850 | 3,950 | 8,850 | 3,950 |
| SQ 14.59 | 1,200 | 3,120 | 7,110 | 2,740 | 4,700 | 550 |
| SQ 19.69 | [5]600 | 2,510 | 3,310 | 1,520 | 900 | 140 |

[1]Scenario A assumes attenuation from channel friction only.

[2] Scenario B assumes bulking to hyperconcentration of 50 percent sediment by volume by mile 8.0 and debulking in overbank sections.

[3] Scenario C assumes a more detailed bulking and debulking scheme determined with the help of areal photographs.

[4]Scenarios B' and C' assume losses to streambanks from mile 8.0.

[5]Discharge is estimated.

photography and involved a more detailed addition and removal of material in the upper reach, as well as removal of material in the lower reach. This scenario did not match the field-calculated discharge in the upper sections as well but did match the lower section values better (table 3).

A last set of scenarios—B' and C'—was run to define dewatering of the flow that could occur with losses to dry streambanks. A ground-water conductivity ($K$) of 900 ft/day was assumed. Head differentials from low-water elevation to peak elevation were defined at each section and volumes of water lost to the system were calculated and subtracted from the flow. Scenario B' (a dewatered scenario B) and C' (a dewatered scenario C) both yielded better results. However, for predictive purposes in the case of the Carver Lake hypothetical breakout, dewatering was not considered because streambank conditions could be saturated if the breach were to occur in spring or early summer.

## Model Sensitivity

It was beyond the scope of this study to do a detailed model-sensitivity study. Prior work done by Laenen and Hansen (1986) did such an analysis for modeled flows in the Mount St. Helens area. However, for the current study, model sensitivity was tested for Mannings' $n$. An average increase of 0.020 for all base values shown in table 2 yielded an average peak magnitude decrease of 15 percent (at the USGS gage and at Sisters), and an average decrease of 0.020 yielded an average peak magnitude increase of 20 percent.

## CONCLUSION

A high potential exists for failure of the moraine dam that impounds Carver Lake. During the last 50 yr, at least three moraine dams have breached in the Three Sisters Wilderness Area, and the resulting floods have traveled down the White Branch, Soda, and Squaw Creek drainages. The probability of a failure for Carver Lake is estimated to be 1 to 5 percent for any given year and would be expected to occur from June to October. The moraine that dams Carver Lake is steep, unvegetated, noncohesive, and loosely consolidated. Small avalanches of ice and rock occur frequently, and a major avalanche into the lake could cause a wave that would overtop and erode the dam; this would cause a catastrophic lake breakout.

A dam-break computer model was used to simulate a hypothetical breach of the moraine dam. Total displacement of the lake water by avalanche material would result almost instantaneously in an initial peak discharge of 180,000 $ft^3/s$. It is assumed that the flow would bulk up to a sediment concentration of 50 percent by volume (hyperconcentration) in the section between the breach and the end of the steeply sloping canyons, a distance of 8 mi. Debulking of the flood is assumed to occur in overflow sections of valley and debris-fan segments. The initial flood hydrograph is routed downstream by using a one-dimensional unsteady-state streamflow model that incorporates field determinations of Manning's $n$ coefficients to allow for hyperconcentrated flow. In the vicinity of the USGS gage (15.4 mi downstream from the lake), routing of the failure scenario simulates an estimated flood peak discharge of 21,000 $ft^3/s$. For comparison, the simulated flood peak discharge is 10 times greater than that of a 100-yr frequency-of-occurrence flood from high precipitation or snowmelt. The 100-yr frequency-of-occurrence flood is used for comparison of peak magnitude only; the probability of occurrence is from a different statistical population.

Three potential channels of flow were defined for the alluvial fan where the community of Sisters is located. Flow could occur almost anywhere on the alluvial fan because of channel shifting that accompanies local scour and dam-

ming. The hypothetical-flood scenario resulted in an estimated discharge of 9,800 $ft^3/s$ in Sisters along the main channel at mile 20.5.

In the remaining channels, about 3,000 and 1,000 $ft^3/s$, respectively, would start to flow down Squaw Creek Ditch, an abandoned channel (now used as a ditch), and down Squaw Creek Canal, but these flows probably would attenuate rapidly. Rising flood water would begin in the community of Sisters about 1.8 h after the dam breach; the flood peak would arrive about 30 min later. The probability of a flood from any breakout of Carver Lake has an estimated 1–5 percent chance of occurring in any given year.

## SELECTED REFERENCES


Andrews, J.T., 1975, Glacial systems: Duxbury Press, North Scituate, Massachusetts, 191 p.

Beverage, J.P., and Culbertson, J.K., 1964, Hyperconcentrations of suspended sediment: Journal of Hydraulics Division, American Society of Civil Engineers, v. 90, HY–6, p. 117–128.

Clague, J.J., Evans, S.G., and Blown, I.G., 1985, A debris flow triggered by the breaching of a moraine-dammed lake, Klattasine Creek, British Columbia: Canadian Journal of Earth Sciences, v. 22, p. 1492–1502.

Costa, J.E., 1985, Floods from dam failures: U.S. Geological Survey Open-File Report 85–560, 54 p.

Costa, J.E., and Schuster, R.L., 1987, The formation and failure of natural dams: U.S. Geological Survey Open-File Report 87–392, 39 p.

Crandell, D.R., and Fahnestock, R.K., 1965, Rockfalls and avalanches from Little Tahoma Peak on Mount Rainier, Washington: U.S. Geological Survey Bulletin 1221–A, 30 p.

DeLong, L.L., 1986, Extension of the unsteady one-dimensional open-channel flow equations for flow simulation in meandering channels with flood plains, *in* Subitzky, Seymour, ed., Selected papers in the hydrologic sciences: U.S. Geological Survey Water-Supply Paper 2290, p. 101–105.

Fread, D.L., 1980, DAMBRK—The dam-break flood forecasting model: Silver Spring, Maryland, National Weather Service, Office of Hydrology, Maryland, 37 p.

Friday, John, and Miller, S.J., 1984, Statistical summaries of streamflow data in Oregon, v. 1, Eastern Oregon: U.S. Geological Survey Open-File Report 84–454, 150 p.

Grove, J.M., 1979, The glacial history of the Holocene: Progress in Physical Geography, v. 3, p. 1–54.

Haeberli, W., and Epifani, F., 1986, Mapping the distribution of buried glacier ice—An example from Lago Delle Locee, Monte Rose, Italian Alps: Annals of Glaciology, no. 8, International Glaciology Society, p. 78–81.

Laenen, Antonius, and Hansen, R.P., 1986, Simulation of three lahars in the Mount St. Helens, Washington area, using a one-dimensional, unsteady-state streamflow model: U.S. Geological Survey Water-Resources Investigations Report 88–4004, 20 p.

Laenen, Antonius, Scott, K.M., Costa, J.E., and Orzol, L.L., 1987, Hydrologic hazards along Squaw Creek from a hypothetical failure of the glacial moraine impounding Carver Lake near Sisters, Oregon: U.S. Geological Survey Open-File Report 87–41, 48 p.

Matthes, F.E., 1939, Report of committee on glaciers: Transactions, American Geophysical Union, v. 20, p. 518–523.

Nolf, Bruce, 1966, Broken Top breaks: Flood released by erosion of glacial moraine: The Ore Bin, October 1966 issue, v. 28, no. 10, Oregon State Department of Geology and Mineral Industries, p. 182–188.

Ostrem, G., 1964, Ice-cored moraines in Scandanavia: Geografiska Annaler, v. 46, p. 282–337.

Porter, S.C., and Denton, G.H., 1967, Chronology of neoglaciation in the North American Cordillera: American Journal of Science, v. 267, p. 177–210.

Scott, K.M., 1988, Lahars and lahar-runout flows in the Toutle-Cowlitz River system, Mount St. Helens, Washington—Origins, behavior, and sedimentology: U.S. Geological Survey Professional Paper 1447–A, A1–A74. p.

———1989, Lahars and lahar-runout flows in the Toutle-Cowlitz River system, Mount St. Helens, Washington—Magnitude and frequency: U.S. Geological Survey Professional Paper 1447–B, B1–B33. p.

Scott, W.E., 1977, Quaternary glaciation and volcanism, Metolius River area, Oregon: Geological Society of America Bulletin, v. 88, January 1977, Document no. 70113, p. 113–124.

Taylor, E.M., 1965, Recent volcanism between Three Fingered Jack and North Sister, Oregon Cascade Range: The Ore Bin, v. 27, no. 7, Oregon State Department of Geology and Mineral Industries, p. 121–148.

Yesenov, U.Y., and Degovets, A.S., 1979, Catastrophic mudflow on the Bol'shaya Almatinka River in 1977: Soviet Hydrology, v. 18, p. 158–160.

U.S. Army Corps of Engineers, 1978, Flood plain information, Squaw Creek, Sisters, Oregon: Department of the Army, Portland District Corps of Engineers, 50 p.

# Ground-Water-Flow Modeling and Optimization Techniques Applied to High-Ground-Water Problems in San Bernardino, California

*By* Wesley R. Danskin *and* John R. Freckleton

**Abstract**

San Bernardino, California, is experiencing destructively high hydraulic heads. Changes in pumping patterns in response to a long-term decrease in agricultural ground-water usage and above-average recharge conditions have caused former marshlands in San Bernardino Valley that had dried to again become saturated. Urbanized areas within a 100-square-mile basin now are experiencing the highest hydraulic heads in 30 years. An increase in hydrostatic pressure near the land surface in a 10-square-mile area has caused a variety of problems, including buckled foundations, severed utility lines, and the threat of soil liquefaction in an area susceptible to earthquakes.

Linear-programming techniques coupled with ground-water response matrices were used to determine the most efficient pumping plan to reduce hydraulic heads in the affected areas. The ground-water system was simulated by using a transient, two-layer, finite-element model. Initial results of the management model indicated that the existing pumpage and capacity of municipal wells and pipelines were insufficient to accomplish an acceptable reduction in hydraulic heads within the required 1-yr timeframe. Therefore, different combinations of existing and proposed facilities were evaluated. Of the pumping plans examined, only the plan that used both existing and proposed extraction and transmission facilities produced an optimal solution that could lower hydraulic heads in the upper model layer to at least 30 ft below land surface within the 1-yr period.

Because soil is saturated close to land surface, the pumpage required to reduce hydraulic heads in the affected area is strongly dependent on changes in the evapotranspiration rate, which decreases with increasing depth to water. To account for these changes, an iterative technique was developed that permits the incorporation of piecewise-linear, source/sink functions, such as evapotranspiration, in an otherwise linear problem. This method combines an optimal pumping solution with the background response of the ground-water system and then adjusts the bounds on individual pumping rates in order to formulate the next iteration of the problem.

## INTRODUCTION

San Bernardino is located in southern California in a semiarid inland valley about 60 mi east of Los Angeles (fig. 1). Over the past 40 yr, the character of the region has changed from predominantly agricultural to mostly urban, and the population has increased. As a result of these changes, the quantities and patterns of water use also have changed. Hydraulic heads, which had declined as a result of intensive agricultural pumping during the 1940's and 1950's, began rising about 1968. By 1980, ground water had reached the land surface in some parts of the city.

The purpose of this study, conducted by the U.S. Geological Survey in cooperation with the San Bernardino Valley Municipal Water District during 1984–85, was to use optimization techniques to determine the minimum pumpage required to reduce hydraulic heads in the area of high ground water and yet maintain acceptably high hydraulic heads near municipal and agricultural wells. Because political injunctions had hampered the implementation of any general recharge and pumping plan, this study was designed to identify the likely short-term success of using specific pumped wells to depressurize the system. A short-term success, although perhaps temporary, would offer an important reprieve from the high-ground-water problems and would provide additional time to resolve the politically more difficult long-term water-management issues. The evaluation of more comprehensive, long-term pumping and recharge plans is the subject of a continuing program with the Water District using similar optimization techniques.

Methods for optimizing pumping from a ground-water system have been studied by several researchers, including Maddock (1972), Aquado and others (1974), and Heidari (1982). The general optimization method used in this study combines linear programming with ground-water response matrices. The method involves using a ground-water-flow model to generate hydraulic-head responses, which are recorded at sites of interest. These responses then can be superposed to simulate the effect of any combination of stresses. When this is done within a linear-programming

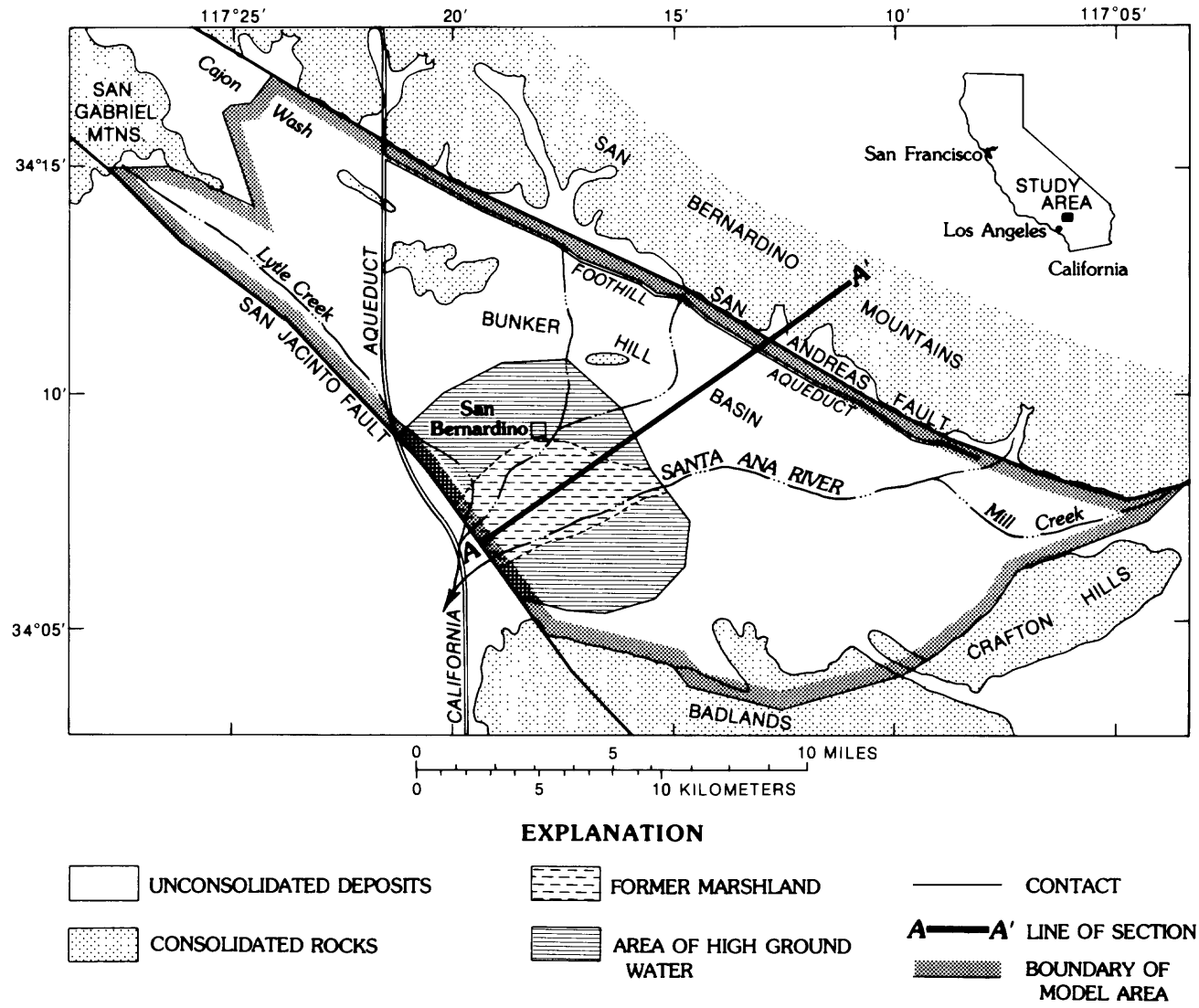


**Figure 1.** Location of study area.

model, constraints can be placed on hydraulic heads at each of the sites, and then an objective, expressed as a mathematical function, can be minimized or maximized. This method, along with other ground-water-management methods that use optimization techniques, is reviewed by Gorelick (1983).

A major extension to the basic procedure used to minimize ground-water pumpage has been incorporated in this study. In order for linear-programming methods to be applied, the ground-water-flow equations that describe the system must be linear with respect to pumping decisions. Recently developed ground-water-flow models, however, routinely include functional relations that are not linear, such as those for evapotranspiration, subsurface drains, and some stream-aquifer interactions. For instance, evapotranspiration may be simulated as a piecewise-linear function of hydraulic head and thus a nonlinear function of pumping decisions. These nonlinearities limit the application of many calibrated flow models in solving hydraulic-optimization problems. To overcome this limitation, an iterative technique was developed for this study so that the effects of a piecewise-linear evapotranspiration function could be included in the management solutions.

## THE AREA

The term "San Bernardino Valley" was first used by Mendenhall (1905, p. 9) to describe an area of indefinite limits beyond the city of San Bernardino. More recently, Dutcher and Garrett (1963, p. 17) restricted the term to that part of the upper Santa Ana Valley between the San Jacinto and San Andreas faults on the southwest and northeast, respectively, and between the San Gabriel Mountains on the northwest and the Crafton Hills and Badlands on the

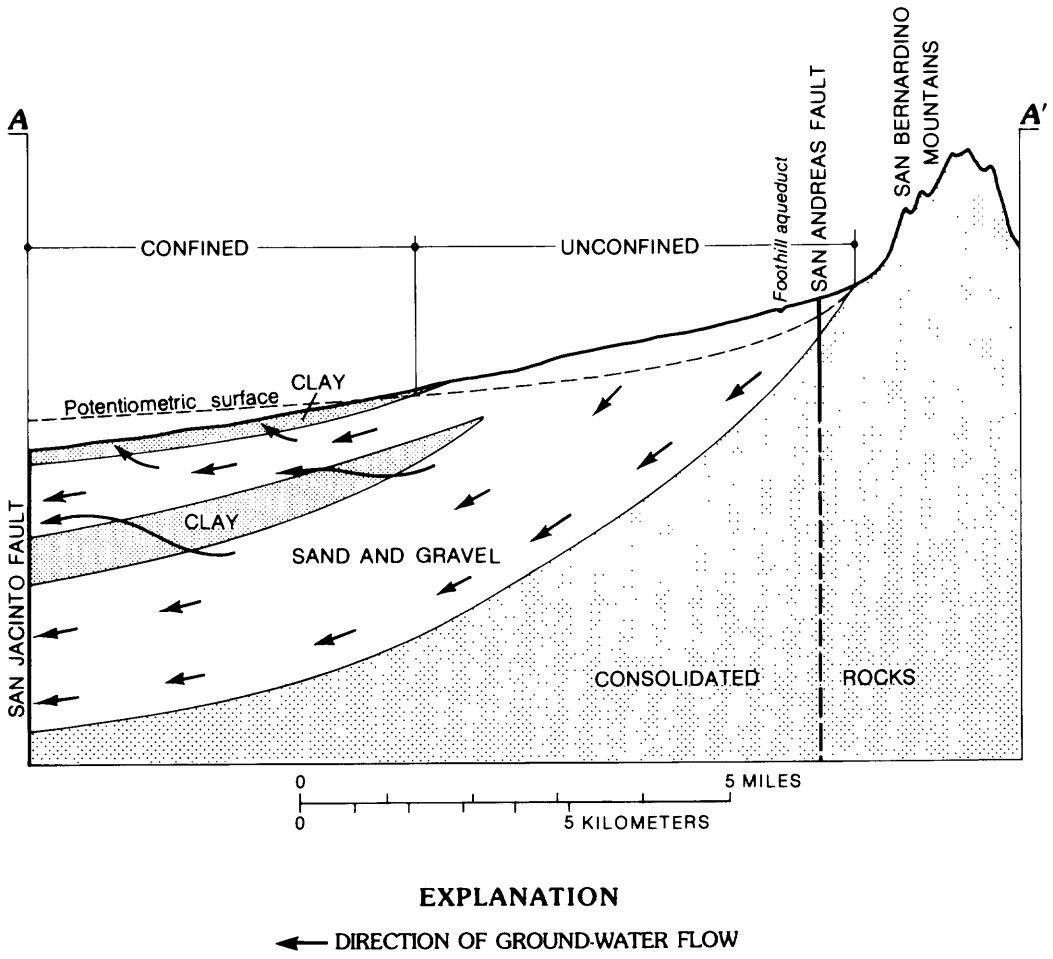


**Figure 2.** Generalized geologic section of the Bunker Hill basin showing confining clay layers and direction of ground-water flow.

southeast (fig. 1). The Bunker Hill ground-water basin lies entirely within the San Bernardino Valley and is the focus of this study.

The basin was formed when an area of about 100 $mi^2$ was downfaulted relative to adjacent areas. Alluvial deposits then filled the basin to a maximum depth of about 1,200 ft (Dutcher and Garrett, 1963, p. 45). The highlands that surround most of the basin are composed of consolidated, virtually nonwater-bearing rocks. These outcrops consist of indurated continental sediments and of igneous and metamorphic rocks, which also form the basement complex underlying the study area. The alluvium within the ground-water basin consists of sand, gravel, and boulders interspersed with lenticular deposits of silt and clay. Figure 2 is a generalized geologic section of the basin showing the major geologic features and directions of ground-water flow. The total thickness of alluvial deposits and the percentage of clay in the deposits increase toward the southwest, reaching their maximums adjacent to the San Jacinto fault. The unconsolidated aquifer materials provide a significant source of water to the valley and locally may yield as much as 4,400 gal/min to individual wells.

Historically, the area near the San Jacinto fault has been the site of marshlands and more recently the site of destructively high hydraulic heads. In the 1870's, test drilling revealed that water-bearing zones underlying the marshland were under significant artesian pressure; some flowing wells in the area had hydraulic heads greater than 50 ft above land surface. Dutcher and Garrett (1963) identified three major clay layers beneath the marshland. These clay layers separate the more permeable aquifer materials and create the confined conditions observed in the aquifer by impeding the vertical movement of ground water. The uppermost clay layer is at land surface and ranges from 30 to 100 ft in thickness. Although the hydraulic head in the aquifer directly beneath the top clay layer historically has been much higher than land surface, the low permeability of the clay slows the upward movement of ground water. As a result, a slow upward seepage of ground water occurred at the land surface, creating

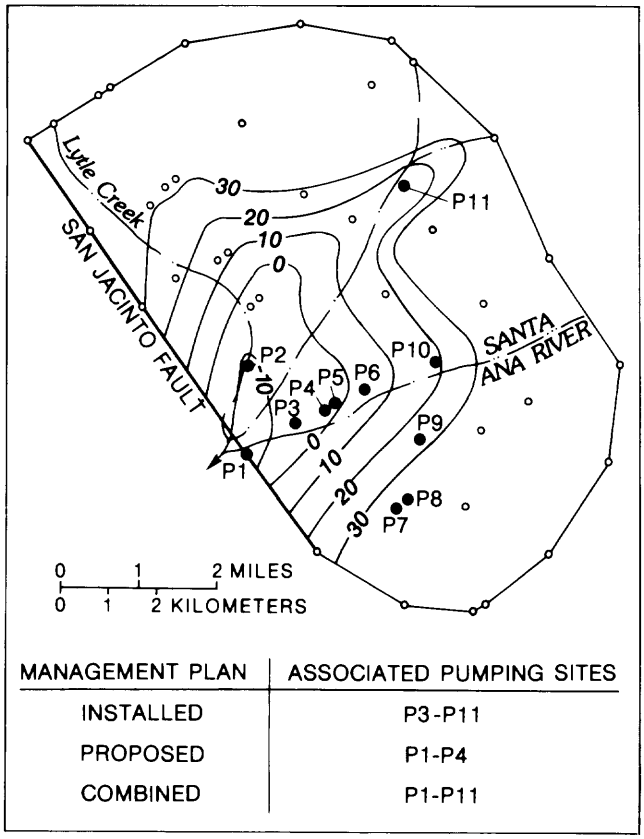


| MANAGEMENT PLAN | ASSOCIATED PUMPING SITES |
|---|---|
| INSTALLED | P3-P11 |
| PROPOSED | P1-P4 |
| COMBINED | P1-P11 |

**EXPLANATION**

—30— LINE OF EQUAL HYDRAULIC HEAD – In feet below land surface. *-10* indicates 10 feet above land surface. Interval 10 feet

●P8 PUMPING SITE AND DESIGNATION

○ HYDRAULIC-HEAD-CONSTRAINT SITE

**Figure 3.** Initial hydraulic-head configuration in the upper model layer within the high-ground-water area. Also shown are the pumping and hydraulic-head-constraint sites.

marshlands. When increased agricultural pumping caused the hydraulic head in the aquifer to drop below land surface, this seepage stopped and the marshlands dried. The areal extent of the uppermost clay layer coincides approximately with the current high-ground-water area shown in figures 1 and 3.

Three main tributary streams—the Santa Ana River, Mill Creek, and Lytle Creek—contribute more than 60 percent of the recharge to the ground-water system. Streamflow originates in mountain areas contiguous to the ground-water basin. For the most part, streamflow that enters the valley is intermittent, averaging 123,000 acre-ft/yr. During storm periods, streamflow emerges from mountain canyons along the valley perimeter and moves down the alluvial fans, where a large part of the flow infiltrates through the permeable surficial deposits on the fans. Some of the infiltrating water is evaporated, and some is transpired by riparian vegetation. However, streamflow records indicate that over long periods of time about 90 percent of the streamflow that enters the valley recharges the ground-water basin. Because most of the streams entering or leaving the valley are gaged, estimates of streamflow recharge are among the most reliable hydrologic data for the basin.

Ground-water movement in the Bunker Hill basin generally follows the surficial-drainage pattern. Surface water enters the aquifer through permeable deposits near the mountain fronts and along stream channels. Ground water generally moves from these areas toward the southwest—except in the Lytle Creek and Cajon Wash areas where it moves toward the southeast—and converges toward a common line of discharge at the San Jacinto fault beneath the Santa Ana River. Underflow of ground water enters along the southeastern edge of the basin through the poorly consolidated deposits of the Badlands. Although ground-water recharge from irrigation return once was significant, it has become less so with the continuing urbanization of agricultural lands. Because of the prevailing semiarid conditions, direct infiltration of precipitation on the basin floor contributes very little to the ground-water system.

Natural ground-water outflow from the basin is controlled by the San Jacinto fault, which acts as a partial barrier and causes ground water to move upward toward the land surface. Prior to intensive pumping, it was this damming effect that contributed to the creation of a 10-mi$^2$ marshland just northeast of the San Jacinto fault (fig. 1). Evapotranspiration from this area originally accounted for most of the ground-water outflow from the basin. Underflow across the San Jacinto fault was less significant; Dutcher and Garrett (1963) estimated underflow to be about 15,000 acre-ft in 1945. In the 1930's, ground-water pumpage became a major component of the ground-water budget. As hydraulic heads in the aquifer declined and vertical hydraulic gradient toward the land surface decreased, evapotranspiration during the 1940's and 1950's decreased. Hydraulic heads continued to decline, but at a slower rate. When rapid urbanization of the valley began, about 1960, ground-water pumpage decreased, recharge increased, and hydraulic heads began to rise.

## THE HIGH-GROUND-WATER PROBLEM

Ground-water storage in the San Bernardino Valley has gone through cycles of decline and replenishment. Prior to significant development in the valley, ground water leaked upward through clay layers and saturated the low-lying areas, creating marshlands (fig. 1). In the early 1930's a combination of ground-water development for agriculture and below-normal precipitation caused the marshlands to dry. These areas subsequently were developed for commercial and industrial uses.

In the 20-yr period 1963 through 1982, recharge to the ground-water basin increased substantially. A sequence of wet years produced greater-than-average natural streamflow and greater percolation through the streambeds. In addition, water agencies upgradient in the basin, acting independently, have been recharging diverted natural streamflow and imported water from the California Aqueduct (fig. 1) in order to reduce pumping costs for their customers in the upland areas. As a result of these increases in recharge, water levels have continued to rise; since about 1980, hydraulic heads have been near or above land surface in the low-lying parts of the valley (fig. 3). Although partial confinement in these areas reduces the rate of upward movement of water, the increase in pore-water pressure beneath the developed areas has caused increasingly severe problems. Streets have buckled, basements have been flooded, and concrete-lined flood-control channels have been damaged. Because traces of two active faults, the San Andreas and San Jacinto, cross the study area, city officials and local residents are concerned also about the potential for soil liquefaction, which can be caused by earthquake-induced shaking. For example, similar geohydrologic conditions existed prior to the 1964 earthquake in Niigata, Japan, in which liquefaction contributed to widespread destruction of buildings (Kishida, 1966; Koizumi, 1966).

A primary management objective for the Water District, in addition to distributing water for use throughout the San Bernardino Valley, is to lower hydraulic heads in the aquifer beneath the problem area, thereby preventing the movement of ground water to the land surface. Meeting this objective has been complicated by the actions of other water agencies, whose goals are to maintain high-ground-water levels. Because long-term recharge to the basin has been greater than discharge, a comprehensive management solution likely would require adjustments in both recharge and discharge quantities. To date, long-term management solutions have not been politically possible. As a short-term solution, the Water District proposed the installation of four new wells designated expressly for depressurizing the high-ground-water area. The purpose of this study was to test the effectiveness of these proposed wells, in combination with the existing, but underutilized, pumping facilities, in meeting the stated objective. Most methods that might be used to solve the problem involve a trial-and-error adjustment of pumping rates and sites. A much more effective method is to formulate the management problem as a hydraulic-optimization model. This approach specifies that total managed pumpage in the area is minimized and that hydraulic heads are maintained within defined limits.

## THE GROUND-WATER-FLOW MODEL

A major component of the hydraulic-optimization technique used to address the high-ground-water problem is the response of hydraulic heads to each of the stresses imposed on the ground-water system. In order to calculate the response, the ground-water-flow model developed by Hardt and Hutchinson (1978, 1980) was used. This model represents the aquifer in the Bunker Hill basin as a two-layer system. Each layer is simulated by using 296 triangular elements and 198 nodes. Within each layer, ground-water flow is assumed to be two dimensional. The hydraulic connection between the layers is simulated by a leakance term that approximates vertical flow through the confining silt and clay layers. The model simulates unconfined conditions in the highland areas of the basin and leaky confined conditions beneath the former marshlands (fig. 2). Discharge of ground water from the upper layer to the land surface is approximated by using an evapotranspiration function. The model assumes that changes in storage occur instantaneously, and the model does not compute the time required for drainage.

A Galerkin finite-element procedure is used to solve the governing equation for each layer,

$$\frac{\delta}{\delta x}\left(T_x\frac{\delta h}{\delta x}\right)+\frac{\delta}{\delta y}\left(T_y\frac{\delta h}{\delta y}\right)-S\frac{\delta h}{\delta t}-\frac{K_z}{b}\left(h-h_a\right)-W-E=0 \quad (1)$$

where

$b$ is thickness of the confining unit [L];
$E$ is evapotranspiration, calculated below [L/T];
$h$ is hydraulic head [L];
$h_a$ is hydraulic head in the adjacent layer [L];
$K_z$ is vertical hydraulic conductivity of the confining bed [L/T];
$S$ is storage coefficient (dimensionless);
$t$ is time [T];
$T$ is transmissivity [$L^2/T$];
$W$ is constant-rate sources and sinks [L/T]; and
$x,y$ are cartesian coordinates [L].

The evapotranspiration rate ($E$) varies with the depth to water. As hydraulic heads decline, the rate decreases, eventually to zero. This relation can be approximated by the piecewise-linear function,

$$E = E_{max}\left(1-\frac{D}{D_o}\right) \qquad \text{for } D < D_o \text{ and} \qquad (2a)$$

$$E = 0 \qquad \text{for } D \geqq D_o \qquad (2b)$$

where

$E$ is evapotranspiration rate at depth $D$ [L/T];
$E_{max}$ is maximum evapotranspiration rate [L/T];
$D$ is depth to water [L]; and
$D_o$ is maximum depth at which evapotranspiration occurs [L].

At the land surface, a maximum evapotranspiration rate is reached. In the San Bernardino area, this is approximately 38 in/yr ($1\times10^{-7}$ ft/s). When hydraulic heads are at

or below a depth of 10 ft, the rate is assumed to be zero.

The ground-water model was used to simulate actual conditions in the basin for the period 1945 to 1974. Additional simulations for the period 1975 to 2000 were used to investigate the effects of above-average-recharge conditions combined with average pumping rates (Hardt and Hutchinson, 1980, p. 61). The usefulness of the model was demonstrated by these simulations, which indicated correctly that ground water would rise to land surface as early as 1980. Hardt and Freckleton (1987) extended previous work by using the model to determine the sensitivity of the ground-water system to different combinations of pumping and recharge.

## THE OPTIMIZATION MODEL

### Formulation

Minimization of total hydraulic-head-reducing pumpage was chosen as the objective function ($z$) for the linear-programming problem:

$$z = \text{Minimize} \sum_{i}^{m} \sum_{j}^{n} Q_{ij} , \qquad (3)$$

where $Q$ is the ground-water pumpage at site $i$ during time period $j$, $m$ is the total number of pumping sites, and $n$ is the total number of time periods.

Constraints imposed on the objective function involve restrictions on hydraulic heads in the upper model layer at 47 sites. In order to prevent the adverse effects of ground-water ponding at land surface and destructive hydrostatic pressures just below land surface, an upper limit on hydraulic head was required. In order to prevent excessive drawdown at municipal and agricultural wells, a lower limit on hydraulic head also was required. These constraints arose from management decisions to lower hydraulic heads to an acceptable degree while at the same time limiting drawdowns in order to lessen the impact of greater pumping lifts. Because the ground-water model simulates regional ground-water flow and does not calculate actual in-well drawdown, measured drawdowns near pumped wells will be greater than values predicted by the model.

Bounds on the decision variables (pumpage $Q_{ij}$) arose from physical limitations of well and transmissionline capabilities and their time-varying excess capacities. Each well and its connecting pipelines have maximum capacities. Part of this capacity is used to satisfy ongoing commitments. The rest is available as excess capacity, which can be used for reducing hydraulic heads. Because water demand varies during the year, the excess capacity also varies. For example, during the months of May through August when water demand is particularly heavy, the existing production and distribution facilities are operated near their maximum capacities. Excess capacity during this period is less than one-fourth that available in winter.

The optimization model was linked to the ground-water system by using response functions. These functions were developed from flow-model simulations of pumpage at each of the pumping sites shown in figure 3. A constant discharge rate was maintained at a pumping site for a 1-month period and then discontinued. Hydraulic-head responses in the upper model layer due to this stress were computed at each of the constraint sites at the end of each month. Because only one stress is imposed on the system at a time, the responses reflect the ability of a single pumping site to produce a reduction in hydraulic head at each of the locations of interest. The response is dependent on the relative positions of the pumping and constraint sites and on the hydraulic properties and geometry of the aquifer system. Because of the coarseness of the ground-water-model grid, individual well sites were not simulated, but rather the pumpage for a particular site was assigned to the nearest model node or nodes.

The effects of the initial conditions, boundary conditions, and unmanaged stresses were developed from separate flow-model simulations and are referred to collectively as background responses. Background responses were developed for different recharge conditions by using identical initial conditions. All other background stresses were assumed to remain constant over time. By uncoupling the background responses from the hydraulic-head constraints, the extra pumping required to reduce hydraulic heads can be determined directly from the linear program.

A difficulty arises in this general linear-programming approach because the ground-water-flow model simulates evapotranspiration as a piecewise-linear function of hydraulic head. The inclusion of this sink term in the model produces nonlinearities in the generated response coefficients. This means that superposition of the background responses with the initial linear-programming solution may not produce an acceptably accurate result. To compensate for this, an iterative approach to the problem was developed. Figure 4 presents a flow diagram of the solution procedure. In this procedure, the results of the linear-programming problem are incorporated in the background simulation, and then the bounds on the pumping rates are modified accordingly. The method is best described by the following example.

If only one well were to be managed, then appropriate bounds on pumpage from the well would be assigned at the beginning of the iterative procedure, such as

$$0 \leqq Q \leqq Q_{max} , \qquad (4)$$

where pumpage $Q$ must be greater than or equal to zero and must be less than or equal to some maximum pumping rate $Q_{max}$, which may be determined by well or pipeline capacities. At the end of the first iteration, a value of pumpage at the well ($Q_1$) would be given by the optimal solution. The second iteration would involve adding $Q_1$ to

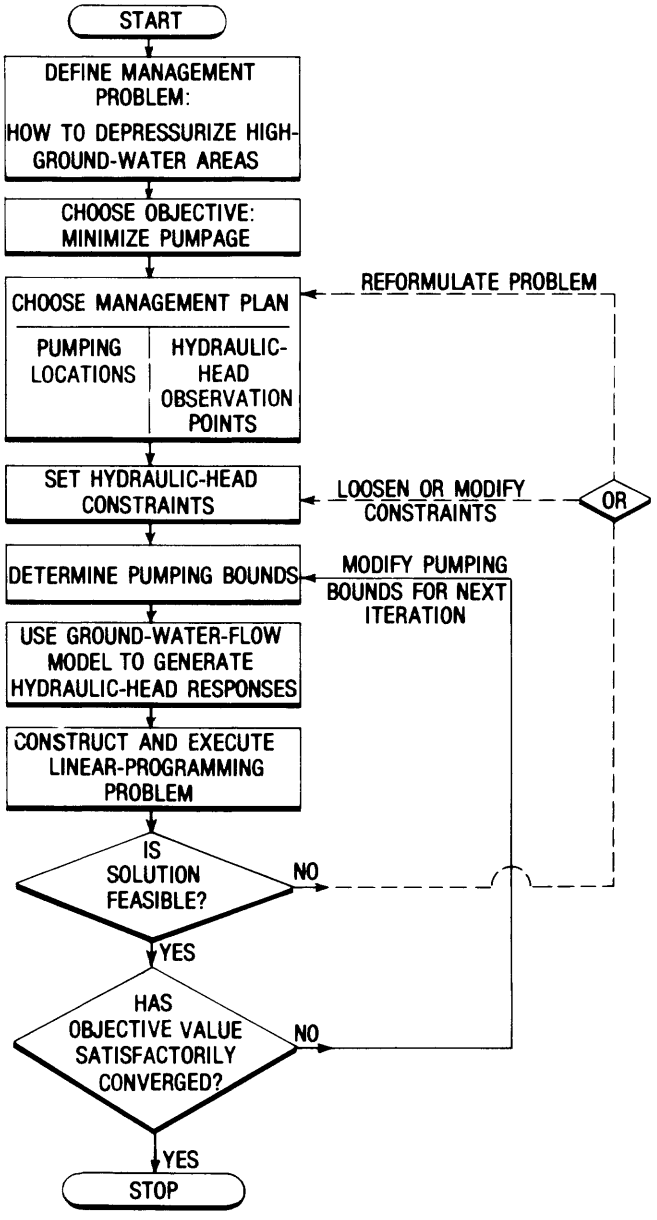


**Figure 4.** Flowchart of iterative solution procedure.

the unmanaged stresses and calculating a new background response. The bounds on $Q$ would be adjusted to compensate for the addition of $Q_1$ to the background responses, so that

$$0-Q_1 \leqq Q \leqq Q_{max}-Q_1. \quad (5)$$

The second optimal solution would yield a new value of pumpage, $Q_2$. Similar modifications would be made to the background responses and pumping bounds, resulting in

$$0-Q_1-Q_2 \leqq Q \leqq Q_{max}-Q_1-Q_2. \quad (6)$$

The optimal total pumpage for the well ($Q_{opt}$) at the end of $n$ iterations would be

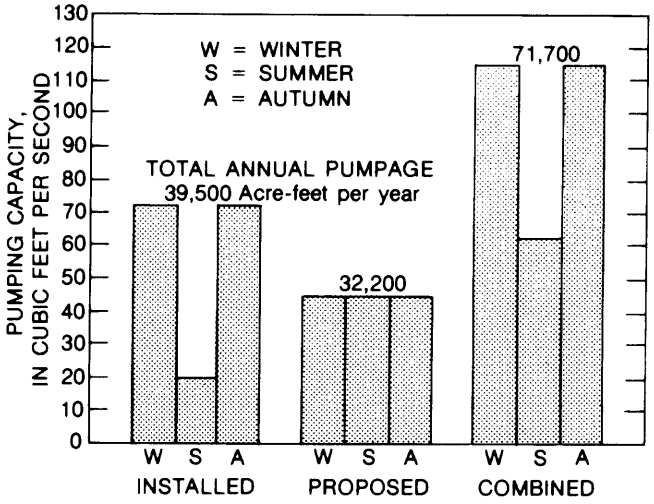


**Figure 5.** Seasonal pumping capacity and total annual pumpage for each management plan.

$$Q_{opt} = \Sigma\, Q_i \text{ for } i=1,2,3 \ldots n. \quad (7)$$

Using this iterative method, the linear-programming solution has the freedom to adjust to the nonlinear effects of evapotranspiration. Convergence to an acceptable solution was assumed if the difference in total pumpage between two successive iterations was less than 3 percent.

## Application

To find the optimal pumping solution to the problem, 26 optimization simulations were performed for different management plans involving existing, proposed, and the combination of existing and proposed facilities. These three management plans will be referred to as INSTALLED, PROPOSED, and COMBINED plans, respectively. The INSTALLED facilities include well fields and pipelines that are currently being used for municipal supplies. As described earlier, these facilities have an excess capacity that varies seasonally but which can be used for reducing hydraulic heads in the affected areas. PROPOSED facilities include the new wells and pipelines that have been proposed by the San Bernardino Valley Municipal Water District. Because these installations are designated for hydraulic-head-reduction purposes only, the capacity does not vary seasonally. The COMBINED plan is simply the sum of installed and proposed capacities. The respective pumping capacities of each plan, by season, are shown in figure 5. (For purposes of this study, winter = January–April; summer = May–August; and autumn = September–December.)

The pumping sites where additional pumpage can occur are defined by the particular management plan and are shown in figure 3. Seasonal pumping capacity for each plan was apportioned by month to the respective pumping sites. Hydraulic heads in the upper model layer were constrained

at all the sites in the problem area. Each of the 11 pumping sites and 47 constraint sites is represented by a node in the ground-water model. Some nodes serve as both a constraint site and a pumping site.

The background responses of the ground-water system are included implicitly in the linear program and exert a significant influence on the quantity of additional pumpage required. A configuration of initial hydraulic heads that represents the existing problem was developed by using the ground-water-flow model and historical data. Average underflow into and out of the basin was estimated to be 7,700 acre-ft/yr and 15,200 acre-ft/yr, respectively. Projected basinwide pumping was assumed to continue at the approximate average of the rate for the past few years (109,000 acre-ft/yr for the period 1974 to 1983). Artificial-recharge efforts were assumed to use all the available entitlement from the California Aqueduct (71,500 acre-ft/yr) to simulate worst case scenarios. Both average natural recharge (96,400 acre-ft/yr) and 120 percent of average natural recharge (116,000 acre-ft/yr) were simulated in order to test the sensitivity of the solutions to different quantities of natural recharge. Under conditions of average natural recharge and no additional pumpage, evapotranspiration was approximately 10,000 acre-ft/yr. It is important to note that, as pumpage is increased and hydraulic heads decline, the amount of water removed from the basin by evapotranspiration decreases. In the management model, this decrease in evaporative losses must be compensated for by additional pumpage.

Because of the critical need to lower hydraulic heads as soon as possible in order to prevent further damage to buildings and utilities, and because another wet year with above-average recharge would compound existing high-ground-water problems, the optimization model was designed to meet hydraulic-head constraints within a 12-month management timeframe. During this management period, hydraulic-head constraints were imposed at different times during the year in order to determine the sensitivity of the management solutions to seasonality. It is important to note that the management period was chosen specifically to investigate the effects on the aquifer system that could be expected within a short period of time. The solutions do not guarantee that satisfactory hydraulic heads will be maintained after the 12-month period or for recharge conditions other than those tested in the model.

The original goal of the management model was to lower hydraulic heads in the upper model layer to at least 30 ft below land surface. At some constraint sites, meeting the 30-ft target would require as much as 45 ft of total drawdown because the initial hydraulic head is considerably above land surface. The reduction in hydraulic head would remove the driving force and possibly prevent further damage to buildings and roads. The reduction also would promote a dewatering of the near-surface environment and thereby decrease the potential for soil liquefaction during an earthquake. However, initial testing of the optimization model revealed that only the COMBINED plan was capable of lowering hydraulic heads to 30 ft below land surface within a 12-month period. Therefore, in simulations involving the INSTALLED and PROPOSED plans, this goal was relaxed to 20 ft. Simulations of the COMBINED plan also used, for purposes of comparison, 10- and 20-ft goals.

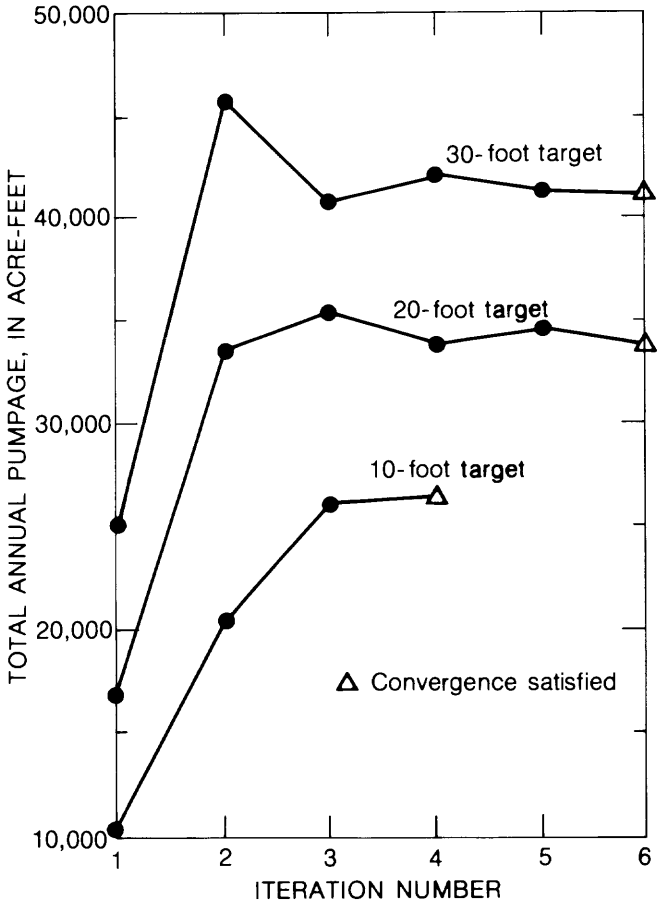


**Figure 6.** Total pumpage required for the COMBINED plan showing convergence of the iterative procedure. Separate graphs indicate the total pumpage required to meet 10- , 20- , and 30-ft drawdown targets during each of the 12 months. Natural recharge was simulated as 120 percent of normal.

The MINOS mathematical programming system (Murtaugh and Saunders, 1983) was used to solve the linear-programming problems on a Prime 9950 mini-computer. Total CPU (central processing unit) time per iteration was about 20 min. Each iteration includes running the ground-water-flow model with 12 time periods to generate the background response, building MINOS data sets, and solving a linear-programming problem with MINOS. Acceptably accurate solutions were achieved within 3 to 4 iterations (fig. 6).

**Table 1.** Comparison of total annual pumpage required for different management plans

[Total pumpage: INF indicates an infeasible solution; asterisk (*) indicates that more detailed data are given in figure 7; implied accuracy is shown for computational purposes only]

| Management plan | Simulation | Drawdown target (ft) | Percent of average recharge | First month constrained | Total pumpage (acre-ft) | |
|---|---|---|---|---|---|---|
| | | | | | Used | Available |
| INSTALLED | 1 | 30 | 120 | 12 | INF | 39,489 |
| | 2 | 20 | 120 | 12 | 34,611 | 39,489 |
| | 3 | 20 | 120 | 11 | INF | 39,489 |
| | 4 | 30 | 100 | 12 | INF | 39,489 |
| | 5 | 20 | 100 | 12 | 27,771 | 39,489* |
| | 6 | 20 | 100 | 11 | 33,551 | 39,489 |
| | 7 | 20 | 100 | 10 | INF | 39,489 |
| PROPOSED | 8 | 30 | 120 | 12 | INF | 32,232 |
| | 9 | 20 | 120 | 12 | 27,922 | 32,232 |
| | 10 | 20 | 120 | 11 | 28,829 | 32,232 |
| | 11 | 20 | 120 | 10 | 29,798 | 32,232 |
| | 12 | 20 | 120 | 9 | 30,659 | 32,232 |
| | 13 | 20 | 120 | 8 | INF | 32,232 |
| | 14 | 30 | 100 | 12 | INF | 32,232 |
| | 15 | 20 | 100 | 12 | 21,652 | 32,232 |
| | 16 | 20 | 100 | 10 | 24,561 | 32,232 |
| | 17 | 20 | 100 | 9 | 26,136 | 32,232 |
| | 18 | 20 | 100 | 8 | 27,624 | 32,232 |
| | 19 | 20 | 100 | 6 | 30,534 | 32,232* |
| | 20 | 20 | 100 | 5 | INF | 32,232 |
| COMBINED | 21 | 30 | 120 | 1 | 42,065 | 71,721 |
| | 22 | 20 | 120 | 1 | 34,512 | 71,721 |
| | 23 | 10 | 120 | 1 | 26,805 | 71,721 |
| | 24 | 30 | 100 | 1 | 40,667 | 71,721 |
| | 25 | 20 | 100 | 1 | 33,942 | 71,721* |
| | 26 | 10 | 100 | 1 | 25,852 | 71,721 |

## EVALUATION OF MANAGEMENT PLANS

The iterative method of including the piecewise-linear evapotranspiration function worked well. Figure 6 shows how the pumpage for the COMBINED pumping plan converges to a solution when solving the 30- , 20- , and 10-ft problems. All the simulations converged to within 3 percent in four to six iterations, and three iterations generally were sufficient to permit comparison of results from different simulations.

A summary of the results from the different simulations is presented in table 1. Each simulation involves a combination of a different management plan, drawdown target, quantity of natural recharge, and the first month during the year when drawdown constraints must be satisfied. The minimum pumpage required to solve the problem is compared to the total pumpage available for that management plan. The accuracy of individual pumpage values is determined by the convergence criteria (3 percent) and is approximately 1,000 acre-ft. Greater precision is shown in table 1 to facilitate comparisons among different solutions.

Of particular interest are those situations that result in an infeasible solution (INF). For example, neither the INSTALLED nor the PROPOSED plans were capable of meeting the 30-ft target, even by the end of 12 months. In other cases, the infeasible solutions were used to bracket the timeframe in which a particular drawdown target could be achieved. Specific results from each of the management plans are discussed below. Figure 7 uses representative simulations to illustrate the most significant conclusions from the study.

### INSTALLED Plan

Although the presently INSTALLED pumping and transmission capacities are not adequate to lower hydraulic heads in the upper model layer to 30 ft below land surface, they can lower hydraulic heads to 20 ft below land surface for both average and above-average-recharge conditions. The difference in total pumpage between the two recharge conditions (simulations 2 and 5 in table 1) is about 7,000 acre-ft; however, the difference in recharge is more than 19,000 acre-ft. This discrepancy between the quantity of water added to the basin and the quantity extracted indicates that a recharge mound will migrate into the problem area in future years unless additional mitigation measures are taken.

It is interesting to note that the INSTALLED plan cannot solve the 20-ft problem before month 11 even

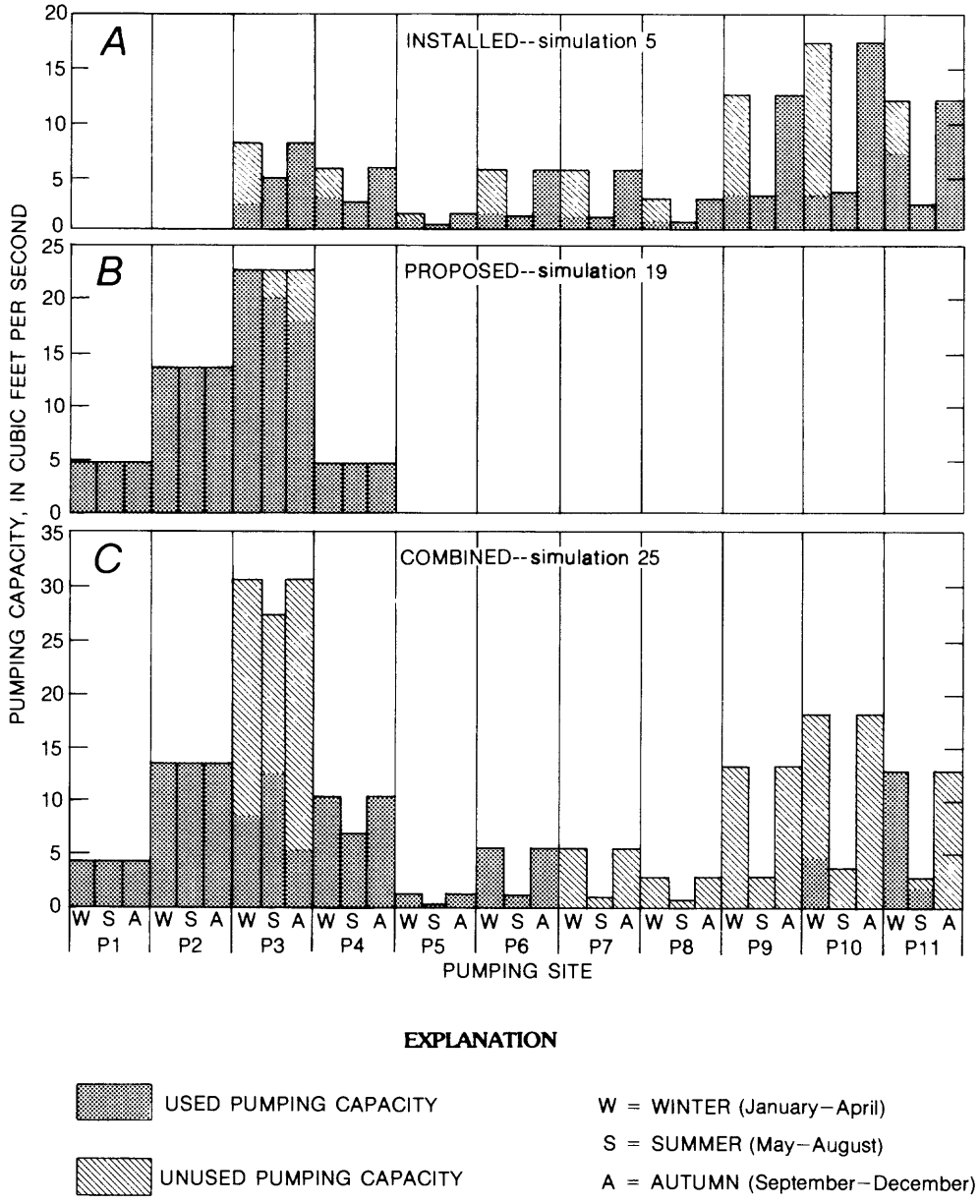


**Figure 7.** Total pumpage required for selected management plans. Graph *A* shows that all of the currently INSTALLED summer pumping capacity is required in order to meet hydraulic-head constraints by the end of autumn. Graph *B* shows that the PROPOSED capacity is almost completely used in order to lower hydraulic heads by midsummer. Graph C demonstrates that the COMBINED plan can meet hydraulic-head constraints in the first month and still have unused capacity at several sites. In each case, hydraulic heads were constrained to at least 20 ft below land surface, and natural recharge was simulated as 100 percent of normal.

though there appears to be sufficient annual capacity. The problem is the low excess capacity available during summer, as shown in figure 5. Because the extractions occur from a confined area with low storage coefficients and high transmissivities, a decrease in pumping permits a rapid recovery of the hydraulic heads. As shown in figure 7*A*, part of the winter capacity and all the summer capacity are used in meeting the hydraulic-head constraints by the end of autumn. The hydraulic heads rebound too far during the four summer months (May through August) when excess pumping capacity is much lower than during either autumn or winter. This result suggests that, if possible, the pumping

rate should not be allowed to vary greatly during the year.

Although pumping sites P7, P8, and P9 lie outside or nearly outside the problem area (fig. 3), they are part of the solution shown in figure 7*A*. In addition, all the unused pumping capacity is present during the winter months. This indicates that the siting of pumping locations is more important than using available pumping capacity earlier in the year.

## PROPOSED Plan

The PROPOSED facilities by themselves are equally incapable of lowering hydraulic heads to 30 ft below land surface within 1 yr. However, as shown in table 1, they can solve the 20-ft problem earlier in the year than is possible under the INSTALLED plan, even though the PROPOSED total annual capacity is less. The reason for this seems to be that the PROPOSED plan has wells located near the center of the problem area and has a more uniform pumping capacity throughout the year.

As the 20-ft drawdown constraint is imposed earlier in the year, the distribution of annual pumpage likewise shifts to earlier months, as would be expected. The inability of the PROPOSED plan to solve the 20-ft problem earlier than the sixth month, or to solve the 30-ft problem at all, appears to result solely from too little total pumping capacity. Another configuration of pumped wells may require less pumpage to solve the same problems; however, this type of analysis is best handled with mixed-integer programming and was not part of this study.

Nevertheless, it can be observed from figures 7*A* and 7*B* that the PROPOSED distribution of pumping capacity is quite different from that of the INSTALLED plan. All the capacity for the PROPOSED plan is focused in the center of the problem area using pumping sites P1–P4. In contrast, capacity for the INSTALLED plan is more broadly distributed. By comparing solutions with identical constraints for each plan (simulations 5 and 15), the preferable distribution of pumping can be identified. As shown in table 1, the INSTALLED plan uses 28 percent more pumpage to solve the identical problem (INSTALLED simulation 5 = 27,771 acre-ft; PROPOSED simulation 15 = 21,652 acre-ft). It seems that concentrating the pumping capacity in the center of the problem area would minimize the pumpage that is required.

The sensitivity of the solution to individual pumping sites can be determined by further analyzing graphs similar to those in figure 7 for different simulations that use the same management plan. Those sites that appear in the solutions with the loosest constraints (for example, constrained in month 12 in comparison with month 6), and those sites that use all the available capacity, are the most effective pumping sites. Graphical analyses such as presented in figure 7 were found to be useful when comparing a range of scenarios.

## COMBINED Plan

The COMBINED plan was the only one that was able to lower hydraulic heads in the upper layer to the original drawdown target of 30 ft below land surface. In fact, this can be done by the end of the first month. Although the COMBINED plan has more than twice the annual pumping capacity of the other plans, the greater success of this plan results primarily from having a slightly higher capacity available throughout the year. For example, the total annual pumpage required by the COMBINED plan to lower hydraulic heads to 30 ft below land surface by the end of month 1 was 42,065 acre-ft. This pumpage is only 6 percent higher than the available capacity of the PROPOSED plan. However, this small additional capacity permits an additional 10 ft of drawdown, 8 months earlier.

The difference between average and above-average recharge did not seem to significantly alter the solutions. For the 30-ft problem, the pumpages required were 40,667 and 42,065 acre-ft for the average and above-average conditions, respectively. Most of the pumpage is used to lower the existing high hydraulic heads. Much less pumpage is used to compensate for additional ground water moving into the problem area as a result of above-average recharge during the management year. This indicates that most of the current problem stems from several years of excess recharge and decreased basin discharge. As discussed earlier, however, a longer management timeframe would be required to investigate the time-lag effects of a large recharge event.

Figure 7*C* shows the pumpage required to satisfy the 20-ft target in 1 month under average-recharge conditions. Pumpage sites P7, P8, and P9 on the periphery of the high-ground-water area (fig. 3) are unused. Pumping sites P10 and P11, also on the periphery, contribute a small amount to the total pumpage. This suggests that, although pumping anywhere within the high-ground-water area would be of use, the greatest effect will be derived from pumping near the San Jacinto fault. In addition to the fact that this area has the highest hydraulic heads, a pumping advantage is achieved by locating wells there. The relatively impermeable boundary formed by the fault magnifies the drawdown for a given pumping rate. According to image-well theory, the closer the well is to an impermeable boundary, the greater the drawdown will be (Lohman, 1979).

## SUMMARY AND CONCLUSIONS

A hydraulic-optimization model was used as part of a study conducted during 1984–85 to investigate solutions to the destructively high hydraulic heads that are occurring in San Bernardino, Calif. Three management plans, which involve additional pumping from the area, were evaluated by using the optimization model. The objective was to minimize the total pumpage while meeting hydraulic-head

constraints. The ground-water system was simulated by a finite-element model and was linked to the optimization model by response functions. An iterative solution procedure was developed that permits incorporation of a piecewise-linear evapotranspiration function in an otherwise linear problem.

The ground-water system includes nonhomogeneous aquifer properties, confined and unconfined conditions, different locations and quantities of recharge, and an undulating hydraulic-head distribution. Because of this complexity, it seems unlikely that the management plans could be fully evaluated without the ground-water optimization model.

The major conclusions that result from this study are as follows:

1. The current lack of sufficient pumping capacity during summer severely limits the ability to maintain lower hydraulic heads throughout the year. The hydraulic characteristics of the confined aquifer permit it to recover quickly whenever pumping is decreased. Therefore, simply having a large annual pumping capacity will not guarantee a solution to the high-ground-water problem.
2. One of the most significant results obtained from the use of an optimization model is identification of the most sensitive elements of different ground-water management plans.
3. The effects of pumping near the center of the area with the highest hydraulic heads would be enhanced by the image-well effects of the San Jacinto fault.
4. Assuming different quantities of natural recharge during a 1-yr period results in relatively minor differences in the total pumpage required to solve the immediate high-ground-water problem. However, results also indicate that the current level of recharge will have a much larger effect in subsequent years.
5. Infeasible solutions that resulted from this short-term analysis were nearly as useful in understanding the management problem as were those feasible solutions that determined an optimal pumpage.
6. The effects of including a piecewise-linear evapotranspiration function in the model were adequately approximated by an iterative procedure. This method may be applicable to similar functional relations used to represent subsurface drains and some stream-aquifer interactions in other ground-water models.

Some limitations in the analysis remain, however. The coarse nodal spacing of the flow model required, in some cases, that groups of wells rather than individual wells be represented by a single node, or that a single well be represented by more than one node. This could diffuse the presumed effectiveness of a management site in the first instance, or enhance it in the second. Additionally, in-well drawdowns are not accurately simulated in large-scale regional models. This indicates that hydraulic-head distributions need to be interpreted cautiously, especially if pumping costs based on local drawdowns are an issue (Gorelick, 1983). Finally, transmissivities that were held constant throughout the analysis actually would decrease in some parts of the basin as hydraulic heads decline. Simulation of water-table conditions creates nonlinearities in the response coefficients and therefore requires a more complex mathematical programming strategy such as that suggested by Maddock (1974) or an iterative optimization technique as used by Danskin and Gorelick (1985). Although each of these limitations may signal caution in applying the results, we feel that none alters the conclusions reached in this study.

Additional aspects of the problem that remain to be addressed include incorporating artificial recharge as part of overall basin management, introducing operating costs into the objective function, and considering the possibility that movement of pollutants in the ground-water system may be accelerated toward municipal wells. These factors can be handled by advanced optimization techniques coupled with the appropriate ground-water-flow or solute-transport model and are topics of an ongoing study of water management in the San Bernardino Valley.

## REFERENCES CITED


Aquado, Eduardo, Remson, Irwin, Pikul, M.F., and Thomas, W.A., 1974, Optimal pumping for aquifer dewatering: American Society of Civil Engineers, Journal of the Hydraulics Division, v. 100, no. HY7, p. 860–877.

Danskin, W.R., and Gorelick, S.M., 1985, A policy evaluation tool: Management of a multiaquifer system using controlled stream recharge: Water Resources Research, v. 21, no. 11, p. 1731–1747.

Dutcher, L.C., and Garrett, A.A., 1963, Geologic and hydrologic features of the San Bernardino area, California—With special reference to underflow across the San Jacinto fault: U.S. Geological Survey Water-Supply Paper 1419, 114 p.

Gorelick, S.M., 1983, A review of distributed parameter groundwater management modeling methods: Water Resources Research, v. 19, no. 2, p. 305–319.

Hardt, W.F., and Freckleton, J.R., 1987, Aquifer response to recharge and pumping, San Bernardino ground-water basin, California: U.S. Geological Survey Water-Resources Investigations Report 86–4140, 69 p.

Hardt, W.F., and Hutchinson, C.B., 1978, Model aids planners in predicting rising ground-water levels in San Bernardino, California: Ground Water, v. 16, no. 6, p. 424–431.

———1980, Development and use of a mathematical model of the San Bernardino Valley ground-water basin, California: U.S. Geological Survey Open-File Report 80–576, 80 p.

Heidari, Manoutchehr, 1982, Application of linear system's theory and linear programming to ground-water management in Kansas: Water Resources Bulletin, v. 18, no. 6, p. 1003–1012.

Kishida, H., 1966, Damage to reinforced concrete buildings in Niigata City with special reference to foundation engineering:

Tokyo, Japan, Soil and Foundation, v. 7, no. 1.
Koizumi, Y., 1966, Change in density of sand subsoil caused by the Niigata earthquake: Tokyo, Japan, Soil and Foundation, v. 8, no. 2.
Lohman, S.W., 1979, Ground-water hydraulics: U.S. Geological Survey Professional Paper 708, 70 p.
Maddock, Thomas, III, 1972, Algebraic technological function from a simulation model: Water Resources Research, v. 8, no. 1, p. 129–134.
———1974, Nonlinear technological functions for aquifers whose transmissivities vary with drawdown: Water Resources Research, v. 10, no. 4, p. 877–881.
Mendenhall, W.C., 1905, Hydrology of San Bernardino Valley, California: U.S. Geological Survey Water-Supply Paper 142, 124 p.
Murtaugh, B.A., and Saunders, M.A., 1983, MINOS 5.0 user's guide: Systems Optimization Laboratory, Department of Operations Research, Stanford University, Technical Report SOL 83–20, 118 p.

# Hydrogeochemical Evidence for Subsurface Inflow to Stagecoach Valley, Lyon County, Nevada

*By* James R. Harrill, Alan H. Welch, *and* Alan M. Preissler

**Abstract**

Stagecoach Valley is a small topographically closed arid basin in western Nevada adjacent to the Carson River. The 70-square-mile basin has been considered to be recharged entirely from local precipitation and to discharge ground water by evapotranspiration and possibly by some subsurface outflow to the river. New water-level contour maps imply more subsurface inflow than was expected through consolidated rocks bordering the southwest part of the basin. Evidence pertaining to subsurface inflow was evaluated as thoroughly as possible because acceptance of this idea would require major conceptual changes regarding the flow system, for development of an accurate ground-water flow model. The resulting evidence includes (1) Indications of permeable consolidated rock in the area where inflow is suspected; (2) water-level contours that imply either greater-than-anticipated local recharge or inflow in the southwest part of Stagecoach Valley; (3) a hydraulic gradient that would permit underflow from the flood plain of the Carson River to the southwest part of Stagecoach Valley; (4) water-budget imbalances that may be explained by subsurface inflow; (5) estimates of flux through the southwest part of Stagecoach Valley that exceed estimates of local recharge; (6) a determination that recharge from local ponding of surface water in the southwest part of the valley is minor under current climatic conditions;(7) indications that the proportions of principal anions in well waters thought to be derived at least in part from inflow could have resulted by mixing of river water and local recharge; and (8) a finding that some ground water in Stagecoach Valley has a deuterium-hydrogen ratio that could result from the mixture of local, precipitation-derived recharge and inflow to the basin from the Carson River.

The collective evidence justifies the conclusion that subsurface inflow moves through consolidated rocks into the southwest part of Stagecoach Valley from the Carson River flood plain.

## INTRODUCTION

Stagecoach Valley is in western Nevada about 20 mi east of Carson City (fig. 1). It is a topographically closed arid basin having a drainage area of about 70 $mi^2$. About half of the area is underlain by unconsolidated basin-fill deposits; the remainder is underlain by consolidated rocks that form relatively low mountains bordering most of the area. The valley is situated just north of the flood plain of the Carson River and is separated from it by low mountains and a low, gently sloping alluvial divide. Information from an earlier study (Glancy and Katzer, 1975, p. 15) was inconclusive regarding hydraulic continuity between basin-fill deposits in Stagecoach Valley and flood-plain deposits of the adjacent Carson River. No specific information was available regarding the permeability of consolidated rocks that border the valley.

This area was selected as one of several ground-water basins to be modeled as part of the Great Basin Regional Aquifer-System Analysis because it is a small arid valley where barriers formed by consolidated rocks were likely to have strong influence on the ground-water flow regimen and the hydrologic response of the basin to pumping. Initially, all consolidated rock bounding Stagecoach Valley was assumed to be impermeable. As the study progressed, however, water-level data suggested that subsurface inflow beneath low mountains initially considered to be consolidated-rock barriers in the southwest part of the area is of significant magnitude. Acceptance of this idea would require major changes in how the flow system was conceptualized for the model; consequently, a specific analysis was made to evaluate the possibility of additional subsurface inflow. Test drilling was ruled out because of timing, cost, and the fact that predevelopment heads in the area of interest had been altered by pumping. Instead, a detailed analysis was made of the available geologic, hydrologic, and geochemical data to determine if these data support or reject the presence of subsurface inflow in the southwest part of Stagecoach Valley. This paper presents the results of that analysis.

The area is arid, with average annual precipitation ranging from 6 in. or less on the valley floor to as much as 20 in. near the crest of the Flowery Range. The annual lake-surface evaporation averages about 48 in. (Meyers, 1962, pl. 3). Most surficial drainage is to the Misfits Flat playa (altitude, about 4,260 ft above sea level) in the

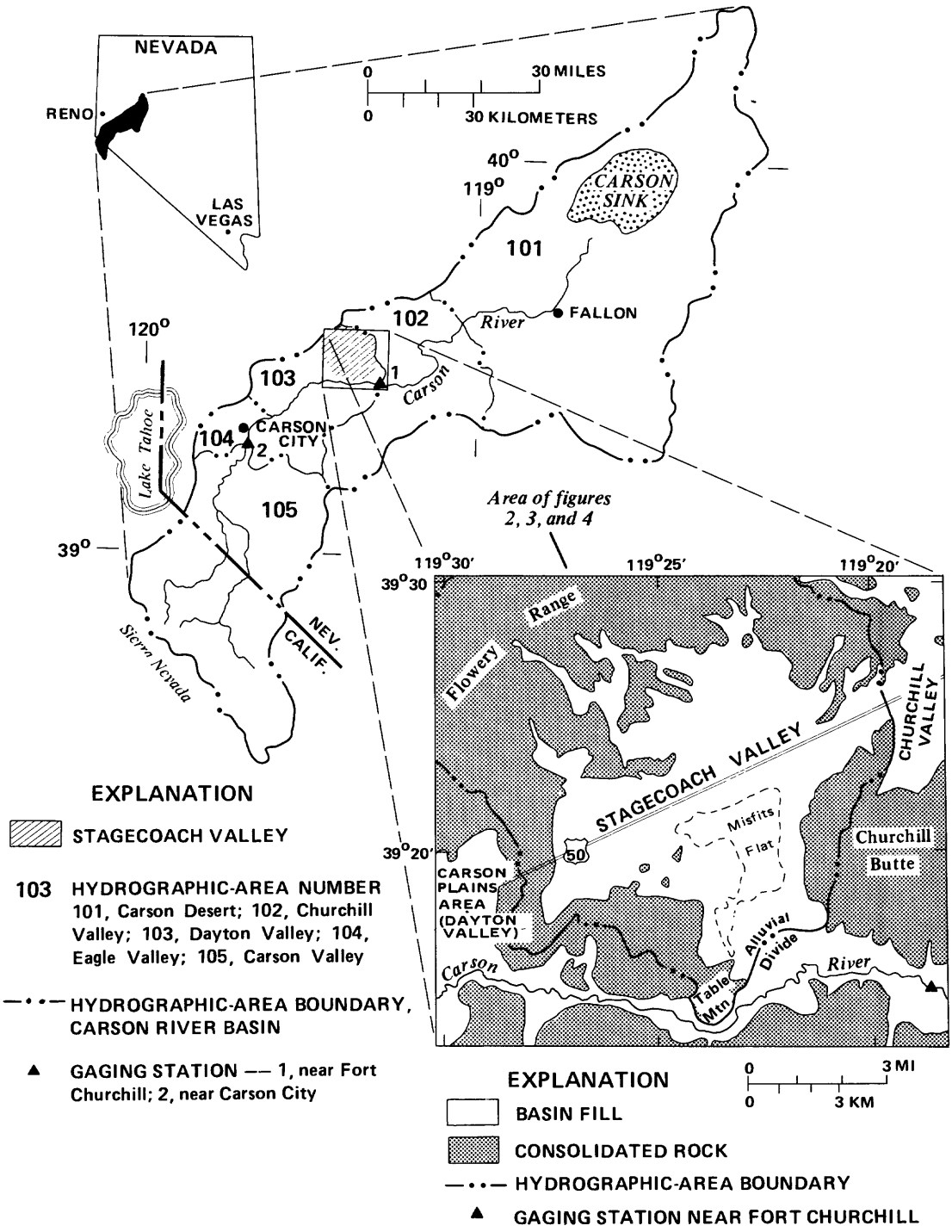


**Figure 1.** Location of the study area.

southern part of the valley (fig. 1). A few minor ephemeral streams drain to a small area of alkali soil and sparse phreatophytes (altitude, about 4,280 ft) in the southwest part of the valley.

The highest parts of the area are in the Flowery Range (maximum altitude, 7,095 ft). Precipitation on the Flowery Range provides most of the locally generated water supply. Low, unnamed mountains bordering the east side of the area have altitudes of less than 5,812 ft, and those bordering the southwest margin of the valley have altitudes of less than 5,221 ft. The low alluviated divide between Misfits Flat and the Carson River has an altitude of about 4,295 ft.

## GEOLOGIC EVIDENCE FOR SUBSURFACE INFLOW

Stagecoach Valley occupies a structural depression that is bounded and underlain by consolidated rocks. The depression is partly filled by fluvial and lacustrine deposits of gravel, sand, silt, and clay derived primarily from the adjacent mountains. These deposits compose the ground-water reservoir in the study area, with units of sand and gravel forming the most productive aquifers. Gravity and seismic-reflection data indicate that more than 1,000 ft of fill underlie the alluvial divide that separates Stagecoach Valley from the flood plain of the Carson River (Schaefer, 1988). This is the area where uncertainty as to hydraulic continuity was indicated by Glancy and Katzer (1975, p. 15); the thick section of alluvial fill confirms continuity through saturated alluvial deposits.

Figure 2 shows the generalized geology of the study area. Rocks along the southern boundary are volcanic—either andesitic or basaltic. The andesitic rocks include flow breccias, flows, and agglomerates interbedded with sediments and would presumably be effective barriers to ground-water flow, unless they have been intensely fractured. The basaltic rocks are predominantly thin flows, with interbeds of scoriaceous basalt breccia and diatomaceous sediments. The breccia and scoria zones may be relatively permeable and may transmit water, as flows may have been intensively fractured by faulting or cooling. Table Mountain is underlain entirely by basalt. Hydraulic continuity between aquifers in Stagecoach Valley and flood-plain deposits of the Carson River may exist if the carbonate rocks between these areas contain interflow or fractured zones below the water table.

Geologic section *A–A′* (fig. 2) shows the probable geologic configuration of the basaltic and andesitic rocks between Stagecoach Valley and the Carson River. This portrayal is based on the assumption that the basalt was deposited on surfaces of andesitic rock that had relatively low relief. The water table beneath the flood plain of the Carson River (as determined from fig. 3) was also projected onto the section. One outcrop of basalt probably extends below the water table, suggesting that at least one interflow zone—between the basalt and the underlying andesitic rocks—also extends below the water table. Moreover, three north-trending, high-angle faults in this same general area also may have significant permeability (fig. 2). The presence of basalt extending below the water table in close proximity to an area of relatively intense faulting suggests that consolidated rocks bordering southwest Stagecoach Valley may be sufficiently permeable to permit subsurface flow into the area. However, flow through these rocks cannot be confirmed on the basis of geologic evidence alone.

## HYDROLOGIC EVIDENCE FOR SUBSURFACE INFLOW

### Ground-Water Flow Patterns in the Basin Fill

The general direction of ground-water flow prior to development is shown in figure 3. The contours were constructed by using the earliest data available; wells used as control points are shown (see explanation, fig. 3). In the north and central parts of the valley, the general pattern of flow is from areas adjacent to the Flowery Range toward the playa. Some flow apparently continues southeast in response to a slight gradient toward the flood plain of the Carson River. This is the pattern that would generally be expected, assuming that most recharge is generated in areas of higher altitude.

In the northeast part of the valley, the ground-water divide is offset about a mile west of the drainage divide (fig. 3). This probably is due primarily to localized development of fracture permeability in consolidated rocks underlying the basin fill. The steep gradients suggest low permeability, and the resulting small outflow to Churchill Valley is supplied by recharge in the northeast part of the valley. This feature probably has only minor indirect effects on inflow-outflow relationships between Stagecoach Valley and flood-plain deposits of the Carson River.

In the western part of the valley, however, the contours indicate that water moves northeast from the southwest boundary of the area toward the main playa. Because most local recharge is generated in the Flowery Range, the expected direction of flow would have been generally eastward or southeastward toward the main playa. The 4,250-ft contour was based on data from three control points for which early water-level measurements were available, and the altitudes of these points were determined by leveling; consequently, the general direction of flow indicated by this contour is considered valid. The flow pattern described for the southwest part of the valley implies that a component other than recharge generated from the local mountains is involved. Subsurface inflow could well be the additional component.

### Hydraulic Potential

For subsurface flow to occur between two areas, two conditions must be satisfied: (1) the materials separating the areas must be permeable enough to transmit water and (2) a hydraulic gradient must exist between the areas. The previous section addressed condition one; this section addresses the second condition. Figure 3 shows contours of ground-water levels in southwestern Stagecoach Valley and along the flood plain of the Carson River. The highest contour shown in southwest Stagecoach Valley is 4,255 ft. Contours along the river flood plain just upstream from

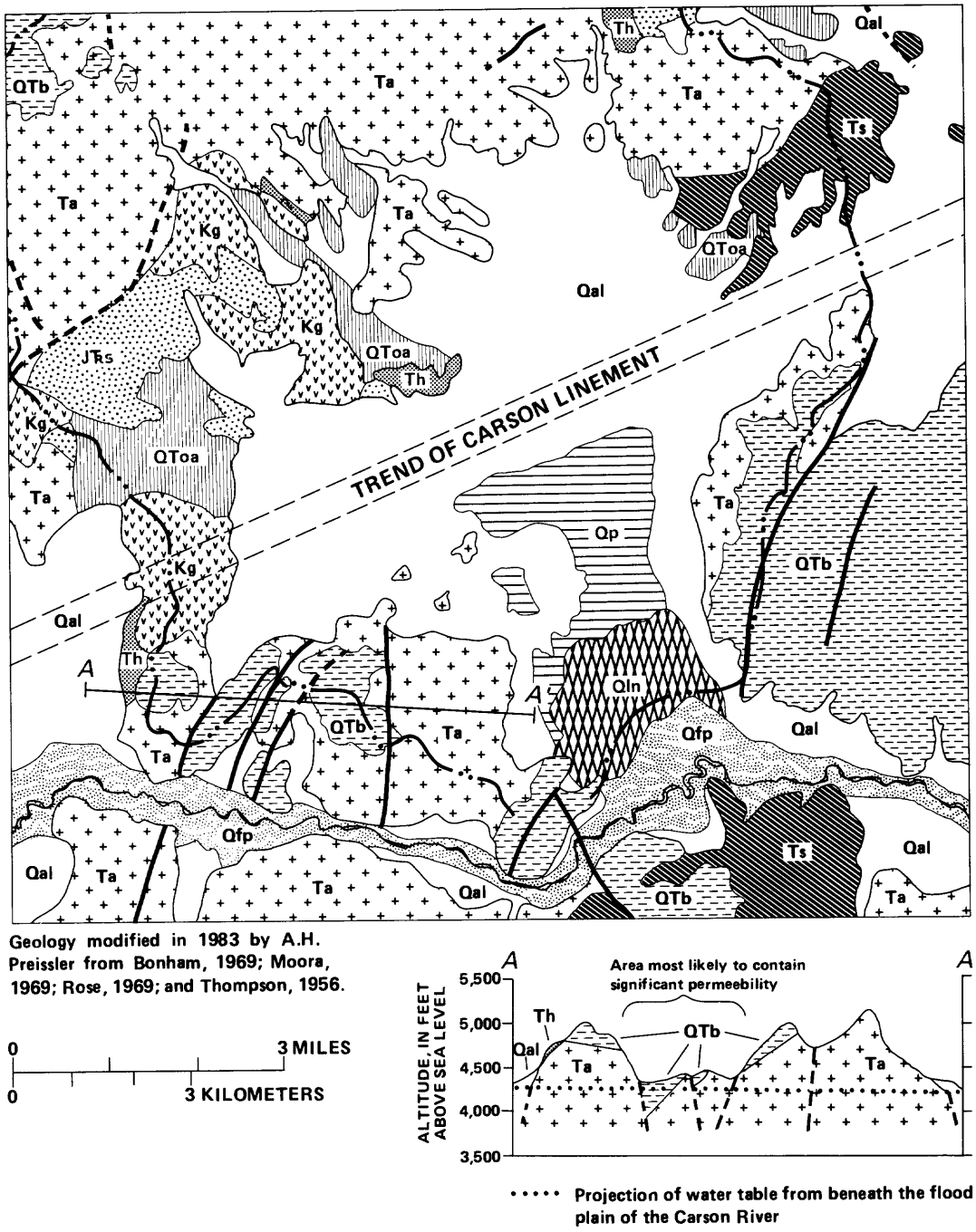


**Figure 2.** Generalized geology of the study area.

Stagecoach Valley, however, range from 4,270 to 4,280 ft. This difference of 15 to 25 ft indicates a hydraulic gradient from the river into Stagecoach Valley. Consequently, if adequate permeability is present, subsurface flow will occur between the two areas.

## Ground-Water Budgets

A water budget for the entire Dayton Valley hydrographic area, which includes Stagecoach Valley, was developed during a reconnaissance study of the Carson River basin (Glancy and Katzer 1975, p. 66). A reconnaissance-type ground-water budget was computed herein for just the Stagecoach Valley area by using primarily the same techniques and data of Glancy and Katzer.

Potential ground-water recharge was estimated by using the general method outlined by Eakin and others (1951, p. 79–81). The potential recharge to Stagecoach Valley from precipitation falling within the drainage area is estimated to be about 600 acre-ft/yr, on the basis of the

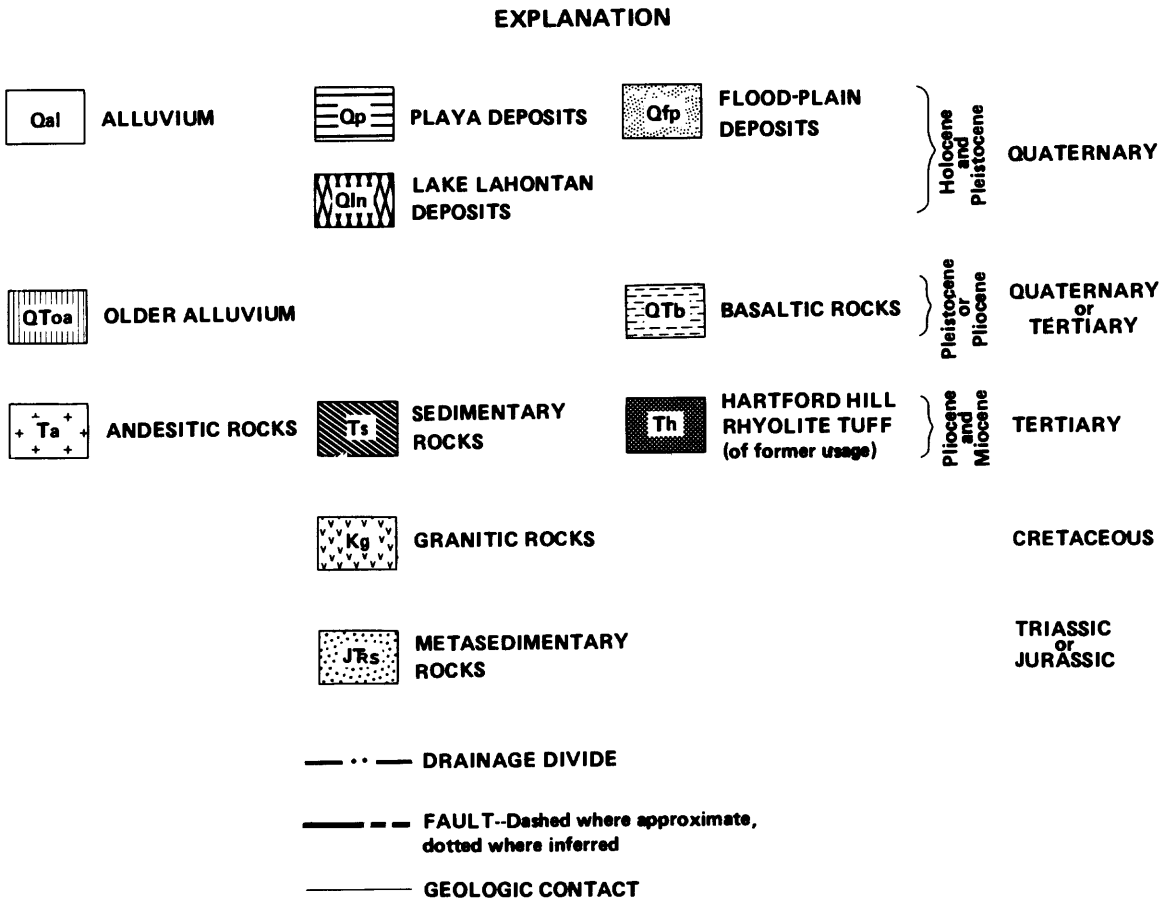


**Figure 2.** Continued.

same distribution of precipitation and recharge coefficients with altitude as was used for the entire Dayton Valley area (Glancy and Katzer, 1975, p. 48).

Areas of phreatophytes were mapped in 1971–72 (P. A. Glancy, U.S. Geological Survey, written commun., 1982); they included about 3,000 acres of primarily low- to moderate-density greasewood and about 1,000 acres of bare playa soil with scattered greasewood mounds. Average rates of ground-water consumption in these areas were estimated at 0.2 and 0.1 ft/yr, respectively. Thus, the total evapotranspiration of ground water is estimated to be about 700 acre-ft/yr.

If the estimates of recharge and discharge by evapotranspiration are both reasonable and the amount of subsurface outflow (if any) to flood-plain deposits of the Carson River in the southeast part of the area is small, then recharge in addition to that supplied by local precipitation may occur. However, the difference of 100 acre-ft/yr could also be due to errors in estimates. These reconnaissance-type water-budget estimates do not conclusively support the presence of subsurface inflow to the area; however, neither do they rule it out.

## Ground-Water Flow from Southwest Corner of Valley

Estimates of the general magnitude of ground-water flow originating from the southwest corner of Stagecoach Valley can be made on the basis of transmissivity, hydraulic gradient, and width of flow section in the basin-fill deposits. Transmissivity in the vicinity of an exploratory hole drilled by Utah International to a depth of 822 ft and completed as a well to a depth of 273 ft, is about 4,000 $ft^2/d$. This value is based on recovery data reported for a pumping test made by Utah International in 1962. This site is identified in figure 3 by the letters UI. The hydraulic gradient between the 4,250- and 4,255-ft contours is about 5 ft/mi, and the width of the flow section originating from the southwest margin of the valley is about 1 mi. Thus, northeastward flow from the southwest part of the valley may be on the order of 170 acre-ft/yr.

Another method of estimating the flux is to estimate the ground-water evapotranspiration from phreatophytes in the southwest part of the valley (fig. 3). About 830 acres of low-density greasewood are present west of the 4,250-ft

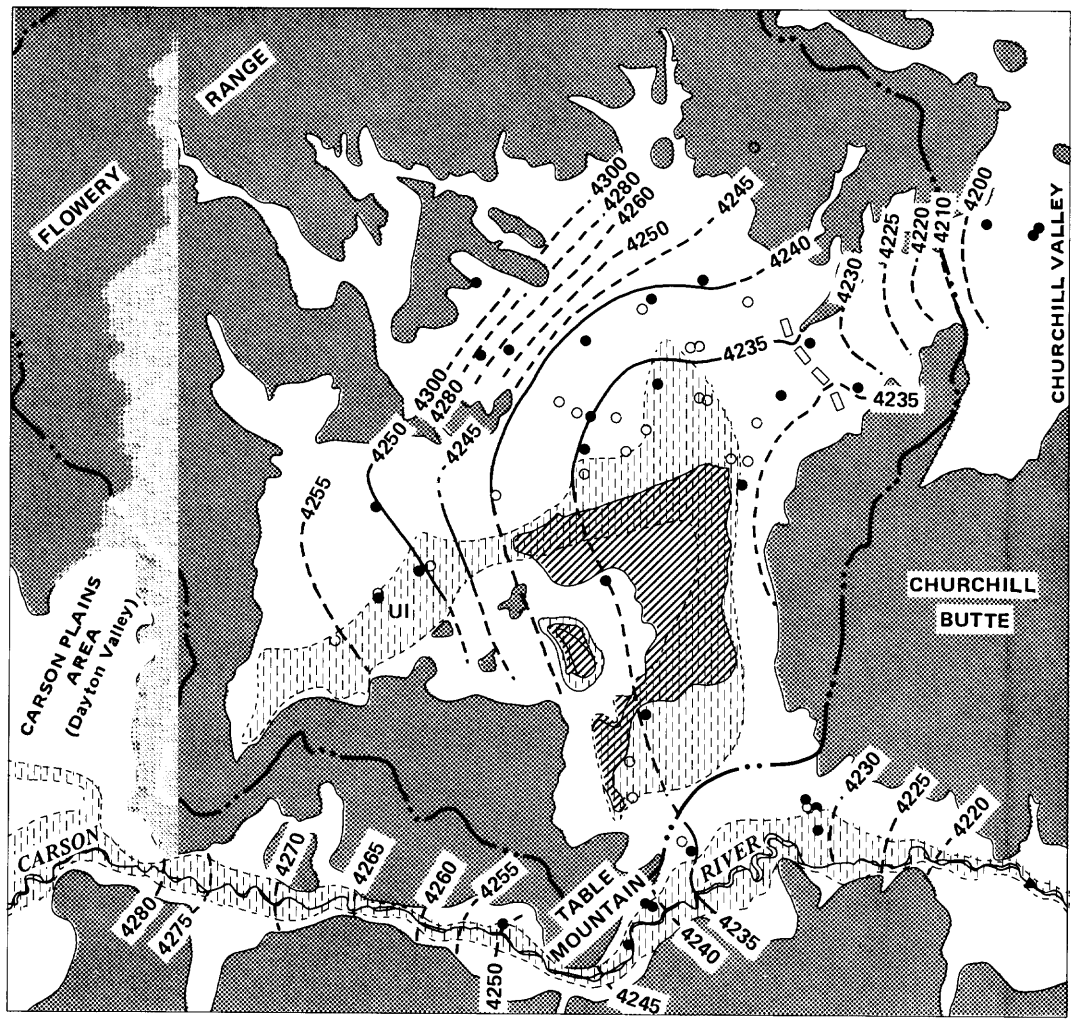


**Figure 3.** Hydrologic features of the study area.

contour along the general flow path followed by ground water originating in the southwest part of the valley. On the basis of the rates of ground-water evapotranspiration mentioned earlier, natural discharge may be on the order of 80–170 acre-ft/yr.

Because the estimate based on hydraulic data does not take into account evapotranspiration upgradient from the 4,250-ft contour, and the estimate based on evapotranspiration does not take into account flow to areas downgradient from the 4,250-ft contour, the actual flux should be slightly greater in both cases. However, these approximate estimates are satisfactory for the purposes of this report inasmuch as both are much greater than the few tens of acre-feet per year of local recharge indicated by calculations using the same techniques employed by Glancy and Katzer (1975, p. 47–48). This is a strong basis for arguing that significant inflow occurs from the flood-plain deposits of the Carson River; however, the possibility of local areas of high recharge from precipitation cannot be excluded, as the technique used to estimate recharge is empirical and best applied to an entire basin.

Seepage from intermittent ponding in the southwest part of the valley is a possible source of additional local recharge. During the late winter and early spring of 1982, an exceptionally wet year, water ponded over an area of 80–100 acres. Water depth probably averaged several tenths of a foot. Recharge could have occurred from this event. Extensive ponding apparently is infrequent, however,

EXPLANATION

BASIN FILL -- Hachures indicate area of playa

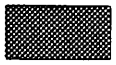

CONSOLIDATED ROCK

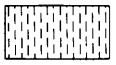

AREA OF NATURAL GROUND-WATER DISCHARGE -- Area covered by low-density stands of phreatophytes, principally greasewood. Based primarily on field mapping by P. A. Glancy, U.S. Geological Survey, 1970-72. Most ground-water discharge areas adjacent to Carson River are situated on flood plain

—4235— – WATER-LEVEL CONTOUR -- Shows altitude of ground-water level. Dashed where approximately located. Contour intervals 5, 10, and 20 feet. Datum is sea level

GROUND-WATER DIVIDE (approximately located)

• WELL USED AS PRIMARY CONTROL POINT -- "UI" indicates the Utah International well where an aquifer test was made in 1962

○ WELL USED AS SUPPLEMENTAL CONTROL POINT -- Generally, sites where predevelopment water levels were estimated from recent measurements that had been adjusted to eliminate effects of pumping

▲ GAGING STATION – Carson River near Fort Churchill

—— • • —— TOPOGRAPHIC DIVIDE

**Figure 3.** Continued.

because most of the area is covered by sparse vegetation that would be killed by repeated flooding. Recharge from this source probably could not account for more than a small part of the fluxes estimated above and this strengthens the argument for subsurface inflow.

## GEOCHEMICAL EVIDENCE FOR INFLOW

Ground water from 19 wells and 4 springs in and immediately adjacent to Stagecoach Valley was sampled for chemical and stable-isotope analysis (table 1). Surface-water samples were collected from the Carson River and from the small, intermittent pond in southwestern Stagecoach Valley. Water samples were passed through a filter of 0.45-μm pore size and stored in plastic bottles for chemical analysis and in glass bottles for isotope analysis. Samples collected for cation analysis were acidified in the field with nitric acid to a pH of about 2. Separate samples were diluted for silica analysis to prevent polymerization. Field measurements were made for pH, specific conductance, water temperature, and alkalinity. Except for Stagecoach Utilities well 6, which was sampled after flowing through a large storage tank, all the wells were pumped for a period that allowed for thorough flushing of the well and, where present, the domestic storage tank. The sample sites are shown in figure 4.

Ground water in Stagecoach Valley is low in dissolved-solids concentration and is a mixed-cation, bicarbonate-sulfate type (fig. 5). The dissolved-solids concentration generally increases as water moves from peripheral recharge areas toward the center of the basin. The ground-water quality in the southwestern part of the valley is similar to that found in the Carson River near Fort Churchill (table 1, fig. 4) during periods of intermediate and high flow. The average chemical quality of recharge from the Carson River is not known, because the relative proportions of recharge during periods of (1) overbank flooding at high flow, (2) infiltration during intermediate flow, and (3) irrigation diversion during low flow cannot be determined from the data presently available. The anion propor-

**Table 1.** Chemical and physical quality of ground water and

[All analyses were made at U.S. Geological Survey Central Laboratory, Arvada, Colo., except as noted. Well data in parentheses

| Site name | Location[2] | Site number (fig. 4) | Total depth of well (ft) | Sampling date (year-month-day) | Sampling depth[3] (ft) | Flow rate[4] | Water temperature (°C)[5] | pH (field) | Calcium (mg/L as Ca) | Magnesium (mg/L as Mg) |
|---|---|---|---|---|---|---|---|---|---|---|
| Schuetz well | N16 E23 03 NE¼ | 1 | 72 | 83-03-03 | 60 | -- | 14.0[a] | 7.5 | 47 | 20 |
| Intermittent pond | N17 E22 24 NE¼ | 2 | -- | 83-02-23 | -- | -- | 5.8 | 8.0 | 2.8 | 1.7 |
| Stagecoach Utilities well 6 | N17 E22 01 SW¼ | 3 | 121 | 81-11-03 | 94.5 | -- | -- | 7.7 | 33 | 7 |
| Chaves well | N17 E22 36 SE¼ | 4 | (115) | 83-03-01 | (98) | -- | 16.8 | 7.2 | 52 | 17 |
| Stagecoach Utilities well | N17 E23 01 SE¼ | 5 | 306 | 81-12-29 | 258 | -- | 21.5[a] | 7.7 | 30 | 8.5 |
| Lawson well | N17 E23 02 SW¼ | 6 | 152 | 81-11-05 | 132 | -- | 16.6 | 7.6 | 37 | 9.4 |
| Hughes well | N17 E23 04 SE¼ | 7 | 339 | 81-12-15 | -- | -- | 22.3[a] | 7.9 | 31 | 15 |
| USGS well | N17 E23 09 SW¼ | 8 | 82 | 81-11-12 | 67 | -- | 17.3[b] | 7.7 | 69 | 17 |
| USGS well | N17 E23 09 SE¼ | 9 | 84 | 81-12-17 | -- | -- | 17.0[b] | 7.8 | 73 | 20 |
| USGS well | N17 E23 10 NE¼ | 10 | 88 | 81-11-18 | -- | -- | 16.0[b] | 7.8 | 35 | 13 |
| Weatherman well | N17 E23 10 NW¼ | 11 | 300 | 81-08-03 | 267 | -- | 18.0[a] | 7.7 | 37 | 15 |
| Page well | N17 E23 11 NE¼ | 12 | 133 | 82-01-18 | 110 | -- | 17.9 | 8.3 | 4 | 0.9 |
| Stanley well | N17 E23 15 SW¼ | 13 | 378 | 81-10-29 | 358 | -- | 20.9 | 7.6 | 54 | 25 |
| Eitell well | N17 E23 17 SW¼ | 14 | (300) | 81-11-16 | -- | -- | 20.8 | 7.8 | 29 | 13 |
| Utah International well | N17 E23 17 SE¼ | 15 | (141) | 81-12-10 | (77) | -- | 19.0 | 7.6 | 100 | 27 |
| Leegard well | N17 E23 19 NE¼ | 16 | 272 | 81-12-01 | 215 | -- | 18.7[a] | 7.9 | 20 | 7.4 |
| Baron well | N17 E23 26 SW¼ | 17 | 176 | 81-10-28 | 166 | -- | 17.1[a] | 8.1 | 22 | 8.4 |
| Kern well | N17 E23 27 NE¼ | 18 | 220 | 81-11-02 | 200 | -- | 22.1[a] | 7.6 | 77 | 28 |
| Cooney Spring | N18 E22 25 SE¼ | 19 | -- | 81-07-29 | 0 | 1 | 17.1[a] | 7.3 | 36 | 13 |
| Spring | N18 E23 29 SE¼ | 20 | -- | 81-12-30 | 0 | 1 | 13.9 | 7.1 | 31 | 17 |
| Spring | N18 E23 32 SE¼ | 21 | -- | 81-11-04 | 0 | 50 | 16.0[a] | 7.7 | 38 | 13 |
| Corral Spring Ranch well | N18 E23 32 SE¼ | 22 | -- | 81-11-19 | -- | -- | 18.0[a] | 7.4 | 34 | 14 |
| Corral Spring | N18 E23 33 SW¼ | 23 | -- | 81-11-04 | 0 | 4 | 18.5[a] | 7.4 | 34 | 14 |
| McHenry well | N18 E23 35 SW¼ | 24 | 215 | 81-10-27 | -- | -- | 18.5[a] | 7.8 | 40 | 12 |
| Carson River near Fort Churchill: | | | | | | | | | | |
| Low flow[δ] | | -- | -- | (δ) | -- | <100 | 16.8 | -- | 53 | 12 |
| Intermediate flow[δ] | | -- | -- | (δ) | -- | 100-1,000 | 9.1 | -- | 27 | 6.4 |
| High flow[δ] | | -- | -- | (δ) | -- | >1,000 | 12.7 | -- | 13 | 3.2 |
| Intermediate flow | | -- | -- | 83-03-07 | -- | 770 | 7.3 | -- | 26 | 7.0 |
| Carson River near Carson City | | -- | -- | 83-04-15 | -- | 540 | 9.6 | 7.4 | 21 | 5.7 |
| do. | | -- | -- | 83-05-20 | -- | 6,400 | 10.0 | 7.4 | 10 | 3.0 |
| do. | | -- | -- | 83-06-30 | -- | 4,300 | 13.6 | 7.5 | 7.6 | 2.1 |
| do. | | -- | -- | 83-08-15 | -- | 764 | 19.1 | 7.6 | 19 | 5.5 |
| do. | | -- | -- | 83-09-21 | -- | 220 | 19.3 | 7.7 | 26 | 7.6 |
| do. | | -- | -- | 83-10-21 | -- | 330 | 12.8 | 8.0 | 21 | 5.4 |
| do. | | -- | -- | 83-12-06 | -- | 750 | 2.0 | 8.0 | 21 | 6.2 |
| do. | | -- | -- | 84-01-13 | -- | 630 | 2.3 | 7.7 | 20 | 5.4 |
| do. | | -- | -- | 84-02-22 | -- | 500 | 4.7 | 7.9 | 24 | 6.2 |
| do. | | -- | -- | 84-05-23 | -- | 2,170 | 13.0 | 7.6 | 7.7 | 2.1 |

[1] Data presented in this table are in the U.S. Geological Survey WATSTORE computer-based storage system. These data, along with other analyses and ground-water information, may be retrieved using a latitude-longitude polygon that includes the area represented in figure 4. Data for the Carson River may be obtained using the WATSTORE site-identification numbers 10311000 and 10312000.

[2] Township and range (Mount Diablo base line and meridian), section and location within section.

[3] Midpoint of screened or cased interval.

[4] Flow rates for springs are in gallons per minute. Rates for the Carson River are in cubic feet per second.

[5] Well- and spring-water temperatures are values measured as pumped or at the spring source, except as noted: *a*, measured after flow through a storage tank or long (>25 feet) discharge line; *b*, down-hole measurement.

selected surface water in Stagecoach Valley and vicinity[1]

were obtained from sources other than drillers' logs and are considered less accurate than the drillers' records; --, no data.]

| Site number | Sodium (mg/L as Na) | Potassium (mg/L as K) | Sulfate (mg/L as $SO_4$) | Bicarbonate (mg/L as $HCO_3$) (field) | Carbonate (mg/L as $CO_3$) (field) | Chloride (mg/L as Cl) | Silica (mg/L $SiO_2$) | Dissolved solids[6] (mg/L) | Delta deuterium[7] (per mil) | Delta oxygen-18[7] (per mil) |
|---|---|---|---|---|---|---|---|---|---|---|
| 1 | 38 | 7.2 | 110 | 200 | 0 | 10 | 45 | 380 | -105 | -14.0 |
| 2 | 93 | 2.2 | 23 | 220 | 0 | 16 | 40 | 290 | - 68 | - 5.9 |
| 3 | 45 | 4.3 | 150 | 180 | 0 | 20 | 55 | 440 | -111 | -14.0 |
| 4 | 46 | 6.4 | 44 | 180 | 0 | 12 | 95 | 330 | -120 | -15.2 |
| 5 | 45 | 4.0 | 57 | 170 | 0 | 10 | 100 | 340 | -121 | -15.4 |
| 6 | 40 | 5.2 | 85 | 140 | 1 | 24 | 55 | 330 | -118 | -15.2 |
| 7 | 40 | 11 | 270 | 160 | 0 | 13 | 40 | 570 | -117 | -15.0 |
| 8 | 22 | 6.1 | 150 | 160 | 0 | 11 | 115 | 440 | -118 | -14.7 |
| 9 | 39 | 7.7 | 210 | 160 | 1 | 12 | 68 | 520 | -117 | -14.7 |
| 10 | 45 | 8.7 | 71 | 180 | 1 | 15 | 110 | 370 | -121 | -15.0 |
| 11 | 42 | 7.2 | 85 | 160 | 0 | 16 | 150 | 420 | -119 | -15.1 |
| 12 | 120 | 2.0 | 41 | 150 | 0 | 25 | 60 | 280 | -124 | -15.6 |
| 13 | 33 | 7.2 | 67 | 200 | 2 | 21 | 75 | 390 | -121 | -15.4 |
| 14 | 33 | 5.4 | 69 | 180 | 0 | 77 | 85 | 470 | -124 | -15.0 |
| 15 | 30 | 7.7 | 72 | 140 | 0 | 11 | 80 | 310 | -115 | -14.9 |
| 16 | 37 | 4.0 | 48 | 130 | 1 | 9.0 | 85 | 280 | -113 | -15.0 |
| 17 | 47 | 5.8 | 55 | 160 | 1 | 12 | 120 | 360 | -113 | -15.1 |
| 18 | 85 | 10 | 190 | 180 | 0 | 140 | 100 | 720 | -118 | -15.3 |
| 19 | 25 | 2.1 | 30 | 180 | 0 | 8.1 | 130 | 330 | -118 | -14.8 |
| 20 | 36 | 10 | 71 | 180 | 0 | 11 | 90 | 360 | -121 | -15.8 |
| 21 | 36 | 4.7 | 53 | 190 | 1 | 11 | 85 | 340 | -118 | -15.5 |
| 22 | 34 | 5.9 | 54 | 180 | 0 | 11 | 90 | 330 | -121 | -15.4 |
| 23 | 34 | 6.1 | 55 | 190 | 0 | 11 | 95 | 340 | -120 | -15.4 |
| 24 | 16 | 4.7 | 35 | 140 | 0 | 14 | 120 | 310 | -121 | -14.9 |
| Carson River near Fort Churchill | | | | | | | | | | |
| -- | 50 | 5.5 | 130 | 180 | 0 | 15 | 27 | 380 | -- | -- |
| -- | 24 | 3.4 | 48 | 110 | 0 | 8.8 | 22 | 200 | -- | -- |
| -- | 8.6 | 2.3 | 17 | 58 | 0 | 3.7 | 16 | 90 | -- | -- |
| -- | 18 | 3.2 | 38 | 100 | 0 | 8.7 | 24 | 170 | -108 | -14.0 |
| Carson River near Carson City | | | | | | | | | | |
| -- | 14 | 2.1 | 30 | 90 | 0 | 5.9 | 22 | 120 | -107 | -14.4 |
| -- | 5.9 | 1.7 | 14 | 47 | 0 | 1.7 | 16 | 60 | -108 | -14.7 |
| -- | 4.1 | 1.3 | 6.0 | 38 | 0 | 1.2 | 14 | 40 | -107 | -14.6 |
| -- | 13 | 5.1 | 19 | 92 | 0 | 7.7 | 23 | 110 | - 95 | -12.8 |
| -- | 23 | 5.3 | 30 | 130 | 0 | 9.8 | 25 | 170 | -104 | -13.7 |
| -- | 17 | 3.0 | 25 | 98 | 0 | 7.1 | 22 | 130 | -107 | -14.4 |
| -- | 17 | 3.0 | 29 | 92 | 0 | 7.2 | 23 | 130 | -104 | -14.0 |
| -- | 15 | 2.1 | 26 | 87 | 0 | 6.0 | 23 | 100 | -105 | -14.3 |
| -- | 19 | 2.5 | 32 | 100 | 0 | 8.7 | 23 | 140 | -105 | -14.2 |
| -- | 4.2 | 1.1 | 5.6 | 39 | 0 | 1.3 | 14 | 55 | -103 | -14.0 |

[6] Sum of constituents, with the bicarbonate values multiplied by 0.492 to make results comparable to values obtained using the "residue-on-evaporation" analytical method (in which carbon dioxide is lost during the evaporation process).

[7] Analyses were made under the supervision of Tyler B. Coplen, U.S. Geological Survey, Reston, Va. The stable isotopes evaluated herein are deuterium (hydrogen-2), relative to hydrogen-1 ($D/^1H$), and oxygen-18, relative to oxygen-16 ($^{18}O/^{16}O$). The ratio is determined for a sampled water, and is then related mathematically to the comparable ratio for Standard Mean Ocean Water (SMOW). By convention, the computed results are expressed as "delta deuterium" and "delta oxygen-18," with the units of measure "per mil" (°/oo). A negative delta value indicates that the sampled water is isotopically lighter than the standard (that is, the sampled water has a smaller proportion of deuterium or oxygen-18, relative to hydrogen-1 or oxygen-16, than the standard).

[8] Values represent numerical means for samples collected by U.S. Geological Survey personnel from October 1970 to May 1983.

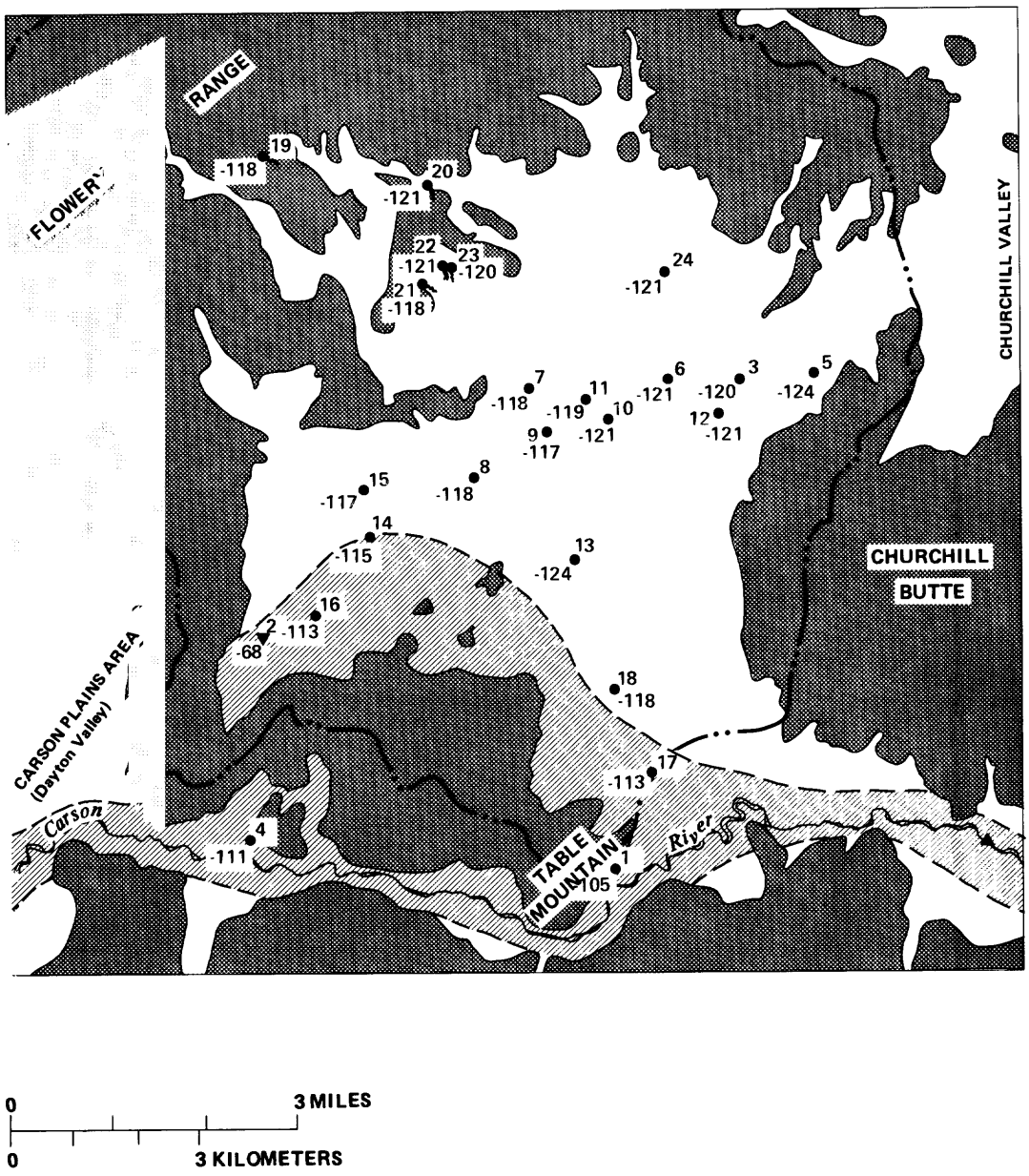


**Figure 4.** Deuterium-hydrogen ratios in ground water and ponded surface water.

tions in the water at wells in the southwestern part of the valley are similar to those found in the Carson River during intermediate and high flow (table 1, fig. 4). Thus, the chemical quality is consistent with that of the river supplying recharge to the southwestern part of the valley.

Hydrologic processes within the valley can also produce anion proportions similar to that found in the southwest. For instance, water at the Weatherman well (11), where ground-water flow is from the north, has anion proportions similar to those in the water at the Eitell well (14) in the southwestern part of the valley. Thus, although the anion proportions are consistent with flow from the river to the valley, precipitation-derived recharge can also produce the observed proportions.

Stable-isotope data were collected to determine the sources of ground water in the valley (see footnote 7, table 1). Ground water derived from recharge of local precipitation (as indicated by water near the base of the mountain block; sites 5 and 19–23 in table 1) has a deuterium-hydrogen ratio of −118 to −124 per mil relative to Standard Mean Ocean Water (SMOW). As can be seen in figure 4, almost all sampled ground water in Stagecoach Valley has values in this range. Because the isotope composition of ground water is not appreciably affected by processes

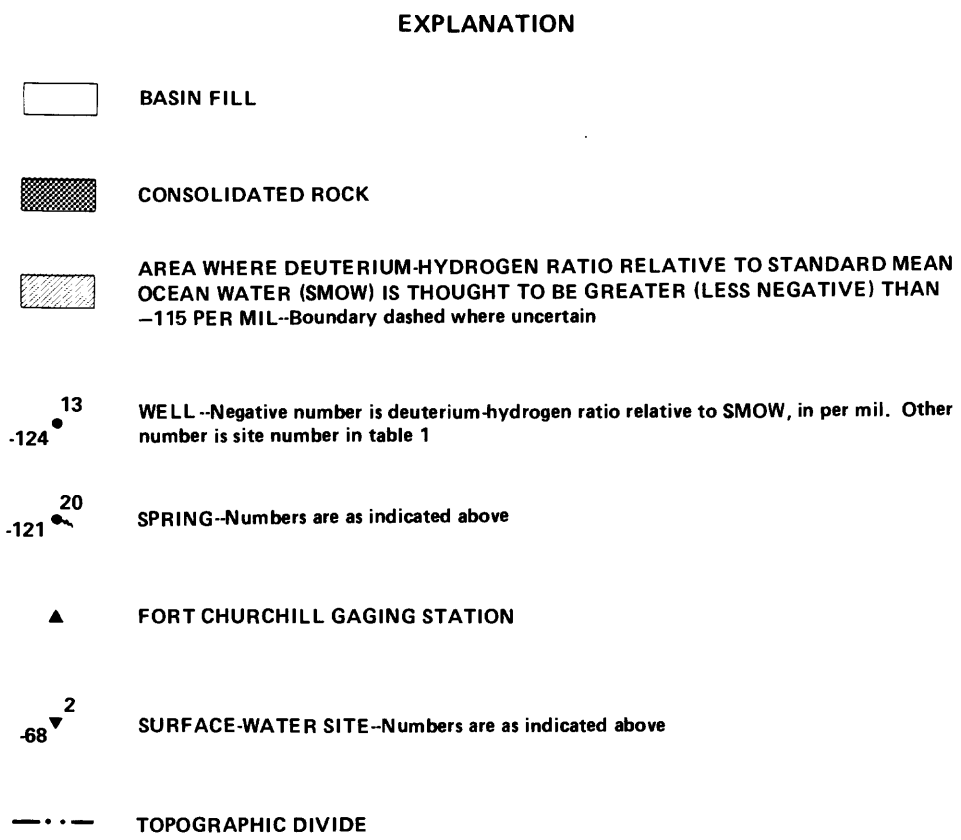


**Figure 4.** Continued.

occurring in a hydrologic setting like Stagecoach Valley, the primary source of recharge appears to be local precipitation.

Ground water with deuterium-hydrogen ratios different from local precipitation-derived recharge (that is, less negative than −117 per mil) occurs in the southwestern part of the valley (sites 14 and 16, table 1) and at riverside wells that probably are recharged at least partly by percolating streamflow (sites 1, 4, and 17, table 1). An isotope composition that is heavier (less negative) than the local recharge could result from inflow to the valley of water with a heavier isotope composition or from partial evaporation of local precipitation prior to recharge.

Evaporation affects the isotope composition of surface water that intermittently covers a small playa in the southwestern part of the valley. During evaporation, the concentration of the lighter isotope is greater in the vapor phase than in the liquid, resulting in a change in the composition of the residual liquid as evaporation proceeds. The equilibrium isotope evolution of a water body is described by the Rayleigh distillation equation, which uses isotope data and concentrations of a conservative constituent (Friedman and others, 1976). By using chloride as a conservative constituent (a solute that remains in solution and is not augmented by appreciable dissolution of salts), and the data for Cooney Spring (site 19) as the initial composition, the evolution of the ponded water is shown in figure 6. The effective alpha[1] of 1.081 for this path is close to the laboratory equilibrium value of 1.092 at 6 °C presented by Friedman and O'Neil (1977, figure 34) and the 1.08 calculated for lakes of the lower Grand Coulee, Wash., by Friedman and others (1976, p. 510). This correspondence supports the validity of using the Rayleigh equation and the associated assumptions.

Accepting that the trend indicated in figure 6 represents the evolution of water evaporating from intermittent ponding, the ground water in the southwest part of the valley could be a result of mixing of locally derived precipitation with water affected by evaporation. Points along tie lines between the local precipitation-derived recharge and the evaporation-affected water, as represented by the Rayleigh curve shown in figure 6, reflect the possible compositions that would result from mixing of these two water types. Because the ground water in the southwestern part of the valley plots between these two sources in figure 6, the observed compositions could result from mixing.

[1] During evaporation the vapor and liquid phases have different isotope compositions. The magnitude of the difference between the composition of the two phases can be expressed by using a fractionation factor, or alpha. The term "effective alpha" is used to distinguish it from the alpha defined on the basis of vapor pressures of $H_2O$ and HDO.

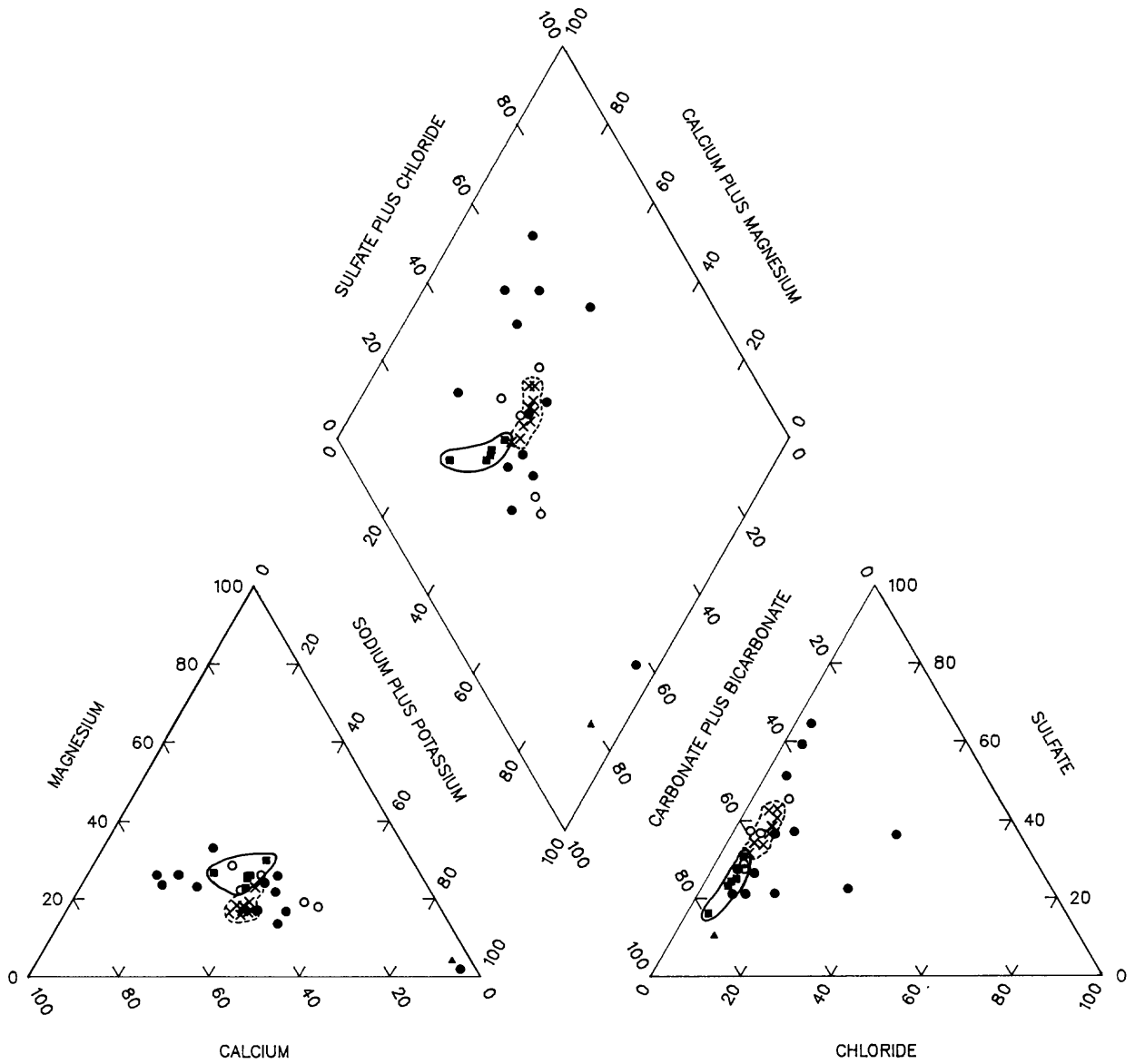


**Figure 5.** Proportions of major dissolved constituents in ground water and surface water. Dashed line encloses field of data for Carson River; solid line encloses field of data for local recharge. Percentages are based on millequivalents per liter. Chemical symbols are given in table 1.

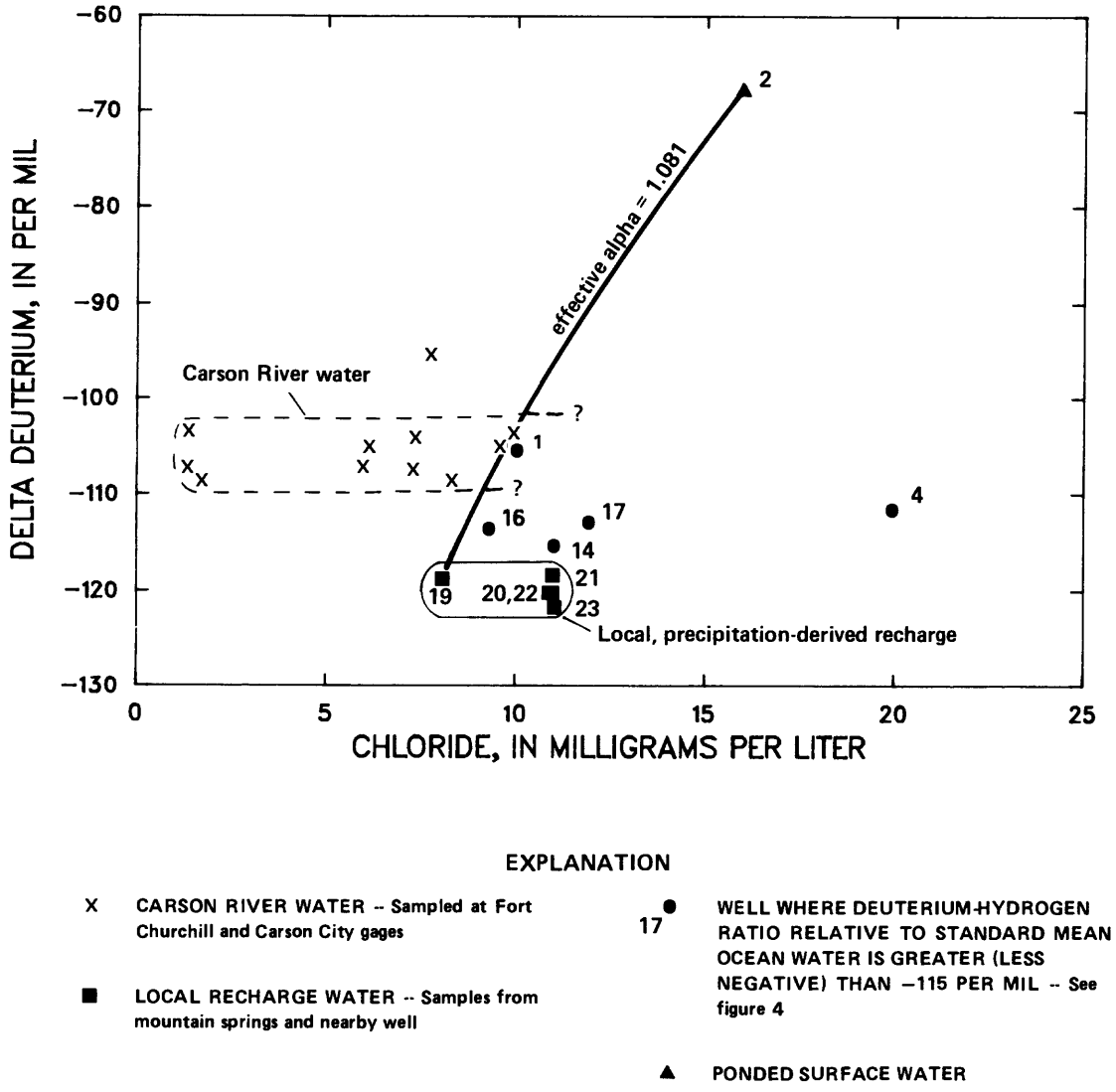


**Figure 6.** Relation between deuterium-hydrogen ratio and chloride in ground water and surface water. Maximum chloride concentrations in the Carson River exceeded those shown here for isotope samples. Water-quality data collected at the Fort Churchill gage since 1962 indicate concentrations consistently in the range from 11 to 20 mg/L at discharges of less than 200 $ft^3/s$. Unfortunately, no stable-isotope data are available at these lower flows.

The Carson River also represents a possible source of isotopically heavy water that, when mixed with locally derived recharge, could produce ground water with a composition like that found in the southwestern part of the basin. As was the case for mixing of evaporation-affected water, the river has a greater deuterium-hydrogen ratio than does the local recharge. Although most of the available isotope data for the Carson River are for samples collected near Carson City (about 25 river miles upstream from Stagecoach Valley), the isotope composition of all samples is heavier than the local recharge. Although evaporation may affect the river water, the isotope composition at Fort Churchill during a period of intermediate flow (−108 per mil) is similar to that found at Carson City under similar flow conditions (table 1). The only process that is likely to alter the isotope composition between Carson City and Stagecoach Valley is evaporation, which would result in a greater (less negative) ratio than found at Carson City. River water, with or without evaporation, could mix with local recharge to form a water with an isotope composition similar to that found for the ground water in the southwestern part of the valley.

In summary, mixing local, precipitation-derived recharge with either Carson River water or local precipitation affected by evaporation could form water with a deuterium-hydrogen ratio like that observed in southwestern Stagecoach Valley.

## CONCLUSIONS

Conclusions about subsurface inflow to Stagecoach cannot be based on any single piece of evidence that is definitive. Instead the conclusions must be based on the evaluation of numerous items. Evidence regarding subsurface inflow to Stagecoach Valley includes the following:

1. Geologic conditions favor the presence of permeable consolidated rock in the area where inflow is suspected.
2. Patterns of flow based on water-level contours indicate either greater-than-anticipated local recharge or ground-water inflow in the southwest part of the valley.
3. A hydraulic gradient exists from the flood plain of the Carson River to the southwest part of the valley.
4. Reconnaissance-type water budgets are not accurate enough to conclusively support the presence of subsurface inflow. However, such inflow would be one explanation for the small budget imbalance in which estimated discharge from the basin is larger than estimated recharge generated within the basin.
5. The estimated quantity of water flowing through the southwest part of Stagecoach Valley substantially exceeds the estimated amount of local recharge. Subsurface inflow or abnormally great localized recharge are two possible explanations.
6. Under current climatic conditions, intermittent ponding of surface water in the southwest part of the valley is not frequent and sufficient enough to account for significant local recharge.
7. The relative proportions of anions in Carson River differ slightly from the proportions in local recharge water. Proportions of anions in samples taken from wells where water may be derived from the river are either similar to the proportions in the river or have anion concentrations that could have formed by the mixing of river water and local recharge. Although the observed water quality could evolve from other processes, the chemical composition of the ground water is consistent with the hypothesis that inflow is from the river.
8. Deuterium-hydrogen ratios for Carson River water are different from ratios for local recharge as represented by samples of ground water in the upper part of the local flow system. Ratios in areas where the presence of river water is suspected have values that can be most satisfactorily explained by simple mixing of river water and local recharge. The observed values also could have been the result of mixing of recharge originating from ponded surface water. As already discussed, however, this process is considered minor, given the existing climatic conditions.

Taken individually, none of the above items conclusively demonstrates the presence of subsurface inflow. However, when considered collectively, the items constitute a body of evidence that strongly supports subsurface inflow and provides adequate justification for modifying the conceptual model of the ground-water flow system in Stagecoach Valley. The argument is strengthened by the fact that evidence based on various disciplines of study, such as geology, hydraulics, and geochemistry, all support subsurface inflow. Hydrogen-isotope data have proven to be of value in helping to characterize the ground-water flow system in and adjacent to the valley. This same technique may be useful in the analysis of flow systems in other river valleys in the Great Basin.

This paper demonstrates the need for careful evaluation of boundary conditions when attempting to simulate ground-water flow in small areas where the geology is complex. Performance of ground-water flow models of these areas will be especially dependent on the incorporated boundary conditions. Considerable time and effort investigating these conditions may be necessary to insure that a model will not be flawed because of conceptual errors in delineating the flow-system boundary.

## SELECTED REFERENCES


Bonham, H.F., 1969, Geology and mineral deposits of Washoe and Storey Counties, Nevada: Nevada Bureau of Mines and Geology Bulletin 70, 140 p.

Eakin, T.E., Maxey, G.B., Robinson, T.W., Fredericks, J.C., and Loeltz, V.J., 1951, Contributions to the hydrology of eastern Nevada: Nevada State Engineer, Water Resources Bulletin 12, 171 p.

Friedman, Irving, and O'Neil, J.R., 1977, Data of geochemistry: U.S. Geological Survey Professional Paper 440–KK, 12 p., 49 fig.

Friedman, Irving, Smith, G.I., and Hardcastle, K.G., 1976, Studies of Quaternary saline lakes—II. Isotopic and compositional changes during desiccation of the brines in Owens Lake, California, 1969–1971: Geochemica et Cosmochimica Acta, v. 40, p. 501–511.

Glancy, P.A., and Katzer, T.L., 1975, Water resources appraisal of the Carson River basin, western Nevada: Nevada Department of Conservation and Natural Resources, Division of Water Resources, Water Resources-Reconnaissance Series Report 59, 126 p.

Meyers, J.S., 1962, Evaporation from the 17 Western States: U.S. Geological Survey Professional Paper 272–D, 100 p.

Moore, J.G., 1969, Geology and mineral deposits of Lyon, Douglas, and Ormsby Counties, Nevada: Nevada Bureau of Mines and Geology Bulletin 75, 45 p.

Rose, R.L., 1969, Geology of parts of the Wadsworth and Churchill Butte quadrangles, Nevada: Nevada Bureau of Mines and Geology Bulletin 71, 27 p.

Schaefer, D.H., 1988, Bouguer gravity anomaly maps of Paradise, Stagecoach, Dixie, Fairview, and Stingaree Valleys, northwestern Nevada: U.S. Geological Survey Geophysical Investigations Map GP–985, 1 sheet.

Schaefer, D.H., Duffrin, B.G., and Plume, R.W., 1986, Principal facts for gravity stations in Paradise and Stagecoach Valleys, Humboldt and Lyon Counties, Nevada: U.S. Geological Survey Open-File Report 85–694, 15 p.

Thompson, G.A., 1956, Geology of the Virginia City quadrangle, Nevada: U.S. Geological Survey Bulletin 1042–C, p. 45–75.

# A Comparison of the Brune and Churchill Methods for Computing Sediment Yields Applied to a Reservoir System

*By* Stanley W. Trimble *and* William P. Carey

**Abstract**

The Tennessee River basin provides an opportunity to determine regional sediment yields by use of available accumulation data from a system of 27 reservoirs throughout the basin. A method of analysis, the Churchill method, that distinguishes between the amount of accumulated sediment that originates from the local contributing drainage area of a reservoir and the amount that has passed through an upstream reservoir has been adapted to analyze data for the series of reservoirs from the headwaters to the mouth of the Tennessee River. The results of the Churchill method of analysis are compared to the results of an alternative method—the Brune method—that does not distinguish between the two sediment sources.

Sediment yields calculated by using the Brune method are all equal to or higher than the Churchill values, but in general the two values are similar. Differences in sediment yields of more than 50 percent between Churchill and Brune values occur at only five reservoirs and indicate that the most uncertainty occurs for reservoirs whose contributing drainage area is only a small percentage of its total drainage area, reservoirs with low trap efficiencies, and reservoirs where a significant amount of accumulated sediment has passed through an upstream reservoir. Differences in sediment yield among the remaining 22 reservoirs range from 0 to 35 percent and average 10 percent. The use of both methods for analyzing a series of reservoirs can delineate areas that require more detailed analysis.

The lower sediment-yield figures for the Churchill analysis are more in agreement with sediment yields derived from measured suspended-sediment data. The Churchill values range from 150 to 2,600 tons per square mile per year, have an areally weighted mean of 630 tons per square mile per year, and indicate that 81 percent of the Tennessee River basin has sediment yields less than 800 tons per square mile per year.

## INTRODUCTION

Although reservoir accumulation data have been used for decades as a means of estimating sediment yield (Gottschalk, 1948), the determination of regional sediment yields using data from a series of reservoirs in a large drainage basin is unique. The numerous reservoirs constructed in the Tennessee River basin provide an excellent opportunity for regional sediment-yield analysis by using accumulation data from a series of reservoirs.

The Tennessee Valley Authority (TVA) began constructing a comprehensive system of multiple-purpose reservoirs on the main stem of the Tennessee River and its tributaries in 1933. At the time TVA began this program, two impoundments were already in place on the Tennessee River, and nine existed in the tributary basins. By 1945, 16 dams were completed, and by 1967 the entire system consisted of 31 reservoirs with storage capacities greater than 25,000 acre-ft. Nine of these reservoirs are on the Tennessee River, and 22 are on tributaries. These large reservoirs make excellent sediment traps because the quiescent waters allow much of the stream's sediment load to settle out. However, in order to assess the amount of sediment accumulating, each reservoir must be resurveyed periodically.

Sediment accumulation data from reservoir surveys are compiled and published every 5 yr. The most recent edition of this compilation, which includes comprehensive coverage of the Tennessee Valley, is the 1975 edition (Dendy and Champion, 1978). A more recent update that contains data reported between 1976 and 1980 was published in 1983 (U.S. Geological Survey, 1983); however, that report contains updated information on only 4 of the 27 reservoirs used in this study. For this study, sediment-accumulation data from 22 major reservoirs having design storage capacities greater than 75,000 acre-ft and 5 smaller reservoirs with contributing drainage areas greater than 50 $mi^2$ have been used.

This paper presents a method of determining regional sediment yields by using sediment-accumulation data from a series of reservoirs. Two existing methods of analysis are applied to sediment-accumulation data from 27 reservoirs in the Tennessee River basin.

## METHODS OF ANALYSIS

### Reservoir Data

Sedimentation-accumulation data from reservoir surveys have both advantages and disadvantages compared to measured suspended-sediment data for calculating sediment yields. The advantages of using reservoir data are as follows:

1. Suspended-sediment samplers cannot get closer than about 3 in. to the streambed, thus a part of the total sediment load transported in this unsampled zone does not get measured. Because most of this material is coarse, reservoirs with high trap efficiencies impound virtually all of the normally unmeasured load.
2. Most of the annual sediment load of a stream is transported during high-flow events, which occur only a small percentage of the time. If suspended sediment is not sampled during these critical high flows, the resulting sediment-yield estimates may be significantly in error. Reservoirs intercept all flow that moves down the channel and, thus, trap some percentage of the sediment being transported by every flow event.

The disadvantages of using reservoir data are as follows:

1. Trap efficiency, the percentage of incoming sediment impounded by the reservoir, is difficult to determine and is probably the greatest element of uncertainty. Although methods are available to estimate average trap efficiency, trap efficiency of a reservoir is expected to change with stream discharge, sediment characteristics, water temperature, and reservoir operation. Especially troublesome are density currents which, under certain conditions of water temperatures and water release from the reservoir, allow direct passage of sediment through the reservoir. A density current is a highly turbid and relatively dense current, which usually moves along the bottom of a body of standing water (U.S. Geological Survey, 1977). The relatively higher density can be caused by suspended sediment, dissolved-solids concentrations, or water-temperature differences. Density currents exist in some TVA reservoirs, but data available are inadequate to determine their significance (Fry and others, 1953).
2. Bulk densities of reservoir sediment are difficult to ascertain, especially in reservoirs with considerable drawdown, where some sediment is dried periodically and thereby compacted. Such dried sediment may have bulk densities twice that of submerged sediment. Bulk densities used in this study were furnished by TVA (Dendy and Champion, 1978), but many of them were clearly estimates.
3. Reservoirs affect downstream sediment movement in a nondeterministic manner when their trap efficiencies are uncertain or highly variable. In order to obtain local sediment yields for a particular reservoir drainage area, the sediment outflow from the upstream reservoir must be subtracted from the total sediment collected during the same time period. A reservoir with a large, gross drainage area, but with another large reservoir a short distance upstream, provides a particular problem because the net contributing drainage area is small and the potential for error is great. Sediment routing procedures through a series of reservoirs are discussed later in this paper.
4. The measurement of sediment accumulation in reservoirs also presents problems. Resurveys usually are done by surveying cross-sectional profiles some distance apart. Each range is assumed to be a representative sample of a zone, and any lack of representation presents an error. The effect of above-crest or delta deposits is also uncertain because it is sometimes difficult to determine where reservoir-induced deposits end and where recent vertical accretion on the flood plains begins.
5. Reservoir sediment data define total yields but do not define the sediment transport dynamics of the inflowing system.
6. Shore erosion may add sediment to the pool. This volume is not always measurable and thus adds uncertainty. For example, fine material may be eroded from the pore space in gravel-rocky soil with little degradation on the banks and thus cause notable accumulation in the deeper part of the reservoir. Wave action primarily affects above-crest areas, but such areas are not always included in reservoir sediment surveys.

Despite the difficulties cited above, reservoirs with high trap efficiencies probably give the best long-term sediment-yield data available. This assumes that both the reservoir and the bulk density of sediment have been properly measured. Reservoir surveys are discussed in detail by Borland (1971).

#### Trap Efficiency Calculations

Estimating trap efficiency (TE) is the greatest problem in sediment-yield analysis from reservoir data. Trap efficiency is defined as the percentage of inflowing sediment that is retained in the reservoir (Vanoni, 1975). There are two basic methods for estimating TE—namely, the Brune method (Brune, 1953) and the Churchill method (Churchill, 1948). The Brune method is the most commonly used.

1. For the Brune method, the reservoir capacity is divided by the average annual inflow, the result being the retention time. This numerical index is then related to trap efficiency (fig. 1).
2. The Churchill method, like the Brune method, uses the retention time, but that value is divided by the average velocity of water in the reservoir, a function of reservoir shape. The result is Churchill's sedimentation

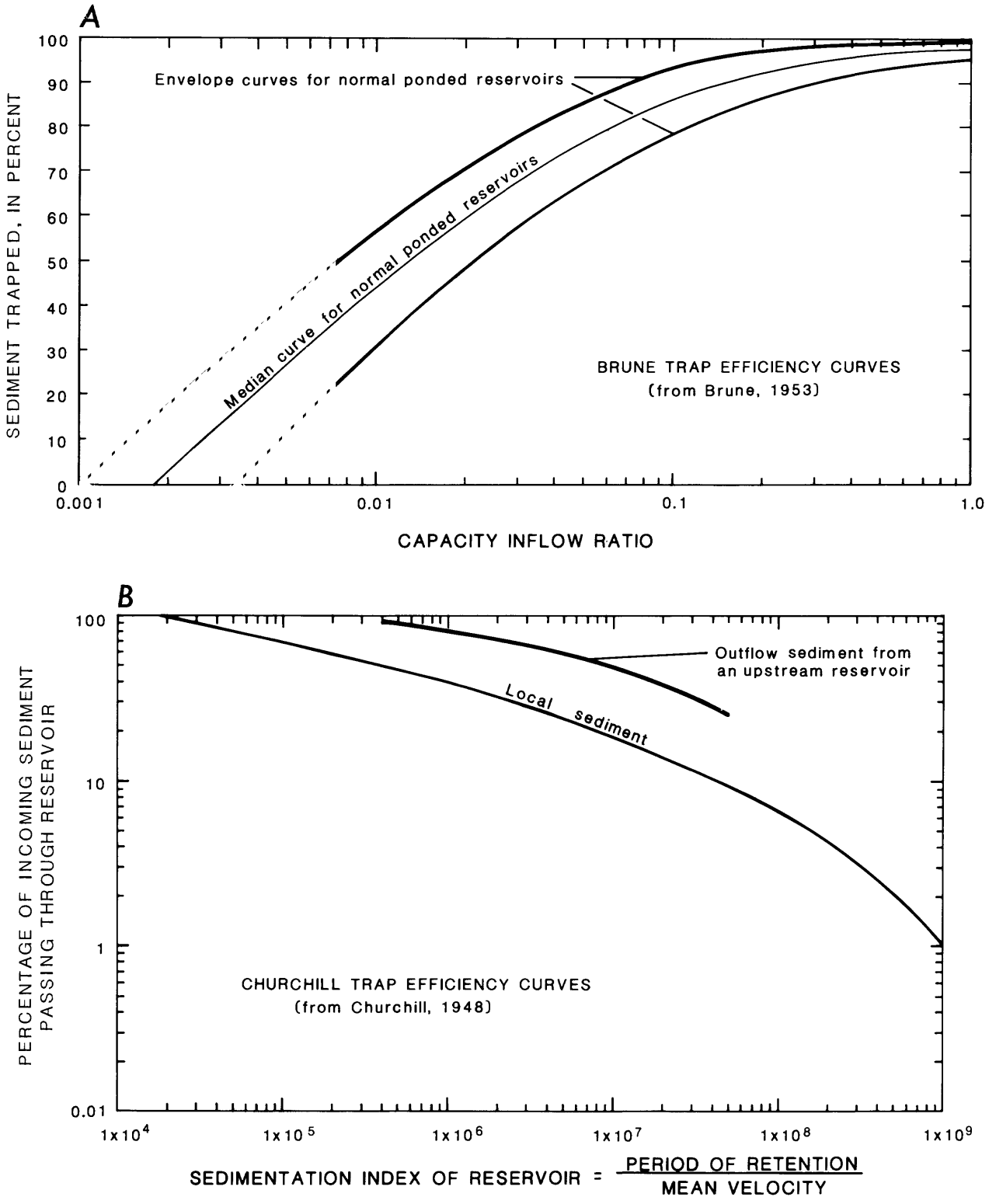


**Figure 1.** Trap efficiency curves: (*A*) Brune trap efficiency curves and (*B*) Churchill trap efficiency curves.

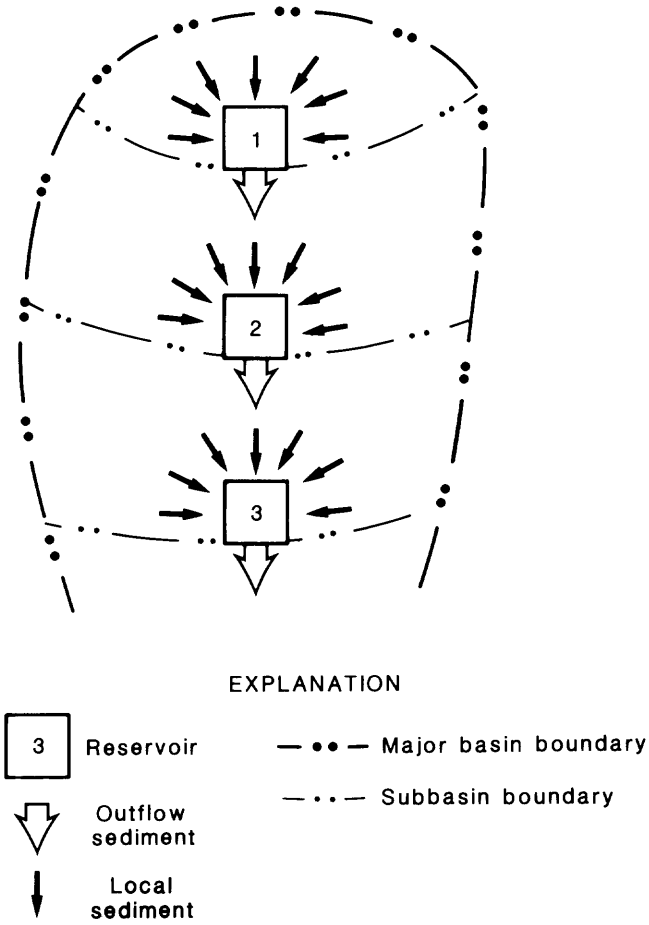


**Figure 2.** Diagrammatic sediment contributions to reservoir series.

index which is related to trap efficiency. The Churchill method accounts for both local sediment and sediment discharged from an upstream reservoir. Sediment that is discharged by an upstream reservoir will be referred to as outflow sediment. Local sediment is sediment that has been delivered to the reservoir from the contributing drainage area.

### Reservoir Calculations

The Churchill method for calculating sediment yield for reservoirs in series is illustrated by the following example. Consider three reservoirs in series as shown by figure 2. Sediment yield is first calculated for the headwater reservoir (reservoir 1 in fig. 2). The local yield for the area contributing to reservoir 1 is computed by:

$$LY = \frac{AA}{LTE} / LDA \ , \qquad (1)$$

where

*LY* is the local yield,
*AA* is the average-annual accumulation,
*LTE* is the local trap efficiency (fig. 1*B*), and
*LDA* is the local contributing drainage area.

The outflow sediment load is then:

$$OSL = \frac{AA}{LTE} - AA \ , \qquad (2)$$

where *OSL* is the outflow sediment load. The outflow sediment load is assumed to be transported downstream to reservoir 2.

The sediment load flowing into reservoir 2 consists of sediment derived from the local contributing area and outflow sediment from reservoir 1. Thus the accumulated sediment in reservoir 2 must be adjusted for the sediment contributed from reservoir 1.

$$NLAR2 = AAR2 - [(OSLR1)(OTER2)], \qquad (3)$$

where

*NLAR2* is the net local accumulation in reservoir 2,
*AAR2* is the average-annual accumulation in reservoir 2,
*OSLR1* is the outflow sediment load from reservoir 1, and
*OTER2* is the outflow trap efficiency (fig. 1*B*) for reservoir 2.

Net local accumulation is then used to compute local yield just as average-annual accumulation was used for reservoir 1. The outflow sediment load from reservoir 2 consists of the sediment from reservoir 1 that was not trapped by reservoir 2 plus that part of the local sediment load that was not trapped by reservoir 2.

$$OSLR2 = (OSLR1)(1-OTER2) + (NLAR2)(1-LTER2) \qquad (4)$$

where *OSLR2* is the outflow sediment load from reservoir 2 and
*LTER2* is the local trap efficiency for reservoir 2.

The computations described for reservoir 2 are repeated for all remaining downstream reservoirs. Thus the analysis cascades sediment from the headwater reservoir down through the reservoir system.The Brune method is much more straightforward, because it does not account for sediment that has already passed through an upstream reservoir. The Brune method assumes that all accumulated sediment has come from the local contributing area. The local-sediment yield is simply:

$$LSY = \frac{AA}{BTE} / LDA \ , \qquad (5)$$

where *BTE* is the Brune trap efficiency. Brune trap efficiencies used in this study were selected from the median curve in figure 1*A*. The envelope curves indicate the range of values plotted by Brune (1953).

## SEDIMENT YIELD

Sediment yields calculated from Churchill curves range from 150 (tons/mi$^2$)/yr at Melton Hill to 2,600

(tons/mi$^2$)/yr at Ocoee No. 3; for Brune curves the range is from 170 (tons/mi$^2$)/yr at Melton Hill to 4,100 (tons/mi$^2$)/yr at Ocoee No. 3 (table 1, fig. 3). The areally weighted mean yield is 630 (tons/mi$^2$)/yr for Churchill values and 740 (tons/mi$^2$)/yr for Brune values. The Brune values are all equal to or higher than the Churchill values, but in general the two values are similar.

Increases of more than 50 percent between Churchill and Brune yields occur at Fort Patrick Henry, Nolichucky, Ocoee No. 3, Ocoee No. 1, and Wilson Reservoirs. The remaining increases range from 0 to 35 percent and average 10 percent. Both Fort Patrick Henry and Wilson Reservoirs have very low net contributing areas compared to their total drainage area. The net contributing area is only 3 percent of the total at Fort Patrick Henry and only 4 percent at Wilson. The calculation of sediment yield for these reservoirs is very sensitive to the amount of outflow sediment from an upstream reservoir. Outflow sediment trapped by Fort Patrick Henry accounts for 43 percent of the total accumulation, and in Wilson it accounts for 70 percent of the total. Reductions in the outflow trap efficiencies of these two reservoirs would result in substantially higher local sediment yields. The Brune yield probably represents a more realistic estimate for Fort Patrick Henry, and a weighted average of Churchill values from Pickwick and Wheeler Reservoirs probably represents a more realistic estimate for Wilson—470 (tons/mi$^2$)/yr.

The difference in the Nolichucky yields is simply a function of the large difference in trap efficiencies that occurs at low TE values. The Brune yield is about two times the Churchill local yield, and the Brune TE is one-half the Churchill local TE. The average of the two yields—610 (tons/mi$^2$)/yr—probably represents a more accurate estimate of the true yield for the Nolichucky drainage.

The Ocoee Reservoirs are downstream of the region known as the Copper Basin in the southeastern corner of Tennessee. Much of the forest in this basin was cut for use as mine timbers in the copper mines and also for use as charcoal in the refining furnaces. Sulfur dioxide fumes created by copper refining subsequently denuded a considerable area in the basin. The Copper Basin drains directly into Ocoee No. 3 and, thus, accounts for the high sediment yields indicated by Ocoee No. 3. Ocoee No. 3 has relatively low TE's of 70 Churchill local and 45 Brune, which indicate that a substantial amount of sediment is passed on to Ocoee No. 1. Ocoee No. 1 has relatively high TE's of 80 Churchill outflow and 85 Brune. Calculation of Churchill local yield for Ocoee No. 1 is sensitive to the high outflow TE combined with the large outflow load from Ocoee No. 3. The result—190 (tons/mi$^2$)/yr—is an apparent underestimation of the true yield. The Brune estimate—2,300 (tons/mi$^2$)/yr—is much too high because it does not account for sediment passed through an upstream reservoir. This case is similar to Wilson Reservoir where errors in the two methods offset the yield estimate in opposite directions. Based on surrounding yield information, the true yield for Ocoee No. 1 probably is in the 300 to 700 (tons/mi$^2$)/yr range. The average of both values for Ocoee No. 3—3,400 (tons/mi$^2$)/yr—can be used as an estimate of the local yield.

Another area of high sediment yield is the Kentucky Lake basin. One possible explanation is that much of the sediment is coming from the west side of the Tennessee River where short, steep streams drain basins composed all or in part of the erodible coastal plain sediments of western Tennessee. Evidence for this comes from six small reservoirs just west of Kentucky Lake near Lexington, Tenn. The combined net drainage area of 40.75 mi$^2$ of these six basins has a weighted average sediment yield of 1,600 (tons/mi$^2$)/yr. These high values would be offset by low sediment yields from the western Highland Rim physiographic province on the east side of Kentucky Lake.

Both the Churchill and Brune yield values for the Melton Hill drainage area appear to be anomalously low. A possible explanation is that Melton Hill has only 7 yr of data and these years had runoff that was 17 percent lower than the long-term (63 yr) average. Additional data from suspended-sediment sampling could help to explain yields from this basin and from the Kentucky Lake area.

## Summary of Sediment-Yield Data

A summary of reservoir sediment-yield data for the Tennessee River basin is shown in table 2. For yields of 0 to 1,000 (tons/mi$^2$)/yr, increments of 100 (tons/mi$^2$)/yr were chosen to present a more detailed picture than figure 3. The total contributing area for the Tennessee basin is 38,860 mi$^2$ (table 2), which is 97 percent of the 40,200 mi$^2$ drainage area for Kentucky Lake. The 3-percent difference is most likely due to measurement and rounding errors.The Churchill data summaries presented in table 2 show that approximately 81 percent of the Tennessee Valley has sediment yields less than 800 (tons/mi$^2$)/yr. The areally weighted mean yield is 630 (tons/mi$^2$)/yr, and the modal class is 400 to 499 (tons/mi$^2$)/yr. The Brune data, which are summarized in table 2, show that approximately 81 percent of the Tennessee Valley has sediment yields less than 1,000 (tons/mi$^2$)/yr. The areally weighted mean yield is 740 (tons/mi$^2$)/yr, and the modal class is 500 to 599 (tons/mi$^2$)/yr.The Brune data reflect not only the general increase in Brune numbers over Churchill numbers but also the influence of the high yields for Ocoee No. 3, Ocoee No. 1, and Kentucky Lake. Therefore, the Brune summary presented in table 2 is biased toward high values. The Churchill data, however, offset the high yield of Ocoee No. 3 and Kentucky Lake, with low yields for Fort Patrick Henry, Ocoee No. 1, and Wilson. Therefore the Churchill data summary given in table 2 is probably a more realistic representation of sediment yields in the Tennessee Valley.The lower Churchill numbers also are closer to the yields derived from

**Table 1.** Sediment yields computed from reservoir data

[(tons/mi$^2$)/yr, tons per square mile per year; *, no sediment accumulation data available; TE, trap efficiency]

| Reservoir | River | Period of record used | Churchill TE | Churchill Outflow TE | Brune TE | Churchill local yield, in (tons/mi$^2$)/yr | Brune yield, in (tons/mi$^2$)/yr | Next reservoir downstream |
|---|---|---|---|---|---|---|---|---|
| South Holston | South Holston | 1950-1964 | 100 | 100 | 100 | 490 | 490 | Boone |
| Wautauga | Wautauga | 1948-1964 | 100 | 100 | 100 | 630 | 630 | Boone |
| Boone | South Fork Holston | 1952-1964 | 95 | 90 | 90 | 520 | 550 | Fort Patrick Henry |
| Fort Patrick Henry | South Fork Holston | 1953-1964 | 75 | 45 | 55 | 220 | 530 | Cherokee |
| Cherokee | Holston | 1954-1964 | 100 | 95 | 95 | 300 | 330 | Fort Loudoun |
| Nolichucky | Nolichucky | 1925-1970 | 60 | 15 | 30 | 410 | 810 | Douglas |
| Douglas | French Broad | 1943-1967 | 100 | 95 | 95 | 550 | 640 | Fort Loudoun |
| Fort Loudoun | Tennessee | 1946-1961 | 80 | 50 | 75 | 490 | 530 | Watts Bar |
| Nantahala | Nantahala | 1950-1969 | 100 | 100 | 95 | 670 | 710 | Fontana |
| Thorpe | West Fork Tuckasegee. | 1941-1969 | 100 | 100 | 100 | 400 | 400 | Fontana |
| Fontana | Little Tennessee | 1944-1967 | 100 | 100 | 95 | 430 | 460 | Calderwood* |
| Norris | Clinch | 1936-1970 | 100 | 95 | 100 | 310 | 310 | Melton Hill |
| Melton Hill | Clinch | 1963-1970 | 85 | 60 | 75 | 150 | 170 | Watts Bar |
| Watts Bar | Tennessee | 1946-1961 | 85 | 60 | 80 | 630 | 710 | Chickamauga |
| Chatuge | Hiwassee | 1942-1965 | 100 | 100 | 100 | 520 | 520 | Hiwassee |
| Nottely | Nottely | 1942-1965 | 100 | 100 | 100 | 540 | 540 | Hiwassee |
| Hiwassee | Hiwassee | 1947-1965 | 100 | 80 | 95 | 310 | 320 | Appalachia |
| Appalachia | Hiwassee | 1943-1965 | 90 | 70 | 75 | 700 | 830 | Chickamauga |
| Blue Ridge | Toccoa | 1944-1968 | 100 | 100 | 95 | 340 | 350 | Ocoee #3 |
| Ocoee No. 3 | Ocoee | 1942-1972 | 70 | 35 | 45 | 2600 | 4100 | Ocoee #1 |
| Ocoee No. 1 | Ocoee | 1954-1968 | 95 | 80 | 85 | 190 | 2300 | Chickamauga |
| Chickamauga | Tennessee | 1954-1961 | 75 | 35 | 70 | 790 | 950 | Guntersville |
| Guntersville | Tennessee | 1940-1961 | 80 | 45 | 75 | 580 | 730 | Wheeler |
| Wheeler | Tennessee | 1947-1961 | 75 | 40 | 70 | 400 | 520 | Wilson |
| Wilson | Tennessee | 1936-1961 | 75 | 40 | 60 | 190 | 800 | Pickwick |
| Pickwick | Tennessee | 1938-1961 | 75 | 40 | 70 | 650 | 880 | Kentucky |
| Kentucky | Tennessee | 1946-1961 | 75 | 45 | 80 | 1200 | 1200 | NONE |

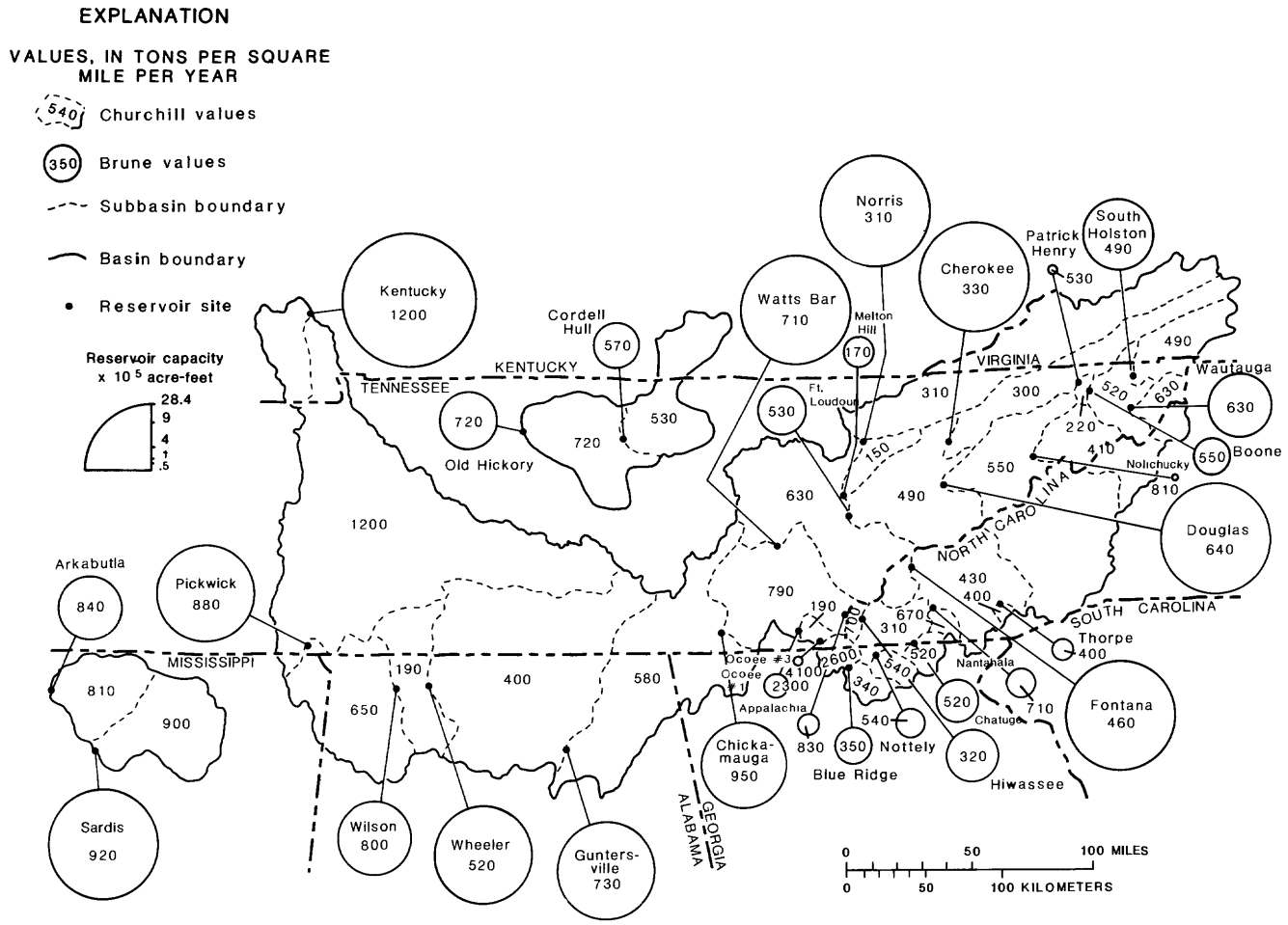


**Figure 3.** Sediment yields computed from reservoir data.

measured suspended-sediment data. Flint (1983) reported sediment yields in southeastern Kentucky that ranged from 250 to 500 (tons/mi$^2$)/yr, except in heavily mined basins, where yields were sometimes greater than 2,000 (tons/mi$^2$)/yr. Unpublished results of a TVA study from 1963 to 1965 (Tennessee Valley Authority, written commun., 1981) showed that for 10 basins in the Valley, 1 had a yield greater than 500 (tons/mi$^2$)/yr, 5 had yields ranging from 250 to 500 (tons/mi$^2$)/yr, and 4 had yields less than 250 (tons/mi$^2$)/yr. Caution should be exercised when comparing sediment yields from stream measurement to those from reservoir data. The reservoir data are longer term, more comprehensive areally, and more comprehensive in terms of inclusion of all sediment-transporting events. Also, the contribution of unmeasured load in the Tennessee River Valley has not been assessed. This contribution is believed to be small, but it cannot be determined easily for channels with coarse and variable bed material.

## CONCLUSIONS

The system of reservoirs that extend from the headwaters to the mouth of the Tennessee River provides an opportunity to assess regional sediment yields. Of the two methods used for analyzing the reservoir accumulation data, the Brune values are all equal to or higher than the Churchill values, but in general the two values are similar. The Churchill method, which accounts for sediment received from an upstream reservoir, probably provides a more realistic estimate of sediment yields for a system of reservoirs than the Brune method. The use of both methods for analyzing a system of reservoirs can delineate areas where the data need closer scrutiny and analysis.

Differences in sediment yields of more than 50 percent between Churchill and Brune yields occur at only four reservoirs. The remaining percentage differences range from 0 to 35 and average 10 percent. Large discrepancies

**Table 2.** Summary of reservoir sediment-yield data for the Tennessee River basin using the Churchill and Brune methods

| Yield class (tons/mi²)/yr | Contributing area Tennesse basin, in mi² | Percent of area Tennessee basin | Cumulative percent Tennessee basin |
|---|---|---|---|
| | **Churchill method** | | |
| 100–199 | 1,653 | 4.2 | 4.2 |
| 200–299 | 62 | .2 | 4.4 |
| 300–399 | 5,066 | 13.0 | 17.4 |
| 400–499 | 9,922 | 25.5 | 42.9 |
| 500–599 | 7,442 | 19.2 | 62.1 |
| 600–699 | 5,468 | 14.1 | 76.2 |
| 700–799 | 1,853 | 4.8 | 81.0 |
| 800–899 | 0 | 0 | 81.0 |
| 900–999 | 0 | 0 | 81.0 |
| 1,000–1,999 | 7,131 | 18.4 | 99.4 |
| 2,000–2,999 | 263 | .7 | 100.1 |
| Total | 38,860 | | |
| | **Brune method** | | |
| 100–199 | 422 | 1.1 | 1.1 |
| 200–299 | 0 | 0 | 1.1 |
| 300–399 | 5,066 | 13.0 | 14.1 |
| 400–499 | 2,151 | 5.5 | 19.6 |
| 500–599 | 7,699 | 19.8 | 39.4 |
| 600–699 | 3,312 | 8.5 | 47.9 |
| 700–799 | 6,553 | 16.9 | 64.8 |
| 800–899 | 4,362 | 11.2 | 76.0 |
| 900–999 | 1,805 | 4.6 | 80.6 |
| 1,000–1,999 | 7,131 | 18.4 | 99.0 |
| 2,000–2,999 | 96 | .2 | 99.2 |
| 3,000 | 263 | .7 | 99.9 |
| Total | 38,860 | | |

between the Churchill and Brune values seem to occur for reservoirs where the contributing drainage area is only a small percentage of the total drainage area, reservoirs with low trap efficiencies, and reservoirs where a significant amount of accumulated sediment has passed through an upstream reservoir.

## REFERENCES CITED


Borland, W.M., 1971, Reservoir sedimentation, *in* Shen, H.W. ed., River mechanics: Fort Collins, Colorado, Shen, v. 2, p. 29–1 to 29–38.

Brune, G.M., 1953, Trap efficiency of reservoirs: American Geophysical Union Transactions, v. 34, no. 3, p. 407–418.

Churchill, M.A., 1948, Discussion of analysis and use of reservoir sedimentation data: Federal Inter-Agency Sedimentation Conference, Denver, Colorado, 1947, Proceedings, p. 139–140.

Dendy, F.E., and Champion, W.A., 1978, Sediment deposition in U.S. reservoirs—Summary of data reported through 1975: U.S. Department of Agriculture Miscellaneous Publication 1362, 82 p.

Flint, R.F., 1983, Fluvial sedimentation in Kentucky: U.S. Geological Survey Water-Resources Investigations Report 83–4152, 75 p.

Fry, A.S., Churchill, M.A., and Elder, R.A., 1953, Significant effects of density currents in TVA's integrated reservoir and river system, *in* Proceedings, Minnesota International Hydraulic Convention: p. 335–354.

Gottschalk, L.C., 1948, Analysis and use of reservoir sedimentation data: Federal Inter-Agency Sedimentation Conference, Denver, Colo, 1947, Proceedings, p. 131–138.

U.S. Geological Survey, 1977, National handbook of recommended methods for water-data acquisition: Office of Water Data Coordination, chap. 3, 100 p.

———1983, Sediment deposition in U.S. reservoirs—Summary of data reported 1976–1980: Office of Water Data Coordination, 32 p.

Vanoni, V.A., ed., 1975, Sedimentation engineering: American Society of Civil Engineers, Manuals and Reports on Engineering Practice, no. 54, 745 p.

# Bubble-Gage Registration Errors Caused by Gas Column Density

*By* Winchell Smith

**Abstract**

Significant manometer-registration errors can occur in installations where there is a wide range of stage and the manometer is placed high above the orifice. These errors will occur unless the weight of the nitrogen in the bubble system is accounted for. The errors are very nearly linear, and can be corrected by changing the gearing between the manometer and the recorder.

## INTRODUCTION

The California District of the U.S. Geological Survey (USGS) accepted responsibility in April 1972 for the operation of a large servo-controlled manometer system designed for monitoring water levels in the new Don Pedro Reservoir. This is a gas-purged bubble-gage system that utilizes a 240-in. temperature-compensated Servomanometer, supplied by Statham Industries, to sense the pressure input to an orifice line 3,000 ft in length and 3/8-in. inside diameter. The manometer is located on the top of the dam at an elevation of 831 ft above mean sea level. The orifice is at an elevation of 600 ft above mean sea level. Two orifice lines were installed; however, only one line is used in the operation. The second line was placed as insurance against possible leakage.

The manometer system was put in operation on April 26, 1972, when the reservoir elevation was 658 ft. During the following months, withdrawals progressively lowered the water level of the reservoir, and it soon became apparent that a cumulative error was developing between staff-gage readings and levels indicated by the manometer. When the lake level had reached an elevation of 610 ft, the manometer was reading 610.5 ft. This same, apparently linear, calibration error persisted as the reservoir refilled, and by January 18, 1973, when a lake surface elevation of 650 ft was reached, the departure was less than 0.1 ft. The system was connected to the second orifice line on this date and reset to agree with the outside staff gage. Periodic inspections made as the reservoir filled during the spring of 1973 showed the same apparent calibration error. When a stage of 735 ft was reached in June, a cumulative error of −0.86 ft was recorded. These data are plotted in figure 1.

This performance of the manometer led to considerable frustration. Staff gages were checked and rechecked by level surveys. The gas-purged system was checked and rechecked for leakage. Isolation of the system (no gas flow into it) for a period of 18 h showed very minor leakage corresponding to a head loss of less than a foot against a total head of 115 ft. Friction losses in the long orifice line were apparently negligible, as indicated by the fact that the manometer readout did not change when purge rates were varied from 20 bubbles per minute to 200 bubbles per minute. The conclusion from all of this study was that there must be a calibration error in the manometer itself, and a field check was made to verify this conclusion. With the cooperation of the manufacturer, the servo unit was checked against a separate mercury manometer and then against another servo device furnished by Statham Industries. These calibration checks indicated that the unit was functioning perfectly; there was no definable error in the instrument calibration over a 100-ft range in stage.

In summary, the calibration of the manometer itself was accurate, friction losses in the system were negligible, there were no leaks in the system, and empirical data indicated a 1 percent underregistration for the system. The system was nearly perfect, yet it did not accurately follow changes in reservoir elevation. What was the problem?

## SYSTEM ANALYSIS

Review of U.S.Geological Survey literature and the bubble-gage manual, in particular, provides no ready

[1]This paper originally was entitled: "Does your bubble gage give you the right answer?" and was printed in 1974 in a U.S. Geological Survey (USGS) internal publication. The subject of the paper continues to be of interest. Although the paper refers to a manometer installation, it is emphasized that any instrument using the bubble gage pressure monitoring system will be subject to these same errors. Changing the sensor from a mercury manometer to a pressure transducer will not change the physics of the bubble gage system. Thus, the author's analysis of the subject still is technically correct, comprehensive, and germane. There appears to be no comparable analysis of the subject available in the hydrologic literature to this day. Editor

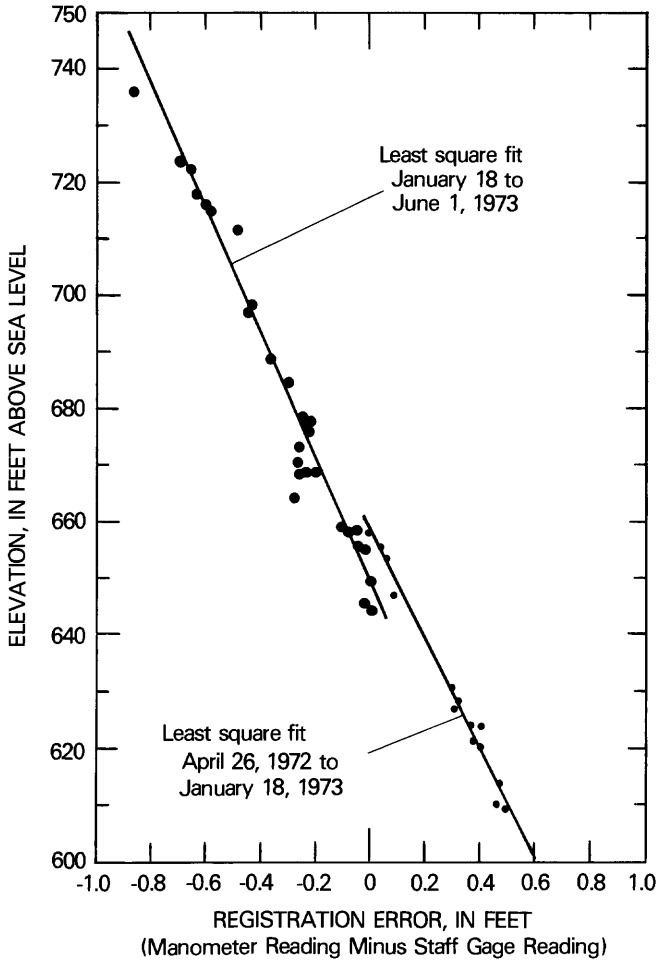


**Figure 1.** Observed performance of manometer at Don Pedro Reservoir.

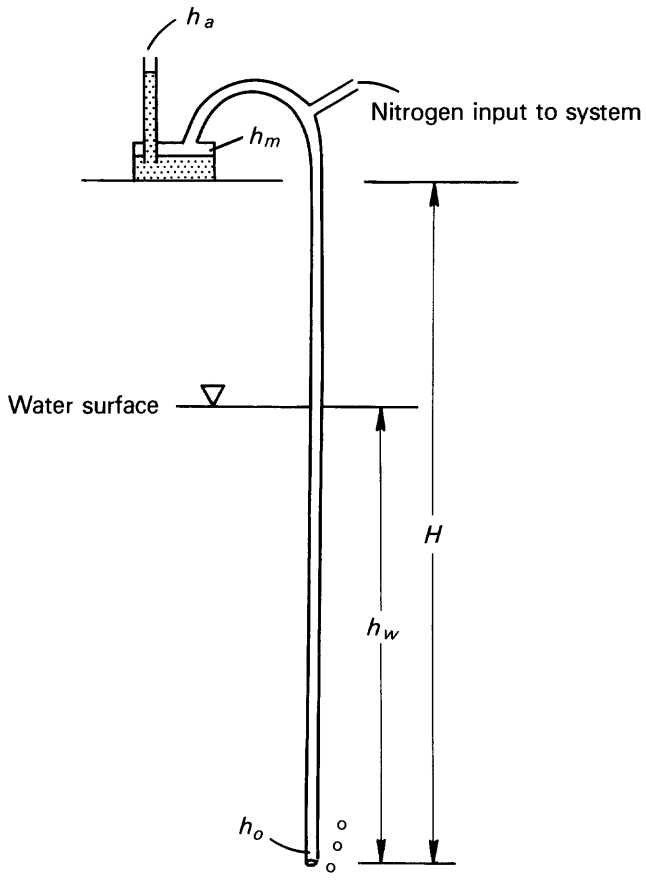


**Figure 2.** Basic manometer system. See text page 205 for explanation of symbols.

answer to the problem found at Don Pedro Reservoir. The following quotation from page 3 of the bubble gage manual (U.S. Geological Survey, Research Section, Columbus, Ohio, written commun., 1962) assures us that errors due to the weight of nitrogen will be small.

> Water is approximately 900 times as heavy as nitrogen (under standard conditions) so that errors due to variations in the weight of the gas will be small. Since the servomanometer assembly can be adjusted to compensate for all errors that vary linearly with stage, the only other error due to variation in the weight of the gas is that due to temperature. Because nitrogen, at atmospheric pressure, has very nearly the same weight as air, and the weight of the atmosphere also varies with temperature, it is only the effect of the difference between the average temperature of the gas in the bubble tube and the air temperature that need be considered. For example, if the recording equipment is mounted 100 feet above the bubble orifice in the river with 2 feet of water over the orifice, and the average temperature of the gas in the bubble tube is constant at 40 °F while the air temperature increases from 40° to 70 °F, the error in the recorded level would be less than 0.01 foot. This error would decrease with the river stage and with the height of the equipment. For the usual height of equipment, this would not seriously affect the accuracy at low water, where greater accuracy is required.[1]

Taken at face value, this quotation indicates that the weight of the nitrogen in the closed system is so small that it can be ignored. This is a convenient assumption, and the success of the USGS's field use of bubble gages attests to the fact that it is generally justifiable. However, the following analysis, which was generated by the frustrations of the Don Pedro system, graphically illustrates that, in some instances, errors due to the weight of nitrogen are neither small nor due only to temperature variations.

Referring to the schematic system shown in figure 2, the following relations hold:

$$h_r = h_m - h_a \tag{1}$$

$$h_O = \gamma h_w + h_a + \Delta h_a \tag{2}$$

$$h_m = h_O - \Delta h_{N_2} \tag{3}$$

[1] *See also* Rantz (1982, p. 74) regarding errors due to variations in the weight of nitrogen in the bubble tube of bubble gages. [Editor.]

$$R_e = h_r - h_w \tag{4}$$

Substituting equations 1, 2, and 3, into equation 4:

$$R_e = \gamma h_w - h_w + \Delta h_a - \Delta h_{N_2} \tag{5}$$

where

$h_r$ is pressure head recorded by the manometer,
$h_m$ is absolute pressure head in closed leg of manom eter,
$h_a$ is atmospheric pressure head at the manometer,
$h_O$ is absolute pressure head at the orifice,
$h_w$ is height of water column above orifice,
$\gamma$ is specific gravity of water,
$\Delta h_a$ is difference in atmospheric pressure head between manometer and the water surface,
$\Delta h_{N_2}$ is difference in pressure head in closed system due to weight of nitrogen in the column of height $H$,
and $R_e$ is the registration error.

The factors $\Delta h_a$ and $\Delta h_{N_2}$ are functions of the altitude of the system, the geometry of the system, temperature, and variations in $h_w$. The specific gravity of water, $\gamma$, also varies with temperature. For this analysis it is assumed that isothermal conditions prevail in the water column, in the closed system, and in the air column above the water surface. Temperature in this air column will certainly not conform to the normal adiabatic lapse rate due to the influence of evaporative cooling at the water surface. The analysis would not be influenced significantly in any case, so, for convenience, an isothermal condition is assumed in both the closed and open parts of the system.

The factors $\Delta h_{N_2}$ and $\Delta h_a$ can be computed by use of gas law relations. Considering the system with origin at the orifice and using normal gas law notation, then:

$$dP = -\rho_{N_2} dH$$

where $\rho$ is the gas density, which is a function of pressure $P$ and temperature $T$.
From the gas laws:

$$\rho = \frac{PM}{RT} = kP \tag{6}$$

where R = the universal gas constant, $M$ is the molecular weight of the gas, and $k = M/RT$, which is a constant for a given gas at a given temperature.

Thus $dP = -k_{N_2} P dH$

and $\frac{dP}{P} = -k_{N_2} dH$

and $\int_{P_O}^{P_m} \frac{dp}{p} = -k_{N_2} \int_O^H dH$

or $\ln P_m/P_O = -k_{N_2} H$ . (7)

Substituting $h_m$ for $P_m$ and $h_O$ for $P_O$ and rearranging equation 7 yields

$$h_m = \exp [\ln h_O - k_{N_2} H] = h_O \exp [-k_{N_2} H].$$

But $\Delta h_{N_2} = h_O - h_m$, from equation 3; thus

$$\Delta h_{N_2} = h_O - h_O \exp [-k_{N_2} H] = h_O(1 - \exp [-k_{N_2} H]). \tag{8}$$

By a similar analysis it can be shown that

$$\Delta h_a = h_a [\exp (k_a (H - h_w)) - 1]. \tag{9}$$

Substitution of equation 2 into equation 8 and of equation 8 and 9 into equation 5 and simplifying yields

$$R_e = \exp(-k_{N_2} H)[\gamma h_w + h_a \exp (k_a(H - h_w))] - h_w - h_a. \tag{10}$$

For the Don Pedro installation with the manometer at elevation 831 ft above mean sea level and the orifice at 600 ft above mean sea level:

$H$= 231 ft,
$h_w$ varies from 0 to 200 ft ±,
$h_a$= 32.87 ft by interpolation from standard atmospheric data,
$\rho_a$= 0.08071 lb/ft$^3$, and
$\rho_{N_2}$= 0.07807 lb/ft$^3$ at 32 °F and 14.67 psia.
Then for any given temperature, $T$

$$k_a = \frac{0.08071}{(14.67)(144)} \left(\frac{492}{T+460}\right)$$

$$= 3.80206 \times 10^{-5} \left(\frac{492}{T+460}\right)$$

and $k_{N_2} = \frac{0.07807}{(14.67)\ (144)} \left(\frac{492}{T+460}\right)$

$$= 3.6957 \times 10^{-5} \left(\frac{492}{T+460}\right)$$

The specific gravity of water varies with temperature as follows:

$\gamma$ = 0.9990 at 60 °F
0.9997 at 50 °F
1.0000 at 39 °F.

Temperature data for Don Pedro Reservoir are not available, but estimates based on downstream records suggest that the average temperature during the period of observation was about 10 °C or 50 °F.

Substitution of the constants listed above in equation 10 yields the following for various values of $h_w$ and $T$.

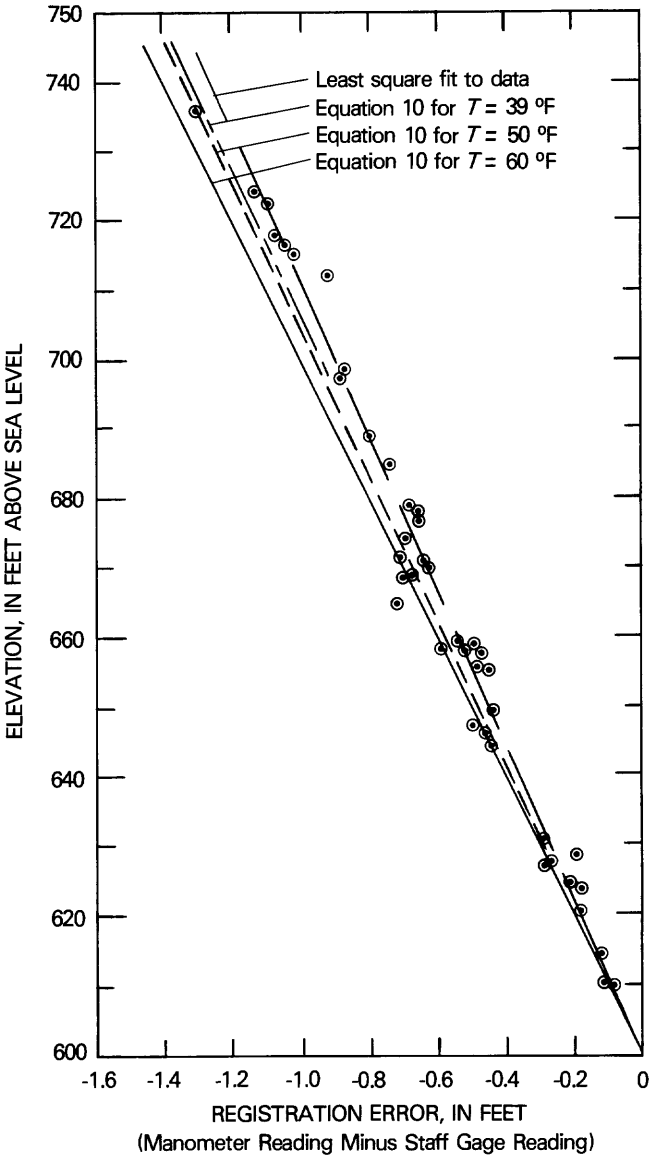


**Figure 3.** Registration errors computed by consideration of gas laws.

| Reservoir elevation (ft) | $h_w$ | $R_e$ | | |
|---|---|---|---|---|
| | | 39 °F | 50 °F | 60 °F |
| 600 | 0 | +0.009 | +0.009 | +0.009 |
| 620 | 20 | −.183 | −.185 | −.196 |
| 650 | 50 | −.471 | −.476 | −.502 |
| 700 | 100 | −.952 | −.962 | −1.013 |
| 750 | 150 | −1.433 | −1.447 | −1.524 |

These computations are plotted in figure 3. Data points shown are those given in figure 1 except that a correction was made for the datum adjustment made on January 18, and the abscissa has been shifted by a constant amount. Shown also in figure 3 is the least-squares line fitted to the data. The difference between this line and the computed 50 °F line is 0.099 ft at elevation 750 ft.

Analysis of the magnitude of the relative error sources included in equation 10 indicates that the recording errors observed at this installation relate primarily to the failure to account for the weight of nitrogen in the closed system. When $h_w$ is 100 ft and $T$ = 60 °F, for example, the error due to variation of the density of water with temperature ($T$ = 60 °F) is −0.100 ft. The error due to the difference in air pressure on the manometer and that on the water surface is +0.156 ft. The error due to the weight of nitrogen is −1.069 ft. Summation of these values yields the value of −1.013 given in the table above. Fortunately, the relationship expressed by equation 10 is very nearly linear, and the readout of the manometer can be easily corrected by a change in the gearing between the servo system and the recording equipment.

## PROBABLE ERRORS IN CONVENTIONAL INSTALLATIONS

The problem discovered at Don Pedro Reservoir represents an extreme case. The USGS does not normally operate bubble gages that cover a range of more than 200 ft with a single orifice and does not normally place manometers 200 ft or more above an orifice. Typically the range of the manometer is 50 or 35 ft, and typically it is placed no more than 75 ft above the orifice.

For reservoirs that have a large range in stage, multiple orifices are generally used, and the manometer is reset each time a change in orifice connections is made. Consequently, the error to be concerned with is that which would be accumulated within a 50-ft range. The following tabulation shows the evaluation of equation 10 for a registration error of a manometer system located near sea level and operating at an ambient temperature of 60 °F.

| Height of manometer, in feet above orifice, ($H$) | Registration error, in feet, for $h_w$ equal to: | | |
|---|---|---|---|
| | 20 | 35 | 50 |
| 50 | −0.077 | −0.137 | −0.196 |
| 75 | −.093 | −.166 | −.239 |
| 100 | −.110 | −.196 | −.282 |
| 150 | −.143 | −.255 | −.366 |

The registration errors tabulated will occur in a manometer system that does in fact record in feet of water the pressure in the purge line at the manometer without compensating for the height of the manometer above the orifice. This is true for the Servomanometer produced by Statham Industries. There is a question in the writer's mind as to whether or not partial compensation for this error source may have been accomplished with the USGS bubble gage by virtue of the techniques employed in laboratory calibration of the device. It is also possible that these errors have not been compensated for.

In the typical river gage, manometers are generally set to agree with an outside staff gage at low water. During flood stages, when there may be as much as 30 to 40 ft of water over the orifice, it is frequently not possible to accurately read the staff-gages, and departures of ± 0.2 ft between manometer dial readings and staff-gage readings are considered acceptable. As a matter of fact, errors are not carried over into the discharge computations because the stage-discharge relations are usually established on the basis of the manometer readings.

Reservoir records, however, present more of a problem and a number of mysteries have developed over the years because manometer readings have tended to drift away from the true stages. It is the expectation of this writer that application of the basic physics of the system, as discussed in this article, would go a long way toward eliminating these mysteries.

## CONCLUSIONS

The results of this study indicate that significant manometer-registration errors can occur in installations in which there is a large range of stage and the manometer is placed high above the orifice. These errors will occur unless the weight of the nitrogen in the bubble system is accounted for. The errors are very nearly linear and can be corrected by changing the gearing between the manometer and the recorder.

## REFERENCE CITED

Rantz, S.E., 1982, Management of stage and discharge, v. 1 *of* Measurement and computation of streamflow: U.S. Geological Survey Water-Supply Paper 2175, 284 p.